

BIRLA CENTRAL LIBRARY

PIHLANI (RAJASTHAN)

Call No. 621.384132

G48E V.1

Accession No. 55392

Acc. No 55392

**ISSUE LABEL**

**Not later than the latest date stamped below.**

--	--	--





# **ELECTRON TUBES**

**Volume I**

---

**(1935-1941)**



# ELECTRON TUBES

## Volume I

---

(1935-1941)

---

*Edited by*

ALFRED N. GOLDSMITH

ARTHUR F. VAN DYCK

ROBERT S. BURNAP

EDWARD T. DICKEY

GEORGE M. K. BAKER

MARCH, 1949

Published by

RCA REVIEW

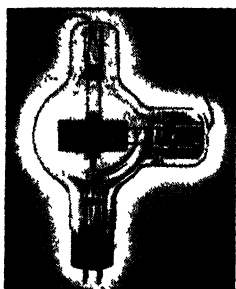
RADIO CORPORATION OF AMERICA

RCA LABORATORIES DIVISION

Princeton, New Jersey

Copyright, 1949, by  
Radio Corporation of America  
RCA Laboratories Division

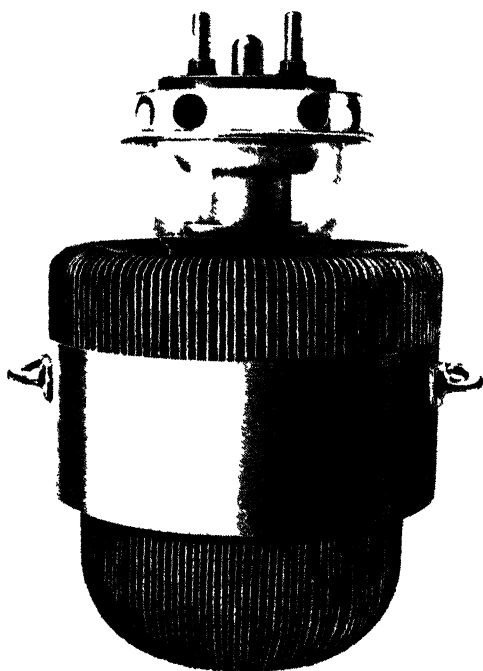
**Printed in U.S.A.**



1920's



EARLY 1940's



# **ELECTRON TUBES** **PAST AND RECENT**



# ELECTRON TUBES

## Volume I

---

(1935-1941)

---

### PREFACE

The wealth of material on the general subject of vacuum tubes and thermionics which was originally published during the years 1935-1948 has required more than one volume for its presentation even though a very stringent selection process has been followed by the editors. Accordingly, two volumes are being published at this time.

This book, ELECTRON TUBES, Volume I, is the ninth volume in the **RCA Technical Book Series** and the first devoted exclusively to tubes. It covers the period 1935-1941; the companion book, ELECTRON TUBES, Volume II, carries the series through 1948.

Papers are presented in four sections: general; transmitting; receiving; and special. As additional sources of reference, the appendices contain a bibliography on vacuum tubes, thermionics, and related subjects and a reference list of Application Notes. The bibliography has been included to insure that applicable material on tubes is available in this volume—at least in reference form. Papers concerning tubes which relate to specific applications or fields such as television, facsimile, UHF, or frequency modulation, are listed in the bibliography; they are covered, however, in other volumes of the Technical Book Series.

\* \* \*

RCA Review gratefully acknowledges the courtesy of the Institute of Radio Engineers (*Proc. I.R.E.*), the American Institute of Electrical Engineers (*Elec. Eng.*), the American Institute of Physics (*Phys. Rev.* and *Physics*), the Society of Motion Picture Engineers (*Jour.Soc. Mot.Pic.Eng.*) and the McGraw-Hill Publishing Company (*Electronics*) in granting to RCA Review permission to republish material by RCA authors which has appeared in their publications. The appreciation of RCA Review is also extended to all authors whose papers appear herein.

\* \* \*

Since the days of the earliest discoveries of Fleming and De Forest, electron tubes have been one of the foundations upon which the entire



structure of modern radio, electronics and television has been built. Progress in tube design and technique has often controlled the rate of advance in various applications in the communications, entertainment and industrial fields.

ELECTRON TUBES, Volume I, is, therefore, being published for scientists, engineers and others whose work involves the design of tubes or their application with the sincere hope that the material here assembled may serve as a useful background text and basic reference source to help speed new tube developments and thus advance the science and art of radio-electronics.

*The Manager, RCA Review*

RCA Laboratories,  
Princeton, New Jersey  
March 4, 1949



# CONTENTS (Continued)

PAGE

## Summaries:

An Electron Oscillator with Plane Electrodes . . . . .	B. J. THOMPSON AND P. D. ZOTTU	288
Description and Characteristics of the End-Plate Magnetron . . . . .	E. G. LINDER	288
Recent Developments of the Class B Audio- and Radio-Frequency Amplifiers . . . . .	L. E. BARTON	289
Magnetron Oscillators for the Generation of Frequencies Between 300 and 600 Megacycles . . . . .	G. R. KILGORE	290
A Push-Pull Ultra-High-Frequency Beam Tetrode . . . . .	A. K. WING	291
The Anode-Tank-Circuit Magnetron . . . . .	E. G. LINDER	291

## RECEIVING

Recent Developments in Miniature Tubes . . . . .	B. SALZBERG AND D. G. BURNSIDE	292
A New Tube for Use in Superheterodyne Frequency Conversion Systems . . . . .	C. F. NESSLAGE, E. W. HEROLD AND W. A. HARRIS	308
Beam Power Tubes . . . . .	O. H. SCHADE	320
Review of Ultra-High Frequency Vacuum-Tube Problems . . . . .	B. J. THOMPSON	365
Development and Production of the New Miniature Battery Tubes . . . . .	N. R. SMITH AND A. H. SCHOOLEY	375

## Summaries:

Recent Trends in Receiving Tube Design . . . . .	J. C. WARNER, E. W. RITTER AND D. F. SCHMIT	382
Vacuum Tubes of Small Dimensions for Use at Extremely High Frequencies . . . . .	B. J. THOMPSON AND G. M. ROSE, JR.	382
A New Converter Tube for All-Wave Receivers . . . . .	E. W. HEROLD, W. A. HARRIS AND T. J. HENRY	383

## SPECIAL

The Secondary Emission Multiplier — A New Electronic Device . . . . .	V. K. ZWORYKIN, G. A. MORTON AND L. MALTER	384
Electron Optics of an Image Tube . . . . .	G. A. MORTON AND E. G. RAMBERG	409
A Review of the Development of Sensitive Phototubes . . . . .	A. M. GLOVER	425

## Summaries:

The Secondary Emission Phototube . . . . .	H. IAMS AND B. SALZBERG	449
Development of Cathode-Ray Tubes for Oscillographic Purposes . . . . .	R. T. ORTH, P. A. RICHARDS AND L. B. HEADRICK	449
The Electron-Image Tube, a Means for Making Infra-red Images Visible . . . . .	G. A. MORTON	450
Theoretical Limitations of Cathode-Ray Tubes . . . . .	D. B. LANGMUIR	450
Vacuum-Tube Engineering for Motion Pictures . . . . .	L. C. HOLLANDS AND A. M. GLOVER	451
The Electrostatic Electron Multiplier . . . . .	V. K. ZWORYKIN AND J. A. RAJCHMAN	452
An Electrically-Focused Multiplier Phototube . . . . .	J. A. RAJCHMAN AND R. L. SNYDER	452
The Behavior of Electrostatic Electron Multipliers as a Function of Frequency . . . . .	L. MALTER	453
The Orbital-Beam Secondary-Electron Multiplier for Ultra-High-Frequency Amplification . . . . .	H. M. WAGNER AND W. R. FERRIS	453
Voltage-Controlled Electron Multipliers . . . . .	B. J. THOMPSON	454

APPENDIX I — Electron Tube Bibliography (1919-1941) . . . . .	455
APPENDIX II — List of Application Notes (1933-1941) . . . . .	472

# THIN FILM FIELD EMISSION\*†

BY

LOUIS MALTER

RCA Manufacturing Company, Inc.,  
Camden, N. J.

*Summary* — Aluminum, oxidized electrolytically, and subsequently treated with caesium and oxygen possesses new and interesting properties when subjected to electron bombardment in the presence of an adjacent collector electrode whose potential is held positive with respect to the aluminum. True secondary electron emission from the treated surface results in the establishment of a positive charge on the surface and a polarization of the oxide film. This positive charge acting through the thin oxide film produces a high gradient, resulting in the emission of electrons through the surface. The emission increases with collector voltage and beam currents, obeying power laws, but exhibits saturation tendencies. The removal of the primary beam does not result in the immediate cessation of the field emission, but rather in a slow decay which is due to the fact that the surface charge takes an appreciable time to leak away. Similar time lags are noticed when the beam is first applied, particularly if the collector voltage has been reversed while the beam impinges on the surface. The surfaces are also light sensitive, in that light causes a decrease in the field emission and a speeding up of decay. Attempts were made to demonstrate this effect for other surfaces, but, with a few exceptions, the results were negative.

## INTRODUCTION

THIS paper constitutes a more extended report of a letter published recently<sup>1</sup> under the title "Anamalous Secondary Electron Emission." Considerable criticism of this name for the phenomenon involved has arisen as not being descriptive of its apparent nature and, consequently, the above title suggested by Dr. J. A. Becker has been adopted.

In a search for a surface possessing a high secondary emission ratio, a considerable number of composite surfaces of various types were investigated. In the case of aluminum oxide treated with caesium and oxygen in a manner to be described below, it was found that a primary electron beam impinging upon the surface caused a current flow to a positive collector which, in certain cases, was several thousand times as great as the primary current. The phenomenon differed from that in the case of normal secondary emission in that the collector current

---

\* Decimal Classification: R138.

† Reprinted from *Phys. Rev.*, July 1, 1936.

<sup>1</sup> Malter, *Phys. Rev.*, 49, 478 (1936)

was dependent upon the collector potential and primary current density. It exhibited very marked time lag characteristics and was also affected by light.

### EXPERIMENTAL PROCEDURE

#### A. Tube and circuit

A diagram of the tube employed, together with the accompanying circuit is shown in Fig. 1.

The cathode was of the barium oxide-strontium oxide type. The electron gun parts were made of tantalum. The electrodes on the walls of the tube were platinum formed by the reduction of Hanovia platinizing solution. The regions around the "side contacts" were coated with silver formed by the reduction of Hanovia silver paste.

The platinum film consisted of two portions, the first serving as the so-called "second anode" of the electron gun. The second portion served to collect the electrons emitted from the target. If a single

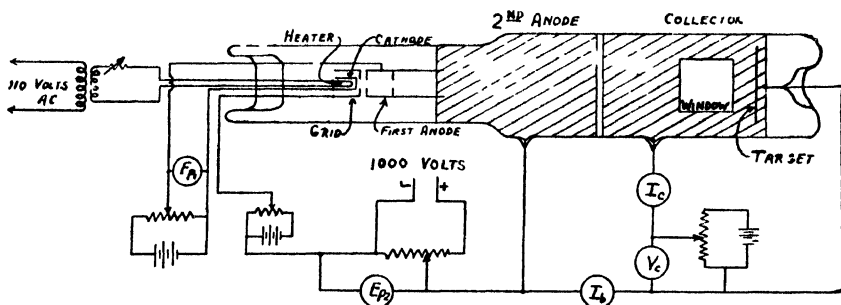


Fig. 1—Schematic diagram of apparatus.

film is used as both second anode and collector, a change in collector voltage ( $V_c$ ) causes a much greater change in beam spot size than if two separate films are employed as shown. This precaution was necessary in view of the dependence of the collector current upon beam spot size.

The caesium was produced by exploding compressed pellets of powdered caesium chromate and zirconium in a side tube.

Two pairs of deflecting coils (not shown in Fig. 1), mounted just beyond the first anode (at right angles to each other), served to position the beam on the target.

#### B. Formation of the oxide film

The aluminum oxide was formed by making the aluminum the anode in a bath wherein the cathode was a platinum foil. Various composition baths were tried. Satisfactory results were obtained with a standard solution of borax and boric acid.

It has been shown<sup>2</sup> that for times of formation in excess of a few minutes the thickness of the oxide film formed is practically independent of the time and the bath employed. The thickness is given by the relation

$$D = 17.0V,$$

where  $D$  is the oxide thickness in Å and  $V$  is the applied potential in volts. However, the resistance of the film does depend upon these factors. No real study of the effect of the nature of the bath upon the film properties appears to have been made.

If at any time during the oxidation process, the applied voltage is gradually reduced, it is found that plots of the logarithm of the applied voltage against the logarithm of the current through the film yield curves of the form shown in Fig. 2. It is seen that below a certain voltage the curve is linear. Güntherschulze and Betz<sup>1</sup> have shown that over this linear region the current is purely electronic, whereas above this point ions move through the oxide lattice and contribute to an increase in its thickness. The portion of the current lying below the extended linear portion of the curve is electronic, whereas that above is ionic.

The prepared aluminum foil was mounted on a nickel plate for support and its edges were painted with willemite in order to permit the position of the beam to be seen by the fluorescence excited. Equally spaced circles were scratched lightly on the willemite in order that it be possible to determine the size of the spot. For intense beams (in excess of 3 to 4 microamperes) a faint blue fluorescence appeared on the oxide surface, permitting of a direct determination of the position and diameter of the electron beam.

The tube was pumped and baked at 475°C until the pressure dropped below  $10^{-5}$  mm of Hg. After cooling, the parts of the electron gun were outgassed by means of high frequency and the oxide cathode activated so as to be thermionically emissive.<sup>4</sup>

Caesium was now introduced into the tube and the tube then baked at 200°C for ten minutes. After cooling, oxygen was admitted into the tube to a pressure of 1 mm of Hg and pumped out after a few seconds. This treatment was sufficient to bring about the appearance of the thin film field emission, or enhance it in cases where it was present prior to any treatment.

---

<sup>2</sup> Güntherschulze and Betz, *Zeits. f. Elektrochemie* 37, 8-9 (1931).

<sup>3</sup> Güntherschulze and Betz, *Zeits. f. Physik* 92, 367 (1934).

<sup>4</sup> Dushman, *Rev. Mod. Phys.* 2, 381 (1930).

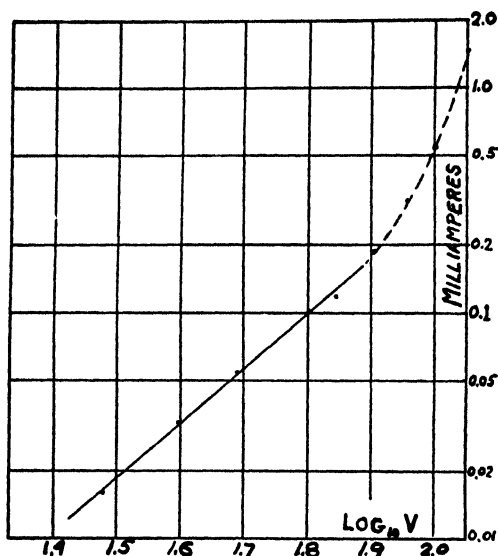


Fig. 2—Current voltage characteristic of aluminum oxide film after formation in saturated borax and boric acid bath for one hour.

It was found impossible to secure completely reproducible results. In an effort to determine the possible reason for this, all chemicals used were recrystallized and the water redistilled, and, in addition, the purest obtainable aluminum was secured from the Rheinische Blattmetall A.G.<sup>5</sup> However, their material was no better in this respect than the available commercial "electrolytic condenser" aluminum.

### EXPERIMENTAL RESULTS

Except where noted the measurement given were obtained from a tube having aluminum with an oxide thickness of 2000A. While the exact results obtained differ from those in other foils with the same oxide thickness, the essential conclusions and laws are the same, the actual magnitudes only being affected.

#### A. Variation of collector voltage ( $V_o$ )

If the beam current ( $I_b$ ), second anode voltage ( $Ep_2$ ) and spot size are held constant, the variation of the collector voltage ( $V_o$ ) causes a rapid variation in the collector current ( $I_o$ ).

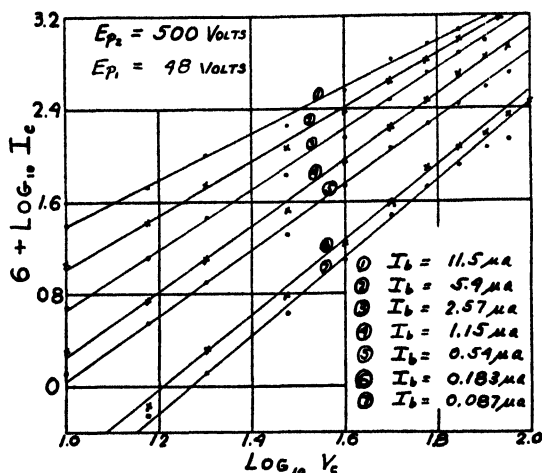
The results for different values of  $I_b$  for the cases wherein ( $Ep_2 = 500$  volts,  $Ep_1 = 48$  volts) and ( $Ep_2 = 250$  volts,  $Ep_1 = 26$  volts) have been plotted in logarithmic coordinates in Figs. 3 and 4. These combinations of  $Ep_1$  and  $Ep_2$  yield the same spot size.

In general, it is seen that:

$$I_o = B(V_o)^m. \quad (1)$$

<sup>5</sup> Rheinische Blattmetall A. G. Grevenbroich (Niederrhein).

At this point, it should be made clear that the results apply to only one region of the target. The values of  $I_o$  obtained from different regions of this surface vary considerably. However, if one restricts oneself to a particular region and is careful not to alter the surface in the manner to be described below, the results are reproducible. In these measurements as well as in those that follow (except where noted) all the data were obtained at the spot on the surface which yielded largest collector currents.



These stabilized  $I_b$ ,  $I_o$  points, which are plotted in Fig. 5, and the curves obtained, are the "repeats" referred to above.

### B. Variation of beam current

A series of readings were taken, everything being held constant except  $I_b$ . The results for  $E_{p2} = 500$  volts,  $E_{p1} = 48$  volts, and different values of  $V_c$  are plotted in Fig. 5. All of these curves are "repeats." It is found that if  $I_b$  is increased in steps, and corresponding values of  $I_o$  obtained, a curve is obtained which does not repeat itself at low values of  $I_b$ . However, after the first run, all succeeding curves do repeat themselves. These stabilized  $I_b$ ,  $I_o$  points, which are plotted in

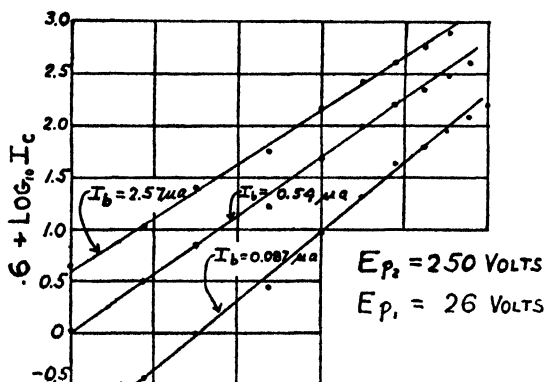


Fig. 3 (above) and Fig. 4 (below)—Variation of collector current with collector potential for different values of beam current. Spot size held constant.

Fig. 5, and the curves obtained, are the "repeats" referred to above.

To illustrate the nature of this deviation for the initial run at low values of  $I_b$ , three successive runs are plotted in Fig. 6. The circles are the first run, the crosses and triangles the second and third, respectively. It is



seen that after the first run, the succeeding runs lie along the same line. The nature of the polarization and time lag effects which give rise to the deviations in the first run will receive more detailed consideration below.

Returning to a consideration of Fig. 5, it is seen that except for low values of  $V_c$  and  $I_b$ , the curves are all straight lines of the same slope. These results can be represented by:

$$I_c = P I_b^{0.71} \quad (2)$$

$\log_{10} P$  as a function of  $V_c$  is plotted in Fig. 7. If  $V_c < 70$  volts,

$$P = 0.145 \times 10^{0.023V_c}. \quad (3)$$

By substituting (3) in (2), there results:

$$I_c = 0.145 \times 10^{0.23V_c} (I_b)^{0.71}. \quad (4)$$

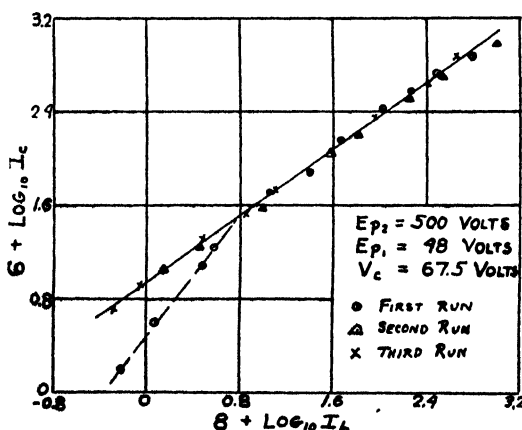


Fig. 6—Demonstration of variation between first and succeeding runs wherein beam current is varied.

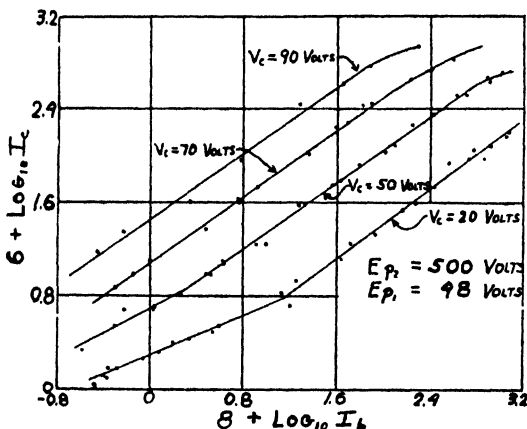


Fig. 5—Variation of collector current with beam current for different values of collector voltage. Spot size held constant.

This relation holds for all values of  $I_b$  and  $I_c$  except for those beyond the linear regions of the curves of Figs. 5 and 6.

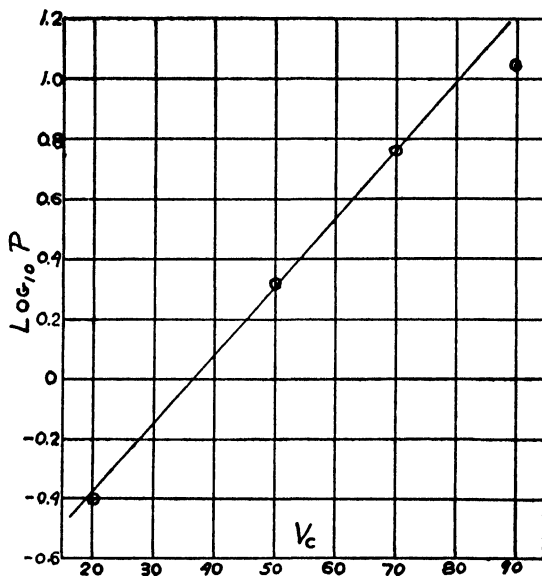


Fig. 7—Plot of intercepts of collector current—beam current characteristics as a function of collector voltage.

### C. Variation of spot size

In order to see whether Eqs. (1) and (4) could be expressed in terms of current density, a series of runs were taken at different spot sizes, the spot sizes being determined by deflecting the spot onto the willemite. Because of a slight misalignment of the first anode, the spot was oval instead of circular. This made the determination of the spot size quite inaccurate, but it was felt that an

approximation of the current density law could certainly be obtained.

In Fig. 8, the values of  $I_c/A$  and  $I_b/A$  for various values of  $I_b$  are plotted on logarithmic scale, where  $A$  is the spot size. When consideration is taken of the large error in the determination of  $A$ , it seems that the best representation of the results is a straight line drawn among the widely scattered points. We have thus:

$$\log 10^6 I_c/A = 1.92 + 0.73 \log 10^6 I_b/A. \quad (5)$$

The fact that the slope is practically the same as that for Eq. (4) indicates that the linear relationship expressed in Eq. (5) is a reasonable representation.

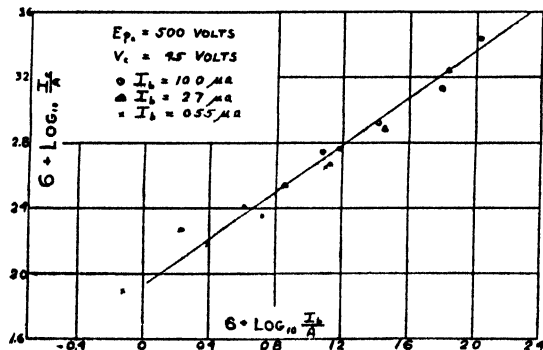


Fig. 8—Variation of collector current divided by spot size with beam current density.

The agreement between Eqs. (4) and (5) is very good and consequently Eq. (4) may be generalized into the form:

$$A(I_c/A) = 0.145(10)^{0.023V_c} A^{0.71} (I_b/A)^{0.71} \quad (6)$$

and since Eq. (4) was derived at  $Ep_2 = 500$  volts,  $Ep_1 = 48$  volts, for which values  $A = 0.72 \text{ cm}^2$ ; we can insert this value of  $A$  in Eq. (6) and obtain:

$$J_c = 0.160(10)^{0.023V_c} J_B^{0.71}, \quad (7)$$

where

$$J_B = I_B/A \quad \text{and} \quad J_c = I_c/A.$$

Eq. (7) is the law representing the collector current as a function of beam current, spot size, and collector voltage for the oxide thickness employed and over the surface region investigated. In general, the law is of the form:

$$J_c = \alpha e^{\beta V_c} J_B^\gamma, \quad (8)$$

where  $\alpha$ ,  $\beta$ , and  $\gamma$  are functions of the oxide thickness and formation conditions. This law does not apply if  $V_c$  and  $I_c$  are above or below certain values. Possible reasons for this will be discussed below.

#### D. Decay characteristics

If  $I_b$  is suddenly reduced to zero by increasing the negative voltage on the grid of the electron gun, it is found that  $I_c$  does not immediately vanish but decreases rapidly at first, and then more slowly, and finally approaches a zero value asymptotically.

Samples of the decay characteristics for the same surface for which the preceding gain studies were made are shown in Fig. 9. Decay characteristics are extremely erratic in that small motions of the spot position cause large changes in the rate of decay. However, in general it is true that the greater the gain, the slower the absolute decay but the more rapid the relative decay. To show the extreme variability of the decay characteristics another curve is shown in Fig. 10. This is the decay characteristic for an entirely different surface, formed at the same voltage as the one previously described. The gains from this surface were slightly higher than from the one studied. Unfortunately, before further measurements could be made, this surface was destroyed by overheating with high frequency. The decay time for this surface was of an entirely different order of

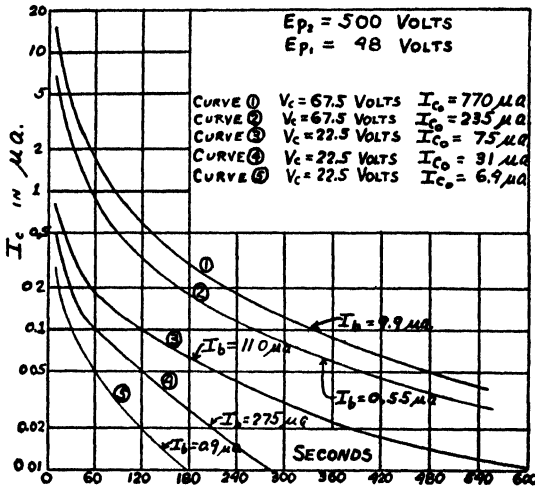


Fig. 9—Typical decay characteristic after removal of primary beam.

corresponding decay time in minutes. This linearity indicates that the neutralization of the surface charge is due primarily to the field emission itself.

If at any time during the decay the lead to the collector is opened momentarily, it is found on closing the circuit that  $I_c$  has dropped to practically zero. If  $V_c$  is reduced at any time during the decay, the rate of decrease of  $I_c$  is not affected unless  $V_c$  is reduced below some definite value, this value being lower the longer the decay period that has elapsed.

A more detailed consideration of the significance of decay characteristics will be given after the theory of the effect.

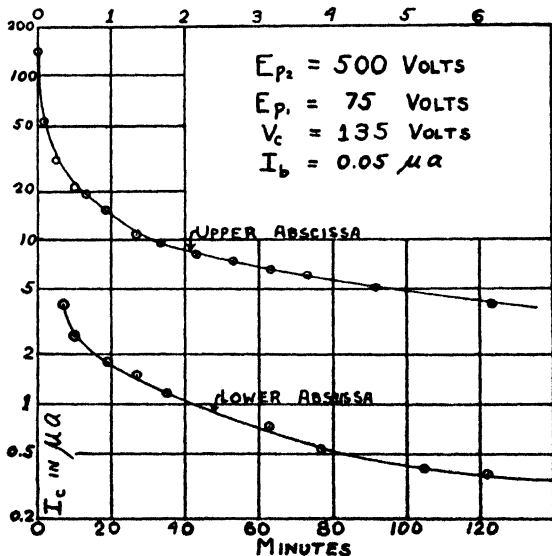


Fig. 10—Example of very slow decay.

magnitude, being measured in minutes rather than seconds. Current to the collector could be detected after 24 hours.

It has been found that if  $\log [-\log (I_c/I_{c0})/T]$  is plotted against  $\log I_{c0}$ , a straight line is obtained. ( $T$  is the decay time). The case corresponding to Fig. 10 is shown in Fig. 11. The small numbers adjacent to the points represent the

### E. "Building-up" characteristics

If, at any time,  $I_b$  is first cut off by an increase in the grid bias, and then after  $I_c$  has dropped to a negligible value,  $I_b$  is suddenly restored to its original value,  $I_c$  returns to its final value very rapidly. If, instead of biasing off  $I_b$ ,  $V_c$  is reduced to zero and then restored to its original value,  $I_c$  also returns to its original value very rapidly.

If, however, instead of reducing  $V_c$  to zero with  $I_b$  unchanged,  $V_c$  is actually reversed in direction so that the collector is negative with respect to the target, upon restoring  $V_c$  to its original positive value, the building-up takes on new and interesting forms. Some of these results are shown in Fig. 12 for cases wherein  $V_c = 22.5$  volts and 45 volts. It is seen that the lower the values of  $I_b$  and  $V_c$ , the slower the building up. A curious feature is the fact that  $I_c$  remains constant for a considerable time before beginning its rise, particularly for low values of  $I_b$  and  $V_c$ .

If, instead of reversing  $V_c$ , a negative voltage ( $V_R$ ) different from  $V_c$  is applied to the collector and then the collector voltage is restored to its original

$V_c$  value, the building-up curves are altered. In Fig. 13 are plotted the building-up characteristics for  $V_R = 0, -22.5, -45$  and  $-67.5$  volts, for the case where  $V_c = 67.5$  volts. As  $V_R$  is made smaller in absolute value, the building-up becomes more rapid. An interpretation of the various building-up curves will be given below.

### F. Scintillations and alteration of characteristics

If  $V_c$  and  $I_b$  are increased beyond certain points, scintillations are observed on the aluminum oxide surface, their number and frequency increasing as  $V_c$  and  $I_b$  are raised. These scintillations alter the surface characteristics and, consequently, in the preceding experimental

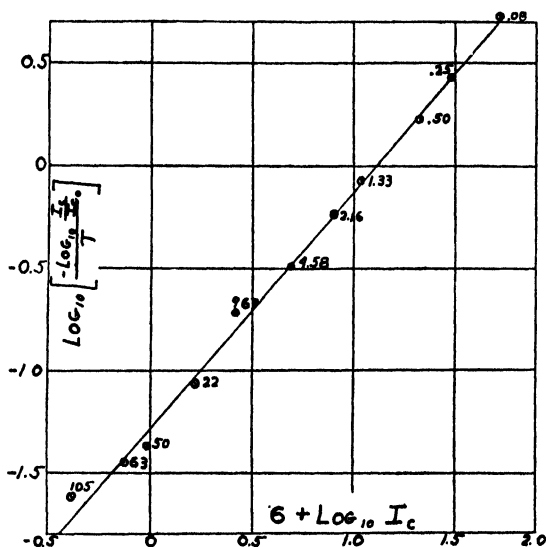


Fig. 11—Illustration of linear relation obeyed by persistent emission.

work, care was taken to keep them at a minimum. Their complete elimination is impossible except for very low values of  $V_c$ . Scintillations are undoubtedly due to momentary ruptures of the oxide film.

Continued scintillation causes a slow decrease in the gain characteristics, but a very rapid alteration in the decay characteristics. Continuous and rapid scintillations finally cause the complete disappearance of the thin film

emission. A surface formed at 12 volts was run with  $V_c = 90$  Volts.

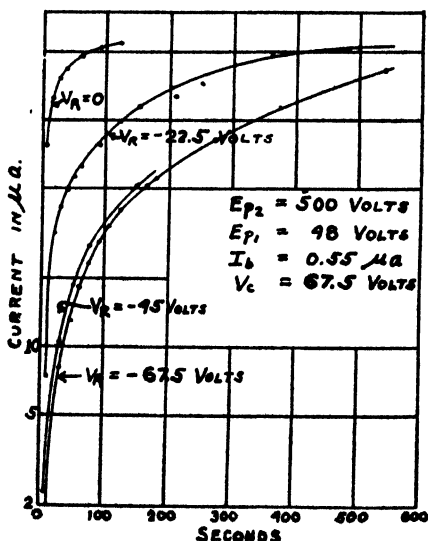


Fig. 13—Building-up curves when collector potentials are reversed to different negative values and subsequently restored to same positive value.

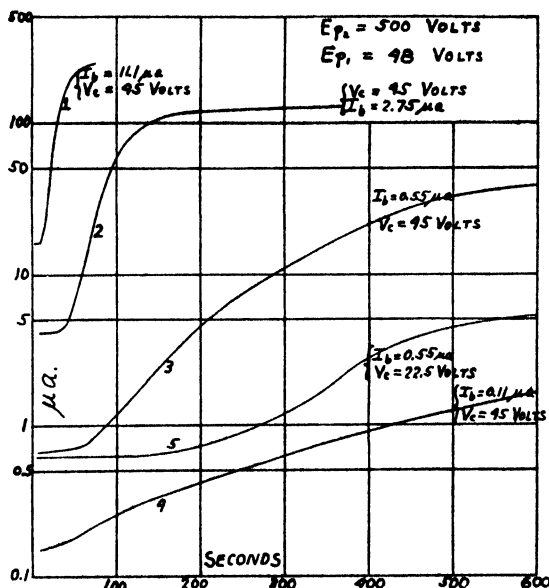


Fig. 12—Building-up curves obtained after reversal of collector potential with beam impinging on target.

Under these conditions, the surface was covered with a uniformly dense distribution of pin-points of scintillation. After one-half hour these scintillations had completely disappeared, but so had the thin film emission.

### G. Light effects

It was noted that the shining of light upon the surface always causes a marked decrease in  $I_c$ . In addition, light causes a marked increase in the rate of decay after  $I_b$  is cut off. The effects upon gain and decay were most marked for tubes with the longest decay. In certain cases a decrease in  $I_c$  of

200 microamperes was observed when a flashlight was shone upon the surface. The same light impinging upon a caesioted silver oxide surface resulted in a current yield of only 10 microamperes. Thus when used in this way the device is many times more "photosensitive" than the best surface heretofore known.

#### DISCUSSION OF EXPERIMENTAL RESULTS AND PROPOSED DESCRIPTION OF THE PHENOMENON

In the case of normal secondary electron emission, the primary electron reacts with the conduction electrons of the substance being bombarded in the presence of the force fields of the atoms or ions constituting the latter, resulting, in certain cases, in the transfer of sufficient backward momentum to conduction electrons to permit of their escape through the surface. The theory for the case of the uniform metallic lattice has been treated by Fröhlich.<sup>6</sup>

Thin film field emission appears to be due to an entirely different mechanism. The phenomenon appears to be closely related to one described by Güntherschulze<sup>7</sup> wherein extremely fine particles of aluminum oxide (among other substances) sprinkled on a semiconductor which serves as the cathode in a gas discharge, emit a copious stream of electrons with velocities corresponding to the cathode-anode difference of potential. In this case, according to Güntherschulze, **positive** ions lodge on the sides of the oxide particles away from the semiconductor and build up a positive charge thereon. If the gradient across any of the particles becomes sufficiently great, electrons will be extracted from the underlying semiconductor. The effect disappears after several hours, apparently due to the mechanical rupture of the oxide particles by the high fields and high current densities present, with a consequent destruction of their insulating structure.

In the case of the thin film field emission the primary electrons impinging upon the treated aluminum oxide surface cause the release of true (i.e., normal) secondary electrons therefrom, these being attracted to the collector electrode. If the secondary emission ratio is greater than unity, more electrons will leave the surface than impinge upon it. Because of the high resistance of the oxide film, a positive charge is built up on the surface, this charge ultimately causing the extraction of electrons from the aluminum and aluminum oxide because of the intense gradients established. Thus in this case the emitted true

---

<sup>6</sup> Fröhlich, *Ann. d. Physik* 13, 229 (1932).

<sup>7</sup> Güntherschulze, *Zeits. f. Physik* 86, 778 (1933).

secondary electrons take the place of the arriving positive ions in Güntherschulze's experiment.

Concomitant with the building up of the surface charge, the oxide becomes polarized, the polarization as well as the surface charge persisting after the removal of the primary beam. Evidence for the persistent polarization of aluminum oxide has been found by Güntherschulze and Betz.<sup>8</sup> In addition, space charges are established within the oxide, the sign of the charge depending upon the sign of the collector.

This picture enables the various manifestations of the phenomenon to be explained in a very convincing manner. These will be considered in turn.

## 1.

The reason for the special treatment required with caesium and oxygen is made clear. This treatment serves to form a thin, nonconducting film on the surface of the aluminum oxide whose true secondary emission ratio is considerably greater than unity, resulting in the rapid building up of the positive charge on the surface when bombarded with primary electrons. It is believed that the layer of caesium oxide is monomolecular. This belief is founded upon the following evidence:

(1) The amount of caesium beyond a certain minimum amount does not appear to affect the magnitude of the phenomenon.

(2) No change can be detected in the appearance of the oxide surface. In the case of silver oxide, on the other hand, the reduction of the oxide to appreciable depths by means of caesium is shown by the decided change in appearance.

(3) The heat of formation of aluminum oxide is so high that it cannot be reduced by metallic caesium. It is quite likely, however, that the heat of adsorption of caesium on aluminum oxide exceeds the heat of formation of the oxide.

The mere formation of the caesium layer on the surface, while it enhances the true secondary emission, does not by itself result in the appearance of the anomalous effect. This is due to the fact that the pure caesium film on the surfaces is conducting and thus prevents the positive charge from being established.

## 2.

The relation between collector current, beam current and collector voltage is expressed by Eqs. (1) and (4). It is of interest to note

---

<sup>8</sup> Güntherschulze and Betz, *Zeits. f. Physik* 73, 580 (1932).



that Eq. (1) is of the same form as the relation between voltage and current for the composition material "Thyrite."<sup>9</sup> For this material the current is given by:

$$I = BV^m, \quad (9)$$

where  $B$  and  $m$  are constants which depend upon the proportions and nature of the constituents. Thyrite is composed of particles of carborundum coated with silica imbedded in a highly resistive matrix. Güntherschulze has ascribed the non-ohmic characteristic to the establishment of high gradients across the particles with a resultant "cold emission" through the particles. This view is borne out by the fact that the "cold emission" through the oxide films in this experiment, i.e., the thin film field emission, obeys a law of the same type.

The identity in form of the Thyrite law, Eq. (9), and the thin film field emission law, Eq. (1), indicates that in the case of this effect, the potential of the front surface of the aluminum oxide surface with respect to the underlying aluminum (denoted by  $(V_s)$ ) is proportional to  $V_c$ , i.e.,

$$V_s \propto V_c.$$

### 3.

The time lags which are a feature of this effect are immediately explained by this picture. If the beam is turned on or increased, it takes an appreciable length of time for the region being bombarded to come to equilibrium under the opposing actions of the charging due to the true secondary emission and discharging due to leakage through the film, as well as for the polarization of the oxide and internal space charge to assume equilibrium values.

The time lag of the space charge is apparently very much greater than that of the surface charge. This belief is borne out by the experiments in which  $V_c$  was reversed with the beam on. On restoring  $V_c$  to its original direction, the surface charge undoubtedly reassumes its original positive value in a time no greater than the building up required when  $V_c$  is not reversed, but merely reduced to zero. Yet, the reversal of  $V_c$  greatly increases the building-up time. This increase can be due only to the fact that the field effective in extracting the electrons is weakened by the presence of negative space charge produced while the collector potential was reversed.

The persistence of the surface charge when the beam is cut off is demonstrated by the slow decay of  $I_c$ . Only a small portion of the

<sup>9</sup> McEachron, U. S. Patent #1,822,742.

field emission serves to neutralize the surface charge. This is also borne out by the virtual disappearance of collector current after a momentary opening of the collector circuit.

#### 4.

The scintillations which appear for intense beams and high collector voltages are due to a violent breakdown of the oxide film. It was thought at first that this rupture would occur only if the surface target potential exceeded the formation voltage of the film. However, it was soon found that scintillations occurred when the collector voltage was less than the formation voltage. It was then believed that scintillations should not occur if the target surface potential were less than the critical potential  $V_b$  in the formation curve. (See Fig. 3.) It would appear that if the surface potential exceeded  $V_b$  there would be a tendency for ions to move through the film. However, since there is no electrolytic bath to supply the loss of ions at the outer surface, a rupture would occur. However, it was found that scintillations occurred when the collector voltage was considerably less than  $V_b$ . Apparently the breakdown is due to there being weak spots in the oxide film. When the sample is in the bath, any tendency to breakdown is overcome by the oxidizing action of the bath. This cannot, of course, occur in the vacuum tube. It is probable that invisible breakdowns occur down to very small values of  $V_c$ . Recently, Zauscher<sup>10</sup> has established a relation between film thickness and breakdown voltage for a film in air. For small thicknesses ( $< 4000\text{\AA}$ ), the relationship is given by:

$$\text{Breakdown Voltage} = 8 \times 10^5 d,$$

where  $d$ , the film thickness, is measured in cm.

Thus for the 2000 $\text{\AA}$  film studied above, the breakdown voltage is 16 volts, whereas  $V_b$  is 78 volts and the formation voltage 116 volts.

The deviations from the laws as expressed in Eqs. (1) and (4) at high values of  $V_c$  may be due to  $V_s$  exceeding some definite value which may be the critical value of Zauscher's relation.

The fact that the deviation from linearity at the upper ends of Fig. 8 occur for approximately the same value of  $I_c$  and appear to be independent of  $V_c$  indicates that  $V_s$  is a function of  $I_c/A$  only.

#### 5.

The sensitiveness of the treated surface to light appears to be explainable only by the ad hoc hypothesis that the aluminum oxide is

---

<sup>10</sup> Zauscher, Ann. d. Physik 23, 597 (1935).

photo-conductive. Light falling upon the oxide causes a decrease in its effective resistance. When the electron beam and light are simultaneously impinging upon the surface, the surface equilibrium potential will take on a smaller value than with the light absent. The light also causes an increase in decay rates by permitting the surface charge to leak away more rapidly through the lessened effective resistance of the oxide film.

#### THIN FILM FIELD EMISSION FROM OTHER SURFACES

Güntherschulze and Fricke<sup>11</sup> obtained field emission from a number of substances in a gas discharge where the positive surface charge was produced by positive ions. A set-up similar to theirs was employed in which finely powdered material was rubbed onto an aquadag surface. The tube was treated with caesium and oxygen in the same manner as for aluminum oxide surfaces. The materials were then bombarded by an electron beam with an adjacent collector highly positive with respect to the aquadag. Field emission would be demonstrated by the presence of scintillations. The following materials were tried in this way:  $Ta_2O_5$ ,  $MgO$ ,  $CaCO_3$ ,  $Al_2O_3$ ,  $Zn_2SiO_4$ , willemite,  $BeCO_3$ ,  $SiO_2$ ,  $ZrO_2$ , and  $ThO_2$ , all of these materials having yielded positive results in the experiments of Güntherschulze and Fricke. Scintillations were observed in the cases of  $Al_2O_3$ ,  $SiO_2$ ,  $MgO$ , and willemite. The non-occurrence of scintillations for the other materials does not indicate that field emission did not occur, but simply that the gradients established were not sufficient to cause breakdown. The coverage of the materials used was too small to enable the demonstration of any field effects as regards the collector current.

In addition, a number of other oxides were tried in tubes, but the results were generally negative. However, E. R. Piore, of the Electronic Research Laboratory of the RCA Manufacturing Company, obtained a pronounced field effect from Be oxidized in a glow discharge, then caesiated, and finally heated to dull redness inside the tube by means of high frequency induction. He has also observed the phenomenon with hot activated barium and strontium oxide cathodes.

The reason for the appearance of the phenomenon only in the case of a few out of a host of oxides tried can be accounted for on the basis of the possible chemical interactions between caesium and oxides. If an oxide is capable of reduction by the caesium, then the introduction of caesium into the tube will cause the destruction of the resistive

---

<sup>11</sup> Güntherschulze and Fricke, *Zeits. f. Physik* 86, 821 (1933).

properties of the oxide film. This will, of course, prevent the appearance of the field effect. In Table I, column one shows the oxide studied, column two its method of preparation, column three the heat of formation of the oxide *per unit atom* of oxygen, and column four the results achieved in an attempt to obtain field emission.

Table I. Field emission from various oxides.

1	2	3	4
OXIDE	MODE OF PREPARATION	HEAT OF FORMATION PER UNIT OXYGEN ATOM (Cal.)	RESULTS FOR ANOMALOUS EFFECT
Al <sub>2</sub> O <sub>3</sub>	Electrolytically in borax plus boric acid bath	126,700	Positive
BeO	Glow discharge in oxygen	?	"
CaO	" " " "	151,900	Negative
CbO	Electrolytically in . IN H <sub>2</sub> SO <sub>4</sub>	?	"
Ag <sub>2</sub> O	Glow discharge in oxygen	7,000	"
CuO	" " " "	37,000	"
NiO	and heating in air Glow discharge in oxygen	57,900	"
Ta <sub>2</sub> O <sub>5</sub>	and heating in air Electrolytically in . IN H <sub>2</sub> SO <sub>4</sub>	60,300	"
WO <sub>3</sub>	" " " "	65,700	"
ZrO	" " " "	86,800	"

Since the heat of formation of Cs<sub>2</sub>O is 82,700 calories, only the oxides of Al, Ca, Mg, Si, and Zr in the above list should show the field effect. The result is believed to be negative in the case of Ca because of the low resistance of the oxide.

An attempt to evaporate SiO<sub>2</sub> from a carbon cup subjected to intense electron bombardment, as described by O'Brien,<sup>12</sup> failed because of the reduction of the SiO<sub>2</sub> by the carbon, with the consequent profuse evolution of CO resulting in a gas discharge. No further attempt was made to evaporate quartz. However, the previously described experiment with the quartz powder indicates that it should yield field emission.

The Zr yielded a negative result, although from the figures cited a positive result should have appeared. However, in heating the tube to 200°C to promote the distribution of the caesium, apparently the heat of formation of the zirconium oxide dropped below that of the caesium oxide. This is evidenced by the decided change in color of the zirconium oxide during caesiation.

This change in the appearance of the oxide upon caesiation occurred whenever field emission failed to occur. The aluminum oxide,

<sup>12</sup> O'Brien, *Rev. Sci. Inst.* 5, 125 (1934).

on the other hand, shows no change in appearance under the same conditions. This is evidence in favor of the belief that the caesium on the aluminum oxide is in the form of a monatomic layer.

#### ACKNOWLEDGMENTS

I wish to express my appreciation to Professor Lloyd P. Smith, under whose direction this work was carried out, for his constant advice and encouragement.

I also wish to express my gratitude to Dr. V. K. Zworykin, of the Electronic Research Laboratory of the RCA Manufacturing Company, for extending to me the facilities of the laboratories for this work, as well as to express my appreciation for his constant advice and encouragement.

I am particularly indebted to Dr. E. G. Ramberg for many valuable discussions and for his contributions to the explanation of the phenomenon.

I wish to express my thanks to Messrs. H. W. Leverenz and H. W. Rhoades for the care in preparing the various oxidizing baths employed.

# EFFECTS OF SPACE CHARGE IN THE GRID-ANODE REGION OF VACUUM TUBES\*†

By

BERNARD SALZBERG AND A. V. HAEFF

RCA Manufacturing Company, Inc., RCA Radiotron Division,  
Harrison, New Jersey

**Summary**—The effects of space charge in the region between grid and anode of a vacuum tube, for the case where the planes of the grid and plate are parallel, are determined from the results of a simple analysis. The main effects of the space charge are (a) to introduce departures from the linear potential distribution of the electrostatic case; (b) to set an upper limit, under certain conditions, for the anode current; (c) to introduce instabilities and hysteresis phenomena in the behavior of the tube; and (d) to increase the electron transit time in this region.

Four modes of potential distribution which may exist in this region are treated: (1) Neither potential minimum nor virtual cathode exist; (2) potential minimum exists; (3) space-charge-limited virtual cathode exists; and (4) temperature-limited virtual cathode exists (negative anode potentials). For each of the various states of operation, expressions are derived for the distribution of potential and electric intensity throughout the region; the time of flight of electrons from grid to anode, and from grid to the plane of zero potential; and the location and magnitude of the minimum potential. An expression is also derived for the dependence of the anode current on the space current, grid-anode distance, grid voltage, and anode voltage. Curves are plotted from these expressions, and it is shown how the behavior of a large variety of practical tubes can be predicted and explained with their aid. The assumptions which underlie the theory are stated, and the effects of the neglected phenomena are discussed qualitatively.

Anode-current vs. anode-voltage and anode-current vs. space-current curves representing observations made on a specially constructed tetrode are presented by way of experimental verification of the theoretical results.

For purposes of illustration, application is made of these results to elucidate the theory of the type of power-amplifier tube which employs a minimum potential, formed in front of the anode as a result of the space charge of the electrons, to minimize the passage of secondary electrons from anode to grid. In addition, it is shown how the decrease of anode current with increasing space current, which occurs when a space-charge-limited virtual cathode is formed in the grid-anode region, may be utilized to provide negative transconductance amplifiers and oscillators.

## I. INTRODUCTION

THE effects of space charge in the region between grid and anode are of fundamental importance in any complete theory of vacuum-tube behavior. This is particularly true for the type of tube in which the anode is preceded by a grid electrode operated at a positive potential. Among such tubes, we may mention the Barkhausen-Kurz triode oscillator, in which the grid is operated at a high positive potential and the anode is either negative or only slightly positive; the common tetrode r-f and a-f amplifiers, in which the screen

\* Decimal Classification: R188.1.

† Reprinted from *RCA Review*, January, 1938.

grid is operated at a relatively high positive potential, and the anode potential is caused to vary from a high positive potential to a smaller positive potential, which may be less than the screen-grid potential; and more recent types of power-amplifier tubes, such as the RCA 6L6, in which a minimum potential which occurs in the space between screen grid and anode at relatively low anode potentials is employed to minimize the passage of secondary electrons (liberated at the anode) to the screen grid.<sup>1, 2, 3, 4</sup>

In this paper we wish to investigate theoretically, somewhat more completely than has been done hitherto, the properties of the grid-anode region.\* The theory is also applicable, with suitable modifications, to the region between two grids, a problem which has also received some attention.<sup>5</sup> To this end, we postulate an idealized situation in which electrons pass through the interstices of a plane-accelerator grid, the effective potential of which is  $V_g$ , towards a parallel-plane anode separated a distance  $a$  from the grid and operated at a potential  $V_a$ . We assume that all of the electrons have been emitted from the cathode with zero velocity, and that they pass through the grid with a uniform velocity corresponding to the potential  $V_g$ . In general, we cannot assume that all of these electrons will pass on to the anode, for the potential distribution in the grid-anode region may be such that some, or even all of the electrons, will be turned back towards the grid at some intermediate point in this region. These returning electrons may be expected to execute excursions about the grid, a portion being absorbed on each passage through the grid.<sup>6, 7, 8, 9</sup> In view of the uncertainty of the exact fractional absorption of the electrons by the grid on each complete passage, and to simplify matters, we shall assume that only two groups of electrons contribute to the space current: one group consists of the electrons which initially pass through the grid towards the anode, corresponding to a current  $I_o$ ; and the second group consists of the electrons which may be turned back at an intermediate point in the grid-anode region, corresponding to a current  $I_o - I_A$ . Generally speaking, we are interested in the dependence of the anode current upon  $V_a$ ,  $V_g$ ,  $a$ , and  $I_o$ ; the time of flight of the electrons; the distribution of potential and electric intensity throughout the region between the grid and anode; and the location and magnitude of the minimum potential which may occur in this region.

As stated above, the problem is only an approximation to the actual

---

1, 2, 3, 4, etc. Numbers refer to bibliography.

\* While we were preparing the results of our investigation for publication, our attention was called to four recent papers dealing with this subject. (Bibliography 13, 14, 15 and 16).

case. The complete treatment of the problem would require taking into account such things as the Maxwellian velocity distribution of emitted electrons; the tangential velocities of the electrons due to grid-wire deflections; the distribution of velocities of the electrons which pass through the grid, due to the variation of the potential in the plane of the grid; the presence of secondary electrons liberated at the anode and accelerator grid; multiple passages of electrons about the grid, etc. However, the solution of the problem set forth will ordinarily suffice for a first-order answer, since the effects of these neglected factors can frequently be inferred, at least, from the physics of the situation.

## II. THEORY

The equation which must be solved to determine the properties we seek is:

$$\frac{d^2V}{dx^2} = 4\pi\rho \quad (\rho \text{ negative}) \quad (1)$$

together with

$$\frac{1}{2} mv^2 = eV \quad (2)$$

and

$$I = \rho v \quad (3)$$

In this problem we do not concern ourselves with the effects of variations of the potential with time. Consequently we may assume that both forward-moving and returning electrons always have the same velocity at any one point, and thus that the total space charge in the grid-anode region depends only upon the absolute values of the corresponding forward and return currents. For these reasons, we may define the quantities used in (1), (2) and (3) as

$V$  = potential at any distance,  $x$

$x$  = distance from grid

$\rho$  = charge density at  $x$

$e$  = electron charge

$m$  = mass of electron

$v$  = absolute value of velocity at  $x$

$I$  = sum of the absolute values of the current densities at  $x$

Further on we shall have occasion to introduce the following additional symbols:

$E$  = electric intensity at  $x$

$H = 16\pi \left( \frac{m}{2e} \right)^{\frac{1}{2}} I_o$ , where  $I_o$  is the current density corresponding to the forward-moving electrons

$\tau$  = transit time for an electron passing from grid to anode

$\tau'$  = transit time for an electron passing from grid to point of zero potential



$$P = \frac{3H^{\frac{1}{2}}x}{4V_g^{\frac{3}{4}}}$$

$$P_a = \frac{3H^{\frac{1}{2}}a}{4V_g^{\frac{3}{4}}}, \quad \left[ P_a = \frac{654 I_o^{\frac{1}{2}} \left( \frac{\text{amp.}}{\text{cm}^2} \right)^{\frac{1}{2}} a \text{ (cm)}}{V_g^{\frac{3}{4}} \text{ (volts)}^{\frac{3}{4}}} \right]$$

$$P_c = \frac{3H^{\frac{1}{2}}c}{4V_g^{\frac{3}{4}}}$$

$$Q_g = \frac{E_g}{H^{\frac{1}{2}} V_g^{\frac{1}{4}}}$$

$$Q = \frac{E}{H^{\frac{1}{2}} V_g^{\frac{1}{4}}}$$

$$Q_c = \frac{E_c}{H^{\frac{1}{2}} V_g^{\frac{1}{4}}}$$

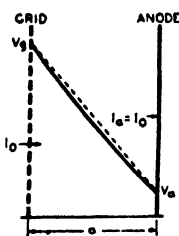


Fig. 1—Potential distribution between grid and anode typical of the case when neither potential minimum nor virtual cathode exists. All of the electrons which pass through the grid are collected at the anode.

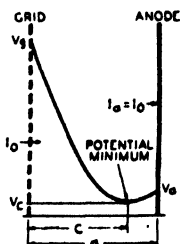


Fig. 2—Potential distribution illustrating the conditions which exist when a potential minimum is formed in the grid-anode region. All of the electrons which pass through the grid are collected at the anode.

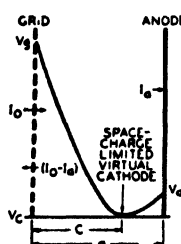


Fig. 3—This potential distribution represents the case when a space-charge-limited virtual cathode exists. Only part of the electrons which pass through the grid are collected at the anode; the others are returned towards the grid at the virtual cathode.

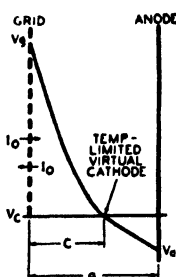


Fig. 4—This potential distribution illustrates the case when a temperature-limited virtual cathode exists. All of the electrons which pass through the grid are subsequently returned towards the grid at the virtual cathode.

The boundary conditions for the various states of operation are given in Figures 1, 2, 3, and 4, which depict typical potential distributions for these states of operation.

By combining (1), (2) and (3), and performing the first integration of (1) from any point  $x_1$ , to another point  $x$ , we get for the electric intensity at  $x$ ,

$$E = \pm [E_1^2 - HV_1^{\frac{1}{2}} + HV^{\frac{1}{2}}]^{\frac{1}{2}} \quad (4)$$

A second integration gives

$$\frac{3H^2}{4} (x - x_1) = \pm [E_1^2 - HV_1^{1/2} + HV_1^{3/2}]^{1/2} \cdot [HV_1^{1/2} - 2(E_1^2 - HV_1^{3/2})] - E_1 [3HV_1^{1/2} - 2E_1^2] \quad (5)$$

The time of flight of an electron from  $x_1$  to  $x$  is

$$\tau - \tau_1 = \int_{x_1}^x \frac{dx}{v} = \left( \frac{m}{2e} \right)^{1/2} \cdot \int_{x_1}^x \frac{dx}{V^{1/2}} \quad (6)$$

From (1), (2) and (3)

$$V^{-1/2} = \frac{1}{4\pi \left( \frac{m}{2e} \right)^{1/2} I} \cdot \frac{dE}{dx}$$

so that (6) becomes

$$\tau - \tau_1 = \frac{1}{4\pi I} \int_{x_1}^x \frac{dE}{dx} \cdot dx = \frac{1}{4\pi I} \cdot (E - E_1) \quad (7)$$

These general equations will now be applied to the various special states of operation.

1—*Neither Potential Minimum Nor Virtual Cathode Exist.*—This mode of operation is depicted in Figure 1. The situation is intermediate between the case when no electrons are present in the grid-anode region, for which condition the potential distribution is linear, and the case when enough electrons are present in this region so that the electric intensity is zero at the grid or anode. In this mode, all of the electrons which pass through the grid are collected at the anode.

Usually,  $I_o$ ,  $a$ ,  $V_g$ , and  $V_a$  are specified, and it is required to determine the distribution of the electric intensity and potential throughout the region and the time of flight of an electron from grid to anode. To start with, we must find  $E_g$ . This can be done by substituting the conditions that  $V = V_a$  when  $x = a$ , and  $E = E_g$  and  $V = V_g$  when  $x = 0$  in (5). Thus,

$$\frac{3H^2 a}{4} = \pm [E_g^2 - H(V_g^{1/2} - V_a^{1/2})]^{1/2} \cdot [HV_a^{1/2} - 2(E_g^2 - HV_g^{3/2})] - E_g [3HV_g^{1/2} - 2E_g^2] \quad (8)$$

This equation allows the determination of  $E_g$  in terms of  $I_o$ ,  $a$ ,  $V_g$ , and  $V_a$ . To put the equation into somewhat more convenient form for

plotting, divide both sides by  $H^{3/2}V_g^{3/4}$ . We get an expression involving the dimensionless parameters,  $P_a$  and  $Q_g$ :

$$P_a = \pm \left[ Q_g^2 - 1 + \left( \frac{V_a}{V_g} \right)^{1/2} \right]^{1/2} \left[ \left( \frac{V_a}{V_g} \right)^{1/2} + 2 - 2Q_g^2 \right] - Q_g [3 - 2Q_g^2] \quad (8a)$$

A curve of  $P_a$  vs.  $\frac{V_a}{V_g}$  for various values of  $Q_g$  may now be obtained

very simply from (8a). This is shown in Figure 5.

For any given set of the four variables,  $Q_g$  can be located in Figure

5. For values of  $\frac{V_a}{V_g}$  greater than unity,  $Q_g$  will range for this case,

from zero to positive values; for values of  $\frac{V_a}{V_g}$  which lie between unity and zero,  $Q_g$  will range from zero to negative values.

The potential distribution can now be determined by means of (5) by substituting the condition that  $E_1 = E_g$  and  $V_1 = V_g$  when  $x_1 = 0$ . Doing this, and rearranging, there results

$$P = \pm \left[ Q_g^2 - 1 + \left( \frac{V}{V_g} \right)^{1/2} \right]^{1/2} \left[ \left( \frac{V}{V_g} \right)^{1/2} + 2 - 2Q_g^2 \right] - Q_g [3 - Q_g^2] \quad (9)$$

This will be recognized as being similar to (8a) except that  $P$  replaces  $P_a$ , and  $V$  replaces  $V_a$ . Therefore, the same data can be utilized

to study the variation of  $\frac{V}{V_g}$  with  $P$ , (to which the distance from the

grid,  $x$ , is proportional) for various values of  $Q_g$ . Figure 5 thus represents, also, generalized potential distribution curves.

The electric intensity at any point may be determined by means of (4) by substituting the condition that  $E_1 = E_g$  when  $V_1 = V_g$ . This gives, after some rearrangement,

$$Q = \pm \left[ Q_g^2 - 1 + \left( \frac{V}{V_g} \right)^{1/2} \right]^{1/2} \quad (10)$$

With the aid of (8a) and (9), (10) can be used to study the variation of  $Q$  (which is proportional to the electric intensity at any point,  $x$ ) as a function of  $P$ , for various values of  $\frac{V_a}{V_g}$ .

The time of flight,  $\tau$ , of an electron passing from grid to anode is, from (7)

$$\tau = \frac{1}{4\pi I_0} (E_a - E_g) \quad (7a)$$

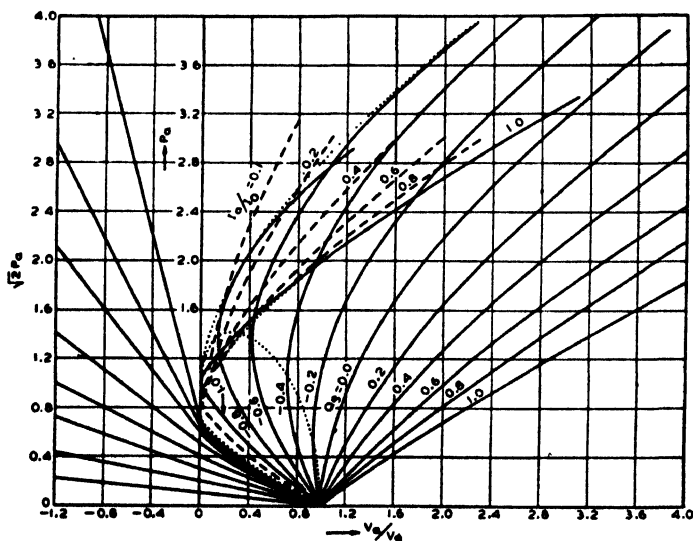


Fig. 5—Generalized potential distribution in the grid-anode region. This plot may be used to determine the particular mode in which the tube is operating, the anode current, and the electric intensity and potential distribution within the grid-anode region. Here,

$$P_a = 654 \cdot \frac{I_0^{1/2} \left( \frac{\text{amp.}}{\text{cm}^2} \right)^{1/2} \cdot a \text{ (cm)}}{V_g^{3/2} \text{ (volts)}^{3/2}}$$

Equation (7a) can be put into more convenient form for plotting by making use of (4). After some rearrangement this gives

$$\tau = \frac{\tau_0}{P_a} \left\{ \pm \left[ Q_g^2 - 1 + \left( \frac{V_a}{V_g} \right)^{1/2} \right]^{1/2} - Q_g \right\} \quad (11)$$

In (11)  $\tau_0 = \left( \frac{m}{2e} \right)^{1/2} \frac{3a}{V_g^{1/2}}$  represents the time of transit of an

electron in a space-charge-limited diode, the electrodes of which coincide with the grid and anode, and for which the electric intensity at the cathode is zero and the anode voltage is  $V_g$ . The ratio  $\frac{\tau}{\tau_0}$  is plotted in Figure 6, the necessary data for the curves being obtained from Figure 5.

It is of interest to note that when  $I_0 \rightarrow 0$ , the limiting case for which the potential distribution is linear, (11) becomes

$$(\tau)_{I=0} = \left( \frac{m}{2e} \right)^{\frac{1}{2}} \cdot \frac{2a}{V_g^{\frac{1}{2}}} \cdot \frac{1}{\left( \frac{V_a}{V_g} \right)^{\frac{1}{2}} + 1} \quad (11a)$$

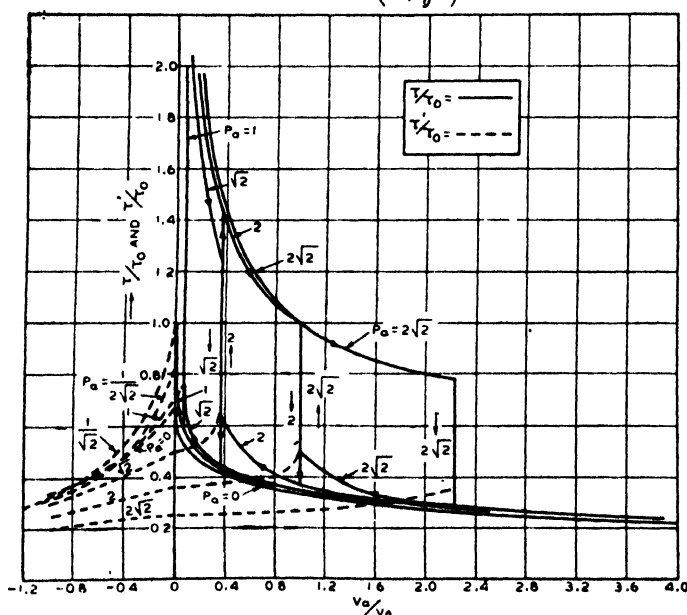


Fig. 6—Dependence of transit time upon anode voltage for various values of parameter  $P_a$ .  $\tau$  is the transit time for electrons which travel from the grid to the anode.  $\tau_0$  is the electron transit time from grid to virtual cathode.

$\tau_0$  (sec) =  $\frac{3a \text{ (cm)}}{5.95 \cdot 10^7 V_g^{\frac{1}{2}} \text{ (volts)}^{\frac{1}{2}}}$  is the electron transit time in a space-charge-limited diode.

The other limiting cases for the potential distributions under consideration here occur when  $E_g = 0$ , representing a potential minimum at the grid, or when  $E_a = 0$ , representing a potential minimum at the anode. In the first case

$$(\tau)_{E_g=0} = \left( \frac{m}{2e} \right)^{\frac{1}{2}} \frac{3a}{V_a^{\frac{1}{2}} + 2V_g^{\frac{1}{2}}} \quad (11b)$$

while in the second case

$$(\tau)_{D_a} = \left( \frac{m}{2e} \right)^{1/2} \cdot \frac{3a}{V_g^{1/2} + 2V_a^{1/2}} \quad (11c)$$

2—*Potential Minimum Exists.*—This mode of operation is shown in Figure 2. The situation existing here is intermediate between the case when enough space current flows through the grid so that the electric intensity is zero at the grid or anode, and the case when the conditions are such that the electric intensity *and* the potential are just zero at either electrode or in the intervening region. In this mode, also, all of the electrons which pass through the grid are collected by the anode.

Here again,  $I_0$ ,  $a$ ,  $V_g$  and  $V_a$  are usually specified, and it is required to find the distribution of the electric intensity and potential throughout the region, the time of flight of an electron from grid to anode, and the value and location of the minimum potential.

We start by substituting the condition that  $V = V_g$  and  $E = E_g$  when  $x = 0$ , and  $V = V_a$  and  $x = a$  in (5). This leads to an expres-

sion identical with (8a); the variation with  $\frac{V_a}{V_g}$  of  $P_a$  for various values of  $Q_g$  is shown in Figure 5. For this mode  $Q_g$  ranges between

0 and  $-1$  for all values of  $\frac{V_a}{V_g}$ , as shown in Figure 5. It is important

to note that for one value of  $\frac{V_a}{V_g}$  there can be two values of  $Q_g$ , corresponding to one value of  $P_a$ . We shall discuss this peculiarity further on.

In the same way, the expression for the potential distribution can be shown to be formally identical to (9), and the variation of  $\frac{V}{V_g}$  with  $P$  for various values of  $Q_g$  can also be studied from Figure 5. For this mode of operation,  $\frac{V}{V_g}$  passes through a minimum, representing the potential minimum.

The expression for the electric intensity is derivable, again, from (4); this is identical with (10). Now  $E$  is negative to the left of the potential minimum, zero at the potential minimum, and positive to the right of the potential minimum.

The time of flight,  $\tau$ , of an electron from grid to anode is again given by (11), and the ratio  $\frac{\tau}{\tau_0}$  is also plotted in Figure 6. It is of interest to note that for the limiting condition, when  $V_c = 0$ , (11) gives

$$\tau = \left( \frac{m}{2e} \right)^{\frac{1}{2}} \cdot \frac{3a}{V_g^{\frac{1}{2}}} \cdot \frac{1}{\left[ 1 - \left( \frac{V_a}{V_g} \right)^{\frac{1}{2}} + \left( \frac{V_a}{V_g} \right)^{\frac{1}{2}} \right]} \quad (11d)$$

The ratio of (11a) to (11d) gives us an estimate of the increase of the transit time for two important limiting cases which may be encountered. This is

$$\frac{(\tau)_{V_c=0}}{(\tau)_{I_0=0}} = \frac{2}{3} \cdot \left[ 1 - \frac{1}{\left( \frac{V_a}{V_g} \right)^{\frac{1}{2}} + \left( \frac{V_g}{V_a} \right)^{\frac{1}{2}}} \right] \quad (12)$$

Thus when  $V_a = V_g$ , the transit time for the case when a zero-potential minimum is just formed is three times larger than the transit time for very low values of anode current.

It is of considerable interest, in any consideration of this particular mode of operation, to determine the value and location of the minimum potential. This may be done indirectly by making use of

Figure 5. Alternately, an implicit expression for the value of  $\frac{V_c}{V_g}$  may be derived from (4) and (5). This is

$$P_a = \pm \left[ 1 - \left( \frac{V_c}{V_g} \right)^{\frac{1}{2}} \right]^{\frac{1}{2}} \cdot \left[ 1 + 2 \left( \frac{V_c}{V_g} \right)^{\frac{1}{2}} \right] \pm \left[ \left( \frac{V_a}{V_g} \right)^{\frac{1}{2}} - \left( \frac{V_c}{V_g} \right)^{\frac{1}{2}} \right]^{\frac{1}{2}} \cdot \left[ \left( \frac{V_a}{V_g} \right)^{\frac{1}{2}} + 2 \left( \frac{V_c}{V_g} \right)^{\frac{1}{2}} \right] \quad (13)$$

The variation of  $\frac{V_c}{V_g}$  with  $\frac{V_a}{V_g}$ , for several values of  $P_a$  is shown in Figure 7.

In the same way, by making use of (4) and (5), the location of

the minimum potential can be expressed in terms of  $\frac{V_c}{V_g}$  and  $P_a$ , i.e.,

$$\frac{c}{a} = \frac{1}{P_a} \cdot \left[ 1 + 2 \left( \frac{V_c}{V_g} \right)^{\frac{1}{2}} \right] \cdot \left[ 1 - \left( \frac{V_c}{V_g} \right)^{\frac{1}{2}} \right] \quad (14)$$

The dependence of  $\frac{c}{a}$  on  $\frac{V_a}{V_g}$ , for various values of  $P_a$  is shown in Figure 8.

Figures 7-11 are of the greatest importance in delineating the properties of the grid-anode region. We shall make extensive use of these curves in our discussion.

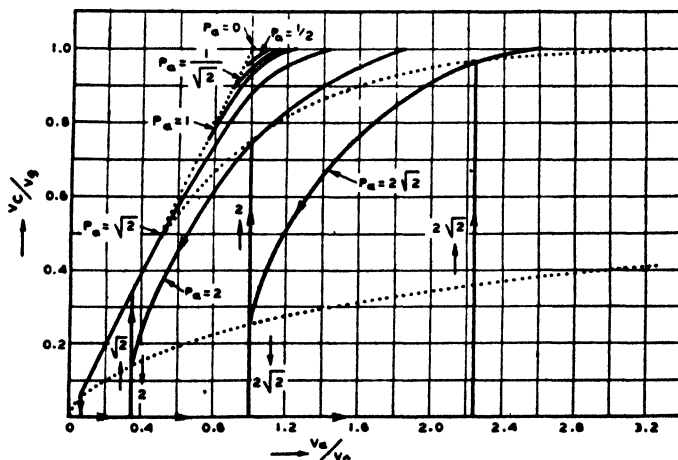


Fig. 7—Variation of the magnitude of the potential minimum with anode potential for several values of the parameter  $P_a$ .

Before proceeding to the next case, let us consider what happens when, with  $V_a$ ,  $V_g$ , and  $a$  fixed, the current density  $I_0$  is increased from zero until the potential minimum which is formed in the grid-anode region descends to the value zero. Figure 9, plotted from (13), shows

the variation of  $\frac{V_c}{V_g}$  with  $P_a^2$  for various values of  $\frac{V_a}{V_g}$ . The rate of

change of the minimum potential with respect to space current is given by the slope of these curves. Differentiating  $P_a$  in (13) with

respect to  $\left( \frac{V_c}{V_g} \right)^{\frac{1}{2}}$ , considering  $\left( \frac{V_a}{V_g} \right)^{\frac{1}{2}}$  fixed, and equating the



derivative to zero tells us that  $(P_a)_{\max}$  occurs when

$$\frac{V_c}{V_g} = \frac{\frac{V_a}{V_g}}{\left[ 1 + \left( \frac{V_a}{V_g} \right)^{\frac{1}{2}} \right]^2} \quad (15)$$

Substituting (15) in (13), we find that the maximum current (density) which can be passed is

$$(I_a)_{\max} = \frac{1}{9\pi a^2} \cdot \left( \frac{2e}{m} \right)^{\frac{1}{2}} \cdot (V_g^{\frac{1}{2}} + V_a^{\frac{1}{4}})^3 \quad (13a)$$

The value of the potential minimum for this maximum current is given by (15). Equation (15) is plotted as a dotted line in Figure 7. Figure

11 is a plot of  $\left( \frac{I_a}{I_o} \right) \cdot P_a^2$  vs.  $P_a^2$  and shows the anode current increasing

directly with the space current until the maximum value, given by (13a), is reached. At this point the potential minimum descends abruptly to zero, and a new state of operation sets in.

3—*Space-Charge-Limited Virtual Cathode Exists.*—This state of operation is shown in Figure 3. The situation existing here is such that at some plane in the region between the two electrodes, or possibly in the plane at either electrode, the electric intensity *and* the potential are zero. Such a point may be called a space-charge-limited virtual cathode, since it turns out that it behaves in many respects like a space-charge-limited thermionic cathode. It is pertinent to call attention to the difference between the virtual cathode of the present case and the potential minimum of the preceding case. In general, the potential minimum merely calls for a zero of electric intensity, but not of potential, since all of the electrons which flow through the grid are collected at the anode. However, when there is a point of zero potential in the region between the two electrodes, some of the electrons passing towards the anode may be turned back towards the grid at this point.

As a digression, we may study briefly the limiting case, when the anode current is exactly equal to the space current. We have, on putting

$$\frac{V_c}{V_g} = 0 \text{ in (13),}$$

$$I_a = \frac{1}{9\pi a^2} \cdot \left( \frac{2e}{m} \right)^{\frac{1}{2}} \cdot (V_g^{\frac{3}{2}} + V_a^{\frac{1}{2}})^2 \quad (13b)$$

This is smaller than the current predicted by (13a), the ratio of (13a) to (13b) being

$$\frac{\left[1 + \left(\frac{V_a}{V_g}\right)^{\frac{1}{2}}\right]^3}{\left[1 + \left(\frac{V_a}{V_g}\right)^{\frac{3}{2}}\right]^2},$$

the maximum value of this ratio occurring when  $\frac{V_a}{V_g} = 1$ . The ratio

is equal to unity when  $\frac{V_a}{V_g} = 0$  or  $\infty$ . The difference between (13a) and

(13b) is the basis of the hysteresis phenomena characteristic of the curves shown in Figures 5-11, and will be discussed further on.

We return now to the general case, for which some of the electrons are turned back towards the grid, and assume for simplicity that such electrons never again re-enter the grid-anode region.\* The anode current is then, in view of (1), (2), (3), and the requisite boundary conditions, given by

$$I_a = \frac{1}{9\pi} \cdot \left(\frac{2e}{m}\right)^{\frac{1}{2}} \cdot \frac{V_a^{3/2}}{(a-c)^2} \quad (16)$$

The total space charge in the region between the grid and the virtual cathode depends upon both the forward-moving and returning electrons, and since these electrons have the same velocity at any one point, we may write

$$2I_o - I_a = \frac{1}{9\pi} \cdot \left(\frac{2e}{m}\right)^{\frac{1}{2}} \cdot \frac{V_g^{3/2}}{c^2} \quad (17)$$

If we divide (17) by  $I_o$ , and put  $H = 16\pi \left(\frac{m}{2e}\right)^{\frac{1}{2}} \cdot I_o$  and  $P_a = \frac{3H^{\frac{1}{2}}a}{4V_g^{\frac{1}{2}}}$  as before, we get, on rearranging,

$$\frac{c}{a} = \frac{1}{P_a \left(2 - \frac{I_a}{I_o}\right)^{\frac{1}{2}}} \quad (18)$$

It is of interest to note that when  $I_a = 0$ , (18) becomes  $\frac{c}{a} = \frac{1}{2^{\frac{1}{2}} P_a}$ .

---

\* The ensuing treatment can easily be generalized to include the multiple-passage case. See, for example, 7, 9 of Bibliography.

That is, when  $V_a = 0$ , the virtual cathode (if one exists) is at a distance

$$c = \frac{a}{2^{1/2} P_a} \text{ cm from the grid.}$$

In order to use (18) to plot the location of the virtual cathode as a function of  $I_o$ ,  $a$ ,  $V_g$  and  $V_a$ , we must first derive an expression for

$\frac{I_a}{I_o}$  as a function of  $\frac{V_a}{V_g}$  and  $P_a$ . This can be done by dividing (17) by

(16) and making use of (18). There results

$$\left( \frac{V_a}{V_g} \right)^{3/2} = \left( \frac{I_a}{I_o} \right)^{1/2} \cdot \left[ P_a - \frac{1}{\left( 2 - \frac{I_a}{I_o} \right)^{1/2}} \right] \quad (19)$$

Equation (19) is used (a) to plot  $P_a$  vs.  $\frac{V_a}{V_g}$  for various values of  $\frac{I_a}{I_o}$ ,

as shown in Figure 5; (b) to plot  $\frac{I_a}{I_o}$  vs.  $\frac{V_a}{V_g}$  for various values of  $P_a$ , as

shown in Figure 10;\* and (c) to plot  $\left( \frac{I_a}{I_o} \right) \cdot P_a^2$  vs.  $P_a^2$  for various

values of  $\frac{V_a}{V_g}$ , as shown in Figure 11. In addition, by making use in

(18) of the data furnished by Figure 10, we are enabled to plot  $\frac{c}{a}$  vs.

$\frac{V_a}{V_g}$  for various values of  $P_a$ , as shown in Figure 8.

The potential distribution within the grid-anode region correspond-

ing to any particular value of  $c$  is  $\frac{V}{V_g} = \left( \frac{c-x}{c} \right)^{4/3}$  to the left of  $c$ , and

$\frac{V}{V_a} = \left( \frac{x-c}{a-c} \right)^{4/3}$  to the right of  $c$ . The corresponding electric intensities

are  $E = -\frac{4}{3} \frac{V}{c-x}$ , and  $E = +\frac{4}{3} \frac{V}{a-c}$ , respectively.

\* Curves similar to those given in Figure 10 have been given by Tonks<sup>7</sup>; his curves however, are restricted to the virtual-cathode case and do not portray the important hysteresis-effects characteristic of the minimum-potential case.

The time of flight of an electron which travels from the grid to the virtual cathode is simply

$$\tau' = \left( \frac{m}{2e} \right)^{1/2} \cdot \frac{3c}{V_g^{1/2}} = \frac{c}{a} \cdot \tau_o \quad (20)$$

The time of flight of an electron which travels from grid to anode is

$$\begin{aligned} \tau &= \left( \frac{m}{2e} \right)^{1/2} \cdot \left[ \frac{3c}{V_g^{1/2}} + \frac{3(a-c)}{V_a^{1/2}} \right] \\ &= \tau_o \cdot \left\{ \left( \frac{V_g}{V_a} \right)^{1/2} + \frac{c}{a} \cdot \left[ 1 - \left( \frac{V_g}{V_a} \right)^{1/2} \right] \right\} \end{aligned} \quad (21)$$

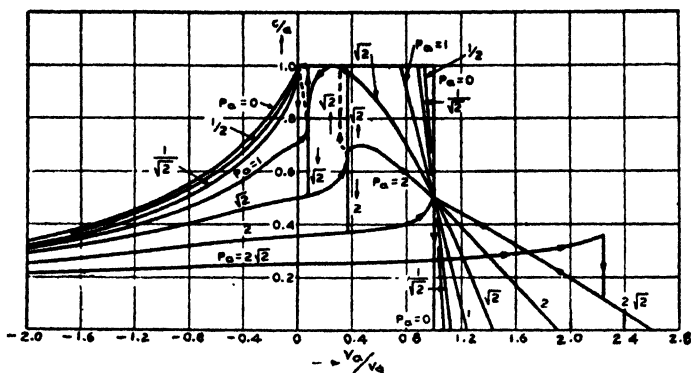


Fig. 8—Position of the potential minimum and virtual cathode as a function of the anode potential for various values of the parameter  $P_a$ .

The time of flight for each class of electrons can be plotted with the aid of (18), as shown in Figure 6.

**4—Temperature-Limited Virtual Cathode Exists (Negative Anode Potentials).**—This state of operation is illustrated in Figure 4. The situation now is such that the electric intensity is negative throughout the region between the two electrodes, and at some intermediate plane the potential is zero. The electrons which move through the interstices of the grid towards the plane of zero potential are gradually decelerated, and finally turned back at this plane toward the grid. Since the electric intensity at this plane is always finite, the potential distribution between  $c$  and  $o$  resembles that of a temperature-limited diode. It turns out, moreover, that the properties of the plane of zero potential are in many respects identical to that of the temperature-limited cathode. Accordingly, we shall designate this plane as a "temperature-limited virtual cathode", by analogy with the "space-charge-limited virtual cathode".

Here  $I_0$ ,  $a$ ,  $V_g$ , and  $V_a$  are specified and it is required to determine the distribution of the electric intensity and potential throughout this region, the position of the virtual cathode, and the time of flight of an electron from the grid to the virtual cathode. We shall not attempt a rigorous treatment, but instead we shall base our analysis on the same assumptions as we have made for the preceding cases.

Since the anode is negative, no electrons will be collected. (This is a consequence of our assumptions regarding the initial velocities of the electrons emerging from the grid plane: in actuality there is always a very small anode current as a result of a distribution of initial veloci-

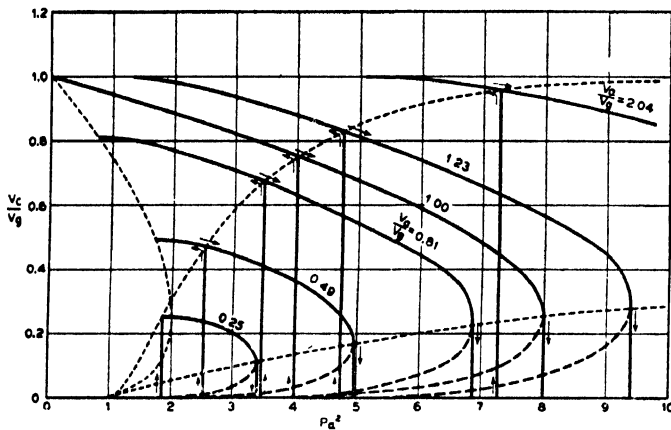


Fig. 9—Variation of the magnitude of the potential minimum with  $P_a^2$  (to which the space current is proportional) for several values of  $\frac{V_a}{V_g}$ .

ties.) Furthermore, since the electric intensity must be continuous, and since there is no charge in the region  $c < x < a$ , the electric intensity,  $E_c$ , at the virtual cathode (and also to the right of this plane) will

be equal to  $\frac{V_a}{a-c}$ .

We now make use of (4) and (5), subject to the appropriate boundary conditions. In (4) we put  $E_1 = E_c$ ,  $E = E_g$ ,  $V_1 = 0$ ,  $V = V_g$ , and  $I = 2I_0$ . There results

$$E_g = -[E_c^2 + 2HV_g^{1/2}]^{1/2} \quad (22)$$

In (5) we put  $x = c$ ,  $x_1 = 0$ ,  $E_1 = E_g$ ,  $V_1 = V_g$ , and  $V = 0$  getting, with the aid of (22)

$$\frac{3H^2c}{a} = \mp [E_c^2 + (E_c^2 - HV_g^{1/2}) \cdot (E_c^2 + 2HV_g^{1/2})^{1/2}] \quad (23)$$

Dividing through by  $2H^{3/2} \cdot V_g^{3/4}$  and making use of our abbreviated symbolism, we get

$$P_c = \frac{Q_c^3 + (Q_c^2 - 1) \cdot (Q_c^2 + 2)^{1/2}}{2} \quad (23a)$$

Now,

$$P_c \cdot Q_c = \frac{3H^{1/2}c}{4V_g^{3/4}} \cdot \frac{V_a}{(a-c)H^{1/2}V_g^{1/4}} = \frac{3}{4} \cdot \left( \frac{V_a}{V_g} \right) \cdot \frac{\frac{c}{a}}{1 - \frac{c}{a}} = P_a \cdot Q_c \cdot \frac{c}{a}$$

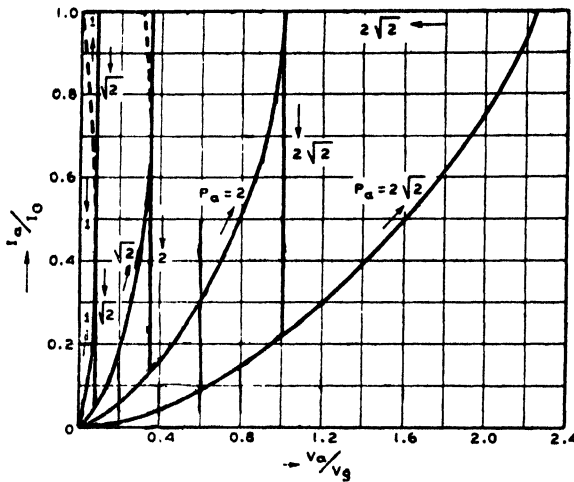


Fig. 10—Dependence of anode current upon anode potential for various values of the parameter  $P_a$ .

so that

$$\frac{c}{a} = \frac{P_c}{P_a} = 1 - \frac{3}{4} \cdot \left( \frac{V_a}{V_g} \right) \cdot \frac{1}{P_a \cdot Q_c} \quad (24)$$

and

$$P_a = P_c + \frac{3}{4} \cdot \frac{1}{Q_c} \cdot \left( \frac{V_a}{V_g} \right) \quad (24a)$$

We may now plot  $P_c$  as a function of  $Q_c$  by means of (23a). The corresponding value of  $P_a$  for any given value of  $\frac{V_a}{V_g}$  may then be

found from (24a). This gives us sufficient information to plot  $\frac{c}{a}$  as a function of  $\frac{V_a}{V_g}$  for various values of  $P_a$ : such curves are included in Figure 8. We are also enabled to plot, from this information,  $P_g$  vs.  $\frac{V_a}{V_g}$  for various values of  $Q_g$ : this is shown in Figure 5, which may be used again as a generalized potential distribution plot.

The electric intensity at any point is given by

$$Q = - \left[ Q_g^2 + 2 \left( \frac{V}{V_g} \right)^{\frac{1}{2}} - 2 \right]^{\frac{1}{2}} \quad (25)$$

The time of transit of electrons from grid to virtual cathode is, from (7) and (25),

$$\tau' = \frac{\tau_o}{2P_a} \cdot [Q_g + (Q_g - 2)^{\frac{1}{2}}] \quad (26)$$

The ratio  $\frac{\tau'}{\tau_o}$  vs.  $\frac{V_a}{V_g}$  for various values of  $P_a$  is shown in Figure 6. The limiting case,  $I_o \rightarrow 0$ , of (26) is

$$\tau' = \tau_o \cdot \frac{2}{3} \cdot \frac{1}{1 - \left( \frac{V_a}{V_g} \right)} \quad (26a)$$

### III. DISCUSSION OF THEORETICAL RESULTS

We now proceed to interpret the results of the foregoing analysis. In the interests of clarity we shall lead up to the general discussion of Figures 5-11 by providing a preliminary verbal description of the results of varying first the space current and then the anode voltage for several representative cases of interest.

#### A—Preliminary Discussion of Several Particular Situations—

1. Effects of Varying  $I_o$ , when  $\frac{V_a}{V_g} = 1$ .

To begin with, let us suppose that the effective grid voltage,  $V_g$ , the anode voltage,  $V_a$ , and the grid-anode distance,  $a$ , are fixed, and that it is required to determine the effects of increasing the space

current,  $I_0$ . This situation corresponds, for example, to the case of a tetrode, the screen-grid voltage and the anode voltage of which are fixed, and the control-grid voltage of which is varied. To fix ideas, we choose  $\frac{V_a}{V_g} = 1$ : a similar interpretation will hold for any other ratio.

When the control-grid bias is adjusted to cut off the cathode current, the potential distribution is linear, as shown by (a) of Figure 12. Decreasing the bias causes electrons to flow into the grid-anode region,

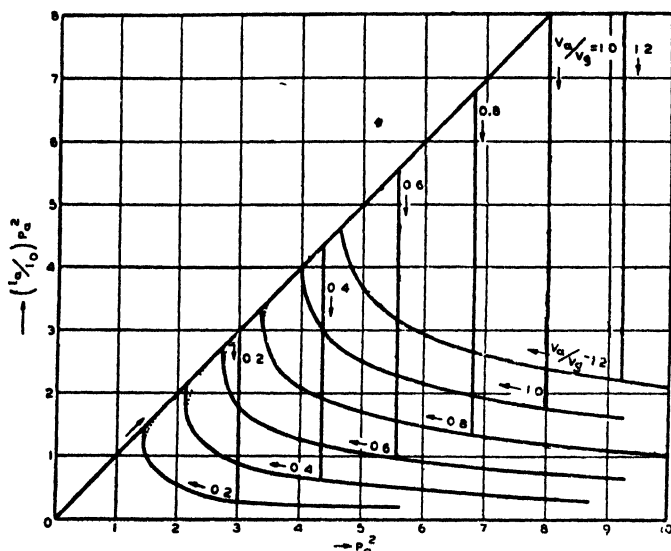


Fig. 11—Variation of the anode current with space current for several values of  $\frac{V_a}{V_g}$

and the potential is depressed, as shown by (b). A potential minimum is formed mid-way between the grid and anode. As the space current is increased, the potential minimum gradually descends until it reaches a value equal to 0.25 times the grid voltage, as shown in Figure 9. Up to this point the anode current increases directly with the space current, as shown in Figure 11. All of the electrons coming through the grid are collected at the anode. If, now, any additional electrons are permitted to pass into the grid-anode region, the potential minimum drops abruptly to zero, mid-way between the grid and anode. This is shown in Figure 9, the rate of change of the minimum potential with space current being infinite at this point. Since the minimum is now zero, some of the electrons are returned towards the grid, thus decreas-



ing the space charge between the potential minimum and the anode, and increasing the space charge between the grid and the potential minimum. This causes an alteration of the potential distribution, the minimum (now a virtual cathode) shifting abruptly towards the grid until it reaches a distance from the grid equal to 0.265 times the grid-anode distance, shown by (d) of Figure 12. Thereafter, as the space current is increased, the anode current decreases gradually, in accordance with Figure 11, and the virtual cathode retreats toward the grid. The effect of increasing the space current on the time of flight of an

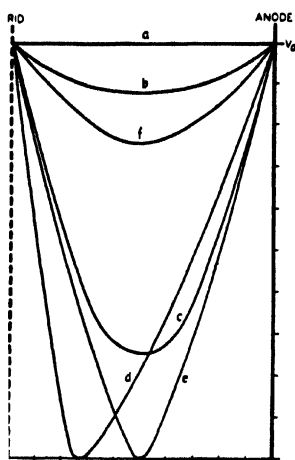


Fig. 12—Potential distribution for several values of space

current.  $\frac{V_a}{V_g} = 1.$

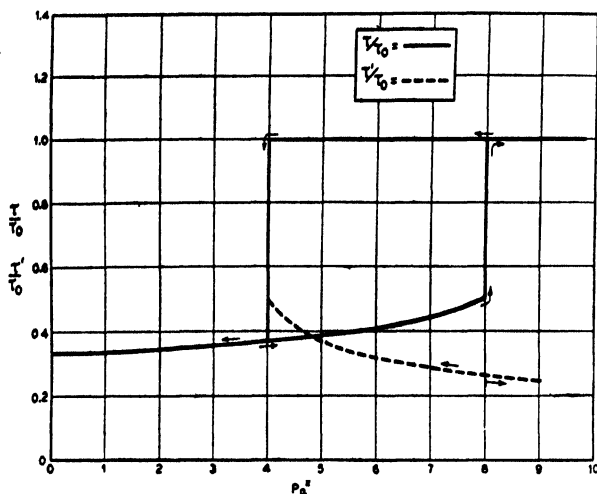


Fig. 13—Variation of electron transit time with

space current.  $\frac{V_a}{V_g} = 1.$

electron from grid to anode, and from grid to virtual cathode, is shown in Figure 13.

It will be observed that the transit time is initially one-third that of a space-charge-limited diode, the electrodes of which coincide with the grid and anode and for which the anode voltage is  $V_g = V_a$ . With increasing space current the transit time rises slowly until a current corresponding to  $P_a^2 = 8$  is reached. At this point a virtual cathode is formed, and the transit time rises abruptly from  $\tau = 0.500\tau_0$  to  $\tau = \tau_0$ . It remains constant thereafter at this value with further increase of space current. The transit time for the electrons which return toward the grid when a virtual cathode is formed is initially  $\tau' = 0.265\tau_0$ , and decreases slowly with increasing space current, since the virtual cathode retreats toward the grid. The time of flight of electrons from grid to virtual cathode and back to grid is twice  $\tau'$ .

If the space current is now gradually decreased, the anode current will be found to increase, as shown in Figure 11. The operation now, however, does not take place entirely along the original curve. This is due to the fact that, originally, operation began with a potential minimum; now it takes place with a virtual cathode. When the space current reaches a value equal to one-half of the current at the transition value, where the potential minimum had previously shifted abruptly into a virtual cathode, the anode current becomes equal to the space current. The virtual cathode is now saturated. At this point the virtual cathode is mid-way between the grid and the anode, as shown by (e) of Figure 12. The slightest further reduction of space current causes the virtual cathode to shift abruptly into a potential minimum, the value of which is 0.75 times the grid voltage, as shown by (f) of Figure 12. Any further reduction of space current is accompanied by a proportionate decrease of anode current, the potential minimum gradually approaching (a) of Figure 12. The effect of decreasing the space current on the time of flight of an electron from grid to anode, and from grid to virtual cathode, is also shown in Figure 13.

The time of flight for electrons moving from grid to anode remains constant until the virtual cathode disappears; this occurs when the space current is decreased to a value corresponding to  $P_a^2 = 4$ . At this point the transit time drops abruptly to a value  $\tau = 0.366\tau_0$ . With further decrease of space current the transit time decreases slowly until the limiting value  $\tau = 0.333\tau_0$  is reached for  $P_a^2 \rightarrow 0$ . The time of flight for the electrons which return from the virtual cathode increases slowly with decreasing space current, because the virtual cathode moves out slowly towards the anode. When  $P_a^2 = 4$ , the virtual cathode disappears and the transit time for the electrons which have been returning for space currents slightly greater than this value, is  $\tau' = 0.500\tau_0$ .

## 2. Effects of Varying $I_0$ , when $\frac{V_a}{V_g} = 0.20$ .

In the foregoing we have described in detail what occurs when the space current between the grid and anode is first increased, and then decreased. But this description was for the particular case when the grid and the anode voltages were equal. Similar phenomena, however,

occur for any other ratio of  $\frac{V_a}{V_g}$ , with only slight differences. For example, suppose  $\frac{V_a}{V_g} = 0.20$ . Beginning with  $I_0 = 0$ , the potential

distribution is linear. As  $I_o$  is increased, the behavior of the grid-anode region is initially characteristic of the first mode of operation, i.e., neither potential minimum nor virtual cathode exist. Further increase of  $I_o$  finally causes a potential minimum to occur at the anode, the value of this potential minimum being equal to the anode potential. The corresponding value of  $P_a$  is given by equation (13) as  $P_a = 1.41$ , the

equivalent space-current density being  $I_o = 4.62 \times 10^{-6} \times \frac{V_g^{3/2} \text{ amp.}}{a^2 \text{ cm}^2}$ .

Reference to Figure 11 tells us that the anode current will increase directly with space current until the space-current density reaches a value

$I_o = 7.00 \times 10^{-6} \times \frac{V_g^{3/2} \text{ amp.}}{a^2 \text{ cm}^2}$ , corresponding to a value of  $P_a^2 = 3.00$ .

This is the maximum anode-current density which can be passed: at this point the potential minimum, which has decreased to a value 0.0956 times the grid voltage, drops abruptly to zero and becomes a virtual cathode. The potential minimum, which had initially been formed at the anode, gradually recedes toward the grid until it reaches a distance equal to 0.776 times the grid-anode distance, given by equation (14). At this point it becomes a virtual cathode, and enables some of the electrons to return toward the grid. The resulting re-distribution of space charge causes the virtual cathode to shift abruptly until it reaches a distance equal to 0.418 times the grid-anode distance, given by equation (18). Any further increase of  $I_o$  results in a decreased anode current, as shown in Figure 11, the virtual cathode retreating still further toward the grid. If the space current is then decreased, the anode current will increase, as shown in Figure 11, and the virtual cathode will move back toward the anode. This behavior will continue until the space-current density reaches a value

$I_o = 3.38 \times 10^{-6} \times \frac{V_g^{3/2} \text{ amp.}}{a^2 \text{ cm}^2}$ , corresponding to a value of  $P_a^2 = 1.45$ .

At this point the virtual cathode is at a distance equal to 0.719 times the grid-anode distance, as given by equation (18). The slightest further reduction of space current permits enough electrons to pass abruptly through the virtual-cathode barrier toward the anode so that the space-charge distribution is radically altered, the virtual cathode disappears, and the anode current rises abruptly to the full value of space current. (An interesting observation about this example is that at this unstable point the virtual cathode does not become a potential minimum, but disappears.) From this point on, any further reduction of space current results in a proportionate reduction of anode current,

as shown in Figure 11, and the potential distribution becomes more and more linear.

### 3. Effects of Varying $V_a$ , when $P_a = 1.0$ .

Let us now suppose that the grid-anode distance,  $a$ , the effective grid voltage,  $V_g$ , and the space-current density,  $I_o$ , are fixed, and that it is required to determine the effects of varying the anode voltage,  $V_a$ . This situation corresponds, for example, to the case of a tetrode, the screen-grid voltage and the control-grid voltage of which are fixed, and the anode voltage of which is varied.

To begin with, we assume that the control-grid voltage is set at a value which provides a space-current density corresponding to a value of  $P_a = 1.0$ . When the anode voltage is negative, the anode current is zero, and all of the electrons are returned toward the grid at the temperature-limited virtual cathode. The potential distribution for

$\frac{V_a}{V_g} = -0.2$  is shown by (a) of Figure 14. The position of the virtual

cathode is given by Figure 8 as  $c = 0.645 a$ . When  $V_a = 0$ , then  $I_a = 0$ , and  $c = 0.707 a$ , as shown by (b) of Figure 14. As  $V_a$  is made more positive, the anode current rises as shown in Figure 10 and the space-charge-limited virtual cathode moves toward the anode. (If there had been no movement of the virtual cathode, the anode current would rise as  $V_a^{3/2}$ .) This continues until  $V_a = 0.068 V_g$ , while the anode current density rises to  $I_a = 0.413 I_o$ , and the virtual cathode moves to  $c = 0.793 a$ , as shown by (c) of Figure 14. The slightest further increase of anode voltage results in an abrupt saturation of anode current, the rate of change of anode current with anode voltage being infinite at this point, as shown by Figure 10. The virtual cathode disappears at this point, and the potential distribution is of the form shown by (c') of Figure 14, characteristic of the mode for which neither potential minimum nor virtual cathode exist. Further increase of anode voltage leaves the anode current, which is now equal to the space current, unaffected. However, when  $V_a$  reaches  $0.75 V_g$ , a potential minimum appears at the anode, as shown by (d) of Figure 14. With increasing anode voltage this minimum recedes toward the grid, approaches  $V_g$  in value, and finally disappears, as shown in Figures 7 and 8.

If the anode voltage is now decreased, the anode current remains at saturation value until  $V_a = 0$ , as shown in Figure 10. The potential minimum re-appears at the grid when  $V_a = 1.23 V_g$ , moves toward the anode as  $V_a$  is decreased, and reaches the anode when  $V_a = 0.75 V_g$ , as before. At this point the minimum disappears. When  $V_a = 0$ , the

potential distribution is abruptly altered, and a virtual cathode is formed at a distance  $c = 0.707 a$ , as shown by (f), (f') of Figure 14.

The time of flight of an electron moving from grid to anode, and from grid to virtual cathode, is shown for increasing and decreasing anode voltages in Figure 6.

#### 4. Effects of Varying $V_a$ , when $P_a = \sqrt{2}$ , $P_a = 2\sqrt{2}$ .

Similar interpretations hold for any other value of the parameter  $P_a$ . As a matter of interest, the various forms of the potential distribution for the particular cases  $P_a = \sqrt{2}$  and  $P_a = 2\sqrt{2}$  are shown in Figures 15 and 16. For the first of these, as the anode voltage is increased from a negative value, the potential distribution

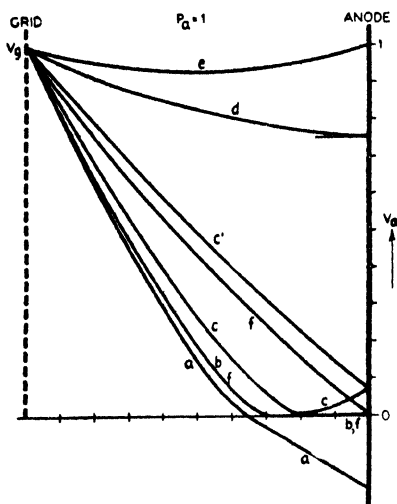


Fig. 14—Potential distribution for various values of anode voltage.  
 $P_a = 1$ .

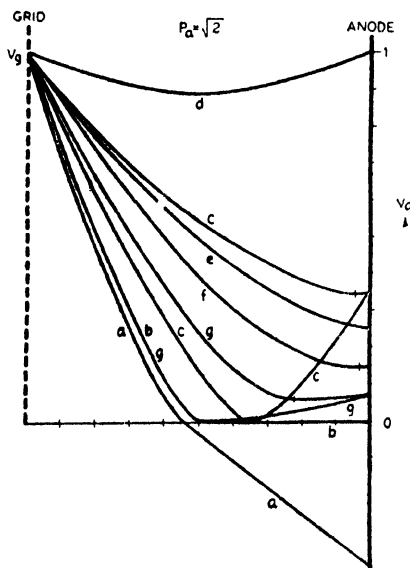


Fig. 15—Potential distribution for various values of anode voltage.  
 $P_a = \sqrt{2}$ .

passes from the state described by Case 4, which is characterized by a temperature-limited virtual cathode, (a), to that described by Case 3—the space-charge-limited virtual cathode case, (b), (c); thence abruptly to that described by Case 2, for which a potential minimum is formed, (c'), (d); and then finally to that described by Case 1, for which neither potential minimum nor virtual cathode exist. The behavior for decreasing anode voltage is successively illustrated by (d), (c'), (e), (f), (g), (g'), (a) of Figure 15. The abrupt decrease in anode current again occurs at a lower value of  $V_a$  than that required for the abrupt rise, as shown in Figure 10.

**B—General Discussion of Curves.**—The four distinct modes of

potential distribution which are treated in the foregoing analysis represent a somewhat arbitrary and simplified division of the potential distributions which may occur in the grid-anode region. This simplification is made possible by the original assumptions that the electrons have all been initially emitted from the cathode with zero velocity and that no velocity distribution has been introduced during the passage of the electrons through the structure. In the rigorous treatment of this problem the separate analyses of the four modes of potential distribution would merge into a single general analysis. However, such a treatment would be considerably more involved, and the main results at least can probably be anticipated by combining the various results found here for the individual states of operation on common graphs. This has been done in Figures 5-11.

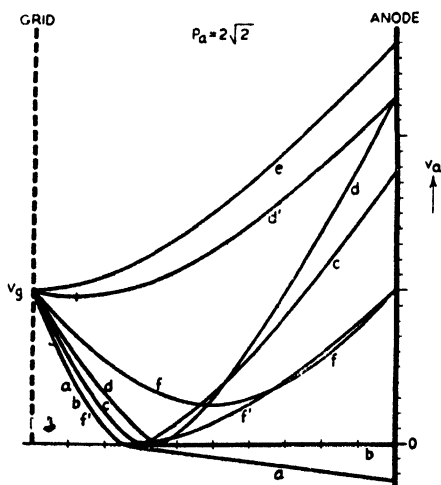


Fig. 16—Potential distribution for various values of anode voltage.  
 $P_a = 2\sqrt{2}$ .

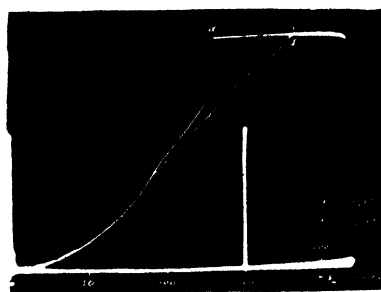


Fig. 17—Anode-characteristic oscillogram of special pentode showing the hysteresis and instability phenomena similar to curve marked  $P_a = 2\sqrt{2}$  in Figure 10.

Figure 5 is a plot of  $P_a$  vs.  $\frac{V_a}{V_g}$ , for various values of  $Q_g$ . If  $I_o$ ,  $V_o$ ,  $V_g$ , and  $a$  are given, this plot enables one to determine the electric intensity at the grid, since  $P_a$  is proportional to  $\frac{aI_o^{3/4}}{V_g^{3/4}}$  and  $Q_g$  is proportional to  $\frac{E_g}{I_o^{1/4}V_g^{1/4}}$ . As was pointed out in the analysis, these curves also represent a generalized potential distribution plot if  $P_a$  is replaced

by  $P$ , which is proportional to  $\frac{xI_o^{1/2}}{V_g^{1/2}}$ , and  $\frac{V_a}{V_g}$  is replaced by  $\frac{V}{V_g}$ . For

the temperature-limited virtual cathode case (negative anode potentials) the scale of ordinates represents  $\sqrt{2} P_a$  instead of  $P_a$ . This results from the fact that all the electrons which pass through the grid toward the anode are turned back toward the grid at the virtual cathode, and the space charge corresponds to a space current of  $2 I_o$  instead of

$I_o$ . The parameter  $Q_g$  is replaced by  $\frac{I_a}{I_o}$  in the space-charge-limited

virtual cathode case because this quantity is of greater practical significance. However, if the electric intensity at the grid is required for this case, it can be found very quickly from the relation

$$Q_g = - \left( 2 - \frac{I_a}{I_o} \right)^{1/2}$$

It will be observed that there occurs a curious overlapping of the various possible states of operation in different regions of the plot.

For example, for  $0 \leq \frac{V_a}{V_g} \leq 1$  and  $\frac{1}{\sqrt{2}} \leq P_a \leq \sqrt{2}$ , there may be a

virtual cathode, a potential minimum, or neither potential minimum

nor virtual cathode. Again, for  $\frac{V_a}{V_g} \geq 0$  and  $P_a \geq \sqrt{2}$ , there may be a

virtual cathode or a potential minimum. To put it in another way, the potential at any point in the region, for certain values of  $I_o$ ,  $V_a$ ,  $V_g$  and  $a$ , is multi-valued. This is a typical hysteresis phenomenon, and in order to determine which of the values of potential is the correct one it is necessary to know, as in all cases of hysteresis, the previous history of the region. This point will be discussed in further detail in connection with the other figures.

Figure 9 is a plot of  $\frac{V_c}{V_g}$  vs.  $P_a^2$ , for various values of  $\frac{V_a}{V_g}$ . The

curves shown in this plot indicate how the minimum potential varies with space current, since  $P_a^2$  is proportional to  $I_o$ . The section of the plot which lies to the left of the lightly-dashed line connecting the

points  $\left( \frac{V_c}{V_g} = 1, P_a^2 = 0 \right)$  and  $\left( \frac{V_c}{V_g} = 0, P_a^2 = 1 \right)$  delineates the

operating region in which neither potential minimum nor virtual cathode occur. The lightly-dashed line which starts at the point

$$\left( \frac{V_c}{V_g} = 0, P_a^2 = 1 \right) \text{ and passes through the point } \left( \frac{V_c}{V_g} = 0.25, P_a^2 = 8 \right)$$

is a parametric line which indicates the points at which the rate of change of the potential minimum with (increasing) space current is infinite. If the grid and anode potentials of a given tube are fixed and the space current is increased from zero, the potential minimum shifts abruptly at these points into a virtual cathode. The lightly-dashed line which starts at the point

$$\left( \frac{V_c}{V_g} = 0, P_a^2 = 1 \right) \text{ and becomes asymptotic to } \frac{V_c}{V_g} = 1 \text{ for very}$$

large values of  $P_a^2$  is a parametric line which indicates the points at which the virtual cathode shifts abruptly, with decreasing space current, into a potential minimum. The heavily-dashed continuations of the individual curves represent mathematical solutions of equation (13) which are probably unrealizable, at least in the steady-state or low-frequency operation of the tube.

These curves exhibit the instabilities and hysteresis phenomena which are characteristic of the grid-anode region, and again illustrate the necessity for a knowledge of the previous history of the operation of the tube in order to predict its future behavior.

Figure 11 is a plot of  $\left( \frac{I_a}{I_o} \right) \cdot P_a^2$  vs.  $P_a^2$  for various values of  $\frac{V_a}{V_g}$ . These curves illustrate the variation of the anode current with

space current for several particular values of the ratio of anode potential to grid potential. It will be observed that if the space current is increased from zero, the anode current bears a linear relation to the space current until a maximum value, given by equation (13a), is reached. At this point a virtual cathode is formed and the anode current is abruptly reduced. Thereafter, the anode current decreases continuously with increasing space current. If the space current is now decreased, the anode current will increase until the virtual cathode disappears. At this point the anode current becomes exactly equal to the space current, the phenomenon being an abrupt one for values

of  $\frac{V_a}{V_g} \leq 1$ . For  $\frac{V_a}{V_g} \geq 1$  this discontinuous phenomenon does not occur.



Further decrease of space current causes the anode current to decrease linearly with space current. The portions of these curves in which the anode current decreases with increasing space current are intimately associated with the presence of a virtual cathode, and can be utilized to provide a negative-transconductance amplifier or oscillator. This matter will be elaborated upon in section *D* of this discussion.

The dotted appendages of the individual curves in this graph represent mathematical solutions of equation (19) which are probably unrealizable in the steady-state or low-frequency operation of the tube. The terminations of these dotted sections upon the linear portion of unit slope, common to all of the curves, are given by equation (13b). On occasion these values have been assumed, incorrectly, as giving the maximum anode-current density which can be obtained.<sup>7</sup>

Figure 7 is a plot of  $\frac{V_c}{V_g}$  vs.  $\frac{V_a}{V_g}$  for various values of  $P_a$ . The curves shown in this plot illustrate the variation of the minimum potential with anode potential for several values of space current. The dotted line connecting the points  $\left( \frac{V_c}{V_g} = 0, \frac{V_a}{V_g} = 0 \right)$  and  $\left( \frac{V_c}{V_g} = 1, \frac{V_a}{V_g} = 1 \right)$  passes through the points on the individual curves at which a potential minimum is suddenly formed when the anode potential is increasing. The dotted line which becomes asymptotic to the value  $\frac{V_c}{V_g} = 1$  passes through the points on the individual curves at which the virtual cathode is abruptly transformed into a potential minimum when the anode potential is increasing. The third dotted line, which starts at the point  $\left( \frac{V_c}{V_g} = 0, \frac{V_a}{V_g} = 0 \right)$  and passes through the point  $\left( \frac{V_c}{V_g} = 0.25, \frac{V_a}{V_g} = 1 \right)$ , is a parametric line which indicates the points on the individual curves at which the potential minimum shifts abruptly, with decreasing anode potential, into a virtual cathode.

The curve which represents the case  $P_a = 0$  degenerates into a point located at  $\left( \frac{V_c}{V_g} = 1, \frac{V_a}{V_g} = 1 \right)$ , since this is the only value

of the ratio  $\frac{V_a}{V_g}$  for which the electric intensity can be zero in the absence of space current. The curves which represent the case  $P_a = 1$  consist of two discontinuous sections, the first being a portion of the axis of abscissas (this corresponding to the virtual cathode), and the second being the curved portion which begins on the first dotted line, which represents the potential minimum. For this case, when the anode potential is increased from negative values, a virtual cathode is first formed which presently disappears abruptly, and then for some greater value of anode potential, a potential minimum is formed. For values of  $P_a \leq \frac{1}{\sqrt{2}}$ , neither potential minimum nor virtual cathode

is formed with increasing anode voltage until  $\frac{V_a}{V_g} \geq 0.888$ . Then a potential minimum is formed.

Figure 8 is a plot of  $\frac{c}{a}$  vs.  $\frac{V_a}{V_g}$  for various values of  $P_a$ . These curves show the position of the virtual cathode and potential minimum for several values of space current plotted against different anode potentials. The sections of the various curves which lie to the left of the axis of ordinates reveal the location of the temperature-limited virtual cathode. The sections of the same curves which lie to the right of the axis of ordinates indicate the location of the space-charge-limited virtual cathode and potential minimum. The dashed-line portions of the curves for  $P_a = 1$  and  $\sqrt{2}$  are mathematical solutions of equation (18) which are probably unrealizable in the ordinary operation of the tube. Figures 7 and 8 together give the location and magnitude of the potential minimum under various operating conditions. This information is of considerable value to a proper understanding of the operation of the tube.

Figure 10 is a plot of  $\frac{I_a}{I_o}$  vs.  $\frac{V_a}{V_g}$  for various values of  $P_a$ . These curves show the variation of the anode current with anode potential for several particular values of space current. It will be observed that as the anode potential is increased from zero, the anode current increases from zero relatively slowly at first and then more rapidly. This rapidity of increase of anode current is more pronounced for the smaller values of space current. The initial variation of anode current with anode potential is approximately a  $\frac{3}{2}$ -power law, such as obtains

in the case of an idealized diode. As the anode potential increases, however, the returning current (corresponding to the electrons which return toward the grid from the virtual cathode) decreases because the anode current increases. This results in a movement of the virtual cathode toward the anode, and thus causes a further increase in the anode current. The net result is similar to that which would exist if the cathode of the idealized diode moved toward the anode with increasing anode potential, i.e., the current would increase more

rapidly than predicted by the  $\frac{3}{2}$ -power law. It will be observed fur-

ther that for the curves which represent the cases  $P_a = 1$  and  $\sqrt{2}$ , the anode current saturates abruptly with increasing anode potential. This action indicates an instability in the plate characteristic for relatively low values of space current. For values of  $P_a$  greater than 2, the saturation of anode current occurs at a finite rate, i.e., the saturation is a stable phenomenon. If the anode potential is decreased toward zero, after the saturated condition has been attained, the anode current does not vary with anode potential entirely as before. For example, in the case  $P_a = 2\sqrt{2}$ , the anode current saturates with

increasing anode potential at the value  $\frac{V_a}{V_g} = 2.24$ . With decreasing

anode potential, the anode current remains saturated until the value  $\frac{V_a}{V_g} = 1.0$  is reached, and thereafter follows the same law of variation

as occurred for increasing anode potential. This "overhang" of anode current illustrates the hysteresis phenomena which occurs in the plate characteristic.

The dashed-line portions of the curves for  $P_a = 1$  and  $\sqrt{2}$ , which indicate a negative-resistance anode characteristic, represent mathematical solutions of equation (19) which are probably unrealizable in the steady-state or low-frequency operation of the tube. The existence of such solutions has been used, unjustifiably, to form the basis of a negative-resistance explanation of Barkhausen-Kurz oscillations.<sup>7</sup> Such oscillations can be explained more satisfactorily by an analysis which takes into account, at the start, the effect of the transit time of the electrons.

Before leaving the discussion of Figure 10, it should be pointed out that curves representing values of  $P_a$  less than 1 have been omitted from this plot, since the analysis indicates the physically unrealizable phenomenon of a saturation current "overhang" into the negative

region of  $\frac{V_a}{V_g}$ . The value  $P_a = \frac{1}{\sqrt{2}}$  represents the limiting case for

which, with increasing anode voltage, the anode current rises gradually.

For values of  $P_a \leq \frac{1}{\sqrt{2}}$ , the anode current saturates abruptly at

$$\frac{V_a}{V_g} = 0.$$

Figure 6 is a plot of  $\frac{\tau}{\tau_0}$  and  $\frac{\tau'}{\tau_0}$  vs.  $\frac{V_a}{V_g}$  for various values of  $P_a$ . These curves show the variation with anode potential of the transit time,  $\tau$ , for the electrons which travel from the plane of the grid to the anode, and of the transit time,  $\tau'$ , for the electrons which travel from the plane of the grid to the virtual cathode. The curves illustrate the magnitude of the effect on the transit time of the electrons which can occur in the presence of space charge.

#### IV. EXPERIMENTAL VERIFICATION

To obtain experimental verification, at least of a qualitative nature, of the main features of the theoretical results, a special pentode was constructed. The tube consisted of an indirectly-heated cathode having an area of 6.3 sq cm; a control grid, the potential of which was varied to alter the space current between the screen grid and anode; and a screen grid spaced 1.5 cm from a suppressor grid located in front of, and very close to an anode having an area of 9 sq cm. The suppressor grid was connected to the anode to prevent any secondary electrons, which might have been emitted from the anode, from seriously disturbing the space-charge conditions in the region between screen grid and anode. The electrodes were made slightly concave to minimize spreading of the electron stream, and large enough in area to minimize edge effects.

Oscillograms of the anode and transfer characteristics of this tube were taken on a special cathode-ray curve tracer built by Mr. O. H. Schade, of this laboratory.\* The characteristics were determined in this way because the heavy currents would have damaged the tube if the tube performance had been observed by the usual point-by-point method.

Figure 17 is an oscillogram record of the variation of anode current with anode voltage, the control-grid voltage being 150 volts and the

---

\* This device was described by Mr. Schade before the Rochester Convention of the I.R.E. on November 20, 1935.

screen-grid voltage being 120 volts. It will be observed that the anode current increases uniformly, as the anode voltage is increased from zero, until the point marked "c" where saturation is reached, and thereafter changes very slowly with further increase of anode voltage. When the anode voltage is decreased, the anode current remains virtually constant until the point "d" is reached, at which point the anode voltage is considerably less than at the point "c". With further decrease of anode voltage, the anode current drops discontinuously and then decreases uniformly on the same curve as obtained with increasing anode voltage. This behavior is qualitatively similar to the theoretical curve marked  $P_a = 2 \sqrt{2}$  of Figure 10.

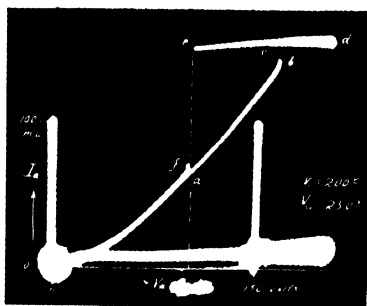


Fig. 18—Anode-characteristic oscillogram of special pentode showing the hysteresis and instabilities similar to curve marked  $P_a = \sqrt{2}$  in Figure 10.

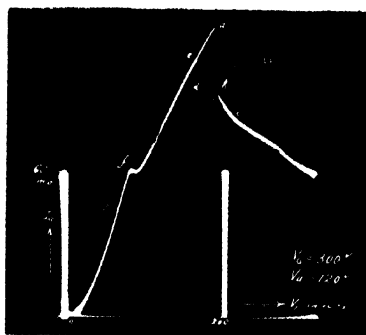


Fig. 19 — Transfer-characteristic oscillogram of special pentode showing the hysteresis and instabilities characteristic of the curve marked  $\frac{V_a}{V_g} = 0.4$  of Figure 11.

Figure 18 is a similar oscillogram record, the control grid now being at 200 volts and the screen grid at 250 volts. This characteristic shows an abrupt increase of the anode current at the point "b" when the anode voltage is increasing, and an abrupt decrease of the anode current at the point "e" when the anode voltage is decreasing. This behavior is qualitatively similar to the theoretical curve marked  $P_a = \sqrt{2}$  of Figure 10. The faint irregular traces which are present at the abrupt changes of anode current are probably mainly due to the unavoidable reactance of the tube connecting leads.

Figure 19 is an oscillogram record of the variation of anode current with control-grid voltage, to which the space current is proportional. The screen grid was maintained at 300 volts and the anode at 120 volts. This record is in qualitative agreement with the curve

for  $\frac{V_a}{V_g} = 0.4$  of Figure 11. It will be observed that the anode current

increases uniformly, except at the point "f", with increasing space current until a virtual cathode is almost formed at the value corresponding to the point "a". Further increase of space current causes the formation of a virtual cathode between screen grid and anode, with an attendant sudden decrease of anode current, as indicated by the point "b". Still further increase of space current is accompanied by a uniform decrease of anode current. (The negative slope of the  $I_a$  vs.  $V_1$  characteristic in this region represents a negative transconductance and can be utilized to form the basis of a novel type of amplifier and oscillator.) If the space current is now decreased, the anode current increases until the point "d" is reached, at which point an abrupt increase of anode current takes place. The point "d" corresponds to a lower value of space current than the point "a", in accordance with theoretical expectations, and marks the sudden disappearance of the virtual cathode and the formation of a potential minimum. Further decrease of space current is accompanied by a decrease of anode current, the same path now being followed as for increasing space current.

The curious kink in the early portion of the curve, indicated by the point "f", may be accounted for as follows: Since the control grid was operated at positive potentials in order to obtain sufficient space current for the experiment, it is to be expected that the possibility of primary and secondary emission from this grid is great. At relatively low values of control-grid voltage, corresponding to relatively low values of space current, these electrons contribute to the anode current. As the control-grid voltage is increased, the space current increases sufficiently so that the value of the potential minimum which has been formed in the region between screen grid and anode becomes less than that of the control grid. As a result the electrons emitted from the control grid are confronted by a potential barrier which they are unable to penetrate and consequently they execute excursions about the screen grid until captured. The slope of the  $I_a$  vs.  $V_1$  curve is greater for values of  $V_1$  corresponding to the range between zero and the point "f" than for the range above "f". This is accounted for by the explanation given above, because for values of  $V_1$  less than those corresponding to "f" the electrons which are emitted from the control grid contribute to the anode current. Beyond this point these electrons do not contribute to the anode current, but instead because of their multiple excursions about the screen grid, they increase the value of space current and actually cause the anode current to increase

at a lower rate with control-grid voltage than before. Approximate calculations which have been made support this explanation, but their reproduction at this point would be out of place.

## V. ILLUSTRATIVE APPLICATIONS

The theoretical results which have been presented in the foregoing treatment are applicable to a wide variety of vacuum-tube problems. For purposes of illustration, we will now discuss two such problems, both of considerable practical interest.

1—*The Type 6L6 Beam Power Tube*.—This tube is a quasi-pentode power amplifier which employs a minimum potential, deliberately formed in front of the anode by utilizing the space charge of the electrons, to minimize the passage of secondary electrons from anode to screen grid. The existence, under certain conditions, of a potential minimum or virtual cathode in the region between screen grid and anode has been known for some time,<sup>6 7 8</sup> and the applicability of the phenomenon to the minimization of the (undesired) passage of secondary electrons from the anode to the grid has also been recognized for some time.<sup>1 7 6 7</sup> Recently, however, the subject has received considerable attention,<sup>2 3 4 10 11</sup> and it appears to us that a number of misconceptions which have arisen concerning the theory of operation of such a tube can be cleared up by means of the foregoing theory with certain modifications, of a quantitative nature, introduced by the factors which we explicitly neglected at the start.

The objectives which were sought in the development of this tube were improvements over a-f power output tubes then available with regard to power output, efficiency, power sensitivity, and distortion. These objectives could best be attained by a high-transconductance tube having an anode characteristic as close as possible to that of an ideal pentode.<sup>4</sup> Although the usual pentode anode characteristic exhibits no trace of the secondary-emission phenomena typical of the conventional tetrode, it is invariably marked by a relatively slow initial rise of anode current with anode voltage and by a rather gradual saturation of the anode current. These undesirable features can be charged mainly to the presence of the suppressor grid, and therefore it was decided to dispense with this grid and replace it, at least as far as its effect on preventing the flow of secondary electrons from the anode to the screen grid was concerned, by a potential minimum. The ultimate result of this development was the 6L6, the anode characteristic of which is reproduced in Figure 20.

In general, the main features of the curves shown in this figure agree qualitatively with those of the idealized curves shown in Figure

10. For example, the curves corresponding to the largest values of space current, i.e., highest values of control-grid voltage, tend to saturate at higher values of anode voltage and also exhibit the abrupt type of saturation predicted by the theory for values of  $P_a$  less than 2. The smooth type of saturation shown in Figure 10 for larger values of  $P_a$ , which was verified experimentally in Figure 17, is also evident in Figure 20. However, there are several discrepancies between the theoretical results for the idealized parallel-plane tube and the curves of Figure 20. One of these lies in the fact that none of the curves saturate immediately, whereas the theory indicates that for  $P_a$  less

than  $\frac{1}{\sqrt{2}}$  the anode current should rise to saturation value for the

smallest positive anode potential. This lack of agreement can be attributed in small part to the Maxwellian distribution of velocities of electron emission, and in much greater part to the angular deflection of the electrons which occurs because of the wire grid structure.<sup>9</sup> This effect is most pronounced at the very lowest values of space current: at the higher space currents, where a virtual cathode is formed, this effect is entirely overshadowed by the behavior predicted by the theory. Another discrepancy is to be observed in the curve for  $E_{c1} = -30$  volts, which exhibits negative anode conductance for anode voltages between 25 and 75 volts. This can doubtless be explained by the existence of a potential minimum, the value of which is too high to provide a suitable retarding field for the proper suppression of secondary electrons which are emitted from the anode. A further discrepancy is to be observed in the fact that all of the curves have a finite slope in the saturation region. This is probably due in main part, to the penetration of the anode field through the screen grid, and perhaps also to the slight contribution to the anode current of primary and secondary electrons from the screen grid. A more serious discrepancy, from an academic point of view, is the relatively narrow area of the hysteresis loops which are to be observed in the curves for  $E_{c1} = +10$  volts and  $E_{c1} = +15$  volts. This may be due to the edge effects introduced by the zero potential "beam-forming" plates.

It may be well to point out here that the behavior of the initial portions of all of the theoretical curves of Figure 10 and also the corresponding portions of the experimental curves of Figures 17, 18, and 20, is at variance with that deduced by J. H. O. Harries,<sup>3</sup> shown in his Figure 9 as curve *G A D E*. Harries invokes the electron-velocity spread at the grid to explain the actual curvature of the rising portion of the anode characteristic, but it appears from the theoretical results that the curvature can be present even in the absence of a



well-defined distribution of velocities of the electrons which pass through the grid. Nor is the suggestion of S. Rodda<sup>11</sup> that the work of Below and Schulze indicates that this curvature is due primarily to the angular deflection of electrons in the neighborhood of the screen grid valid, except (as we have mentioned above) for very low values of space current. As Harries pointed out,<sup>11</sup> this is because Below explicitly neglected the possibility of the formation of a virtual cathode.<sup>9</sup> The suggestion of Bell<sup>10</sup> that the "detailed mechanism" of the anode characteristic of tubes, ostensibly utilizing a potential minimum to mini-

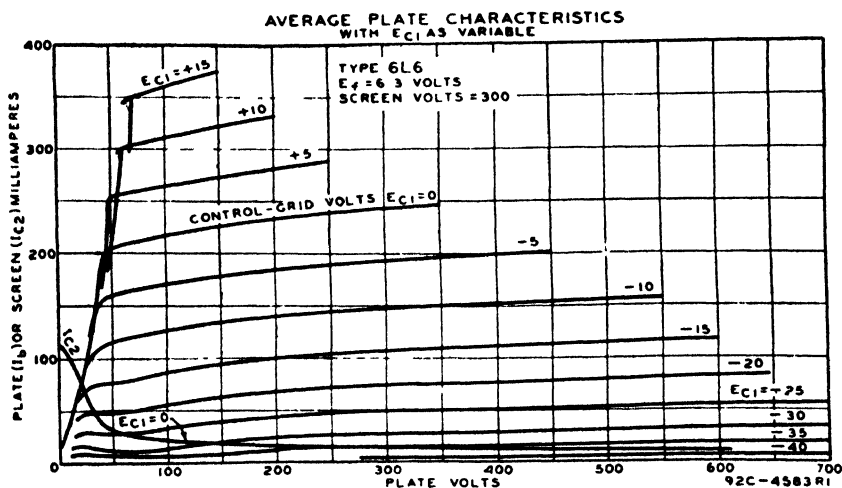


Fig. 20—Anode characteristic of RCA-6L6.

mize the passage of secondary electrons from the anode to the screen grid, may be due largely to the inherently steep initial rise of the tetrode plus the somewhat reduced secondary emission of electrons from the anode is interesting, but hardly satisfying as a complete theory. Finally, in passing, we wish to call attention to the possibilities of obtaining misleading results when using long glass tubes such as that of the "sliding-anode" tube employed by Harries.<sup>2,3</sup> This has been pointed out by I. Langmuir<sup>12</sup>, in a discussion of Lilienfeld's work.

2—*Negative-Transconductance Amplifiers and Oscillators.*—To illustrate the application of the negative-transconductance features of Figure 11, in which the anode current decreases with increasing space current<sup>6</sup>, a special pentode capable of operation with negative control voltage was constructed. The relative spacings of the electrodes were  $K-G_1: G_1-G_2: G_2-G_3: G_3-A = 0.6: 0.6: 1.0: 8$ . The first grid was used as a negative-control electrode, the second grid as a positive-

accelerator electrode, the third grid as a positive electrode for controlling the velocity of the electrons entering the  $G_3$ -A region where a virtual cathode was formed, and the anode was used as the output electrode. The tube could be used as an amplifier and as an oscillator having several unique properties.

For an oscillator application, a typical circuit is shown in Figure 21. The control grid is coupled to the plate circuit by means of a large blocking condenser,  $C_{AG1}$ , the negative bias being supplied to the grid through a high resistance  $R_g$ . The grid excitation is adjusted by sliding

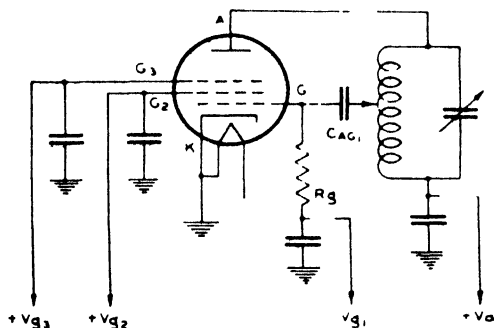


Fig. 21—Schematic circuit of negative-transconductance oscillator.

the tap along the plate inductance. In this circuit the grid voltage is essentially in phase with the anode voltage, so that the tube oscillates only when the transconductance is negative. The condition for oscillation requires that the negative transconductance be greater than the sum of the internal anode conductance and the external circuit conductance, which includes the anode circuit proper and the reflected conductance of the grid resistor. Typical operating conditions were:  $g_m = -2500 \mu\text{mhos}$ ,  $g_p = 500 \mu\text{mhos}$ ,  $g_r = 200 \mu\text{mhos}$ ,  $V_a = 210$  volts,  $I_a = 55$  ma,  $V_3 = 200$  volts,  $I_3 = 25$  ma,  $V_2 = 200$  volts,  $I_2 = 25$  ma,  $V_1 = -12$  volts,  $I_1 = -0.2$  milliamperes,  $\lambda = 30$  meters,  $V_{rf} = 15$  volts.

In order to obtain a larger plate swing without destroying the virtual cathode, and also to obtain a larger effective negative conductance by reducing the anode conductance, an additional screen grid may be placed in front of the anode. In this way the space-charge conditions in the  $G_3$ - $G_4$  region can be adjusted independently of the output circuit impedance by control of the potential of the screen grids  $G_3$  and  $G_4$ . A tube of this type with relative electrode spacings of 0.6:0.6:1.0:8.0:2.0 showed an anode conductance of only  $40 \mu\text{mhos}$  in the negative-transconductance region.

## VI. CONCLUSIONS

The effects of space charge in the region between grid and anode are of fundamental importance in determining the behavior of vacuum tubes, particularly when the anode is preceded by a grid operated at a positive potential. The effects of space charge between the grid and anode of a parallel-plane vacuum tube have been determined in this study from the results of a simple analysis. The assumptions which underlie this analysis necessarily introduce modifications of the theory, but as the experimental verification indicates, these do not invalidate the main results, and their effects can be taken into account in a qualitative way.

The principal effects of the space charge in the grid-anode region are: (a) to introduce departures from the linear potential-distribution characteristic of the electrostatic case; (b) to set an upper limit to the current which can be collected at the anode, the limiting current density being

$$(I_a)_{\max.} = 2.33 \times 10^{-6} \times \frac{(V_g^{3/4} + V_a^{3/4})^3}{a^2} \text{ amp per cm}^2$$

where  $V_g$  and  $V_a$  are the effective grid and anode voltages, respectively, and  $a$  is the distance between grid and anode; (c) to introduce instabilities and hysteresis phenomena in the behavior of the tube; and (d) to increase the electron-transit time in this region.

For the four modes of potential distribution which have been treated, expressions have been derived for the distribution of potential and electric intensity throughout the grid-anode region; the time of flight of electrons from grid to anode, and (when a zero-potential plane is formed) also from grid to this plane of zero potential; and the location and magnitude of the minimum potential. A formula has also been derived for the dependence of the anode current on the space current, grid-anode distance, grid voltage and anode voltage. These expressions have been plotted, using dimensionless parameters, in Figures 5-11.

The experimental verification of these theoretical results indicate that the theory can be employed in a qualitative way at least, to predict and explain the behavior of a large variety of vacuum tubes. This has been done for the 6L6 "beam power" tube, and for amplifier and oscillator tubes which make use of the decrease of anode current with increasing space current which the theory predicts.

## BIBLIOGRAPHY

- <sup>1</sup> G. Holst and B. D. H. Tellegen, U. S. Patent 1,945,040.
- <sup>2</sup> J. H. O. Harries, U. S. Patents 2,045,525; 2,045,526; 2,045,527.
- <sup>3</sup> J. H. O. Harries, "The Anode to Accelerating Electrode Space in Thermionic Valves", *Wireless Engineer*, 13, pp. 190-199, April, 1936.
- <sup>4</sup> O. H. Schade, "Beam Power Tubes", to be published in *Proc. I.R.E.*
- <sup>5</sup> E. W. B. Gill, "Distribution of Electric Forces in Spaces Traversed by Electrons", *Phil. Mag.*, 10, pp. 134-139, July, 1930.
- <sup>6</sup> E. W. B. Gill, "A Space Charge Effect", *Phil. Mag.*, 49, pp. 993-1005, May, 1925.
- <sup>7</sup> L. Tonks, "Space Charge as a Cause of Negative Resistance in a Triode and its Bearing on Short Wave Generation", *Phys. Rev.*, 30, pp. 501-511, October, 1927.
- <sup>8</sup> D. C. Prince, "Four-Element Tube Characteristics as Affecting Efficiency", *Proc. I.R.E.*, 7, pp. 805-821, June, 1928.
- <sup>9</sup> F. Below, "Zur Theorie der Raumladegitterröhren", *Zeitschrift für Fernmeldetechnik*, 8, pp. 113-143.
- <sup>10</sup> D. A. Bell, "Secondary Emission in Valves", *Wireless Engineer*, 13, pp. 311-313, June, 1936.
- <sup>11</sup> Discussion by S. Rodda and J. H. O. Harries, *Wireless Engineer*, 13, pp. 315-316, June, 1936.
- <sup>12</sup> I. Langmuir, "Fundamental Phenomena in Electron Tubes Having Tungsten Cathodes", *G. E. Review*, 23, pp. 503-513, June, 1920, and pp. 589-596, July, 1920.
- <sup>13</sup> G. Plato, W. Kleen, and H. Rothe, "Die Raumladegleichung für Elektronen mit Anfangsgeschwindigkeit", *Zeitschrift für Physik*, 101, No. 5, pp. 509-520.
- <sup>14</sup> H. C. Calpine, "Conditions in the Anode Screen Space of Thermionic Valves", *Wireless Engineer*, 13, No. 156, pp. 473-474, September, 1936.
- <sup>15</sup> W. Lukoshkow, "Electron Space Charge and the Theory of the Triode", *Technical Physics of the U.S.S.R.*, 3, No. 5, pp. 408-432.
- <sup>16</sup> W. Kleen and H. Rothe, "Die Raumladegleichung für Elektronen mit Anfangsgeschwindigkeit. II. Teil", *Zeitschrift für Physik*, 104, Nos. 11 and 12, pp. 711-723.

# FLUCTUATIONS IN SPACE-CHARGE-LIMITED CURRENTS AT MODERATELY HIGH FREQUENCIES \*†

By

B. J. THOMPSON, D. O. NORTH AND W. A. HARRIS

RCA Manufacturing Company, Inc.,  
Harrison, New Jersey

## PART I—GENERAL SURVEY

By B. J. Thompson

**Summary**—This paper is presented in five parts of which this is the first, serving as an introduction to the others which present detailed analyses of fluctuations in space-charge-limited currents in diodes and negative-grid triodes, in multi-collector tubes, and in tubes with appreciable collision ionization, and of the fluctuations in vacuum-tube amplifiers under operating conditions. The purpose of this part is to present the theoretical and historical backgrounds for the other parts.

Previous work led to a recognition of the fact that fluctuations in space-charge-limited currents are less than in temperature-limited currents. Attempts were made to explain the actual magnitude of such residual fluctuations in terms of thermal agitations in the internal resistance of the tube at cathode temperature. Agreement between such explanation and experimental results was not observed, the observed mean-square value of fluctuations being only about six-tenths of the predicted value.

It is clear that the thermodynamic reasoning on which the thermal agitations argument is based cannot properly be applied to a case such as a vacuum tube in which the drift velocities of the electrons greatly exceed the thermal velocities. A microscopic examination of the mechanism of space-charge reduction of shot effect is required, therefore.

The number of emitted electrons having velocities greater than any fixed value fluctuates at random. If the retarding potential (virtual cathode) established near the cathode by the space charge were fixed in magnitude, the current passing to the anode would show fluctuations identical with those observed in temperature-limited currents of the same value. Since this is not the case, it is apparent that the retarding potential fluctuates with fluctuations in emission in such a way as to oppose the changes in anode current.

The method of analysis is to determine the effect on the potential minimum of a small pulse of electrons of each velocity group from zero to infinite velocity, and from this effect the change in anode current. The average rate of emission of electrons of each velocity group is known for a given cathode temperature. The mean-square fluctuations in number emitted is proportional to the average number. From this and from the effect of electrons of different velocities on the anode current, the total current fluctuations may be determined by integration.

---

\* Decimal Classification: R138.1.

† Reprinted from *RCA Review*, January 1940 et seq.

*It has been observed that fluctuations in positive-grid tubes exceed those in triodes. This difference must be due to fluctuations in division of current between positive grid and anode. Such fluctuations in division can be accounted for by the fact that, for each pulse of excess emission confined to a small area of the cathode, there must be a compensating reduction of anode current extending over a considerable area. The initial excess pulse will flow chiefly to the grid or to the anode, while the compensating pulse will divide between the two.*

*Fluctuations in anode current caused by collision ionization have been observed, but are of little importance under practical conditions. Ballantine's analysis is incomplete because of difficulties arising from the study of the effect of a single ion. It is more convenient to treat the ion flow as a continuous stream as is done in the case of electron currents.*

*The application of the methods of approach outlined in this part will be given in the later parts of this paper.*

#### A—INTRODUCTION

FEW technical problems have been the subject of so much discussion over such a long period without general agreement as that of the random fluctuations in plate current of a space-charge-limited vacuum tube. Until recently this lack of agreement embraced experimental fact as well as theory. In this situation, it was natural that the theories should be nearly as numerous and as dissimilar as the authors thereof. Now, however, it appears that there is something approaching general agreement on the observed facts. The time seems ripe, therefore, for agreement on theory. It is the hope of the present writer and his collaborators to present in this series of papers a reasonably complete theoretical analysis of fluctuations in vacuum-tube amplifiers under operating conditions, and experimental confirmation thereof.

The work on which these papers are based extends over a period of more than ten years. While we have found ourselves in disagreement with many of the papers which have appeared on this subject, we have delayed presenting our work in published form until repeated experimental verification and continued analytical refinement, together with the acceptance of our conclusions by others, have convinced us of the soundness of our results. In the course of preparation of these papers, we have received further assurance from the publication by distinguished German workers of results closely similar in part to ours.

The extensive literature on the subject of current fluctuations is, to some extent, an indication of its importance. Vacuum-tube amplifiers enable us to perceive extremely minute electrical impulses, the minuteness being limited only by the magnitude of the inevitable extraneous background of "noise". This application of amplifiers is of major importance and "noise" is the only serious technical limitation at present.

The desired signal which is introduced into an amplifier is not, in itself, free from noise. The amplifier, however, introduces additional noise which often is greatly in excess of the inherent noise of the signal. It is recognized that both the circuits and the vacuum tubes of the amplifier contribute to the amplifier noise. In many circumstances, circuit noise predominates; in other cases—notably of late, television amplifiers—tube noise is the limiting factor.

The extraneous background noise produced by a vacuum tube may be divided into three general classifications:

1. Disturbances caused by wall charges, vibration of electrodes, faulty contacts, etc. These are largely confined to the lower frequencies and may be reduced without theoretical limit by more careful tube design and construction.

2. Flicker effect, caused by random changes in surface conditions of the emitter. This disturbance is confined chiefly to frequencies below 500 cycles per second, and may be reduced by choice and treatment of the emitter.

3. Fluctuations in space-charge-limited currents associated with the random emission of electrons. These disturbances are distributed uniformly over the whole frequency spectrum from zero to frequencies such that the electron transit time is comparable with the period. They are of a fundamental nature.

Because the first two effects are largely confined to the lowest frequencies and because they may be controlled by well-known means, this part and subsequent parts of the paper will deal solely with the third class of fluctuations.

In an attempt to present our work in the form most convenient to possible readers, whose interests may vary from the purely theoretical to the intensely practical, we shall divide the material into several parts, of which this is Part I. These parts will, in effect, be independent papers which may be read separately, though, of course, each part will use without repetition of proof the pertinent conclusions of other parts. These parts are as follows:

Part I. General Survey, by B. J. Thompson.

Part II. Fluctuations in Diodes and Triodes, by D. O. North.

Part III. Fluctuations in Multi-Collector Tubes, by D. O. North.

Part IV. Fluctuations Caused by Collision Ionization, by B. J. Thompson and D. O. North.

Part V. Fluctuations in Vacuum-Tube Amplifiers, by W. A. Harris.

The titles of Parts II, III, and IV list the major sources of noise which will be treated separately.

It is the purpose of this general survey to present the historical and theoretical backgrounds for the individual analyses. Those who are concerned solely with the application of the results will be interested chiefly in Part V, since the rest of this part and Parts II, III, and IV describe how the results are obtained.

## B—FLUCTUATIONS IN SPACE-CHARGE-LIMITED DIODES AND TRIODES

### 1. HISTORICAL SURVEY

Historically, the first publication concerning current fluctuations was the classic paper by Schottky<sup>1</sup> in 1918 in which he predicted that there would be fluctuations in the plate current of a temperature-limited diode, the mean-square value of which is proportional to the plate current, the electron charge, and the frequency interval over which the measurement is made. Subsequently this prediction was verified experimentally.

In 1928, Nyquist<sup>2</sup> and Johnson<sup>3</sup> published their important papers showing that there are fluctuations in voltage across the terminals of an open-circuited resistor, the mean-square value of which is proportional to the resistance, the absolute temperature, and the frequency interval over which the measurement is made.

It was recognized that these two types of fluctuations set a minimum limit to the magnitude of signal which may be perceived by means of a vacuum-tube amplifier. As early as 1925, however, it was recognized that the shot-effect formula of Schottky does not apply directly to space-charge-limited currents, the careful measurements of Hull and Williams<sup>4</sup> having shown a reduction to as low as 16 per cent of the root-mean-square temperature-limited shot effect. The question then arose as to the lowest magnitude of fluctuations to be expected under operating conditions.

One view, attractive in its simplicity, was that in the presence of "complete space charge" the fluctuations would be zero. The fact that they were not found to be zero was taken to be an indication of the lack of complete space charge.

The first attempt at a complete analysis of the problem was that of Llewellyn<sup>5</sup> in 1930. The fluctuations were divided into two component parts: that resulting from the lack of complete space charge (measured by the rate of change of plate current with emission current) and appearing as a fraction of the temperature-limited shot effect, and that produced by thermal agitations in the plate resistance of the tube, demonstrated by thermodynamic considerations to be effectively at the cathode temperature.



This analysis was widely accepted, but came to be recognized as suffering from the grave defect that the predicted values of shot effect or of thermal agitations taken alone often considerably exceeded the total measured fluctuations. The published measurements of Pearson<sup>6</sup> and of F. C. Williams<sup>7</sup> and unpublished work of others established this fact clearly and led to an attempt to obtain agreement between theory and measurement by dropping the shot-effect component and making the quite reasonable substitution of cathode resistance for plate resistance in computing the thermal agitations of a triode.<sup>8</sup> This still left an excess of "theoretical" over measured fluctuations.

F. C. Williams<sup>7</sup> appears to have been the first to point out in a published paper the fallacy of viewing the anode current fluctuations as thermal agitations in the internal anode resistance. It seems clear that thermodynamic reasoning cannot be applied to a situation where the drift velocities of the electrons are greatly in excess of their thermal velocities.

In November, 1936, Dr. North and I presented at the Rochester Fall Meeting of the I. R. E. a brief summary of our theoretical and experimental work which will form a considerable part of the present contribution.<sup>9</sup> As relates to diodes and triodes, it was shown by a microscopic study of the actual mechanism of reduction of shot effect by space charge that the magnitude of mean-square current fluctuations should be approximately six-tenths of the thermal agitations in a resistor equal in magnitude to the cathode resistance at the cathode temperature. This result was stated to be in agreement with experimental observations.

At about the same time Schottky published the first<sup>10</sup> of a projected series of papers;<sup>11</sup> this constituted the first published attempt to analyze the actual mechanism of space-charge reduction of shot effect. Unfortunately, the different effects of different velocity classes of electrons were ignored, leading to an erroneous result.

A subsequent paper by Schottky and Spenke<sup>12</sup> has corrected the errors and omissions of the earlier papers. So far as relates to fluctuations in space-charge-limited diodes and triodes, these writers are now in substantial agreement with the results presented by us in 1936 and now published in detail.

Rothe and Engbert<sup>13</sup> have published a large number of measurements on a variety of tubes which establish more firmly the experimental facts.

## 2. NATURE OF THE PROBLEM

The analysis of fluctuations in temperature-limited currents (to be called true shot effect) is based on the assumptions that the emission of any one electron is an independent event determined solely by

chance and uninfluenced by the emission of other electrons at that or any other time, and that all emitted electrons instantaneously pass to the anode. Under such conditions, it is shown that the number of electrons emitted in successive equal time intervals varies according to the laws of probability and that this variation in number constitutes a spectrum of alternating-current components having constant amplitude independent of frequency. A tuned circuit through which the anode current flows will develop a voltage the mean-square value of which is proportional to the plate current, the square of the resonant impedance, and the band width over which the circuit responds. To give a numerical example, a circuit of 50,000 ohms impedance having an effective band pass of 10,000 cycles per second through which a temperature-limited current of one milliamperere flows will develop a voltage of 89 microvolts across its terminals, independent of the resonant frequency. This prediction has been accurately verified.

The assumption of complete randomness of electron emission applies equally well to the space-charge-limited case, of course. It is obvious that the second assumption of instantaneous passage of all electrons to the anode is not justified, however. The mechanism of space-charge limitation of anode current is such that part of the emitted electrons are turned back to the cathode. As the total emission is arbitrarily increased—by increasing cathode temperature, for example—a larger fraction of the electrons is turned back. This results from the mutual repulsion between electrons, the presence of one electron tending to turn back following electrons. It is to be expected, then, that when an instantaneous excess of electrons over the average number happens to be emitted, a greater fraction of the total number of electrons will be returned to the cathode. It follows that the anode current fluctuations will be reduced by the action of the space charge to a value less than the true shot effect. We shall call this value the reduced shot effect.

It seems clear that it will be necessary to examine minutely the mechanism of space-charge limitation of anode current in order to determine the effect of space charge on shot effect.

Before proceeding with a discussion of the problem, it may be well to pause here and clear up several points which have tended to becloud the technical issues in the past, both by leading to experimental error and by confusing theoretical discussion.

It has been erroneously stated that, since shot effect is produced by the arrival of individual discrete electrons at the anode, nothing may be expected to reduce its magnitude for a given current. Shot effect is not a matter of the discreteness of the electron, directly. A current of 1.0 milliamperere corresponds to a flow of nearly  $10^{16}$  elec-

trons per second. If they were to arrive at the anode at a uniform rate, there would be no frequency component below  $10^{16}$  cycles per second.

It has been erroneously stated that shot-effect currents are the same in the presence of space charge as with temperature limitation of emission and that the reduction in shot-effect voltage results only from the shunting effect of the lower anode resistance in the case of space-charge limitation.

On the other hand, experimental results have frequently been published in which the varying shunting effect of the anode resistance was ignored.

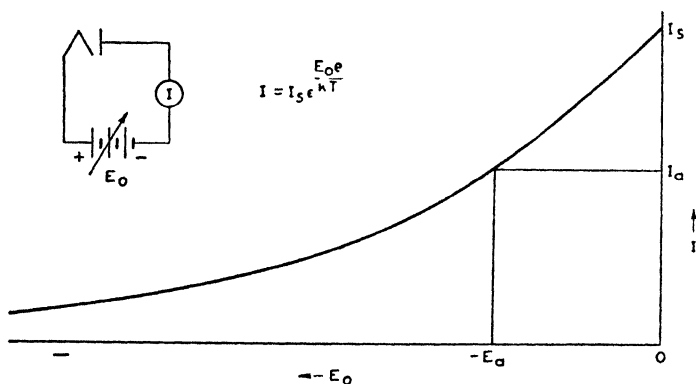


Fig. 1

Shot effect is essentially the varying rate of flow of electrons between cathode and anode brought about by the random rate of emission of electrons. The study or discussion of current flow in a vacuum tube is expedited by assuming no external impedance in any electrode circuit. We shall, therefore, make this assumption, unless otherwise stated. The fluctuation voltage in the anode circuit for any fluctuation current may be obtained in the same manner as for varying currents of other origin: by multiplying the alternating component of current by the effective anode impedance, including the internal anode resistance in parallel with the external circuit. The internal anode resistance has no unique influence on shot effect. Of course, measurements of shot effect require an impedance in the circuit. The experimental results presented in these papers represent either the current which would flow in the electrode circuit without impedance, or the voltage developed across a stated impedance, including the internal electrode resistance.

## 3. GENERAL THEORETICAL CONSIDERATIONS

In a temperature-limited diode, there is an accelerating field at the cathode and all emitted electrons pass over to the anode. According to the well-known formula for true shot effect, the mean-square fluctuation current  $\bar{i}^2$  produced by an anode current  $I$  is  $\bar{i}^2 = 2eI \Delta f$  where  $e$  is the electron charge and  $\Delta f$  is the frequency band over which the measurement is made. *If the total temperature-limited current  $I$  is divided in any arbitrary fixed manner, the mean-square fluctuation current of any part of the current is in proportion to that part, thus corresponding to true shot effect.* This is stated axiomatically, and will be called the principle of fixed division. It applies to divided

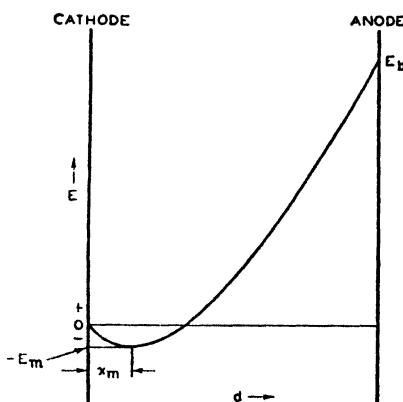


Fig. 2

cathodes, divided anodes, selected velocity groups, or any other fixed division.

Let us consider the velocity distribution of the emitted electrons, shown in Figure 1. This is really a plot of the current which would flow to a negative electrode closely surrounding the cathode, the potential of the electrode being  $E_0$  and the current flowing to it,  $I$ . As the electrode is made more negative, fewer electrons have sufficient velocity of emission to reach the electrode against the retarding field. If the potential be set at  $-E_a$ , a current  $I_a$  will flow to the electrode, electrons having lower velocity being turned back. Since we are fixing the division of the total current by the retarding potential  $-E_a$ , there will be true shot-effect fluctuations in current  $I_a$ .

The potential distribution in the space between cathode and anode in a parallel-plane diode with space-charge-limited current is represented in Figure 2. Near the cathode there is a potential minimum of magnitude  $E_m$  (negative) at a distance  $x_m$  from the cathode. Between this potential minimum and the cathode, all electrons having an initial velocity of emission  $E_0$  normal to the cathode less than  $E_m$  (expressed

in electron volts, the actual velocity being given by  $v = \left( \frac{2E_0 e}{m} \right)^{\frac{1}{2}}$

where  $v$  is the velocity,  $e$  is the electron charge, and  $m$  is the mass of the electron) are turned back to the cathode. All electrons with greater initial velocity pass to the anode. The values of  $x_m$ ,  $E_m$ , and plate current  $I_p$ , may be determined for given cathode temperature, electron emission, electrode spacing, and anode potential from well-known analyses.<sup>14</sup>

From our discussion of the fluctuations in current flowing to a retarding electrode, we must conclude that, if  $E_m$  remains constant, the fluctuations in plate current of the space-charge-limited diode must be

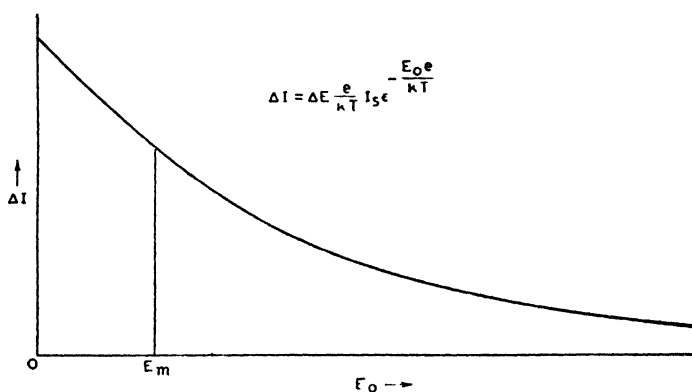


Fig. 3

equal to the true shot-effect value. The study of the effect of space charge on shot effect is then the study of the behavior of the potential minimum with fluctuations in emission.

Qualitative considerations show that  $E_m$  does not remain fixed, however. Its value is determined at any instant by the instantaneous space-charge distribution between cathode and anode. When the number of electrons having velocities of emission in excess of the mean value of  $E_m$  is momentarily in excess of the average, the number of electrons passing across the cathode-anode space increases and, as a result of their space-charge effect,  $E_m$  becomes more negative, thus turning back a certain number of electrons which would otherwise have passed to the anode. When the number of high-velocity electrons is less than the average,  $E_m$  becomes less negative than the mean value and some of the lower-velocity electrons are permitted to pass over to the anode.

To determine the magnitude of the reduced shot effect it is necessary to analyze the quantitative relations between instantaneous velocity distribution and instantaneous value of potential minimum.

Let us consider again the velocity distribution of emitted electrons. Figure 3 shows the current corresponding to the average number of electrons in each velocity group ( $E_o + \Delta E$ ), where velocity of emission  $E_o$  is expressed in volts as before. The total area under the curve (on to infinity) is equal to the total average emission from the cathode. The area under the curve to the right of  $E_m$  (the potential minimum) is equal to the average anode current. The area to the left of  $E_m$  represents the current turned back to the cathode by the potential minimum. This curve represents average conditions, only. From our previously stated principle of fixed division, we know that the current corresponding to *each* velocity group of electrons fluctuates at random. If the velocity increment is made small enough, all electrons in a given

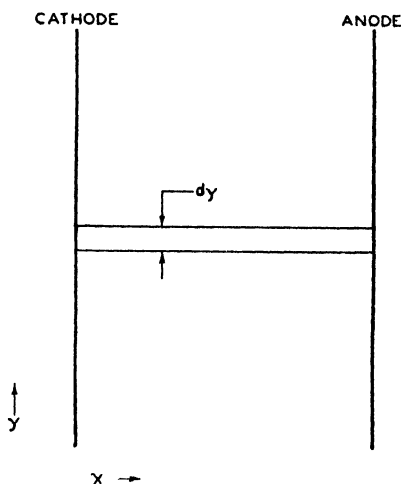


Fig. 4

velocity group have the same space-charge effect on the potential distribution and, hence, on the potential  $E_m$ . Knowing as we do the fluctuations in number of electrons in each group and being able to calculate the effect of each group on the potential  $E_m$ , we are in a position to determine the over-all net fluctuations.

To simplify the physical viewpoint in this analysis, let us consider a vacuum tube in cross-section, Figure 4. We may say that, since the fluctuations in current are small compared to the average current, the fluctuations in  $E_m$  are small compared to the average value of  $E_m$ . We may then apply the principle of superposition. Let us say that the emission is constant outside of the differential strip  $dy$ . Within  $dy$  it fluctuates at random.  $E_m$  is, of course, constant except for infinitesimal changes produced by fluctuations in emission within  $dy$ . An excess number of electrons of any velocity group emitted within  $dy$  will pass

to the anode if their initial velocity  $E_0$  is greater than  $E_m$  or will be returned to the cathode if it is less than  $E_m$ . Whichever course they take, their effect on  $E_m$  (an infinitesimal effect) may be calculated. Suppose a group of electrons having a velocity greater than  $E_m$  be emitted. These electrons pass on to the anode and, on their way, add to the space charge and depress the potential  $E_m$  over a considerable area. This lowering of  $E_m$  turns back some of the lower velocity electrons in the region adjacent to  $dy$ , so that, in effect, there is a compensating current flowing in the opposite direction which reduces the effect of the original group of electrons.

If the velocity of this group of electrons is less than  $E_m$ , none of the electrons reach the anode but  $E_m$  is depressed by the additional space charge, with the result that there is a reduction in anode current.

For each velocity group of electrons in  $dy$  which reaches the anode there is, then, a compensating current in the opposite direction the magnitude of which depends on the velocity of the electrons. The net current pulse due to this group of electrons is the difference between the current flow corresponding to the electrons and the compensating current.

For each velocity group of electrons which fails to reach the anode, there is a negative pulse of anode current, the magnitude of which depends on the velocity of the electrons.

By integrating in the proper way the effect of each velocity group of electrons in  $dy$  on the resulting anode current we may find the net fluctuations produced by the random emission of all the current in  $dy$ . Integrating over the entire cathode area will then give us the total fluctuations in current.

Simple considerations show that it is really unnecessary to integrate over the whole cathode surface, however. The effect of a given velocity group of electrons emitted in one place is the same as that of a similar group distributed over the entire cathode surface, so long as the group is infinitesimal in size. We may, then, for analytical purposes equally well consider the velocity groups distributed over the entire cathode surface. The actual mathematical process to be followed will then be the dividing of the total cathode emission into an infinite number of velocity groups, the multiplying of the mean-square fluctuation current corresponding to each velocity group by a factor indicating the relative effect of electrons of each velocity on the anode current, and the integrating of the product for the entire range of velocities. The result is the total mean-square fluctuation in anode current.

In the above discussion it is implicitly assumed that a fluctuation involving a given velocity group of electrons persists long enough for a new equilibrium to be established. This simplifies the analysis, but renders it inapplicable to frequencies such that the transit time of an electron is comparable with the period—frequencies of several hundred megacycles per second in usual tubes.

The application of the diode analysis to triodes is obvious. We see that the addition of a negative grid between cathode and anode has little effect on the fluctuation current for a given anode current, but chiefly serves to alter the internal anode resistance of the tube.

It has been customary to view reduced shot effect and thermal agitation as identical, or at least closely related. The above discussion had laid the background for an analysis without mention of thermal agitations nor has any mechanism for establishing thermal equilibrium between the electron stream and the cathode been found or assumed. Does this mean that the thermal-agitations viewpoint is considered false?

The answer is yes to the extent that that viewpoint is used as a means of predicting the reduced shot effect without detailed microscopic analysis. Reduced shot effect is essentially shot effect in the presence of space charge and should be approached from the shot-effect and space-charge viewpoints. The thermal-agitations viewpoint is useful only in the interpretation and application of the results.

Part II continues the above analysis and presents an experimental verification of the results.

## C—FLUCTUATIONS IN POSITIVE-GRID TUBES.

### 1. HISTORICAL INTRODUCTION.

Comparatively little attention has been accorded to the question of current fluctuations in screen-grid tubes, it being generally implicitly assumed that, where the cathode current divides between two electrodes such as the screen and the anode, the fluctuations would divide in the same manner. (Here I ignore the question of thermal agitations in the plate resistance, for so far as I know this concept has never been seriously applied to screen-grid tubes.) It was fairly generally recognized, however, that triodes were "quieter" than tetrodes and pentodes, though a very great deal of confusion was introduced by a general failure to take into proper consideration the greater shunting effect of the lower plate resistance of triodes.

About 1933, Mr. Stuart Ballantine very courteously told me of his experimental results which showed greater fluctuations in the anode current of screen-grid tetrodes than in that of triodes. He was able to account for this by the fluctuations in emission of secondary elec-



trons from the screen grid. Measurements which I undertook as a result of this with suppressor-grid pentodes seemed to show that this explanation, while undoubtedly based on an existing phenomenon, was incomplete, since no important difference in fluctuations appeared to exist between tetrodes and pentodes although it was known that the suppressor grid effectively prevented secondary emission.

In 1935, Messrs. S. W. Seeley and W. S. Barden called to the attention of Dr. North and me their ingenious measurements<sup>17</sup> with suppressor-grid pentodes in which a resistance in the cathode circuit (see Figure 5) should "degenerate" practically all cathode-current fluctuations, and, therefore, should eliminate the component of anode-current fluctuations resulting therefrom. Nevertheless, they observed

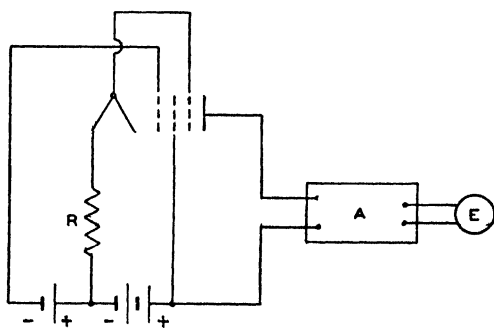


Fig. 5

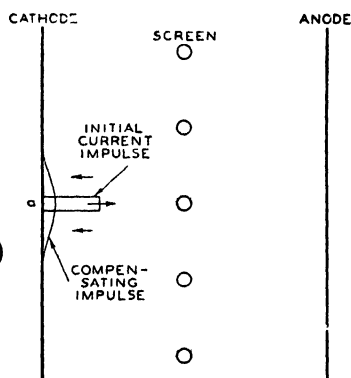


Fig. 6

large fluctuations in the anode current. These could not be accounted for by thermal agitations in the cathode resistor. The conclusion was, therefore, that there was a fluctuation in division of current between screen and anode. That this was so they verified by direct measurement.

On the explanation of the Seeley and Barden effect is based the analysis presented in Part III by North. This analysis was made immediately after the discussion with Messrs. Seeley and Barden. It was presented in brief at the Rochester Fall Meeting of I. R. E. in November, 1936.<sup>9</sup>

In December 1937, Rothe and Engbert<sup>17</sup> published a qualitative theory which explains the fluctuations in division of current between screen and anode as resulting from the chance determination of the destination of the electrons which either strike close to edges of the screen wires or pass on to the anode after narrowly missing the wire. The measurements which they report are in agreement with those reported by us.

## 2. THEORETICAL CONSIDERATIONS

The explanation of the fluctuation in division of the current between screen and anode which was offered (and later developed in detail by Dr. North) is as follows:

Consider a vacuum tube as shown in cross section in Figure 6. Suppose that an excess number of electrons of high velocity is emitted over some short period of time at point (a). These electrons will pass through the region of potential minimum and will pass on to the positive screen-grid wire directly before them (the negative control grid is omitted for simplicity). On their way, they increase the space charge of the space through which they pass to greater than the normal value. This increase in space charge depresses the potential of the potential minimum, thus bringing about a reduction in current below the normal value in the area surrounding the closely confined initial impulse in the manner discussed under (C). This reduction in current is in effect a compensating current flowing in the opposite direction to the initial impulse. The difference between the two currents is the net fluctuation which would exist in a diode.

In the case of the positive-grid tube, however, the initial impulse just considered went entirely to the screen grid. The compensating current, being distributed over a considerable area, divides between screen and anode almost as the average current divides. If the screen-grid current is a small fraction of the anode current, the screen-current fluctuations will be almost uncompensated and it would, therefore, be expected that the magnitude of these fluctuations would be given by the formula for true shot effect. If the net cathode-current fluctuations are small, the plate-current fluctuations must be approximately the same as the screen fluctuations.

Of course, this explanation ignores the effect of the cathode resistor in the Seeley and Barden experiment. The degenerative fluctuation voltage fed back to the grid through the action of this resistor merely makes more certain that the compensating current is distributed over a large cathode area.

Rothe and Engbert<sup>13</sup> have assumed that the arrival of a certain class of electrons at the screen is entirely fortuitous. That is, electrons emitted directly under the edge of the screen wire have the same chance of reaching the screen wire as of reaching the anode. This leads to the conclusion that some fraction of the current in the screen should fluctuate at random.

This last analysis should lead to correct results for extremely minute grid wires, such that the motions of electrons in directions parallel to the cathode as the result of random velocities of emission would be large compared to the grid wire diameter. It appears, how-

ever, that it would be difficult to apply quantitatively in the practical case. The analysis presented by North should give quantitatively correct results in the case of infinitesimal as well as of finite collectors.

In the event that an intermediate collector of current intercepts a large continuous area, the conclusions arrived at by North would be invalid. This is because the fluctuation in distribution of current could occur only at the boundaries of the large area.

#### D—FLUCTUATIONS CAUSED BY COLLISION IONIZATION

No vacuum tube is perfectly evacuated. The residual gas molecules will occasionally be struck by an electron on its way from cathode to anode. If the velocity of the electron is sufficient, the molecule may lose an electron, thus becoming a positive ion. The effect of the positive ion is well known to be that of increasing the electron current which may flow across the space. Inasmuch as the formation of positive ions is a random event, the current produced by them must fluctuate at random, and thus be a source of noise.

The existence of such an effect has long been recognized. Ballantine<sup>16</sup> in 1933 analyzed the effect of a single ion and from that arrived at the nature of the qualitative relationship between ion current and plate-current fluctuations. He found experimentally that this relationship was correct. It was not possible, however, to determine analytically the magnitude of fluctuations to be expected.

In Part IV of this paper, I present an analysis which was carried out in 1933. This treats the flow of positive ions toward the cathode as the movement of a positively charged continuous stream through the negatively charged electron stream, in the same manner as is conventionally done in treatments of electron-space-charge effects. This is a great simplification as compared with Ballantine's analysis of the effects of a single ion. It is justified because it may readily be shown that the average distance between ions is extremely small as compared with electrode spacings, even under conditions most unfavorable to the assumption.

#### E—OTHER SOURCES OF FLUCTUATIONS

We have already considered the fluctuations caused by random emission of electrons from the cathode, by inconstant division of current between positive electrodes, and by varying production of positive ions. There are other sources of fluctuations.

It is well known that positive ions may be emitted from a hot cathode or may be formed at its surface and that these ions cause fluctuations in cathode current.<sup>17</sup> Experimentally, we have detected

the effects of such ions only in special cases. Under normal conditions this source of fluctuations need not be considered.

Flicker effect, wall charges, microphonics, etc., have been mentioned and dismissed from our present consideration.

Secondary emission from the screen grid plays a small part in determining the fluctuations in current of screen-grid tetrodes. The prevailing use of suppressor-grid pentodes makes it unnecessary to concern ourselves with this.

Grid current produced by gas ionization will develop a fluctuation voltage in an impedance in the grid circuit according to the shot-effect formula. With usual values of grid current this fluctuation voltage may be ignored, though it may readily be taken account of if necessary.

The analyses which have been made do not apply at the highest frequencies. Further, at ultra-high frequencies there are other sources of noise. These matters we hope to discuss in another paper.

#### F—CONCLUSION

This introductory part of our paper has, by its nature, been devoid of results. The succeeding parts, of which the next is Part II, Fluctuations in Diodes and Triodes, by D. O. North, will continue the analyses by more rigorous methods and will present the results.

#### REFERENCES

- <sup>1</sup> W. Schottky, "Spontaneous Current Fluctuations In Various Conductors", *Ann. Physik*, 57, pp. 541-567, (1918).
- <sup>2</sup> H. Nyquist, "Thermal Agitation of Electric Charge in Conductors", *Phys. Rev.*, Vol. 32, No. 1, pp. 110-113, July, (1928).
- <sup>3</sup> J. B. Johnson, "Thermal Agitation of Electricity in Conductors", *Phys. Rev.*, Vol. 32, No. 1, pp. 97-109, July, (1928).
- <sup>4</sup> A. W. Hull and N. H. Williams, "Determination of Elementary Charge  $e$  from Measurements of Shot Effect", *Phys. Rev.*, Vol. 25, No. 2, pp. 147-173, February, (1925).
- <sup>5</sup> F. B. Llewellyn, "A Study of Noise in Vacuum Tubes and Attached Circuits", *Proc. I.R.E.*, Vol. 18, No. 2, pp. 243-265, February, (1930).
- <sup>6</sup> G. L. Pearson, "Shot Effect and Thermal Agitation in an Electron Current Limited by Space Charge", *Physics*, Vol. 6, No. 1, pp. 6-9; January, (1935).
- <sup>7</sup> F. C. Williams, "Fluctuation Voltages in Diodes and in Multi-electrode Valves", *Journ. I.E.E.*, Vol. 79, No. 477, pp. 349-360; September, (1936).
- <sup>8</sup> This method of calculating the fluctuations in a triode was suggested by Mr. W. A. Harris in a discussion of a paper at the Rochester Fall Meeting of I.R.E., November, (1935).
- <sup>9</sup> B. J. Thompson and D. O. North, "Shot effect in space-charge-limited vacuum tubes", *Electronics*, Vol. 9, No. 11, p. 31, November, (1936). (Summary)
- B. J. Thompson, *Electronics*, Vol. 10, No. 2, p. 34, February, (1937). (Letter)
- <sup>10</sup> W. Schottky, "Shot Effect and the Virtual Cathode", *Die Telefunkenröhre*, Vol. 8, pp. 175-195, (1936).

<sup>11</sup> W. Schottky, "The Connection Between Corpuscular and Thermal Fluctuations in Electron Tubes"; *Z. Physik*, Vol. 104, pp. 248-274, (1937).

<sup>12</sup> W. Schottky and E. Spenke, "The Space-Charge Reduction of Shot Effect", *Wissenschaftliche Veröffentlichungen aus den Siemens-Werken*, Vol. 16, No. 2, pp. 1-41; July, (1937).

<sup>13</sup> H. Rothe and W. Engbert, "The Fluctuation Noise of Amplifier Tubes in the Range between 150 and 15,000 Kilocycles per second", *Die Telefunken-Röhre*, No. 11, pp. 183-212, December, (1937).

<sup>14</sup> I. Langmuir and K. T. Compton, "Electrical Discharges in Gases; Part II"; *Reviews of Modern Physics*, Vol. 3, No. 2, pp. 241-245, April, (1931).

<sup>15</sup> S. W. Seeley and W. S. Barden, a paper presented at the Rochester Fall Meeting of I.R.E., November, (1935).

<sup>16</sup> S. Ballantine, "Fluctuation Noise Due to Collision Ionization in Electronic Amplifier Tubes", *Physics*, Vol. 4, No. 9, pp. 294-306; September, (1933).

<sup>17</sup> J. S. Donal, Jr., "Abnormal Shot-Effect of Ions of Tungstous and Tungstic Oxide", *Phys. Rev.*, Vol. 36, pp. 1172-1189, October 1st, (1930).

## PART II—DIODES AND NEGATIVE-GRID TRIODES

BY DWIGHT O. NORTH

*Summary*—A quantitative theory of shot effect in the parallel-plane diode is formulated for any degree of space charge, and for frequencies such that transit-time effects are of no concern. Beginning with the steady-state description of a diode showing a Maxwell-Boltzmann distribution of emission velocities, the theory is founded upon a determination of the new steady state which results from the injection of a small additional emission comprised of electrons of a specified velocity.

The fluctuations in a diode current  $I$  are expressed by

$$\overline{i^2} = I^2 \cdot 2eI\Delta f.$$

For a temperature-limited diode it has long been known that  $\Gamma^2 = 1$ . For a diode with anode potential sufficiently negative (retarding field),  $\Gamma^2 = 1$  also. For the usual space-charged-limited case, i.e., any instance in which there is a virtual cathode,  $\Gamma^2$  is less than unity, but in this paper  $\Gamma^2$  is computed by numerical integration for only those instances in which the anode current is a small fraction of the emission.

In this last case the shot-effect formula is also written, phenomenologically, to correspond with Nyquist's well-known expression for thermal agitation in a passive network of conductance  $g$ , thus:

$$\overline{i^2} = \theta \cdot 4kTg\Delta f.$$

Here  $T$  is absolute cathode temperature and  $g$  is diode conductance. The

dimensionless factor  $\theta$  is found to be virtually a constant  $\left( \theta \approx \frac{2}{3} \right)$

for the whole range of normal anode potentials with asymptotic value,

$$\theta \sim 3 \left( 1 - \frac{\pi}{4} \right)$$

in the limit of high anode potential. That is, the mean-square noise generated by emission fluctuations is roughly numerically equal to two-thirds of the noise of thermal agitation generated by a resistance of magnitude equal to the a-c resistance of the diode and possessing a temperature equal to the cathode temperature.

The theory is extended to cover shot effect in the anode circuit of a triode with negative grid. Unless the amplification factor  $\mu$  is very low, the same formulas apply, except that  $g$  is now interpreted as the con-

ductance of the "equivalent diode". Following recent practice, the anode-circuit shot effect is expressed in terms of an ohmic resistance  $R_{||}$  at room temperature  $T_0$  in the grid circuit, the thermal agitation of which produces an equal fluctuation in the anode circuit, thus:

$$R_{||} = \frac{\theta}{\sigma} \cdot \frac{T}{T_0} \cdot \frac{1}{g_m},$$

where  $g_m$  is the transconductance and  $\sigma = \frac{g_m}{g}$ . For modern tubes,  $\sigma$  lies between 0.5 and unity.

The diode in thermal equilibrium (diode of any geometry, all at one temperature, no source of energy) is analyzed to show that the fluctuations can be quantitatively reckoned as either shot effect or thermal agitation with the same numerical results. It is argued that here only can these distinct concepts be merged into one.

Diode measurements show noise consistently higher than the theoretical predictions, the factor of disagreement amounting to an order of magnitude at high currents. This is qualitatively accounted for in a satisfactory manner in terms of a small amount of elastic reflection of electrons at the anode, an hypothesis supported by published experimental work.

Negative-grid triodes are usually not subject to such complications; this is evidenced by good agreement between the triode formulas and measurements of a variety of modern tubes, including not only the usual quasi-cylindrical structures, but even one flat structure with a V-type filament. The theory is, therefore, believed to be extensively valuable as a guide to low-noise amplifier design.

## THEORY

### INTRODUCTION AND REVIEW OF STEADY STATE

IN PART I it was shown that an adequate analysis of space-charge-reduced shot effect must recognize that the reduction associated with fluctuations in emission of electrons having a specified emission velocity is, *inter alia*, a function of that velocity. This investigation will, therefore, be confined initially to ascertaining the net fluctuations in current which occur as a consequence of true shot fluctuations in the emission of electrons of a *specified velocity*. The total reduced shot effect, measurable in a suitably connected circuit, will then be established by summing over the whole gamut of initial velocities.

It can be seen immediately that the character of the results will be determined largely by the Maxwell-Boltzmann (M-B) laws of distribution. At the same time it becomes apparent that the theory will have to be founded upon a *steady-state* description which embodies these laws. As often happens, the processes of analysis are impeded least by confining ourselves to a parallel-plane model, for the desired

description of the steady state is well known.<sup>1,2,3,4</sup> Whether or not the results obtained can be applied to other types of structure is a question relegated to subsequent experimental studies. The treatment and notation of Fry and of Langmuir will be employed here inasmuch as these references are likely to be most accessible. To conserve space and to avoid unreasonable repetition of these published works, it will be assumed henceforth that the reader is acquainted with the general nature of these papers, particularly the work of Fry.

The steady-state potential within a space-charge-limited parallel-plane diode, the cathode of which produces an unlimited supply of electrons with zero emission velocity, is represented by the well-known expression,

$$E = \left( 9\pi \sqrt{\frac{m}{2e}} \right)^{2/3} x^{4/3}, \quad (1)$$

in which  $E$  is the potential at a distance  $x$  from the cathode,  $I$  is the cathode current per unit area,  $m$  is the mass of an electron, and  $e$  its charge (throughout, this symbol implies a positive quantity). The potential of such a hypothetical case is illustrated by curve  $A$  of Figure 1.

In actuality there is a finite emission current  $I_s$  per unit area possessing a M-B distribution described by the usual exponential law. If we let  $v_s$  be the normal component of an electron's initial velocity, and if we define two useful equivalent potentials, thus:

$$\frac{1}{2} m v_s^2 = e V_s, \quad \frac{kT}{e} = V_c, \quad (2)$$

one aspect of the M-B distribution can be written

$$dI_s = \frac{I_s}{V_c} e^{-\frac{V_s}{V_c}} dV_s. \quad (3)$$

In (2),  $k$  is Boltzmann's constant ( $= 1.37 \times 10^{-16}$  ergs/°K), and  $T$  is the absolute cathode temperature. Equation (3) defines the portion

<sup>1</sup> P. S. Epstein, "Theory of Space-Charge Effects," *Verh. d. Deut. Phys. Gesell.*, Vol. 21, p. 85, (1919).

<sup>2</sup> T. C. Fry, "The Thermionic Current Between Parallel Plane Electrodes: Velocities of Emission Distributed According to Maxwell's Law," *Phys. Rev.*, Vol. 17, p. 441, (1921).

<sup>3</sup> I. Langmuir, "The Effect of Space Charge and Initial Velocities on the Potential Distribution and Thermionic Current Between Parallel Plane Electrodes," *Phys. Rev.* Vol. 21, p. 419, (1923).

<sup>4</sup> I. Langmuir and K. T. Compton, "Electrical Discharges in Gases," *Rev. Mod. Phys.*, Vol. 3, p. 191, (1931).



$dI_e$ , of the total emission current  $I_e$ , composed of electrons whose initial normal velocities, expressed in terms of the equivalent potential  $V_e$ , lie within the narrow limits  $V_e$  and  $V_e + dV_e$ . The actual potential function, therefore, has the appearance of curve *B*, the potential minimum  $E_m$  adjacent to the cathode serving as a gate which permits electrons of higher velocity to proceed to the plate. These constitute the cathode (or anode) current  $I$ . The rest of  $I_e$ , consisting of electrons whose emission velocities are such that  $\frac{1}{2} m v_e^2 < |e E_m|$ , is returned

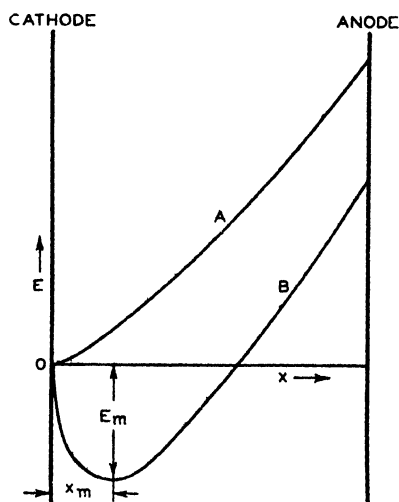


Fig. 1—Potential functions in a space-charged-limited diode.

to the cathode without having crossed the potential minimum or “virtual” cathode.

The potential function in this case is best described by replacing  $E$  and  $x$  by quantities  $\eta$  and  $\xi$ , respectively, having the following definitions

$$\eta = \frac{E - E_m}{V_e} \quad (4a)$$

$$\xi = 4 \left( \frac{\pi}{2kT} \right)^{3/4} m^{1/4} e^{1/2} I^{1/2} (x - x_m). \quad (4b)$$

It should be noted that the origin of coordinates is thereby shifted to the potential minimum. In the  $\alpha$ -space, to the left of the virtual cathode,  $\xi$  is negative; in the  $\beta$ -space, to the right of the virtual cathode,  $\xi$  is positive; while  $\eta$  is positive in both spaces. The steady-

state potential distribution then appears, in Fry's notation, as the solution of the cryptic differential equation,

$$\left( \frac{d\eta}{d\xi} \right)^2 = \phi(\eta), \quad (5)$$

$\phi(\eta)$  being shorthand for either of two expressions,

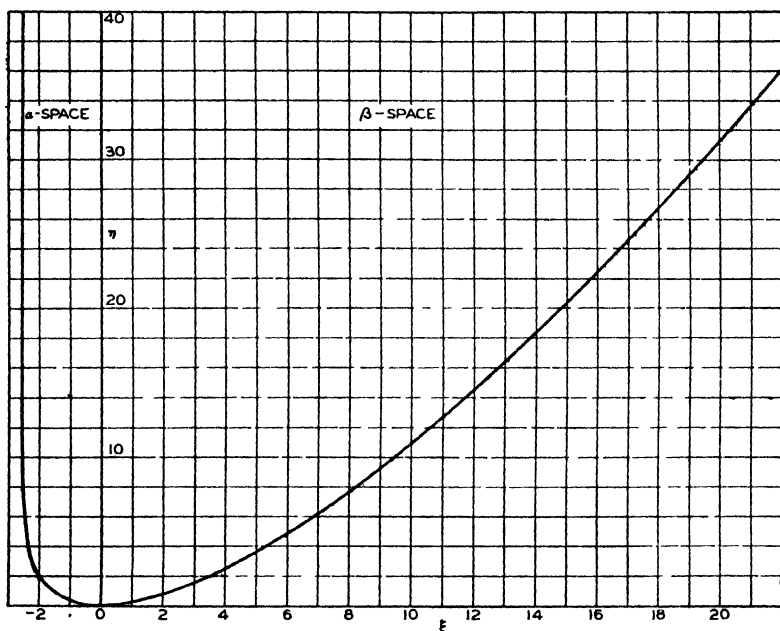


Fig. 2—Solutions of the differential equation:  $\left( \frac{d\eta}{d\xi} \right)^2 = \phi(\eta)$ .

$$\phi(\eta) = \epsilon\eta - 1 \mp \left( \frac{2}{\sqrt{\pi}} \eta^{1/2} - \epsilon\eta \operatorname{erf} \eta^{1/2} \right). \quad (6)$$

The upper sign is used for the  $\alpha$ -space, the lower sign for the  $\beta$ -space, and the error function is defined:

$$\operatorname{erf} y = \frac{2}{\sqrt{\pi}} \int_0^y e^{-x^2} dx \quad (7)$$

The solution of this equation has already been effected by mechanical means, with the assistance of series approximations. It is plotted in Figure 2 which, in terms of  $\eta$  and  $\xi$ , embodies all plots of  $E$  against  $x$ , such as curve  $B$ , Figure 1. The solution is tabulated in Table I,

taken intact from Langmuir's paper.<sup>1</sup> In Table II there are listed the values of  $\phi_\alpha$  for values of  $\eta < 10$ , and of  $\phi_\beta$  for values of  $\eta < 100$ . These were calculated directly from (6) with the help of tables of the error function, except for values of  $\phi_\beta$  for  $\eta > 1$  which were computed from the asymptotic series. The series expansions are very valuable in checking the tables, and, in addition, give much information as to the behavior of the functions.

TABLE I

$\eta$	$-\xi_\alpha$	$\xi_\beta$	$\eta$	$-\xi_\alpha$	$\xi_\beta$	$\eta$	$-\xi_\alpha$	$\xi_\beta$
0.00	0.0000	0.0000	3.0	2.2338	4.4750	20	2.5538	14.8260
0.05	0.4281	0.4657	3.2	2.2650	4.6524	25	2.5539	17.1931
0.10	0.5941	0.6693	3.4	2.2930	4.8261	30		19.4253
0.15	0.7167	0.8296	3.6	2.3183	4.9963	35		21.5522
0.20	0.8170	0.9674	3.8	2.3410	5.1634	40		23.5939
0.25	0.9028	1.0909	4.0	2.3615	5.3274	45		25.5643
0.30	0.9785	1.2042	4.5	2.4044	5.7259	50		27.4740
0.35	1.0464	1.3098	5.0	2.4376	6.1098	60		31.141
0.40	1.1081	1.4092	5.5	2.4634	6.4811	70		34.642
0.45	1.1648	1.5035	6.0	2.4834	6.8416	80		38.007
0.50	1.2173	1.5936	6.5	2.4990	7.1924	90		41.258
0.6	1.3120	1.7636	7.0	2.5112	7.5345	100		44.412
0.7	1.3956	1.9224	7.5	2.5206	7.8690	150		59.086
0.8	1.4704	2.0725	8.0	2.5280	8.1963	200		72.479
0.9	1.5380	2.2154	9.0	2.5382	8.8323	300		96.877
1.0	1.5996	2.3522	10	2.5444	9.4465	400		119.185
1.1	1.6561	2.4839	11	2.5481	10.0417	500		140.068
1.2	1.7081	2.6110	12	2.5504	10.6204	600		159.885
1.4	1.8009	2.8539	13	2.5518	11.1845	700		178.861
1.6	1.8813	3.0842	14	2.5526	11.7355	800		197.146
1.8	1.9515	3.3040	15	2.5531	12.2747	900		214.850
2.0	2.0134	3.5151	16	2.5534	12.8032	1000	2.5539	232.054
2.2	2.0681	3.7187	18	2.5537	13.8313			
2.4	2.1168	3.9158						
2.6	2.1602	4.1071						
2.8	2.1990	4.2934						

When  $\eta \ll 1$ ,

$$\phi_\beta^\alpha(\eta) = \left[ \eta + \frac{1}{2} \eta^2 + \frac{1}{6} \eta^3 + \dots \right] \pm \frac{2}{\sqrt{\pi}} \eta^{1/2} \left[ \frac{2}{3} \eta + \frac{4}{15} \eta^2 + \dots \right]$$

When  $\eta \gg 1$ ,

$$\left. \begin{aligned} \phi_\alpha(\eta) &\sim 2e^\eta - \frac{2}{\sqrt{\pi}} \eta^{1/2} - 1 - \frac{1}{\sqrt{\pi} \eta^{1/2}} \left[ 1 - \frac{1}{2\eta} + \frac{3}{4\eta^2} - \frac{15}{8\eta^3} + \dots \right] \\ \phi_\beta(\eta) &\sim \frac{2}{\sqrt{\pi}} \eta^{1/2} \left[ 1 + \frac{1}{2\eta} - \frac{1}{4\eta^2} + \frac{3}{8\eta^3} - \frac{15}{16\eta^4} + \dots \right] - 1 \end{aligned} \right\} (3)$$

<sup>1</sup> Langmuir, loc. cit.

TABLE II

$\eta$	$\phi_a(\eta)$	$\phi_\beta(\eta)$	$\eta$	$\phi_\beta(\eta)$
0.00	0.0000	0.0000	10	2.75
0.01	0.0109	0.0093	15	3.51
0.02	0.0224	0.0180	20	4.17
0.03	0.0345	0.0265	25	4.75
0.04	0.0469	0.0347	30	5.29
0.05	0.0599	0.0427	35	5.77
0.06	0.0731	0.0505	40	6.23
0.07	0.0867	0.0583	45	6.65
0.08	0.1009	0.0657	50	7.06
0.09	0.1153	0.0731	60	7.81
0.1	0.1300	0.0804	70	8.51
0.2	0.2944	0.1484	80	9.15
0.3	0.4897	0.2101	90	9.77
0.4	0.7164	0.2672	100	10.32
0.5	0.9764	0.3210		
0.6	1.2722	0.3720		
0.7	1.6068	0.4208		
0.8	1.9836	0.4674		
0.9	2.4067	0.5125		
1.	2.8806	0.5560		
2.	11.846	0.932		
3.	36.94	1.23		
4.	105.68	1.50		
5.	293.1	1.77		
6.	802.8	1.99		
7.	2,190	2.20		
8.	5,960	2.39		
9.	16,200	2.57		

It will be convenient to use Subscripts 1 and 2 to denote values of quantities such as  $\xi$  or  $\eta$  at the cathode and anode, respectively. This brief description of the steady state is then completed by observing that

$$I/I_s = \varepsilon^{-\eta_1}. \quad (9)$$

When  $I$ ,  $I_s$  and  $T$  are specified, the operating voltage ( $E_2 - E_1$ ) can be found<sup>1</sup> by first evaluating  $\eta_1$  from (9). The value of  $\xi_1$  is then located in Table I. Knowledge of the distance ( $x_2 - x_1$ ) between electrodes permits  $\xi_2$  to be derived from (4b). The value of  $\eta_2$  is then located in Table I, and the desired ( $E_2 - E_1$ ) from (4a). The process of finding  $I$ , when the operating potential is specified, follows the same tactics; various values of  $I$  are assumed and the corresponding potentials determined; the  $I$  which corresponds to the specified ( $E_2 - E_1$ ) is then located by interpolation or read from a current-voltage plot.

<sup>1</sup> Langmuir and Compton, loc. cit.

## ANALYSIS OF SHOT FLUCTUATIONS

Upon this steady-state foundation the succeeding analysis of fluctuations will be constructed. Inasmuch as all of the work entails numerical integration, one very important simplifying assumption will be made. It will be supposed that

$$I/I_s \rightarrow 0. \quad (10)$$

In effect, this means that  $\xi_1$  will always be assigned the asymptotic value,  $-2.554$ , which is suggested by Figure 2 and tabulated in Table I. Although this may at first appear to be a most severe limitation, it is not, in fact. For example, reference to Table I shows that  $\xi_1$  is only 16% below its asymptotic value when  $\eta_1 = 3.0$ , which is to say, in view of (9), when  $I/I_s = \epsilon^{-3} \sim 1/20$ . One may expect to run across disagreement between theory and measurement on this account in case thoriated or pure-tungsten emitters are used. But, ordinarily, oxide-coated cathodes produce enough emission to place  $I/I_s$  far below the figure cited, so that, in such applications, the assignment of discrepancies to this limitation of theory will not be just. Nevertheless one should not lose sight of the assumption, for it is tantamount to what might be termed "complete space-charge limitation", and the final expressions to be evolved are valid only in this domain. If, for instance, the noise is measured while the cathode temperature (emission) is slowly dropped, one should expect the measured shot effect to depart eventually from the theoretical value given in this paper, and to move to higher levels through an uncharted region, finally arriving at a magnitude prescribed by Schottky's original formula for true temperature-limited shot effect simultaneously with the disappearance of the last vestige of a virtual cathode. The transition region is left unanalyzed in this paper, not because it is not understood, but simply because it requires much crank turning, yet promises little of practical interest.

The only further limitation of note is the confinement of discussion to frequencies low compared with the reciprocal of the electron transit time. Although there is every need for an understanding of shot fluctuations at ultra-high frequencies, it comes not on the wings of the morning, but only through a comprehension of the phenomena at frequencies unmolested by transit angles. This particular limitation simplifies the treatment tremendously. For, as pointed out in Part I, we shall consequently be concerned with fluctuations of a duration great enough that the analysis need only search for the description of the new *equilibrium state* into which the diode settles when, in addition to its original emission  $I_s$ , one admits a *small steady incre-*

ment  $i_s(v_s)$  possessing a specified normal emission velocity  $v_s$ . Despite the fact that fluctuations in emission really do occur at random over the surface of the cathode, so that, to be exact, every emerging electron should be regarded as a "noise" electron, we shall nevertheless suppose  $i_s$  to be spread uniformly over the cathode area, even as  $I_s$  itself. That no precision is sacrificed through use of this artifice was proven in Part I, where the question was discussed in detail.

Hereafter, for brevity, we shall suppose the cathode potential to be zero ( $E_1 = 0$ ). As before, we shall replace  $v_s$  by an equivalent potential  $V_s$  defined in the manner of (2),

$$\frac{1}{2} m v_s^2 = e V_s. \quad (11)$$

Let us further define a dimensionless quantity,

$$\lambda = \frac{V_s + E_m}{V_c}, \quad (12)$$

it being understood that  $E_m$  is negative. This quantity can be used in place of  $v_s$  to designate the emission velocity of electrons comprising  $i_s$ . If  $v_s$  be chosen so that  $i_s$  crosses the potential minimum to strike the anode ( $V_s > -E_m$ ),  $\lambda$  is positive. For smaller choice of  $v_s$  such that the electrons proceed only part way to the potential minimum, stop, and return to the cathode,  $\lambda$  is negative; in fact,  $-\eta_1 \leq \lambda \leq 0$ , the lower limit corresponding to  $v_s = 0$ . In the  $\eta, \xi$  diagram, Figure 2, the turning point for these electrons will, of course, be a function of  $\lambda$  and will be that point for which  $\eta = -\lambda$ .

We are now prepared to construct a—for the moment—purely formal expression for the space-charge-reduced shot current fluctuations in the anode circuit. For every  $i_s(\lambda)$  we shall find the new equilibrium current  $I$  (identified with a fixed emission  $I_s$ , and therefore *not* including  $i_s(\lambda)$  itself) which flows in the presence of  $i_s(\lambda)$ . This permits a determination of the net increase in anode current over the steady-state  $I$  which flows in the absence of  $i_s(\lambda)$ . Both  $I$  and  $I$  are to be evaluated under the assumption that the electrode spacing and operating voltage are held fixed.\* The ratio of this net increase in anode current to the quantity  $i_s(\lambda)$  will, for small  $i_s$ , be a function of  $\lambda$  and not  $i_s$ . It will be denoted by  $\gamma(\lambda)$  and is of value

---

\* In Part I it was shown that the basic quantity to be determined is the fluctuation current. The voltage it produces across a connected circuit is only a simple problem in algebra involving both the external circuit and the internal impedance of the tube. Fluctuations of the latter, although certainly present, being initiated by fluctuations in space charge, represent a negligible contribution to the fluctuation voltage and will not be further discussed.

in that it represents the linear reduction factor by which a change in emission is converted into a change in plate current. Now confining our attention to the emission current  $dI_e$  composed of electrons whose normal emission velocities lie between  $\lambda$  and  $\lambda + d\lambda$ , we find from (3), (9), and (12) that its magnitude is

$$dI_e = I \epsilon^{-\lambda} d\lambda \quad (13)$$

This differential-sized emission current exhibits true shot fluctuations, expressible by the following well-known formula for the mean-square fluctuation current  $\overline{i^2}$  in a band width  $\Delta f$ :

$$d(\overline{i^2})_e = 2e(dI_e)\Delta f, \quad (14)$$

or, in terms of (13)

$$d(\overline{i^2})_e = 2eI\Delta f(\epsilon^{-\lambda} d\lambda). \quad (15)$$

But every variation in emission is, as we have said, *linearly* reduced at the anode by the factor  $\gamma(\lambda)$ . The resulting fluctuations in anode current to be associated with electrons of this velocity class are, therefore,

$$d(\overline{i^2}) = 2eI\Delta f [\gamma^2(\lambda) \epsilon^{-\lambda} d\lambda]. \quad (16)$$

Since the fluctuations in emission of one velocity class are presumably independent of fluctuations in all other classes, the total fluctuation current in the anode circuit is the integral of (16) over  $\lambda$ :

$$\overline{i^2} = 2eI\Delta f \int_{-\eta_1}^{\infty} \gamma^2(\lambda) \epsilon^{-\lambda} d\lambda. \quad (17)$$

The quantity  $2eI\Delta f$  is recognized as the true shot effect to be expected from a temperature-limited current  $I$ . The mean-square fluctuations in the present space-charge-limited current  $I$  are, therefore, reduced below the true shot effect by the factor,

$$\Gamma^2 = \int_{-\eta_1}^{\infty} \gamma^2(\lambda) \epsilon^{-\lambda} d\lambda. \quad (18)$$

This is the quantity of principal interest. The evaluation of the integral will be treated in two sections, thus:

$$\left. \begin{aligned} \Gamma^2 &= \Gamma_a^2 + \Gamma_b^2 \\ \Gamma_a^2 &= \int_{-\eta_1}^0 \gamma^2(\lambda) \epsilon^{-\lambda} d\lambda, \quad \Gamma_b^2 = \int_0^{\infty} \gamma^2(\lambda) \epsilon^{-\lambda} d\lambda. \end{aligned} \right\} \quad (19)$$

The subscripts  $\alpha$  and  $\beta$  are appropriately used to signify the reduction factors associated with the two main groups of electrons, those whose emission velocities are insufficient to take them across the virtual cathode and out of the  $\alpha$ -space, and those whose velocities permit them to enter the  $\beta$ -space and thus proceed to the anode. It should be observed that there is an intrinsic distinction to be made here, namely, fluctuations  $i_s(\lambda > 0)$  contribute *directly* to the anode current, whereas fluctuations  $i_s(\lambda < 0)$  do not.

More precisely,

$$\left. \begin{aligned} \gamma(\lambda) &= \frac{I - I}{i_s(\lambda)}, \quad -\eta_1 \leq \lambda \leq 0, \quad \alpha\text{-group}, \\ \gamma(\lambda) &= 1 + \frac{I - I}{i_s(\lambda)}, \quad 0 \leq \lambda \leq \infty, \quad \beta\text{-group}. \end{aligned} \right\} \quad (20)$$

Inasmuch as the great majority of  $\alpha$ -group electrons are returned before coming very near to the potential minimum, we should expect to find  $\Gamma_\alpha^2 \ll \Gamma_\beta^2$ . This will be borne out in the succeeding analysis. Furthermore, for either group, one should expect  $\lim_{\lambda \rightarrow 0} \gamma(\lambda) = -\infty$ ,

since an electron which comes permanently to rest\* in the virtual cathode produces a permanent decrease in plate current. And yet, for the  $\beta$ -group,  $\lim_{\lambda \rightarrow \infty} \gamma(\lambda) = 1$ , since the influence of an electron in transit

must be a monotonic decreasing function of its transit time. It follows that there must be a certain  $\lambda > 0$  such that  $\gamma(\lambda) = 0$ . One should reasonably expect this  $\lambda$  to correspond to a velocity at the virtual cathode *roughly* equal to the mean velocity of the M-B current  $I$  at the same point. In other words, one should predict  $\gamma(\lambda) = 0$ , for  $\lambda \sim \pi/4$ . This also will be verified.

#### EVALUATION OF $\Gamma_\beta^2$

When, in addition to the M-B emission  $I_s$ , a current  $i_s(\lambda > 0)$  is produced at the cathode, the anode current  $I$  which is derived from  $I_s$  can be represented as the solution of

$$\left( \frac{d\eta}{d\xi} \right)^2 = \frac{i_s}{I} \cdot \frac{2}{\sqrt{\pi}} \left[ \sqrt{\eta + \lambda} - \sqrt{\lambda} \right] + \phi(\eta) \quad (21)$$

---

\* The nature of the potential function in the vicinity of the virtual cathode, (8), permits this view, for it shows that an electron just able to reach the potential minimum requires an infinite transit time.



or

$$\left(\frac{d\eta}{d\xi}\right)^2 = \frac{i_s}{I} F(\eta, \lambda) + \phi(\eta) \quad (22)$$

where

$$F(\eta, \lambda) = \frac{2}{\sqrt{\pi}} \left[ \sqrt{\eta + \lambda} - \sqrt{\lambda} \right]. \quad (23)$$

This expression is valid in both the  $\alpha$ - and  $\beta$ -spaces, with the understanding that the appropriate form of  $\phi(\eta)$  be employed in each case, cf. (6). The construction of (21) will not be entered into; the reader will find it simple enough if he avails himself of the methods employed by Fry in developing the basic equation (5). That (21) is correct can be *inferred* from the following useful identity:

$$\int_0^\infty F(\eta, \lambda) e^{-\lambda} d\lambda = \phi_\beta(\eta). \quad (24)$$

This means, naturally, that if, instead of confining  $i_s$  to a specified velocity  $\lambda$ , we distribute its velocities so that at the virtual cathode  $i_s$  has the same velocity distribution as  $I$ , (21) reduces to the same form as (5) in the  $\beta$ -space, which not only is absolutely necessary, but should be sufficiently convincing that (21) is properly constructed.

Now, since we always assume  $i_s \ll I$ , and  $I$ , we shall continually neglect all but the lowest power of  $i_s/I$  or  $i_s/I$ . The differential equation can, therefore, be written

$$d\xi = \pm \left[ 1 - \frac{1}{2} \frac{i_s}{I} \frac{F(\eta, \lambda)}{\phi(\eta)} \right] \frac{d\eta}{\phi(\eta)^{1/2}}, \quad (25)$$

where the proper sign is to be used for each space.

For the  $\beta$ -space:—

Integrate (25),  $0 < \xi < \hat{\xi}_2$ ,  $0 < \eta < \hat{\eta}_2$ .

$$\hat{\xi}_2 = \int_0^{\hat{\eta}_2} \frac{d\eta}{\phi_\beta(\eta)^{1/2}} - \frac{1}{2} \frac{i_s}{I} \int_0^{\hat{\eta}_2} \frac{F(\eta, \lambda)}{\phi_\beta(\eta)^{3/2}} d\eta. \quad (26)$$

Solution of the unperturbed problem, (5), gives

$$\xi_2 = \int_0^{\eta_2} \frac{d\eta}{\phi_\beta(\eta)^{1/2}}. \quad (26a)$$

The differences  $(\hat{\eta} - \eta)$  and  $(\hat{\xi} - \xi)$  evaluated at end points are also to be looked upon as first-order infinitesimals. The difference between (26) and (26a) is, therefore,

$$\hat{\xi}_2 - \xi_2 = \frac{\hat{\eta}_2 - \eta_2}{\phi_\beta(\eta_2)^{1/2}} - \frac{1}{2} \frac{i_s}{I} \int_0^{\eta_2} \frac{F(\eta, \lambda)}{\phi_\beta(\eta)^{3/2}} d\eta \quad (27)$$

For the  $\alpha$ -space:—

A similar treatment shows

$$\hat{\xi}_1 - \xi_1 = -\frac{\hat{\eta}_1 - \eta_1}{\phi_\alpha(\eta_1)^{1/2}} + \frac{1}{2} \frac{i_s}{I} \int_0^{\eta_1} \frac{F(\eta, \lambda)}{\phi_\alpha(\eta)^{1/2}} d\eta \quad (28)$$

We shall set up the difference between (27) and (28). First, however, we define

$$D \equiv \frac{1}{2} (\xi_2 - \xi_1) + \phi_\beta(\eta_2)^{-1/2} + \phi_\alpha(\eta_1)^{-1/2} \quad (29)$$

Then observe that, for small variations, and with the aforementioned stipulation that the operating potential is invariant, there follows from the definitions. (4a) and (4b) .

$$\left. \begin{aligned} \hat{\eta}_2 - \eta_2 = \hat{\eta}_1 - \eta_1 = \frac{E_m - \hat{E}_m}{V_e} = \log \frac{I}{I} = -\frac{I - I}{I} \\ (\hat{\xi}_2 - \hat{\xi}_1) - (\xi_2 - \xi_1) = (\xi_2 - \xi_1) \left( \sqrt{\frac{I}{I}} - 1 \right) = \frac{1}{2} (\xi_2 - \xi_1) \frac{I - I}{I} \end{aligned} \right\} \quad (30)$$

When (29) and (30) are used in taking the difference of (27) and (28), rearrangement of terms shows

$$\frac{I - I}{i_s} = -\frac{1}{2D} \left[ \int_0^{\eta_1} \frac{F(\eta, \lambda)}{\phi_\alpha(\eta)^{3/2}} d\eta + \int_0^{\eta_2} \frac{F(\eta, \lambda)}{\phi_\beta(\eta)^{3/2}} d\eta \right].$$

The negative sign confirms the view that every transit of an electron of this group effects a momentary drop in the  $M$ - $B$  space current. With regard to (20), we have finally:

$$\gamma_{\lambda > 0}(\lambda) = 1 - \frac{1}{2D} \left[ \int_0^{\eta_1} \frac{F(\eta, \lambda)}{\phi_\alpha(\eta)^{3/2}} d\eta + \int_0^{\eta_2} \frac{F(\eta, \lambda)}{\phi_\beta(\eta)^{3/2}} d\eta \right]. \quad (31)$$

From this point evaluation of  $\gamma(\lambda)$  proceeds, perforce, numerically. And there is now introduced, for simplicity, the previously discussed assumption that the emission  $I_v$  is copious enough to warrant postulating

$$I/I_s = 0,$$

which reduces in (31) to the equivalent statements,

$$\eta_1 = \infty, \quad \xi_1 = -2.554, \quad \phi_\alpha(\eta_1) = \infty,$$

so that

$$D = \frac{1}{2}(\xi_2 + 2.554) + \phi_\beta(\eta_2)^{-1/2}, \quad (32)$$

a function of  $\eta_2$  alone. Likewise  $\gamma(\lambda)$  itself reduces to a function of  $\eta_2$  and  $\lambda$  alone.

The numerical work was carried out with the help of a computing machine and Tables I and II, together with auxiliary tables constructed from these, e.g.,  $\phi_\alpha(\eta)^{3/2}$  and  $\phi_\beta(\eta)^{3/2}$ . The details are for the most part uninteresting and will be described only in brief. After a value of  $\lambda$  was chosen,  $\gamma(\lambda)$  was found from (31) for a series of values of  $\eta_2$ ,  $5 \leq \eta_2 \leq 100$ , by trapezoidal integration. This computation was repeated for a large number of selected  $\lambda$ 's,  $0.05 \leq \lambda \leq 5$ . Both of the integrands in (31) become infinite at the origin; hence, in the range  $0 \leq \eta \leq 0.01$ , these integrals were evaluated directly, using the series expansions (8). The outcome is a numerical representation of  $\gamma$  as a function of two parameters,  $\eta_2$  and  $\lambda$ , in the domain:

$$5 \leq \eta_2 \leq 100$$

$$0.05 \leq \lambda \leq 5.$$

The representation cannot be carried to  $\lambda = 0$ , for  $\gamma$  exhibits a logarithmic discontinuity at this point. It could have been carried to zero for  $\eta_2$ , but there is little point in it for when  $\eta_2 = 0$ , the virtual cathode has moved over to the anode and there is no "gate" action—hence no reduction in shot effect—so that we know *a priori* that  $\Gamma^2 = \Gamma_\beta^2 = 1$ . More will be said of this situation later. The range of  $\eta_2$  was limited to values thought to be of practical interest. For example,  $V_g$  is about

0.1 volt for oxide-type cathodes, whereas the operating potential is typified by 3 volts, in which event  $\eta_2$  is approximately 30.

This stage of the calculations, being intermediate, merits only momentary attention to the nature of the function  $\gamma$ . In Figure 3, curve B shows  $\gamma(\lambda)$  when  $\eta_2 = 30$ . The unbroken line contains the calculated values; the dashed line shows the logical extrapolation in both directions. As predicted, the point for which  $\gamma = 0$  lies near  $\pi/4$ . Plots of  $\gamma$  for other choices of  $\eta_2$  show precisely the same qualitative character and need not be exhibited. It is now patent from Figure 3

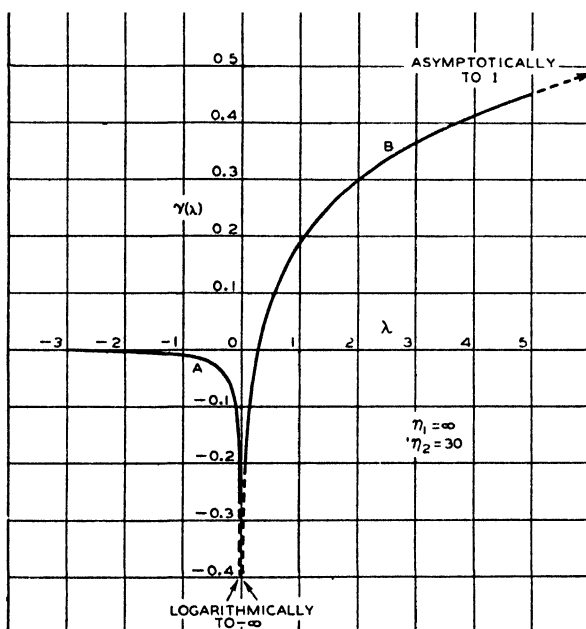


Fig. 3—Shot-effect reduction factor  $\gamma$  as a function of  $\lambda$  (velocity) for A—the  $\alpha$ -group of electrons which fail to reach the virtual cathode. B—the  $\beta$ -group of electrons which traverse the virtual cathode.

that the reduction factor varies so widely with the emission velocity of the electrons that it is absolutely necessary to investigate each velocity class separately. The point is emphasized by the offensive behavior of fluctuations associated with electrons barely able to cross the virtual cathode ( $\lambda$  slightly  $> 0$ ), these fluctuations proving to be so over-compensated ( $\gamma < -1$ ,  $\gamma^2 > 1$ ) that their *net fluctuations are in excess of the true or temperature-limited shot effect*.

This portion of the analysis is completed with a numerical integration of (19), giving  $\Gamma_\beta^2$  as a function of  $\eta_2$ . For example, the value of  $\Gamma_\beta^2$  when  $\eta_2 = 30$  was found by squaring the ordinates of curve B, Figure 3, multiplying by  $e^{-\lambda}$  and making a trapezoidal integration over

the range  $0.05 \leq \lambda \leq 5$ , for which numerical values of  $\gamma(\lambda)$  had been computed. The additional contributions,  $0 \leq \lambda \leq 0.05$  and  $5 \leq \lambda \leq \infty$ , were calculated by direct integration from series approximations. The former can be handled in no other way because of the logarithmic discontinuity at the origin; the latter is a relatively insignificant contribution since  $e^{-\lambda}$  vanishes rapidly. The result is tabulated in Table III and plotted in Figure 4. The heavy line contains the calculated values, while the light line shows the logical extrapolation. The dashed

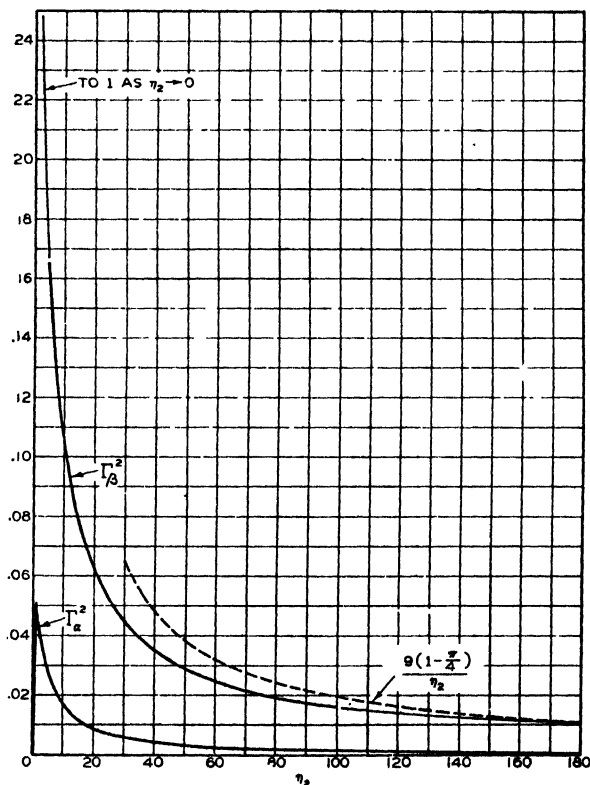


Fig. 4—Shot-effect reduction factors for the case,  $I/I_0 \ll 1$ .

line shows the asymptotic form approached for large  $\eta_2$ . This is found from (31) through consideration of the largest  $\eta_2$ -terms only, and use of the asymptotic form of  $\phi_\beta(\eta)$  as given in (8). In brief, for large  $\eta_2$ , the first indicated integral in (31) vanishes in comparison with the second, and  $2D$  can be replaced by  $\xi_2$ . The second integral has already been shown to possess a logarithmic discontinuity for  $\lambda = 0$ . This can be overlooked, however, for the integral is otherwise an increasing function of  $\eta_2$  so that, for any finite  $\lambda$ , choice of a sufficiently large  $\eta_2$  permits that portion of the integral which depends

on  $\eta_2$  to overshadow the portion which depends on  $\log \lambda$ . Assuming finally that  $\lambda \ll \eta_2$ , one finds

$$\begin{matrix} \gamma \sim -\frac{3}{\sqrt{\eta_2}} \\ \lambda > 0 \\ \eta_2 \rightarrow \infty \end{matrix} \left( \sqrt{\lambda} - \frac{1}{2\sqrt{\pi}} \right). \quad (33)$$

It is quite apparent that this form bears only a very slight resemblance to the curve of Figure 3 and approaches incorrect limits for both large and small  $\lambda$ . The difference in appearance means only that  $\eta_2 = 30$  is too small to permit the use of (33). Of the incorrect lower limit enough has just been said to justify the omission from (33) of the additive term which contains the proper logarithmic discontinuity. That the upper limit is incorrect is only natural in view of the assumption  $\lambda \ll \eta_2$ . In spite of this, relation (33) may be used to find the asymptotic form of  $\Gamma_{\beta}^2$  because of the rapid attenuation furnished by  $e^{-\lambda}$ . The result of putting (33) into (19) is

$$\begin{matrix} \Gamma_{\beta}^2 \sim -\frac{9}{\eta_2} \left( 1 - \frac{\pi}{4} \right) \\ \eta_2 \rightarrow \infty \end{matrix} \quad (34)$$

#### EVALUATION OF $\Gamma_{\alpha}^2$

This study parallels the other so closely that its description can be made brief. Since the current  $i_{\lambda}$  consists, in this case, of electrons which have normal emission velocities insufficient to carry them over the virtual cathode ( $-\eta_1 < \lambda < 0$ ), and since those electrons of a specified velocity  $\lambda$  turn about at the point  $\eta = -\lambda$ , it will be understandable that, in contrast with (21), there are now three distinct differential equations, the simultaneous solution of which determines the *M-B* anode current  $I$  derived from the *M-B*  $I_s$  when an additional  $i_s$  ( $\lambda < 0$ ) is produced at the cathode.

$$\left. \begin{aligned} \text{For the } \beta\text{-space: } \left( \frac{d\eta}{d\xi} \right)^2 &= \phi_{\beta}(\eta), \quad 0 \leq \eta \leq \hat{\eta}_2 \\ \text{For the } \alpha\text{-space: } \left( \frac{d\eta}{d\xi} \right)^2 &= \phi_{\alpha}(\eta), \quad 0 \leq \eta \leq -\lambda \\ \left( \frac{d\eta}{d\xi} \right)^2 &= \frac{i_s}{I} G(\eta, \lambda) + \phi_{\alpha}(\eta), \quad -\lambda \leq \eta \leq \hat{\eta}_1 \end{aligned} \right\} \quad (35)$$

where

$$G(\eta, \lambda) = \frac{4}{\sqrt{\pi}} \sqrt{\eta + \lambda}. \quad (36)$$

As before, the construction of these equations will not be described: it is simple, but lengthy. The stamp of credibility is affixed by noting

$$\int_{-\eta}^0 G(\eta, \lambda) e^{-\lambda} d\lambda = -2 \left[ \frac{2}{\sqrt{\pi}} \eta^{1/2} - e^{-\eta} \operatorname{erf} \eta^{1/2} \right] = \phi_{\alpha}(\eta) - \phi_{\beta}(\eta), \quad (37)$$

which the reader can interpret, like (24), to mean that under the proper conditions (*M-B* distribution of  $i_s$ ) the set (35) reverts to the form (5).

Repeating the process of taking the infinitesimal difference between the solution of (35) for  $I$  and the unperturbed solution of (5) for  $I$ , we arrive by familiar stages at the statement,

$$\gamma(\lambda) = -\frac{1}{2D} \int_{-\lambda}^{\eta_1} \frac{G(\eta, \lambda)}{\phi_{\alpha}(\eta)^{3/2}} d\eta. \quad (38)$$

Again it is convenient to suppose the emission  $I_s$  very copious, so that  $D$  takes the form (32) and the upper limit of the integral above is made infinite. The integral then becomes a function of  $\lambda$  alone, and one numerical integration, therefore, suffices to permit representation of  $\gamma$  for all values of  $\eta_2$ , since  $\eta_2$  influences the function only through the definition of  $D$ .

These integrations were performed for chosen values of  $\lambda$  in the range  $0.01 \leq -\lambda \leq 3$ , observing the same precautions at discontinuities and methods similar to those outlined earlier. A sample plot for  $\eta_2 = 30$  is shown in Figure 3, curve A.

Finally  $\Gamma_{\alpha}^2$  is determined from a numerical integration of (19) with the result:

$$\Gamma_{\alpha}^2 = \frac{0.729}{D^2}. \quad (39)$$

This function has a marked maximum at  $\eta_2 \approx 0.8$ , when  $\Gamma_{\alpha}^2 \approx 0.0513$ , but vanishes rapidly, of course, as  $\eta_2$  approaches zero. The values of  $\Gamma_{\alpha}^2$  versus  $\eta_2$  are also listed in Table III and plotted in Figure 4. The expectation that  $\Gamma_{\alpha}^2 \ll \Gamma_{\beta}^2$  is confirmed. For a practical instance, say  $\eta_2 = 30$ ,  $\Gamma_{\alpha}^2/\Gamma_{\beta}^2 = 0.11$ ; for larger  $\eta_2$ , the ratio diminishes slowly.

## COMPOSITION AND INTERPRETATION

The measuring device cannot discriminate between  $\Gamma_\alpha^2$  and  $\Gamma_\beta^2$ . The important quantity, their sum  $\Gamma^2$ , is shown in Table III. And in Figure 5,  $\Gamma$  is plotted against  $\eta_2$ . This curve, in effect, describes the ratio of r-m-s current fluctuations appearing in the anode current of a space-charge-limited parallel-plane diode to the fluctuations in an equal temperature-limited current. Once more, the heavy line contains the calculated values, while the light line shows a reasonable extrapolation. The asymptotic curve for large  $\eta_2$  is again included for comparison. The trend with both temperature and applied potential should be self-explanatory.

Rough agreement with experience is already noticeable, for most reports of noise measurements on modern amplifying tubes indicate an r-m-s reduction of 1/3 to 1/5. But Figure 5 is an inconvenient basis for comparison because the parameter  $\eta_2$  is difficult to ascertain. It requires knowledge of the depth of the potential minimum, which, in turn, requires a determination of the ratio  $I/I_s$ . A plot of  $\Gamma$  against  $(\eta_2 - \eta_1)$  is hardly an improvement because of serious errors that may arise when the applied voltage is not corrected for contact potential. A much more useful universal parameter is found as follows. Starting with

$$\eta_2 - \eta_1 = \frac{E_2}{V_c}$$

$$\xi_2 - \xi_1 \propto I^{1/2}$$

$$\eta_1 = \log \frac{I_s}{I},$$

and defining the diode conductance by  $g \equiv \frac{\partial I}{\partial E_2}$  (i.e., the reciprocal

of the a-c diode resistance), one can demonstrate that, under the assumption of invariance of  $I_s$  and  $T$  when  $I$  is altered by varying  $E_2$ ,

$$\frac{I}{gV_c} = D\phi_\beta(\eta_2)^{1/2}. \quad (40)$$

The quantity on the left will become our new parameter, replacing  $\eta_2$  and being defined by (40) which is principally a function of  $\eta_2$  only, and becomes *entirely* independent of  $\eta_1$  if it is again supposed that  $I/I_s \rightarrow 0$ . This assumption was made in plotting  $I/gV_c$  against  $\eta_2$  in Figure 5.



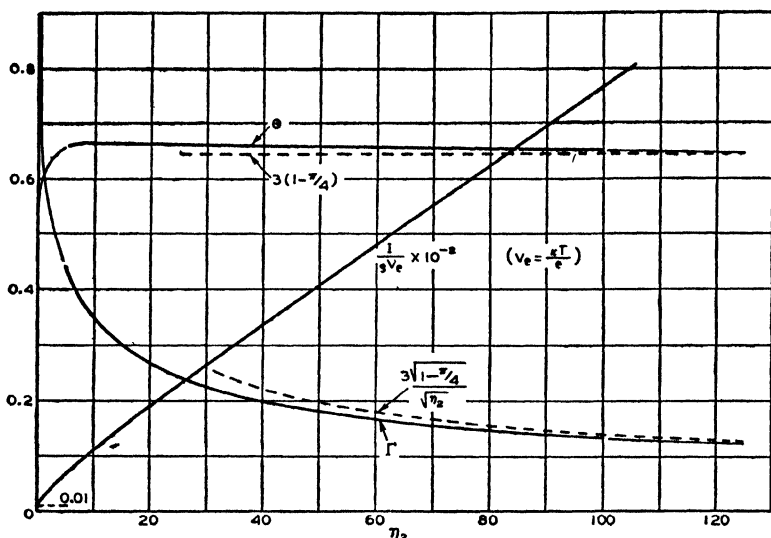


Fig. 5—Shot-effect reduction factors for the case,  $I/I_s \ll 1$ .

From the two curves of Figure 5, the plot of  $\Gamma$  in Figure 6 was made. This curve is entirely suitable for experimental checks of the analysis since current, conductance and cathode temperature are accessible parameters. Too, the reader has no doubt foreseen that representation of  $\Gamma$  in this way permits a test of the theory against non-planar structures.

The analysis might logically terminate at this point were it not for widespread curiosity over the connection (if any) between this type of shot effect and the current fluctuations of thermal origin (Brownian movement) known to exist in any short-circuited ohmic resistance. According to Nyquist's formula,<sup>1</sup> the thermal current fluctuations in an ohmic resistance whose conductance is  $g$ , and whose temperature is  $T$  are represented by

$$\bar{i}^2 = 4kTg\Delta f.$$

( $k$  = Boltzmann's constant,  $f$  = band width)

Let us then suppose that our space-charge-limited diode exhibits pseudo-thermal fluctuations (that they cannot be considered truly thermal has been emphasized in Part I). We, therefore, describe the space-charge-reduced current fluctuations by the empirical formula.

$$\bar{i}^2 = \theta \cdot 4kTg\Delta f, \quad (41)$$

<sup>1</sup>H. Nyquist, "Thermal Agitation of Electric Charge in Conductors," *Phys. Rev.*, Vol. 32, p. 110, July, (1928).

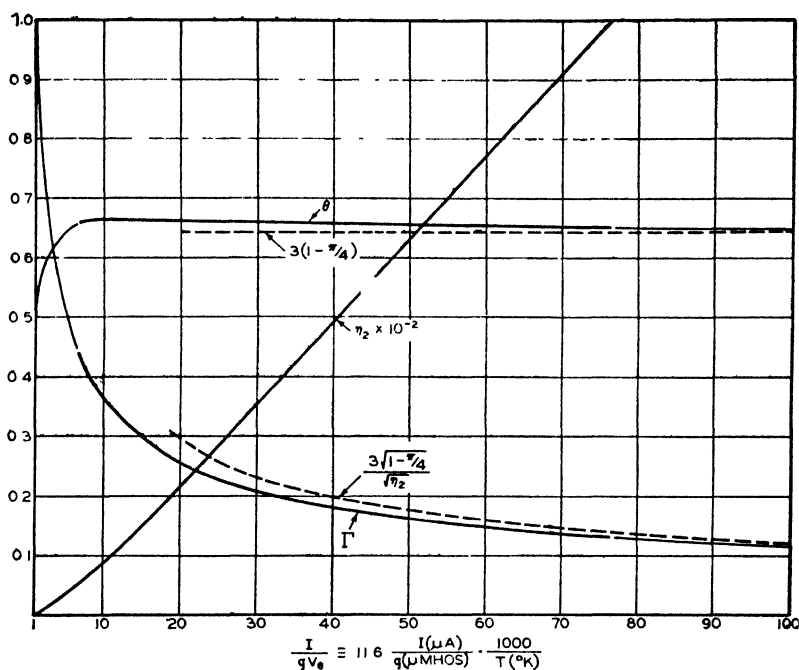
Fig. 6—Shot-effect reduction factors for the case,  $I/I_s \ll 1$ .

TABLE III

$\eta_2$	$\xi_2$	$\phi_\beta(\eta_2)^{1/2}$	D	$\Gamma_\alpha^2$	$\Gamma_\beta^2$	$\Gamma^2$	$\Gamma$	$\frac{I}{gVe}$	$\theta$
0	0	0	$\infty$	0	1	1	1		
5	6.110	1.33	5.08	0.0282	0.1663	0.1945	0.441	6.76	0.657
10	9.447	1.66	6.60	0.0167	0.1043	0.1210	0.348	10.96	0.663
15	12.275	1.87	7.95	0.0115	0.0775	0.0890	0.298	14.9	0.663
20	14.826	2.04	9.18	0.0086	0.0621	0.0707	0.266	18.7	0.661
25	17.193	2.18	10.33	0.0068	0.0519	0.0587	0.242	22.5	0.660
30	19.425	2.30	11.43	0.0056	0.0448	0.0504	0.224	26.3	0.663
35	21.55	2.40	12.47	0.0047	0.0394	0.0441	0.210	29.9	0.659
40	23.59	2.50	13.47	0.0040	0.0352	0.0392	0.198	33.7	0.661
45	25.56	2.58	14.45	0.0035	0.0319	0.0354	0.188	37.3	0.660
50	27.47	2.66	15.39	0.0031	0.0291	0.0322	0.179	40.9	0.658
60	31.14	2.79	17.21	0.0025	0.0248	0.0273	0.165	48.0	0.655
70	34.64	2.92	18.94	0.0020	0.0217	0.0237	0.154	55.3	0.655
80	38.01	3.02	20.61	0.0017	0.0192	0.0209	0.145	62.2	0.650
90	41.26	3.13	22.23	0.0015	0.0173	0.0188	0.137	69.6	0.654
100	44.41	3.21	23.80	0.0013	0.0157	0.0170	0.130	76.4	0.649

$I/I_s \rightarrow 0$  so that  $\xi_2 = -2.55$ ,  $\eta_1 \rightarrow \infty$

and our problem is to discover the relationship between  $\theta$  and  $\eta_2$  or  $I/g V_e$ . Since we have formerly written

$$\bar{i}^2 = \Gamma^2 \cdot 2eI\Delta f, \quad (42)$$

identification of (41) with (42) shows that

$$\theta = \frac{1}{2} \Gamma^2 \frac{I}{g V_e} = \frac{1}{2} \Gamma^2 D\phi_\beta(\eta_2)^{1/2}. \quad (43)$$

The right-hand side is a combination of known functions of  $\eta_2$  and serves to define  $\theta$ . Values of  $\theta$ , calculated in this manner, are listed in Table III and plotted in Figures 5 and 6 against  $\eta_2$  and  $I/g V_e$ , respectively. The asymptotic value is also shown (dashed line); its magnitude is found from (34) together with

$$\frac{I}{g V_e} = D\phi_\beta(\eta_2)^{1/2} \sim \frac{2}{3} \eta_2, \quad (\eta_2 \rightarrow \infty) \quad (40a)$$

so that

$$\theta \sim 3 \left(1 - \frac{\pi}{4}\right) = 0.6438. \quad (\eta_2 \rightarrow \infty) \quad (44)$$

In this place it should be recorded that the asymptotic solution was first developed by W. A. Harris of these laboratories. Working along similar lines and independently, he arrived at the above expression in March, 1936, prior to the completion of the author's analysis. Indeed, the simplicity of his result, together with its substantial accord with contemporary experimental work,<sup>1</sup> added incentive to the more detailed study just described.

The value of  $\theta$  for vanishing  $\eta_2$  (incipient retarding field condition) is also found easily from the following limit values:

$$\lim_{\eta_2 \rightarrow 0} \left\{ \begin{array}{l} \frac{I}{g V_e} \equiv D\phi_\beta(\eta_2)^{1/2} = 1 \\ \Gamma\alpha^2 = 0, \Gamma^2 = \Gamma_\beta^2 = 1, \text{ so that} \\ \theta = \frac{1}{2}. \end{array} \right. \quad (45)$$

<sup>1</sup>G. L. Pearson, "Shot Effect and Thermal Agitation in an Electron Current Limited by Space Charge," *Physics*, Vol. 6, p. 6, January, (1935).

It is interesting to note how rapidly  $\theta$  rises and how closely it corresponds to the asymptotic value (44) throughout the whole practical working range. (Slight fluctuations in the tabulated values are to be attributed wholly to small errors arising in the numerical work.) Because of this fortunate property, equation (41) recommends itself as the formula for space-charge-reduced shot noise most useful in engineering application; and for most purposes sufficient accuracy will be obtained by assuming  $\theta(\eta_2)$  to be simply a constant equal to the asymptotic value, namely, 0.644. Although, whenever one is principally interested in the noise *reduction* attributable to space charge, it will be convenient to revert to (43):

$$\Gamma^2 = 2\theta \frac{g V_c}{I} \sim 1.29 \frac{g V_c}{I}. \quad (43a)$$

Inasmuch as  $I$  increases more rapidly than  $g$  as (say) voltage is raised, it is apparent that although  $\Gamma^2$  becomes smaller it decreases more slowly than the true shot effect increases so that the net result is a steadily increasing noise proportional to the diode conductance. It may be said then that *the mean-square noise generated by emission fluctuations in a space-charge-limited diode is roughly numerically equal to two-thirds of the noise of thermal agitation generated by a resistance of magnitude equal to the a-c resistance of the diode and possessing a temperature equal to the cathode temperature*<sup>1</sup>. Yet the two phenomena must not be confused in concept. For, thermal agitation is known to be a form of Brownian movement, and finds its origin in the equipartition of energy among the various mechanical and electrical degrees of freedom of a substance in thermal (i.e., kinetic or statistical) equilibrium. The diode, on the other hand, while clearly in a stationary state, cannot be regarded as a system in a condition of thermal equilibrium so long as there is a battery providing plate voltage and energy. The mechanics of the two phenomena are, therefore, distinct; the formulas alone exhibit a resemblance. The only instance in which complete identification can be made is that in which the plate voltage is zero and the whole diode (anode as well as cathode) is brought to a common temperature. This interesting situation will be discussed briefly in a later section.

It is of interest to perfect the picture of shot noise by considering the case of a retarding field. The mean-square noise at the threshold

<sup>1</sup> In our oral report of this week (Rochester Convention, November, 1936), we quoted "six-tenths" instead of the present "two-thirds," (cf. *Electronics*, Vol. 9, No. 11, p. 31, November, 1936). The alteration follows discovery of a numerical error which required that all values of  $\Gamma_a^2$  be raised by the factor 16/3.

of a retarding field condition has already been shown, (45), to be precisely half the thermal-agitations value. One can easily demonstrate that equations (45) are all valid throughout the retarding-field region. There is no virtual cathode, hence no space-charge reduction; and since  $I/g V_e = 1$ , it is numerically immaterial whether one regards the noise as true shot effect expressed by

$$\overline{i^2} = 2eI\Delta f,$$

or half-thermal fluctuations expressed by

$$\overline{i^2} = \frac{1}{2} \cdot 4kTg\Delta f.$$

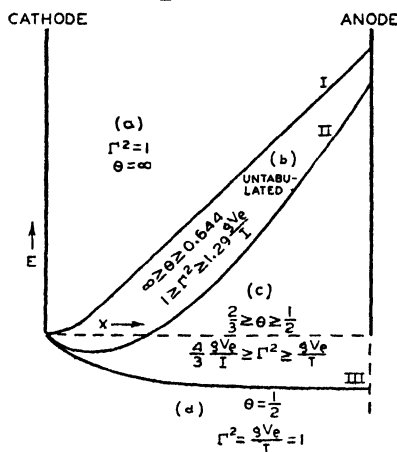


Fig. 7—Schematic survey of shot effect in a parallel-plane diode, all modes of operation.

This identification was first remarked in print by F. C. Williams,<sup>1</sup> who also showed good experimental agreement with the theory, and pointed out the nature of the modifications necessary when the formulas are to be adapted to cylindrical structures. These modifications are of no great consequence unless the ratio of anode to cathode diameter is much larger than customary in conventional equipotential-cathode structures.<sup>2</sup>

We are now in a position to diagram the shot effect for virtually all modes of operation of a diode which approximates a parallel-plane structure. The applicable formulas will be either or both of (41) and (42). In Figure 7 four operating regions, (a)—(d), are schematically demarcated by three curves of space potential. Curve I represents

<sup>1</sup> "Fluctuation Noise in Vacuum Tubes Which Are Not Temperature-Limited," *Journ. I.E.E.*, Vol. 78, No. 471, p. 326, March (1936).

<sup>2</sup> Cf. footnote, p. 468.

that potential distribution for which the virtual cathode coincides with the cathode  $\left(\frac{\partial E}{\partial x} = 0 \text{ at cathode}\right)$ ; curve *I* shows qualitatively a

mode of operation such that  $I/I_s = 1/5$  (say); curve *III* gives the potential distribution for which the virtual cathode coincides with

the anode  $\left(\frac{\partial E}{\partial x} = 0 \text{ at anode}\right)$ , which is the condition of incipient re-

tarding field. Region (a): there is no virtual cathode, and the diode is, therefore, temperature-limited so that the classical shot-effect formula obtains, i.e.,  $\Gamma = 1$ . No significance can be attached to (41) for, except for field currents or other anomalous behavior,  $g = 0$ . Region (b): no tabulation has been made for this region where  $I/I_s$  is not sufficiently small that the present analysis can be used with negligible error. Close study is so lengthy and provides so little additional engineering information that mention will be made here of only a few rough estimates of error incurred if the tabulated values of  $\Gamma^2$  and  $\theta$  are employed. The value  $I/I_s = 1/5$  is of course an arbitrary choice for the boundary curve *II*. If  $\eta_2 = 10$  (anode potential approximately 1 volt, for a cathode temperature of  $1000^\circ\text{K}$ ), the tabulated value of  $\Gamma^2$  is low by approximately 1 per cent and  $\theta$  is low by approximately  $1\frac{1}{2}$  per cent, when  $I/I_s = 1/5$ . Larger values of  $\eta_2$  (higher anode potentials or lower cathode temperatures) reduce the error. For  $I/I_s = 1/3$  and the same  $\eta_2$ , the errors in  $\Gamma^2$  and  $\theta$  are approximately 4 and 6 per cent, respectively. And for  $I/I_s = 1/2$  the errors are only about 10 and 15 per cent, respectively. It is clear, then, that  $\Gamma^2$  departs appreciably from the tabulated values only when the tube is nearly temperature-limited and then climbs rapidly to unity as *I* approaches  $I_s$ .<sup>1</sup> Region (c): this is the region of practical operation of virtually all biased diodes giving high emission. The virtual cathode effects a reduction in emission fluctuations, and the tabulated values of  $\Gamma^2$  and  $\theta$  should show negligible error. Region (d): with the appearance of a monotonic retarding field, the virtual cathode and, therefore, the reduction of shot effect simultaneously vanish. Throughout this region  $\Gamma^2 = 1$ ,  $\theta = 1/2$ , and when used in their respective formulas, they produce identical numerical results.

<sup>1</sup>Spence has carried out the complete numerical integration for two examples and shows for them the sharp rise of  $\Gamma$  to unity described here; E. Spence, "The Space-Charge-Reduction of Shot Effect," *Wiss. Veröff. aus den Siemens-Werken*, Vol. 16, No. 2, p. 19, July, (1937). In a more recent study, Rack has shown graphically the influence of the ratio  $I/I_s$  for the complete range,  $0.05 \leq I/I_s \leq 1$ ; A. J. Rack, "Effect of Space Charge and Transit Time on the Shot Noise in Diodes," *B.S.T.J.*, Vol. 17, No. 4, p. 592, October, (1938).

## THE DIODE IN THERMAL EQUILIBRIUM

It was mentioned above that one could expect the shot effect in a diode to be completely identified with the thermal agitations of its resistance only when the diode is unenergized and the whole of it put at one temperature. Let us demonstrate this identity by showing that the formula for shot effect proves to be, in this instance, identical with Nyquist's expression for the thermal agitation. Consider an electrode (1) surrounded by an electrode (2), the material of which each is constructed being unimportant. The electrodes are short-circuited and the diode is maintained at temperature  $T$ . Both surfaces emit, but at rates which are not necessarily equal, since, for example, the work functions are not prescribed. Yet the current  $I_1$ , that portion of the emission from the first electrode which is absorbed by the second, must be equal to  $I_2$  (similarly defined) *on the average*. This statement will be recognized as a direct outcome of the second law of thermodynamics. The average current through the short-circuiting link is therefore zero, but fluctuations are present nevertheless. If these fluctuations are traced back to variations in emission, they are properly labeled "shot effect"; yet, if they are simply accepted as a manifestation of Brownian motion, they are just as properly termed "thermal agitation".

Adhering for the moment to the latter point of view, we find that Nyquist's formula provides a valid measure of the fluctuations. For, we need only observe that we have here a two-terminal, unenergized circuit element at a uniform temperature. Its short-circuit fluctuations are, therefore,

$$\overline{i^2} = 4kTg\Delta f, \quad (46)$$

where  $g$  is the real part of the diode admittance at the frequency in question. Confining ourselves, as usual, to frequencies at which transit-time effects are negligible, we may say that  $g$  is simply the low-frequency conductance. It is not difficult to obtain an expression for  $g$ . Suppose that a voltage  $E$  is included in the circuit, making the outer electrode more positive. In case the situation is not complicated by individual collisions,<sup>1</sup> it can readily be shown by kinetic theory that

$$I_1/I_2 = e \frac{E}{V_e}, \quad (47)$$

<sup>1</sup> This assumption is reasonable, except for exceedingly high space-charge densities, not likely to be encountered in practice. Cf. I. Langmuir and K. T. Compton, "Electrical Discharges in Gases," *Rev. Mod. Physics*, Vol. 3, No. 2, p. 220, (1931).

regardless of the geometrical configuration, coefficients of reflection, contact potential, etc. Consider now variations of  $I_1$  and  $I_2$  against  $E$  with  $T$  fixed:

$$\frac{\partial I_1}{I_1} - \frac{\partial I_2}{I_2} = \frac{\partial E}{V_e}.$$

The conductance is, therefore,

$$g = \left[ \frac{\partial (I_1 - I_2)}{\partial E} \right]_{\substack{E=0 \\ I_1=I_2=I}} = \frac{I}{V_e}, \quad (48)$$

where  $I$  is the equilibrium current emitted by either electrode and absorbed by the other. And this expression is valid whether or not there exists a virtual cathode in the equilibrium state. Consequently, the thermal fluctuations can be written

$$\overline{i^2} = 4Ie\Delta f \quad (49)$$

Turning now to the kinematic viewpoint, we note that the emission current from either electrode exhibits true shot effect, so that the mean-square current fluctuations in the short-circuiting link are simply the sum of the separate shot effects associated with the currents  $I_1$  and  $I_2$ . To calculate this sum, we must first determine the space-charge-reduction factor  $\Gamma$  for each current. Suppose that the equilibrium state is perturbed by the injection of an additional small steady emission  $i_s$  from the first electrode. The emission velocities of the electrons comprising  $i_s$  will be permitted any values whatever. The question is: In what way is the original equilibrium affected? Now except for individual encounters, which we suppose highly improbable, the electrons in  $i_s$  disturb the equilibrium only in so far as they introduce a potential field superimposed upon that which existed initially. The diode, therefore, settles into a new equilibrium state such that the space-charge density is everywhere slightly altered, yet, except for the injected electrons  $i_s$ , at every point in space the M-B distribution still obtains. The originally equal equilibrium currents  $I_1$  and  $I_2$  are now somewhat reduced, but still equal. It follows that whatever fraction of  $i_s$  is absorbed on the second electrode is accompanied by no net increment in the equilibrium current, and this is true whether or not there exists a virtual cathode in the equilibrium state. There is consequently no space-charge reduction of noise,  $\Gamma = 1$ , and

$$\overline{i^2} = 2e(I_1 + I_2)\Delta f = 4eI\Delta f. \quad (50)$$



In the equilibrium case, then, the two viewpoints are only alternative aspects of the same phenomenon. The identification is logical and complete. Where space-charge densities are low enough to make individual collisions unimportant, all of the dynamical processes which maintain the electrons in thermodynamical equilibrium occur within the electrode material. The space between electrodes is only a passageway through which electrons travel without incident.

With this in mind, we can now understand thermodynamically that the shot effect of a normal diode operating in the retarding-field condition should have turned out to be precisely half-thermal. Consider a diode in thermal equilibrium, and, if there is a virtual cathode, let the emission from the electrode of higher work function become smaller by raising the work function until the virtual cathode has disappeared. If the diode is parallel-plane, this emission is now temperature-limited, i.e., it contributes nothing<sup>1</sup> to the conductance  $g$  given by (48). On the other hand, it is *still* responsible for half the shot effect as represented by (50), because  $I_1 = I_2$  is still valid, nothing having been done yet to destroy thermal equilibrium. But now we remove the temperature-limited current altogether, say, by lowering the emitter to room temperature. The noise is halved, the conductance is unaltered, and the half-thermal fluctuations of a parallel-plane diode operating in retarding-field condition are provided with thermodynamical significance.

#### NEGATIVE-GRID TRIODES

The foregoing study is, of course, but a preliminary to the problem of chief interest, namely, noise in amplifying tubes. To see how the theory of diodes can be adapted to a triode, imagine the conversion of a parallel-plane diode by adding grid wires one at a time. When only two or three grid wires are in place, and biased negatively, the space potential is badly disrupted. Moreover, electrons on the plate side of the grid wires still contribute materially to the potential in the vicinity of the virtual cathode. Noise analysis at this stage would be painfully difficult. Hence, there is little to be said about very low- $\mu$  tubes, except,

---

<sup>1</sup> It should be noted that this statement is partly hypothesis. If the coefficient of reflection is a function of velocity, the conductance of any unilateral current flow will be affected, whether the field be accelerating or retarding. The nature, even the existence of such a function, is still moot (cf. Compton and Langmuir, *Rev. Mod. Phys.*, Vol. 2, No. 2, p. 171, 1930; also W. B. Nottingham, *Phys. Rev.*, Vol. 49, p. 83, 1936). Overlooking this difficulty as well as the possibility of field emission, the reader should observe that the statement is still not applicable to all geometrical configurations. As long as there are any electrons which, from an energy standpoint alone, would fall on the collector, but which fail to do so because of momentum considerations, the conductance is finite for a temperature-limited current, and is not easily formulated for any mode of operation. It is on this account that the present analysis is restricted to parallel-plane structures.

perhaps, to set limits for the noise. When, with the addition of more grid wires, the control grid stands complete, with a  $\mu$  of say, 5 or more, the space potential can generally be considered very regular again, except in the immediate neighborhood of the grid wires. A first approximation to the shot current fluctuations, exact in the limit of an infinite  $\mu$ , would then amount to neglecting the grid-plate region altogether, and applying the diode analysis directly to the grid-cathode space. The anode potential of the diode,  $E_2$ , would have to be interpreted now as the "effective" potential of the grid plane,  $E_a$ , i.e., that potential which, when applied to a solid sheet in the grid-plane, would draw the same cathode current. In addition,  $g$  would now be viewed as the conductance of this equivalent diode. This procedure recognizes the contribution which electrons in the grid-plate space make to the steady-state space potential on the other side of the grid, but does not take account of their contribution to  $\Gamma^2$ . For this reason, theoretical values of shot effect so determined should be a little too high. The error, however, should be practically unimportant where high- $\mu$  tubes are concerned. For, in the first place, an electron's contribution to noise reduction must vary inversely as its velocity and its distance from the virtual cathode. Second, the grid mesh is a good electric shield.

$$\left. \begin{aligned}
 E_a &= \sigma \left( E_{c1} + \frac{1}{\mu_o} E_b \right) \\
 \sigma &= \left\{ 1 + \frac{1}{\mu_o} \left[ 1 + \frac{4}{3} y (1 + h) - \frac{1}{3} h^2 (6 + 4h + h^2) \right] \right\}^{-1} \\
 y &= \frac{x_p}{x_c} = \frac{\text{grid-anode spacing}}{\text{cathode-grid spacing}} \\
 h &= \frac{\tau_p}{\tau_c} = \frac{\text{grid-anode transit time}}{\text{cathode-grid transit time}} \\
 \mu_o &= \mu \left( 1 - \frac{h^3}{y} \right) \\
 \mu &= \text{"cold", i.e., electrostatic amplification factor}
 \end{aligned} \right\} \quad (51)$$

To put this procedure into effect, one must relate  $E_a$  and  $g$  to the grid and anode voltages. It will be assumed throughout that the grid has negative bias so that the plate alone collects electrons. The best

formulation of  $E_a$  to date is (51), derived by Llewellyn,<sup>1</sup> which takes into account the influence of space charge upon space potential, but assumes zero emission velocities.

The grid-plate transconductance (for negligible transit angles) is, therefore,

$$g_m = \sigma g, \quad (52)$$

and since it is easily measured, whereas  $g$  cannot be measured at all,  $g_m$  will be used in place of  $g$  in the expressions for shot effect. Thus

$$(41) \text{ becomes } \bar{i}^2 = \frac{\theta}{\sigma} \cdot 4kTg_m\Delta f, \quad (41a)$$

$$\text{and (43a) becomes } \Gamma^2 = 2 \frac{\theta}{\sigma} \frac{g_m V_c}{I} \sim \frac{1.29}{\sigma} \frac{g_m V_c}{I}. \quad (43b)$$

Under ordinary circumstances  $\sigma$  will decrease somewhat with an increase in current, because  $h$  increases. This behavior may be marked for low- $\mu$  tubes, but becomes less pronounced as  $\mu$  is increased, since

$$\lim_{\mu \rightarrow \infty} \sigma = 1.$$

It will not in general be correct, therefore, to assume that  $\sigma$  is strictly a constant; for conventional tubes, it will usually lie between 0.5 and 1. Inasmuch as  $h$  is usually less than 0.5, rough estimates of  $\sigma$  for parallel-plane structures may be made by supposing  $h = 0$ , whence<sup>2</sup>

$$\sigma \sim \left\{ 1 + \frac{1}{\mu} \left[ 1 + \frac{4}{3} y \right] \right\}^{-1}. \quad (51a)$$

No rigorous formula analogous to (51) has yet been developed for cylindrical structures. The analogue of (51a), however, has long been known:<sup>2</sup>

$$\sigma_{\text{cyl.}} \sim \left\{ 1 + \frac{1}{\mu} \left[ 1 + \frac{2}{3} \log \frac{r_p}{r_g} \right] \right\} \quad (51b)$$

This expression is limited to structures in which the ratio of grid to cathode radius is larger than about 10. For smaller ratios the formula for plane structures will suffice.

The current fluctuations in the plate circuit (without load) are now seen to be principally a function of conditions between cathode and grid. And in contrast with the diode fluctuations, it is no longer pos-

<sup>1</sup> F. B. Llewellyn, "Operation of Ultra-High-Frequency Vacuum Tubes," *B.S.T.J.*, Vol. 14, p. 659, October, (1935).

<sup>2</sup> B. D. H. Tellegen, "The Value of Cathode Current in a Triode," *Physica*, Vol. 3, p. 801. (1925).

sible to find a simple empirical relation between triode shot effect and thermal agitation in an ohmic resistance of magnitude equal to the anode resistance. Following (41a), attention is more properly focused upon the transconductance.

The shot voltage  $\overline{e_o^2}$  appearing across a load  $Z$  in the output circuit of a negative-grid triode whose plate resistance is  $r_p$ , is from (41a),

$$\overline{e_o^2} = \frac{\theta}{\sigma} \cdot 4kTg_m\Delta f \cdot \left| \frac{r_p Z}{r_p + Z} \right|^2 \quad (53)$$

Inasmuch as the principal sources of local noise in amplifiers are thermal agitation in the input circuit and shot effect in the first tube, it has often been remarked that, instead of (53), a more useful formula for shot effect is found by referring the plate-current fluctuations back to the input circuit. This effective input fluctuation voltage is then that voltage which, applied between cathode and grid, produces in the output fluctuations equal in magnitude to those actually generated by shot effect. The effective input shot effect can then be compared directly with the thermal agitation of the input circuit. In fact, instead of expressing the shot effect as a voltage, we may symbolize it by a resistance  $R_{eff}$ , i.e., that resistance which, at ambient temperature, exhibits a thermal agitation voltage equal to the effective input shot voltage of the tube. This we do as follows. Since the transconductance,  $g_m$ , represents the ratio of output current (without load) to input voltage, we have from (41a),

$$\frac{\overline{i^2}}{g_m^2} = \frac{\theta}{\sigma} \cdot \frac{4kT}{g_m} \cdot \Delta f. \quad (54)$$

Nyquist's expression for thermal agitation voltage across a resistance  $R_{eff}$  at room temperature  $T_o$  is

$$\overline{e_i^2} = 4kT_o R_{eff}\Delta f. \quad (55)$$

Equating the two voltages, we obtain

$$R_{eff} = \frac{\theta}{\sigma} \cdot \frac{T}{T_o} \cdot \frac{1}{g_m} \quad (56)$$

A brief numerical estimate will serve to indicate the order of magnitude of  $R_{eff}$ . Using figures typical of coated-cathode receiving tubes, let us choose  $T = 1000^\circ K$ ,  $T_o = 300^\circ K$ ,  $\theta = 2/3$ ,  $\sigma = 3/4$ . Then,

$$R_{eff} \approx 3/g_m.$$

With transconductances of 1000, 1500, and 10,000 micromhos, respectively, such a tube would exhibit shot effect equivalent to the fluctuations arising from thermal agitation in resistances connected between grid and cathode of magnitude 3000, 2000, and 300 ohms, respectively.

(The close approximation of these estimates to measured values of  $R_{eff}$  already published at once attests the validity of the theory and implies its successful adaptation to cylindrical structures.) So long as the input impedance actually employed presents a real component  $R$  ( $Z = R + jX$ ) two or three times greater than  $R_{eff}$ , the limit of useful amplification is set by thermal agitation; this is generally the state of affairs in the case of sharply tuned circuits and high-gain tubes, e.g., in broadcast receivers properly designed. When the reverse is true, and  $R_{eff} \cong R$ , the shot-effect problem becomes acute and anything which can be done to restore the original inequality,  $R_{eff} \ll R$ , without slighting performance requirements will increase the intelligibility of small signals. A case in point is the television receiver; in brief, the requirement of a pass-band width of several megacycles necessitates a low tuned-input impedance comparable in magnitude to the  $R_{eff}$  of conventional tubes, so that shot effect may be a serious concern.

A more detailed study of this and other noise problems is postponed (Part V) until we have completed our analysis with a description of shot-effect phenomena peculiar to multi-collector tubes, i.e., those in which the cathode-current stream is collected at two or more electrodes (Part III). For the present it will be sufficient simply to note the obvious recommendations of (56). As stated previously,  $\theta$  is practically a constant and little can be done to reduce it. Similarly  $\sigma$  is practically a constant and generally offers, at most, a maximum of 50 per cent improvement. Furthermore,  $T$  is at present confined to rather limited regions in the vicinity of  $1000^\circ K$  for coated cathodes and  $1900^\circ K$  for thoriated tungsten. Other things being equal, coated cathodes are, therefore, to be preferred. It is, of course, possible to lower the temperature below the recommended value and still maintain performance, but in general a drop of  $200^\circ$  or so brings the tube so near the temperature-limited condition that the formulas given are vitiated, and the signal-to-noise ratio decreases sharply (see Figure 11). Fortunately, there always seem to be ways to improve transconductance; although the mean-square output noise is proportional to  $g_m$ , the equivalent input noise varies as  $1/g_m$ , so that it is profitable to use as high a transconductance as possible. This notion is hardly novel, for it has long been recognized that increase in gain, *per se*, would improve the input signal-to-noise ratio. The derived proportionality of mean-square output noise to  $g_m$  serves to render this expected improvement not inexistent, but simply smaller than conceived in dreams. Other things being equal, then, a change in structure which doubles  $g_m$  should cut the mean-square input noise of a triode in half—not a magnificent improvement, but the only thoroughly practical method available.

## EXPERIMENT

## APPARATUS AND METHODS

ALL measurements were made at a frequency of about one megacycle. This is low enough to avoid transit-time complications and high enough to escape the "flicker effect" which contaminates shot-effect studies at audio frequencies. In design and construction of the special four-stage tuned amplifier,<sup>1</sup> extraordinary care was given to shielding, so as to minimize errors attributable to regeneration. The outfit was housed in a tight copper box, the false bottom of which contained thoroughly filtered supply leads; the upper portion was partitioned so that each tuned circuit was isolated. The partitions were constructed so that the tubes, themselves surrounded by shields, projected obliquely through the walls. Feedback was thus reduced to coupling between grid and plate elements in the type 57 pentodes. And even this source of regeneration was minimized by coupling each output to its tuned circuit through a large inductance which presented to the plate a capacitive reactance, varying but little with frequency. Each compartment was made accessible by a tight-fitting sliding cover. In this way voltage gains of over  $10^6$  were obtained without appreciable regeneration, and controlled by grid-bias adjustment of a type 58 pentode in the third stage. A fifth stage was alternatively employed as a vacuum-tube detector for preliminary work such as alignment, or as an additional stage of amplification feeding a thermocouple for accurate work. In the latter instance, a power tube was used to drive the couple to avoid cutting off the peaks. For detection the thermocouple was

---

<sup>1</sup>The amplifier and most of its associated equipment were constructed by L. I. Potter of these laboratories. Its continuously reliable performance must be credited entirely to his careful workmanship.

preferred in order to avoid any question as to whether the detector was really "square-law". A frequency-calibrated signal generator with calibrated attenuator provided measured signal accurate to 0.1 microvolt for alignment and calibration of the amplifier. It also provided, in one procedure, a comparison signal for noise measurement. Finally, the whole outfit was operated in a doubly screened room equipped with filters for all power lines.

The tube under observation was housed, together with its tuned coupling circuit ( $Z$ ), in the first compartment of the amplifier box. All components of this unit were mounted on a removable false bottom, so that changes in tube, circuit, or connections could be made rapidly and conveniently. A small hole in the lid of this and each amplifier compartment permitted insertion of a condenser-tuning rod to allow adjustments in tuning without upsetting the shielding. The pass-band of the amplifier was about 10 kilocycles, and the " $Q$ " of the coupling impedance  $Z$  was lowered by adding shunt resistance until it could be assumed

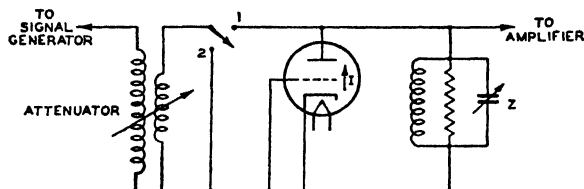


Fig. 8—Schematic shot-effect test circuit using signal generator.

that the over-all frequency-response curve was defined by the amplifier alone. This procedure simplified computation tremendously, since the pass-band could always be considered fixed, independent of whatever variations in the coupling circuit might occur in the course of measurement. The impedance  $Z$  was measured *in situ* by the familiar dynatron method, and fixed throughout the work at  $45.5 \times 10^3$  ohms.

The early measurements were conducted in a manner explained schematically by Figure 8, which depicts only the essential radio-frequency connections. The signal-generator frequency was centered on the amplifier pass-band. Then, with the switch in position 2, and the tube operating, the amplifier gain was set at a point which gave a suitable reading on the output ammeter. This reading was a measure of the sum of tube noise and thermal agitation in  $Z$ . Then the switch was thrown to position 1, and that signal ( $V$ ) found which brought the ammeter reading back to its original value. (Inasmuch as the output impedance of the attenuator was negligible, it was immaterial whether or not the tube remained on.) The signal voltage was then a direct measure of the noise voltages integrated over the pass-band ( $\Delta f$ ) of the amplifier. A measure of the noise per unit band width

therefore required a determination of  $\Delta f$ , and this was accomplished in the usual way by running through a response curve. Thus, if  $V$  is the input voltage at frequency  $f$  which produces a fixed output meter reading, then

$$\Delta f = V_{\min}^2 \int \frac{df}{V^2}.$$

Making a correction for thermal agitation in  $Z$ , one would finally evaluate  $\Gamma^2$ , for example, from

$$\Gamma_{\text{exp.}}^2 = \frac{V^2 \left( \frac{1}{Z} + \frac{1}{r_p} \right) - \frac{4kT_o}{Z}}{2eI} \quad (57)$$

In this expression  $r_p$  is the output resistance of the tube under test, in parallel with the circuit impedance  $Z$ , and  $I$  is the current, the fluctuations in which are under study. The second term in the numerator

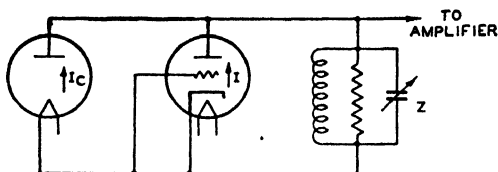


Fig. 9—Schematic shot-effect test circuit using comparator diode.

is the correction for thermal agitation in  $Z$ , and is almost always nearly negligible. No correction for background noise in the amplifier proper is in order since it affects both meter readings equally.

Straightforward variations in the circuit of Figure 8 permitted measurements of noise in not only the plate circuit, but grid and cathode circuits also. Yet for the latter, and for work with diodes, the method was not wholly satisfactory, for when the output resistance of the tube was small, the equivalent signal voltage  $V$  diminished in consequence, until inaccuracies in reading  $V$  led to adoption of a different procedure.

The second method replaced the signal generator by a temperature-limited diode, whose fluctuations could be calculated directly ( $\Gamma = 1$ ) from a measure of its anode current. One example of its use is shown in Figure 9 which, again, emphasizes only the radio-frequency connections. With input shorted, the amplifier had its gain adjusted at a point which gave an output reading  $R_1$ , a measure of the background produced by the amplifier proper. With the tube under test operating



as desired, and with the comparator diode in the circuit but not operating (cold), a second reading  $R_2$  was a measure of the sum of the shot effect under study plus amplifier noise. From a calibration curve of the output circuit, there was rapidly located a reading  $R_3$  which would represent double the mean-square input to the amplifier. The filament of the comparator diode was then brought to that temperature at which the temperature-limited diode current  $I_c$  supplied additional noise sufficient to establish the reading  $R_3$ .

Just as in the first method, a correction for thermal agitation in  $Z$  will enter a determination of  $\Gamma$  from these data. And yet the working formula will be very simple because, first, all current fluctuations involved can legitimately be assumed to have a uniform frequency distribution; second, the input impedance remains unaltered when the comparator diode is in operation, the conductance of a temperature-limited diode being effectively nil. It turns out, then, that

$$\Gamma_{\text{exp}}^2 2eI + \frac{4kT_o}{Z} = 2eI_c,$$

or, for the impedance used,

$$\Gamma_{\text{exp}}^2 = \frac{I_c - 1.14}{I}, \quad (58)$$

where  $I_c$  and  $I$  are expressed in microamperes.

The correction for thermal agitation is generally negligible. In comparison with the first method, this scheme has the disadvantage of necessitating a careful calibration of the output circuit, but this is not difficult and is permanent—until the thermocouple leaves in a puff. It has a distinct advantage in requiring no determination of the amplifier pass-band, a measurement which is always subject to correction as a result of aging, or other uncontrollable causes.

A third method, not employed in these studies, is worth mentioning inasmuch as it has proved very rapid and reliable whenever a measure of  $R_{\text{eff}}$  (see p. 471) was the chief objective. It is found directly by inserting resistance in the input of the tube until the mean-square input noise is doubled. Again taking into account a small correction for thermal agitation, it should be clear that this resistance is precisely  $R_{\text{eff}}$ . The method is probably unequalled as a swift, accurate scheme for rating tubes for signal-to-noise ratio. Its adaptation to studies of diodes has obvious drawbacks. For this reason, and because the present work is mostly concerned with testing theory, the other methods were preferred as more direct.

The comparator diode was essentially a copy of miniature diodes previously designed in this laboratory for short-wave work.<sup>1</sup> A nickel anode 6 millimeters long, and having a diameter of 15 mils, surrounded a 3-mil tungsten filament. With about 80 volts on the anode, currents of 2 or 3 milliamperes were unquestionably temperature-limited. For most measurements on radio-frequency receiving tubes, this proved to be ample current.

Although  $\Gamma_{\text{exp}}$  can be compared with  $\Gamma_{\text{theor}}$ , it is somewhat simpler to find  $\theta_{\text{exp}}$  and compare this with  $\theta_{\text{theor}}$ , which has been shown to be essentially a constant. At least it does not exhibit the wide variation that  $\Gamma_{\text{theor}}$  shows with change in operating conditions. The value of  $\theta_{\text{exp}}$  can be computed from, e.g., (58) and (43a) or (43b).

To make either test of theory, it is necessary to determine cathode temperature. Now this is one of the most awkward tasks if high accuracy is demanded. But if, as in the present studies, one is satisfied with experimental errors of 4 or 5 per cent, estimates of temperature accurate to well within these limits can be procured, at least for the more conventional structures which have a not-too-uneven temperature distribution. Filament temperatures were, therefore, computed from information found in "The Characteristics of Tungsten Filaments as Functions of Temperature".<sup>2</sup> A Leeds and Northrup optical pyrometer was used for early estimates of the temperature of sleeve-type cathodes. This was soon discarded; it was virtually impossible in many instances to get a direct line of sight. The temperature was subsequently computed from a measurement of heater power by means of the equation for temperature radiation. Extensive studies by E. G. Widell of these laboratories had shown that the fourth-power law was essentially valid for this type of cathode, and had permitted determination of emissivities. The working formula, developed from his studies and applicable to the present investigation, is

$$\frac{T}{1000} = \left[ 533 \frac{W}{dl} \right]^{1/4},$$

where  $W$  is heater power in watts,  $d$  is diameter in mils, and  $l$  is length in millimeters. This formula accurately applies only to the center "brightness" temperature of a type 6C6 cathode coated with a particular spray. Error due to cooling at the ends ( $50^\circ$  to  $100^\circ$ ) is largely offset by the fact that "brightness" temperature runs about  $30^\circ$  to  $40^\circ$  below true temperature. The formula is naturally somewhat altered

<sup>1</sup> L. S. Nergaard, "Electrical Measurements at Wave Lengths Less Than Two Meters", *Proc. I.R.E.*, Vol. 24, p. 1207, September, (1936).

<sup>2</sup> H. A. Jones and I. Langmuir, *Gen. Elec. Rev.*, June-August, 1927.

by changes in length, diameter, percentage of uncoated area at ends, type of base material, thickness and type of spray, and proximity of other bodies. For all sleeve-type cathodes discussed in the present paper such changes are minor, and the formula is believed to give their true average temperature with an error of less than 3 per cent.

Although the noise analysis is based upon a parallel-plane model, tests were conducted on cylindrical structures alone. Simplicity of con-

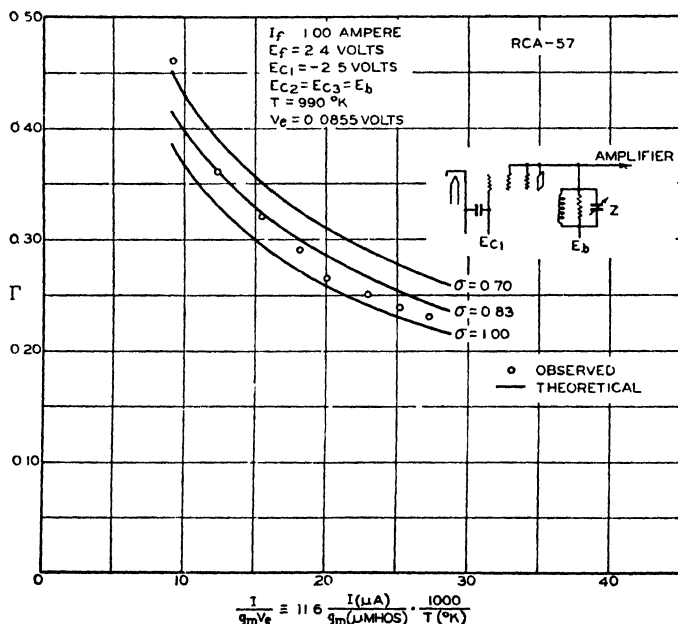


Fig. 10—Reduction of shot effect in cathode current of RCA-57 operated as a triode. The cathode current ranges from  $\frac{1}{2}$  to 4 milliamperes.

struction, minimum end effects, and ease of temperature determination all suggested the choice. Then, too, since commercial tubes are in the main cylindrical, it was hoped that the theory might be shown adequate for engineering purposes. Of course, many cylindrical tubes would be expected to behave essentially according to parallel-plane theory. The question becomes acute only in certain instances, e.g., filamentary cathodes, or especially large diameter ratios.

## RESULTS

From a large group of observations on many commercial tube types, the following examples are chosen as typical. And although diodes would naturally be expected to receive first discussion, regular ampli-

fying tubes will be given precedence, for reasons which will shortly be self-evident.

A precise test of theory against performance of amplifiers demands a determination of  $\sigma$ . It is unfortunate that there is no apparent way to measure this quantity directly; one is consequently forced to make estimates of  $\sigma$  from expressions such as (51), and tests of theory lose rigor thereby. However, it has been mentioned that  $\sigma$  will ordinarily lie between narrow limits, and estimates made for tubes of even very irregular design can be presumed accurate to well within 15 per cent.

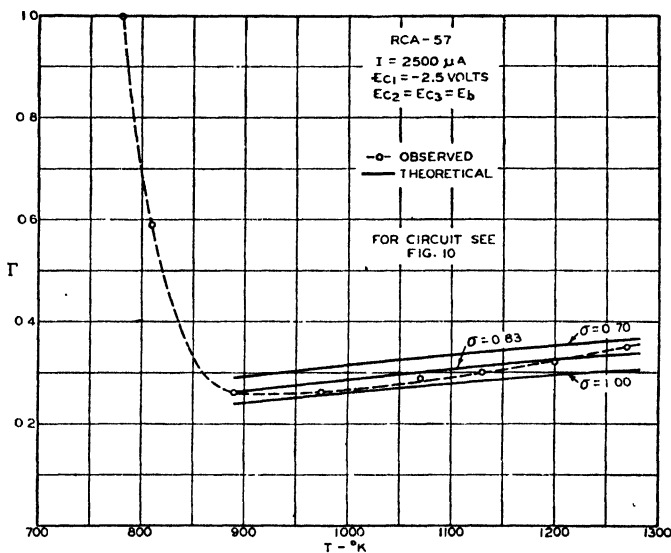


Fig. 11—Reduction of shot effect in cathode current of RCA-57 operated as a triode, for  $I = 2.5$  ma and various cathode temperatures.

If, with this tolerance, there is seen to be good agreement with theory, there is much to recommend it, in view of the order-of-magnitude discrepancies typical of the past.

Tables IV and V and Figures 10, 11, and 12 all refer to the same tube, a regular RCA-57. This is a radio-frequency pentode amplifier which, for these measurements of cathode-current fluctuations, was operated in triode fashion, the screen, suppressor and plate being tied together as shown in Figure 10. Although the first two grids are elliptical, it is possible to make a good estimate of  $\sigma$  from (51). And because the  $\mu$  is high (approximately 20 as a triode) and the transit-time ratio small, the estimated value ( $\sigma \approx 0.83$ ) is not much below the ideal value of unity, and is virtually constant over the range of measurement.

TABLE IV  
RCA-57 (Serial No. F-10)

$I_f = 1.00$ ampere						$V_s = 0.0855$ volts			
$E_f = 2.4$ volts						$E_{c1} = -2.5$ volts			
$T = 990^\circ\text{K}$						$E_{c2} = E_{c3} = E_b$			
$E_f$ volts	$I$ $\mu\text{a}$	* $g_m$ $\mu\text{mhos}$	$I_c$ $\mu\text{a}$	$I/g_m V_s$	$\Gamma_{exp}$	$\Gamma_{theor}$			$\theta_{exp}$ $\sigma = 0.83$
						$\sigma = 0.70$	$\sigma = 0.83$	$\sigma = 1.00$	
75	500	640	108	9.14	0.46	0.45	0.415	0.38	0.81
85	1000	950	150	12.3	0.36	0.39	0.36	0.33	0.66
95	1500	1140	150	15.4	0.32	0.35	0.325	0.30	0.64
103	2000	1290	165	18.1	0.29	0.33	0.30	0.27	0.62
108	2500	1460	175	20.0	0.26	0.31	0.285	0.26	0.58
115	3000	1530	185	22.9	0.25	0.29	0.265	0.24	0.58
121	3500	1630	200	25.1	0.24	0.28	0.25	0.23	0.59
127	4000	1720	205	27.2	0.23	0.26	0.24	0.22	0.58

\* As triode

$$\dagger \theta_{exp} = \frac{\sigma}{2} \cdot \frac{\Gamma_{exp}}{\Gamma_{theor}} \cdot \frac{I}{g_m V_s}, \text{ from (43b).}$$

TABLE V  
RCA-57 (Serial No. 7-10)

$I = 2500 \mu\text{a}$									
$E_{c1} = -2.5$ volts									
$E_{c2} = E_{c3} = E_b$									
$T$ $^\circ\text{K}$	$E_b$ volts	* $g_m$ $\mu\text{mhos}$	$I_c$ $\mu\text{a}$	$I/g_m V_c$	$\Gamma_{exp}$	$\Gamma_{theor}$			$\theta_{exp}$ $\sigma = 0.83$
						$\sigma = 0.70$	$\sigma = 0.83$	$\sigma = 1.00$	
780†	250	75	2500	430	1.0	1	1	1	‡
810	128	1050	880	34.1	0.59		1		‡
890	114	1400	165	23.3	0.26	0.29	0.26	0.24	0.63
975	108	1460	175	20.4	0.26	0.31	0.28	0.255	0.59
1070	103	1500	205	18.1	0.29	0.325	0.30	0.27	0.62
1130	99	1530	230	16.8	0.30	0.34	0.31	0.28	0.64
1200	95	1540	250	15.7	0.32	0.35	0.325	0.295	0.65
1270	91	1590	300	14.4	0.35	0.365	0.335	0.305	0.72

\* As triode.

† Lowest  $T$  which, for  $E_b = 250$ , gave  $I = 2500 \mu\text{a}$ . The tube was, therefore, essentially temperature-limited, as indicated by the low  $g_m$ .

‡ Not within the scope of the present analysis, since  $I/I_c$  is not sufficiently small. Following figures are evaluated under assumption that the analysis does apply, i.e.,  $I/I_c < 1$ .

With fixed control-grid bias and constant cathode temperature, the currents shown in column 2 of Table IV were procured by adjusting anode voltage, column 1. The transconductance was measured, column 3, and the noise measurement is represented by the comparator-diode current in column 4. Column 6 was computed from (58), and column 5 from the data shown. If now a value is assigned to  $\sigma$ , and it is multiplied by values in the fifth column,  $\Gamma_{\text{theor.}}$  can be read directly from Figure 6, since

$$\frac{\sigma I}{g_m V_c} = \frac{I}{g V_c}.$$

The next three columns were constructed in this manner and, together with  $\Gamma_{\text{exp}}$ , are plotted in Figure 10. The curves for  $\sigma = 1.00$  (ideal) and  $\sigma = 0.70$  are included to indicate the spread occasioned by varia-

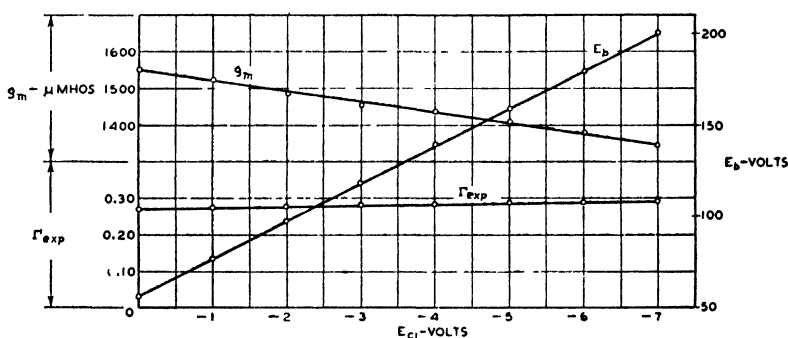


Fig. 12—Reduction of shot effect in cathode current of RCA-57 operated as a triode, for  $I = 2.5$  ma,  $T = 990^\circ\text{K}$ , and various control-grid biases.

tions in  $\sigma$ , or the possible discrepancies arising from inaccuracies in making its estimate.

Since  $I_s$  for this cathode temperature is well over 150 milliamperes, the current  $I$  could have been carried higher but was kept low on principle to avoid any doubt as to the observance of the stipulation,  $I/I_s \ll 1$ . The temperature,  $990^\circ\text{K}$ , is normal for this tube. Many similar runs of this kind at neighboring temperatures showed equally good agreement with theory.

In order to illustrate the course of  $\Gamma$  when  $T$  is varied, and also to show the transition from temperature-limited to fully space-charge-limited currents, the data of Table V and Figure 11 are presented as a typical example selected from many similar groups of data. The circuit was unchanged. But in this instance, with a fixed  $I$  (maintained

by adjustment of  $E_b$ , the cathode temperature was varied, column 1. For the lowest temperature, the tube was virtually temperature limited.<sup>1</sup> For the two lowest temperatures no comparison with the theory of this paper is permissible, in view of the high value of  $I/I_s$ . The remaining data agree very well with theory, even exhibiting the predicted upward trend of  $\Gamma$  with increasing  $T$ . It is evident that, for this current, the tube should be operated with a cathode temperature of about 950°K, but that there is only a minor departure from the optimum  $\Gamma$  if  $T$  is permitted to deviate 100° to either side. The undesirability of too low a cathode temperature is impressively patent in the sharp rise to unity which characterizes the extreme left portion of this and all other  $\Gamma$ -curves of similar construction.

The plot is carried to only 1300°K for the simple reason that at higher temperatures measured noise exceeds the theoretical prediction by steadily increasing amounts. In itself this is hardly an excuse for discarding the phenomenon as non-pertinent, particularly after it is remarked that the behavior is characteristic of *all cathodes operated at temperatures several hundred degrees above normal*; this is true of tungsten, thoriated-tungsten, and coated cathodes alike. It has often been conjectured that the anomaly can be ascribed to emission of positive ions which, while pursuing a leisurely and long-lived course through the virtual cathode, control the destiny of multitudes of electrons. Evidence supports the view: (a) large-scale impulses appear simultaneously in the output meter; (b) the noise still approaches that predicted for true shot effect when the tube is made temperature-limited, i.e., when there is no virtual cathode upon which ions may react; (c) the change in excess noise with variation of temperature, and with time at a fixed temperature, is, in a qualitative manner, precisely that which would be expected on this hypothesis. Since the ion currents involved are much too small to detect by ordinary means, and since a quantitative analysis of the interaction of such ions with space-charge is much too laborious to promise immediately useful results, the theory remains in a semi-speculative state. The supporting evidence nevertheless appears to the author to justify exclusion of such data from tests of the theory of this paper. In Figure 11 it may be that part of the rise in  $\Gamma_{\text{exp}}$  with increasing temperature can, even here, be ascribed to this source.

---

<sup>1</sup> The fact that  $g_m$  is not precisely zero does not contradict this assertion. A phenomenon of this nature, probably akin to Schottky effect is characteristic of coated cathodes. In contrast with the behavior of metallic emitters, coated cathodes exhibit no decisive saturation voltage, but only a gradual change in slope of the  $I$  vs.  $V$  curve. Measurements of  $I_s$ , which would perfect the picture presented by Tables IV and V, are for this reason doubtful and deliberately omitted.

Table V deserves final comment. The reader may already have wondered why, with  $I$  fixed,  $E_b$  continues to decrease,  $g_m$  to increase, even after  $I_s \gg I$ . This behavior is best seen in terms of the equivalent diode which, stripped to essentials only, consists of the space between the virtual cathode and the control grid. Roughly speaking, then,

$$I \propto (E_a - E_m)^{3/2} \cdot d_{am}^{-2}$$

$$g_m \propto I^{1/3} \quad d_{am}^{-1/3}.$$

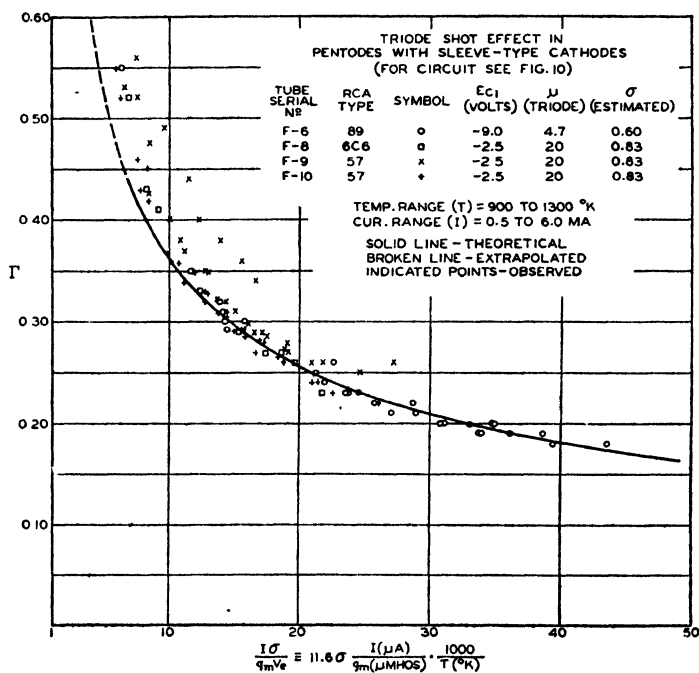


Fig. 13—Collected shot-effect data for a representative group of tubes with sleeve-type cathodes.

With constant  $I$ , an increase in  $T$  and  $I_s$  makes  $E_m$  more negative and decreases  $d_{am}$  (space between control grid and virtual cathode). The latter change accounts for an increase in transconductance. In the first expression both changes tend to increase  $I$ , and this necessitates a reduction in  $E_a$ , which, in turn, accounts for the decrease in  $E_b$ .<sup>1</sup> In order that the reader may have a correct appreciation of the magnitude and position of the virtual cathode, he may imagine a parallel-plane analogue to the equivalent diode of a type 57 under normal operating

<sup>1</sup> Unpublished work of H. R. Nelson of these laboratories suggests that the drop in potential may also be traced, in part, to thermo-electric emf's between cathode base metal and coating.



conditions. Assuming  $I = 3$  milliamperes per square centimeter,  $I/I_s = 1000^1$ ,  $d = 0.05$  centimeters, and  $T = 1000^\circ\text{K}$ , the effective anode potential will be about 0.6 volt ( $E_a = 0.6$ ), and the virtual cathode will be approximately 0.6 volt deep ( $E_m = -0.6$ ) and will be found at about  $\frac{1}{5}$  the distance from cathode to grid.

Figure 12 is included to demonstrate that, for fixed  $I$ , measured shot effect is independent of negative grid bias. This is in agreement with theory, for the quantity  $I/gV_c$  which determines  $\Gamma_{\text{theor}}$  depends, not upon  $E_{c1}$  and  $E_b$  in themselves, but upon  $V_a$  which, if the current is to be held constant, must be invariant against alteration in electrode potentials. The course of  $E_b$  and of  $g_m$  is also shown. A small drop in the latter with increasing negative grid bias is normal, arising simply from non-uniformity of  $\mu$ , i.e., effects due to grid support rods and grid ellipticity.

The agreement with theory which this tube exhibits is duplicated by tests on other tubes of the same general design. Figure 13 permits comparison of theory with approximately 100 observations of cathode-current fluctuations in four tubes. The 6C6 differs significantly from the 57 only in its heater resistance; the 89, on the other hand, is a low- $\mu$  power-amplifier pentode operated at well below its rated current, and is included to demonstrate the applicability of theory to tubes having a  $\mu$  as low as even 5. Its grids are also elliptical, but a reasonably accurate estimate indicates that  $\sigma$  is about 0.6. This figure is lower than the 0.83 estimate given for the type 57 simply because the  $\mu$  is much lower. The series of seven observations on F-9 showing the largest discrepancy on the left-hand side of the figure were all taken with  $T = 1280^\circ\text{K}$  which is 70 higher than any other temperature for the data of this figure, and roughly  $300^\circ$  higher than the rated temperature for this tube. The discrepancy is, therefore, ascribed to incipient positive-ion emission. Although  $\sigma$  was assumed constant in constructing the plot, it should be remembered again that this is not exactly true. The common tendency of all points on the left-hand side to surmount their theoretical positions is possibly due to a lowering of  $\sigma$  for small currents as a result of the non-uniformities in  $\mu$  mentioned above.

No such general accord with theory can be found in observations on these tubes operated as diodes. (In "diode" operation, all electrodes

---

<sup>1</sup> That this is a reasonable choice of  $I_s$ , and representative of conventional oxide-coated cathodes, is supported by actual measurement; cf. B. J. Thompson, "High Efficiencies of Emission from Oxide-Coated Filaments", *Phys. Rev.*, 36, p. 1415; October, (1930). Although these measurements give too high a value of zero-field emission, on account of Schottky effect and surface inhomogeneities, they are probably high by a factor no greater than 10.

but the cathode were tied together; in other respects the circuit was unaltered.) Although the shot effect is still reduced by space-charge, it always exceeds the predicted amount. For very small currents, at the threshold of region (d) in Figure 7, the predicted shot effect is closely approached; with increasing current the mean-square noise exceeds the theoretical value by a steadily increasing factor. Figure 14 is representative of the relative behavior of "diode" as compared

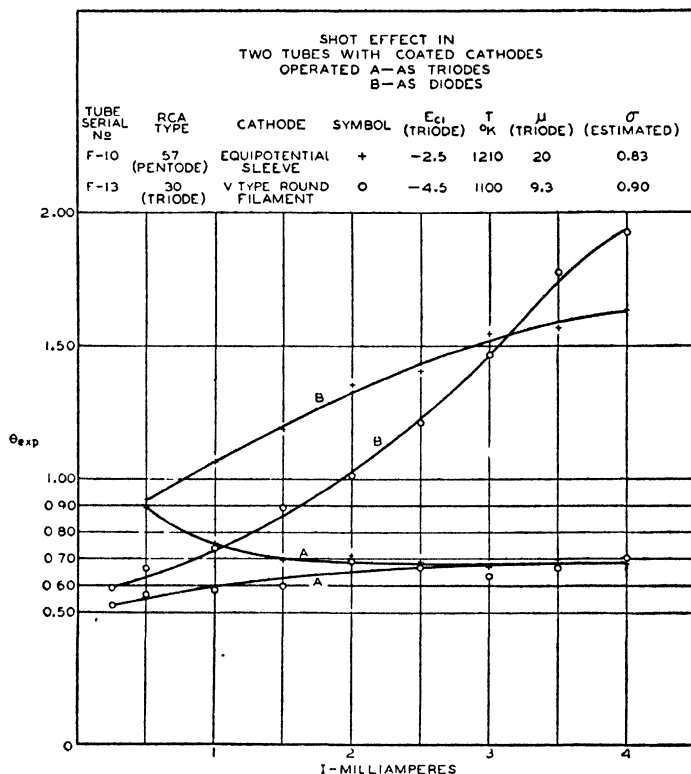


Fig. 14—Comparison of "diode" and "triode" shot effect in two regular tubes with coated cathodes.

with "triode" shot effect in amplifying tubes. Considering first the curves for F-10 (the same RCA-57 discussed above), note that the "triode" noise shows a  $\theta_{exp}$  which agrees closely with the theoretical value of approximately  $\frac{2}{3}$ . The "diode" noise, on the other hand, shows a  $\theta_{exp}$  which steadily increases with current. It should be remarked that, although the same  $\sigma = 0.83$  was assumed for plotting, the "diode"  $\sigma$  should properly have been chosen very slightly smaller on account of an increase in "h", (51); but this correction, while in the right direction, would by no means account for even a

significant fraction of the excess noise. The second pair of curves belongs to a triode with a coated V-filament (RCA-30). The same extraordinarily high noise for large (but not abnormally high) currents is evident in the "diode" case. For both tubes the factor of disagreement is, at 4 milliamperes, not trivial, but rather an order of magnitude. The curve for "triode" noise of the RCA-30 is, incidentally, of interest in its own right, for it indicates that the parallel-plane formula applies to a structure even so remotely related as this one which, despite a flat grid and plate, has a cathode similar in no respect to the plane surface employed for analysis.

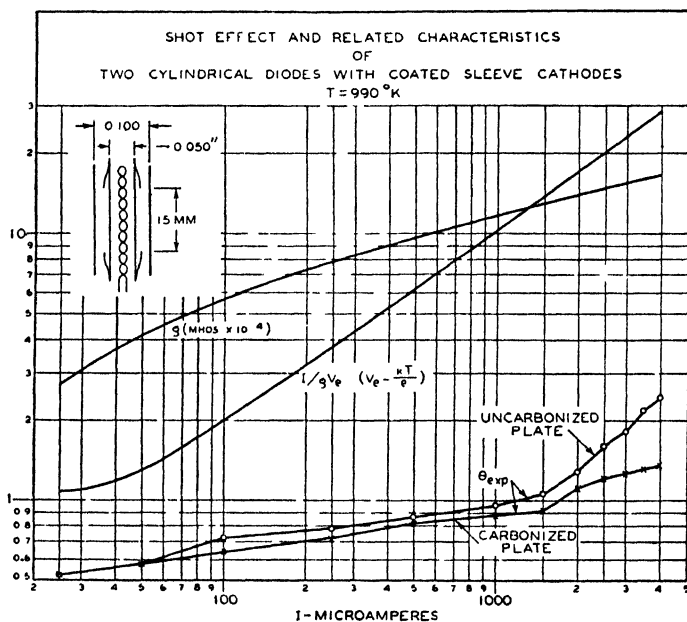


Fig. 15

Although one might conjecture that the anomalous "diode" noise is somehow obscurely connected with the presence of grids, such a notion is disqualified by measurements on actual diodes. Essentially the same results were observed in every instance. In an attempt to duplicate the theoretical model as closely as could be achieved with a cylindrical structure, two diodes were built as designed in Figure 15. A cylindrical coated cathode of 50 mils diameter was fitted at each end with short guard sleeves of thin nickel tubing, leaving a central exposed length of 15 millimeters. Both anodes were nickel of 100 mils diameter; one was hydrogen-fired at about  $1100^\circ\text{C}$ , the other carbonized. Both tubes gave ample emission at  $T = 990^\circ\text{K}$ , and their current-voltage curves were so nearly alike that the plots of  $g$  and  $1/gV_e$  in Figure 15

refer to either. The general course of these curves agrees very well with predictions based upon the steady-state equations for parallel-plane structures discussed above. No plot of voltage is shown since accurate absolute measurements were difficult in view of the small voltages required. The maximum voltage ( $I = 4$  milliamperes) was estimated to be about 3.2 volts, corrected for contact potential. Calculation shows that currents below about 50 microamperes were collected in a retarding field. The curves for  $I/g V_c$  and  $\theta_{\text{app}}$  approach the theoretical limits 1 and  $1/2$  quite closely at the lowest current measured, 25 microamperes. There was, therefore, every reason to expect the shot effect to follow theory for larger currents. And yet  $\theta_{\text{app}}$  is seen to rise steadily with current for both diodes just as it did for amplifying tubes in diode connections.

This strange behavior can, in the writer's opinion, be interpreted wholly in terms of a small amount of elastic reflection at collecting surfaces. Electrons returned to the vicinity of the virtual cathode as a result of either scattering or reflection will, of course, alter its potential and tend to decrease the steady-state flow of emission current across the barrier in a fashion strictly analogous to the process by which temperature-limited shot fluctuations are compensated and reduced by space-charge. The reflection hypothesis is chiefly concerned with those electrons which are elastically reflected or nearly so; an electron which loses more than a fraction of a volt on collision can not return sufficiently close to the virtual cathode to do damage at all comparable to the havoc promoted by those which actually pass through the virtual cathode a second time. It is impossible to handle this problem with quantitative rigor, but a crude notion of magnitude may be had. Consider a unit increase in the emission of electrons in a particular velocity class. Without space-charge compensation there would follow a unit increase in anode current. Our analysis has shown, however, that in the presence of a virtual cathode, there flows a compensating current  $-(1-\gamma)$ . The net increase in anode current is then  $[1-(1-\gamma)] = \gamma$ . But suppose, to exaggerate a little, that all of the original electrons are reflected back to the cathode to start out again and finally be captured on the second attempt. The net increase in anode current will be, in this event, something like

$$[1-(1-\gamma)-(1-\gamma)-(1-\gamma)] = -2 + 3\gamma.$$

If  $\gamma$  for this velocity class is, say 0.25, the net increase in anode current turns out to be  $-1.25$  instead of  $+0.25$ . On a mean-square basis, the reflection of electrons has resulted in over-compensation to such an extent that the noise has been increased twenty-five fold. Now a brief calculation along these lines shows that if so little as 10 per cent of the

*total* anode current is reflected as described, the *total* mean-square shot effect is increased by a factor of 3 or more in a diode comparable to those of Figure 15 and carrying three or four milliamperes current. It is logical that the factor should increase with  $I$ , for the quantity  $\Gamma$  decreases (see Figure 5), so that, supposing the coefficient of reflection to vary but little with an increase in anode potential, in the light of the example just discussed, the trend is obvious.

The precise amount by which noise will be increased by electron reflection depends upon too many factors to permit accurate prediction. Structure, nature of the electric field, electrode potentials, character of the reflecting surfaces, all are involved in a complex manner. Yet the chief features of the experimental difference between "diode" and "triode" noise are thus simply interpreted. For in the first place, a negative grid leaves smaller opportunity for anode-reflected electrons to return to the virtual cathode. But, more important, above a certain low critical potential a fairly high percentage of elastically reflected primaries drops to practically nothing. It is difficult to find much experimental evidence in point amongst the quantities of literature concerned with secondary emission, most of which is devoted to inelastic encounters and to emission of true secondaries, characterized by very low energies. But in one of Farnsworth's papers<sup>1</sup> the precise experimental information desired may be found. Of several conclusions which he draws from his measurements of the energy distribution of secondaries from *Cu*, *Fe*, *Ni*, and *Ag* the second is of present concern: "For primary voltages below a certain limiting value, which varies with the metal, most of the secondary electrons have energies approximately equal to the primary energy". Measurements of secondary energies for these four metals are much alike, and of the four *Ni* appears to reflect least. The table given here is constructed from his data for *Ni* and shows for each primary voltage  $V$  the per cent of the primary stream which appears in the secondary stream as electrons possessing within one-half volt of the primary energy.

$V$	6.2	10.4	18.6	33.5	50.0
%	12	11	9	6	5

It must be remembered that these data apply only to a specific surface put through a specific heat treatment, and cannot be considered

<sup>1</sup> H. E. Farnsworth, "Energy Distribution of Secondary Electrons from Copper, Iron, Nickel, and Silver", *Phys. Rev.*, Vol. 31, p. 405, March, (1928). In Compton and Langmuir's "Electrical Discharges in Gases", *Rev. Mod. Phys.*, Vol. 2, p. 171, April, (1930) will be found a brief factual background, but elastic and inelastic reflections are not clearly distinguished.

strictly representative of other samples. But the order of magnitude supports the hypothesis under discussion.

One might naturally expect to ascribe the difference between  $\theta_{\text{exp}}$  for the two tubes of Figure 15 to a reduction in elastic reflection as a result of carbonization. Subsequent experiments supported the notion. To separate out the possible alteration of reflection coefficient as a result of deposition of cathode material during activation, two diodes were constructed with dimensions similar to those of Figure 15, except that these had slidable nickel anodes. One anode was wholly carbonized; of the other, one-half was carbonized and the remainder was left "clean". The first showed substantially the same noise for

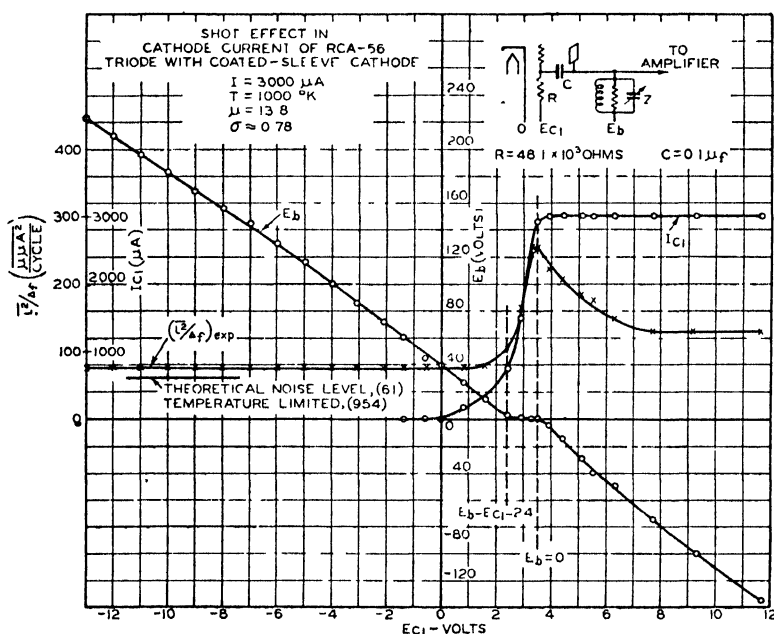


Fig. 16—Effect of electron reflection and scattering upon space-charge-reduced shot effect in a triode: constant cathode current.

either position of the anode, indicating that deposition of cathode material upon a carbonized anode during normal activation alters the reflection coefficient (of the kind in question) a negligible amount. The other, activated with the carbonized section exposed to the cathode, showed a slightly higher noise when the "clean" section was used. Even here, just as in Figure 15, the carbonized anodes showed noise far in excess of theoretical estimates; it is concluded that slow speed (2- or 3-volt) electrons are *reflected elastically* almost as profusely from a carbonized surface as from a clean one.

Further support for the hypothesis of noise augmented by reflected electrons is found in Figure 16. By operating a triode with grid positive and anode negative, one obtains an artificial electron reflection. All electrons that miss the grid on first passage are returned, and many of these may miss a second time and continue back to the cathode. The figure shows in panorama the entire course of shot effect in a constant cathode current for anode voltages running from high positive to high negative values. The construction of the RCA-56 differs little from that of the RCA-57 except that a carbonized anode replaces the 57's screen grid, and a smaller  $\mu$  (13.8) brings  $\sigma$  down from an estimated 0.83 to 0.78. The circuit sketch shows how grid and anode could be given individual bias voltages and yet operated as a unitary electrode for radio frequencies so that, even though the cathode current was at times divided between the two, fluctuations in cathode current ( $I$ ) were measured under all circumstances. Bias voltages were measured at the electrodes, were not corrected for contact potential, and for small values are therefore not precise. The trend of  $E_b$  vs.  $E_{c1}$  is normal; in particular the kink accompanying the approach of  $E_b$  to zero from the positive side is familiar and has long been correctly attributed to a sudden lowering of space potential due to the abrupt return of much of the anode-directed current to the vicinity of the virtual cathode. The noise, which for normal biases remains very constant and approximates the theoretical value, rises sharply to a peak at precisely the point at which it would be expected to do so. This maximum is considerably higher than the "diode" noise, at  $E_b = E_{c1} = 2.4$  volts. The ultimate decline as more and more electrons are trapped at the grid on first passage, and the finally levelling off need little comment.

Finally, some observations on diodes with thoriated-tungsten cathodes should be mentioned. A 4-mil filament was used with a nickel anode of 100 mils diameter, either carbonized or not. At temperatures providing emission sufficient to remove suspicion from the ratio  $I/I_s$ , the behavior was much the same as that exhibited in Figure 15, including a decrease in noise with carbonization. Further,  $\theta_{\text{exp.}}$  for these was, for the higher currents, always a little less than shown in Figure 15; with  $I = 3.5$  milliamperes,  $\theta_{\text{exp.}} = 1.95$  and 1.15 for these diodes, uncarbonized and carbonized, while  $\theta_{\text{exp.}} = 2.19$  and 1.31 for their coated-cathode brothers. A reflected electron finds the virtual cathode less easily when the cathode has a diameter of 4 mils instead of 50 mils.

However unsatisfying it may be that the theory should agree but poorly with measurements on the simplest structures patterned closely after the model upon which the analysis was based, we conclude that there is generally excellent agreement between theory and observations

of cathode-current shot effect in tubes operated with negative control grids. The formulas developed serve well as accurate engineering guides to construction of low-noise tubes for class A operation. And where experiment has shown the theory to be inapplicable, the hypothesis of elastic reflection appears adequate to account for discrepancies. The nature of cathode-current fluctuations, for small transit angles, is now thought to be well understood. The complexities which are added to the situation when the cathode current is divided and the noise measured in one portion only, for example in the plate current of a pentode, form the subject of the succeeding pages.



## PART III—MULTI-COLLECTORS

BY DWIGHT O. NORTH

*Summary*—The fluctuations in cathode current ( $I_a$ ) due to true shot effect in cathode emission are

$$\overline{i_k^2} = \Gamma^2 (I_a \cdot 2e\Delta f).$$

$\Gamma$  is a factor, evaluated in Part II, equal to unity when the current is temperature-limited, but ordinarily only about 0.2 under normal space-charge-limited conditions.

Theory here presented shows that fluctuations in the current ( $I_n$ ) to the  $n^{\text{th}}$  collector of a device possessing several collectors for the cathode current are, in general, improperly represented by the expression,

$$\overline{i_n^2} = \frac{I_n}{I_a} \overline{i_k^2},$$

but correctly by the following formula:

$$\overline{i_n^2} = \left[ 1 - \frac{I_n}{I_a} (1 - \Gamma^2) \right] (I_n \cdot 2e\Delta f).$$

In connection with suppressor-grid pentodes, for which it is generally true that  $\Gamma^2 \ll I_{c2}/I_b$ , the formula for shot effect in either screen or plate lead (with input grounded) is

$$\overline{i_{p2}^2} \approx \overline{i_p^2} \approx \frac{I_{c2} I_b}{I_a} \cdot 2e\Delta f.$$

The noise in the plate lead is, then, usually higher than that in the cathode lead, and this fact accounts in large measure for prevalent observations that pentodes are usually inferior to triodes from purely a noise standpoint.

Experimental work is described, supporting the theory.

Combination of this theory with that of Part II yields a practical working formula for the apparent input shot effect of a conventional pentode amplifier with coated cathode and negative control grid. Expressed in terms of an ohmic resistance ( $R_{eff}$ ) at room temperature (300°K), the thermal agitation of which is equal to the apparent input shot effect, the formula is

$$R_{eff} \text{ (pentode)} = \left[ 1 + 8.7 \sigma \frac{I_{c2}}{g_m} \cdot \frac{1000}{T} \right] \cdot R_{eff} \text{ (triode)}$$

$$\text{where } R_{eff} \text{ (triode)} = \frac{2.2}{\sigma} \cdot \frac{T(^{\circ}\text{K})}{1000} \cdot \frac{I_s}{I_a} \cdot \frac{1}{g_m}$$

*T* is cathode tempature in  $^{\circ}\text{K}$ ,  $g_m$  is pentode transconductance in micromhos,  $I_a$  is the screen current in microamperes, and  $\sigma$  is the ratio of total transconductance to conductance of the "equivalent diode."

### THEORY

THE phenomena peculiar to shot-effect fluctuations in a space-charge-limited device which possesses more than one collector have been outlined in Part I. If a pentode, for example, is space-charge-limited, the shot effect in the anode lead is often much in excess of an estimate based upon a simple division of cathode current fluctuations similar to the division of the cathode current itself. In *tetrodes* such a behavior might *ab initio* be ascribed, at least in part, to additional noise associated with secondary-emission current circulating among the collecting electrodes. The analysis and experiment presented below are confined to arrangements in which secondary emission plays no role. In fact we shall be concerned with only an extension of the concepts and formulas of Parts I and II.

Any electron in transit alters the potential of the virtual cathode as explained earlier. This slight depression of the potential minimum is by no means localized but extends over a region the linear dimensions of which are, loosely speaking, comparable to the distance between cathode and anode of the "effective diode". It is beyond the purposes of this paper to examine the precise geometrical scope of the potential variation at the virtual cathode, but it should be evident that the concomitant variation in the steady-state cathode current  $I$  possesses a comparable geometrical spread. In this way it comes about that, at times, the compensatory flow of current which accompanies and tends to reduce an initial fluctuation in emission (yielding the  $\Gamma$  of Part II) does not all arrive at the same collecting electrode to which the initial fluctuation may be consigned, but is divided among the several collectors. Consequently, the fluctuation in the electrode named is not fully reduced, while in the other electrodes there flows simultaneously a "compensating" current for which there is no antecedent. The mean-square fluctuations in each electrode are, therefore, in excess of an estimate based upon a simple apportioning of the cathode current fluctuations. At any instant the sum of the linear fluctuations in all collector currents is still, naturally, equal to the fluctuation in cathode current. But the sum of the mean-square current fluctuations in the former is *greater than* in the latter.

Let us consider in detail two extreme examples of cathode-current division. The behavior of these will set natural limits encompassing the performance of all others. In Figure 1a the collectors are to be considered so close to the cathode (in comparison with their linear dimensions) that there is virtually no region of the cathode from which current is delivered to both collectors. Except in the immediate vicinity of the boundary common to the collectors this will be strictly true. Hence, by extending the cathode and collectors laterally the ideal can be approached as closely as desired. These collectors now operate independently and their performance will be altered in no way whatsoever if the cathode be split also and the two diode systems sep-

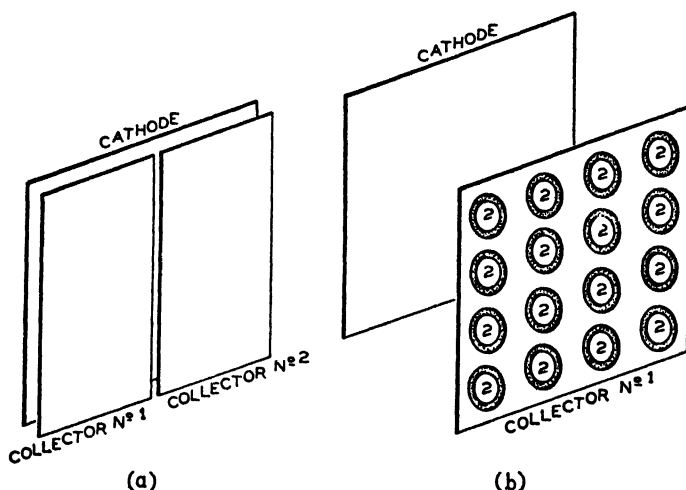


Fig. 1.—Extreme examples of a multi-collector.

arated. Employing the notation of Part II, we may therefore write the shot effect in each collector as follows:

$$\left. \begin{aligned} \overline{i_1^2} &= \Gamma_1^2 \cdot 2eI_1\Delta f = \theta_1 \cdot 4kTg_1\Delta f \\ \overline{i_2^2} &= \Gamma_2^2 \cdot 2eI_2\Delta f = \theta_2 \cdot 4kTg_2\Delta f. \end{aligned} \right\} \quad (1)$$

In short, there is nothing novel here; each collector current shows a shot effect prescribed by the analysis of Part II, and the sum of the mean-square fluctuations in the two anode currents, measured separately, is equal to the mean-square fluctuation in the anode current of the device when the two collectors are tied together.

Proceeding to the opposite extreme, we find in Figure 1b a scheme in which all the little discs (2) constitute one collector, the other consisting of the remanent sheet. If now the number of discs is thought to become exceedingly large while, at the same time, the area of each

is proportionately diminished so that the currents  $I_1$  and  $I_2$  are unaltered, another ideal situation is approached. It has the following significant properties:

1. The current to either collector is composed of electrons which, at the virtual cathode, exhibit a *precise* Maxwell-Boltzmann distribution of velocities.

2. The depression of virtual-cathode potential which accompanies the passage of any electron (from whatever point on the cathode it emerges) gives rise to a "compensating" current which is *always* divided between the collectors in proportion to their steady-state currents  $I_1$  and  $I_2$ .

The scheme can be generalized to  $N$  collectors, and this we shall analyze. The cathode current will be

$$I = \sum_1^N I_n. \quad (2)$$

Assuming that all electrodes are grounded with respect to noise frequencies, let us determine the net current fluctuations in the  $n^{\text{th}}$  collector. It is composed of three parts: A, fluctuations associated with true shot effect in those  $\beta$ -electrons<sup>1</sup> which are collected at the  $n^{\text{th}}$  electrode; B, fluctuations associated with true shot effect in those  $\beta$ -electrons which are collected at all other electrodes; C, fluctuations associated with true shot effect in the  $\alpha$ -electrons<sup>1</sup>.

A. Were it not for compensating action at the virtual cathode, the shot effect in  $I_n$  would be true shot effect originating wholly in random fluctuations in the emission of those  $\beta$ -electrons which reach  $I_n$ , namely,

$$\overline{i_n^2} = I_n \quad 2e\Delta f. \quad (4)$$

In the presence of a virtual cathode, it was shown in Part II that for each emission velocity  $v_s$ , there is a compensating action such that each fluctuation which contributes to (4) is *linearly* reduced by a factor  $\gamma_\beta$  (itself a function of  $v_s$ ). However, in contrast with the simple diode, it cannot now be said that an initial fluctuation of unit amplitude (1) gives rise to a "compensating" current *in the  $n^{\text{th}}$  electrode* of amplitude— $(1 - \gamma_\beta)$ . For the compensating flow is divided in proportion to the steady-state current distribution. Rather, each

---

<sup>1</sup> See Part II, pp. 444 and 451. The  $\alpha$ -electrons are those emitted with velocity insufficient to carry them over the virtual cathode. The remainder, the  $\beta$ -electrons, constitute the normal cathode current which is divided and collected at the  $N$  electrodes.

initial fluctuation which contributes to (4) is here linearly reduced by the factor  $\left[1 - \frac{I_n}{I}(1 - \gamma_\beta)\right]$ . The net fluctuations in  $I_n$ , due to true shot fluctuations in  $I_n$ , and averaged over the appropriate range of emission velocities,\* are, therefore,

$$\overline{i_n^2} = \left[1 - 2\frac{I_n}{I}(1 - \overline{\gamma}_\beta) + \left(\frac{I_n}{I}\right)^2 (1 - 2\overline{\gamma}_\beta + \overline{\gamma}_\beta^2)\right] I_n \cdot 2e\Delta f. \quad (4a)$$

B. A similar treatment starts with initial true shot fluctuations in the current to all collectors but the  $n^{\text{th}}$ , namely,

$$(I - I_n) \cdot 2e\Delta f. \quad (5)$$

Again, for each fluctuation which contributes to (5), there is a compensating flow which, for unit amplitude of the initial fluctuation,

produces a current in the  $n^{\text{th}}$  electrode of amount  $-\frac{I_n}{I}(1 - \gamma_\beta)$ .

Averaged over the same range of emission velocities, the contribution from this source to fluctuations in the  $n^{\text{th}}$  electrode is

$$\overline{i_n^2} = \left[\left(\frac{I_n}{I}\right)^2 (1 - 2\overline{\gamma}_\beta + \overline{\gamma}_\beta^2)\right] (I - I_n) \cdot 2e\Delta f. \quad (5a)$$

C. The initial true shot effect in the  $\alpha$ -electron current is

$$(I_s - I) \cdot 2e\Delta f, \quad (6)$$

where  $I_s$  is the total emission, so that  $(I_s - I)$  is simply that portion of the emission current which fails to cross the virtual cathode. And once more, for each fluctuation which contributes to (6) there is a disturbance of the virtual cathode potential and a consequent flow of current to the collectors, each collector receiving its share in proportion to the steady-state current it carries. Averaged over the appropriate range of emission velocities, the contribution from this source to fluctuations in the  $n^{\text{th}}$  electrode is

---

\* The averaging process will not be elaborated here. It is explained in detail in Part II, p. 450, from which it will be recognized that the  $\overline{\gamma_\beta^2}$  of (4a) is simply  $\Gamma_\beta^2$ , and that the  $\overline{\gamma_\alpha^2}$  of (6a) is similarly  $\Gamma_\alpha^2$ .

$$\overline{i_n^2} = \left[ \left( \frac{I_n}{I} \right)^2 \frac{1}{\gamma_n^2} \right] I \cdot 2e\Delta f. \quad (6a)$$

Provided there is no secondary emission, nor elastic reflection of the sort described in Part II, the total shot effect in the  $n^{\text{th}}$  collector is the sum of these three contributions, (4a), (5a), (6a). Remembering that

$$\Gamma^2 = \Gamma_n^2 + \Gamma_\beta^2,$$

we find for the total fluctuation:

$$\overline{i_n^2} = \left[ 1 - \frac{I_n}{I} (1 - \Gamma^2) \right] I_n \cdot 2e\Delta f. \quad (7)$$

The fluctuation in the cathode current is

$$\overline{i^2} = \Gamma^2 I \cdot 2e\Delta f. \quad (8)$$

Part II was devoted to a determination of  $\Gamma^2$ . At this point one needs only to recall that it runs from unity in the absence of a virtual cathode to the neighborhood of 1/20 for normal space-charge-limited operation of modern medium-gain receiving tubes.

The sum of the separately measured shot effects in all  $N$  collectors is

$$\sum_1^N \overline{i_n^2} = \left[ \Gamma^2 I + \frac{(1 - \Gamma^2)}{I} \sum_1^N I_n (I - I_n) \right] 2e\Delta f,$$

substantiating the remark above that the sum of the mean-square current fluctuations in the collector leads is greater than that in the cathode lead—unless either  $\Gamma=1$  (no virtual cathode, no compensating action), or one collector takes the entire cathode current (no problem).

Inspection of (7) leads to the following observations:

1. No fluctuation is greater than the true shot effect for the current considered.
2. The smaller fraction of the total current an electrode collects the more nearly the noise in that current approaches true shot effect.
3. For vanishingly small  $\Gamma$ , the mean-square fluctuation in the current collected at any electrode is equal to the product of the true shot effect for said current and the fraction of the cathode current *not* collected at said electrode.

4. The ratio of actual noise to true shot effect in a divided portion of the cathode current *exceeds* the corresponding ratio for the total cathode current.

5. The noise in a divided portion  $I_n$  of the cathode current *exceeds* the noise in the total cathode current provided

$$\frac{\Gamma^2}{1 - \Gamma^2} < \frac{I_n}{I} < 1.$$

In conventional tubes this is usually true for all collectors.

6. With constant  $\Gamma$ , the noise in a given collector current  $I_n$  is a maximum (against variations in  $I_n$ ) when

$$\frac{I_n}{I} = \frac{1}{2(1 - \Gamma^2)}.$$

In other words, provided  $\Gamma^2 < 1/2$ , the noise in *no* collector lead should exceed

$$\frac{1}{4(1 - \Gamma^2)} I \cdot 2e\Delta f.$$

#### APPLICATION TO PENTODES

The conventional suppressor-grid pentode is expressly designed to inhibit exchange of secondaries between screen grid and plate. Its performance can, therefore, be expected to lie within the extremes just discussed, provided there is no appreciable secondary emission from insulating surfaces, e.g., the envelope. The suppressor grid will be supposed to collect no current. It will also be supposed that the control grid is given a negative bias; from the viewpoint of this section a positive control grid would, of course, be regarded as just another collector, but it will generally introduce further complexities because of possible secondary emission to other electrodes, and, more important yet, the likelihood of elastic reflection resulting in an indeterminate increase in  $\Gamma$  of the sort described at length in Part II.

Tubes designed with no intent to align grids so as to produce electron beams, or, more specifically, to reduce the screen-grid current, would be expected *a priori* to perform very nearly like the idealized scheme of Figure 1b. For, scattering of electrons under the influence of the control-grid field, together with the lack of alignment, are sufficient reasons for supposing that the two important properties (p. 247) of the idealized structure are closely approximated. Even some tubes

of beam-forming design can be placed in the same category, but, in general, each device of this class should be accorded an individual examination.

Since subsequent experiments support these conjectures, it will be useful to cast (7) into pentode nomenclature. With the cathode current divided as follows,

$$I_a = I_{c2} + I_b, \quad (9)$$

and with all electrodes grounded with respect to noise frequencies, the shot effect in the cathode, the screen-grid, and the plate leads,<sup>1</sup> respectively, is

$$\left. \begin{aligned} \overline{i_k^2} &= \Gamma^2 (I_a \cdot 2e\Delta f) \\ \overline{i_{c2}^2} &= \frac{\Gamma^2 I_{c2} + I_b}{I_a} (I_{c2} \cdot 2e\Delta f) \\ \overline{i_p^2} &= \frac{\Gamma^2 I_b + I_{c2}}{I_a} (I_b \cdot 2e\Delta f) \end{aligned} \right\} \quad (10)$$

It should be noted carefully that these formulas will serve directly to predict the noise voltage appearing across an impedance in any lead, but only provided no noise voltages appear on other electrodes. For example, if the screen is grounded for radio frequencies, the noise voltage appearing across an impedance  $Z$  in the plate lead is simply

$$\overline{e_p^2} = \overline{i_p^2} \left| \frac{r_p Z}{r_p + Z} \right|^2, \quad (11)$$

where  $r_p$  is the plate resistance of the tube. If, however, there is impedance in both screen and plate circuits, the screen-plate transconductance (and, to a lesser extent the plate-screen transconductance), together with the fact that the current fluctuations in screen and plate are partly in phase, partly random, necessitates a return to fundamentals and construction of entirely new expressions to take the place of (10) and (11). These are not difficult to obtain but lie beyond the aim of this paper which refers specifically to normal pentode amplifiers only. To these the expressions above are usually applicable.

<sup>1</sup> Different methods of attack have led to the same formula, e.g., W. Schottky, "On the Theory of Electron Noise in Multiple-Grid Tubes," *Ann. d. Physik*, Vol. 32, p. 195, May, (1938). C. J. Bakker, "Current Distribution Fluctuations in Multi-Electrode Radio Valves," *Physica*, Vol. 5, No. 7, p. 581, July, (1938).



Now it will ordinarily be found that  $\Gamma^2 \ll \frac{I_{c2}}{I_b}$ . The formulas

(1C) then approach the following limiting forms:

$$\left. \begin{aligned} \overline{i_k^2} &= \Gamma^2 (I_a \cdot 2e\Delta f) \\ \overline{i_{g2}^2} &= \overline{i_p^2} = \frac{I_{c2}I_b}{I_a} \cdot 2e\Delta f. \end{aligned} \right\} \quad (10a)$$

If it is also true that  $I_{c2} \ll I_b$ , the noise in both screen and plate circuits is approximately equal to the true shot effect for a current equal to the screen current  $I_{c2}$ . The noise in the plate circuit may then exceed that in the cathode lead by an order of magnitude. This undesirable behavior is illustrated by the measurements below, and is in accord with the prevalent impression that conventional pentodes are usually inferior to triodes from purely a noise standpoint.

The most valuable figure of merit is the effective input noise, namely, that voltage applied between grid and cathode which produces output current fluctuations equal in magnitude to those actually generated by shot effect. The effective input noise is expressed by

$$\overline{e_i^2} = \frac{\overline{i_p^2}}{g_m^2},$$

where  $g_m$  is used here to denote control grid-to-plate transconductance. The symbol  $g_t$  will be used to denote total (or cathode) transconductance. In brief,

$$g_m \equiv \frac{\partial I_b}{\partial E_{c1}}, \quad g_t \equiv \frac{\partial I_a}{\partial E_{c1}},$$

and, since it is normally true, we shall assume

$$g_t = \frac{I_a}{I_b} g_m.$$

Using (10), we then have

$$\overline{e_i^2} = \left[ 1 + \frac{I_{c2}}{\Gamma^2 I_b} \right] \frac{\Gamma^2 I_a \cdot 2e\Delta f}{g_t^2}. \quad (11)$$

The term without brackets will be recognized as the equivalent input noise of the tube operated as a triode (both screen and plate working into the same radio-frequency circuit). The term within brackets is, therefore, the factor by which the effective input noise is increased when the tube is employed as a pentode.

For engineering purposes a more valuable formula expresses the input noise simply as the effective resistance  $R_{eff}$  which, at room temperature  $T_o$ , exhibits a thermal-agitation voltage equal to the effective input shot voltage of the tube. This development parallels that of p. 471, Part II, to which reference may be made for details. We also need (43b) of Part II, namely,

$$\Gamma^2 = 2 \frac{\theta}{\sigma} \frac{g_t V_e}{I_a} \quad (12)$$

In this expression  $\theta$  is a pure number, practically equal to  $2/3$  over the whole range of space-charge-limited operation, provided the ratio of cathode current to emission is small;  $\sigma$  is the ratio of total transconductance  $g_t$  to the conductance  $g$  of the "equivalent diode", and is

given more explicit definition in (51) of Part II:  $V_e = \frac{kT}{e}$ , where

$T$  is cathode temperature,  $k$  is Boltzmann's constant,  $e$  is electron charge. Assuming that  $\theta = 2/3$  and  $T_o = 300^\circ K$ , we find

$$\left. \begin{aligned} R_{eff}(\text{pentode}) &= \left[ 1 + 8.7\sigma \frac{I_{c2}}{g_m} \cdot \frac{1000}{T} \right] \cdot R_{eff}(\text{triode}) \\ \text{where } I_{c2} \text{ is in microamperes, } g_m \text{ in micromhos, and } T \text{ in } ^\circ K, \\ \text{and where} \\ R_{eff}(\text{triode}) &= \frac{\theta}{\sigma} \cdot \frac{T}{T_o} \cdot \frac{1}{g_t} = \frac{2.2}{\sigma} \cdot \frac{T}{1000} \cdot \frac{I_b}{I_a} \cdot \frac{1}{g_m} \end{aligned} \right\} \quad (13)$$

For tubes with oxide-coated cathodes, it has been shown in Part II that  $\theta = 2/3$  for practical purposes, so that (13) may be considered valid. However, whenever there is any question as to the validity of (12), (11) should be used in place of (13), and  $\Gamma^2$  should be found experimentally from a measurement of noise in the cathode lead.

As an example of the magnitude of pentode shot noise as predicted by (13), consider a typical radio-frequency pentode for which

$$T = 1000^\circ K$$

$$I_t = \frac{4}{5} I_a = 2 \text{ milliamperes}$$

$$g_m = 1200 \text{ micromhos}$$

$$\sigma = 0.83$$

Then  $R_{eff} \text{ (triode)} = 1770 \text{ ohms}$

$$R_{eff} \text{ (pentode)} = 4.0 R_{eff} \text{ (triode)} = 7100 \text{ ohms.}$$

In concluding the theory it is worth observing that, although (10) and (11) are developed with the understanding that  $0 < \Gamma < 1$ , and that  $\Gamma$  is simply a manifestation of fluctuations in virtual-cathode potential elicited by and tending to compensate true shot fluctuations in electron emission, they are equally valid in at least two further instances in which  $\Gamma$  may be greater than unity. Whenever positive ions are evaporated from the cathode (discussed in Part II) or whenever they are formed within the tube by collisions between electrons and molecules of residual gas (the subject of Part IV), if the ion currents are small enough their sole contribution to the current fluctuations in the plate circuit is due simply to the fact that the ions alter the potential of the virtual cathode, so that fluctuations in ion current bring about fluctuations in cathode current.<sup>1</sup> The mechanics of this process is strictly parallel to that discussed at length in Part II. Fluctuations observed in the cathode lead may even here be expressed empirically in the usual fashion:

$$i_k^2 = \Gamma^2 I_a \cdot 2e\Delta f.$$

But now the former analytical expression,

$$\Gamma^2 = \Gamma_a^2 + \Gamma_\beta^2,$$

must be extended to include, phenomenologically, the noise produced by positive ions, so that we have

$$\Gamma^2 = \Gamma_a^2 + \Gamma_\beta^2 + \Gamma_{pos.}^2 \quad (14)$$

Exceedingly small ion currents can make  $\Gamma > 1$ . Nevertheless, when

<sup>1</sup> Assuming, as before, that the control grid is grounded with respect to noise frequencies. If not, gas current to the grid introduces additional noise, cf. Part IV.

$\Gamma$  is defined as stated, the noise in screen and plate leads is still properly described by (10). An observed example of such a situation will be presented in the following section.

### EXPERIMENT

All measurements were conducted at a frequency of about one megacycle. The apparatus and techniques are fully detailed under this heading in Part II, and the signal substitution method described therein was employed throughout.

Since the chief purpose of this work was a direct test of multi-collector theory as enunciated in (10), there was no attempt to make use of the theoretical value of  $\Gamma$ . In brief the procedure was as follows. A two-collector tube was operated at any chosen point on its characteristic. The fluctuations in cathode current were measured to permit an experimental determination of  $\Gamma$ . At the same operating point the fluctuations in plate and screen current were successively measured. These two values were then compared with their corresponding theoretical estimates, using the experimental  $\Gamma$  in the calculation.

The control grid was biased to a negative potential in every instance, and the suppressor, if any, was connected directly to the cathode. Measurement always showed no significant current to either of these electrodes. When plate-current fluctuations were being measured, all electrodes but the plate were grounded for noise frequencies with blocking condensers, and a known impedance was placed in the plate lead; the voltage fluctuations appearing across this impedance were amplified and measured. A similar procedure yielded screen-current fluctuations. Cathode-current fluctuations were obtained in this way also whenever screen and plate were operated at the same potential so that they could be tied together. Otherwise, known impedances with conductive branches were inserted in both screen and plate leads, and the screen and plate were tied together (as regards noise frequencies) with a blocking condenser. Screen and plate, therefore, operated as a unitary electrode at one megacycle, and the voltage fluctuations at the plate were a direct measure of fluctuations in cathode current. (A schematic circuit of this type, used for the same purpose, is given in Part II, Figure 16.)

Voltage fluctuations are plotted here, but these can be interpreted immediately in terms of current fluctuations because all voltages refer to a common impedance ( $45.5 \times 10^3$  ohms) and band width (9.50 kilocycles)—these being the magnitudes of circuit impedance used, and amplifier pass-band, respectively. Thus the fundamental quantity,

the mean-square current fluctuations per unit band width  $\left( \frac{\bar{i}^2}{\Delta f} \right)$  corresponding to any rms noise voltage  $\sqrt{\bar{e}^2}$  ( $\mu v$ ) shown in Figures 2-4 can be obtained from

$$\frac{\bar{i}^2}{\Delta f} \left( \frac{\mu \mu a^2}{kc} \right) = \frac{\bar{e}^2}{Z^2 \Delta f} = 50.9 \bar{e}^2 (\mu v^2).$$

The three sets of data exhibited were selected from measurements on several types of tube, and may be considered truly representative

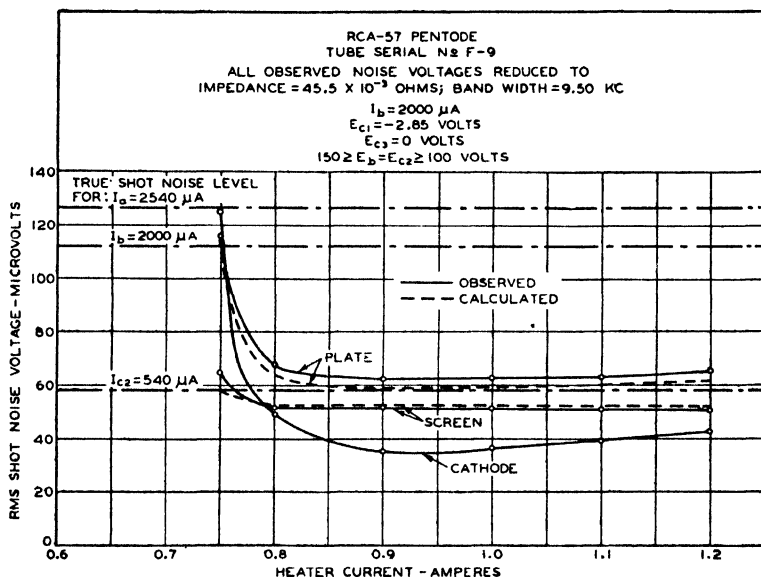


Fig. 2—Comparison between theory and observation of fluctuations in screen and plate leads of a typical radio-frequency pentode. Constant plate current, maintained by adjusting  $E_{c1}$  and  $E_b$ .

of the extent to which (10) may be employed in predicting noise behavior of similar tubes. In each figure the course of noise is traced while, with constant plate current and fixed control-grid bias, the heater temperature is altered so that the tube moves from an essentially temperature-limited condition to one in which the emission is considerably higher than the cathode current.  $\Gamma$  (measured), therefore, runs from unity rapidly to a minimum and then rises again with increasing temperature, in general accord with the theoretical representations of Part II.  $\Gamma$  is not plotted but may be evaluated in any instance by taking the ratio of cathode noise to the true shot noise level for the cathode current, plotted in each figure. This procedure

implies that the cathode current was constant for each plot, which is not strictly true, but the variations are small enough that they cause no material error in this connection.

Figure 2 exhibits the behavior of an RCA-57, a typical radio-frequency pentode with coated cathode and a screen current equal to about one-fifth of the cathode current. The plate and screen were operated at the same potential which was varied from 150 to 100 volts in order to keep  $I_b$  constant as  $T$  was increased.  $I_{c2}$  ran simultaneously from 540 to 530 microamperes. The theory is seen to agree very well with the data. For minimum cathode current fluctuations,

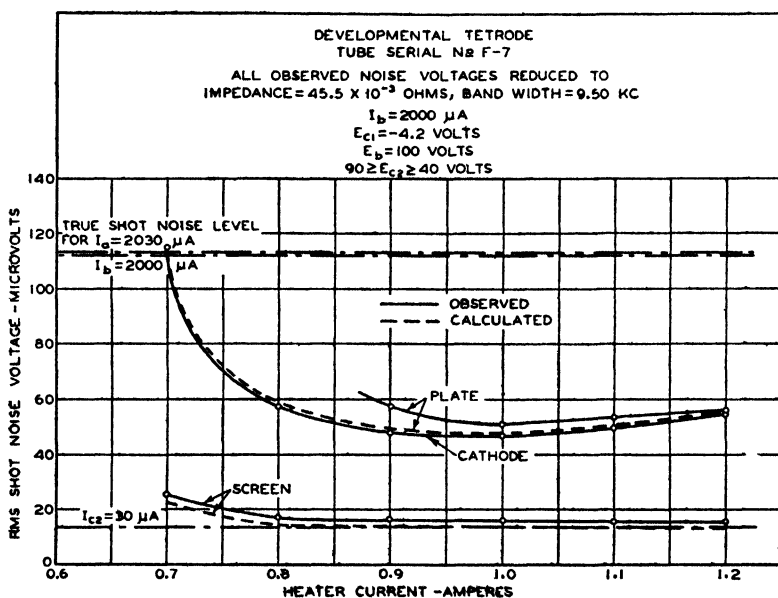


Fig. 3—Comparison between theory and observation of fluctuations in screen and plate leads of a special beam-type tetrode with aligned grids. Constant plate current maintained by adjusting  $E_{c2}$ .

$$\Gamma^2 = 0.077$$

$$\frac{I_{c2}}{I_b} = 0.27,$$

so that

$$\Gamma^2 < \frac{I_{c2}}{I_b}$$

and the limit (10a) is approached, both screen and plate noise approximating the true shot effect for a current equal to the screen current. Due simply to the presence of a screen grid, the rms plate noise in this

tube has roughly twice the magnitude which would be observed if the screen grid were absent.

The data shown were duplicated in tests wherein the plate was held at 250 volts and the screen-grid potential assigned whatever lower value (100 — 200 volts) would set  $I_b = 2000$  microamperes.

The tube concerned in Figure 3 was a special developmental tetrode made by Mr. Otto Schade of these laboratories during studies culminating in the RCA-6L6, a beam power tube.<sup>1</sup> The exceptionally low

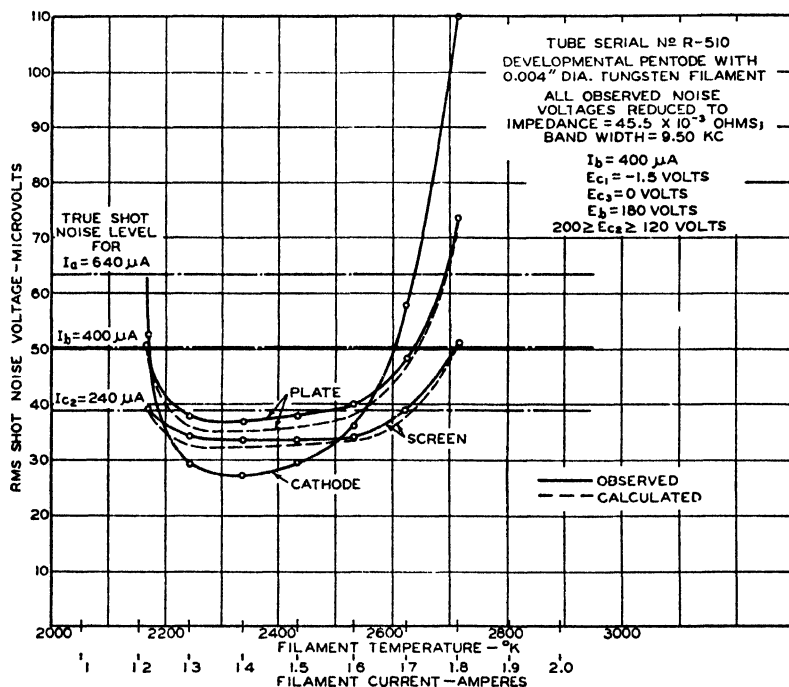


Fig. 4—Comparison between theory and observation of fluctuations in screen and plate leads of a special pentode with tungsten filament, illustrating region for which  $\Gamma > 1$  as a result of positive-ion emission. Constant plate current, maintained by adjusting  $E_{c2}$ .

screen current, 1.5 per cent of the cathode current, is obtained through alignment of control-grid wires with those of the screen grid. Actually the screen-grid current was about 100 microamperes in the temperature-limited condition, and dropped to a nearly constant value of 30 microamperes for all other points. The increase in screen-grid noise above the true shot noise level may be due in part to exchange of secondaries between screen and plate. The course of plate noise is

<sup>1</sup> O. H. Schade, "Beam Power Tubes," *Proc. I.R.E.*, Vol. 26, No. 2, p. 137, February, (1938).

shown for only that portion of the total range in which the emission is far in excess of cathode current, i.e., the noise is independent of emission.<sup>1</sup> At the time plate noise was measured, the emission was increasing slowly with constant heater current; hence, measurements for nearly temperature-limited currents could not be expected to agree well with theoretical estimates based upon subsequent measurements of noise in the cathode current. In any event, only the region of "complete" space-charge limitation is practically important. And here the agreement between theory and observation is again good. In this region the screen potential is less than 50 volts, so that, in view of the extremely small screen current, noise originating in secondary emission cannot be serious.

The plate noise is practically equal to the cathode noise, simply because the screen current is negligible. At a casual inspection these data might be considered a none-too-convincing confirmation of (10), inasmuch as the plate noise would naturally approach that of the cathode if the screen current were to vanish. The proper focal point, however, is the screen noise, which agrees well with (10) but is, on the other hand, more than twice the magnitude predicted by (1).

Finally, Figure 4 is presented to demonstrate the extension of (10) to instances in which positive-ion production raises the noise level. The 4-mil tungsten filament of this pentode was formed from wire of ordinary commercial purity. Furthermore, there was never any detectable ion current, and yet at around 2600°K enough ions evaporated from the filament to raise  $\Gamma$  above unity. The behavior is typical of all cathodes but is especially marked in tungsten filaments merely because the operating temperature is high. The first ions evaporated (about 2500°K) are probably surface contaminations, largely potassium. Subsequently (about 3000°K) tungsten ions, themselves, predominate. Reasonably enough, the ion emission always falls off slowly with age at a fixed temperature, and is also greatly diminished by flashing at a higher temperature, even though the temperature increment be as little as 10° to 50°. This performance is reflected in fluctuation measurements. Consequently, the three plots of noise in Figure 4 do not represent precisely the same cathode conditions for the same temperature. The cathode noise, measured last, yields a value of  $\Gamma$  smaller than that prevailing in prior measurements; and this accounts for a portion of the small discrepancy between observed and calculated noise. The important point, however is the good agreement in the range for which  $\Gamma > 1$ .

On the whole there appears to be thorough experimental support for the hypothesis that shot effect in conventional multi-collectors

---

<sup>1</sup> See Part II.



adheres closely to the performance, summarized in (10), of the idealized structure depicted in Figure 1b. In conjunction with the evidence of Part II, and subject to the following summarized group of conditions:

- a)  $I/I_s \ll 1$
- b) No positive ion emission
- c) No secondary emission
- d) No elastic reflection of electrons into the virtual cathode
- e) Current collected at plate and screen only. The expressions (11) and (13) can be relied upon to give an accurate estimate of the effective input shot noise of modern amplifying tubes, and thus serve a useful purpose in analysis and design.

## PART IV—FLUCTUATIONS CAUSED BY COLLISION IONIZATION

BY

B. J. THOMPSON AND D. O. NORTH

*Summary*—An expression is derived for the number of electrons released from the virtual cathode by each positive ion formed by collision. The plate-current fluctuations originating in the random formation of such ions are then formulated for a simplified, parallel-plane model approximating conventional sleeve-cathode structures. The formula does not require a knowledge of gas pressure, and thus is especially useful in connection with sealed-off tubes. Calculations from the theory, under the assumption that the chief constituent of residual gas is carbon monoxide, compare favorably with a series of measurements. It is concluded that the "gas" component of noise may generally be ignored when grid gas-current is less than a few hundredths of a microampere.

### INTRODUCTION

IN EVERY vacuum tube there are free gas molecules some of which are converted into positive ions by collision with electrons in those regions where the potential exceeds the ionization potential. Throughout its lifetime each ion affects the virtual cathode, if one exists, in such a way that the electron current is increased. Inasmuch as the formation of ions is a matter of chance, the increase in electron current caused by the ions must fluctuate at random. Thus, the plate current exhibits a "gas" component of noise in addition to the normal shot fluctuations investigated in Parts II and III. The results of an analytical and experimental study of this ionization noise are presented in this part.

It should be noted at the outset that no significant ionization noise is found in modern high-vacuum receiving tubes. The subject of this part of the series is, therefore, not of such serious import as it was so little as ten years ago. This is a direct tribute to present-day exhaust technique, particularly the use of effective new getters. Today's new

tube with an estimated gas pressure of perhaps  $10^{-4}$  micron has a grid current of less than  $10^{-8}$  ampere, a value so small that it may be due as much to photoelectric emission as to the collection of positive ions. Under the circumstances, the objective of this investigation has been primarily to establish a sound quantitative understanding of the phenomena involved, a result of greater theoretical than practical interest.

In 1933 Ballantine<sup>1</sup> studied this same problem. Because he did not attempt to determine the number of electrons released from the virtual cathode by an ion during its lifetime, his analysis led to conclusions which can be quantitatively applied only to tubes in which both the gas

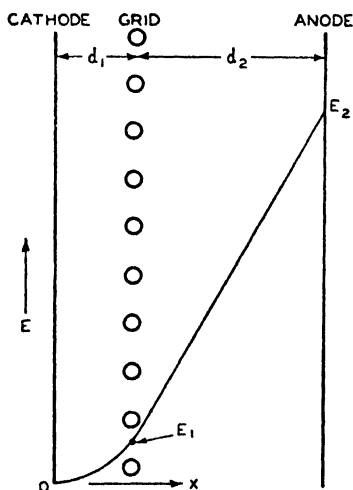


Fig. 1—Space potential in a model triode.

pressure and the increment in plate current caused by ionization are known. His qualitative predictions were well demonstrated in a series of careful observations of the noise produced by controlled amounts of mercury vapor, argon, and gas evolved from the tube structure.

The analysis below, begun in 1933, determines the number of electrons released per ion and leads to an end-formula which relates the noise to the grid gas-current, tube geometry, and electrode potentials, but, unlike Ballantine's, does not require a knowledge of the increment in plate current. Instead, this increment is also obtained as a function of the above parameters. One of the chief merits of this work is that it bears directly upon the performance of sealed-off tubes in which the gas pressure is not directly observed.

<sup>1</sup> S. Ballantine, "Fluctuation Noise due to Collision Ionization in Electronic Amplifier Tubes", *Physics*, Vol. 4, No. 9, pp. 294-306; September (1933).

## THE ANALYTICAL MODEL

For simplicity only the parallel-plane case is considered, and, unless otherwise specified, this will be a triode with negative grid bias. The space distribution of the gas is considered uniform in the regions where ionization occurs. It is assumed that each ion is formed with zero velocity, moves in a straight line under the acceleration of the electric field, and is collected (or neutralized) at first encounter with an electrode. Since carbon monoxide is known to be the chief component of residual gas in tubes with coated cathodes and since it has been found to have a representative probability of ionization, we shall confine our analysis to this gas. It is then proper<sup>2</sup> to ignore collision products other than the singly charged ion,  $CO^+$ ; we can also ignore multiple collisions altogether.

The ionization potential of  $CO$  is about 14 volts<sup>2,3</sup>. With reference to Figure 1, the effective potential  $E_1$  of the grid surface in conventional tubes is well below this figure. It will, therefore, be supposed that no ion is formed in the cathode-grid space and that the division of ion current between grid and cathode can be approximated in terms of the fraction  $\alpha$  of open grid surface.

To avoid discussing transit-time effects, the analysis is limited to conditions in which the transit time of an ion is short in comparison with the period of the measuring circuit. Our conclusions will, therefore, be applicable only to frequencies less than about ten megacycles in conventional receiving tubes. However, the threshold effect of increasing transit angles is known to be a reduction of plate-current noise, so that we are, for small transit angles, calculating an upper limit.

As we have previously stated, ionization increases not only the fluctuations, but also the average electron current. It will be supposed that the ion-dependent increment in electron current is small, so that the actual operating parameters of the tube, such as transconductance, are satisfactorily approximated by their ion-free values.

The gas current to the grid will, of course, produce a shot voltage across the input circuit. In comparison with the plate-current fluctuations this source of noise can usually be ignored in radio-frequency amplifiers. It must be reckoned with in high-input-impedance d-c

---

<sup>2</sup> A. L. Vaughan, "Mass Spectrograph Analysis and Critical Potentials for the Production of Ions by Electron Impact in Nitrogen and Carbon Monoxide", *Phys. Rev.*, Vol. 38, pp. 1687-1695; November (1931).

<sup>3</sup> John T. Tate and P. T. Smith, "The Efficiencies of Ionization and Ionization Potentials of Various Gases Under Electron Impact", *Phys. Rev.*, Vol. 39, pp. 270-277; January (1932).

amplifiers, where it may become the dominant noise source.<sup>4</sup> But since the calculation in the d-c case is straightforward, following the standard formula for temperature-limited shot effect, it will also be ignored at this time. Our model tube will have its grid at ground potential for currents at the operating frequency.

The space potential in the model is shown in Figure 1. Electrons are emitted with zero velocity. The familiar three-halves-power law is used in the cathode-grid space and the field is approximately uniform in the grid-anode space. Hence, for the symbols shown in Figure 1, the space potential  $E$  is determined by

$$\left. \begin{aligned} \frac{E}{E_1} &= \left( \frac{x}{d_1} \right)^{4/3} & 0 \leq x \leq d_1 \\ \frac{\partial E}{\partial x} &= \frac{E_2 - E_1}{d_2} & d_1 \leq x \leq d_2 \end{aligned} \right\} \quad (1)$$

Because  $E_1$  is small in comparison with the ionization potential, every ion which enters the cathode-grid space is assumed to move therein with a constant velocity equal to its terminal velocity at the cathode.

If the amplification factor ( $\mu$ ) is large enough, the grid may be regarded as a perfect shield (permeable membrane), inhibiting the influence which each ion exerts upon the virtual cathode until the moment when the ion has penetrated the grid surface. We have found, however, that  $\mu$ 's of conventional tubes are *not* large enough to permit this approximation, and thus the influence of both ions and electrons in the grid-anode space has to be admitted. The extended analysis is too lengthy to warrant presentation; hence the end-formulas alone will be listed. The analysis detailed below refers merely to the simplified, high- $\mu$  tube, but the procedure followed to extend it will be outlined.

#### INCREMENT IN ELECTRON CURRENT

- Let  $I$  = average cathode (or anode) electron current in the absence of gas.  
 $\delta I$  = increment in  $I$  as a consequence of ionization.  
 $v_e$  = electron velocity at the grid.  
 $v_i$  = terminal ion velocity at the cathode.  
 $\alpha$  = fraction of open grid surface.

<sup>4</sup> E.g., L. R. Hafstad, "The Application of the FP-54 Pliotron to Atomic Disintegration-Studies", *Phys. Rev.*, Vol. 44, pp. 201-213; August (1933).

$I_i$  = total average ion current arriving at grid surface.

$I_{ig}$  = total average ion current absorbed at the grid.

$I_{ik}$  = total average ion current absorbed at the cathode.

Then we have  $I_i = I_{ig} + I_{ik}$

and assume  $I_{ik}/I_i \approx \alpha$ .

Let  $m_i$  = mass of an ion.

$m_e$  = mass of an electron.

$M$  = molecular weight of an ion (28 for CO).

Then  $\left( \frac{m_i}{m_e} \right) = 1833 M \quad (5.13 \times 10^4 \text{ for CO}).$

Our first objective is to determine the ratio of the increment in electron current caused by the ions to the ion current flowing to the cathode from a point of ion formation (potential  $E$ ) in the grid-anode space. The calculation pivots around two principles. First, the net surface charge on the cathode must be zero (no field) at every instant. Second, the ion flow may be regarded as a movement of charge continuously distributed in space exactly as is customary for electron-current analyses.

Let us suppose that the cathode ion current  $I_{ik}$  consists of ions of just one common velocity (all formed at points having space potential  $E$ ). The charge it induces on the cathode is

$$q_i = - \int_0^{d_1} \frac{I_{ik}}{v} \left( 1 - \frac{x}{d_1} \right) dx = - \frac{1}{2} \frac{I_{ik} d_1}{v_i}.$$

The charge induced on the cathode by the electrons comprising the increment  $\delta I$  in electron current elicited by the presence of ions is

$$q_e = \int_0^{d_1} \frac{\delta I}{v} \left( 1 - \frac{x}{d_1} \right) dx = \frac{\delta I}{v_e} \int_0^{d_1} \left( \frac{d_1}{x} \right)^{2/3} \left( 1 - \frac{x}{d_1} \right) dx = \frac{9}{4} \frac{\delta I d_1}{v_e}.$$

If the field at the cathode is zero,

$$q_e + q_i = 0,$$

and

$$\frac{\delta I}{I_{ik}} = \frac{2}{9} \frac{v_e}{v_i} = \frac{2}{9} \left( \frac{m_i}{m_e} \right)^{1/2} \left( \frac{E_1}{E} \right)^{1/2} = 9.53 M^{1/2} \left( \frac{E_1}{E} \right)^{1/2}$$

Since the ions are singly charged, the ratio likewise signifies the num-

ber of electrons  $N(E)$  released from the virtual cathode by each ion of this terminal velocity,

$$N(E) = \frac{\delta I}{I_{ik}} = 9.53 M^{1/2} \left( \frac{E_1}{E} \right)^{1/2} \quad (2)$$

indicating approximately 10 electrons for each CO ion which reaches the cathode.

Equation (2) shows the increment in electron current under the assumption that all ions have the same velocity (formed at potential  $E$ ), but it also shows the increment in electron current actually caused by the ions in each velocity class (formed between potentials  $E$  and  $E + dE$ ). Knowing the number of ions formed at each potential, we may then determine the total increment in electron current. Let  $P(E)$  be the average number of ions formed by each electron of energy  $E$  for each centimeter of its path<sup>5</sup>. The total increment in electron current as a consequence of ionization is, therefore,

$$\delta I = \alpha I \int_0^E N(E) P(E) dx = \frac{\alpha I}{\left( \frac{\partial E}{\partial x} \right)} \int_0^E N(E) P(E) dE. \quad (3)$$

Here  $\left( \frac{\partial E}{\partial x} \right)$  is the uniform field in the grid-anode space, and the lower limit to the integration is set at zero merely for convenience. There is, of course, no contribution to the integral from potentials below the ionization potential.

Similarly, the total ion current is

$$I_i = \frac{I}{\left( \frac{\partial E}{\partial x} \right)} \int_0^{E_1} P(E) dE,$$

and the grid gas-current is

$$I_{ig} = (1 - \alpha) I_i = \frac{(1 - \alpha) I}{\left( \frac{\partial E}{\partial x} \right)} \int_0^{E_1} P(E) dE. \quad (4)$$

<sup>5</sup> Tate and Smith, Reference 3, have measured this quantity for a number of gases. Their data for CO will be used.

By combining (3) and (4), and using (2), we obtain

$$\delta I = 9.53 M^{1/2} \frac{\alpha}{1 - \alpha} E_1^{1/2} \frac{\int_0^{E_2} \frac{P(E)}{E^{1/2}} dE}{\int_0^{E_2} P(E) dE} I_{1g}.$$

Let us define a quantity

$$E_t^{1/2} = \frac{\int_0^{E_2} P(E) dE}{\int_0^{E_2} \frac{P(E)}{E^{1/2}} dE}. \quad (5)$$

We then find

$$\delta I = 9.53 M^{1/2} \frac{\alpha}{1 - \alpha} \left( \frac{E_1}{E_t} \right)^{1/2} I_{1g}. \quad (6)$$

$E_t$  is, in a sense, a "mean" potential at which ions are formed. Since  $P(E)$  appears in both numerator and denominator of (5),  $E_t$  is independent of the gas density. The experimental values of  $P(E)$  published by Tate and Smith are shown for CO in Figure 2. The data refer to a gas density corresponding to a pressure of one millimeter and a temperature of zero Centigrade.  $E_t$  was computed from these data and is plotted as a function of  $E_2$  in Figure 3.

### THE FLUCTUATIONS

It is illuminating to express the plate current fluctuations in terms of the temperature-limited diode current which exhibits equal fluctuations. In a diode current  $J$  the fluctuations are expressed<sup>6</sup> by

$$\overline{i^2} = 2eJ\Delta f.$$

Since the ion current exhibits random fluctuations they can be described in the same way.

We have observed that a given velocity class of ions produces an increment in electron current proportional to the ion current within the class and depending on the velocity of the ions [see Equation (2)].

<sup>6</sup> See Part II, p. 450; April (1940).



The ion current within each velocity class will fluctuate at random. The increment in electron current caused by each class will fluctuate by a proportional amount. Therefore, we may represent that portion of the plate-current fluctuations due to ion effects by a temperature-limited diode current  $J_1$  as follows:

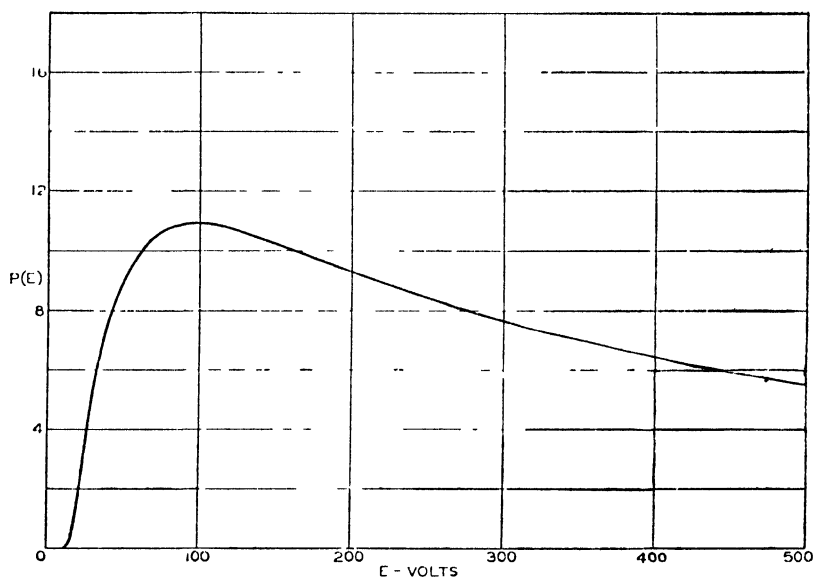


Fig. 2—Average number of  $\text{CO}^+$  ions formed by each electron of energy  $E$  for each centimeter of its path in carbon monoxide at one millimeter pressure, zero degrees Centigrade. Data from Tate and Smith.

$$J_1 = \alpha I \int_0^{E_s} N^2(E) P(E) dE = \left( \frac{\alpha I}{\frac{\partial E}{\partial x}} \right) \int_0^{E_s} N^2(E) P(E) dE. \quad (7)$$

By combining (3) and (7) and defining a quantity,

$$E_s = \frac{\int_0^{E_s} P(E) dE}{\int_0^{E_s} \frac{P(E)}{E} dE}, \quad (8)$$

we find

$$J_1 = 90.8 M \frac{\alpha}{1 - \alpha} \left( \frac{E_1}{E_s} \right) I_{10}. \quad (9)$$

$E$  is, in another sense, a "mean" potential at which ions are formed. It is also plotted in Figure 3 for CO.

Formally, this simplified analysis of high- $\mu$  structures is now complete, and can be tested by inserting a comparator diode across the

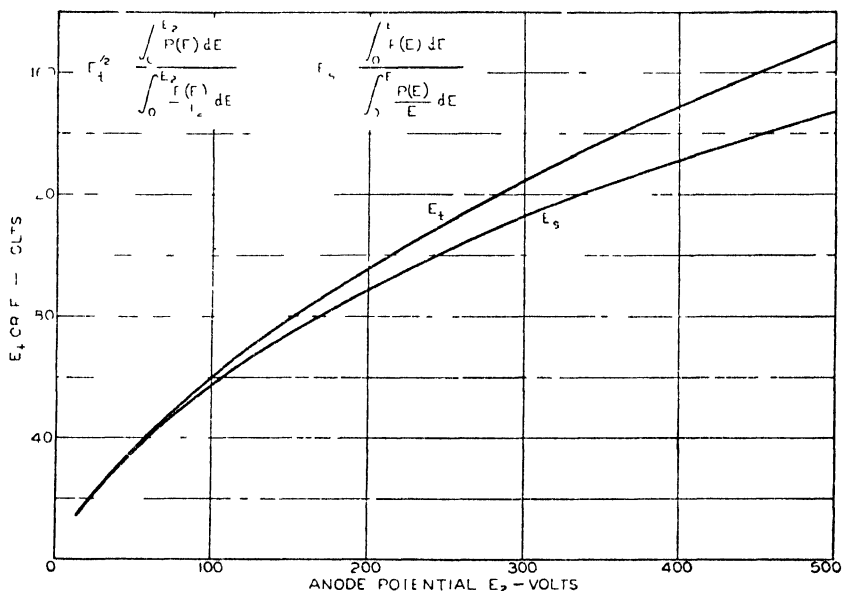


Fig. 3—Effective potentials of ion formation in carbon monoxide, as a function of anode potential.

plate circuit and determining  $J_1$  experimentally. The quantities appearing on the right hand side of (9) can all be determined to a fair approximation.  $E_1$  cannot be measured directly, but, in view of the three-halves-power law, can be expressed in terms of current and transconductance by

$$E_1 = \frac{3}{2} \frac{I}{g_m} \quad (10)$$

#### EXTENSION OF ANALYSIS TO STRUCTURES WITH FINITE $\mu$

The space-charge-free electrical equivalent of a three-electrode tube structure is a combination of three capacitances which may, with equal generality, be represented in either delta or star connection. The delta concept is commonly employed in tube engineering because the capaci-

tances so defined (Maxwell's coefficients of induction) are easily measured and blend without struggle into networks attached to the tube. But for all problems relating to the distribution of the images of a charge moving through the structure, the star connection is far superior<sup>7</sup>. In Figure 4 the central connection  $A$  is not accessible, but plays an important rôle in that its potential corresponds to the "equivalent-diode potential". When a tube approximates the ideal parallel-plane structure, the capacitances (per unit area) are closely approximated by the following simple expressions:

$$C_k = \frac{1}{4\pi d_1}, \quad C_p = \frac{1}{4\pi d_2}, \quad C_g = \mu C_p \quad (11)$$

Adaptation of these expressions to simple structures without plane symmetry is functionally obvious.

A charge  $e$  in transit may now be regarded as moving, first, through a space ( $C_k$ ) bounded by the cathode and a hypothetical "permeable membrane" at  $A$ , then through a similar grid-anode space ( $C_p$ ). Its images ( $q$ ) in the three electrodes can therefore be written with ease. For the parallel-plane structure they are

$$\begin{aligned} -\frac{q_k}{e} &= \left\{ \begin{array}{c} \frac{(\mu+1)(d_1-x)+d_2}{(\mu+1)d_1+d_2} \\ \frac{\mu x}{(\mu+1)d_1+d_2} \\ \frac{x}{(\mu+1)d_1+d_2} \end{array} \right\} = \left\{ \begin{array}{c} \frac{d_1+d_2-x}{(\mu+1)d_1+d_2} \\ \mu \frac{d_1}{d_2} \frac{d_1+d_2-x}{(\mu+1)d_1+d_2} \\ \mu \frac{d_1}{d_2} \frac{(x-d_1)+x}{(\mu+1)d_1+d_2} \end{array} \right\} \quad (12) \\ &\quad 0 \leq x \leq d_1 \qquad \qquad \qquad d_1 \leq x \leq d_2 \end{aligned}$$

With these formulas, the extension of the simple ionization analysis is readily accomplished. To express the end-formulas concisely, we need a few additional parameters which are defined as follows:

<sup>7</sup> See, e.g., F. B. Llewellyn, "Operation of Ultra-High-Frequency Vacuum Tubes", *B.S.T.J.*, Vol. 14, p. 659; October (1935).

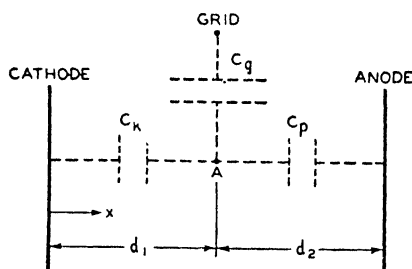
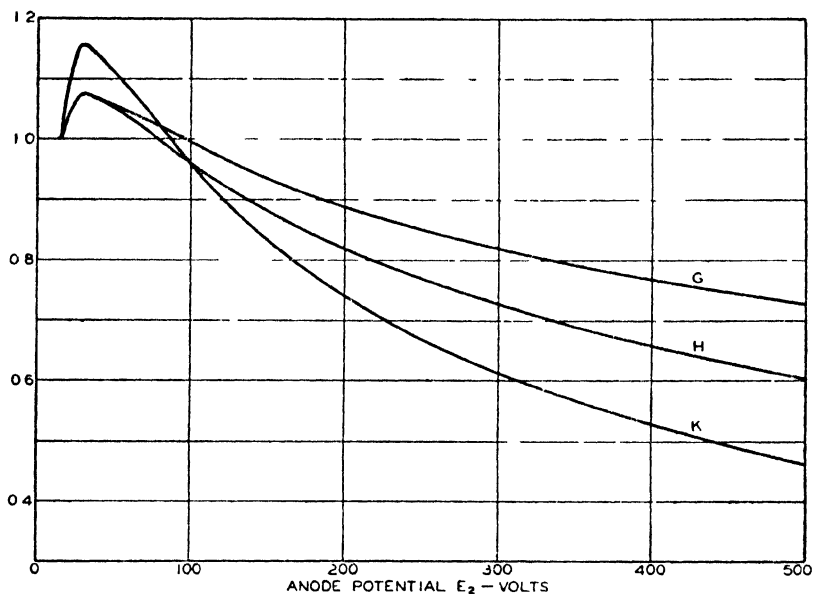


Fig. 4—Electrostatic representation of a triode.

$$\begin{aligned}
 h &= \frac{\tau_2}{\tau_1} = \frac{\text{grid-anode electron transit time}}{\text{cathode-grid electron transit time}} \\
 \sigma &= \frac{\mu}{1 + \mu + \frac{4}{3} \frac{d_2}{d_1} (1 + h) - \frac{1}{3} h^2 (6 + 4h + h^2)} \\
 &= \frac{g_m}{g} = \frac{\text{transconductance}^8}{\text{conductance of equivalent diode}} \\
 \lambda &= \frac{1 + \mu + 2 \frac{d_2}{d_1}}{1 + \mu + \frac{4}{3} \frac{d_2}{d_1} (1 + h) - \frac{1}{3} h^2 (6 + 4h + h^2)} \\
 \beta &= \frac{4}{3} \frac{\left( \frac{d_2}{d_1} \right)^2}{1 + \mu + 2 \frac{d_2}{d_1}}
 \end{aligned} \tag{13}$$

We shall also use the following dimensionless functions, which are plotted in Figure 5 for  $CO$ :

<sup>8</sup> Cf. Part II, p. 469.

Fig. 5—Functions  $G$ ,  $H$ ,  $K$  evaluated for carbon monoxide

$$\left. \begin{aligned}
 G(E_2) &= \frac{\int_0^{E_2} \left( \frac{E}{E_2} \right) \left( 3 - 2 \frac{E}{E_2} \right) \frac{P(E)}{E^{1/2}} dE}{\int_0^{E_2} \frac{P(E)}{E^{1/2}} dE} \\
 H(E_2) &= \frac{\int_0^{E_2} \left( \frac{E}{E_2} \right) \left( 3 - 2 \frac{E}{E_2} \right) \frac{P(E)}{E} dE}{\int_0^{E_2} \frac{P(E)}{E} dE} \\
 K(E_2) &= \frac{\int_0^{E_2} \left( \frac{E}{E_2} \right)^2 \left( 3 - 2 \frac{E}{E_2} \right)^2 \frac{P(E)}{E} dE}{\int_0^{E_2} \frac{P(E)}{E} dE}
 \end{aligned} \right\} \quad (14)$$

In these terms, the number of electrons released from the cathode for each ion which originates at some point of potential  $E$  in the grid-anode space, and ends its career at the grid, is

$$N_g(E) = 9.53 M^{1/2} \left( \frac{E_1}{E} \right)^{1/2} \cdot \lambda \beta \left( \frac{E}{E_2} \right) \left( 3 - 2 \frac{E}{E_2} \right). \quad (15)$$

But, if the ion goes through to the cathode, the total number is

$$N_h(E) = 9.53 M^{1/2} \left( \frac{E_1}{E} \right)^{1/2} \cdot \lambda \left[ 1 + \beta \left( \frac{E}{E_2} \right) \left( 3 - 2 \frac{E}{E_2} \right) \right]. \quad (16)$$

Superseding (6), the increment in electron current becomes

$$\delta I = 9.53 M^{1/2} \frac{\alpha}{1 - \alpha} \left( \frac{E_1}{E_t} \right)^{1/2} I_{ig} \cdot \lambda^2 \left[ 1 + \frac{\beta}{\alpha} G \right]. \quad (17)$$

Superseding (9), the plate-current fluctuations are given by

$$J_1 = 90.8 M \frac{\alpha}{1 - \alpha} \left( \frac{E_1}{E_s} \right)^{1/2} I_{ig} \cdot \lambda^2 \left[ 1 + 2\beta H + \frac{\beta^2}{\alpha} K \right]. \quad (18)$$

Superseding (10),  $E_1$  is now to be computed from

$$E_1 = \sigma \cdot \frac{3}{2} \frac{I}{g_m}. \quad (19)$$

In general, the extended formula indicates a several-fold increase in  $J_1$  over that derived in (9). The reason is that, although the electrical shielding action of the grid may be great, the ions spend most of their lives approaching the grid and but very little of their lives (if any) in the cathode-grid region.

The extension of this analysis to multi-collector structures is straightforward, following the pattern of Part III. But so little material of additional value accrues that it does not invite elaboration.

The experimental work described below is a direct test of (18). However, in making an advance rough estimate of the fluctuations, the rather large number of unsubstantiated premises and approximations which enter into the calculations probably does not justify all of the refinement. For such a purpose it is accurate enough to assume that  $\lambda$ ,  $\beta$ ,  $\sigma$ ,  $G$ ,  $H$ , and  $K$  all have the value unity, and that  $\alpha = 0.9$ . We then have, for CO gas,

$$J_1 \sim 1.4 \times 10^5 \frac{I}{g_m E_s} I_{ig}. \quad (20)$$

Reference to Figure 3 suggests that 70 volts is a representative figure for  $E_s$ . If, in addition, we suppose  $I$  to be about 5 milliamperes, and  $g_m$  about 2,000 microhmos,

$$J_1 \approx 5 \times 10^3 I_{ig}.$$

From the treatment of the gas-free space-charge-limited triode in Part II, we know that the normal shot effect in such tubes can be expressed in terms of a temperature-limited-diode current  $J_o$ :

$$J_o = \Gamma^2 I \quad (21)$$

where<sup>9</sup>

$$\Gamma^2 \approx \frac{1.29}{\sigma} \frac{g_m V_e}{I} \quad (22)$$

and  $V_e = \frac{kT}{e}$ ,  $T$  being cathode absolute temperature,  $k$  Boltzmann's constant. In typical tubes,  $\Gamma^2$  is about 0.05. For the representative tube under consideration the ratio of mean square ion-elicited fluctuations to the ion-free space-charge-reduced shot fluctuations is

$$\frac{J_1}{J_o} \approx 10^5 \frac{I_{ig}}{I} = 2 \times 10^7 I_{ig}.$$

If the ion noise is to be kept below, say, twenty per cent of the normal shot effect, the grid gas-current should not rise above one hundredth microampere. So low a figure suggests a basic reason for the poor experimental agreement amongst studies of space-charge-limited shot effect before the advent of modern getters. Even today it represents a severe manufacturing tolerance. It should be pointed out again that, for a constant gas-current, ion noise decreases at higher frequencies. The expectation that large ion-transit-angles will reduce the theoretical value of  $J_1$  has already been confirmed by a few rough comparative measures of  $J_1$  at one and ten megacycles.

Ion-free noise in multi-collector tubes runs higher than in triodes<sup>10</sup>. The mean-square plate fluctuations in receiving-type pentodes run two to four times greater than the figure for triodes expressed by (21). For pentodes, then, the threshold gas currents are proportionately larger.

#### MEASUREMENT

The standard RCA-56 structure was used. This is a cylindrical mount having a 0.050-inch cathode, a 0.255-inch anode, and an oval

<sup>9</sup> Part II, p. 470, Eq. (43b).

<sup>10</sup> See Part III, pp. 244-260; October (1940).

grid with a minor diameter of 0.095 inch and a major diameter (between side rods) of 0.170 inch. It was anticipated that this structure, representative of many in common use, would correspond closely enough to that of the parallel plane model to permit comparisons, particularly since the bulk of the current is concentrated in a sector in the vicinity of the minor grid diameter, and  $d_1$  and  $d_2$  can, therefore, be estimated with confidence despite grid ellipticity. The structural parameters, (13), were then assigned the following approximate values on the basis of design data:

$$\alpha = 0.88, \beta = 0.81, \sigma = 0.72, \lambda = 1.16.$$

The last two, although functions of the transit-time ratio  $h$ , are virtually constant over the range of operation, and were computed for  $h = \sigma$ .

Noise was measured with the equipment described in Part II at a frequency of about one megacycle, over a band of about ten kilocycles. Original plans called for use of a comparator diode, but it was found difficult to maintain sufficiently high impedance in diodes carrying saturated currents in the order of ten milliamperes. The current fluctuations in such cases are believed to obey the standard formula for true shot effect. But in the presence of the strong fields necessary to produce saturation the emission becomes field-sensitive (Schottky effect), so that accurate work demands recognition of the finite contribution of the diode to the total circuit impedance. We found it less awkward, therefore, to use the signal substitution method, also described in Part II.

Into some of the tubes CO was introduced by heating calcium oxalate in a side arm;  $\text{Ca}(\text{COO})_2 \rightarrow \text{CaO} + \text{CO} + \text{CO}_2$ . A liquid air trap removed the  $\text{CO}_2$ . After being flushed with about 2 centimeters of gas, the tubes were sealed off at a pressure of about 5 microns. Gas currents, read directly after sealing off, were always several microamperes. All such tubes showed a tendency to "clean up" during operation, but the rate was not sufficient to interfere with measurement. Indeed, the effect could be reversed by overheating the cathode or the plate a small amount, a welcome phenomenon for studies of performance versus gas density.

Into the other tubes studied no gas was introduced. But, after sealing off, high-frequency heating was applied until the gas current rose to the desired value. Gas so evolved was presumably representative of the residual gas in commercial tubes.

Exact interpretation of the data requires a measure of the normal space-charge-limited fluctuations which exist in the absence of gas. To this end both groups of tubes were provided with getters which, at the end of the ionization studies, could be relied upon to clean up the gas.



Measurement of the residual fluctuations agreed well enough with the theoretical expectation (21) on the two occasions in which this procedure was followed, so that, for the rest, the measurement was not considered necessary.

In every respect the performance of the tubes with evolved gas coincided with that of the tubes into which  $CO$  had been introduced. This tends to confirm the findings of many gas analyses that  $CO$  is a chief constituent of residual gas. There is, however, the possible alternative, that the constituents of the evolved gas had such an average molecular weight and ionization probability<sup>11</sup> as to simulate  $CO$ . The question was not pursued.

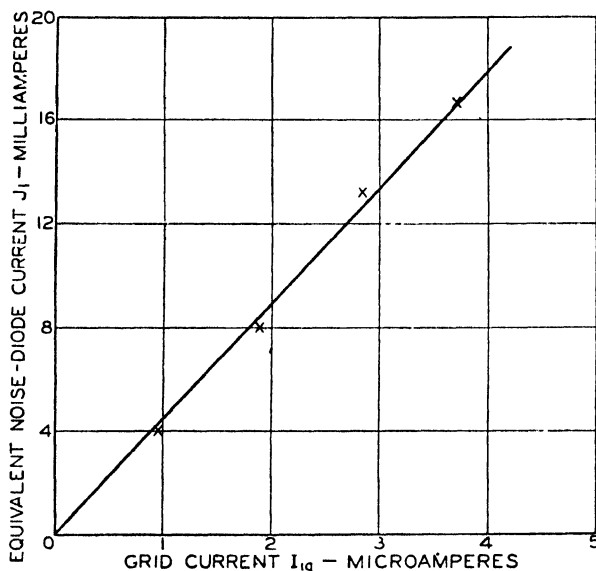


Fig. 6—Measured values of ionization noise versus ion current to the grid of a triode containing carbon monoxide

Juggling the gas content, as described above, yielded the data of Figure 6, demonstrating that ion-provoked noise is proportional to gas current, as one would expect. In this instance, gas was released by raising the cathode temperature in steps from an estimated  $980^{\circ}K$  to  $1180^{\circ}K$ , meanwhile holding anode potential at 250 volts, and maintaining a constant cathode current of 8 milliamperes by means of minor adjustments of the grid bias.

Figures 7 and 8 illustrate a representative set of observations of the kind used to test the analysis. This tube contained evolved gas. The anode potential was fixed at 250 volts. Cathode current was varied from 0.5 to 9.0 milliamperes by running the grid bias up from  $-17$  to

<sup>11</sup> E.g., Any mixture of  $CO$ ,  $N$ ,  $NO$ , and  $O_2$ ; cf. Tate and Smith, loc. cit.

-10 volts. Grid current, transconductance, and noise were measured simultaneously<sup>12</sup>. The experimental values of  $J_0$  were obtained after the run by flashing a getter. Failure to obtain a closer fit to the theoretical curve for  $J_0$  may be due largely to incomplete gettering; the residual gas current amounted to 0.009 microampere for the largest cathode current. Plotted values of  $J_1$  are measured noise corrected by subtraction of the theoretical  $J_0$ . From (17), the largest fractional increment in ion-free cathode current was estimated to be 5 per cent, corresponding to a  $\delta I$  of 420 microamperes for an  $I$  of 9.0 milliamperes. It, therefore, appears justifiable to ignore the influence of the ions upon transconductance, space potential, etc.

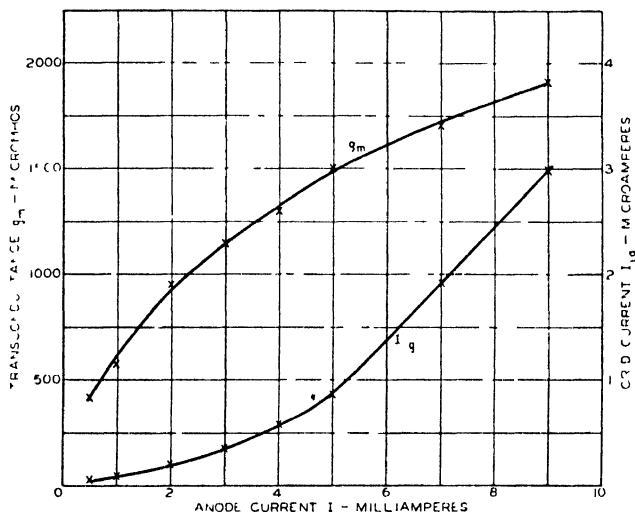


Fig. 7—Transconductance and evolved-gas current to the grid of a triode as a function of anode current. Anode potential fixed at 250 volts.

Measured mean-square noise always exceeded prediction in the manner typified by Figure 8. The most reliable comparison of theory and measurement is made for large  $J_1$ , where the measuring sensitivity was best, experimental error least likely, and the importance of the correction  $J_0$  negligible. For the lowest point, the ratio of observed to calculated  $J_1$  is 2.5; for the highest, 1.2. In consideration of the many obvious analytical departures from reality, the fit along the upper, most accurate part of the curve is considered a rather good agreement.

It should particularly be noticed that the expression for  $J_1$  depends greatly upon the ratio  $d_2/d_1$ . In actuality, the virtual cathode in close-

<sup>12</sup> It is certain that the gas density was not constant, but increased with current. Precise information on this point was not essential and was not sought. However, by putting the analysis into reverse, one can estimate from (4) that the gas pressure ( $^{\circ}$ C) rose from about 0.2 to about 0.7 micron.

spaced tubes may be so positioned that the proper  $d_1$  differs significantly from the cathode-grid spacing. A correction of this sort would further improve the agreement. While provisions for this, as well as for other refinements, could be arranged, they appear hardly justified at present.

### CONCLUSIONS

We have attempted to provide a sound quantitative understanding of the basic fluctuation phenomena in conventional vacuum tubes con-

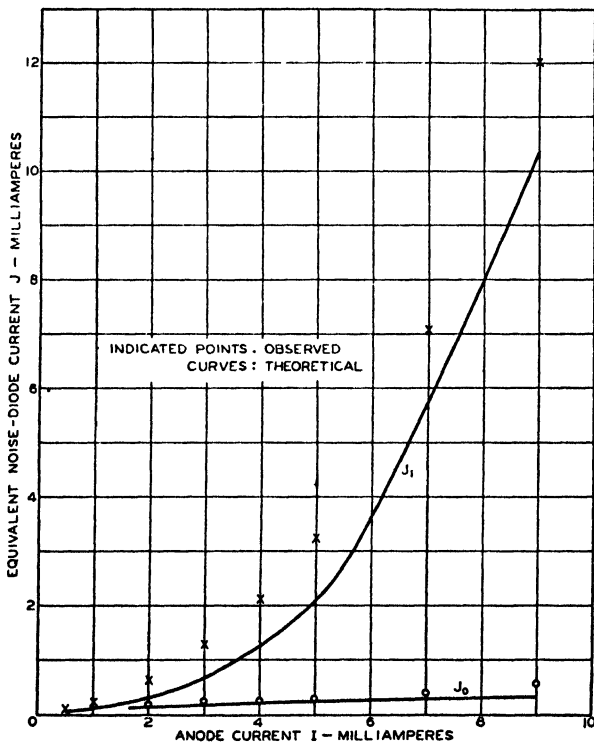


Fig. 8—Fluctuations ( $J_1$ ) in the anode current of the triode of Figure 7 containing evolved gas, corrected by subtraction of the residual fluctuations ( $J_0$ ) measured after flashing a getter. Curves calculated from theory.

taining small amounts of gas. We conclude that it is proper, at least for coated-cathode types, to regard  $CO$  as a representative gas for this purpose, and that it is possible hereby to predict the noise performance of such tubes in terms of structural constants, normal electrical characteristics, and the control-grid gas current. Both calculation and measurement suggest that the ionization component of noise may generally be ignored when the grid gas-current is less than a few hundredths of a microampere.

## PART V — FLUCTUATIONS IN VACUUM TUBE AMPLIFIERS AND INPUT SYSTEMS

BY

W. A. HARRIS

*Summary*—The determination of fluctuation-noise magnitudes in amplifiers can be accomplished by comparing the amplifier circuits with equivalent circuits including noise generators which simulate the fluctuation-noise sources. Noise-equivalent resistance or noise-equivalent conductance values based on thermal-agitation formulas may be used to represent the voltage-squared or current-squared outputs of these generators. In this PART V applications of the "noise generator" method of analysis to various systems using vacuum-tube amplifiers are illustrated. Formulas, based on the theoretical analyses of the preceding Parts, are given for noise-equivalent resistance values applicable to space-charged-limited vacuum tubes. These formulas are arranged for use with published tube data. A table of noise-equivalent resistance values for a number of tube types is included. Formulas for the noise-equivalent conductance values applicable to phototubes and television camera pick-up tubes are given.

It is shown that noise picked up by the antenna of a radio receiver can be represented by a noise-equivalent resistance proportional to (but in general, not equal to) the antenna-radiation resistance.

The effect of feedback on signal-to-noise ratio is discussed. Even when the feedback does not affect the signal-to-noise ratio to a serious degree, the possibility of the presence of feedback must be taken into account before inferences are drawn from experimental data as to the relative importance of noise sources.

### INTRODUCTION

IN THE preceding Parts of this series it is shown that there is a definite, predictable fluctuation in the plate current of a space-charge-limited vacuum tube; detailed theoretical studies are presented and formulas, verified by experimental work, are given to permit the calculation of fluctuation magnitudes and the prediction of the results of changes in tube parameters and operating conditions. The present section is written with the object of illustrating the application of the results and formulas of the preceding sections in the design of vacuum-tube amplifier systems and in the prediction and explanation of their performance.

The method of presentation followed will be based on the discussion of examples and problems of types encountered in design work. In

most cases the fluctuation phenomena are of interest because they produce noise, so the term "noise" will usually be used instead of the expression "fluctuation phenomena." Formulas for tube noise, based on those given in the preceding Parts, will be presented in simplified forms with, at times, some sacrifice in accuracy. This does not detract in any way from the importance of the more rigorous forms of the equations. It is our knowledge of the soundness of the underlying theory which gives us confidence in the approximate formulas, within their limitations, and when discrepancies and doubts do arise we can turn to the complete forms to find out whether the difficulties are due to the approximations made or to some other cause. Reference to the historical summary given in Part I should be sufficient to suggest the result of the absence of detailed analytical studies in the past.

Tube noise is one of three major components of the fluctuation noise in an amplifier system, the others being thermal-agitation noise in the input circuit and noise entering the system with the input signal. The grid of the first tube in an amplifier system is a convenient reference point for comparing the effects of noise from these sources and for comparing the resulting total noise level with the signal level at which the system is designed to operate.

#### EQUIVALENT CIRCUITS AND NOISE GENERATORS

In the consideration of an amplifier system, we want to be able to identify sources of fluctuation noise and to evaluate the contributions from these sources without concerning ourselves each time with such details as the mechanism by which the shot-effect fluctuations in the emission of electrons from the cathode of a tube are related to fluctuations in the plate current. One method of avoiding these details is to treat an amplifier as if all the fluctuation noise comes from "noise generators" connected at appropriate points in the circuit. These "noise generators" may have the noise-producing properties of resistors or of temperature-limited diodes. The equations describing these properties are the shot-effect and thermal-agitation formulas discussed in the preceding Parts.<sup>1</sup>

The mean-square fluctuation current  $\overline{i^2}$  from a temperature-limited diode, measured in a frequency band  $\Delta f$ , is given by the equation:

$$\overline{i^2} = 2eI\Delta f$$

where  $e$  is the electronic charge,  $1.59 \times 10^{-19}$  coulomb, and  $I$  is the diode current. Consequently,

$$\overline{i^2} = 3.18 \times 10^{-19} I \Delta f$$

<sup>1</sup> Part II, pp. 450, 460-471, April (1940) *RCA Review*; Part III, pp. 245-255, Oct. (1940) *RCA Review*. See also Part I, p. 272 and references, Jan. (1940) *RCA Review*.

when  $I$  and  $i$  are expressed in amperes and  $\Delta f$  is expressed in cycles per second. We can describe a constant-current noise generator producing an output of  $3.18 \times 10^{-10}$  current-squared units per kilocycle of bandwidth by stating that "the noise-equivalent diode current of the generator is one milliamperere". We retain the current-squared unit because the noise power output of a system including a noise generator of this type is proportional to the mean-square current output of the generator and noise power outputs are quantities which can be added directly. Two noise generators connected in parallel, each having a noise-equivalent-diode-current rating of one milliamperere, would produce the same results as a single generator with a noise-equivalent-diode-current rating of two milliampereres.

A short-circuited resistor produces a mean-square fluctuation current  $\bar{i}^2$  in a frequency band  $\Delta f$  in accordance with the equation:

$$\bar{i}^2 = 4kTg\Delta f$$

where  $g$  is the conductance of the resistor, or the reciprocal of its resistance;  $k$  is Boltzmann's constant,  $1.372 \times 10^{-23}$  joule per degree; and  $T$  is the temperature, degrees Kelvin. We can compare the mean-square current output of one of our noise generators with that of a short-circuited resistor at a given temperature; for a temperature of  $290^\circ$  K the mean-square current from a resistor with conductance  $g$  is

$$\bar{i}^2 = 1.59 \times 10^{-20} g \Delta f$$

The temperature  $290^\circ$  K is near enough to "room temperature" for practical purposes, so the relation between the "room-temperature" noise-equivalent-conductance rating and the noise-equivalent-diode-current rating of a constant-current noise generator can be written<sup>2</sup>

$$g_{eq} = 20 I_{eq}$$

The symbols  $g_{eq}$  and  $I_{eq}$  will be used for "noise-equivalent conductance" and "noise-equivalent diode-current", respectively. The constant-current noise generator referred to above ( $I_{eq} = 1$  milliamperere) would have a noise-equivalent conductance of 20 milliampereres per volt, or 20,000 micromhos.

The mean-square thermal-agitation voltage  $\bar{e}^2$  across the terminals of a resistor in a frequency band  $\Delta f$  is

$$\bar{e}^2 = 4kTR\Delta f$$

or, for a temperature of  $290^\circ$  K

$$\bar{e}^2 = 1.59 \times 10^{-20} R \Delta f$$

<sup>2</sup> It is of little consequence whether we say that the coefficient 20 is obtained by using  $290^\circ$  K for room temperature, or that it is obtained by rounding the coefficient obtained for some other assumed temperature. The coefficient is actually  $5800/T$ , so "room temperatures" of  $300^\circ$ ,  $294^\circ$ , and  $290^\circ$  give coefficients 19.3, 19.7, and 20.0, respectively. The corresponding Fahrenheit temperatures are  $81^\circ$ ,  $70^\circ$ , and  $68^\circ$ .

The choice of a "noise-equivalent resistance" value to represent the output of a constant-voltage noise generator is made for the same reasons as those given above. The symbol  $R_{cq}$  will be used for "noise-equivalent resistance" in this Part<sup>3</sup>. A constant-voltage noise generator with a noise-equivalent resistance of 100,000 ohms produces a fluctuation-noise output of  $1.59 \times 10^{-12}$  voltage-squared units per kilocycle of bandwidth.

The application of the usual circuit theorems in connection with the noise-equivalent diode current, conductance, or resistance values assigned to our "noise generators" becomes evident when we remember that these values correspond to current-squared and voltage-squared outputs. Thus, a constant-voltage noise generator with a noise-equivalent-resistance value  $R_{cq}$  at the grid of a tube produces the same result as a constant-current noise generator at the plate with a noise-equivalent conductance value  $g_{cq}$  when

$$g_{cq}(\text{plate}) = g_m^2 R_{cq}(\text{grid})$$

The symbol  $g_m$  is the tube transconductance.

Since the numerical value of the noise-equivalent diode current is one-twentieth of the value of the noise-equivalent conductance, we have

$$I_{cq}(\text{plate}) = 20g_m^2 R_{cq}(\text{grid})$$

and by definition<sup>4</sup>

$$I_{eq}(\text{plate}) = \Gamma^2 I_L$$

where  $\Gamma^2$  is the shot-effect reduction factor for the tube.  $\Gamma^2$  is the factor determined from theoretical considerations in Parts II and III.

A constant-current noise generator  $g_{cq}$  in parallel with an admittance  $Y$  is equivalent to a constant-voltage noise generator

$$R_{eq} = \frac{g_{cq}}{|Y|^2}$$

in series with an impedance  $1/Y$  in any frequency band  $\Delta f$  small enough so that  $Y$  can be considered constant in that band; and conversely, a constant-voltage noise generator  $R_{eq}$  in series with an impedance  $Z$  is equivalent to a constant-current noise generator

$$g_{eq} = \frac{R_{eq}}{|Z|^2}$$

in parallel with an admittance  $1/Z$  in any frequency band  $\Delta f$  small enough so that  $Z$  can be considered constant in that band.

The diagrams of Figure 1 illustrate the use of "noise generators".

<sup>3</sup> The symbol  $R_{eq}$  and the name "effective resistance" used in Parts II and III in connection with tube noise are ambiguous when applied to circuit noise. The effective resistance of a circuit may be an entirely different quantity than the noise-equivalent resistance applicable to the circuit.

<sup>4</sup> Part II, Summary, p. 441; Apr. (1940) *RCA Review*.

The first diagram (Figure 1-a) represents an amplifier system consisting of an input circuit, the first vacuum tube, an amplifier including the output circuit of the first tube and additional stages, and an output system which might include a loudspeaker or a television screen, or alternatively a load circuit and a power-output meter. Noise in the output system is due to the combined effect of fluctuation voltages from tubes, input-circuit thermal agitation, and noise from external sources; the major part of the tube noise is due to reduced shot-effect fluctuations in the plate current of the first tube, as discussed in Parts II and III. When the gain of the first stage is low, it may be necessary to take into account the noise introduced by the interstage coupling circuit and by the second tube.

Figure 1-b indicates the substitution of a noise-free tube and a constant-current noise generator for the tube of Figure 1-a. The "generator" can have the characteristics of a temperature-limited diode; then we can determine the noise-equivalent diode current, which is the product of the plate current and the shot-effect reduction factor  $\Gamma^2$ , as determined by such equations as (43-a), Part II, and assign this current to the noise generator. The fluctuation-noise output from the "diode" noise generator is similar in both frequency-distribution and amplitude-distribution characteristics to the fluctuation-noise output of the actual tube. Thus, we can obtain the same noise-power output and at the same time produce noise which "sounds" the same as the noise from the original tube by this substitution. We describe the generator by stating that it has the characteristics of a temperature-limited diode which introduces the same current fluctuations into the circuit as did the original tube. The use of a noise generator of this type in our hypothetical equivalent circuit is directly comparable to the use of a "comparator diode" for the measurement of tube noise.<sup>5</sup>

It is also feasible to represent the plate-current fluctuations as if they were derived from thermal-agitation in a resistor. Since we want a "constant-current" (i.e. infinite-impedance) generator we cannot draw a noise-producing resistor as part of the circuit, but we can assign the appropriate noise-equivalent-conductance value to the noise generator of Figure 1-b. If we must draw a resistor we can draw a noise-free negative resistance of equal magnitude in parallel with it.

The third diagram (Figure 1-c) is a more useful representation for many purposes, since it shows tube noise introduced by a noise generator at the grid of the tube.<sup>6</sup> This noise generator can be represented as having the noise-equivalent-resistance value  $R_n$ , and other noise can be represented as coming from a second noise generator

<sup>5</sup> Part II, pp. 108-110, Aug. (1940) *RCA Review*.

<sup>6</sup> Part II, p. 471, July (1940) *RCA Review*.



having the noise-equivalent-resistance value  $R_b$ ; then it is correct to say that the total noise from these two sources corresponds to the noise-equivalent-resistance value  $(R_a + R_b)$ . The ideal tube substituted in this case should have infinite input impedance so the voltages supplied by the noise generators will not be short-circuited or reduced. The impedance of the real tube can be considered as part of the input circuit.

The circuit of Figure 1-d may represent conditions in an actual amplifier more accurately. The noise generators are assumed to produce noise distributed in accordance with the thermal-agitation law, in a uniform manner at all frequencies, but the frequency distribution of noise in various parts of the system is controlled by selectivity factors. The filter shown between the two noise generators  $R_b$  and  $R_a$  in Figure 1-d is assumed to have a selectivity characteristic corresponding to that of the input circuit of Figure 1-a. If we assume that  $R_a$  and  $R_b$  are approximately equal, that the amplifier passes a frequency band of width 8 kc and the filter passes a band of width only 4 kc, the output noise will contain contributions from both generators (i.e. tube and circuit) in the 4-kc band, but noise from  $R_a$  only (tube) in the range between the limits of the 4-kc band and those of the 8-kc band. The noise would sound differently than the same total noise power in either the 4-kc or the 8-kc band.

When the object of drawing or considering an equivalent circuit is to facilitate the computation of noise-power output or signal-to-noise ratio, the question of the exact frequency distribution of the noise may be of little consequence. Then the circuit of Figure 1-e would be preferred to 1-d, since direct addition of the noise-equivalent-resistance values for the noise generators is possible in Figure 1-e.  $R_a'$  (Figure 1-e) is made enough greater than  $R_a$  to compensate for the effect of the filter; consequently, it does not represent the tube noise directly. The noise generators in Figures 1-c, 1-d, and 1-e become identical when the effect of the filter is negligible ("broad" input circuit, "sharp" amplifier).

Noise from the second tube and the coupling circuit can be taken into account by the addition of another "generator",  $R_c$  (Figure 1-f). Since the noise-equivalent resistance represents the mean-square voltage produced by the noise generator, a factor equal to the square of the stage gain is used to refer the noise-equivalent-resistance value for a noise generator at the second grid, to the first grid. The method indicated can be extended to any number of stages, but it is not likely that tubes beyond the second will make an appreciable contribution to the total noise. In Figure 1-f,  $R_a$  and  $R_b$  represent noise-equivalent-resistance values for the first tube and the input circuit;  $R_c$  can be

described as representing the noise-equivalent-resistance value for the additional (second tube and circuit) amplifier noise, referred to the grid of the first tube. The total noise-equivalent resistance (excluding noise which might be introduced from external sources) is

$$R_{eq} = R_a + R_b + R_c$$

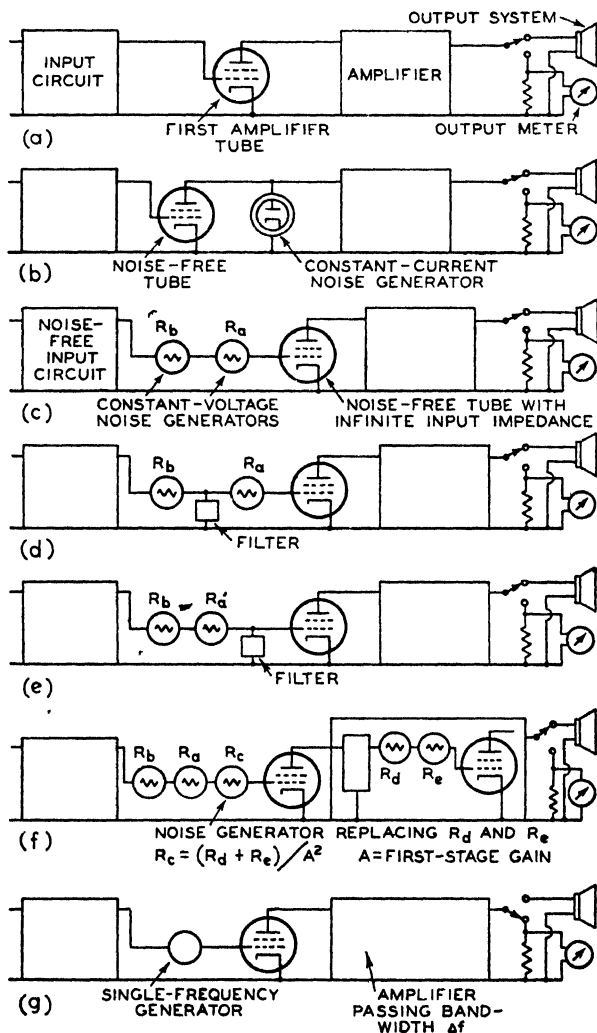


Fig. 1

The noise generators introduced in Figures 1-b to 1-f have an important property in common with the noise sources which they replace, in that they produce noise distributed in a uniform manner over a wide frequency band. However, there are some cases in which

we prefer to consider constant-frequency generators equivalent to the others in the sense that they cause the same output-meter deflection as the original noise sources of the amplifier. In such cases, we can use the equivalent circuit shown in Figure 1-g, and assume the substitution of an amplifier with a rectangular band-pass characteristic of bandwidth  $\Delta f$  and a noise-equivalent voltage generator operating at a frequency inside this passed band. The bandwidth  $\Delta f$  must be determined from the frequency characteristic of the amplifier in such a manner as to satisfy the relation

$$\sqrt{\overline{e^2}} = \sqrt{4kTR_{eq}\Delta f}$$

or,  $\Delta f = \overline{e^2}/4kTR_{eq}$

The quantity  $\Delta f$  will be referred to as the effective bandwidth of the amplifier.

In these equations  $\sqrt{\overline{e^2}}$  is the rms voltage of the new generator and  $R_{eq}$  is the total noise-equivalent resistance used in the previously discussed method of representation. When room-temperature noise-equivalent-resistance values are considered, the equations become

$$\sqrt{\overline{e^2}} = 1.3 \times 10^{-10} \sqrt{R_{eq}\Delta f} \quad (1)$$

or,  $\Delta f = 0.6 \times 10^{20} \overline{e^2}/R_{eq}$

If we want to assume separate generators corresponding to the separate noise sources, we must also assume that each operates at a different frequency inside the passed band so that their contributions to the power output will be added in the proper manner. Generally, it is easier to determine the noise-equivalent-resistance values first, add them, and obtain the noise-equivalent voltage from this result.

The effective bandwidth of an amplifier can be determined from a curve of power output against frequency by dividing the area under that curve by the ordinate corresponding to the chosen "noise-equivalent-voltage" frequency. When a curve of output voltage against frequency is available, the same result is obtained by using the squares of the ordinates of that curve. An approximate value obtained by measuring the frequency difference between the half-maximum ordinates of the curve of power output against frequency or between the corresponding (0.707 maximum) ordinates on the curve of power output against voltage can be used in many cases. An effective-bandwidth determination is referred to in the description of the amplifier used for measurements, Part II.<sup>7</sup>

The effective bandwidth determined for fluctuation-noise computa-

<sup>7</sup> Part II, p. 108, July (1940) *RCA Review*.

tions is generally considerably less than the bandwidth which represents the "frequency range" of an amplifier. This difference can be illustrated by a comparison of two amplifiers, one "cutting off" sharply at, say, 3000 cycles and the second giving some attenuation at 3000 cycles, but some response at 6000 cycles. The two amplifiers will not sound alike, although they may produce the same noise-power outputs when they are connected to similar input systems.

#### APPLICATION TO RADIO RECEIVERS

The generality of the method of analysis discussed is illustrated by considering its application to a radio receiver of the superheterodyne type. In a receiver the output system passes a band of frequencies from possibly 100 to 5000 cycles. To represent a superheterodyne receiver the amplifier shown as a block in Figures 1-a to 1-g must include a frequency-conversion stage for converting the signal to the intermediate frequency and a detector for producing the audio-frequency output. The detector makes noise analysis quite troublesome when we try to predict the noise-power output in the absence of any signal, but this is not an important condition. When a signal is being received the "carrier" component of the signal establishes the receiver gain because it determines the detector sensitivity, and the amount of avc voltage developed. With a given carrier voltage, the audio-frequency voltage output is proportional to the sideband amplitudes, and the ratio between output and sideband amplitude is substantially constant so long as the modulation does not exceed 100 per cent and the audio system is not overloaded. The sidebands do not have to be those produced by modulation of the signal at its source. If we introduce a second signal differing by an audio frequency from the carrier we observe that the output is proportional to the amplitude of the second signal when this amplitude is not too great. Moreover, when the carrier is present we can introduce a second signal differing by an audio frequency from the intermediate frequency, into the i-f amplifier and obtain a similar result. The noise generators in Figures 1-a to 1-g produce signals corresponding to the "second signal" referred to, so the receiver functions as a linear amplifier with respect to the noise when a carrier is present.

The signal-to-noise ratio in a radio receiver depends on the relation between the sidebands of the received signal and the outputs of the noise generators. Consequently, when we decide to turn from consideration of noise-equivalent resistances to noise-equivalent voltages (as in Figure 1-g) it is proper to refer to the noise-equivalent rms voltage as the "equivalent-noise sideband input." This expression is

generally abbreviated to "ensi" when it is used in receiver-measurement discussions. In a double-side-band system the effective bandwidth to be used in making the conversion from noise-equivalent resistance to noise-equivalent voltage (ensi) is twice the effective audio-frequency bandwidth. The effective audio-frequency bandwidth can be obtained from a curve of power output against modulation frequency by dividing the area under the curve by the ordinate chosen to correspond to the noise-generator frequency. In this case the actual noise-generator frequency is the carrier frequency plus or minus the chosen audio-frequency value.

### NOISE FORMULAS

Use of the method of analysis described in the preceding sections depends on assignment of noise-equivalent-resistance and noise-equivalent-conductance values to the "noise generators" shown in the diagrams. The following equations are recommended for this purpose:

For triode amplifiers

$$R_{eq} = \frac{2.5}{g_m} \quad (2)$$

For pentode amplifiers

$$R_{eq} = \frac{I_b}{I_b + I_{c2}} \left( \frac{2.5}{g_m} + \frac{20I_{c2}}{g_m^2} \right) \quad (3)$$

For triode mixers

$$R_{eq} = \frac{4}{g_c} \quad (4)$$

$$\text{or, } R_{eq} = \frac{2.5\overline{g_m}}{g_c^2} \quad (4a)$$

For pentode mixers

$$R_{eq} = \frac{I_b}{I_b + I_{c2}} \left( \frac{4}{g_c} + \frac{20I_{c2}}{g_c^2} \right) \quad (5)$$

$$\text{or, } R_{eq} = \frac{I_b}{I_b + I_{c2}} \left( \frac{2.5\overline{g_m}}{g_c^2} + \frac{20I_{c2}}{g_c^2} \right) \quad (5a)$$

For multigrid converters and mixers

$$R_{eq} = 20 \frac{I_b(I_c - I_b)}{I_c g_c^2} \quad (6)$$

The following approximate relations for triode and pentode mixers are useful when the data required for Equations (4) and (5) are not available. The values "as amplifier" refer to conditions at the peak of the assumed oscillator cycle.

$$g_c \text{ (as converter)} = \frac{1}{4} g_m \text{ (as amplifier)} \quad (7)$$

$$I_b \text{ (as converter)} = \frac{1}{4} I_b \text{ (as amplifier)} \quad (8)$$

$$I_{c2} \text{ (as converter)} = \frac{1}{4} I_{c1} \text{ (as amplifier)} \quad (9)$$

$$R_{eq} \text{ (as converter)} = 4R_{eq} \text{ (as amplifier)} \quad (10)$$

Equation (10) applies to pentode mixers only. For triode mixers, use Equations (7) and (4) to obtain  $R_{eq}$ .

The noise from phototubes and television camera pick-up tubes operating without internal (gas or secondary-emission) current amplification can be represented by constant-current noise generators with outputs corresponding to noise-equivalent conductances as follows:

$$g_{eq} = 20I \quad (11)$$

The equation for a similar device with an internal current-amplification factor  $N$  (to a first approximation) is

$$g_{eq} = 20NI \quad (12)$$

Conversion from noise-equivalent resistance to noise-equivalent rms voltage is effected by use of Equation (1):

$$\sqrt{\overline{v^2}} = 1.3 \times 10^{-10} \sqrt{R_{eq} \Delta f} \quad (1)$$

Conversion from noise-equivalent conductance to noise-equivalent rms current is effected by use of the corresponding equation:

$$\sqrt{\overline{i^2}} = 1.3 \times 10^{-10} \sqrt{g_{eq} \Delta f} \quad (1-a)$$

The relation between noise-equivalent conductance and noise-equivalent diode current is

$$I_{eq} = 0.05 g_{eq} \quad (13)$$

Most of the symbols used in these equations have been defined or have conventional significance. The definitions are:

$R_{eq}$ , noise-equivalent resistance

$g_{eq}$ , noise-equivalent conductance

$I_{eq}$ , noise-equivalent diode current

$g_m$ , grid-plate transconductance

$\overline{g_m}$ , average transconductance (frequency converters and mixers)

$g_c$ , conversion transconductance (frequency converters and mixers)

- $I_b$ , average plate current  
 $I_{c2}$ , average screen-grid current  
 $I_{a0}$ , average cathode current  
 $\sqrt{\overline{e^2}}$ , noise-equivalent rms voltage for bandwidth  $\Delta f$   
 $\sqrt{\overline{i^2}}$ , noise-equivalent rms current for bandwidth  $\Delta f$   
 $\Delta f$ , effective bandwidth  
 $I$ , Equations (11), (12), average output current  
 $N$ , Equations (11), (12), ratio of output current to photo-emission current.

Equations (2) to (6) are derived from the equations for fluctuation noise in triodes and pentodes given in Parts II and III and from equations for fluctuation noise in converters and mixers given by E. W. Herold.<sup>8</sup> Equations (7) to (10) are approximations derivable from certain idealized tube characteristics.

Equation (2) is derived from Equation (56) of Part II,

$$R_{eff} = \frac{\theta T}{\sigma T_o g_m}$$

In Part II it is demonstrated that the quantity  $\theta$  has a value of approximately  $\frac{2}{3}$  (the asymptotic value is 0.644). The quantity  $\sigma$  will be near unity for triodes likely to be of interest in input-circuit applications. Assignment of the value  $8/9$  to  $\sigma$ ,  $1000^\circ \text{ K}$  to  $T$  (for an oxide-coated cathode), and  $300^\circ \text{ K}$  to  $T_o$  gives Equation (2). The coefficient 2.5 is reasonably accurate over most of the expected range of variation for the significant quantities. Substitution of a tungsten filament for the oxide-coated cathode would make the use of a different coefficient necessary, but practically all tubes of current interest use oxide-coated cathodes operating at temperatures near  $1000^\circ \text{ K}$ .

Equation (3) is derived from Equation (13), Part III. In this case the original equation was first written as the sum of two terms. The coefficient 20 is the quotient  $e/2kT_o$  which determines the relation between noise-equivalent conductance and noise-equivalent diode current.

Equations (4), (4-a), (5), and (5-a) are developed from equations given by Herold.<sup>8</sup> Equations (4) and (5) apply for approximately optimum oscillator voltage and (4-a) and (5-a) may be used for conditions deviating considerably from optimum conditions. Herold's equations are given in terms of conditions at the peak of the assumed oscillator cycle, but the ratios between average and peak values for

<sup>8</sup> E. W. Herold "Superheterodyne Converter System Considerations in Television Receivers," *RCA Review*, Vol. IV, pp. 324-337, Jan. (1940).

currents and transconductances given in the same paper enable us to rewrite the equations in terms of the average quantities. As a final step, the coefficients for Equations (4) to (5-a) were adjusted slightly to make them consistent with those of Equations (2) and (3).

Use of Equation (6) amounts to the substitution of the factor

$$\frac{I_a - I_b}{I_a} \text{ for the factors } \frac{I_a - \overline{I_b^2}/I_b}{I_a} \text{ and } F^2 \text{ used in Herold's equations}$$

for heptodes and hexodes, for outer-grid and inner-grid injection, respectively. The substitution gives values for  $R_{eq}$  which are higher than Herold's values by as much as 30 or 40 per cent under some conditions, but use of Equation (6) has an advantage over an arbitrary choice of  $F^2$  in that it predicts "full shot-effect" for  $I_b$  as the limiting condition for high signal-grid biases.

There is a difference in meaning for a noise-equivalent resistance value applicable to an amplifier and for a value applicable to a frequency converter or to a mixer. In either instance the noise-equivalent-resistance value can be considered as derived from a noise-equivalent-conductance value representing the plate-current fluctuations, but in the case of a converter or a mixer this derivation (division by conversion transconductance squared) yields a noise-equivalent-resistance value which is applicable only in a frequency band which centers at the chosen signal frequency and which does not extend half way to the intermediate frequency or half way to any adjacent image frequency. An equivalent circuit of the type of Figure 1-e is implied with a band-pass filter between the noise generator and the grid of the tube.

Use of Equations (11) and (12) amounts to the assumption that photoelectric emission is subject to shot-effect fluctuations, an assumption adequately justified by theory and experiment.<sup>9</sup> Equation (12) neglects additional noise from the amplification mechanism.

#### TUBE NOISE: TABULATED VALUES OF $R_{eq}$

The data in the following table were obtained by using Equations (1) to (9). The noise computations for each type were made by using published data conditions (as noted) with the appropriate equations; the values for triode and pentode converters were obtained by use of Equations (7) to (9) for currents and conversion-transconductance values and Equations (4) and (5) for noise-equivalent resistance. In some instances it is possible to obtain higher transconductance values by changing operating conditions, but this does not

<sup>9</sup> V. K. Zworykin, G. A. Morton, and L. Malter, "The Secondary Emission Multiplier—A New Electronic Device" *Proc. I. R. E.*, Vol. 23, No. 3, pp. 351-375, March (1936).



## TUBE NOISE VALUES

Type	Application	Voltages			Currents			Transcon- ductance Micromhos	Noise-Equivalent Resistance		Noise- Equivalent Input Voltage (d) Microvolts
		Plate Volts	Screen Volts	Bias Volts	Plate ma	Screen ma	Cathode ma		Calculated Ohms	Measured Ohms	
6SK7	Pentode Amplifier	250	100	-3	9.2	2.4	11.6	2,000	10,500	9,400-11,500	0.94
6SJ7	Pentode Amplifier	250	100	-3	3	0.8	3.8	1,650	5,300	5,300	0.70
6SG7	Pentode Amplifier	250	125	-1	11.8	4.4	16.2	4,700	3,300		0.53
6AC7/1852	Pentode Amplifier	300	150	-2	10	2.5	12.5	9,000	720	600-760	0.25
956	Pentode Amplifier	250	100	-3	5.5	1.8	7.3	1,800	9,400		0.90
1T4	Pentode Amplifier	90	45	0	2.0	0.65	2.65	750	20,000		1.3
6SA7	Frequency Converter	250	100	0	3.4	8.0	11.9	450 (c)	240,000	210,000	4.5
6K8	Frequency Converter	250	100	-3	2.5	6.0	8.5 (b)	350 (c)	290,000		4.9
1R5	Frequency Converter	90	45	0	0.8	1.8	2.75	250 (c)	170,000		3.8
6L7	Pentagrid Mixer	250	100	-3	2.4	7.1	9.5	375 (c)	255,000	210,000	4.6
6J5	Triode Amplifier	250	—	-8	9.0	—	—	2,600	960	1,250	0.28
955	Triode Amplifier	180	—	-5	4.5	—	—	2,000	1,250		0.32
6AC7/1852	Triode Amplifier	150	150	-2	—	—	12.5	11,200	220	200	0.14
6AC7/1852	Pentode Mixer	300	150	-1 (a)	5.2	1.3	6.5	3,400 (c)	2,750	3,000	0.48
6SG7	Pentode Mixer	250	125	-1 (a)	3.0	1.1	4.1	1,180 (c)	13,000		1.0
956	Pentode Mixer	250	100	-1 (a)	2.3	0.8	3.1	650 (c)	33,000		1.7
6J5	Triode Mixer	100	—	-1 (a)	2.1	—	—	620 (c)	6,500		0.74
6AC7/1852	Triode Mixer	150	150	-1 (a)	—	—	6.5	4,200 (c)	950		0.28
955	Triode Mixer	150	—	-1 (a)	2.8	—	—	660 (c)	6,100		0.72

(a) At peak of oscillator cycle.

(b) Hexode section only. Triode section takes its current from a separate part of the cathode.

(c) Conversion transconductance value.

(d) For effective bandwidth of 5000 cycles.

result in any radical change in the noise-equivalent resistance values. The noise-equivalent voltage input values were obtained by using Equation (1) and are included to facilitate comparisons with experimental data. It is generally preferable to use the noise-equivalent resistance values for circuit computations.

Most of the measured values in the table are from data supplied by E. W. Herold. The acorn types (955, 956) are seen to have about the same noise-equivalent values as Types 6J5 and 6SK7 respectively, as might be expected. Type 6AC7/1852 is in a class by itself with respect to noise because of its very high transconductance.

### POSITIVE-ION NOISE

The fluctuation-noise component produced by collision ionization, discussed in Part IV, is quite properly omitted from the equations for noise-equivalent resistance. Residual gas in sufficient quantity to cause an appreciable increase in the fluctuation noise is not desirable from any point of view connected with normal tube operation. It is desirable, however, that we be able to determine the conditions under which residual gas will cause an appreciable increase in the noise power output of a system.

An estimate of the effect of residual gas can be obtained from the equation,

$$R_{eq}(\text{gas}) = \left( 20R^2 + A_1 \frac{I_a}{g_m^3} \right) I_{ig} \quad (14)$$

where

$R$  = grid-circuit resonant impedance

$I_a$  = cathode current

$I_{ig}$  = positive-ion current to grid

$g_m$  = transconductance

$A_1$  is a coefficient of the order of 40,000

The term  $20R^2 I_{ig}$  represents shot-effect voltage fluctuations produced by the gas current in the grid circuit. It may be increased several fold by induction effects connected with ion-transit time, even at frequencies of a few megacycles. The second term is derived from Equation (20), Part IV.<sup>10</sup>

When  $A_1$  is 40,000, the two terms are equal for

$$R^2 = 200 I_a / g_m^3$$

By substituting typical values for  $I_a$  and  $g_m$ , we find that the first term is probably the greater when  $R$  exceeds 20,000 ohms.

<sup>10</sup> Part IV, p. 384, Jan. (1941) *RCA Review*.

The noise-equivalent resistance value for thermal agitation in the grid-circuit resonant impedance is numerically equal to that impedance at frequencies near resonance. The total noise-equivalent resistance component depending on this impedance (neglecting transit-time effect) is

$$R_{eq} = R + 20R^2I_g = R(1 + 20RI_g)$$

The fluctuation noise due to gas exceeds that due to thermal agitation when the product  $RI_g$  exceeds one-twentieth of a volt. When the grid-circuit impedance is one-tenth megohm a positive-ion grid current of one-half microampere doubles the mean-square fluctuation noise.

When the grid-circuit impedance is low, the second term of Equation (14) predominates and at the same time the tube noise is likely to predominate over the circuit thermal-agitation noise. An equation for fluctuation noise in a system using a pentode amplifier connected to an input circuit with resonant impedance  $R$  can be written

$$R_{eq} = R + 20R^2I_g + \frac{I_b}{I_b + I_{c2}} \left( \frac{2.5}{g_m} + 20 \frac{I_{c2}}{g_m^2} \right) + A_1 \frac{(I_b + I_{c2})I_{tq}}{g_m^3}$$

and the most important terms can be compared for any conditions which may be of interest.

#### INPUT-CIRCUIT NOISE

The input circuit used with an amplifier can introduce noise because of thermal agitation in the resistance of that circuit, and it can also transfer the noise generated in or picked up by the microphone, phototube, antenna, or any other input device to the grid of the first amplifier tube. It is evident that the noise from either cause may be the controlling factor in the choice of the first amplifier tube, since there is little object in using a tube with an inherent noise level much lower than that introduced by the input circuit. When the input-circuit noise is predominantly that due to thermal agitation, the determination of the noise level and the comparison with the amplifier noise are fairly simple matters. The general method to be used in such cases has already been indicated.

#### MICROPHONE AMPLIFIER

As a specific illustration we can consider the case of a microphone amplifier (Figure 2). The microphone is assumed to be of a type having a definite internal resistance; it may be one of the types using a ribbon or a moving coil as the voltage-generating element. Noise will be generated in this element in accordance with the thermal-

agitation law. The input transformer shown in Figure 2 can have a ratio high enough to make the noise from this source at the secondary of the transformer considerably greater than the noise-equivalent input voltage applicable to the first amplifier tube. This condition is realized when the reflected resistance at the secondary terminals (microphone resistance times voltage ratio squared) is considerably greater than the noise-equivalent resistance of the first tube.

As an example, let the first tube be a Type 6SJ7 pentode operated under resistance-coupled amplifier conditions. Reference to a table containing data for this method of operation<sup>11</sup> shows that for a supply voltage of 300 volts a plate-load resistor of 0.1 megohm followed by a second-tube grid resistor of 0.5 megohm, and a screen resistor of approximately 0.5 megohm give suitable operating conditions. The voltage gain is approximately 100. The value of the transconductance indicated by this gain and these specified load resistors is 1200 micromhos.

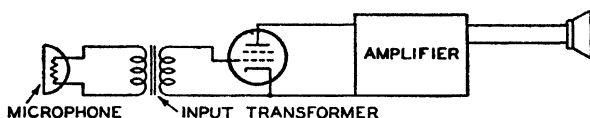


Fig. 2

The currents may be estimated by assuming that the plate-voltage drop is about one-half the supply voltage and that the screen current is about one-fourth of the plate current; resulting values are 1.5 milliamperes and 0.37 milliampere, respectively. The noise-equivalent resistance, determined by using Equation (3), is approximately 6000 ohms. The reflected impedance at the transformer secondary is likely to be of the order of 100,000 ohms, so the tube fluctuation noise is not important.

The noise-power level in the input circuit can be determined from the thermal-agitation formula when the effective bandwidth is known or assumed. The equation for the mean-square thermal-agitation voltage across the terminals of a resistor is

$$\bar{e}^2 = 4kTR\Delta f$$

and the average power  $\bar{e}^2/R$ , is, therefore,

$$\bar{P} = 4kT\Delta f$$

For a temperature of 290° K, the equation becomes

$$\bar{P} = 1.6 \times 10^{-20} \Delta f$$

<sup>11</sup> RCA Receiving Tube Manual RC-14; resistance-coupled amplifier chart.

The noise-power level in decibels, referred to a standard 10-milliwatt level is

$$\text{Noise (db)} = 10 \log \Delta f - 178$$

When  $\Delta f = 10,000$  cycles, the noise power output is 138 db below 10 milliwatts.

The microphone signal output level is likely to be of the order of  $-40$  or  $-50$  db. The fluctuation-noise level is, therefore, 70 or 80 db below the signal. In some amplifiers a multigrid tube, Type 6L7 or 1612, is used because it offers the advantage of a second control grid for volume-control use. The noise-equivalent resistance of such a type as a resistance-coupled amplifier might be 100,000 ohms at maximum gain and a megohm or more when the gain is reduced by application of negative bias, but even these values permit satisfactory signal-to-noise ratios. The choice of a first tube for an audio-frequency amplifier quite evidently depends on factors other than fluctuation noise. Hum, microphonics and mechanical or leakage noises are generally far more important.

#### PHOTOTUBE INPUT CIRCUITS

A high-vacuum phototube produces noise in accordance with the shot-effect law,

$$\begin{aligned} \overline{i^2} &= 2eI\Delta f \\ \text{Consequently } I_{cq} &= I \\ \text{and } g_{cq} &= 20I \end{aligned} \quad (11)$$

Here  $\overline{i^2}$  is the mean-square fluctuation current and  $I$  is the average phototube current.

When the light input to the phototube is modulated in a sinusoidal manner the relation between the mean-square signal current and the average current is

$$\overline{I^2} = \overline{I} M^2 / 2 = \frac{1}{2} \overline{I^2} M^2$$

The factor  $M$  is the modulation factor for the light input or the current output.

The signal-to-noise power ratio (or current-squared ratio) is, therefore,

$$\overline{I^2} / \overline{i^2} = \frac{1}{2} I M^2 / e \Delta f$$

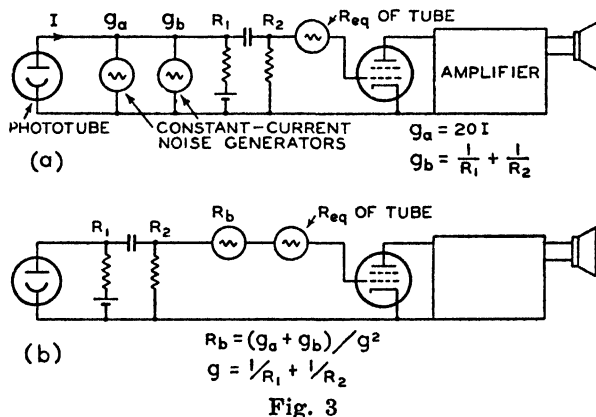
For values  $I = 1$  microampere,  $\Delta f = 10,000$ , and  $M = 1$ ,

$$\overline{I^2} / \overline{i^2} = 1.6 \times 10^8, \text{ or } 82 \text{ db.}$$

The phototube noise can be considered as coming from a constant-current generator with a noise-equivalent conductance value of twenty times the average phototube current. Equivalent circuits for this substitution are shown in Figures 3-a and 3-b.

When the phototube load resistance is one megohm, the fluctuation-noise contributions from phototube and resistor are equal for a phototube current of 0.05 microampere. At higher current levels the phototube noise predominates, but the current of 0.05 microampere gives noise 69 db below the signal level for a 10,000-cycle effective bandwidth and 100 per cent modulation.

Direct amplification of the current emitted by the photo cathode can be accomplished by "gas amplification" or by secondary-emission amplification. The effect of such amplification is to increase the signal and the noise outputs in the same ratio, except for the addition of a small amount of noise associated with the amplification mechanism.<sup>9</sup> If we assume as a first approximation that the signal-to-noise ratio in



the phototube output is unchanged by this amplification we find that the noise-equivalent conductance would be

$$g_{eq} = 20 IN \quad (12)$$

$N$  is the current-amplification ratio. When  $N = 5$ , the phototube noise becomes equal to the noise from a one-megohm load resistor for an output current of only 0.01 microampere. This value corresponds to a photo-emission current of only 0.002 microampere. If we were interested in a tube working at audio frequencies at such a low output level we would still obtain a signal-to-noise ratio of 55 db for 100 per cent modulation and a 10,000-cycle bandwidth from the tube itself. Subtraction of 3 db for the added resistor noise and 10 db as an allowance for lower modulation levels leaves a 42-db signal-to-noise ratio as an approximate theoretical value for the assumed conditions. Use of a high-vacuum phototube without current amplification, with the same load and the same light input, would result in a total noise reduction of 3 db and a signal reduction of 14 db, so the result would be a 31-db

ratio with the same allowances as in the other case. At these low operating levels the signal-to-noise improvement with current amplification would be quite marked, but the assumed outputs are considerably below those usually encountered in practice. The real value of gas amplification in phototubes used for sound work comes from the fact that the input signal to the amplifier becomes greater in comparison to the hum, microphonics, or other disturbances which might be present. The high assumed load resistor permits us to ignore normal tube fluctuation noise in this case also. The one-megohm value is not inconsistent with the assumed 10,000-cycle effective bandwidth if the input-circuit capacitance, including that of the phototube, does not exceed 15  $\mu\text{f}$ .

#### TELEVISION CAMERA PICK-UP TUBE

The output signals from an Iconoscope or from other television camera pick-up tubes have certain characteristics in common with those of phototube-output signals. The output current is proportional to the light input; the signal which we wish to amplify appears as modulation of this current; and fluctuation current is produced in the pick-up tube in accordance with the shot-effect law. The major difference is in the effective band width, which is of the order of 5 megacycles in the television case.

When the capacitance of the pick-up tube and the first amplifier tube total 20  $\mu\text{f}$ , a resistor of 1600 ohms could be used to obtain approximately uniform response over a 5-megacycle band. It would be practical to use an amplifier tube with less than 1600 ohms for its noise-equivalent resistance, thus insuring that the amplifier tube does not contribute seriously to the noise level. However, the thermal-agitation noise of the resistor would exceed the pick-up tube noise for all pick-up tube currents less than 30 microamperes, and would seriously limit the sensitivity of the system.

This thermal-agitation noise can be greatly reduced by the substitution of a resistor of considerably greater value. The signal voltage developed in the input circuit then becomes greater at low frequencies than at high frequencies, but this effect can be compensated for by using an inductance as the plate load for the first amplifier tube. A resistance in series with this inductance balances the effect of the resistance in parallel with the input-circuit capacitance. This circuit arrangement is indicated in Figure 4-a; additional refinements, such as circuit elements to provide the right amount of damping at the plate-circuit resonance frequency, are not considered.

Figure 4-b is an equivalent circuit showing the pick-up-tube noise and the resistor noise introduced by constant-current noise generators

with noise-equivalent conductance values of  $20I$  and  $1/R$ , respectively. The tube noise is shown as introduced by a constant-voltage noise generator  $R_{eq}$ . The diagram gives a correct indication of the noise-frequency distribution; noise current from  $g_a$  and  $g_b$  is amplified in a uniform manner over the amplifier-frequency band since it enters the system in the same manner as the signal, while noise from  $R_{eq}$  is amplified in the manner indicated by the plate load of the first tube.

The noise voltage produced by  $R_{eq}$  could also be produced by a constant-current noise generator represented by a noise-equivalent

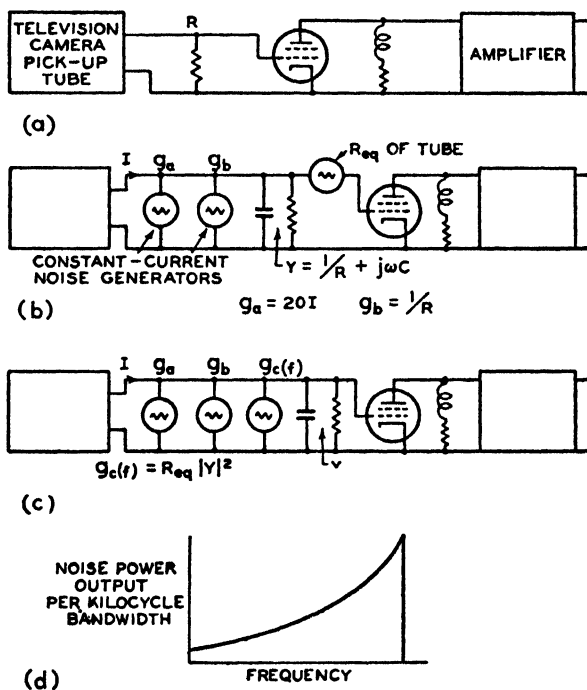


Fig. 4

conductance varying in the proper manner with frequency. This "generator" is represented as  $g_c(f)$  in Figure 4-c. The mean-square voltage delivered by  $R_{eq}$  in a small frequency band  $df$  is

$$d\bar{e}^2 = 4kT R_{eq} df$$

The square of the admittance of the input circuit is

$$|Y|^2 = \left( \frac{1}{R} \right)^2 + \omega^2 C^2 = g^2 + \omega^2 C^2$$

The mean-square current in  $Y$  which would produce the mean-square voltage  $d\bar{e}^2$  is

$$d\bar{i}^2 = d\bar{e}^2 |Y|^2 = 4kT R_{eq} |Y|^2 df$$



The mean-square current produced by a conductance  $g_c$  is

$$d\bar{i}^2 = 4kT g_c df$$

Consequently, the required noise-equivalent conductance to produce the same noise-equivalent mean-square voltage as that from  $R_{eq}$ , in a specified narrow frequency band, is

$$g_c = R_{eq} (g^2 + \omega^2 C^2)$$

We can symbolize this by the equation

$$g_{eq(f)} = R_{eq} |Y|^2$$

The total noise-equivalent conductance represented in Figure 4-c is

$$g_{eq(f)} = g_a + g_b = g_{c(f)}$$

or, substituting values,

$$g_{c(f)} = 20I + \frac{1}{R} + \frac{R_{eq}}{R^2} + R_{eq} \omega^2 C^2$$

The noise power output per unit bandwidth for the system is proportional to  $g_{eq(f)}$  so it can be represented by the curve of Figure 4-d. An average noise-equivalent conductance value can be obtained readily from this equation. It is

$$\overline{g_{eq}} = 20I + \frac{1}{R} + \frac{R_{eq}}{R^2} + \frac{1}{3} R_{eq} \omega^2_{max} C^2$$

The total noise-power output will be proportional to this value.

Let  $R = 50,000$  ohms

$C = 20 \mu\mu\text{f.}$

$R_{eq} = 720$  ohms

$f_{max} = 5 \times 10^6$  cycles per second

Then, when  $I$  is given in microamperes,

$$\begin{aligned} \overline{g_{eq}} &= (20I + 20 + 0.29 + 96) \times 10^{-6} \\ &= (20I + 116) \times 10^{-6} \text{ mho} \end{aligned}$$

The corresponding equation for the circuit using the 1600-ohm resistor is

$$\begin{aligned} g_{eq} &= 20I + \frac{1}{R} + \frac{R_{eq}}{R^2} \\ &= (20I + 625 + 281) \times 10^{-6} \\ &= (20I + 906) \times 10^{-6} \text{ mho} \end{aligned}$$

At low current inputs an advantage of about 9 db in signal-to-noise ratio is indicated for the circuit of Figure 4-a. The current input required to produce noise equal to the fixed noise under the assumed conditions in the circuit of Figure 4-a is 5.8 microamperes and the rms fluctuation current in a 5-Mc band with this current flowing is 0.0043 microamperes; the rms fluctuation current with no signal input ( $I=0$ ) is 0.003 microampere. Since noise is evidently not at a prohibitive level with the 5.8-microampere signal, operation at lower levels may be assumed. At low-input levels the first amplifier tube is the principal noise source.

The frequency-distribution curve for the circuit, shown in Figure 4-d, will quite evidently produce a different effect on the television screen than would a uniform distribution. Fluctuation "noise" on a television screen gives somewhat the appearance of a snow storm. When the noise is concentrated in the high-frequency portion of the band to the extent indicated in Figure 4-d the result is finer "flakes." Tests have shown that greater noise power outputs can be tolerated under this condition than under the condition of uniform frequency distribution. Therefore, the effective improvement obtained from the circuit of Figure 4-a (under the assumed conditions) over the circuit using the 1600-ohm load resistor would be even greater than the 9-db power-output-ratio improvement.

#### RECEIVER INPUT CIRCUITS

The noise from the input circuit of a radio receiver can be divided into that produced by thermal agitation in the circuit itself and that picked up by the antenna. The first part is readily determined. An equivalent circuit such as the circuit of Figure 1-d\* can be used to represent the system, with a noise-equivalent resistance value equal to the resonant impedance of the circuit assigned to the noise generator  $R_n$ . When the input circuit does not have much effect on the overall selectivity of the receiver the "filter" of Figure 1-d can be eliminated and the noise-equivalent resistance for the amplifier can be added directly to that for the circuit.

When the first circuit is selective enough to have an effect on the overall selectivity, the noise-equivalent resistance for the amplifier should be multiplied by the ratio of the effective bandwidth determined for the amplifier only, to that for the complete system. The noise-equivalent resistance value thus obtained corresponds to the value for the noise generator  $R'_n$  of Figure 1-e.\* It can be added to the noise-equivalent-resistance value for the input circuit as before and the

---

\* See page 511, RCA REVIEW, April, 1941.

noise-equivalent sideband input for the receiver can be determined by using the total noise-equivalent resistance and the overall effective bandwidth.

*Example:* Let the first tube be an r-f amplifier with a noise-equivalent resistance of 10,000 ohms. Assume an effective bandwidth of 6000 cycles with the first circuit disconnected and 4000 cycles with the first circuit in use; an input circuit operating at 600 kilocycles with a "Q" of 100 could produce this result. Let the resonant impedance of the input circuit be 50,000 ohms. The resulting total noise-equivalent resistance is 65,000 ohms. "Ensi" for this receiver, referred to the grid of the first tube, would be 2.1 microvolts.

Of course, we could obtain the same result by using the effective bandwidth and the noise-equivalent resistance of the amplifier as reference values and assigning a correspondingly reduced noise-equivalent resistance to the circuit. The total noise-equivalent resistance would then be 43,000 ohms and the effective bandwidth 6000 cycles; "ensi" would still be 2.1 microvolts.

An extension of the same idea can be applied in the analysis of a receiver using an "untuned r-f" stage ahead of a frequency converter. A circuit for such an arrangement is shown in Figure 5-a, and a representation of a curve of power output against frequency for a constant-current "sideband" signal introduced at point "A" is shown in Figure 5-b. This curve applies when the receiver is adjusted for a signal of 1000 kc; the assumed intermediate frequency is 455 kc and the corresponding oscillator frequency is 1455 kc. The dotted curve (Figure 5-b) represents the response of the interstage coupling circuit, and the relations between the heights of the rectangles and the dotted curve represent the relative gains (squared) of the converter itself at the different frequencies indicated. The squares of the relative overall gains determined for one such system were as follows:

	<i>I-f</i>	<i>Signal</i>	<i>Image</i>	<i>2d-harmonic Images</i>	
Frequency	455	1000	1910	2455	3365
(Relative gain) <sup>2</sup>	1.72	1.00	0.75	0.22	0.15

Small responses could be observed at higher frequencies but their importance with respect to the total noise output was small.

Additional data for this system were:

Converter noise-equivalent resistance .....	240,000 ohms
R-f gain .....	5
R-f tube noise-equivalent resistance .....	10,800 ohms
Circuit resistance (1000 kc) .....	100,000 ohms

Converter noise-equivalent resistance values are referred to the signal frequency only; the value of 240,000 ohms referred to the r-f grid (divide by 25) gives 9600 ohms.

The r-f tube produces noise at all the response frequencies, but comparison is to be made with a circuit operating at only one of those frequencies—1000 kc. Consequently the noise-equivalent-resistance value to be added on account of the r-f tube is obtained by adding the

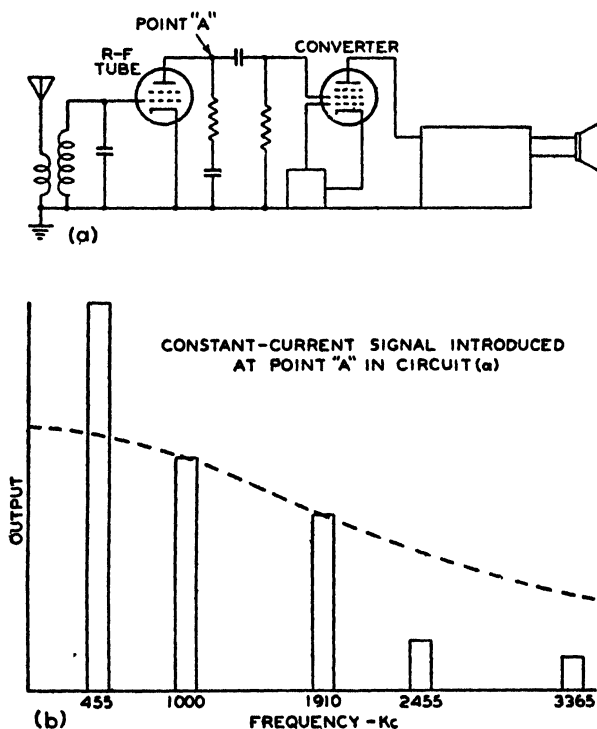


Fig. 5

(relative gain)<sup>2</sup> factors and multiplying their sum by the noise-equivalent resistance for the r-f tube; the resultant product is 41,500 ohms. The total noise-equivalent resistance for the system is consequently 151,000 ohms. A "broad" input circuit is assumed.

### ANTENNA NOISE

An antenna can be regarded as a transformer coupling the input circuits of a receiver to "space". In this sense, the radiation resistance of an antenna is the reflected resistance of "space" measured at the antenna terminals, and the efficiency is the ratio of the radiation resistance to the total resistance of the antenna. There will be a

thermal-agitation voltage at the terminals of an antenna of the magnitude determined by the antenna temperature and the ohmic or dissipative resistance of the antenna, but noise associated with the "radiation resistance" component does not originate in the antenna; it is properly classified as "received" noise.

There is one situation in which this received noise can be calculated. If we imagine an antenna in a large enclosure, with the boundaries and the contents of the enclosure maintained at a constant temperature, we know that the antenna must then be in thermal equilibrium with any resistor connected across its terminals. This condition means that the thermal-agitation law must apply to the radiation resistance of the antenna as well as to the dissipative resistance.

When a resistor is connected to the antenna, part of the thermal-agitation energy is radiated into the enclosure. Maintenance of thermal equilibrium requires that an equal amount of energy be received by the antenna; otherwise the resistor would be cooled by the loss of thermal energy to the surrounding space. The thermal-agitation voltage associated with the radiation resistance would be a measure of this received energy. If the boundaries of the enclosure were cooled to a temperature below that of the resistor, the resistor could actually lose heat by radiation, no thermodynamic principle would be violated and the thermal-agitation voltage association with the radiation resistance would be reduced. We could take this into account by using a noise-equivalent resistance for the antenna equal to the sum of the dissipative resistance and the proper fraction of the radiation resistance; or if the temperature of the enclosure was higher than that of the antenna and the resistor, we could use a suitable multiple of the radiation resistance.

Unfortunately, since we cannot locate any boundaries for the space enclosing a real antenna, this method of noise calculation cannot be used. An experimental approach would require a determination of the amount of noise picked up by antennas of known characteristics at various frequencies. Perhaps analysis of the results of such an investigation would reveal a steady component of noise which could be classified as thermal agitation. Our real interest, however, would be in the determination of that minimum noise level which could be expected to persist for time intervals long enough to permit the reception of useful signals. We need not be greatly concerned as to whether or not the name "thermal agitation" is properly applicable to that minimum noise.

The "transformer" analogy indicates that the received noise power will be proportional to the radiation resistance when other factors (such as directivity) remain constant. If we assume that the relation between radiation resistance and noise input is known for a particular system

we can represent this component of noise by a noise-equivalent resistance such as  $R_c$  in the circuit of Figure 6-b;  $R_c$  will be a multiple (or fraction) of that component of the circuit resistance measured at the grid, which is due to the antenna radiation resistance. This component is indicated as  $R_2$  in Figure 6-b. Its magnitude can be calculated by transformer theory and the ratio of its magnitude to the total resistance ( $R_2/(R_1 + R_2)$ , Figure 6-b) determines the efficiency of the system as a whole. The ratio of " $R_c$ " to the total  $R_{eq}$  determines the efficiency of the system with respect to signal-to-noise ratio, for if  $R_c$  is much greater than  $(R_a + R_b)$  the signal-to-noise ratio in the receiver approaches equality with the signal-to-noise ratio existing in "space." It is evident that this desirable condition can be realized most readily

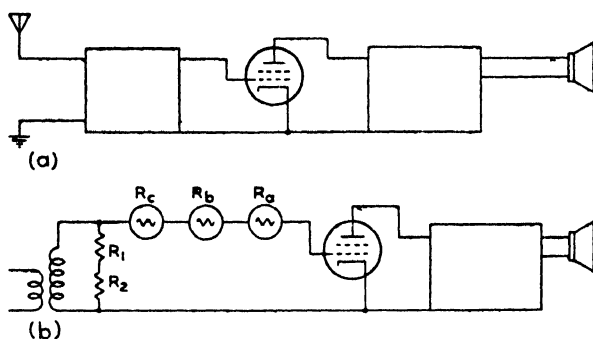


Fig. 6

if the ratio of the noise-equivalent-resistance value corresponding to the radiation resistance, to the radiation-resistance value happens to be large; but this is no more significant than a statement that a quiet receiver is of no particular value in a noisy location. When it is found that the ratio is small in a given situation, we are justified in doing everything possible to improve the coupling between the antenna and the grid of the first tube and to reduce circuit losses to a minimum.

In most home receivers operating at low frequencies the component of circuit impedance derived from the radiation resistance is so small that noise picked up by the antenna under quiet conditions is negligible in comparison with the internally-generated fluctuation noise. At higher frequencies, however, it is practical to build efficient antennas of reasonable dimensions. Consequently the determination of minimum values for the ratio of radiation resistance to noise-equivalent resistance at the higher frequencies may become a matter of considerable importance.

## FEEDBACK

A simple circuit involving feedback is shown in Figure 7. A signal current  $i$  is introduced from a high-impedance source. A voltage  $e_g$  is developed between the grid and the cathode of the tube. The plate current  $i_b$  flowing through the "tickler coil" induces a voltage in the grid circuit. This induced voltage has the same effect as a second current

$$i_1 = -\frac{M}{L} i_b = -\frac{M}{L} g_m e_g$$

introduced into the circuit in the same manner as the signal current, and the value of  $e_g$  is the resultant of the effect of these two currents in the grid circuits. Represent the impedance of the grid circuit as  $Z$ . Then,

$$e_g = \left( i + \frac{M}{L} g_m e_g \right) Z$$

$$\text{or } e_g = \frac{iZ}{1 - \frac{M}{L} g_m Z}$$

$$\text{and } i_b = \frac{ig_m Z}{1 - \frac{M}{L} g_m Z}$$

A spurious current component originating in the plate circuit will be represented by  $i'_b$  and a spurious component originating in the input circuit will be represented as  $i'$ . Inclusion of these components gives the total current into the grid circuit as

$$i_{\text{total}} = i + i' + \frac{M}{L} i'_b + \frac{M}{L} g_m e_g$$

$$\text{consequently } e_g = Z \left( i + i' + \frac{M}{L} i'_b \right) + \frac{M}{L} g_m Z e_g$$

$$\left( i + i' + \frac{M}{L} i'_b \right) Z$$

$$\text{or } e_g = \frac{\quad}{1 - \frac{M}{L} g_m Z}$$

$$\text{and } i_b = g_m e_q + i'_b$$

$$= \frac{(i + i') g_m Z}{1 - \frac{M}{L} g_m Z} + i'_b \left[ 1 + \frac{\frac{M}{L} g_m Z}{1 - \frac{M}{L} g_m Z} \right]$$

$$= \frac{(i + i') g_m Z + i'_b}{1 - \frac{M}{L} g_m Z}$$

The numerator represents just the plate-current components which would be observed in the absence of feedback, so it is evident that the signal component and both spurious components are affected to the same degree. The result should not be surprising; it is difficult to see how feeding part of the output back into the input could affect the relation between the desired signal and spurious signals introduced

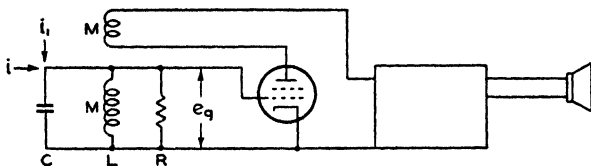


Fig. 7

with the desired signal or generated between the "input" and "output" points.

It is conceded that situations of greater complexity, to which the above statement does not apply, can be developed in vacuum-tube amplifier circuits. However, the circuit of Figure 7 can be used to illustrate some of the effects of feedback on signal-to-noise ratio and particularly on the measurement of noise.

(1) When a second amplifier stage following the circuit of Figure 7 produces a significant amount of fluctuation noise, the amount of feedback affects the signal-to-noise ratio by its effect on the first-stage gain.

(2) The feedback in the circuit of Figure 7 changes the effective bandwidth of the circuit and, consequently, it may change the effective bandwidth of the whole system. The signal-to-noise ratio in the plate circuit of the tube would be unchanged if the signal power were distributed uniformly over the frequency band passed by the system, or if the frequency band passed by the following amplifier was so narrow that  $Z$  could be replaced by  $R$  in the equations for Figure 7 for that



band; otherwise, the total signal-to-noise ratio in the output of the amplifier of Figure 7 would change with the amount of feedback.

(3) The frequency distribution of the output noise changes when feedback changes the effective bandwidth by a significant amount.

In the measurement of noise it is common practice to make a measurement of noise-power output with the input circuit of the first tube effectively shorted (a "carrier" signal is introduced when necessary) and to compare the result of this measurement with the noise-power output observed with the input circuit in use. With the circuit of Figure 7 the feedback is eliminated when the input circuit is shorted. Shorting the input circuit might result in a considerable change in the noise-power-output component due to tube noise, especially when the feedback is regenerative. It is evident, therefore, that the ratio of the noise-power output measured with the input circuit shorted to that measured with the input circuit operative does not always represent the ratio of tube noise to total noise. When there is regenerative feedback into the input circuit there will be a decrease in noise-power output when the input circuit is shorted, even though the circuit noise is entirely negligible.

The principal limitation to the scope of this series is implied by the title phrase "At Moderately High Frequencies." There is a source of current fluctuations associated with the component of tube-input conductance produced by electron transit-time effects, a source which becomes important when the input frequency is high enough to make the transit-time input conductance relatively large.<sup>12</sup> There are also complications introduced at high frequencies by electron-transit angles, which make it more difficult to take feedback into account in noise determinations. The lower limit of frequencies at which these effects become important depends on the high-frequency operating characteristics of the first amplifier tube; the limit may range from about 30 to 200 megacycles. The theory and application methods presented in this series are believed adequate to permit the complete determination of the more important manifestations of fluctuation phenomena at lower frequencies.

---

<sup>12</sup> D. O. North and W. R. Ferris, "Fluctuations Induced in Vacuum Tube Grids at High Frequencies." *Proc. I.R.E.*, Vol. 29, pp. 49-50, February (1941).

# ELECTRON BEAMS AND THEIR APPLICATIONS IN LOW VOLTAGE DEVICES\*†

BY

HARRY C. THOMPSON

RCA Radiotron Division, RCA Manufacturing Company, Inc.,  
Harrison, New Jersey

**Summary**—A study has been made of the segregation into beams of the space current in devices of the over-all size of commercial receiver tubes and at potentials less than 300 volts. Electrode coatings of luminescent material were used to make the beam traces apparent on any or all electrodes. Qualitative relationships between beam formations and relative electrode potentials are stated. Space currents of a few milliamperes have been concentrated into beams less than 0.010 inch wide in simple structures. Special control grids associated with conventional cathodes have been found to combine good space current control with effective beam formation. These effects together with control of beam width and direction can be obtained in a single device.

Simple structures are used to segregate the electron discharge from a single cathode into a few or many similar electron beams. Between such structures and the outermost electrodes are placed perforated positive electrodes with their openings disposed to receive and pass the electron beams. Such electrodes are found to receive as little as two per cent of the current computed from their projected area. Such perforated electrodes include conventional type grids.

The relationships between beam widths and electrode potentials have been found to be such that mutual volt-ampere relations can be radically different from those hitherto utilized. Linear, saturation type, or special volt-ampere relations can be obtained. Individual electrode volt-ampere relations can be altered by utilizing the action of the field of such an electrode to change the width and direction of the beam impinging upon that electrode independently of interelectrode coupling. A variety of negative conductance devices have been made on this principle.

## I. INTRODUCTION

THE high vacuum devices in which electron beams have been used previously, such as the X-ray tube and the cathode-ray oscillograph, have employed, for the most part, small space currents, single beams of circular cross section produced by essentially spherical electrostatic or magnetic lens systems, and high electrode potentials. Attempts to take advantage of the properties of beams for other purposes have usually resulted in structures more or less like those employed in the above devices and evidently derived therefrom. Such structures, as compared with receiving tubes and small power tubes, tend to be expensive to make, large in size, inefficient in their use of cathode power, and inadequate in their ability to carry current.

\* Decimal classification: R138.

† Reprinted from *Proc. I.R.E.*, October, 1936.

The present investigation represents a different approach to the subject, and was begun as the result of an observation made more than ten years ago on a commercial form of triode whose anode had been coated with luminescent material. With a certain ratio of potentials on grid and anode there appeared on the latter narrow, sharp-edged luminous lines opposite the openings between grid wires, indicating a nearly complete segregation of space current into beams. The space current so segregated was many milliamperes at anode voltages of two or three hundred and the widths of the luminous bands could be controlled by the electrode potentials.

These observations suggested that electrodes of various kinds, located in the noncurrent carrying spaces between beams and used for control purposes, might have a high input impedance even though operated at positive potentials, and that screening electrodes similarly placed might receive and waste very little space current. It was also thought that the variation of beam width might make possible, by redistribution of space current between various positive electrodes suitably placed, transconductance and conductance characteristics of kinds unobtainable in devices utilizing the space-charge phenomenon alone.

Such expectations have been fulfilled in a variety of devices which are characterized by compactness, relative simplicity, high current carrying ability at low potentials, the use of rectangular section beams produced by cylindrical lens systems, the use of several beams from a common cathode, and structural forms adapted to assembly methods more nearly like those for amplifier and small power tubes than those for devices of the cathode-ray oscillograph type.

The devices here presented belong, with one exception, to a class of devices in which the advantages of segregation of the discharge into beams and of variation of beam width and focus are utilized. Two other classes of devices dependent upon the deflection of the median planes of rectangular section beams and upon the use of magnetic fields are excluded from this discussion.

The work along these lines was begun a number of years ago, and the elementary principles and potentialities of it were established. Later it was learned that work of a somewhat similar kind was being done in Germany by Knoll and Schloemilch.<sup>1,2</sup>

<sup>1</sup> M. Knoll and J. Schloemilch, "Electron optical current distribution in electron tubes with control electrodes," *Arch. für Elektrotech.*, vol. 28, pp. 507-516; August 18, (1934).

<sup>2</sup> M. Knoll, "Amplifying and transmitting valves considered as a problem in electron optics," *Zeit. für. Tech. Phys.*, vol. 51, no. 12, pp. 584-591, (1934).

## II. METHODS OF OBSERVATION

In structures for the study of beam phenomena appropriate electrodes were coated with a thin and uniform layer of fine particles of a luminescent material such as willemite. Such a layer becomes luminous where and only where electrons of sufficient energy arrive at a sufficient rate. If the space current is divided into beams, there appears on a coated and bombarded electrode a luminous pattern corresponding to the cross section of the beams at the surface of the electrode. Observations of that pattern can often be made with the potential of the bombarded electrode as low as twenty volts. In cases where it was not clear from the luminous pattern of beam traces just what had happened to the cross section of the beam in transit to the target, a low pressure of gas and the consequent glow made it possible to observe the beam throughout most of its path. The pressure of the gas introduced for this purpose was always insufficient to cause observable change in the trace patterns and hence the observed beam paths were only slightly different from those in high vacuum. It will be seen from the data below that this method of study is of practical utility in the design of beam devices.

The first ten figures illustrate the beam-forming properties of simple structures in association with conventional forms and sizes of cathodes and certain elementary properties of the beams thus formed. The remaining figures show some typical devices for the utilization of such beam properties.

## III. OBSERVATIONS

Fig. 1 shows scale sections of a triode with parallel plane electrodes and indicates the observed beam traces on the anode or No. 2 electrode at 250 volts for four different grid or No. 1 electrode potentials. The shapes of the equipotential surfaces in the grid openings are roughly indicated. With the grid at seventy-six volts positive, approximately geometrical shadows of the grid wires appear as indicated on the anode with temperature-limited space current. The grid is here approximately at its space potential, the calculated value of which is seventy-eight volts. A similar trace pattern was observed with space-charge-limited current with the grid at its correspondingly lower space potential. In both cases the equipotential surfaces are parallel planes except in regions very close to individual grid wires. In the same figure, the traces for twenty-two and five-tenths volts positive and for zero volts on the grid correspond, respectively, to focus of the electron beam on the anode and between the anode and grid. These two cases are for space-charge limitation of the current. The fourth section of the figure shows

the result of placing the grid above its space potential at 172 volts whereby the grid opening becomes a diverging lens and the traces of adjacent beams overlap, as indicated, on the anode.

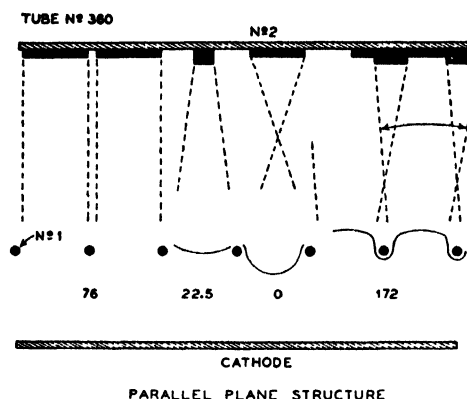


Fig. 1—Beam formation by grid openings.

<i>No. 1 volts</i>	<i>No. 2 volts = 250</i>	<i>Beam Focus</i>
0		Before No. 2
22.5		On No. 2
22.5-76		Beyond No. 2
76		At infinity
172		Virtual

The actual appearance of the beam traces for these four cases is shown in Fig. 2, which is a group of four photographs of the anode of the triode of Fig. 1 for the above four conditions. The preceding two

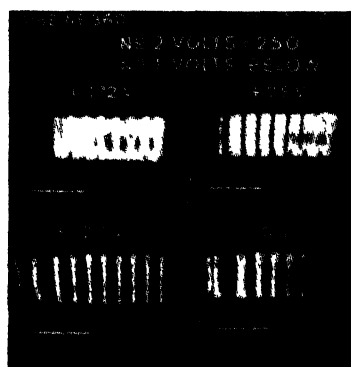
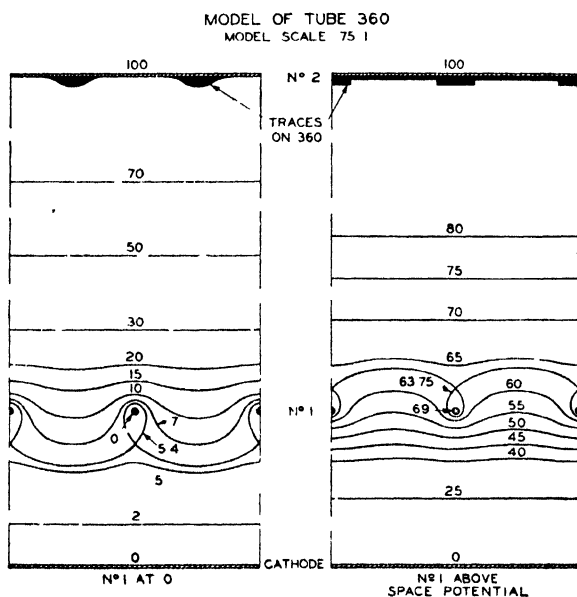
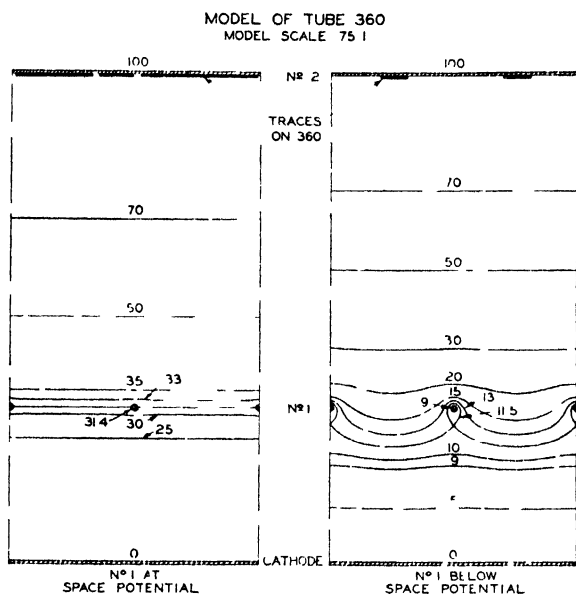


Fig. 2—Beam traces on an anode.

figures are representative of the manner of beam formation not only for the plane grid structure, but for a helical grid in a cylindrical structure at different but corresponding potentials. In the cylindrical case,



the traces for focus often have a width one tenth or less of the distance between traces and are very sharp edged.

Figs. 3 and 4 are maps of the equipotential surfaces obtained by means of a field-mapping apparatus on a 75-to-1 scale model of the triode of Figs. 1 and 2. The potentials are there shown as percentages of the anode potential; the grid potentials correspond in percentage to the actual potentials of Figs. 1 and 2. The field maps for the grid potentials of nine and zero per cent cannot, of course, correspond accurately to those existing in the observations of beam traces above, be-

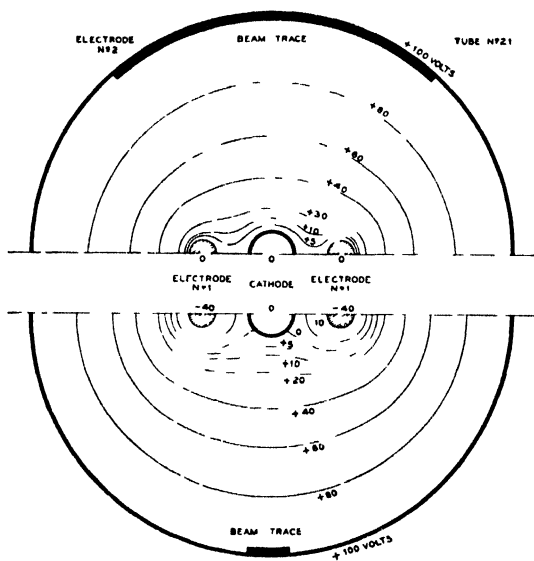


Fig. 5—Beams by a longitudinal element grid

cause, as stated, those two particular observations were made for the space-charge-limited condition which is not simulated by the field-mapping apparatus. The two maps indicate the kind of field in the grid opening which constitutes a converging lens. The above figures and data illustrate the fact that the space current can be segregated into beams without the cutting off of emission from any part of the cathode.

Fig. 5 shows a cylindrical anode, or No. 2 electrode, a coaxial cathode, and two longitudinally placed wires constituting the beam-forming or No. 1 electrode. With the latter at forty volts negative bias, two narrow beams are formed. The anode trace of one of them is indicated. The location of the intersections of the zero equipotential surface with the cathode surface for that case indicates that a considerable part of the cathode is cut off as regards emission, unlike the case of the first-

mentioned device for similarly narrow beams. The map for zero bias of No. 1 electrode shown in the upper half of the figure indicates no cutoff of emission at the cathode.

In Fig 6, a typical instance of the manner in which the width of the beam trace varies with anode potential is shown. The unlabeled electrode is the cathode in this and all following figures. For a positive

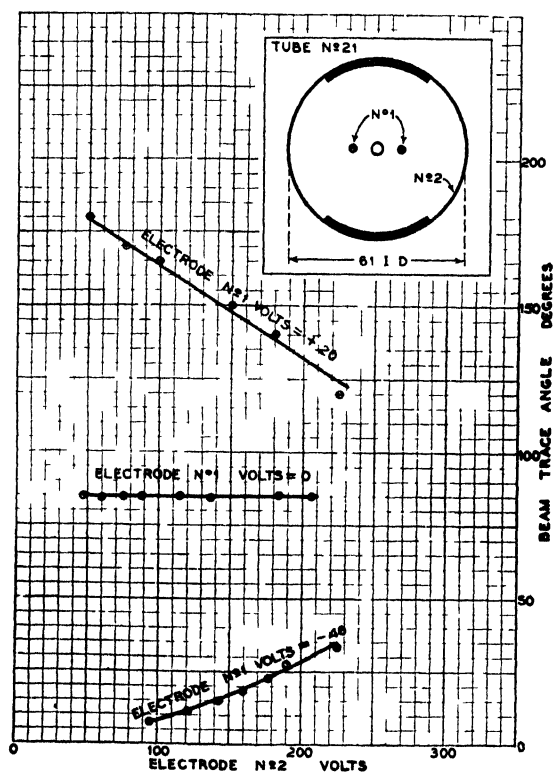


Fig. 6—Beam width and anode potential

bias on the beam-forming electrode, an increase of anode potential causes a decrease of beam width, while for a negative bias the reverse is true. This illustrates a behavior which proves to be general except in such structures and at such potentials that a crossover or focus of the beam occurs before it reaches the anode. The constancy there shown of the beam width for zero bias of No. 1 electrode is typical of closely spaced structures for anode potentials above a certain value for each particular structure. At anode potentials lower than that value the traces are observed to increase in width in some cases, before they become invisible. There are several causes tending to spread the beam at



such low potentials, and it cannot be said at once which of these predominates.

Corresponding beam formations by longitudinal wires have been observed for numbers of wires from one to eight, and for a wide range of wire diameters and spacings from the cathode.

Fig. 7 shows a case in which the two wires are much larger than the cathode. It also shows the constancy of beam width when the ratio of the potential on No. 2 to that on No. 1 is kept constant. This illustrates another general behavior subject to qualification for low potentials as above.

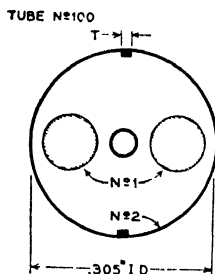


Fig. 7—Constant ratio of electrode potentials.

$$\frac{\text{No. 2 volts}}{\text{No. 1 volts}} = 3$$

No. 1 volts	No. 2 volts	No. 1 ma	T (inches)
-20	60	0.8	0.02
-30	90	2.0	0.02
-40	120	3.3	0.02
-60	180	7.2	0.02
-80	240	12.1	0.02
-100	300	15.5	0.02

Fig. 8 shows an example of the way in which beam width and current vary simultaneously with negative bias on a two-wire beam-forming electrode. Fig. 9, derived from Fig. 8, shows the constancy of the current-to-width ratio over a considerable range. It should not be concluded from this that the current per unit width is constant throughout the beam. Actually a "piling-up" of current at the sharp edges of a wide beam is often observed. No generalization of current-to-width ratio or of current distribution in beams can be made at present.

Such two-wire structures, while useful for beam formation alone, have a very poor control over the space current. In Fig. 10, however, a beam-forming structure No. 1 is shown which gives a transconductance more nearly of the conventional order and also a segregation into a rather narrow beam. The coated area of the cathode is about seventy-five per cent of that of an RCA-57 cathode of the same size. The struc-

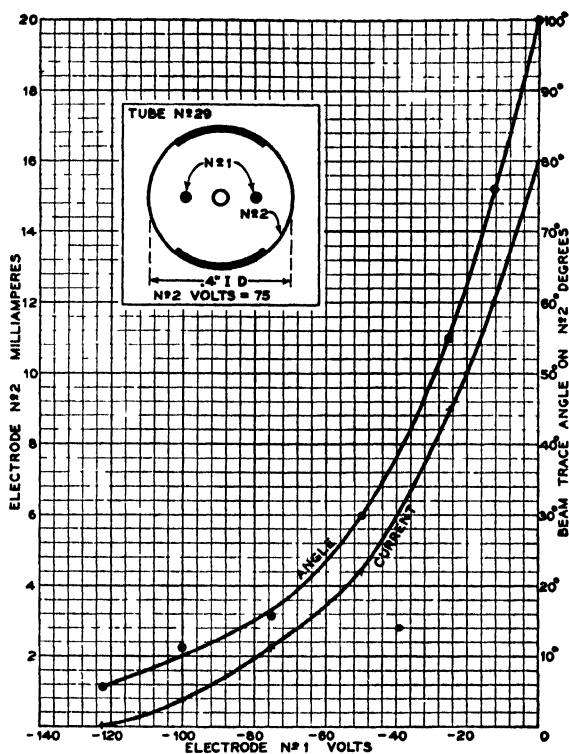


Fig. 8—Beam width and current.

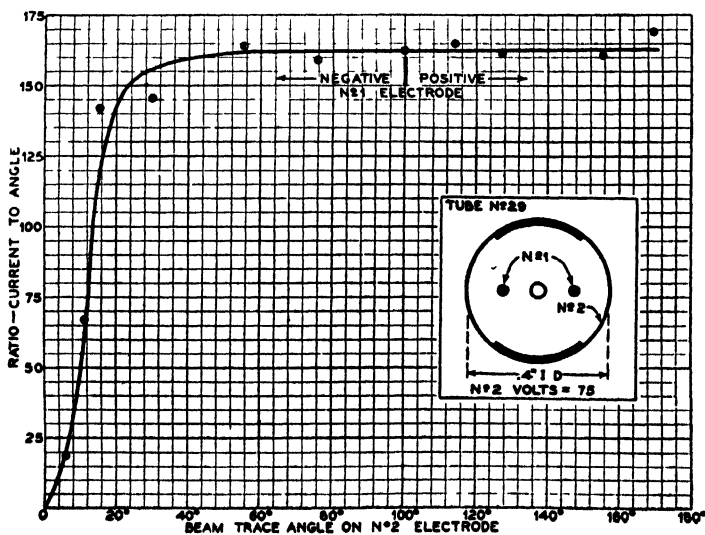


Fig. 9—Current-to-width ratio of a beam.

ture consists of a helical wire grid enclosed in a sheet-metal cylinder with a slit as indicated. The wires of the grid are thus transverse with respect to the longer dimension of the rectangular section beam formed by the slit and, while they cause the beam trace to be divided up into sections along that dimension, they do not seriously distort it in its shorter dimension.

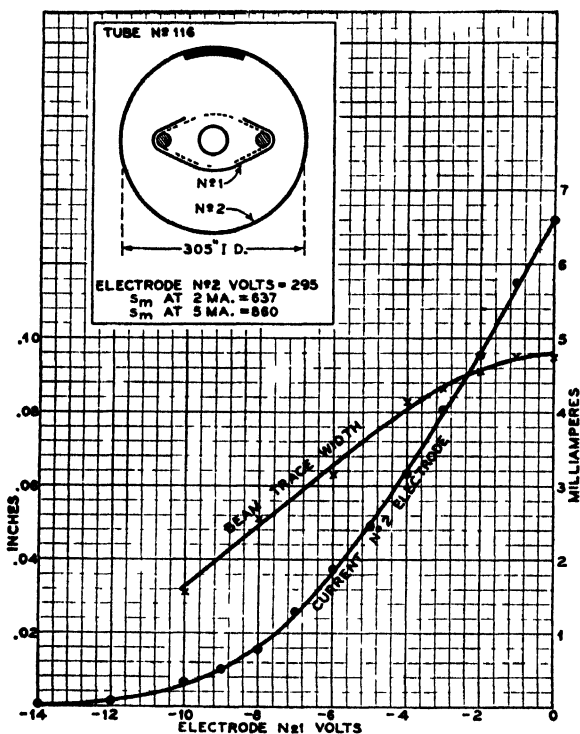


Fig. 10—Beam formation and normal transconductance.

#### IV. DISCUSSION OF OBSERVATIONS

From the above and many other observations, certain simple principles can be formulated which are sufficiently general in their applicability to constitute a valuable basis for the design of beam devices of the kind presented here. With reference to small triode structures operated space-charge limited and to anode potentials above a value which varies with the structure but which is usually of the order of twenty volts, the observations support the following statements:

(1) A nonemitting electrode operating at cathode potential and constituting a part of the cathode or intervening between it and the

anode determines, on the anode, trace patterns which are constant with varying anode potential.

(2) If the ratio of the potential of the intervening electrode to that of the anode is kept constant, the beam traces are also constant. This generalization, of which the preceding is a special case, is consistent with a corresponding mathematical generalization on electron paths where initial electron velocities are zero, as expressed by Langmuir and Compton.<sup>3</sup> The error caused by initial velocities has been too small to be observed in the small structures used except, as mentioned above, at low electrode potentials.

(3) If a thin electrode containing an opening is introduced between cathode and anode in such a way as to conform to a previously existing equipotential surface, the opening acts upon the electron stream through it as a converging or a diverging lens, according to whether the electrode is below or above its space potential, respectively. The opening has approximately no deviating effect upon the stream when the electrode is at its space potential. In the latter case a grid is observed to form on the anode a shadow pattern which is a geometrical projection of itself.

In many structures, the converging effect of an opening may be such, at suitable potentials, as to give a focus or crossover of the electron stream either at or before the anode as in Fig. 1. In other structures such as that of Fig. 5, the divergence of the beam entering the opening may be so great as to prevent the formation of such a focus at potentials less negative than those at which there is complete cutoff of the space current.

(4) In structures according to (3) and at such potentials that no focus occurs, it can be said that an increase of anode potential decreases the dimensions of the beam trace when the apertured electrode is positive and increases them when that electrode is negative. For the range of potentials in which one crossover of the beam occurs the reverse statement is true.

(5) For low positive, zero, or negative biases of the beam-forming electrode there may be faint, sharp-edged beam traces on the anode corresponding to a minor beam system which behaves somewhat differently from the accompanying major beam system. This minor system, often clearly distinguishable from any distortion fringing of the major traces, has its origin in a virtual source formed by those electrons which go directly toward a beam-forming element at which they cannot arrive because of its zero or negative potential. Such

<sup>3</sup> I. Langmuir and K. T. Compton "Electrical discharges in gases," Part II, *Rev. Mod. Phys.*, vol. 3, p. 252; April, (1931).

electrons are diverted at some region relatively close to the element and thus form a weaker trace pattern which behaves differently from the major traces. This minor pattern disappears abruptly at some low positive potential on the beam-forming element, indicating that the electrons in question are absorbed by that element. Some structures of the type of Fig. 1 show this minor system clearly. The current in such a minor system is usually a small percentage of that in the major system. Suitably placed screen grids and other electrodes at positive potentials may, for practical purposes, be sufficiently nearly "currentless" without resort to suppression of the minor beam system. Where the beam-forming electrode is an integral part of the cathode base structure, the minor beam system may be entirely absent. Such an arrangement constitutes a means for avoiding these undesired beam formations.

(6) Another effect which can be misleading in the investigation of beam behavior is the appearance on an anode of a general diffused luminescence which is characterized by the absence of sharp boundaries. The conclusion which has sometimes been drawn that this diffused bombardment is evidence of inefficient beam formation is erroneous in many cases. Such diffused glow is usually present and is caused by high velocity secondary electrons originating at the major traces and returning to the same electrode with sufficient velocity to cause luminescence. The conclusive evidence in certain cases is that, when a beam of cross section determined by the major trace on an anode is let through a slightly larger opening in a similar anode and collected by a more remote electrode at higher potential, there is no *diffused* luminescence on the apertured first anode and its current is very small. Moreover, in the development of devices having positively operated low-current screen and control electrodes the suppression of secondary emission from the anode by slotting or by coating it with soot from a flame results in a large reduction in the residual current to those electrodes even when they are from twenty to forty volts below anode potential. Other observations on specially made devices have confirmed the above interpretation.

(7) Insulator surfaces close to the electron stream act as additional electrodes. Observations by means of beam traces show very clearly the effects of adjacent mica, glass, or other insulators. The effects of such surfaces are consistent with those of so-called "floating" conductors similarly placed. If an insulator surface has, under particular conditions, the ability to emit secondaries in excess of the impinging primaries then it can be made to assume either of two stable "floating" potentials. One of these is close to cathode potential, the other is some

positive potential usually less than that of the highest potential electrode in the device. A transient rise of potential of the insulator can be communicated to it inductively so as to shift it abruptly from its lower to its higher stable value. A sudden change of beam-trace pattern results. It was by means of such observations that a certain erratic behavior of developmental forms of the RCA-58 and other tubes was found to be associated with the polarization of the glass envelope at

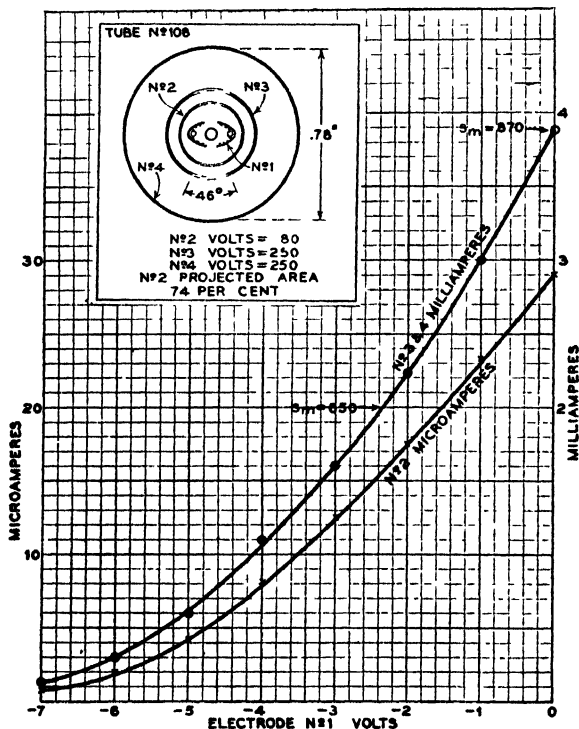


Fig. 11—Low screen current in a two-beam structure.

the higher of the two "floating" potentials. Reduction below the one-to-one value of the secondary emissivity of the interior surface of the glass by coating it with finely divided material such as carbon eliminated the existence of the upper floating potential and the behavior associated therewith.

## V. DEVICES UTILIZING ELECTRON BEAMS

### (1) Low-current positive potential electrodes.

In Fig. 11 is shown a two-beam device employing a beam-forming and space-current controlling electrode No. 1 according to Fig. 10.

The No. 2 electrode may be regarded as the equivalent of a screen grid. For the data shown, the No. 3 electrode is combined with the No. 4 cylinder as an anode. The cathode is of the RCA-57 size, but with a coated length seventy-five per cent of normal. With this in mind, it is apparent that the transconductance of 870 micromhos shown is only moderately lower than normal while the space current is segregated into two beams so that the No. 2, or screen, electrode at 150 volts receives only 0.7 per cent of the space current of four milliamperes at a No. 1 bias of zero. This occurs although the projected area of No. 2 electrode is seventy-four per cent.

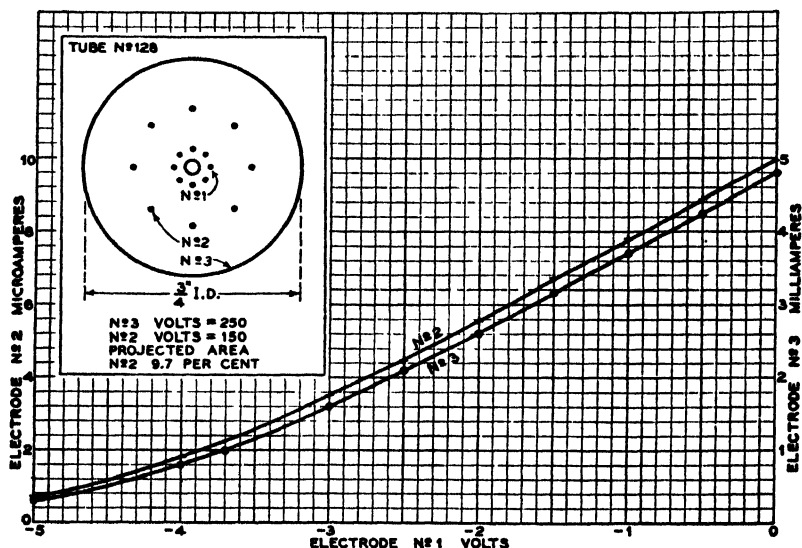


Fig. 12—Anode and screen current in an eight-beam structure.

In the device of Fig. 12, an eight-wire No. 1 electrode has its elements in register with the eight wires of the No. 2 or screen electrode. At the voltages shown the No. 2 electrode receives only 0.2 per cent of the space current at five milliamperes although its projected area is 9.7 per cent. A grid-plate transconductance of 1100 micromhos is observed at five milliamperes.

The device of Fig. 13 has the wires of its No. 2 electrode 2.67 times as large as those in the preceding device but is otherwise the same. One curve shows the anode current as a function of the potential of the No. 2 electrode over a positive range. Such an electrode is thus an example of a low-current positively operated control electrode but its transconductance is extremely poor. Considered as a screen electrode at 150 volts, it receives 0.7 per cent of the anode current although its

projected area is 25.9 per cent. The increase of current to electrode No. 2 above 150 volts is due almost entirely to secondary electrons from the anode. The low current to No. 2 below 150 volts might be thought to be due to loss of secondary electrons from it. That part of the characteristic (not shown) shows very little indication of the flattening observed where secondary emission is considerable. There is ample other evidence that segregation and not secondary emission is the cause of the low current to No. 2.

In the device of Fig. 14, a four-wire longitudinal No. 1 electrode has its openings in register with the four slits of a cylindrical screen or No.

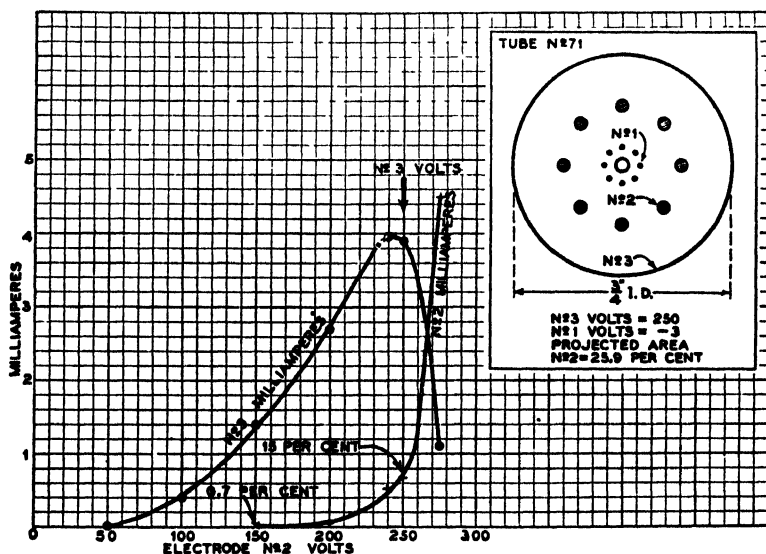


Fig. 13—Low screen current in an eight-beam structure.

2 electrode with a projected area of fifty-nine per cent. The No. 3 and No. 4 electrodes are used together as an anode for the data shown and their peculiar form has no significance for this discussion. Current to the No. 2 electrode at 100 volts positive is about one per cent of the space current when the latter is ten milliamperes.

In the device of Fig. 15, a cylindrical cathode has its emitting area confined to a helical band flush with the equal intervening nonemitting area. The helical emitting band is in register with the openings of a helical wire grid or No. 1 electrode. The helical nonemitting area of the cathode is essentially a beam-forming electrode combined with the cathode and has the effect of confining the beams from the emitting area to the spaces between grid wires. In addition to this nonemitting portion of the cathode two uncoated wires are placed along the cathode



in register with the two support wires of the grid in order to shield them from electron reception. Both No. 1 and No. 2 electrodes are sooted to suppress secondary emission. Grid and anode currents are shown for a positive range of grid potentials. At a grid potential equal to anode potential, only 0.7 per cent of the space current is taken by the grid although its projected area is 10.7 per cent. It will be readily accepted

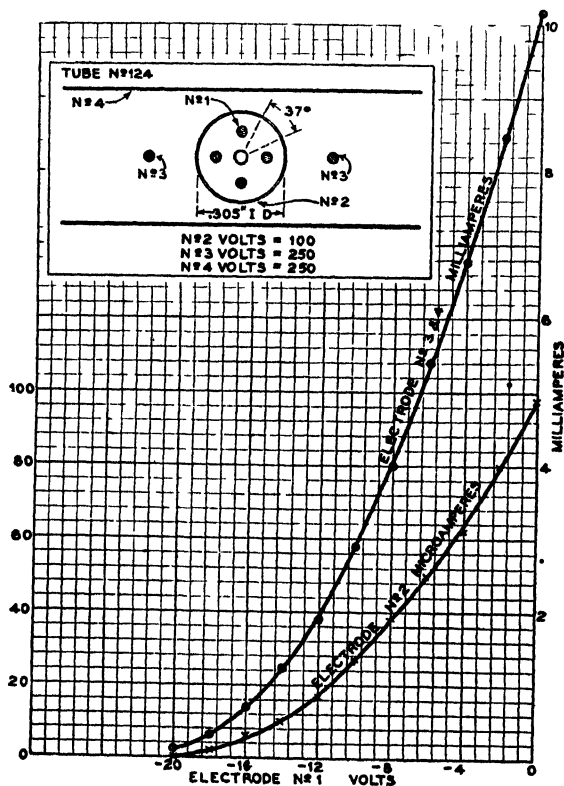


Fig. 14—Low screen current in a four-beam structure.

that the grid at three hundred volts, or fifty volts above the anode potential, does not lose an appreciable percentage of its current by means of secondary emission. Nevertheless the grid there receives only 1.4 per cent of the space current. This constitutes convincing evidence that there is efficient segregation of the space current into beams in the device. It is to be noted that the space current thus segregated and utilized is considerable, being 180 milliamperes to an anode one inch long and three quarters of an inch in diameter, at 250 volts, with the grid at 300 volts. Structures with similar properties have been

made in which the grid elements are all parallel to the cathode axis and in register with corresponding nonemitting strips on the cathode. Such devices can be used as amplifiers of classes B and C with diminished input loss and distortion. In cases where secondary emission from the anode can be effectively suppressed, a new range of operability is made possible, that in which the positive peak voltage of the grid oscillation is greatly in excess of the simultaneous anode potential.

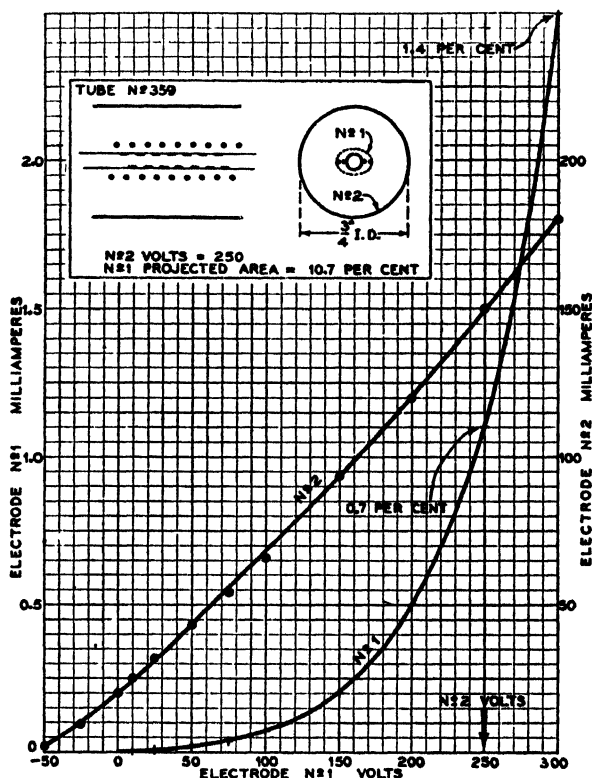


Fig. 15—Low current to a control grid operating at positive potentials.

(2) *Special mutual characteristics by means of varying beam width.*

In the device of Fig. 16, the beam-forming and controlling electrode No. 1 is of the two-wire longitudinal type. The electrode No. 2 has two slits registering with the openings of No. 1. The anode consists of Nos. 3 and 4 in combination and their peculiar form may be disregarded for the purposes of this figure. The graph shows that, for large negative bias of No. 1, the two beams formed by it pass through the slits of No. 2 without contributing appreciable current to the latter. As the bias on No. 1 is decreased, current begins to flow to No. 2 when the beams

become too wide to pass through the slits, whereupon the increment of space current with decreasing No. 1 bias is transferred entirely from the anode combination to the No. 2 electrode as is clearly shown. This result is consistent with the constancy of the ratio of current to beam width shown in Fig. 9. Such a device is typical of a class of devices in which variation of beam width is used to redistribute the space current among positive electrodes in a manner which can be predetermined so

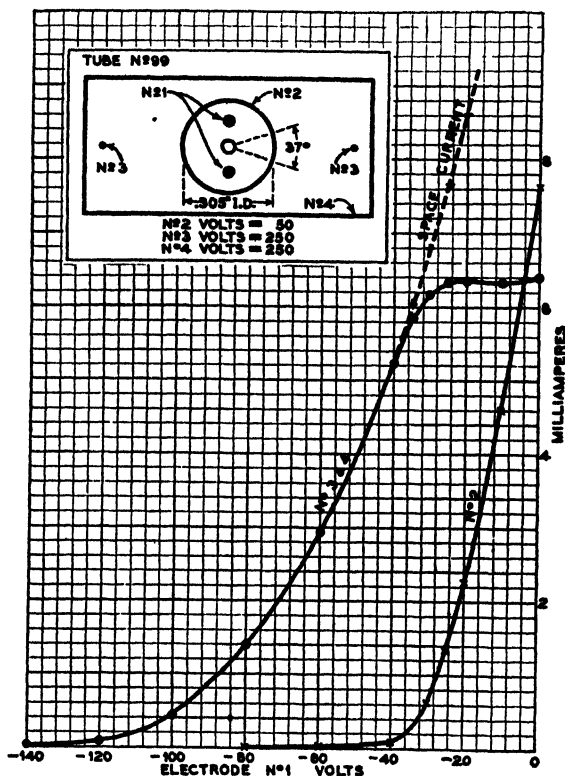


Fig. 16—Special mutual characteristic by varying beam width.

as to give those electrodes mutual and impedance characteristics of various kinds desirable for special purposes. Such characteristics are, in many cases, quite impossible to attain with devices depending on space-charge properties alone. In the above device, for instance, the current to Nos. 3 and 4 shows an upper limit equivalent in effect to emission saturation but not subject to the impracticality of the latter condition. It also illustrates the sharpening of the cutoff on the No. 2 characteristic which results from the rejection onto Nos. 3 and 4 of the smaller values of space current while No. 1 is very negative. Devices

similar in principle but with larger numbers of No. 1 elements have been made and found to operate in similar fashion but with higher transconductance. The electrode No. 2 has been replaced by one consisting of slats placed normally to the beam paths and occupying the positions of the slits in the device shown. Thereby the functions of the No. 2 electrode and the anode are inverted. Suitable shaping of the boundaries of the openings in the No. 2 electrode in that case can be made to alter the relation of anode current to No. 1 voltage, making it either linear or some other predetermined form.

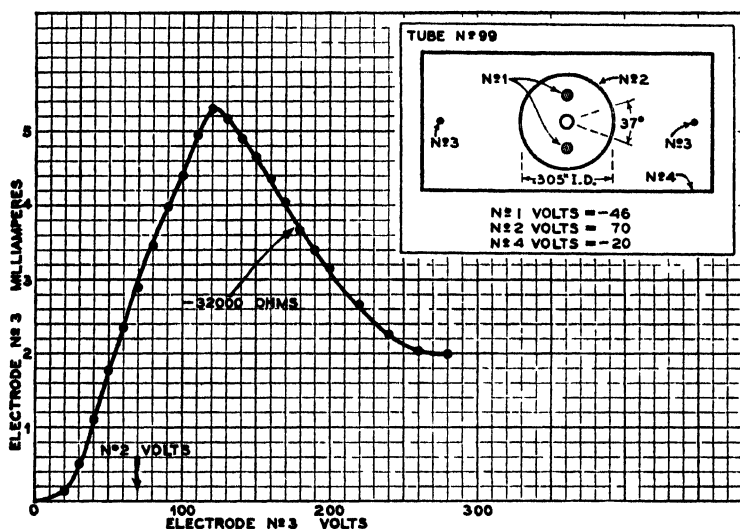


Fig. 17—Negative impedance by change of focus.

(3) *Special impedance characteristics—Negative impedance devices.*

The device of Fig. 17 is identical with that of the preceding figure, but is used differently as indicated. The volt-ampere characteristic of electrode No. 3 is shown with the other potentials as there stated. No. 3 consists of two wires of 0.020-inch diameter placed parallel to the cathode and in register with the slits of No. 2. For the potentials shown, the field outside of No. 2 is decelerating and focusing in its effect upon the beams emerging therefrom. A beam is focused before reaching a No. 3 wire when the latter is at low positive potential and the electrons passing through this focus return to No. 2 by orbital paths and form thereon traces readily seen on each side of the slit. As No. 3 potential rises, the focus of a beam approaches and finally arrives on No. 3, when its current becomes the maximum value shown by the graph. The further rise of No. 3 potential gives the falling or negative imped-

ance portion of the characteristic as shown. This decrease of current to No. 3 is caused by the recession of the beam focus to a region between Nos. 3 and 4 and the consequent return of most of the electrons to No. 2. Thus, the negative impedance of No. 3 may be said to be due to a process of defocusing with respect to that electrode. A variety of devices are operable upon this principle. It is noteworthy that the negative slope occurs while the potential of No. 3 is higher than that of any other electrode in the device, thus entirely excluding the possibility that secondary emission from No. 3 is responsible for its negative impedance.

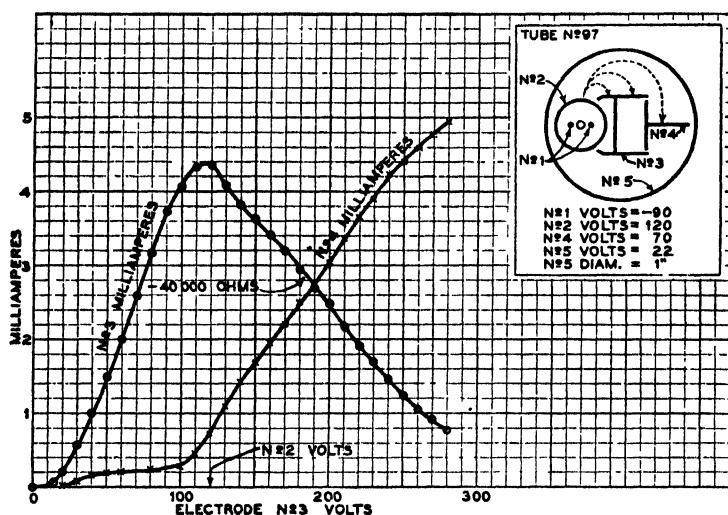


Fig. 18—Negative impedance by change of electron trajectories.

In the device of Fig. 18, the two-beam electron "gun" projects its beams tangentially with respect to the equipotential surfaces of a roughly radial electric field existing between Nos. 3 and 5. The latter is shown at a positive potential of twenty-two volts but has also been used at zero and negative potentials. No. 4 may have any positive potential in a wide range. As the potential of No. 3 is increased, the electron trajectories increase in length as indicated by the successively longer dotted lines shown on the drawing of the device. Eventually, the beams miss No. 3 entirely and are received on No. 4. During the transition of the beams from No. 3 to No. 4, the former has a negative impedance as shown. As in the preceding device, such negative impedance cannot be caused by secondary emission. This device was rendered slightly gassy and the beam paths were clearly seen to behave as stated.

Another negative impedance device, not shown, has been made in which the property stated under Section IV, Subsection (4), is utilized. The structure consists of, in order: a cathode, a beam-forming electrode used at a positive potential, a registering slit electrode used at a higher positive potential, and an anode or collector used at a still higher potential. At some potential on the slit electrode, each beam passes through its corresponding slit and the current to the electrode is small. As the potential of the slit electrode is decreased, each beam becomes too wide to pass through the corresponding slit; hence the current to the electrode increases and a negative impedance results.

The last three devices are examples of a class of devices in which the negative impedance of an electrode is due to its direct electrostatic effect upon the electron paths in such a way as to divert current from itself as its potential increases. No co-operating changes of potential on other electrodes are necessary and the device is functionally equivalent to a secondary-emission dynatron and has the advantage that the constancy of its negative impedance is dependent on geometrical constancy of the structure and not upon the sometimes unreliable secondary emissivity. Such devices have been made to oscillate at audio frequencies and at fifty megacycles. The starting and stopping of oscillation are accompanied by visible changes in the trace patterns.

#### (4) *Luminous trace voltmeters.*

The width of a beam trace, or of the dark space between traces, is a measure of the potential of the beam-forming electrode relative to the potentials of other electrodes in the device. This property is illustrated in Figs. 1 and 8. It has found application in tube voltmeters in which the "pointer" is the edge of a luminous trace, and the scale is the surface of the electrode carrying the trace. Such a device, the RCA 6E5, is now used commercially as a tuning indicator and for other purposes. The convenient form of the structure in this case is largely due to H. M. Wagner. The beam-forming electrode is here actuated by the output of a triode amplifier included in the tube.

## VI. CONCLUSION

A new array of properties of electron discharge devices is introduced by systematically utilizing beam formation. The combination of these new properties with those already in use furnishes an augmented supply of means for the improvement of existing types of devices, and for the creation of devices having entirely new properties to fulfill the new requirements which inevitably arise.

Experience with such structures as represented here indicates that

the utilization of beam formations is consistent with economy of cathode power and with the attainment of conductances and transconductances of magnitudes within the useful range even at low voltages. The difficulties of design of such structures are considerable in the present stage of the art. The difficulties of construction are, in many cases, not extraordinary.

#### ACKNOWLEDGMENT

The writer wishes to express his appreciation of the sponsorship of this work by Mr. B. J. Thompson, and also of the valuable co-operation of Mr. H. M. Wagner in the later stages of it.

## NEGATIVE RESISTANCE AND DEVICES FOR OBTAINING IT\*†

By

E. W. HEROLD

RCA Manufacturing Co., Inc.,  
Harrison, N. J.

### Summary

*By the use of a concept due to Crisson, negative resistance is shown to be a phenomenon controlled by either current or voltage but not by both together. Thus, two main classes are found differing in the shape of the volt-ampere characteristic, in the conditions for stability, in the effect of an added positive resistance, and in the effect of an internal time lag. Reliability, good power conversion efficiency, and a low ratio of the unavoidable self-reactance to the negative resistance are mentioned as being desirable characteristics of any negative resistance. A figure of merit for the voltage controlled type is shown to be  $1/\omega C_o R_o$ , where  $C_o$  is the unavoidable effective shunt capacitance. In the current controlled case  $R_o/\omega L_o$  is shown to be a merit factor,  $L_o$  being the effective series inductance. The addition of external positive resistance lowers the figure of merit for the combination.*

*A number of well-known devices are discussed after classifying them in three groups according to principle of operation. The simple group includes such devices as the dynatron and arc which produce negative resistance between two elements. The direct-coupled group comprises primarily vacuum tubes having negative transconductance in which negative resistance is produced by a direct connection between the controlling and controlled electrodes. The general properties of the negative transconductance tube as a negative resistance are detailed, including the effect of interelectrode capacitances. The third group, the reverse-phase-coupled group, is included but not treated in detail. It comprises vacuum-tube arrangements requiring a phase reversing means for coupling the controlling to the controlled electrodes.*

*Applications of negative resistance to the production of sinusoidal and relaxation oscillations, to circuits having special properties, and to measurement work, are mentioned with frequent reference to the bibliography. In addition, the features of a tube having negative transconductance as an amplifier are pointed out.*

*In conclusion a section is devoted to the characteristics of the type 57 tube which has negative transconductance between the third and the second grid. As a voltage controlled negative resistance, this tube will produce a negative resistance of 3500 ohms with a total cathode current of only seven milliamperes. This performance is believed to be better than that of most dynatrons.*

(23 pages; 8 figures)

---

\* Decimal Classification: R139.

† *Proc. I. R. E.*, October, 1935.



## ANODE MATERIALS FOR HIGH VACUUM TUBES\*†

BY

E. E. SPITZER

RCA Manufacturing Company, Inc.,  
Harrison, N. J.*Summary*

*Continued development of the high vacuum tube has played an extremely important part in the development of radio communication. Since the power output of a tube is proportional to the amount of heat that may be dissipated safely from its anode, the anode is one of the most vital parts of high vacuum tubes especially those used for transmitting purposes. Several materials have been found suitable for the anodes of transmitting tubes, depending upon the requirements of specific applications and the type of cooling adopted; these materials and their characteristics are discussed in this paper.*

(7 pages; 6 figures)

\* Decimal Classification: R331.

† *Elec. Eng.*, November, 1935.ANALYSIS OF THE EFFECTS OF SPACE CHARGE  
ON GRID IMPEDANCE\*†

BY

D. O. NORTH

RCA Manufacturing Company, Inc.,  
Harrison, N. J.*Summary*

*Previous theory of transit-time phenomena in high vacuum diodes is extended and augmented to provide an explanation of the high-frequency behavior of high- $\mu$  amplifiers with parallel plane electrodes. For mathematical reasons the analysis is restricted to triodes with plate at alternating-current ground and to tetrodes with screen grid at alternating-current ground. Expressions for internal input loading and capacity are derived, showing the dependence upon frequency, voltages, and tube dimensions, and it is shown how the theory in its present form can be made quantitatively applicable to many commercial tubes of cylindrical design.*

*In agreement with both elementary theory and observation, the theory shows that at the threshold of the effect the input loading varies as the square of the frequency. For the RCA-57 there is calculated an internal input resistance of 21 megohms at one megacycle, dropping to 2100 ohms*

\*Decimal Classification: R130.

† *Proc. I. R. E.*, January, 1936.

at 100 megacycles. These figures are in excellent agreement with actual measurement, and illustrate the tremendous importance of transit times in the design of tubes for ultra-high frequencies. It is likely that internal input power losses of this character, together with closely allied losses in transconductance, are primarily responsible for high-frequency failure of both amplifiers and oscillators.

"Hot" input capacity exceeds the "cold" value. The magnitude and dependence upon tube parameters is given, the increase is primarily due to space charge but also depends upon  $\tau_2/\tau_1$ , the ratio of the electron transit time between control grid and plate to the transit time between cathode and control grid. In agreement with observation, the theory indicates very slight frequency dependence.

There is included a brief account of temperature-limited diodes, illustrating their possibilities as a source of high-frequency negative resistance.

(29 pages; 3 figures; 1 appendix)

## INPUT RESISTANCE OF VACUUM TUBES AS ULTRA-HIGH-FREQUENCY AMPLIFIERS\*†

BY

W. R. FERRIS

RCA Manufacturing Company, Inc.,  
Harrison, N. J.

### Summary

Vacuum tubes which when operated as voltage amplifiers at low frequency require no measurable grid input power have been found to take very serious amounts of power at ultra-high frequencies. The grid input conductance is shown to be very accurately represented for electrodes of any shape by the expression

$$g_g = K s_m f^2 \tau^2$$

where  $g_g$  is the input conductance,  $s_m$  the grid-plate transconductance,  $f$  the frequency, and  $\tau$  the electron transit time.  $K$  is a parameter which is a function of the geometry of the tube and the voltage distribution. A physical picture of the effect, a simple theoretical derivation, and experimental proof with conventional tubes are given.

The magnitude of  $g_g$  is such that it is the principal limitation for amplifiers at frequencies of the order of 100 megacycles, and it seriously affects the amplification at frequencies as low as fifteen megacycles. The input resistance of a typical commercial tube, the RCA-57, is approximately 20,000 ohms at thirty megacycles. Other commercial tubes, being of the

\*Decimal Classification: R132.

†Proc. I. R. E., January, 1936.

same general construction and size, have input resistance of the same order. The use of very small tubes, such as the RCA-954, with correspondingly short transit times is shown to be a practical means of increasing the amplification obtainable with conventional circuits.

Input capacity variation with frequency is found to be negligible with the RCA-57 even up to eighty megacycles and higher. However, the grid-cathode capacity is a function of the applied voltage; the ratio of this capacity under operating conditions to that with the tube cold having a value of four thirds for its minimum. The change in input capacity from cold to hot is of the order of one micromicrofarad for RCA-57. No change in grid-screen capacity is indicated.

The plate resistance of screen-grid tubes is found to vary with frequency but with the RCA-57 at eighty megacycles it is over twenty times the grid resistance and thus constitutes a negligible amount of the total loss in the circuit.

(24 pages; 13 figures; 1 table)

## EFFECT OF ELECTRON PRESSURE ON PLASMA ELECTRON OSCILLATIONS\*†

BY

ERNEST G. LINDER

RCA Manufacturing Company, Inc.,  
Camden, N. J.

### Summary

A general equation for electron motion in a plasma is developed which includes a term arising from electron gas pressure. The resulting expression is

$$\partial^2 \xi / \partial t^2 + (4\pi ne^2/m)\xi = (kT/m)\nabla^2 \xi,$$

where  $\xi$  is electron displacement,  $n$  electron density, and  $T$  electron gas temperature. From this it is found that the possible frequencies of free vibration form a series given by  $f_i = (kT/\lambda_{De}^2 m + ne^2/\pi m)^{1/2}$ . The lower limit corresponds to the Tonks-Langmuir value  $(ne^2/\pi m)^{1/2}$ , while the other frequencies depend upon the possible standing waves which may exist. The theory explains the observed variation of frequency with electron gas temperature.

(2 pages; 1 figure)

\* Decimal Classification: R214.1.

† *Physical Review*, May 15, 1936.

# AN ANALYSIS OF ADMITTANCE NEUTRALIZATION BY MEANS OF NEGATIVE TRANSCONDUCTANCE TUBES\*†

By

E. W. HEROLD

RCA Radiotron Division, RCA Manufacturing Company, Inc.,  
Harrison, N. J.

## Summary

The reduction of capacitance by feedback from the anode of a negative transconductance tube has frequently been considered an attractive method for compensating for the drop in impedance at high frequencies of a circuit consisting of  $R$  and  $C$  in parallel. Experimentally, however, the results of previous investigators have never been exceptional. This paper presents a theoretical analysis of the problem on the assumption that an ideal tube is used for admittance neutralization only. The results indicate that approximately flat response of the circuit up to cutoff is obtained when

$$\frac{C_m}{C_s} = \frac{1}{\sqrt{-2 \frac{R_p}{R_s} (1 + g_m R_p) - (1 + g_m R_p)}}$$

where  $C_m$  is the feed-back capacitance,  $C_s$  is the original shunt capacitance, and  $R_s$  is the effective resistance (see Fig. 1(c)). An interdependence between cutoff frequency  $C_s$ ,  $R_s$ , and the closeness to oscillation is found for a given control-electrode-to-anode transconductance. The effective resistance (and hence the gain of a preceding tube) in the ideal case can be raised several fold over that of the conventional inductance compensated circuit for the same cutoff and shunt capacitance; the greater the increase and consequent improvement, the smaller the safety factor (defined as the fractional increase in transconductance needed to produce oscillation). For the inductance compensated case  $\omega_0 C_s R_s = 1$ , while for the tube compensated circuit, the relations is approximately

$$\omega_0 C_s R_s = 1.5 + \frac{1}{S}$$

where  $\omega_0$  is the cutoff angular frequency and  $S$  the safety factor. However,  $S$  and  $R_s$  are not independent, being related by the approximation

$$g_m R_s = -2 \frac{S + 1}{S^2}.$$

A minimum  $S$  of about 0.2 would seem reasonable: such a value gives an improvement over inductance compensation of six and one-half times for the ideal tube considered. With a practical tubes and circuit, the improvement will probably be much less, possibly one half.

Under ideal conditions, the relations found for the single tube case, apply also to the case of two, cascaded, conventional tubes with feedback from the anode of the second tube to the grid of the first tube.

(15 pages; 6 figures)

\* Decimal Classification: R139.

† Proc. I.R.E., November, 1937.

## "BATALUM", A BARIUM GETTER FOR METAL TUBES\*†

By

E. A. LEDERER AND D. H. WAMSLEY

RCA Manufacturing Company, Inc.,  
Harrison, N. J.

### *Summary*

*In the manufacture of vacuum tubes, it is generally desirable to remove residual gases by a chemical process known as gettering. Various methods of gettering are reviewed. A new getter, called "Batalum", consisting of a length of tantalum wire coated with a mixture of barium carbonate and strontium carbonate is described. In the manufacture of metal tubes, "Batalum" gettering shows a marked advantage over the older methods.*

(7 pages; 4 figures)

---

\* Decimal Classification: R331.

† RCA Review, July, 1937.

## THE RATE OF EVAPORATION OF TANTALUM\*†

By

D. B. LANGMUIR AND L. MALTER

RCA Manufacturing Company, Inc.,  
Harrison, N. J.

### *Summary*

*The rate of evaporation of tantalum was determined by measuring the change of resistance and the change of weight of uniform filaments. Temperatures were held constant throughout each run by adjustments of voltage  $V$  and current  $A$  so that  $VA^{1/2}$  remained approximately unchanged. The rate of evaporation can be expressed by  $\log_{10} M = 7.86 - 39,310/T$ , where  $M$  is the rate of evaporation in grams per  $\text{cm}^2$  per second and  $T$  is the temperature on the Kelvin scale.*

(2 pages; 1 figure; 1 table)

---

† Physical Review, April 15, 1939.

\* Decimal Classification: R331.

## RECENT ADVANCES IN BARIUM GETTER TECHNIQUE\*†

BY

E. A. LEDERER

RCA Manufacturing Company, Inc.,  
Harrison, N. J.

### Summary

*Barium metal of high purity and without undesirable by-products can be obtained by chemically reducing barium berylliate. Barium berylliate, the barium salt of the hypothetical dibasic beryllic acid, has been discovered only recently. It is stable in air, but can be easily reduced by tantalum or similar reducing agents at about 1300°C with approximately 60 per cent efficiency. The resulting barium metal is of silvery appearance and is very active in the clean-up gas. The preparation of barium berylliate and methods for testing it are briefly outlined. The design, manufacture, and use of a simple, inexpensive, but highly efficient getter for the controlled production of barium metal from barium berylliate are described.*

(9 pages; 6 figures; 2 tables)

---

\* Decimal Classification: R331.

† RCA Review, January, 1940.

## SPACE-CHARGE LIMITATIONS ON THE FOCUS OF ELECTRON BEAMS\*†

BY

B. J. THOMPSON AND L. B. HEADRICK

RCA Manufacturing Company, Inc.,  
Harrison, N. J.

### Summary

*A calculation has been made of the effect of space charge in the region between the lens and the focal point on the focus of electron beams of rectangular and circular cross section under conditions of zero velocity of electron emission and with the lenses free from spherical aberration.*

*The results show that for an electron beam of circular cross section having a given current and voltage, and included in a cone of a given initial angle, there is a resultant minimum beam diameter at the focal point a given distance from the lens which cannot be reduced by changing the radial force, or focusing component, of the lens. The value of the minimum beam diameter is nowhere zero and it increases more rapidly than the distance between the lens and focal point. Thus, for the production of a television picture with a given angle of deflection the definition should improve as the screen approaches the lens.*

---

\* Decimal Classification: R583.

† Proc. I. R. E., July, 1940.

For a beam of circular cross section the factors determining this minimum spot size at a given distance from the lens are the initial beam radius  $R_0$ , the beam velocity  $V_0$ , and the current  $I$ . The spot size may be reduced only by increasing  $R_0$ , increasing  $V_0$ , or decreasing  $I$ .

For a rectangular beam with one dimension infinite, the minimum beam thickness depends upon the perpendicular force or focusing component supplied by the lens. The beam thickness may be zero up to a given distance from the lens and beyond this distance the minimum beam thickness increases with distance from the lens. To increase the distance from the lens at which the beam thickness or in the beam velocity or a decrease in current would be required.

The spreading of the electron beam between the final lens and the luminescent screen, caused by space charge, is a small fraction of the spot size obtained in direct-viewing kinescopes as used for television reception. However, this is not necessarily true of the projection-type kinescope where much higher values of beam current density are generally employed. Because at such high values of beam-current density the position of the focal point will change considerably with beam current or with picture-signal modulation there may be a large change in spot size at the screen.

(7 pages; 10 figures)

## SPACE-CHARGE EFFECTS IN ELECTRON BEAMS\*†

BY

ANDREW V. HAEFF

RCA Manufacturing Company, Inc.,  
Harrison, N. J.

### Summary

The effects of space charge in long, magnetically focused electron beams directed parallel to positively charged sheath electrodes are determined from a simple analysis. The main effects of space charge are: (a) to introduce departure from the potential distribution of the electrostatic case; (b) to set an upper limit for the beam current; and (c) to introduce instabilities and hysteresis phenomena in the behavior of the tube. It is shown that in a long beam the longitudinal potential gradient is negligible throughout the major portion of the beam length so that the upper limit for beam current is independent of beam length and of potentials of end electrodes, but depends only upon the relative transverse dimensions of the beam and of the surrounding sheath electrode and upon the sheath-electrode potential. The analysis gives expressions for maximum beam current, for space-potential distribution and for the minimum value of the focusing magnetic field, in terms of the beam and sheath-electrode dimensions and the sheath-electrode potential.

The use of multicellular sheath electrodes to minimize the effects of space charge is discussed. Thin "sheet" beams and "thin-walled" tubular beams are treated separately by a simplified "capacitance" method and expressions for maximum current, space potential, and for minimum-focusing magnetic field are derived.

The effect of space-charge interaction between multiple beams inside a common sheath electrode is considered and a method of control of current

\* Decimal Classification: R188.1.

† Proc. I. R. E., September, 1939.

*in one beam by the current in the adjacent beam is analyzed and also illustrated by experimental data. The effect of modulation of sheath-electrode voltage on the space potential for constant beam current, and the effect of beam-current modulation on the space potential, are discussed.*

*Application of the theory to the cases of beam focused electrostatically is discussed. The experimentally found characteristics of tubes utilizing long magnetically focused electron beams are presented and compared to those predicted by the theory and a satisfactory agreement is demonstrated.*

*(17 pages; 32 figures; 4 tables)*

## FLUCTUATIONS INDUCED IN VACUUM-TUBE GRIDS AT HIGH FREQUENCIES\*†

BY

D. O. NORTH AND W. R. FERRIS

RCA Manufacturing Company, Inc.,  
Harrison, N. J.

### *Summary*

*A theoretical formula for the noise induced in the input circuit of vacuum-tube amplifiers by fluctuations in the electron stream is compared with measured values. The results are found to be in substantial agreement.*

*(2 pages)*

---

\* Decimal Classification: R132.

† *Proc. I. R. E.*, February, 1941.

## A NEW SERIES OF INSULATORS FOR ULTRA-HIGH-FREQUENCY TUBES\*†

BY

L. R. SHARDLOW

RCA Manufacturing Company, Inc.,  
Harrison, N. J.

### *Summary*

*The electrical properties of power factor and dielectric constant, and the physical properties of porosity and firing shrinkage have been determined on an alumina-talc-silica series of ceramic bodies. The effect of body composition and firing temperature on the above properties is shown, and some theoretical considerations of these are discussed. It is shown that while small amounts of flux may be advantageous, large amounts are detrimental to the electrical properties. On the other hand large amounts of flux may be beneficial in the production of the desirable physical properties.*

*(7 pages; 3 figures; 2 tables)*

---

\* Decimal Classification: R331.

† *RCA Review*, April, 1941.



# SIMPLIFIED METHODS FOR COMPUTING PERFORMANCE OF TRANSMITTING TUBES\*†

By

W. G. WAGENER

RCA Radiotron Division, RCA Manufacturing Co., Inc.,  
Harrison, N. J.

**Summary**—Simplified methods are given for quickly computing with reasonable accuracy the performance of transmitting tubes in the usual radio-frequency and audio-frequency applications. These applications cover the cases where the current wave shapes within the tube are pulses of current which flow for less than the full cycle.

The factors controlling the shape of these pulses are discussed and a simplified analysis of the pulses is presented.

The problems of choosing the optimum conditions for a transmitting tube are discussed and the conditions for fully utilizing a tube's capabilities in the different classes of service are presented. These methods are illustrated thoroughly by calculations for a standard transmitting tube.

## I. INTRODUCTION

IN designing equipment, or in studying the actual performance of existing installations, it is invaluable to have knowledge of the capabilities of the individual component parts. The performance of standard types of transmitting tubes as component parts in the usual power amplifier services can be computed with a very useful accuracy. When the user has the ability to calculate a tube's capabilities and requirements, the design of the associated circuit and equipment becomes definite and straightforward. At the same time, an appreciation of what a transmitting tube should do and why, will aid greatly in analyzing trouble or in clarifying observed behavior in practical installations. Similarly, the attainment of modulation characteristics of greater linearity will be greatly aided by a knowledge of the tube requirements. Fortunately when performance of transmitting tubes in the usual modes of operation is to be calculated, a number of simplifying assumptions are reasonable and justifiable. The accuracy of the results will probably be well within the accuracy with which tube circuit conditions are known and within the reasonable variations of individual tubes from the average of a group.

If a complete and exact computation of any individual tube is desired, an understanding of the simpler methods will indicate just what more thorough mathematical or graphical solutions are needed. These exact solutions may be made readily as an extension of the

---

\* Decimal classification: R253.

† Reprinted from *Proc. I.R.E.*, January, 1937.

simplified methods to be presented. However, for more practical purposes the accuracy desired does not justify such exact analysis.

Because all radio-frequency power amplifiers operate in such a manner that plate and grid currents flow for only a fraction of the cycle, the wave forms are not those of simple direct or sine wave currents. It is this complicating factor that has discouraged the application of the standard electrical circuit methods of analysis to transmitting tubes. However, such pulses can be broken down easily into their equivalent direct-current and alternating-current components. All calculations will then follow the familiar simple methods.

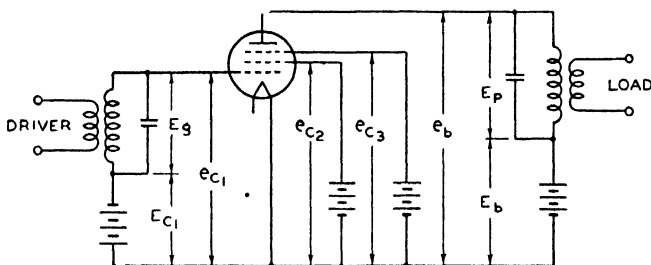


Fig. 1—Schematic radio-frequency power amplifier circuit.

In order to understand the behavior of tubes operated in this manner, it will be necessary to investigate the composition of these pulses of current. In general the principal features that must be known are:

1. The shape of the current pulse.
2. The peak value, or greatest instantaneous current.
3. The direct-current component.
4. The fundamental alternating-current component.
5. The higher harmonic component in cases of frequency multiplication.

## II. FACTORS CONTROLLING THE CURRENT PULSE

In order to ascertain the shape of the current pulses, it will be necessary to investigate the action of a typical power amplifier circuit and to see how a vacuum tube will respond to the various voltages acting within such a circuit. Fig. 1 represents a typical radio-frequency power amplifier circuit and indicates the voltages acting on the tube. For completeness a five-electrode tube is shown; for a tetrode or triode analysis, the surplus electrodes are omitted. It is seen that each electrode has a direct voltage applied to it. In addition, the input and output circuits each have a parallel resonant circuit in series with the supply voltages.

Because the resonant circuits store oscillating energy and because this energy is many times the energy extracted each cycle by the loading, the voltages developed across the circuits will be practically pure sine waves over the full cycle. Thus, the control grid and the plate of the tube can be considered as having applied to them by the outside circuit a combined direct voltage and fundamental sine wave voltage.

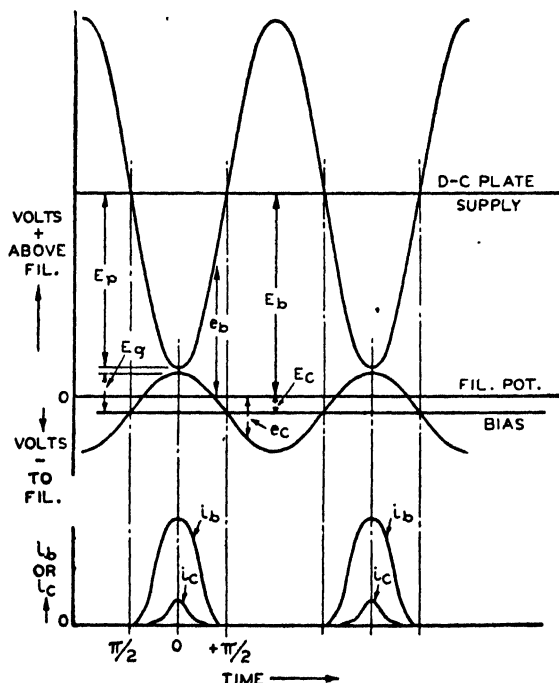


Fig. 2—Typical plate and grid voltages developed in a class C radio-frequency power amplifier, and the resultant tube currents.

In the case of two tubes operated as class B audio-frequency amplifiers, the sine wave analysis is also permissible because the two tubes are known to develop an almost pure fundamental sine wave in the output transformer and to have this voltage applied to the plate of each tube throughout a full audio cycle.

Fig. 2 shows the typical magnitude and phase of the instantaneous plate and grid voltages throughout a radio-frequency cycle. These voltages acting on the tube cause the pulses of plate and grid current to flow with the shapes as indicated. It will be seen that the plate voltage has a sine wave of peak value ( $E_p$ ) superimposed on the direct-current component ( $E_b$ ). The resultant instantaneous voltage is  $e_b$ .

Similarly, the instantaneous grid voltage ( $e_c$ ) is the resultant of a sine wave with a peak value of  $E_g$  superimposed on the negative direct-current bias ( $E_c$ ). The plate current flows as a result of the combined action of these two instantaneous grid and plate voltages ( $e_c$  and  $e_b$ ). As can be seen, the plate current generally flows for less than half a cycle. The grid current flows for a shorter period of time than the plate current.

Aside from the incidental electrostatic capacities of the electrodes which become part of the associated circuit, the vacuum tube is a pure resistive device at all ordinary frequencies and has no reactive impedances. This statement follows logically because the tube does not store appreciable electrostatic or electromagnetic energy. Further, the associated circuits are normally operated close to resonance so that the developed fundamental alternating voltages are in phase with the tube currents. Thus, the problem of the tube and the applied circuits can be treated solely on the basis of pure resistances. At the instant the grid voltage is at its most positive crest, the plate voltage has dropped to its lowest value.

It will now be advisable to see how such voltage combinations, acting on the plate and grid of a tube along with any direct voltages applied to the screen or suppressor, if either is present, will control the flow of plate current. The total space current ( $i_s$ ) from the cathode emitter depends on the geometry of the tube and the combined effect of the electrode voltages acting in the plane of the control grid as follows:

$$i_s = G \left[ e_{c_1} + \frac{e_{c_2}}{\mu_2} + \frac{e_{c_3}}{\mu_3} + \frac{e_b}{\mu_b} \right]^{3/2}$$

where,

$e_{c_1}$  is the control grid voltage.

$e_{c_2}/\mu_2$  is the effect of the No. 2 grid (screen) voltage ( $e_{c_2}$ ) at the control grid as reduced by the amplification factor ( $\mu_2$ ) of grid No. 1 with respect to grid No. 2.

$e_{c_3}/\mu_3$  is the effect of the No. 3 grid voltage ( $e_{c_3}$ ) at the control grid as reduced by the amplification factor ( $\mu_3$ ) of grid No. 1 with respect to grid No. 3.

$e_b/\mu_b$  is the effect of the plate voltage ( $e_b$ ) at the control grid as reduced by the over-all amplification factor ( $\mu_b$ ).

This equation assumes that the voltages are sufficiently positive to form no virtual cathode between the control grid and plate. The space current will flow only while the total effective voltage expressed by the brackets is positive.

In the case of a tetrode or a pentode, the factors  $\mu_3$  and  $\mu_b$  are sufficiently large so that the effect of the suppressor voltage and the plate voltage can usually be neglected. Thus, for a tetrode or pentode, the space current is governed almost solely by  $e_{c1} + (e_{c2}/\mu_2)$ . This formula does not cover the case where the suppressor voltage is sufficiently low or negative to control the space current by forming a virtual cathode in the vicinity of the suppressor.

Because the plate current is less than the cathode space current by the current drawn to other grids and is also influenced in a small way by space charges in front of the plate at low plate voltages and by secondary electrons from other grids, the current that reaches the plate seldom follows a three-halves power law and can be represented by

$$i_b = G_1 \left( e_{c1} + \frac{e_{c2}}{\mu_2} \right)^x \quad \text{for a multigrid tube}$$

or,

$$i_b = G_1 \left( e_{c1} + \frac{e_b}{\mu} \right)^x \quad \text{for a triode}$$

where  $x$  is an exponent fairly close to 1.0.

As was shown earlier,  $e_{c1}$  and  $e_b$  are composite voltages and can be represented by

$$\begin{aligned} e_{c1} &= E_{c1} + E_g \cos \omega t \\ e_b &= E_b - E_p \cos \omega t. \end{aligned}$$

The negative sign indicates that the alternating-current plate component is a voltage drop and hence is 180 degrees out of phase with the applied alternating grid voltage. Thus, for a triode,

$$i_b = G_1 \left[ E_{c1} + E_g \cos \omega t + \frac{E_b - E_p \cos \omega t}{\mu} \right]^x.$$

The solution for a multigrid tube will not be carried further because it is always a simplification of the triode case. Thus,  $(E_b - E_p \cos \omega t)/\mu$  can be replaced by  $e_{c2}/\mu_2$  and will usually have no alternating-current component.

The above equation becomes

$$i_b = G_1 \left[ E_{c1} + \frac{E_b}{\mu} + \left( E_g - \frac{E_p}{\mu} \right) \cos \omega t \right]^x$$

or,

$i_b = G_1$  (direct voltage component and alternating voltage component)\*.

If now the direct voltage component is negative, as it is in class

C amplifiers, no current will flow until the alternating voltage component becomes sufficiently positive to overcome the direct component. This action is shown in Fig. 3 where the portion of the cycle during which the resultant effective voltage is positive is indicated by the shaded portion. At the instant the effective voltage rises above the zero effective voltage level and becomes positive, the plate current begins to flow as shown by the typical plate current pulse. The grid current flows over a smaller portion of the cycle because the zero effective voltage level occurs at the plate current "cutoff" point where the

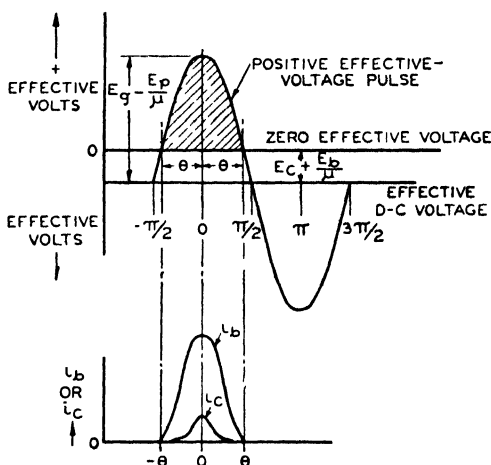


Fig. 3—Resultant effective voltage acting at cathode of tube to cause the flow of space current.

instantaneous grid voltage is always still negative. The grid voltage then rises into the positive region for a shorter duration of the cycle.

Because the alternating-current cycle is represented as a cosine wave, the effective voltage is maximum at  $\omega t = 0$ . As  $\omega t$  increases toward  $\pi/2$ , the zero effective voltage level is crossed at some angle  $\theta$  each side of maximum. At this point, the value of the cosine wave is just equal to the negative direct-current component and hence

$$\left(E_g - \frac{E_p}{\mu}\right) \cos \theta = - \left(E_{c_1} + \frac{E_b}{\mu}\right)$$

or,

$$\cos \theta = \frac{- \left(E_{c_1} + \frac{E_b}{\mu}\right)}{E_g - \frac{E_p}{\mu}}$$

Thus, the analysis of the output from the standpoint of two tubes is complete when the operating load line is a straight line drawn on these composite curves. The analysis of the currents in a single tube must be taken from the single tube curves with the voltages obtained from the composite curves.

From the composite curves, it is easily seen that the required load resistance value for each tube is

$$\frac{E_b - e_{b\min}}{i_{b\max} - 0} = \frac{E_p}{i_{b\max}}.$$

Hence, for this case,

$$R_{r\text{ per tube}} = \frac{1050}{0.550} = 1910 \text{ ohms.}$$

On the per tube basis again, and from Fig. 8, we find  $e_{c\max} = +115$  volts, and  $i_{c\max} = 80$  milliamperes. Then,

$$\begin{aligned} E_g &= -(E_c) + e_{c\max} = 45 + 115 = 160 \text{ volts} \\ \cos \theta_{\text{grid}} &= 45/160 = 0.272 \\ \theta_{\text{grid}} &= 74 \text{ degrees.} \end{aligned}$$

From Fig. 5,  $i_{c\max}/I_c = 4.8$ . Therefore,

$$I_c = 80/4.8 = 16.7 \text{ milliamperes.}$$

We have, then,

$$\begin{aligned} \text{average driving power per tube} &= 0.9 \times 0.0167 \times 160 \\ &= 2.4 \text{ watts} \\ \text{average driving power two tubes} &= 4.8 \text{ watts.} \end{aligned}$$

In order to understand the grid circuit requirements, it is advisable to plot a curve of instantaneous  $i_c$  values. This curve for the 203-A analysis is shown in Fig. 13. On this curve are also shown the values of plate output, power input, and plate dissipation averaged over a full audio cycle and plotted against peak signal amplitude. It is essential to note that the maximum plate dissipation occurs at a signal less than the maximum.

### VIII. CONCLUSION

In conclusion it is seen that the performance of vacuum tubes in power amplifier service can be computed in a straightforward manner. The requirements for linear modulation have been indicated and the application of these requirements demonstrate why in grid modulation

Thus, for analysis of the plate current pulse and the plate circuit performance, it is quite reasonable to treat  $x$  as 1.0 for the peak, direct-current, and alternating-current values. For  $x$  to be unity is the same as ascribing to the tube the quality of linear performance. That this is reasonable is also borne out by the well-recognized experience that class B audio-frequency amplifiers and class B linear power amplifiers can be made to operate with a small degree of distortion. In class B work, the cutoff angle ( $\theta$ ) is constant and linearity is due to the effective first power exponent in the equation relating plate current and effective voltage.

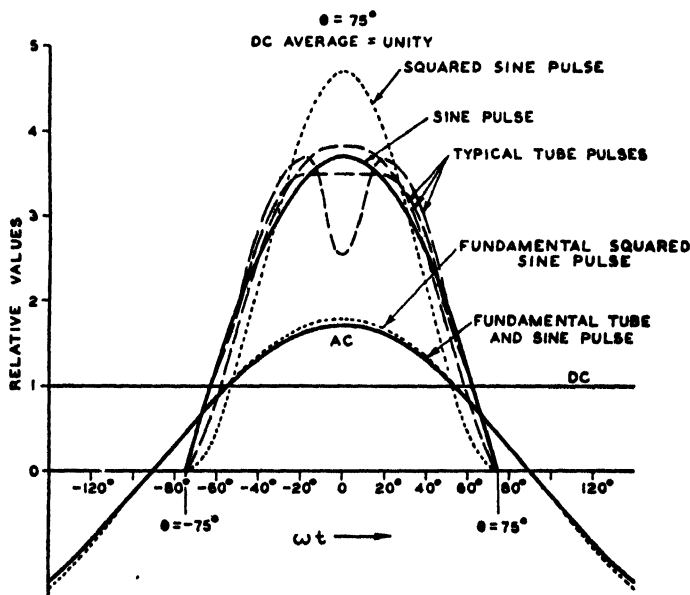


Fig. 4—Typical plate current pulses having the same direct-current values.

Analyses of various pulse shapes as a function of the cutoff angle and degree of linearity of the pulse have been made frequently. Perhaps the most recent and most complete for the immediate purpose of class B and C computations are those made by F. E. Terman and J. H. Fern,<sup>1</sup> and by F. E. Terman and W. C. Roake.<sup>2</sup> The former gives the harmonic components as a function of angle of flow and is valuable for computations of harmonic operation. A solution which is also

<sup>1</sup> F. E. Terman and J. H. Ferns, "The calculation of class C amplifier and harmonic generator performance of screen-grid and similar tubes," *Proc. I.R.E.*, vol. 22, pp. 359-373; March, (1934).

<sup>2</sup> F. E. Terman and W. C. Roake, "Calculation and design of class C amplifiers," *Proc. I.R.E.*, vol. 24, pp. 620-632; April, (1936).



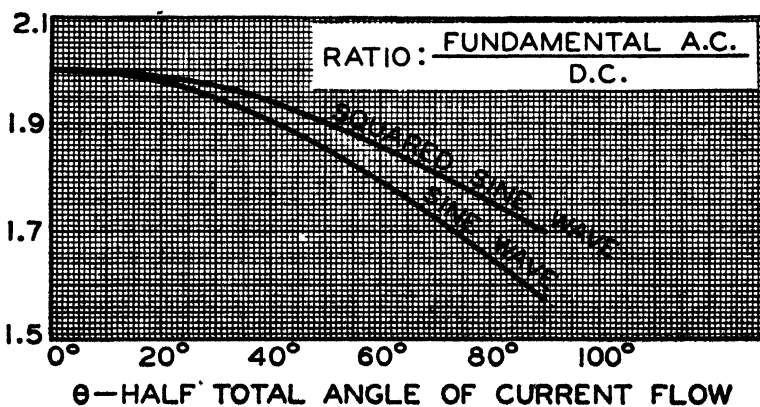
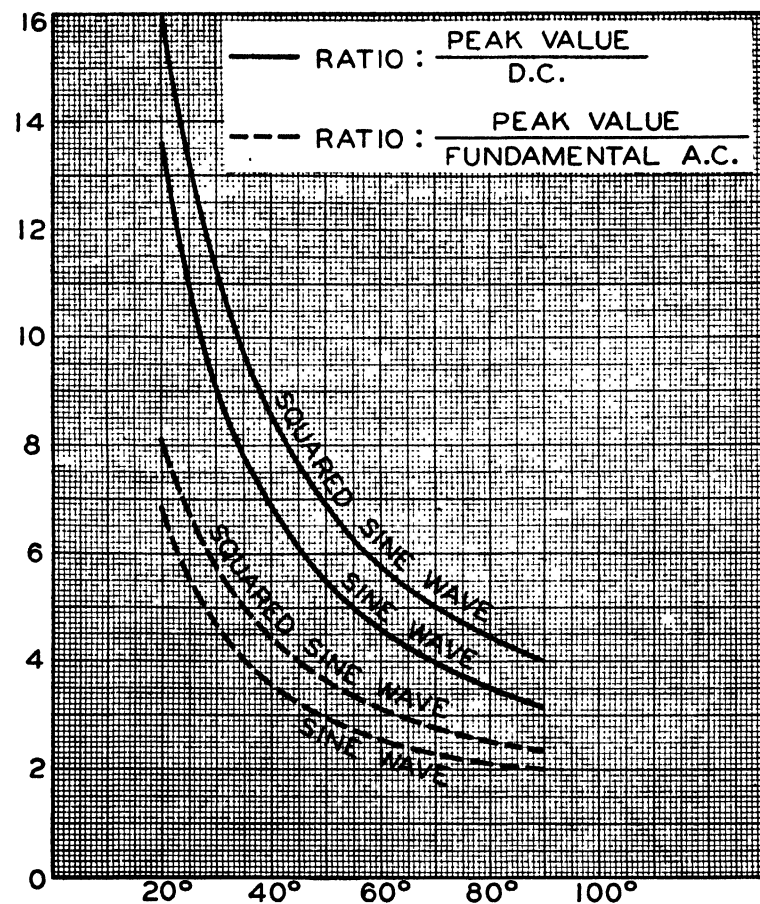


Fig. 5—Principal components of simple pulses.

applicable to class AB work, or to waves with flat tops such as might be obtained with limited emission, has been given by Yuziro Kusunose.<sup>3</sup> For convenience, the curves of the ratio of peak value to direct-current component, peak value to alternating-current component, and the ratio of alternating-current to direct-current component for a cut-off sine wave and a squared cutoff sine wave ( $x=2.0$ ) are given in Fig. 5 as a function of  $\theta$ . For completeness, the basic formulas for the analysis of these two pulses with all harmonic components are given in the Appendix.

In case the exact graphical or mathematical analysis of these pulses is desired in an individual case, the results may be applied in the same manner in these computations as the results of this simplified analysis. The final results will then be quite accurate because the assumption of the sinusoidal variation of input and output radio-frequency voltage is very reasonable. The analysis of the actual current pulses that would be picked off step by step as indicated in Fig. 8 could be made by a graphical Fourier analysis. A simple way of doing this has been outlined by I. E. Mouromtseff and H. N. Kozanowski.<sup>4</sup>

#### IV. OPTIMUM TUBE OPERATING CONDITIONS

Now that a full knowledge of the important components of the current pulses expected in a transmitting tube is at hand, it is necessary to determine how such pulses are developed in a tube in order to utilize fully the capabilities of the tube. Because the power in the output resonant circuit is proportional to both the alternating voltage developed across the impedance of this circuit and the alternating-current component of current flow into this impedance, an individual tube's capabilities will be most fully developed when these alternating-current factors are at their maximum values. This brings up the question of the inherent limitations of a vacuum tube which will determine the maximum values of the alternating-current components.

The principal limitations are the maximum voltage that can be applied, the peak value of the current that can be drawn continuously from the emitter, and the maximum power losses that can be permitted within the tube consistent with the full life expectancy of the tube. These values are established by the manufacturers whose experience is incorporated in the ratings given the tube. Thus, a solution that is consistent with the tube requirements and the normal operation as

<sup>3</sup> Yuziro Kusunose, "Calculations on vacuum tubes and the design of triodes," Bulletin No. 237 of the Researches of the Electrotechnical Laboratory, Tokyo, Japan, September, (1928).

<sup>4</sup> I. E. Mouromtseff and H. N. Kozanowski, "Analysis of the operation of vacuum tubes as class C amplifiers," Proc. I.R.E., vol. 23, pp. 752-778; July, (1935).

expected in the hands of qualified persons is given in the maximum rated values of direct plate voltage, direct plate current, direct-current plate power input, plate dissipation, direct-current grid bias, and direct grid current, as listed under the various classes of operation.

It will now be interesting to see what happens in a triode operating as a class C amplifier with a fixed amount of input power (with both  $E_b$  and  $I_b$  constant), as the plate load impedance is varied. Variation of the load impedance means that the developed alternating plate voltage will vary and that the grid circuit conditions must be adjusted to keep the direct plate current constant. Fig. 6 shows how the power output increases to a maximum and the grid driving current rises very rapidly in the neighborhood of the maximum output region.

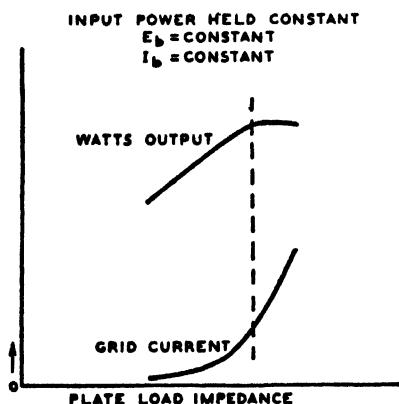


Fig. 6—Power amplifier performance with constant power input.

Thus, an optimum operating impedance is indicated. This optimum operating impedance is the value which develops the maximum output with the lowest grid current and, hence, the lowest driving power.

It is possible to calculate the optimum load impedance from the desired voltage value and current value required in the plate circuit. As explained previously, the maximum or peak value of the current pulse occurs at the instant the grid is at its maximum positive value ( $+e_{c\max}$ ) and the plate voltage is at its minimum value ( $e_{b\min}$ ). This point of maximum current on the static tube curves defines the upper limit of the operating curve which is traced across the static curves during a full radio-frequency cycle. It is point (A) in Fig. 8. From the location of this point in terms of  $i_{b\max}$ ,  $e_{c\max}$ , and  $e_{b\min}$ , the full operation of the tube may be forecast.

In the triode, the optimum operating impedance indicated in Fig. 6 corresponds to the impedance necessary to place the maximum

current point at  $e_{c\max} = e_{b\min}$ . In this region if  $e_{b\min}$  is allowed to fall below  $e_{c\max}$ , no further increase in peak plate current occurs although the grid current rises very rapidly. This is then the point at which the top of the plate current pulse begins to develop depressions or valleys due to the very low value of the instantaneous plate voltage compared to the other voltages in the tube. In a tetrode or pentode, this point may be found by an inspection of the static plate  $i_b$  vs.  $e_b$  curves in the region of low plate voltage and positive grid voltage, and where a further increase in positive grid voltage does not raise the plate current but only results in an increase of grid current.

Thus, a tube is fully utilized when the largest downswing of plate voltage is developed and when this downswing does not result in a serious dip in the crest value of the plate current pulse. The location of this maximum current point may frequently be varied in individual cases in view of the fact that a small change in plate circuit efficiency results in large changes of grid driving power since the peaks of grid current drawn vary so rapidly at this balance point.

#### V. CHOICE OF TUBE MAXIMUM CURRENT POINT AND PLATE CIRCUIT ANALYSIS

It is the location of the maximum current point on the tube characteristics which is the key to the complete solution of any operating problem. This point can be found directly from the desired or actual operating conditions.

In the first place the power input to the tube is usually known for any application in terms of the plate voltage and plate current. Depending on the type of operation, the operating angle ( $\theta$ ) will be known approximately. From  $\theta$  the ratio of the peak value of the current pulse to the direct-current component is established and may be found from Fig. 5. This factor times the plate current ( $I_b$ ) fixes the desired peak plate current. This peak plate current ( $i_{b\max}$ ) is then located on the static curves, and its position fixes the maximum value of the instantaneous grid voltage. The minimum value of the instantaneous plate voltage will also be determined with the choice of this point.

As has been stated for the triode, the location of this point is most favorably fixed in the region where the instantaneous values of grid and plate voltage are about equal. The exact location depends on the amount of grid current one wishes to draw. For the tetrode or pentode, this point is set at the lowest possible value of plate voltage before the individual curves on the  $i_b$  vs.  $e_b$  characteristics begin to knee over rapidly. Again, the exact point varies slightly with the amount of grid current desired. In a tetrode or pentode, the point lies roughly in

the region in which the minimum value of plate voltage approaches the screen voltage or the positive suppressor voltage, respectively.

From the location of this peak value of plate current on the tube curves, the swing of the plate voltage ( $E_p$ ) from the direct plate voltage is known. The swing of the positive grid voltage above the filament potential is fixed. From the expression for the cosine of the cutoff angle, the plate voltage components, and the grid swing above filament, it is possible to calculate the required grid bias. Thus,

$$\cos \theta = \frac{-\left(E_c + \frac{E_b}{\mu}\right)}{E_g - \frac{E_p}{\mu}}$$

but,

$$E_g = c_{\max} + (-E_c).$$

By rearrangement,

$$E_c = \frac{1}{1 - \cos \theta} \left[ \left( -c_{\max} + \frac{E_p}{\mu} \right) \cos \theta - \frac{E_b}{\mu} \right].$$

It is now possible to calculate the alternating grid voltage ( $E_g$ ) as the sum of the absolute values of  $+c_{\max}$  and the negative grid bias.

From the cutoff angle  $\theta$ , the ratio of alternating fundamental current ( $I_p$ ) to the direct current ( $I_b$ ) is known. Hence,  $I_p$  is determined. The power output, the power input, and the efficiency may now be computed as follows:

$$\text{Power output, P.O.} = \frac{I_p}{\sqrt{2}} \frac{E_p}{\sqrt{2}} = 1/2 I_p E_p$$

$$\text{Power input, P.I.} = I_b E_b$$

$$\text{Plate circuit efficiency} = \frac{1/2 I_p E_p}{I_b E_b}.$$

Thus, the maximum current point is determined and the plate circuit analysis is complete.

## VI. ANALYSIS OF GRID CIRCUIT

As may be seen by reference to Fig. 2, the rapid rise of grid current produced as the plate voltage swings down in the region of the grid voltage gives the pulse of grid current quite a peaked form. The form of the pulse, as well as its total magnitude, varies rapidly. Such peaked pulses have been found to be fairly close to a squared sine wave form

(exponent equal to 2.0). See Fig. 7, where two sample grid current waves are drawn alongside a squared sine wave of the same peak value and angle of flow. Although this squared sine wave is only an approximation of the exact wave, it is reasonable in view of the rapid variation of the direct grid current with slight changes of adjustments. Hence, the approximation is of real value in estimating the values of direct grid current from the known peak values.

In the complete solution, the total alternating grid voltage swing is known and the direct grid current can be calculated from the peak value reached at the known maximum current point and the ratio of peak to direct current for the angle of grid current flow. The power represented by these values is quite close to the product,  $E_g I_c$ , where

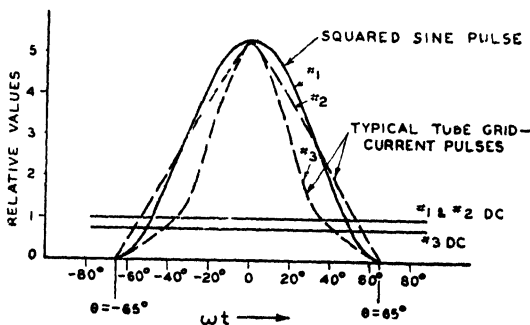


Fig. 7—Typical grid current pulses having the same peak values.

$E_g$  is the crest amplitude of the alternating voltage in the grid circuit, and  $I_c$  is the direct grid current. This relation has been demonstrated recently by H. P. Thomas,<sup>5</sup> though he shows that probably  $0.9 E_g I_c$  is a closer approximation. As was pointed out by F. E. Terman,<sup>6</sup> this result follows logically from the fact that practically the whole grid current flows while the alternating grid voltage is near its peak amplitude ( $E_g$ ).

## VII. TYPICAL TUBE PERFORMANCE CALCULATIONS

To show the complete calculations for a typical transmitting tube, let us take a type 203-A triode. For class C operation, the angle  $\theta$  is usually in the neighborhood of 60 to 80 degrees as a practical balance between plate circuit efficiency, grid driving power, and reasonable peak emission requirements of the filament or cathode.

<sup>5</sup> H. P. Thomas, "Determination of grid driving power in radio-frequency power amplifiers," *Proc. I.R.E.*, vol. 21, pp. 1134-1141; August, (1933).

<sup>6</sup> F. E. Terman, "Radio Engineering," p. 234, McGraw-Hill Book Company, Inc., (1932).

## 1. Calculation of Radio-frequency Power Amplifier

### (a). Class C Telegraphy.

In this service, the type 203-A tube has the following maximum ratings:

Direct plate voltage;  $E_b = 1250$  volts

Direct plate current,  $I_b = 175$  milliamperes

Direct-current plate power input,  $P. I. = 220$  watts

Direct grid current,  $I_c = 60$  milliamperes

Plate dissipation = 100 watts

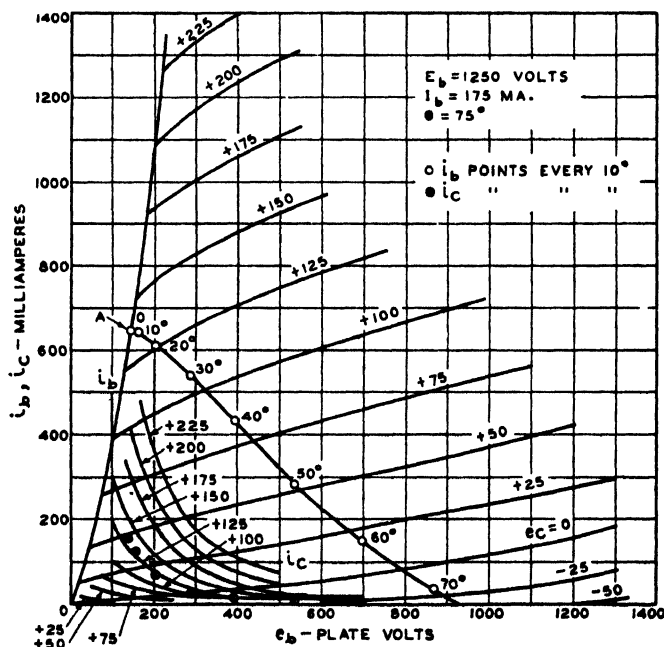


Fig. 8—Typical operating points plotted on static plate and grid curves of a type 203-A tube.

Let us take the following conditions for the computations:

$E_b = 1250$  volts,  $I_b = 175$  milliamperes, and  $\theta = 75$  degrees

The tube maximum current point will be established on the line where  $+e_{r\max} = e_{b\min}$ . Referring to Fig. 5, at  $\theta = 75$  degrees for the sine wave case, it is seen that the ratio of peak to direct-current value ( $i_{b\max}/I_b$ ) is 3.7, and the ratio of alternating-current component to direct-current component ( $I_p/I_b$ ) is 1.7. Hence,

$$i_{b\max} = 3.7 \times 175 = 647 \text{ milliamperes.}$$

At this point, the voltage requirements are found from the  $i_b$  vs.  $e_b$  curves of Fig. 8 to be

$$e_{c\max} = 140 \text{ volts, and } e_{b\min} = 140 \text{ volts}$$

Using these voltages, and from Fig. 8, we find  $i_{c\max} = 160$  milliamperes. Then,

$$E_p = E_b - e_{b\min} = 1250 - 140 = 1110 \text{ volts}$$

and,

$$\begin{aligned} E_c &= \frac{1}{1 - \cos \theta} \left[ \left( -e_{c\max} + \frac{E_p}{\mu} \right) \cos \theta - \frac{E_b}{\mu} \right] \\ &= \frac{1}{1 - 0.260} \left[ \left( -140 + \frac{1110}{25} \right) 0.260 - \frac{1250}{25} \right] \\ &= -101 \text{ volts.} \end{aligned}$$

Therefore, the total grid swing is

$$E_g = e_{c\max} + (-E_c) = 140 + 101 = 241 \text{ volts.}$$

As  $I_p/I_b = 1.7$ , we have

$$I_p = 1.7 \times 175 = 297 \text{ milliamperes}$$

$$\text{P.O.} = 1/2 I_p E_p = 1/2 \times 0.297 \times 1110 = 165 \text{ watts}$$

$$\text{P.I.} = I_b E_b = 0.175 \times 1250 = 219 \text{ watts}$$

$$\text{Efficiency} = \frac{\text{P.O.}}{\text{P.I.}} = \frac{165}{219} = 75 \text{ per cent.}$$

In the grid circuit, we have

$$\begin{aligned} \cos \theta_{\text{grid}} &= \frac{-E_c}{E_g} = \frac{+101}{241} = 0.42 \\ \theta_{\text{grid}} &= 65 \text{ degrees.} \end{aligned}$$

From the squared sine wave, wave,  $i_{c\max}/I_c = 5.4$ . Therefore,

$$I_c = 160/5.4 = 30 \text{ milliamperes.}$$

$$\text{Grid driving power} = 0.9 \times 241 \times 0.030 = 6.5 \text{ watts.}$$

#### (b). Class C Telephony, Plate Modulated.

In this service, the tube is operated in a manner similar to that of the previous class C telegraphy application. However, the plate supply voltage ( $E_b$ ) instead of being a pure direct voltage has superimposed on it an audio-frequency voltage. The amplitude of the audio voltage



varies with the intensity of the modulating signal. The largest signal that can be superimposed without introducing serious distortion is that whose alternating-current amplitude equals the direct plate voltage. This signal acts to drive the supply voltage up to twice its normal value and down to zero, during the audio cycle.

An idea of the tube capabilities may be obtained by carrying out calculations at the carrier, or zero-modulating signal condition, and at the crest of the cycle of the largest permissible audio signal where the plate voltage has been doubled and the tube conditions are at

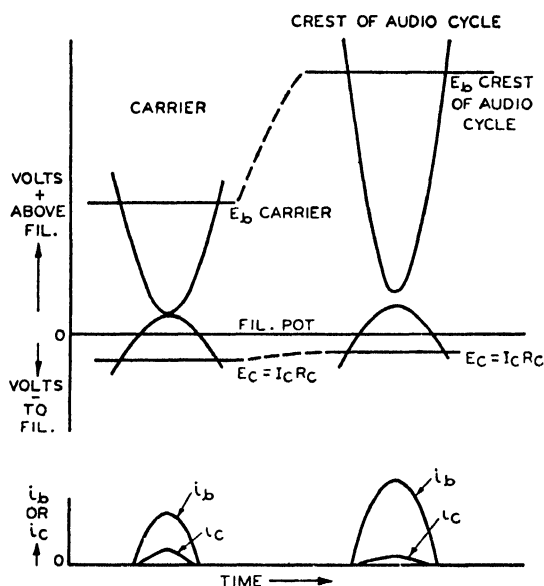


Fig. 9—Typical tube voltages and currents developed in a plate modulated class C radio-frequency power amplifier.

their maximum. These relations are shown in Fig. 9 for the carrier and crest conditions. In this maximum modulation state, the ratio of audio-frequency signal crest amplitude to direct plate voltage supply ( $E_b$ ) is 1.0. This ratio is the modulation factor.

In order to obtain distortionless modulation, we must have a linear relationship between currents and voltages. Thus, as the plate supply voltage ( $E_b$ ) is doubled, the radio-frequency output voltage and current must double. Likewise, as  $E_b$  is driven to zero, the input and output currents and voltages must fall to zero. Averaged over an audio cycle, however, the direct supply voltage and current ( $E_b$  and  $I_b$ ) remain constant because the superimposed audio variations are symmetrical about the direct-current values. For a modulation factor

of 1.0, the superimposed audio-frequency crest voltage and crest current become equal to the direct supply voltage and current ( $E_b$  and  $I_b$ ). Hence, their root-mean-square values are equal to  $E_b/\sqrt{2}$  and  $I_b/\sqrt{2}$  and the audio-frequency modulating power required is  $1/2 E_b I_b$ . Thus, when a tube is being modulated with a modulation factor of 1.0, the total input power is the sum of the direct-current input and audio-frequency input, or  $E_b I_b + 1/2 E_b I_b$  or  $3/2 E_b I_b$ . The radio-frequency modulated carrier power also goes up 50 per cent with complete modulation because the energy in the side bands is then 50 per cent of the carrier energy. Since the tube efficiency remains almost constant, the tube plate dissipation losses rise 50 per cent. In order to allow for this level of dissipation, it is necessary for the carrier losses to equal two thirds of the maximum rated dissipation of the tube. These factors have usually been considered in specifying the maximum rated values of a transmitting tube type for different services.

Plate modulated service usually requires a higher grid bias voltage than the unmodulated class C service. This will be seen readily at the completion of the calculations which show that the bias must change with the modulation in the plate circuit. This variation is more easily obtained where it is not too large a fraction of the total bias, and hence it is well to assume a large bias voltage. Such values reduce the total angle of plate current flow and the cutoff angle to less than that for the usual class C telegraph service. Calculations may be made by assuming initially either an operating angle ( $\theta$ ) or a specific value of bias. To demonstrate the latter type of calculation and to assure the large value of bias voltage, these calculations will be made on the basis of an assumed grid bias voltage.

As a plate modulated radio-frequency power amplifier, the type 203-A has the following maximum ratings at the carrier:

Direct plate voltage,  $E_b = 1000$  volts

Direct plate current,  $I_b = 175$  milliamperes

Direct-current plate power input,  $P.I. = 175$  watts

Direct grid current,  $I_c = 60$  milliamperes

Plate dissipation = 65 watts (two thirds of telegraph rating)

Let us take the following conditions for the computations:

$E_b = 1000$  volts,  $I_b = 175$  milliamperes, and  $E_c = -200$  volts

With the bias stipulated, it is necessary to make first an approximation of  $\theta$  in order to establish the voltages involved. These voltages will then permit  $\theta$  to be calculated to a sufficiently correct final value.

Say  $\theta = 60$  degrees. From Fig. 5,  $i_{b\max}/I_b = 4.6$ . Hence,

$$i_{b\max} = 4.6 \times 175 = 805 \text{ milliamperes.}$$

Assume that the maximum current point is on the line of equal grid and plate voltages. Then, from the  $i_b$  vs.  $e_b$  curves of Fig. 8,  $e_{c_{\max}} = +160$  volts and  $e_{b_{\min}} = 160$  volts. Therefore,

$$E_g = 200 + 160 = 360 \text{ volts}$$

$$E_p = 1000 - 160 = 840 \text{ volts}$$

$$\cos \theta = \frac{- \left( -200 + \frac{1000}{25} \right)}{360 - \frac{840}{25}} = 0.50$$

and,

$$\theta = 60 \text{ degrees.}$$

The original estimate of  $\theta$  is seen to have been satisfactory.

At 60 degrees, from Fig. 5,  $I_p/I_b = 1.79$ . Therefore,

$$I_p = 1.79 \times 175 = 313 \text{ milliamperes}$$

$$\text{P.O.} = 1/2 \times 0.313 \times 840 = 131 \text{ watts}$$

$$\text{P.I.} = 0.175 \times 1000 = 175 \text{ watts}$$

$$\text{Plate dissipation} = 44 \text{ watts}$$

$$\text{Efficiency} = 75 \text{ per cent.}$$

At the audio signal maximum (modulation factor of 1.0), the values become for no distortion:

$$E_b = 2 \times 1000 = 2000 \text{ volts}$$

$$E_p = 2 \times 840 = 1680 \text{ volts}$$

$$I_p = 2 \times 313 = 626 \text{ milliamperes.}$$

These values must be attained with the same load circuit impedance and usually with the same grid circuit radio-frequency driving voltage. It is then desirable for the grid bias voltage to be permitted to vary over the audio cycle in order to attain this linear modulation.

At the crest, a trial value of  $\theta$  is found to be 78 degrees. From Fig. 5,  $I_p/I_b = 1.67$ , and  $i_{b_{\max}}/I_b = 3.5$ . Therefore,

$$I_b = \frac{I_p}{1.67} = \frac{626}{1.67} = 375 \text{ milliamperes}$$

and,

$$i_{b_{\max}} = 3.5 \times 375 = 1310 \text{ milliamperes.}$$

From the crest values, we have

$$e_{b_{\min}} = 2000 - 1680 = 320 \text{ volts.}$$

From the  $i_b$  vs.  $e_b$  curves for  $i_{b_{\max}} = 1310$  and  $e_{b_{\min}} = 320$ , it is found that  $+e_{c_{\max}}$  must be 220 volts.

Because  $E_g$  is the same as for the carrier condition, the bias voltage ( $E_c$ ) must be reduced to have  $e_{c\max}$  shift from +160 volts at the carrier to +220 volts at the crest of the audio cycle. Therefore,  $E_g = 360$  volts  $= -E_c + 220$  volts, and  $E_c = -140$  volts.

Practically this variation may be obtained quite well by the use of a grid leak resistor to develop the bias voltage. Let us compare the carrier and crest conditions of the grid circuit to see how the bias shifts can occur. The maximum current points to attain this with a given value of grid resistor ( $E_c$ ) have been found and are given below:

	Carrier	Crest	
$E_g$	360	360	volts
$e_{c\max}$	+160	+220	volts
$E_c$	-200	-140	volts

From Fig. 8 at the maximum current point and from Fig. 5

$i_{c\max}$	220	133	milliamperes
$\theta_{grl}$	56.5	67	degrees
$i_{c\max}/I_c$	6.0	5.2	
$I_c$	36.6	25.6	milliamperes
$R_c$	5460	5460	ohms
$I_c R_c$	-200	-140	volts
Driving power	11.9	8.3	watts

It is seen that as  $e_{b\min}$  rises, it must pull away from  $e_{c\max}$  so that the peak grid current is reduced; hence, the direct grid current may develop less bias in the grid resistor. It is thus seen that a poor regulation source of bias is desirable for plate modulated telephony. This bias may preferably be a combination of fixed and grid leak bias as is discussed in an article on this subject by I. E. Mouromtseff and H. N. Kozanowski.<sup>4</sup>

### (c). Class C Telephony, Grid Modulated.

In the grid modulated radio-frequency power amplifier, the grid excitation is an unmodulated radio-frequency voltage and the direct-current grid bias has an audio-frequency signal superimposed on it. Thus, for the analysis of a single radio-frequency cycle, the grid bias may be considered to have been shifted by the audio-frequency signal. The analysis is similar to that for class C amplifiers except that the carrier maximum current point must be chosen so that sufficient operating leeway is allowed to permit the plate circuit radio-frequency voltage to double at the crest of an audio cycle. In order to assure that the tube will be fully utilized, it is best to make the initial calculations at the crest of the audio cycle.

Fig. 10 shows the developed radio-frequency voltages and the plate and grid circuit current pulses. It should be noted that the direct plate

voltage is the same at both the carrier and crest conditions, and hence the developed plate voltage swing ( $E_p$ ) at the carrier can utilize only about half the direct voltage. Then, at the crest of the audio cycle when the radio-frequency voltages and currents must be doubled, the plate voltage swing can approach the full direct plate voltage amplitude without driving  $e_{bmin}$  down below the instantaneous positive peak grid voltage. The limited plate voltage swing at the carrier means that the radio-frequency output is low and that the plate circuit efficiency is only about half that of a class C telegraph amplifier.

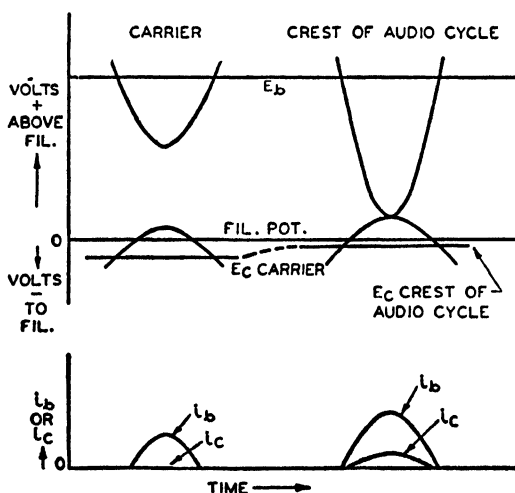


Fig. 10—Typical tube voltages and currents developed in a grid modulated class C radio-frequency power amplifier.

At the crest of the audio cycle, the grid bias ( $E_c$ ) has been reduced in magnitude to raise the peak grid voltage and to drive a much greater peak plate current through the tube. Let us assume the cutoff angle at this point has increased to 90 degrees. At the crest of the audio cycle,  $I_b$  rises to a little more than double.

In class C radio-frequency power amplifier service with grid modulation, the maximum ratings are the same as in class B radio-frequency power amplifier telephony service where the modulation also appears in the grid circuit. For the 203-A, the maximum ratings at the carrier are:

Direct plate voltage,  $E_b = 1250$  volts

Direct plate current,  $I_b = 150$  milliamperes

Direct-current plate power input, P.I. = 150 watts

Plate dissipation = 100 watts.

For 150 watts input, let us take  $E_b = 1250$  volts and  $I_b = 120$  milliamperes. As  $I_b$  more than doubles at the crest of the audio cycle, assume  $I_{b\text{crest}} = 270$  milliamperes.

Thus, at the crest,  $E_b = 1250$  volts,  $I_b = 270$  milliamperes, and  $\theta = 90$  degrees. From Fig. 5,  $i_{b\text{max}}/I_b = \pi$ , and  $I_p/I_b = 1.57$ . Therefore,

$$i_{b\text{max}} = \pi \times 270 = 848 \text{ milliamperes}$$

$$I_p = 1.57 \times 270 = 424 \text{ milliamperes.}$$

Taking the maximum current point of 848 milliamperes on the line of equal grid and plate voltages from Fig. 8, we have  $e_{c\text{max}} = e_{b\text{min}} = 165$  volts. Then,

$$E_p = 1250 - 165 = 1085 \text{ volts}$$

$$E_c = \frac{-E_b}{\mu} \text{ at } 90 \text{ degrees} = -50 \text{ volts}$$

$$E_g = 50 + 165 = 215 \text{ volts}$$

$$\text{P.O.} = 1/2 I_p E_p = 1/2 \times 0.424 \times 1085$$

$$= 230 \text{ watts at crest of audio cycle.}$$

At the carrier,  $E_p$  and  $I_p$  must be cut to half values. Therefore,  $I_p = 424/2 = 212$  milliamperes, and  $E_p = 1085/2 = 542$  volts.

Say  $\theta = 65$  degrees as an approximation to determine voltages. From Fig. 5,  $i_{b\text{max}}/I_b = 4.2$ , and  $I_p/I_b = 1.76$ . Then,

$$I_b = 212/1.76 = 120 \text{ milliamperes}$$

$$i_b = 4.2 \times 120 = 504 \text{ milliamperes}$$

$$e_{b\text{min}} = E_b - E_p = 1250 - 542 = 708 \text{ volts.}$$

From the  $i_b$  vs.  $e_b$  curves of Fig. 8, in order to attain  $i_{b\text{max}}$  at  $e_{b\text{min}} = 708$  volts,  $e_{c\text{max}}$  must be  $+80$  volts, and  $i_{c\text{max}}$  is found to be 25 milliamperes.

Since the radio-frequency grid voltage is constant,  $E_g = 215$  volts and since  $E_c = -(215 - 80) = -135$  volts, we have

$$\cos \theta = \frac{-(-135) + \frac{1250}{25}}{215 - \frac{542}{25}} = 0.44$$

and,

$$\theta = 64 \text{ degrees.}$$

This value of  $\theta$  is in satisfactory agreement with the assumed value.

Then,

$$\text{P.O.} = 1/2 \times 0.212 \times 542 = 57.2 \text{ watts}$$

$$\text{P.I.} = 0.120 \times 1250 = 150 \text{ watts}$$

$$\text{Efficiency} = 38 \text{ per cent}$$

$$\text{Plate dissipation} = 92.5 \text{ watts}$$

$$\cos \theta_{\text{grid}} = 135/215 = 0.627$$

and,

$$\theta_{\text{grid}} = 51 \text{ degrees.}$$

From Fig. 5,  $i_{c\text{max}}/I_c = 6.6$ . Therefore,

$$I_c = 25/6.6 = 3.8 \text{ milliamperes.}$$

This current, however, does not indicate the peak driving condition. At the crest,  $e_{c\text{max}} = 165$  volts,  $e_{b\text{min}} = 165$  volts, and from Fig. 8,  $i_{c\text{max}} = 200$  milliamperes. We also find  $\cos \theta_{\text{grid}} = 50/215 = 0.232$  and  $\theta_{\text{grid}} = 76.5$  degrees. From Fig. 5,  $i_{c\text{max}}/I_c = 4.6$ . Therefore,

$$I_c = 200/4.6 = 43.5 \text{ milliamperes.}$$

and,

$$\begin{aligned} \text{driving power} &= 0.9 \times 0.0435 \times 215 \\ &= 8.4 \text{ watts at crest of audio cycle.} \end{aligned}$$

Since the bias at the crest is  $-50$  volts, and at the carrier is  $-135$  volts, the audio voltage peak swing must be the difference, or  $85$  volts. The audio supply must be capable of supplying  $43.5$  milliamperes of current at the peak and of not distorting under the varying load throughout the remainder of the cycle. The radio-frequency excitation must be  $215$  volts and capable of good regulation under the varying load. Similarly, the source of carrier bias of  $-135$  volts must be of good regulation because it must pass this same varying grid current.

Over an audio cycle, the direct plate current from the supply rises and falls almost linearly so that the direct-current average is practically equal to the direct plate current drawn at the carrier. Thus, the input power to the plate circuit is practically constant. As modulation occurs, the power in the radio-frequency output increases by the amount of the side-band energy. Since the plate dissipation is the difference of the direct-current input power and the radio-frequency output power, the plate loss is maximum at zero modulation, or under carrier conditions.

#### (d). Class B Telephony.

This case is very similar to the grid modulated class C power amplifier except that  $\theta$  is maintained close to  $90$  degrees. The bias is practically constant at the cutoff point, and the radio-frequency exci-

tation is a modulated carrier whose amplitude varies about the carrier level with the changes in the audio signal. The currents and voltages acting in the tube throughout a radio-frequency cycle are pictured in Fig. 11 and show that the carrier efficiency must be low since only half the available plate voltage swing can be developed at the carrier. Calculations should be made at the crest of the audio cycle to assure that the tube is fully utilized.

This mode of operation is freer from distortion than the grid modulated case since the angle ( $\theta$ ) does not change appreciably throughout the audio cycle. The bias and direct plate voltage remain practically

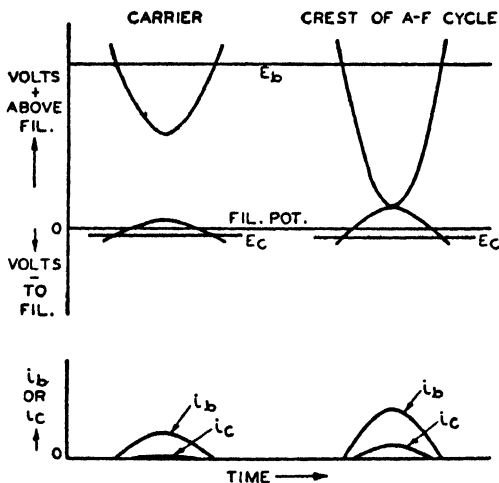


Fig. 11—Typical tube voltages and currents developed in a class B radio-frequency power amplifier (telephony).

constant at values that reduce the effective direct component voltage in the basic equation to approximately zero. Hence, any variation of the alternating-current component cannot change the angle much from 90 degrees.

In this service the maximum ratings for the 203-A at the carrier are:

Direct plate voltage,  $E_b = 1250$  volts

Direct plate current,  $I_b = 150$  milliamperes

Direct-current plate power input, P.I. = 150 watts

Plate dissipation = 100 watts.

Let us take  $I_{b \text{ at the carrier}} = 120$  milliamperes, and  $E_b = 1250$  volts for a carrier input of 150 watts. At the crest, the tube output currents are doubled, and since  $\theta$  is constant, the input current is also doubled.



At the crest, then,  $I_b = 240$  milliamperes,  $E_b = 1250$  volts, and  $\theta = 90$  degrees. From Fig. 5,  $i_{b\max}/I_b = \pi$ , and  $I_p/I_b = 1.57$ . Therefore,

$$i_{b\max} = \pi \times 240 = 755 \text{ milliamperes.}$$

From the  $i_b$  vs.  $e_b$  curves of Fig. 8, take the maximum current point on the limiting line of  $e_c = e_b$ . For  $i_b = 755$  milliamperes,  $e_{c\max} = e_{b\min} = 155$  volts. Then,

$$E_p = 1250 - 155 = 1095 \text{ volts.}$$

At the carrier,  $I_b = 120$  milliamperes,  $E_b = 1250$  volts, and  $\theta = 90$  degrees. So

$$i_{b\max} = \pi \times 120 = 377 \text{ milliamperes.}$$

but,

$$E_p = 1/2 \times 1095 = 547 \text{ volts.}$$

Therefore,

$$e_{b\min} = 1250 - 547 = 703 \text{ volts.}$$

From Fig. 8, at  $i_{b\max} = 377$  milliamperes and  $e_{b\min} = 703$  volts,

$$e_{c\max} = +60 \text{ volts.}$$

If  $E_c$  is adjusted to the cutoff point at the carrier,  $E_c = -50$  volts and  $E_p = 60 + 50 = 110$  volts. At the crest,  $E_p$  must be double and, therefore,  $E_p = 2 \times 110 = 220$  volts.

However, it has already been shown that for the required plate current at the crest,  $e_{c\max}$  must be  $+155$  volts. Thus,  $E_c = -(220 - 155) = -65$  volts. This small change in bias from the carrier point is usually made up in the regulation of the bias or excitation sources, since the grid current loading varies greatly over the audio cycle. The resulting crest angle will vary only slightly from 90 degrees.

A tabulation of the grid circuit calculations follows:

	Carrier	Crest	
$E_p$	110	220	volts
$E_c$	-50	-65	volts
$i_{b\max}$ (from Fig. 8)	20	190	milliamperes
$\cos \theta_{\text{grid}}$	$\frac{50}{110} = 0.455$	$\frac{65}{220} = 0.295$	
$\theta_{\text{grid}}$	63	73	degrees
$i_{c\max}/I_c$ (from Fig. 5)	5.5	4.8	
$I_c$	3.6	39.5	milliamperes
$R_c$ (assumed)	420	420	ohms
$I_c R_c$	-1.5	-16.5	volts
$E_{c\text{used}}$	-48.5	-48.5	volts
$E_{c\text{total}}$	-50	-65	volts
Driving power	—	$0.9 \times 0.0395 \times 220 = 7.8$	watts

It should be noted that a very small degree of regulation (due to  $R_c = 420$  ohms) in the grid bias supply aids the linearity of performance.

Finally, we have

$$I_{p_{\text{carrier}}} = 1.57 \times 120 = 188.5 \text{ milliamperes}$$

$$\text{P.O.} = 1/2 \times 0.1885 \times 547 = 51.5 \text{ watts}$$

$$\text{P.I.} = 0.120 \times 1250 = 150 \text{ watts}$$

$$\text{Efficiency} = 34.4 \text{ per cent}$$

$$\text{Plate dissipation} = 98.5 \text{ watts.}$$

As in the case of the grid modulated class C amplifier, the plate dissipation is maximum at the carrier, and the direct plate current averaged over the audio-frequency cycle remains constant.

## 2. Calculation of Class B Audio-Frequency Power Amplifier.

In class B service the operating angle is 90 degrees, and hence a tube carries plate current for 2 $\theta$  or 180 degrees of the cycle. By using two tubes, one for each half of the cycle, it is possible to obtain the complete sine wave of current. However, the analysis of each individual tube can be made in the manner that has been presented.

At maximum signal, the maximum ratings for each 203-A in this service are:

$$\text{Direct plate voltage, } E_b = 1250 \text{ volts}$$

$$\text{Direct plate current, } I_b = 175 \text{ milliamperes}$$

$$\text{Direct plate power input, } P.I. = 220 \text{ watts}$$

$$\text{Plate dissipation} = 100 \text{ watts}$$

Let us take  $E_b = 1250$  volts,  $I_b = 175$  milliamperes, and  $E_c = -45$  volts. From Fig. 5,  $\theta = 90$  degrees,  $i_{b_{\text{max}}}/I_b = \pi$ , and  $i_{b_{\text{max}}} = \pi \times 175 = 550$  milliamperes. Arbitrarily take  $e_{b_{\text{min}}} = 200$  volts. Then,  $E_p = 1250 - 200 = 1050$  volts.

Proceeding as for radio-frequency circuits, we have from Fig. 5,  $I_p/I_b = 1.57$ , and  $I_p = 275$  milliamperes. Therefore,

$$\text{P.O.} = 1/2 \times 0.275 \times 1050 = 144.5 \text{ watts}$$

and,

$$\text{P.O.}_{\text{two tubes}} = 2 \times 144.5 = 289 \text{ watts}$$

A simpler and more direct method, however, is to calculate the power output from the sine waves of voltage and current present. The maximum plate current ( $i_{b_{\text{max}}}$ ) calculated above is the amplitude of the full sine wave of current from the two tubes. Since the developed amplitude of the alternating voltage in the plate circuits of the two tubes is a full alternating-current sine wave, the usual alternating-current power computations may be applied. Hence,

$$\text{P.O.} = 1/2 i_{b_{\text{max}}} \times E_p$$

$$\text{P.O.}_{\text{two tubes}} = 1/2 \times 0.550 \times 1050 = 289 \text{ watts}$$

and the total power input is

$$P.I._{\text{two tubes}} = 2 \times 0.175 \times 1250 = 438 \text{ watts.}$$

Therefore,

$$\text{efficiency} = 66 \text{ per cent.}$$

Some confusion is apt to occur in the detailed analysis of two tubes operating in class B due to the fact that they are not operated at complete cutoff with zero signal and to the fact that the tubes interact through the common magnetic circuit of the output transformer. Thus, for small signals the tubes operate as push-pull class A amplifiers, with large signals as class AB push-pull amplifiers, and with very large signals almost as pure class B amplifiers.

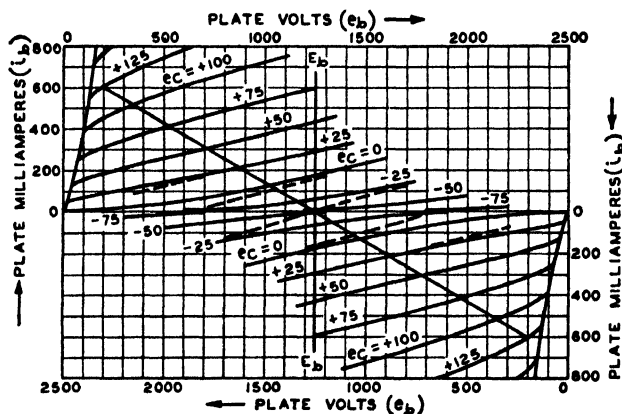


Fig. 12—Composite plate characteristic for combined tubes and transformer as used in class B audio-frequency power amplifier under the following conditions:  $E_b = 1250$  volts,  $E_c = -25$  volts, and  $I_b = 175$  milliamperes.

This confusion can be completely dispelled by referring to the graphical method outlined by B. J. Thompson.<sup>7</sup> In this method the static  $i_b$  vs.  $e_b$  curves of the two tubes are placed so as to form a composite plate circuit characteristic curve of the combined tubes and transformer, as reproduced in Fig. 12. Operation of the 203-A's at  $E_c = -25$  volts has been chosen for the illustration. Because the plate currents from the two tubes flow through opposite halves of the output transformer, their magnetizing forces cancel and only their differences act usefully in the secondary output. Hence, the composite plate circuit curves for corresponding signal grid voltages are formed from the differences of the plate currents and are shown as broken lines.

<sup>7</sup> B. J. Thompson, "Graphical determination of performance of push-pull audio amplifiers," *Proc. I.R.E.*, vol. 21, pp. 591-600; April, (1933).

Thus, the angle of plate current cutoff ( $\theta$ ) is defined as the angle whose cosine equals the ratio of the direct-current component amplitude to the alternating-current component amplitude. For simplicity,  $\theta$  will be called the cutoff angle. The plate current flow then occurs over a portion of the cycle equal to  $2\theta$ . Similarly, the flow of grid current occurs over twice the angle ( $\theta_{\text{grid}}$ ) where

$$\cos \theta_{\text{grid}} = \frac{-E_{c_1}}{E_g}$$

because the alternating-current component ( $E_g \cos \omega t$ ) overcomes the bias ( $E_{c_1}$ ) at  $\omega t = \theta_{\text{grid}}$ .

Thus, the angles ( $\theta$  and  $\theta_{\text{grid}}$ ) specify when the resultant effective voltage governing plate current flow, and the actual grid voltage governing grid current flow, become positive. Hence, the plate current flows over  $2\theta$  of the cycle and grid current flows over  $2\theta_{\text{grid}}$  of the cycle. It remains now to establish the approximate shape of the plate current pulse that must flow between  $-\theta$  and  $+\theta$  and the grid current pulse that flows between  $-\theta_{\text{grid}}$  and  $+\theta_{\text{grid}}$ . In other words, what is the exponent  $x$  in the equation and is it a constant?

### III. SHAPE AND ANALYSIS OF THE CURRENT PULSE

Analysis of several actual plate current pulses, that are typical of the pulses obtained in tubes, shows that although  $x$  is not constant it may be treated as practically equal to unity in establishing the ratio of the peak to the direct-current value, and the ratio of fundamental alternating-current component to direct-current component as a function of the angle of flow ( $2\theta$ ). Fig. 4 shows a pure sine pulse with  $x = 1.0$  for  $\theta = 75^\circ$ . The direct-current component and the fundamental alternating-current component (which with the higher order harmonics form the pulse) are also shown. The ratio of the peak to the direct-current value is 3.7 and the ratio of the alternating-current fundamental crest amplitude to the direct-current amplitude is 1.70. The pulses shown by dashes are actual plate current pulses which have been drawn with the same direct-current component and whose alternating-current fundamental is the same within the accuracy of the solid line curve (AC). Note that the maximum values are quite close to the pure sine wave maximum. For comparison the extreme case in which the pulse is a squared sine wave ( $x = 2.0$ ) with the same angle and same direct-current component is also shown in dots. It is interesting to see that the alternating-current fundamental is not widely different. In fact this ratio of alternating-current to direct-current component varies relatively slowly with both  $\theta$  and  $x$ .

the plate efficiency of the tube must inherently be low. From a study of the conditions to be met at the carrier and at the crest of the audio cycle, the importance of the amount of regulation of the various voltages and power supplies can be seen.

The results of these simplified computations should indicate what items are important in obtaining the most satisfactory results from transmitting tubes. Of course, the best way to study the practical overall modulation characteristics of a power amplifier system is to use an

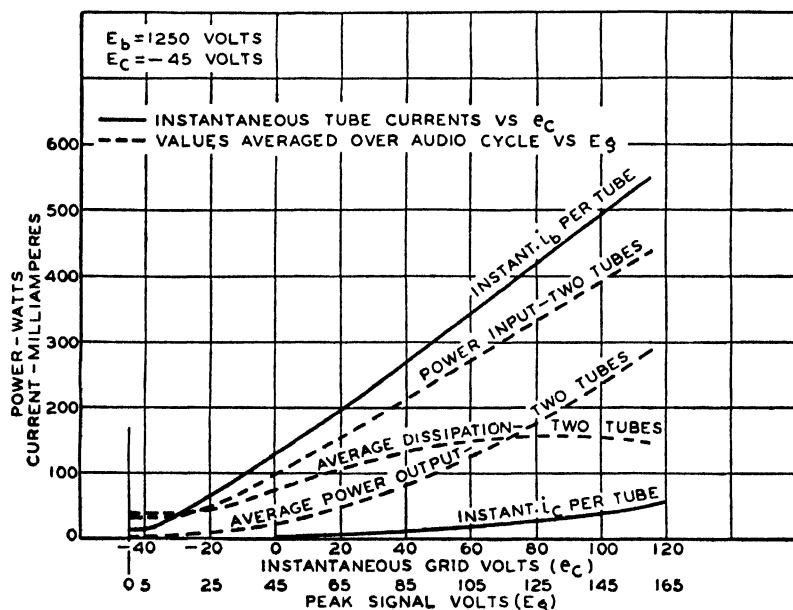


Fig. 13—Instantaneous current curves of a class B alternating-frequency power amplifier and power performance curves vs. signal amplitude.

indicating device such as a cathode-ray oscillograph. To interpret and control the results, however, it is always well to be able to estimate the relative importance and effects of the factors influencing performance.

## APPENDIX

### 1. Results of Fourier Analysis of Simple Pulses.

#### (a). Sine Wave Pulse.

$$\text{Current pulse} = i = \cos \omega t - \cos \theta$$

where positive current flows during each cycle between  $\omega t = -\theta$  and  $\omega t = +\theta$ .

$$\text{Direct-current component} = 1/\pi (\sin \theta - \theta \cos \theta)$$

$$\text{First harmonic} = 1/\pi (\theta - 1/2 \sin 2\theta) \cos \omega t$$

$$\begin{aligned} n\text{th harmonic} = \frac{1}{\pi} \left[ \frac{\sin (n+1)\theta}{n+1} + \frac{\sin (n-1)\theta}{n-1} \right. \\ \left. - \frac{2}{n} \cos \theta \sin n\theta \right] \cos n\omega t. \end{aligned}$$

(b). *Squared Sine Wave Pulse.*

$$\text{Current pulse} = i = (\cos \omega t - \cos \theta)^2$$

where positive current flows during each cycle between  $\omega t = -\theta$  and  $\omega t = +\theta$ .

$$\text{Direct-current component} = 1/2\pi (\theta - (3/2) \sin 2\theta + 2\theta \cos^2 \theta).$$

$$\text{First harmonic} = 1/\pi (-2\theta \cos \theta + 3/2 \sin \theta + 1/6 \sin 3\theta) \cos \omega t$$

$$\begin{aligned} \text{Second harmonic} = 1/\pi \left[ 1/4(1 + 6 \cos^2 \theta) \sin 2\theta \right. \\ \left. - 2(\sin \theta + 1/3 \sin 3\theta) \cos \theta + \theta/2 \right] \cos 2\omega t \end{aligned}$$

$$\begin{aligned} n\text{th harmonic} = 1/\pi \left\{ 2/n (1/2 + \cos^2 \theta) \sin n\theta \right. \\ \left. - \cos \theta \left[ \frac{2 \sin (n-1)\theta}{n-1} \right. \right. \\ \left. + \frac{2 \sin (n+1)\theta}{n+1} \right] + \frac{\sin (n-2)\theta}{2(n-2)} \\ \left. + \frac{\sin (n+2)\theta}{2(n+2)} \right\} \cos n\omega t. \end{aligned}$$

## 2. Extrapolation of Vacuum Tube Static Curves.

It sometimes happens that the static curves of a vacuum tube need to be extended to aid in making the computations. With certain requirements maintained, this can be done quite well by using the three-halves power law relating currents and voltages. Provided the relative magnitudes of all electrode voltages are not changed, but are each varied by the same percentage, the distribution of total current to the electrodes will not be altered, and all currents will rise and fall as the three-halves power of the voltage changes.

This follows from the fact that the shape of the voltage fields within the tube is not disturbed. Thus, the magnitudes of the currents are affected and not the distribution to the different electrodes. The application of this rule is limited to regions that do not approach the limit of cathode emission. The accuracy may also be adversely affected somewhat by high secondary emission currents.

# EXCESS-ENERGY ELECTRONS AND ELECTRON MOTION IN HIGH-VACUUM TUBES\*†

BY

ERNEST G. LINDER

RCA Manufacturing Company, Inc.,  
Camden, N. J.

*Summary*—In the development of magnetron oscillators, one of the principal difficulties has been the overheating of the cathode. The present article discusses an effect which is at least partially responsible for this, and which consists in the gaining of excess energy by some electrons, which then bombard the cathode. The effect is of importance also because of its bearing on transit time, orbit shape, tube noise, shape of cutoff curve, etc.

Experimental results indicate that a Maxwellian distribution of velocities is superimposed on the orbital velocities, the energy of the random motion being derived from the orbital motion. This leads to the formation of a new type of virtual cathode about the real cathode. The properties of this type of cathode are discussed.

Subjects related only indirectly to cathode overheating, but necessary to its understanding, also are discussed, such as current flow and space-charge phenomena for cases in which electrons execute cyclic orbits. Extensive experimental data are included.

## INTRODUCTION

THE overheating of the cathode in magnetrons, which occurs to some extent at all times during operation, but becomes especially troublesome at high plate voltages, has been one of the principal difficulties in the development of a satisfactory oscillator of this type. The present article is an outgrowth of a study of this effect, undertaken as a part of a development program of centimeter-wave oscillators. The work broadened out somewhat as it progressed, to include subjects related only indirectly to cathode overheating, since it became evident that cathode overheating, and magnetron behavior in general, involved some concepts not associated with more common types of vacuum tubes. For example, no detailed discussion seems previously to have been given of current and space-charge phenomena for the case in which electrons execute cyclic orbits, as in magnetrons and positive-grid tubes. It is clear that current and space charge must be vitally affected by the fact that the direction of motion of an electron may reverse many times. This reversal gives rise to such concepts as "returning current," and "number of electron oscillations." As a further example, it has been found that electrons in such tubes inter-

---

\* Decimal classification: R138.

† Reprinted from *Proc. I.R.E.*, March, 1938.



act so that energy exchanges occur, resulting in a Maxwellian distribution of velocities superimposed on the orbital motion. This has led to the application of the technique and terminology developed by Langmuir for the investigation of gaseous electrical discharges by probe electrodes, to the electron swarms occurring in electron-transit-time oscillators.

Any adequate treatment of magnetron or positive-grid-tube electronics must necessarily involve ideas and terms foreign to conventional tube theory. An attempt has been made in this article to state these concepts in mathematical terms appropriate to the discussion of short-wave oscillators. Extensive experimental tests have been carried out and checks of the theory made wherever possible.

The first observation of excess-energy electrons was made several years ago. In 1925 Irving Langmuir<sup>1</sup> observed that in certain types of high-vacuum tubes some electrons possessed the ability to pass to an electrode having a more negative potential than the cathode from which they originated. Several types of tubes were used. In one the anode consisted of a few small-sized wires close to, and paralleling, the cathode. A surrounding cylindrical electrode was negatively charged with respect to the cathode. An electron current was observed to flow to this cylinder in spite of its negative potential. Another tube was of the cylindrical magnetron type, having negatively charged end plates. A magnetic field was applied parallel to the filament, of such strength that an electron, influenced only by it and the electrostatic field, would be unable to reach the plate. In this case small electron currents flowed to the cylinder in spite of the magnetic field, and to the end plates even when they were twenty to fifty volts negative with respect to the cathode. The effect appeared not to be due to oscillations since they rarely could be detected. Langmuir showed that the electrons appeared to have a Maxwellian distribution of velocities, the temperature of which was proportional to the anode voltage.

More recently similar phenomena have been observed by several other investigators, but the true nature of the effect has not always been recognized. These recent observations have resulted from the large amount of work which has been done during the last few years on magnetron oscillator tubes for the generation of ultra-short electromagnetic waves. E. C. S. Megaw<sup>2</sup> noticed that the filaments of such tubes underwent electronic bombardment of sufficient intensity to cause a visible increase in brightness. However he attributed the effect

<sup>1</sup> I. Langmuir, "Scattering of electrons in ionized gases," *Phys. Rev.*, vol. 26, p. 585; November, (1925).

<sup>2</sup> E. C. S. Megaw, "Cathode secondary emission: A new effect in thermionic valves at a very short wave length," *Nature*, vol. 132, p. 854; December, (1933).

entirely to oscillations. Slutzkin, Leljakow, and Kopilowitsch<sup>3</sup> observed a similar heating of magnetron filaments, but attributed it to thermal radiation from the hot plate of the tube. Later investigations by Slutzkin, Braude, and Wigdortschik<sup>4</sup> led to the conclusion that the effect was caused by oscillations. E. Pierret, and C. Biguenet<sup>5</sup> attributed it to oscillations. G. R. Kilgore<sup>6</sup> recognized filament bombardment as the cause of the effect, but offered no explanation. O. Pfetscher and W. Puhlmann<sup>7</sup> concluded that the bombardment was induced by oscillations. Two papers by I. M. Wigdortschik<sup>8</sup> have very recently appeared in which experiments similar to those of Langmuir are described. Evidence for a Maxwellian distribution is given, but no explanation is offered. The writer has mentioned the effect in several previous publications.<sup>9,10,11,12</sup>

In the cases of Pfetscher and Puhlmann, and also Megaw, definite proof has been given indicating that oscillations may cause, or augment, electron bombardment of the cathode. However, there is ample evidence that a similar effect can occur also in the absence of oscillations. The writer has observed, in the case of magnetron oscillators for nine-centimeter waves, that very marked bombardment occurs, when the tube is oscillating, but when the oscillations are stopped, considerable bombardment persists, and in some cases is even greater than during oscillation.

When gas is present in sufficient quantity, bombardment by positive ions also may occur. The intensity of this type of bombardment

<sup>3</sup> Slutzkin, Leljakow, and Kopilowitsch, "Factors influencing the output and efficiency of magnetron oscillators," *Phys. Zeit. der Sowjetunion*, vol. 5, p. 887, (1934).

<sup>4</sup> A. A. Slutzkin, S. J. Braude, and I. M. Wigdortschik, "Production of an ion current in high vacuum by means of a magnetic field," *Phys. Zeit. der Sowjetunion*, vol. 6, p. 268, (1934).

<sup>5</sup> E. Pierret and C. Biguenet, "On the ultra-short waves obtained with a magnetron," *Jour. de Phys. et le Radium*, vol. 6, p. 67; April, (1935).

<sup>6</sup> G. R. Kilgore, "Magnetron oscillators for the generation of frequencies between 300 and 600 megacycles," *Proc. I.R.E.*, vol. 24, pp. 1140-1157; August, (1936).

<sup>7</sup> O. Pfetscher, and W. Puhlmann, "Über Habann-Generatoren grosser Leistung für Ultrakurzwellen," *Hochfrequenz. und Elektroakustik*, vol. 47, p. 105; April, (1936).

<sup>8</sup> I. M. Wigdortschik, "Die Geschwindigkeitsverteilung der Elektronen unter dem Einfluss eines Magnetischen Feldes im Hochvakuum," *Phys. Zeit. der Sowjetunion*, vol. 10, p. 245, (1936), and "A study of the surplus heating of a cathode in a magnetron," vol. 10, p. 634, (1936).

<sup>9</sup> E. G. Linder, "Improved magnetron oscillator for the generation of micro-waves," *Phys. Rev.*, vol. 45, p. 656; May, (1934).

<sup>10</sup> I. Wolff, E. G. Linder, and R. A. Braden, "Transmission and reception of centimeter waves," *Proc. I.R.E.*, vol. 23, pp. 11-23; January, (1935).

<sup>11</sup> E. G. Linder, "Excess energy electrons in high vacuum tubes," *Phys. Rev.*, vol. 49, p. 860; June 1, (1936). (Abstract.)

<sup>12</sup> E. G. Linder, "Description and characteristics of the end-plate magnetron," *Proc. I.R.E.*, vol. 24, pp. 633-653; April, (1936).

depends upon the amount of gas present. In the work described here it was negligible, as will be shown later.

The existence of these three different types of bombardment, i.e., (1) that due to oscillations, (2) that due to positive ions, and (3) that due to the effect discussed in this paper (scattering), is no doubt largely responsible for the divergent opinions among different investigators, and the apparent inconsistency of some previous results. The present paper will deal only with the third type of bombardment, the first two being considered comparatively well-known and understood phenomena.

No previous investigators appear to have studied the effect in very great detail. Langmuir's work seems to have been the most comprehensive, but his published account is brief, and no data are given. A small amount of data appear in the articles by Megaw, Pfetscher and Puhlmann, Wigdortschik, and the writer.

#### CURRENT FLOW AND SPACE CHARGE IN A MAGNETRON

The present discussion will be confined to magnetrons. Much of it obviously will be directly applicable to tubes of the positive-grid type, but no attempt will be made to point this out or discuss it in this paper. We shall consider first a simple tube consisting of a cylindrical plate  $P$ , Fig. 1, and a concentric filamentary cathode  $C$ , mounted within an evacuated envelope. A uniform magnetic field is applied normal to the plane of the figure.

In the absence of a magnetic field, electrons emitted by the cathode travel along radial paths to the plate. If a weak field is applied these paths become curved. At a certain value of field, known as the "critical" magnetic field, the curvature becomes so great that electrons are unable to reach the plate, and after approaching it closely, return again toward the cathode as shown by  $T$ . Further increase in magnetic field strength causes a contraction of the dimensions of this path but no essential change in its shape until the path dimensions become comparable with the cathode diameter. The latter case will not be considered here. The path  $T$  represents that of an undisturbed electron. It will be shown later that disturbances modify electron paths, especially near the cathode. However, the theory discussed in this section is independent of path shape, it being assumed only that electrons return periodically to the neighborhood of the cathode.

When the magnetic field exceeds the critical value, so that electrons are unable to reach the plate, the plate current is said to be "cut off." It is under this circumstance that excess-energy electrons appear. The

conditions which then exist in the tube are of considerable interest, and importance.

The simplest case is that in which each electron traverses a path such as  $T$  but once, and is then recaptured by the cathode. The current  $I_f$  emitted by the cathode is then equal to the returning current  $I_r$ . The net current is zero. If electrons are emitted at the constant rate  $dN/dt$ , and if  $\tau$  is the time required for one complete traversal of the path  $T$ , or radial oscillation, the number of electrons contained within the interelectrode space at any instant will be

$$N = \tau \frac{dN}{dt} \quad (1)$$

The case in which the electrons make on the average but one radial oscillation before returning to the cathode probably seldom actually occurs. Measurements made by the writer indicate that the average number of oscillations is of the order of one hundred in the tubes used in the present work. Furthermore some current always flows to the plate in spite of the magnetic field. (This will be discussed later.) Equation (1) must therefore be modified.

Assume that  $dN$  electrons are emitted in an interval of time  $dt$  short in comparison with the transit time  $\tau$ . In general during any one oscillation a fraction  $\beta_1$  of these will be collected by the plate, and as they return to the vicinity of the cathode another fraction  $\beta_2$  of the initial total will be collected. Denote by  $\beta = \beta_1 + \beta_2$  the total fraction collected in the first revolution. Then the fraction which starts from the cathode upon a second revolution will be  $\alpha = 1 - \beta$ . The time required for their passage of the cathode will be  $dt$ . During that interval another group of  $dN$  electrons will be emitted. Hence the total number starting on the second cycle will be  $(1 + \alpha)dN$ . Similarly after  $m$  cycles the total number leaving the cathode will be  $(1 + \alpha + \alpha^2 + \dots + \alpha^{m-1})dN$ . We shall consider only cases for which  $\alpha < 1$ , and make no distinction between reflected and secondary electrons. If there is a large amount of secondary emission  $\alpha$  will exceed unity and the above series will not converge. However, if  $\alpha < 1$  and  $m$  is infinite this becomes  $dN/(1 - \alpha)$ . It is assumed here that the fraction lost on successive revolutions is a constant. This is probably not strictly true, so that  $\alpha$  should be regarded as a mean value.

The total number of electrons in the interelectrode space may be found by taking the sum of all the above groups each leaving the cathode during an interval  $dt$  of the total period  $\tau$ . These intervals are  $\tau/dt$  in number. However it must be remembered that of each group leaving the cathode a fraction  $\beta_1$  makes only one half a revolution.

Hence, while  $dN/(1-\alpha)$  electrons travel from cathode to plate, only  $(1-\beta_1)dN/(1-\alpha)$  travel back from plate to cathode. The average number making the entire trip is

$$\frac{1}{2} \left( \frac{dN}{1-\alpha} + (1-\beta_1) \frac{dN}{1-\alpha} \right) = \frac{2-\beta_1}{2} \frac{dN}{(1-\alpha)},$$

and the total number  $N$  in the interelectrode space at any instant is  $\tau/dt$  times this, or

$$N = \frac{2-\beta_1}{2} \frac{\tau}{1-\alpha} \frac{dN}{dt}; \quad (2)$$

Some special cases are of interest. (a) If no electrons are collected by the plate and all are collected by the filament, then  $\beta_1 = \alpha = 0$ . In this case, (2) reduces to (1). (b) If all are collected by the plate, i.e.,  $\beta_1 = 1$ ,  $\alpha = 0$ , then

$$N = \frac{\tau}{2} \frac{dN}{dt}.$$

This is just one half the value given by (1), since all electrons make only one half a revolution. (c) As  $\alpha \rightarrow 1$ ,  $N$  becomes very large, since only a small fraction of the electrons are collected by either plate or cathode. This means that a very small filament emission may cause a large space charge by virtue of the electrons making many oscillations before being captured.

It is evident from (2) that  $\tau/(1-\alpha)$  represents the total average time  $D$  that an electron remains in the interelectrode space, if  $\beta_1 = 0$ . Since  $\tau$  is the time required for one radial oscillation,  $1/(1-\alpha)$  is the number of radial oscillations. This is valid regardless of the path shape. Hence we have

$$D = R\tau = \frac{\tau}{1-\alpha} \quad (3)$$

where  $R$  is the total number of radial oscillations.

Multiplying (2) by  $e$  and dividing by  $D$ , we may write the following relation between the various currents:

$$I_f = I_r + I_p = \frac{Ne}{D}, \quad (4)$$

for the case  $\beta_1 = 0$ .

Unfortunately a simple tube such as is shown in Fig. 1 is of little use experimentally since it does not permit the measurement of either  $I_f$  or  $I_r$ . In most of the work described below a modified design was employed in which the single filament  $C$  was replaced by two identical

tungsten wires  $C_1$  and  $C_2$  close together near the center of the tube, as in Fig. 2. Only one of these was heated and served as an electron source. The other served as a probe electrode. The distance between them was small in comparison to the plate diameter so that the electrostatic field was not greatly different from that in the tube of Fig. 1. Two tubes of this type were employed. They will be referred to as numbers I and II. They were of Pyrex 16.5 inches long and 1.5 inches in diameter. The plate, which was 10 inches long, consisted of a silver coating painted and baked on the inside of the glass. Electrodes  $C_1$  and  $C_2$  were pure tungsten wires of 0.0125-centimeter diameter, held taut by spiral tungsten springs. The tube had also disk-shaped tan-

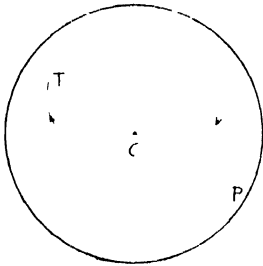


Fig. 1—Trajectory of an undisturbed electron in a magnetron, for the case when the magnetic field slightly exceeds cutoff value.

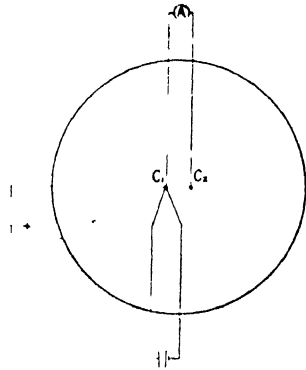


Fig. 2—Schematic diagram of the circuit for tubes I and II.

talum end plates positioned near the ends of the plate, but these played no part in the measurements except when specifically mentioned. The magnetic field was supplied by a solenoid, which was built in sections, permitting the field to be applied only to the middle five inches of the tube, or to the entire tube, as was desired. By applying the field to only the central section, cyclic orbits were produced only in that section. However, current flowing radially from cathode to plate in the end sections produced potential distributions there not greatly different from that in the middle section, and thus errors due to end effects were reduced.

With this type of tube, measurements of the returning current  $I_r$  could be made. If  $C_1$  be taken as the emitting electrode, electrons leave it, traverse cyclic orbits, then are collected by either  $C_1$ ,  $C_2$ , or the plate. The probability of collection is assumed equal for both of the filaments if at the same potential, because of their proximity and identical

form, and also, as will be shown later, because the electrons are subjected to disturbances during their motion. The current collected by  $C_2$  is indicated by meter  $A$  and is equal to one half of the total returning current.

The circuit was essentially as shown in Fig. 2. In order to eliminate the effect of the potential drop along the filament, a commutator was used with tubes I and II so that current collected by  $C_2$  was measured only during intervals when no heating current was flowing through  $C_1$ . With tubes III and IV, which were of a different type, to be described later, no commutator was used since the filament drop was only about 0.2 per cent of the plate potential.

In Fig. 3 data are plotted illustrating the occurrence of space-charge limitation of current in tube I for small filament-emission currents with

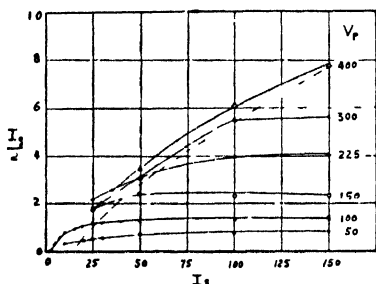


Fig. 3—Variation of probe current (milliamperes) with temperature-limited emission (milliamperes) and plate potential (volts).  $I_p/2$  is the current actually indicated by meter  $A$ , Fig. 2, because of the use of a commutator it must be multiplied by two to get the total probe current. Tube I.

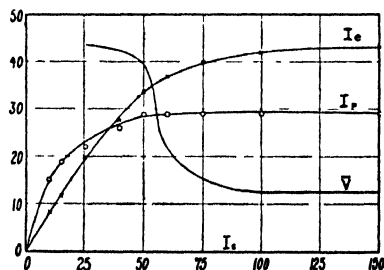


Fig. 4—Variation of end-plate current (milliamperes), plate current (microamperes) and mean random electron energy (electron volts), with temperature-limited filament emission (milliamperes).  $V_p = V_e = 400$ . Tube II.

the magnetic field exceeding the cutoff value.  $I_s$  is the saturated emission from the filament, measured by applying about 1000 volts to the plate in the absence of a magnetic field. The current collected by the probe electrode  $C_2$  is indicated by  $I_p/2$ . Each curve is labeled with the corresponding plate potential in volts. All of these curves show space-charge limitation except the 400-volt one. A dashed line has been drawn approximately through the upper bend of each so that the region under this line represents the condition of space-charge limitation. Another set of similar data for tube II is shown in Fig. 4. This tube was identical with the first, but the magnetic field was applied to the entire length of the plate, and the end-plate current also was measured. Both plate

current  $I_p$  and end-plate current  $I_e$  are shown. As should be expected these limit at substantially the same value of  $I_e$ .  $I_e$  limits somewhat indefinitely since the end plates draw current from portions of the filament, which are at varying distances from them.

In this case practically all the current flowed to the end plates. The plate current (microamperes in the figure) was comparatively small. The current  $I_p$  to the probe was of the order of one milliampere. Therefore it is seen that space-charge limitation occurs for a filament emission of approximately 45 milliamperes, whereas emission of about 1500 milliamperes would be required in the absence of a magnetic field, as calculated from the Langmuir-Childs law.

The effect is more striking in the previous case of Fig. 3. Here all currents are negligibly small except  $I_p$ . Space-charge limitation occurs at  $I_e = 0.25$  milliampere, i.e.,  $I_p = I_e = 0.5$  milliampere, for a plate voltage of 100. Without the magnetic field a current of about  $I_p = 98$  milliamperes would be required. This typical numerical case will be referred to repeatedly in the following pages.

The distributions of potential and charge which produce space-charge limitation in the presence of a magnetic field greater than the cutoff value are not the same as those in the absence of a magnetic field. However the difference is not very great,<sup>13</sup> except close to the cathode. It follows that a fair approximation to  $N$  can be obtained from the Langmuir-Childs law. Using as an example the above-mentioned case of Fig. 3, in which  $I_p$  is negligible, so that we may put  $\beta_1 = 0$ , we obtain  $N = 15 \times 10^8$  and from (4)  $D = N_e/I_p = 4.8 \times 10^{-7}$  seconds.

The time required for an undisturbed electron to execute a complete cycle is given by  $\tau_0 = 6.5 \times 10^{-8} r / \sqrt{V}$ , which yields in the present case  $6 \times 10^{-9}$  seconds. Thus if the electron paths resemble those of undisturbed electrons, the number of cycles per electron is  $D/\tau_0$  or 80. This result is typical for tubes such as I or II.

The relation between  $D$  and the plate voltage  $V_p$  may be determined from (4), and the experimental data of Fig. 3. From the latter it is evident that  $I_e$ , i.e.,  $I_p$ , varies as the first power of  $V_p$  in the space-charge-limited region. Since  $N$  also changes as  $V_p$  for space-charge limitation, it follows from (4) that  $D$  must remain constant as  $V_p$  is changed. This conclusion can be drawn only for the case in which  $H$  is varied so as to maintain an electron swarm of constant size, as was done experimentally.

<sup>13</sup> H. G. Möller, "Electronenbahnen und Mechanismus der Schwingungserregung im Schlitzanodenmagnetron," *Hochfrequenz. und Elektroakustik*, vol. 47, p. 115; April, (1936).



### ACTION OF A CYLINDRICAL COLLECTOR ELECTRODE IN AN ELECTRON SWARM IN WHICH SCATTERING OCCURS

The theory will be developed for a probe in an electron swarm in which energy exchanges between electrons occur. The resulting equations will then be applied to the experimental data.

If a fraction of the orbital energy of an electron is converted into energy of random motion, the electron will, in general, not be able to return to the cathode surface. For the present no hypothesis will be made regarding the mechanism of this energy conversion, but it will be assumed that a mean amount of energy of  $\bar{V}$  electron volts per electron is changed from the orbital to the random type, the total average

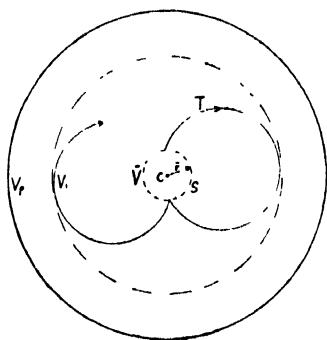


Fig. 5—Schematic diagram showing virtual cathode  $S$  and type of electron orbit outside virtual cathode.

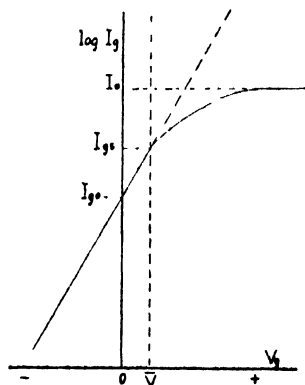


Fig. 6—Theoretical collector characteristic according to (10).

energy per electron remaining constant. On the average then, electrons will be able to travel towards the cathode only up to a limiting distance at which the potential is  $\bar{V}$ . Electrons approaching the cathode will thus have zero orbital energy upon reaching an equipotential cylindrical surface  $S$  surrounding the cathode, the potential of this surface being  $\bar{V}$ , and its distance from the cathode  $\bar{r}$ , see Fig. 5. Electrons on this surface retain their random motion, which, due to the assumed random nature of the energy exchanges, is Maxwellian in nature.

It is evident that  $S$  possesses the properties of a virtual cathode. To determine its temperature, it is only necessary to equate the random energy to the kinetic energy of a gas in terms of temperature; i.e.,

$$ne\bar{V} = \frac{3}{2} nkT$$

or,

$$T = \frac{2}{3} \frac{eV}{k}. \quad (5)$$

The surface  $S$  and the cathode  $C$  form a diode, in which a current  $I_f$  flows from  $C$  to  $S$ , and a current  $I_r$  flows from  $S$  to  $C$ . Under the condition that the plate current is negligible,  $I_f = I_r$ .

To compute  $I_r$  we use the expression developed by I. Langmuir and H. M. Mott-Smith,<sup>14</sup> for the current from a cylindrical cathode at temperature  $T_0$  to an internal cylindrical collector against a retarding field. This is

$$I_r = 2\pi r_0 l I \epsilon^{-e\bar{V}/kT_0} \quad (6)$$

where  $r_0$  is the radius of the collector and  $l$  its length,  $I$  the saturated current density at  $S$ ,  $e$  the electronic charge,  $k$  Boltzmann's constant, and  $T_0$  the electron temperature due to the cathode heat.

If  $I_0$  is the space-charge-limited current we have in the present instance  $I = I_0/2\pi\bar{r}l$ . Also the temperature of  $S$  is given by (5) plus that due to the real cathode. Hence,

$$I_r = \frac{r_0 I_0}{\bar{r}} \epsilon^{-e\bar{V}/k(T+T_0)}. \quad (7)$$

When a probe is inserted near the cathode, the returning current  $I_r$  divides between cathode and probe, and sheaths  $S_1$  and  $S_2$  form about each respectively. For simplicity these sheaths will be assumed to have circular cross section. The currents to each will be in the same ratio as their sheath areas, hence the probe current  $I_p$  is, from (7)

$$I_p = \frac{\bar{r}_2}{\bar{r}_1 + \bar{r}_2} I_r = \frac{r_0 I_0}{\bar{r}_1 + \bar{r}_2} \epsilon^{-e\bar{V}/k(T+T_0)} \quad (8)$$

where  $r_1$  and  $r_2$  are the sheath radii about cathode and probe, respectively. This expression must be further modified if the probe potential  $V_p$  differs from that of the cathode. In that case we must substitute for  $\bar{V}$  the term  $V_p - \bar{V}$  since that is the actual potential difference.

The radius of the sheath about the probe may vary with probe potential, the sheath being forced farther away as the probe becomes more negative. If probe and cathode are of the same size, and both at zero potential,  $\bar{r}_1 = \bar{r}_2$ , but as the probe becomes negative  $\bar{r}_2$  increases by an amount  $\Delta r$ . Hence in place of  $\bar{r}_1 + \bar{r}_2$  we may write  $2\bar{r}_1 + \Delta r$ .

Reflections of electrons from the collector also must be considered. No distinction will be made between reflected and secondary electrons,

<sup>14</sup> H. M. Mott-Smith, and I. Langmuir, "The theory of collectors in gaseous discharges," *Phys. Rev.*, vol. 28, p. 727; October, (1926).

and only the case will be considered in which the ratio of secondaries to primaries is low, i.e., less than unity. Thus the only effect of reflections or secondary emission will be to increase the number of oscillations. In case reflections occur, the factor  $(1-f)$ , where  $f$  is the coefficient of reflection, must be introduced. Hence the final expression for probe current is

$$I_o = \frac{(1-f)r_o I_0}{2\bar{r}_1 + \Delta r} e^{e(V_o - \bar{V})/k(T+T_o)}, \quad (9)$$

or,

$$\log I_o = \log \frac{(1-f)r_o I_0}{2\bar{r}_1 + \Delta r} + \frac{e(V_o - \bar{V})}{k(T+T_o)}. \quad (10)$$

The Langmuir—Mott-Smith relation (6) used in deriving (9) is applicable in the presence of a magnetic field, providing the proper expression for the saturation current be introduced. The method used above of expressing this current in terms of  $I_0$ , is applicable for all values of magnetic field, and gives the proper value of the saturation current.

If (10) be applied to space-charge-limited cases,  $I_0$  will be constant, if  $V_p$  is constant. As  $V_o$  is varied  $\Delta r$  will change, but not greatly, and the logarithm of the term containing  $\Delta r$  will be but slightly affected. The reflection coefficient is in general a function of the incident electron energy, i.e., temperature. However, changes of  $V_o$  do not affect this, hence  $f$  is constant. It follows that (10) gives a nearly linear relation between  $\log I_o$  and  $V_o$ .

The slope of the line obtained by plotting  $\log I_o$  against  $V_o$  is  $e/k(T+T_o)$ . Hence the electron temperature may be determined. In the experimental work  $T$  is so much greater than  $T_o$  that the latter may usually be neglected.

Fig. 6 gives the collector characteristic according to (10),  $\log I_o$  being plotted against  $V_o$ . It is linear only for  $V_o < \bar{V}$ . For  $V_o = \bar{V}$ ,  $\Delta r = -\bar{r}_1 + r_o$ , and  $I_o = [(1-f)r_o I_0]/(\bar{r}_1 + r_o)$ . As  $V_o$  increases above  $\bar{V}$  the current approaches the limiting value,  $I_0$ . This is the limiting value only if the filament temperature is sufficiently high to maintain a space-charge-limited condition; otherwise the limiting value will be lower. For very high positive probe potentials  $I_0$  will depart considerably from the value for low probe potentials since the potential distribution in the tube will be considerably distorted, and secondary emission may become important. For these reasons (10) probably is not valid unless  $V_o$  is small compared to  $V_p$ , and also sufficiently small that secondary emission may be neglected. The actual characteristic would

therefore likely differ considerably from that of Fig. 6 for large positive values of  $V_g$ .

The potential distribution near the probe or cathode for retarding potentials may be obtained by making use of Poisson's equation for cylinders

$$\frac{1}{r} \frac{d}{dr} \left( r \frac{dV}{dr} \right) = 4\pi n e, \quad (11)$$

and Boltzmann's law,

$$n = n_0 e^{V e / k T}, \quad (12)$$

which governs the charge distribution between the electrode and the virtual cathode. Inserting (12) in (11) and expanding gives

$$\frac{d^2 V}{dr^2} + \frac{1}{r} \frac{dV}{dr} = 4\pi n_0 e e^{V e / k T}. \quad (13)$$

The solution of this for  $V=0$ , and  $dV/dr=0$ , when  $r=0$ , is

$$V = -\frac{4}{3} \bar{V} \log \left[ 1 - \left( \frac{r}{4\lambda} \right)^2 \right], \quad (14)$$

where  $\lambda$ , the Debye distance for the electron swarm near the collector where the density is  $n_0$ , is given by

$$\lambda^2 = \frac{kT}{8\pi n_0 e^2}. \quad (15)$$

The electron density distribution is obtained by substituting (14) in (12), which gives

$$n = n_0 \left[ 1 - \left( \frac{r}{4\lambda} \right)^2 \right]^{-2}. \quad (16)$$

The radius of the virtual cathode is found by putting  $V = \bar{V}$  in (14). Thus,

$$\bar{r} = \sqrt{1 - e^{-3/4}} 4\lambda = 2.9\lambda. \quad (17)$$

Similarly,

$$\bar{n} = 4.48 n_0. \quad (18)$$

In applying these equations to the numerical case mentioned previously it is necessary to compute  $n_0$ . This may be done by use of the expression<sup>15</sup>

$$n_0 = 2 \times 10^{13} I_1 T_0^{-1/2}$$

<sup>15</sup> I. Langmuir and K. T. Compton, "Electrical discharges in gases," *Rev. Mod. Phys.*, vol. 3, p. 242; April, (1931).

where  $I_1$  is the emission current density in amperes per square centimeter, and  $T_0$  the cathode temperature. This yields  $n_0 = 5 \times 10^8$ , whence

$$\lambda = 0.049 \text{ centimeter,}$$

and

$$\bar{r} = 0.14 \text{ centimeter.}$$

Expanding (14) in a power series we have

$$V = \frac{4}{3} \bar{V} \left[ \left( \frac{r}{4\lambda} \right)^2 + \frac{1}{2} \left( \frac{r}{4\lambda} \right)^4 + \frac{1}{3} \left( \frac{r}{4\lambda} \right)^6 + \dots \right],$$

whence it is evident that near the cathode  $V$  varies as  $r^2$ , and as an increasingly higher power as the virtual cathode is approached. Beyond the virtual cathode the variation must approach the logarithmic-

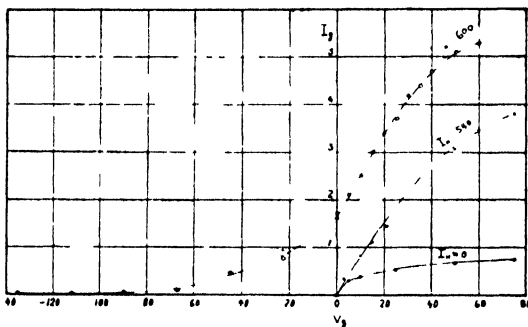


Fig. 7—Probe-current (milliamperes) curves for several values of magnetic field, versus probe potential (volts). Tube III.

law characteristic of concentric cylinders, it being remembered that although the current from the real cathode is space-charge limited, that from the virtual cathode is not.

Fig. 7 illustrates the typical behavior of a magnetron under various magnetic field strengths, and shows the existence of excess-energy electrons. The tube used here was smaller than those previously described, having a cylindrical tantalum plate of 2 millimeters radius, and 8 millimeters length. Two tungsten wires 0.0125 centimeter in diameter and 0.05 centimeter apart were positioned near the central axis and served as cathode and probe. This will be referred to as tube III. Its behavior was qualitatively the same as that of the larger tubes I and II.

In the figure, probe current  $I_p$  is plotted against probe potential  $V_p$ , and curves are labeled with their corresponding magnet current  $I_H$ . If the magnetic field is zero, the probe collects no current when it is

at negative or zero potential, and a small, slowly increasing current as it becomes more positive. For a field a little below cutoff ( $I_H = 540$ ) the behavior is unchanged qualitatively, but the current collected is larger. As the magnetic field passes through the cutoff value there is a sudden change in that the probe begins to collect electrons when it is negative, as is shown by the curve for  $I_H = 600$ .

As the probe becomes increasingly negative the current collected approaches zero. If positive ions were present in appreciable numbers a point would eventually be reached where the electron current would be

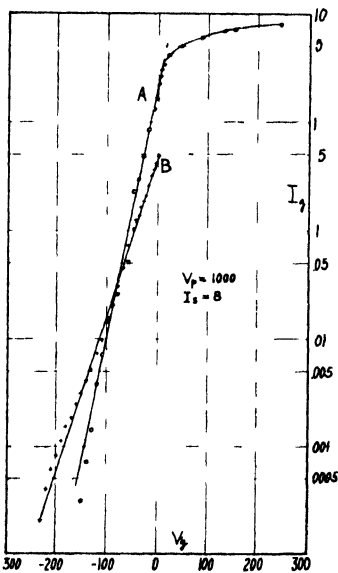


Fig. 8—Probe current characteristics. A, axial probe. B, end-plate probes with greater tilt. Tube III.

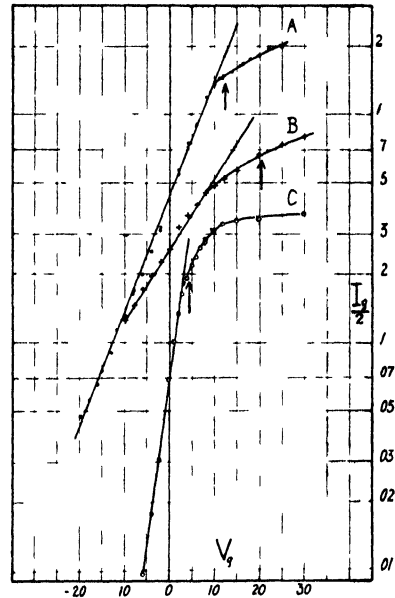


Fig. 9—Collector characteristics showing extension of linear portion into region of positive potentials. Curve A, space-charge limited,  $V_p = 300$ . Curve B, not space-charge limited,  $V_p = 300$ . Curve C, space-charge limited,  $V_p = 150$ ,  $I_c$  divided by 2.45 before plotting. Tube II.

negligible and the positive-ion current comparatively large. The curve would cross the horizontal axis, the actual crossing taking place when the electron and positive-ion currents were equal. This effect was observed in only a few cases when the plate voltage and emission current were both high. However the amount of positive-ion current was always too small to play any important part in the tube behavior.

Such curves as those of Fig. 7 should obey the relation (10). Two

examples are shown in Fig. 8, in which  $I_p$  is plotted versus  $V_p$  on a semilog scale, yielding straight lines. These were obtained with tube IV, which was similar to tube III except for having disk-shaped end plates. Curve *A* was obtained with the plate at 1000 volts, the end plates at zero potential, and a temperature-limited filament emission of 8 milliamperes. For curve *B* the end plates were used as probes. In this case the tilt of the tube in the magnetic field was not the same as in case *A*. It will be noted that for curve *A*, an appreciable number of electrons have excess energy equivalent to over 130 volts, while for *B*, energies over 220 volts appear. The mean random energy of the Maxwellian distribution in case *A* is found to be  $\bar{V} = 27$  equivalent volts, which corresponds to a temperature of about 210,000 degrees centigrade. Although this would be considered a very high temperature for an electron swarm in a plasma, it is not unusually high for a swarm in a high-vacuum magnetron, such as those described here. Cases have been observed in which the temperature exceeded one-half million degrees.

Equation (6) from which (9) was derived is valid only for retarding fields. Hence (9) should hold only for  $V_p < \bar{V}$ . For  $V_p > \bar{V}$  the linear relation between  $\log I_p$  and  $V_p$  should no longer hold. Departures from this linear relation are shown in Fig. 8, curve *A*, and Fig. 9. Curves *A* and *C*, Fig. 9, were made under identical conditions except that the plate voltage and magnetic field were changed, as mentioned elsewhere, to maintain a constant electron swarm size. The cathode was held at a sufficiently high temperature to give space-charge limitation of emission current. The arrows indicate the points at which  $V_p = \bar{V}$ , the value of  $\bar{V}$  being determined from the slope of the line. In curves *A* and *C* the break occurs as near the arrow as could be expected in view of the assumptions made in deriving (10). These results indicate that the energy of random motion is derived at the expense of the orbital motion of the electrons themselves, and not from some external source such as oscillations.

Curve *B* shows the effect of reducing the filament temperature until space-charge limitation does not exist. Except for a lower cathode temperature the conditions were identical with those of curve *A*. The decrease of slope of the linear portion indicates a higher electron random energy. This effect will be discussed later. The arrow indicates the point where  $V_p = \bar{V}$ . It is evident that the break does not occur at this point if space-charge limitation is not maintained.

In connection with these characteristics it should also be noted here that there is no abrupt increase in the probe current as  $V_p$  passes through zero. Such an increase would occur if appreciable numbers of

electrons did not undergo scattering, since they would possess sufficient energy just to reach the probe when it was at zero potential. The absence of any break in the curve at that point is evidence that essentially all electrons are scattered.

The change of the quantity  $\Delta r$  is unimportant when  $\bar{V}$  is large compared to  $V_g$  for then  $\bar{r}$  is large compared to  $\Delta r$ . However, if  $\bar{V}$  is small, the effect of the change in  $\Delta r$  may become noticeable. This is illustrated in Fig. 10. The decreasing slope with increasing plate potential indicates increasing electron random energy  $\bar{V}$  as is evident from (10).

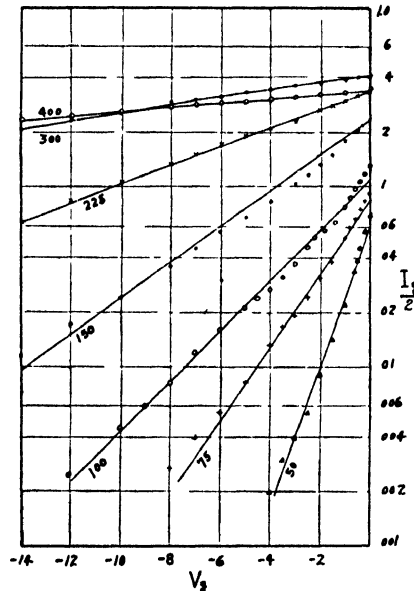


Fig. 10—Probe current (milliamperes) against probe potential (volts) for various plate potentials. Tube 1.

It will be noticed that for high random energy (small slope) the points lie closer to straight lines than for low random energy. The plots for plate potentials from 50 to 150 volts show  $\log I_p$  increasing more rapidly than linearly as  $V_g$  approaches zero. This is interpreted as due to the decrease of  $\Delta r$  in (10), which causes the right-hand logarithmic term to increase slightly instead of remaining constant.

To apply (9) to the computation of the current for  $V_g = 0$ , put  $\bar{V} = 3/2 kT/e$ , then

$$I_{g0} = \frac{(1-f)r_0 I_0 e^{-3/2}}{2\bar{r}_1}.$$

For the reflection coefficient  $f$  use the experimental data of H. E. Farns-



worth.<sup>16</sup> The space-charge-limited current  $I_0$  is obtained by means of the Langmuir-Childs law. The virtual cathode radius  $\bar{r}_1$  is calculated from (17), as shown above. Values of  $I_0$  thus computed from the data of Fig. 10 are shown as crosses in Fig. 11. Values of  $f$  were not available to permit calculation over a larger range. The points lie on a good straight line through the origin, although that such should be the case is not evident from the above equation. The experimental points, indicated by circles, are in very good agreement with the calculated ones in view of the approximations made. The point for  $V_p = 400$  lies outside the space-charge-limited region (see Figs. 3 and 13) and hence should not follow the same law as the others.

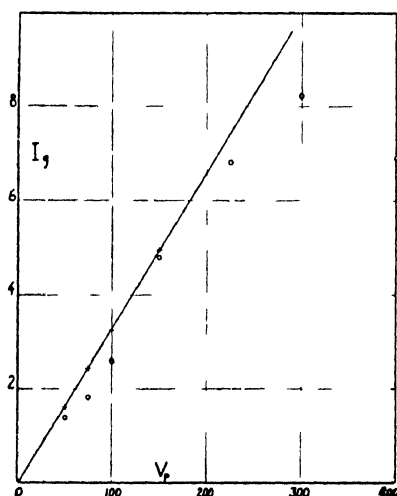


Fig. 11—Probe currents for  $V_g = 0$ . Experimental (O) from data of Fig. 10; computed (+) from (9).

The above theory is therefore in good agreement with the experimental results since it explains (1) the linear relation between  $\log I_0$  and  $V_p$ , (2) the existence of the linear relation for positive values of  $V_p$  up to  $\bar{V}$ , (3) the curvature of the  $\log I_0$ -versus- $V_p$  plots for small  $\bar{V}$ , and (4) the current  $I_0$  for  $V_p = 0$ .

#### RELATION BETWEEN ELECTRON TEMPERATURE AND OTHER VARIABLES

It has been found that the mean random electron energy or temperature is a function of the plate potential, the filament emission, the magnetic field, and the end-plate potential. Graphs showing the varia-

<sup>16</sup> H. E. Farnsworth, "Electronic bombardment of metal surfaces," *Phys. Rev.*, vol. 25, p. 41; January, (1925).

tion with respect to plate potential are shown in Fig. 10. These were obtained with tube I, applying the magnetic field to the middle section only, so that the end plates played no part. The temperature-limited filament emission was 50 milliamperes. The magnetic field strength was varied with the plate potential in such a way as to confine the elec-

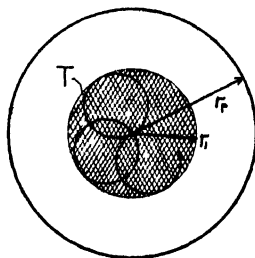


Fig. 12—Schematic diagram of cross section of magnetron showing electron swarm (crosshatched) and undisturbed electron path  $T$

trons (i.e., undisturbed ones) within a cylindrical sheath of constant radius, as is shown in Fig. 12. This diagram represents a cross section of the tube, the probe not being shown. The cross-hatched area indicates the electron swarm in which individual undisturbed electrons

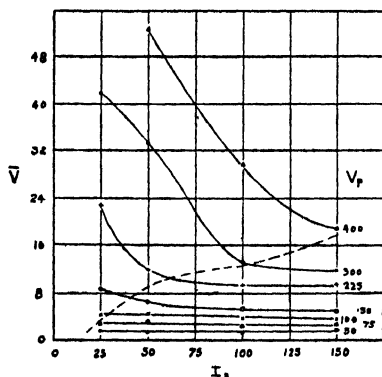


Fig. 13—Variation of electron mean random energy (electron volts) with plate potential (volts) and temperature-limited emission (milliamperes) Tube I

execute trajectories outside the virtual cathode approximately as illustrated by curve  $T$ . The ratio of the plate radius  $r_p$  to the swarm radius  $r_1$  was maintained at the arbitrary value of 2.7. This was done to insure that the changes observed would be due to plate-potential changes alone and not to other factors associated with change of swarm size. The graphs of Fig. 10 are similar to those of Fig. 8 but are taken for a variety of plate potentials, as indicated by the figures on each curve.

The electron random energy is inversely proportional to the slope, hence the decreasing slope with increasing plate potential indicates increasing random energy

A more comprehensive set of data, which shows the variation of random energy with both plate potential and temperature-limited filament emission, is given in Fig. 13. These curves are related to those of Fig. 3, being derived from the same set of data. The dashed lines in the two figures correspond to each other, and divide the space-charge-limited regions from the nonlimited regions. It will be observed that the graphs are essentially horizontal straight lines in the limited regions, indicating that changes in  $I_s$  (i.e., filament temperature) have little or no effect upon  $\bar{V}$  if space-charge limitation exists. However, if

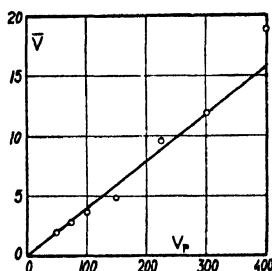


Fig. 14—Linear relation between electron random energy and plate potential when current is space-charge limited.

space-charge limitation does not exist, a decrease in  $I_s$  results in a rapid rise in  $\bar{V}$ , within Hence it appears that the random energy drops as space charge increases, until a limiting value is reached when the current becomes space-charged limited.

These same data show that  $\bar{V}$  varies directly as the first power of  $V_p$  in the space-charge-limited region. Outside that region the variation is as some higher power. This is illustrated in Fig. 14 in which are plotted data from Fig. 13 for  $I_s = 150$ . It is seen that the points lie fairly well along a straight line except at  $V_p = 400$ . The latter point, however, lies outside the space-charge-limited region. If we had taken the points for some lower  $I_s$ , say 75, they would have departed from the straight line much sooner, in fact at about  $V_p = 200$ .

The variation with respect to the magnetic field strength  $H$  is somewhat more complicated, as is evident from Fig. 15. These curves were made with tube II, which was a duplicate of tube I, except for having a somewhat better vacuum. The plate voltage was 225, the end-plate voltage zero, the temperature-limited filament emission was 25 milliamperes.

To obtain curve *A* the magnetic field was applied to the entire tube. This was done only to determine the cutoff point. (No cutoff is obtained when the field is applied to only a section of the tube, since then electrons merely execute long spirals from the section in the magnetic field to a field-free section where they may reach the plate. Under this condition the plate current changes but slightly as the critical value of magnetic field is passed through.) After curve *A* was obtained, the solenoid was reconnected so as to apply field to the mid-section only, as described above, and curves *B* and *C* were taken with that arrangement.

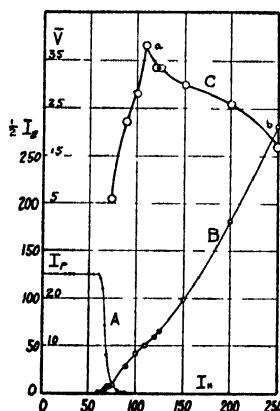


Fig. 15—A. Cutoff characteristic of plate current (milliamperes).

B. Probe current (microamperes).

C. Corresponding electron mean random energy (electron volts). Tube II.

Curve *B* indicates the change of probe current with magnetic field, while curve *C* shows the change of electron random energy. These curves will be discussed more fully later, but it is desired to point out here that for values of magnetic field such that the electron sheath is well clear of the plate and yet large compared to the cathode-probe spacing, as section *ab* of *C*, the electron temperature appears to vary as the inverse first power of  $H$ . This is indicated if section *ab* be plotted on log-log paper. The departure from this relation below  $I_H = 120$  may be due to the elimination of the higher-energy electrons by the plate and the consequent reduction of temperature. As the field becomes stronger the sheath shrinks farther away from the plate, fewer high-energy electrons are lost, and the inverse first-power law then becomes apparent.

The variation of the electron random energy with end-plate potential is qualitatively the same as with plate potential. That is, there is an increase of  $\bar{V}$  with  $V_a$ , but the law of variation is not as simple as in the former case and has not been determined. A less simple law is

to be expected since the electrostatic field distribution is complicated by end plates. A similar dependence upon space charge also exists, for it can be shown that if there is space-charge limitation of current, variations of  $I_s$  have no effect on  $\bar{V}$ . However, if space-charge limitation of current does not exist then an increase of  $I_s$  causes a decrease of  $\bar{V}$ .

Experimental data illustrating this are given in Fig. 16. Here  $\bar{V}$  is plotted as a function of  $I_s$  for different values of  $V_e$ . This figure is analogous to Fig. 13 in which the same quantities are plotted for different values of  $V_p$ . As in the former case, the graph can be divided into two regions as by the dashed line. Below this line  $\bar{V}$  is seen to be substantially independent of  $I_s$ , the temperature-limited emission, while

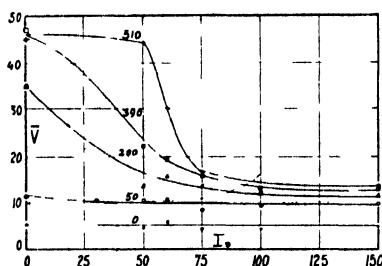


Fig. 16—Variation of electron random energy (electron volts) with respect to end-plate potential (volts) and temperature-limited filament emission (milliamperes). Tube II.

above the line there is a marked dependence. It can be shown, as was done in the case of Fig. 13, that the region below the line represents the cases in which the cathode emission is space-charge limited whereas in the region above, space-charge limitation does not occur. The position of the line cannot be sharply determined, of course, since the transition is a gradual one. In the figure it was roughly drawn through those points where the horizontal straight lines first show some upward trend.

Evidence that this upward trend of the curve arises from a departure from the space-charge-limited condition is given in Fig. 4. Here a curve of  $\bar{V}$  (at  $V_e = 400$ ) is plotted on the same sheet as curves of  $I_s$  and  $I_p$  against  $I_s$ . It is seen that the downward trend of  $\bar{V}$  begins as  $I_s$  and  $I_p$  commence to level off, and that the sharpest drop in  $\bar{V}$  occurs approximately at the knee of the other curves, where space-charge limitation occurs.

#### RELATION BETWEEN ENERGY OF ORBITAL MOTION AND ELECTRON TEMPERATURE

To compute the orbital energy of the undisturbed electrons we refer again to Fig. 12. An undisturbed orbit is represented by  $T$ , in which

the distance of maximum excursion of the electron from the cathode is  $r_1$ . We shall determine the potential at  $r_1$ , for the general case when the potential distribution is given by

$$V = V_p \left( \frac{r}{r_p} \right)^\mu, \quad (19)$$

where  $\mu$  is determined by the amount of space charge; e.g., it is equal to two thirds for space-charge limitation.<sup>13,17</sup> This expression is used mainly to give a qualitative idea of the effect of space charge. It is only approximately correct, but is a good approximation especially near the space-charge-limited region in which we are principally interested. Even when the electron swarm does not fill the entire interelectrode space the approximation is sufficiently good.

Making use of Hull's<sup>18</sup> differential equation for electron motion,

$$\left( \frac{dr}{dt} \right)^2 = \frac{2eV(r)}{m} - \left( \frac{He}{2m} \right)^2 r^2,$$

we get the maximum value of  $r$  (i.e.,  $r_1$ ) by putting  $dr/dt=0$ . This yields, after substituting from (19),

$$\frac{r_1}{r_p} = \left( \frac{8mV_p}{H^2 e r_p^2} \right)^{1/(2-\mu)} \quad (20)$$

The critical cutoff value of  $H$  is found by putting  $r_1 = r_p$ , hence

$$H_c^2 = \frac{8mV_p}{e r_p^2},$$

and therefore

$$\frac{r_1}{r_p} = \left( \frac{H_c}{H} \right)^{2/(2-\mu)} \quad (21)$$

Substituting this in (19) yields

$$V_1 = V_p \left( \frac{H_c}{H} \right)^{2\mu/(2-\mu)}. \quad (22)$$

In the space-charge-limited case  $\mu = 2/3$ , so that

$$V_1 = V_p \frac{H_c}{H}.$$

<sup>17</sup> For a discussion of electron paths in magnetrons as a function of space charge, see E. G. Linder, "Description and characteristics of the end-plate magnetron," *Proc. I.R.E.*, vol. 24, pp. 633-653; April, (1936).

<sup>18</sup> A. W. Hull, "The effect of a uniform magnetic field on the motion of electrons between coaxial cylinders," *Phys. Rev.*, vol. 18, p. 31; July, (1921).

Thus it is seen that the maximum orbital energy  $eV_1$  of the undisturbed electrons is directly proportional to  $V_p$  and inversely proportional to  $H$  as is the electron random energy  $\bar{V}$ , as determined experimentally. We may therefore write  $\bar{V} = \text{constant } V_1$ , for space-charge limitation.

For cases in which space-charge limitation is not attained,  $\mu$  is less than two thirds. The relation (19) then less accurately represents the potential distribution but does so sufficiently well for the present purposes. As  $V_p$  is increased,  $\mu$  decreases, and the factor  $(H_c/H)^{2\mu/(2-\mu)}$  increases, instead of remaining constant as in the previous case. Hence  $V_1$  increases at a rate greater than the first power, as was found experimentally for  $\bar{V}$  in non-space-charge-limited cases.

It has been found that tilting the tube slightly so that its axis is no longer parallel to the direction of the magnetic field causes an increase in electron temperature. This is due to the resulting decrease in space charge by virtue of electrons reaching the plate by traveling along spirals whose axes parallel the field. The decrease in space charge causes a decrease in  $\mu$ , resulting as above in an increase of  $V_1$ .

#### POSSIBLE CAUSES OF SCATTERING

In the preceding discussion of electron motion and collector theory it was assumed that electron scattering existed, but no assumptions were made regarding its cause. The above theory is valid regardless of the source of the scattering; nevertheless some consideration of various possible causes is desirable, even though a satisfactory explanation has not been found.

It has been shown that the electron random energy is derived from the orbital energy of the electrons themselves and not from some external source. It has also been shown that the scattering is such as to yield a Maxwellian distribution when the orbital energy is subtracted. Any satisfactory mechanism must meet these conditions.

Oscillations in the external circuits connected to the tube could conceivably yield a Maxwellian distribution; however, the energy would not be supplied by the electrons themselves. Consequently no virtual cathode would be formed, and the law for the current to a probe would differ from that found. However this possibility was carefully investigated since it has been so frequently suggested as an explanation.

Experimental tests for such oscillations were made. With tubes of type III and IV oscillations were searched for down to wavelengths of several centimeters. A conventional radio wavemeter was used for the longer waves, while for the shorter ones a Lecher wire system, coupled to the tube, was employed. Audio-frequency modulation was applied to the magnetron, and a crystal detector in the shorting bridge was con-

nected to an audio-frequency amplifier. Excess-energy electrons were easily observed when no oscillations could be detected with this apparatus. Further tests were made by connecting large condensers across the leads of the tube; no effect whatsoever was observed upon the excess-energy-electron current.

Additional evidence that oscillations are not the cause of this effect lies in the stability and reproducibility of the phenomena, and the smoothness of the curves obtained. If oscillations were present a more erratic behavior would be expected.

Scattering by gas molecules would result in random energy being supplied at the expense of orbital energy. This type of scattering has been studied in detail by Langmuir<sup>1</sup> and Langmuir and Jones<sup>10</sup>, who found a relationship between collector current and voltage of a different type from that of (9). Furthermore the number of collisions between electrons and molecules may be computed, and is found to be far too small. If the data of Langmuir and Jones<sup>20</sup> for nitrogen and 75-volt electrons are used, and the pressure be assumed to be  $10^{-5}$  millimeters of mercury, it is found that for an electron path of 90 centimeters the probability of a collision is only about 0.02.

Energy exchanges due to collisions between electrons satisfy all the assumed conditions. An expression for the mean-square angular deflection due to multiple impacts by an electron traversing a swarm of electrons has been derived by H. A. Wilson<sup>21</sup> in connection with  $\beta$ -ray scattering. It has been applied to electron scattering by Langmuir and Jones.<sup>20</sup> The equation is

$$\bar{\phi}^2 = \frac{2\pi e^2 n L}{V^2} \log \frac{P_1}{P_0}.$$

Knowing the angle  $\phi$ , the mean transverse energy for small angles is given by  $\bar{V} = \bar{\phi}^2 V$ , where  $V$  is the energy before impact. Thus  $\bar{V} = (2\pi e^2 n L / V) \log (P_1 / P_0)$ , where  $n$  is electron density,  $L$  is total path length, and  $P_1$  and  $P_0$  are the maximum and minimum distances of approach between the orbits of colliding electrons which need be considered. Their method of determination is given by Langmuir and Compton.<sup>22</sup> Application of this expression to the numerical example

<sup>10</sup> I. Langmuir and H. A. Jones, "Collisions between electrons and gas molecules," *Phys. Rev.*, vol. 31, p. 357; March, (1928).

<sup>20</sup> I. Langmuir and H. A. Jones, "Collisions between electrons and gas molecules," *Phys. Rev.*, vol. 31, p. 390; March, (1928).

<sup>21</sup> H. A. Wilson, "On the scattering of  $\beta$ -rays," *Proc. Roy. Soc.*, A102, vol. 9, October, (1923).

<sup>22</sup> I. Langmuir and K. T. Compton, "Electrical discharges in gases," *Rev. Mod. Phys.*, vol. 3, p. 219; April, (1931).



used above gives  $\bar{V} = 0.055$  volt whereas the experimental value is 4.2 volts.

This same equation applies to scattering by positive ions. However, since the positive-ion density is much smaller than the electron density, the scattering also will be much less.

Electron oscillations similar to plasma electron oscillations<sup>23</sup> may exist in swarms of electrons, since the existence of positive ions is not necessary. There is no direct experimental evidence of their presence, in such swarms, but it is of interest that such oscillations have been suggested as a possible cause of electron scattering in strongly ionized gases,<sup>24</sup> where the free electrons are found to possess a Maxwellian velocity distribution which cannot be accounted for on the basis of ordinary collisions.

<sup>23</sup> K. T. Compton and I. Langmuir, "Electrical discharges in gases," *Rev. Mod. Phys.*, vol. 2, p. 239; April, (1930).

<sup>24</sup> I. Langmuir, "Oscillations in ionized gases," *Proc. Nat. Acad. Sci.*, vol. 14, p. 627; August, (1928).

# EFFECT OF ELECTRON TRANSIT TIME ON EFFICIENCY OF A POWER AMPLIFIER\*†

BY

ANDREW V. HAEFF

RCA Radiotron Division, RCA Manufacturing Company, Inc.,  
Harrison, N. J.

*Summary*—Measurements of the plate efficiency of a neutralized triode amplifier operated at high frequencies are reported. The results are compared with those obtained for an oscillator operated at the same frequency. At a frequency at which the oscillator efficiency approaches zero the amplifier efficiency is found to be reduced to only 50 per cent of the low-frequency value. It is shown that the difference in efficiency is primarily due to a large phase angle between the plate current and the grid voltage produced by the electron transit time.

IN a recent paper<sup>1</sup> W. G. Wagener discusses the effect of electron transit time on amplifier efficiency and presents generalized curves of transit-time-efficiency factors for triode oscillators and amplifiers. Wagener refers to the work done early in 1936 by the author, who at that time suggested that in a neutralized amplifier, or in any amplifier in which the phase of output voltage is independent of the phase of input voltage, the efficiency of a tube as an amplifier will be higher than as a triode oscillator at higher frequencies when, as a result of electron transit time, appreciable phase difference may exist between grid voltage and plate current. In order that this suggestion might be checked, curves of plate efficiency versus transit angle were obtained for a push-pull cross-neutralized amplifier. These curves clearly demonstrated the improved performance of a tube as an amplifier and indicated the possibility of extending the high-frequency limits of conventional tubes. It is the purpose of the present paper to present the original data on amplifier efficiency as affected by electron transit time and to discuss the significance and usefulness of such information for the design of high-frequency power-amplifier tubes.

The study of the effect of electron transit time on the performance of tubes at high frequencies has been the subject of many recent publications. Starting with the original work of Benham<sup>2</sup> and other investigators,<sup>3,4,5,6</sup> we find that a satisfactory theory confirmed by experiment, has been developed for analyzing the high-frequency performance of conventional diodes and triodes. However, application of

---

\* Decimal Classification: R1385 X R334.

† Reprinted from *RCA Review*, July, 1939.

this theory is limited to receiving tubes because small radio-frequency signal amplitudes are assumed in the theory. The problem of high-frequency power tubes where r-f voltages comparable with the d-c voltages are involved, still is in need of an adequate theoretical treatment, although attempts to find a solution have already been made.<sup>7</sup> Lacking an adequate theory, a researcher and designer has to resort to experiment to obtain the quantitative information necessary for design of high-frequency power tubes.

The purpose of the author's original work was to determine the effect of electron transit time on the plate efficiency of a tube operated as an amplifier and to compare it directly with the transit-time effect in the case of an oscillator. For this comparison to be sufficiently

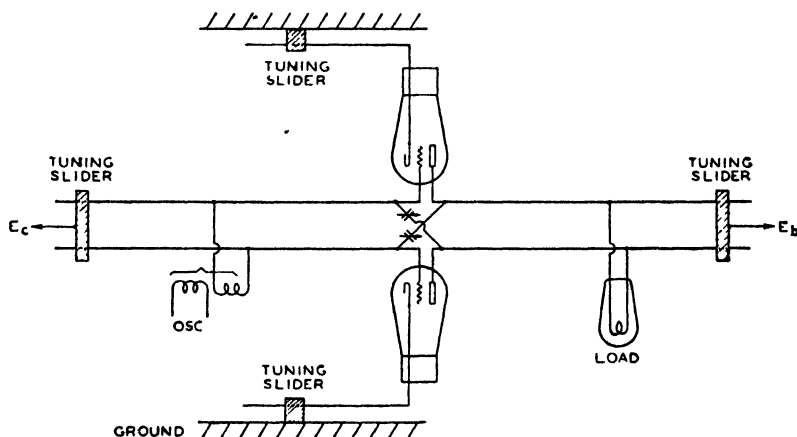


Fig. 1—A schematic diagram of the amplifier circuit.

significant, it was necessary to use the same tube, under the same operating conditions, and to use the same circuit both for the amplifier and for the oscillator tests, except for the addition of neutralizing condensers for the amplifier tests. The circuit is shown in Figure 1. Two developmental h-f triodes (similar to RCA-834) were used. Variable air condensers connected to grids and plates by short low-inductance leads were used for capacitive cross-neutralization. Low-loss, parallel-wire, tuned transmission lines were used as circuit elements to facilitate tuning and loading adjustments. The filaments were also tuned by means of half-wave lines. The excitation for the amplifier was obtained from an oscillator coupled inductively to the grid lines. The load consisting of one or two ten-watt lamps was placed across the plate line and the value of output impedance was adjusted by varying the position of the load lamps along the plate line. It was found necessary to change the adjustments of the neutralizing con-

densers when the frequency was changed because of lead inductance. For each frequency, the setting was adjusted to obtain a minimum transfer of energy from input to output circuit. The plate voltage was reduced below normal so that an increased power dissipation on the plate would not be a limitation at higher frequencies.

First, oscillator-efficiency data for a frequency range from 180 to 300 megacycles were obtained with the neutralizing condensers removed, and then the amplifier-efficiency data were taken. To obtain results which would directly indicate the relative plate efficiency of

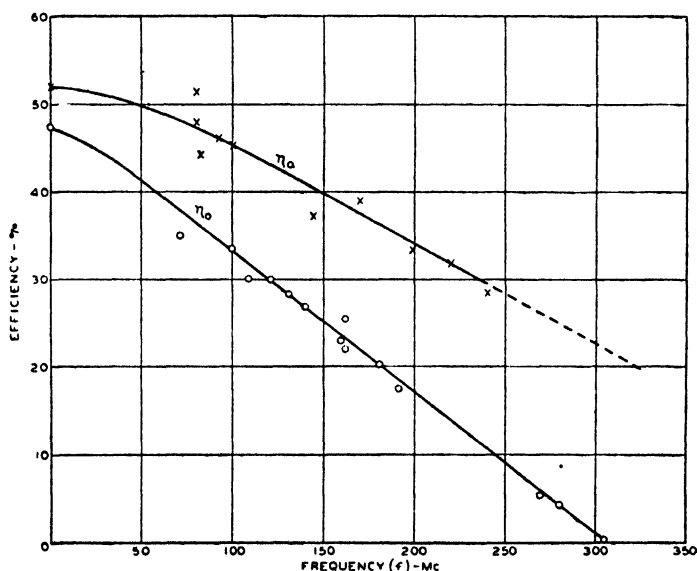


Fig. 2—Variation with frequency of amplifier ( $\eta_a$ ) and oscillator ( $\eta_o$ ) efficiency.

oscillator and amplifier, the following procedure was adopted. The low-frequency performance as oscillator or amplifier was checked against the performance calculated from the static characteristic curves of each tube used in the experiment. The grid and plate currents were noted so that for amplification tests at high frequency, the grid excitation could always be adjusted to give approximately the same average grid and plate currents. This adjustment was considered to indicate approximately the same input voltage, the error due to variation in magnitude and phase of plate voltage being small because of the high amplification factor of the tube ( $\mu = 10$ ). The negative bias on the grid was adjusted so as to obtain approximately class B operation at low frequency and was kept the same at higher frequencies.

Figure 2 shows the curves of oscillator efficiency ( $\eta_o$ ) and amplifier efficiency ( $\eta_a$ ) versus frequency ( $f$ ). The oscillator-efficiency curve extends practically to a limit of oscillations, i.e.,  $f = 810$  Mc, where the efficiency approaches zero. The amplifier curve was measured only up to a frequency of 240 Mc because of the difficulties in neutralization at higher frequencies. It can be seen that at the limit, when oscillator efficiency approaches zero, the power-amplifier efficiency is reduced to only one-half of the normal efficiency obtained at low frequencies. (The difference in efficiencies at  $f = 0$  is due to grid power required for excitation in the case of an oscillator.)

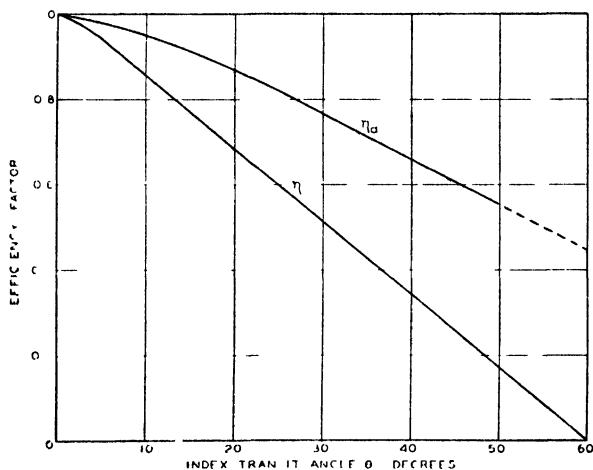


Fig. 3—Efficiency factors for amplifier ( $\eta_a$ ) and oscillator ( $\eta_o$ ) plotted against the index transit angle ( $\theta$ ).

To make the above information on variation of efficiency with frequency more generally useful, the curves were replotted as shown in Figure 3. Here the "transit-time efficiency factor"  $\eta'(\theta_i)$  is plotted against the electron transit angle ( $\theta_i$ ). The transit-time efficiency factor  $\eta'(\theta_i)$  is defined as the ratio of efficiency at a given first (cathode-grid) transit angle to the efficiency at low frequency, i.e.,

$$\eta'(\theta_i) = \frac{\eta(\theta_i)}{\eta(0)} \quad (1)$$

The transit angle  $\theta_i$ , referred to above, can be called the index transit angle and is defined as the product of the operating angular frequency and the transit time between cathode and grid computed for peak grid voltage at low frequency. Experience indicated that this generalized representation of experimental results, while not wholly justified

theoretically, is very useful in analyzing and predicting the performance of tubes at high frequencies.

It is realized, of course, that the index transit time is a fictitious transit time and does not correspond to the actual electron transit time at high frequencies. However, it has been selected as a convenient transit-time index, easily calculable from tube dimensions and voltages. The formulas and chart, given by W. R. Ferris<sup>6</sup> are very useful for this calculation. The actual transit time varies during the r-f cycle when the r-f voltage amplitudes are large compared with direct volt-

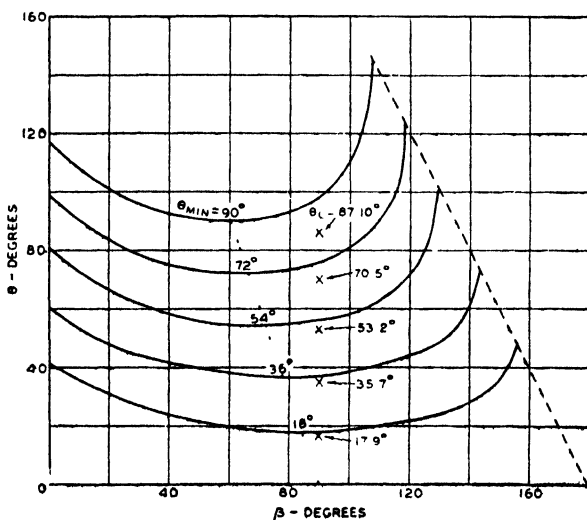


Fig. 4—Variation of electron transit angle in a temperature limited diode during a positive half-cycle for different values of index transit angle.  $\beta$  expresses the time at which electrons leave the cathode.

ages. To give an idea of variation of transit time during an r-f cycle, the curves of Figure 4 may be of interest. They represent the variation of transit angle in a temperature-limited diode during a positive half-cycle computed for the case of class B operation. The crosses indicated in the figure correspond to the values of the index transit angle calculated for the peak voltage.

One may expect that qualitatively an analogous situation exists in the case of a space-charge-limited tube. The transit time for electrons starting in the beginning and near the end of the positive half-cycle will be greater than for electrons starting near the peak of the voltage wave. Some electrons starting near the end of the half-cycle will not reach the grid at all and will be returned to the cathode with appreciable velocity to produce cathode bombardment. The actual

shape of the current pulse has not been calculated, but a qualitative description given by Wagener<sup>1</sup> is sufficient to explain the drop in efficiency of an amplifier.

The decrease in efficiency with frequency of an oscillator is more rapid than in the case of an amplifier. Two effects contribute to this difference in performance. First, due to increased input-circuit losses and electron-input loading the driving power increases with frequency. Since it is derived from the plate output of the oscillator the apparent plate efficiency will be lower. However, an estimate of the additional driving power at the highest frequency indicated that it would account for only a 10 per cent reduction in output power as compared with the low-frequency performance.

The second effect is the change in phase of plate current with respect to plate voltage due to electron transit time. In an oscillator employing grid-plate capacity for feed-back the coupling admittance at high frequencies is so high that the best adjustment that can be obtained is the one in which the grid-plate voltage phase does not differ materially from 180°. Therefore in the oscillator the phase shift in plate current due to electron transit time cannot be corrected. In the neutralized amplifier, however, the phase of output voltage can be adjusted for optimum condition, that is, a 180° phase angle between plate current and plate voltage can be realized even for large transit angles. If the electron loading effect is neglected and one assumes that the shape of the current pulse is a function of transit angle only and is the same for both the amplifier and oscillator, then one might consider that the difference in efficiency in the case of an oscillator is due primarily to the uncorrected phase angle between the plate current and plate voltage.

The efficiency of an oscillator and amplifier can be expressed as

$$\eta_o = \frac{I_p E_p}{I_b E_b} \cos \phi \quad (2)$$

$$\eta_a = \frac{I_p E_p}{I_b E_b} \quad (3)$$

where

$\phi$  = phase angle between the plate current and plate voltage of an oscillator due to electron transit time.

$I_p$  = fundamental component of r-f plate current.

$E_p$  = fundamental component of r-f plate voltage.

$I_b$  = average plate current.

$E_b$  = average plate voltage.

If the magnitudes of currents and voltages are assumed to be the same in oscillator and amplifier, then the ratio of efficiencies will be

$$\frac{\eta_o}{\eta_a} = \cos \phi \quad (4)$$

As a first approximation, it may be assumed that the phase angle is directly proportional to transit angle, i.e.,

$$\phi = K\theta_i \quad (5)$$

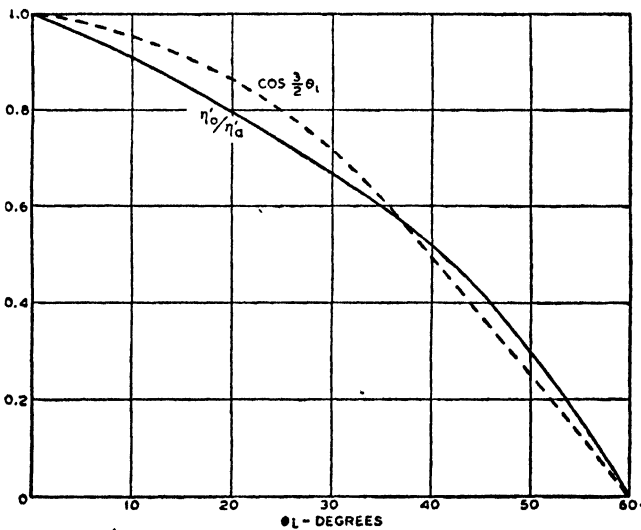


Fig. 5—The experimental curve of  $\eta_o/\eta_a$  and the function  $\cos \frac{3}{2} \theta_i$  plotted against the index transit angle.

Since at  $\theta_i = 60^\circ$ ,  $\eta_o/\eta_a = 0$ , we conclude that the constant of proportionality  $K = 3/2$ . Therefore,

$$\frac{\eta_o}{\eta_a} = \cos \frac{3}{2} \theta_i \quad (6)$$

In Figure 5 the experimental curve of  $\frac{\eta_o}{\eta_a}$  computed from data of Figure 3 is shown together with the curve representing the relationship (6). In view of the experimental error, the agreement between the simple theory and the experiment is quite satisfactory. One may



consider, then, that the difference in efficiency of oscillator and amplifier is primarily due to the plate-current phase lag caused by finite electron transit time and that, as a first approximation, the efficiency of an amplifier can be calculated from the relationship (6) when the oscillator efficiency is known.

The above information, although not complete and not as accurate as might be desirable, can be used as a first approximation in the design of high-frequency tubes. To illustrate its use, suppose it is desired to design a triode amplifier to be operated at a frequency  $f$ . Ordinarily from mechanical considerations a minimum grid-cathode spacing will be selected. Then the design will be carried out as is usually done for low-frequency tubes. The required peak grid voltage will be calculated and then an estimate of the grid-cathode angle at the operating frequency will be made. From the curve of Figure 3, the transit-time efficiency factor can be found and the previously assumed values of plate efficiency and plate dissipation corrected accordingly. The tube dimensions are corrected to correspond to the new value of plate dissipation. A second approximation can then be made.

In conclusion, it may be stated that at present empirical data are the only guide for the designer of high-frequency power tubes. The author is hopeful that a more refined experimental technique will make it possible to separate and evaluate accurately the different effects (circuit losses, grid-plate transit time) influencing the high-frequency performance of power tubes. Such an experimental analysis would greatly aid in the design of high-frequency tubes. In addition, the development of a satisfactory theory is also highly desirable and important, particularly when a design of tubes differing materially from the conventional is contemplated.

#### REFERENCES

- <sup>1</sup> W. G. Wagener, "The Developmental Problems and Operating Characteristics of Two New Ultra-High-Frequency Triodes," *Proc. I.R.E.*, Vol. 26, No. 4, pp. 401-414; April (1938).
- <sup>2</sup> W. E. Benham, "Theory of the Internal Action of Thermionic Systems at Moderately High Frequencies," Part I, *Phil. Mag.*, p. 641; March (1928); Part II, *Phil. Mag.* Vol. II, p. 457; February (1931).
- <sup>3</sup> J. Müller, "Electronenschwingungen in Hochvacuum," *Hochfrequenztechnik u. El. ak.*, Vol. 41; May (1933).
- <sup>4</sup> F. B. Llewellyn, "Vacuum Tube Electronics at Ultra-High Frequencies," *Proc. I.R.E.*, Vol. 21, No. 11, pp. 1532-1573; November (1933).
- "Note on Vacuum Tube Electronics at Ultra-High Frequencies," *Proc. I.R.E.*, Vol. 23, No. 2, pp. 112-127; February (1935).
- "Operation of Ultra-High-Frequency Vacuum Tubes," *The Bell System Tech. Jour.*, Vol. XIV, pp. 632-665; October (1935).

<sup>5</sup> D. O. North, "Analysis of the Effects of Space Charge on Grid Impedance," *Proc. I.R.E.*, Vol. 24, No. 1, pp. 108-136; January (1936).

<sup>6</sup> W. R. Ferris, "Input Resistance of Vacuum Tubes as Ultra-High-Frequency Amplifiers," *Proc. I.R.E.*, Vol. 24, No. 1, pp. 82-107; January (1936).

<sup>7</sup> G. Grünberg, "On the Theory of the Operation of Electron Tubes With Rapidly Varying Anode Voltages," *Techn. Phys. of the USSR*, Vol. 3, No. 1, pp. 65-80; (1936).

"On the Initial Current Flowing Through an Electron Tube at the Sudden Application of an Impulse Voltage," *Techn. Phys. of the USSR*, Vol. 3, No. 2, pp. 101-110; (1936).

## AN ELECTRON OSCILLATOR WITH PLANE ELECTRODES\*†

By

B. J. THOMPSON AND P. D. ZOTTU

RCA Radiotron Company, Inc.,  
Harrison, N. J.

### Summary

*This paper describes a new types of thermionic tube capable of producing ultra-high frequencies by means of electron oscillations. Tubes of this type are characterized by having paralleled plane electrodes, instead of cylindrical electrodes as in the conventional Barkhausen-Kurz tubes, and a fourth element called a backing plate.*

*The relations between wavelength and amplitude of oscillation and the various electrode potentials are shown by measurements on a typical tube. It is found that in these tubes the filament voltage is not critical, space-charge-limited operation being satisfactory, and that only one mode of oscillation is obtained. Both of these factors appear to give these tubes an advantage in stability over cylindrical Barkhausen-Kurz tubes.*

*A tube of the flat type is described which has produced oscillations at a wavelength of less than 10 centimeters in the fundamental mode with a positive grid potential of 150 volts.*

(12 pages; 14 figures)

---

\* Decimal Classification: R334.

† *Proc. I. R. E.*, December, 1934.

## DESCRIPTION AND CHARACTERISTICS OF THE END-PLATE MAGNETRON\*‡

By

ERNEST G. LINDER

RCA Manufacturing Company, Inc.,  
Camden, N. J.

### Summary

*A new type of magnetron is described which is especially adapted to the generation of centimeter waves. It possesses several advantages over the simple magnetron, namely: (1) greater stability with respect to fluctuations of supply voltages, (2) less tendency to oscillate at undesired long*

---

\* Decimal Classification: R331.

‡ *Proc. I. R. E.*, April, 1936.

wavelengths, (3) greater efficiency, (4) greater output, and (5) greater ease of adjustment. Static and dynamic characteristics are discussed. The effect of space charge on electron motion and tube performance is treated mathematically, and supporting experimental data are presented. Evidence is given that for best operation an optimum space-charge condition is required, which can conveniently be established and maintained by the use of end plates. Power output is limited by a type of instability involving electron bombardment of the filament, and apparently initiated by excessive space charge.

(21 pages; 18 figures)

## RECENT DEVELOPMENTS OF THE CLASS B AUDIO- AND RADIO-FREQUENCY AMPLIFIERS\*†

BY

LOY E. BARTON

RCA Manufacturing Company, Inc.,  
Camden, N. J.

### Summary

*Class B audio-frequency and radio-frequency amplifiers have many applications and distortion can be kept to a very low value if the necessary precautions are taken to prevent nonlinearity of such amplifiers. Undoubtedly, the most important factor in the design of a class B amplifier for low distortion is the characteristic of the driver system. Tube characteristics and the use of a proper load are also important but are more definite and more generally understood.*

*The purpose of this paper is to present the results of recent developments of the class B audio and radio amplifiers to reduce distortion. The results of the investigations indicate that a heavily loaded driver system in general is undesirable because of the power consumed and because such loading results in greater distortion than obtainable by other means.*

*The general procedure adopted to reduce distortion was to prevent distortion in each unit of the amplifier system. Distortion balancing schemes are not only critical to adjust but are likely to introduce higher order harmonics and sum and difference tones which may be more objectionable than a higher measured value of lower order harmonics. Actual performance data are presented for medium and relatively high powered audio and radio systems. The necessary input requirements to permit the performance obtained are discussed.*

*Sufficient theory is given to make the paper complete and to show that the actual performance of such amplifiers can be quite accurately predicted if the necessary tube characteristics are known.*

(22 pages; 15 figures)

---

\* Decimal Classification: R363.1.

† *Proc. I. R. E.*, July, 1936.

## MAGNETRON OSCILLATORS FOR THE GENERATION OF FREQUENCIES BETWEEN 300 AND 600 MEGACYCLES\*†

BY

G. R. KILGORE

RCA Manufacturing Company, Inc.,  
Harrison, N. J.

### *Summary*

*The need for vacuum tube generators capable of delivering appreciable power at frequencies from 300 to 600 megacycles is pointed out and the negative resistance magnetron is suggested as one of the more promising generators for this purpose.*

*An explanation of the negative resistance characteristic in a split-anode magnetron is given by means of a special tube which makes possible the visual study of electron paths. In this manner it is demonstrated how most of the electrons starting toward the higher potential plate reach the lower potential plate.*

*From the static characteristics it is shown how the output, efficiency, and load resistance can be calculated, and from this analysis it is concluded that the negative resistance magnetron is essentially a high efficiency device at low frequencies.*

*Measurements of efficiency at ultra-high frequencies are given for several magnetrons under various operating conditions. It is concluded from these measurements that the decrease of efficiency at very high frequencies is mainly due to electron-transit-time effects. A general curve is given showing efficiency as a function of the "transit-time ratio." This curve indicates that for a transit time of one-fifteenth of a period, approximately fifty per cent efficiency is possible; for one-tenth of a period, thirty per cent; and for one-fifth of a period, the efficiency is essentially zero.*

*Two methods are described for increasing the plate-dissipation limit. One method is that of increasing the effective heat-dissipating area by the use of an internal circuit of heavy conductors. The other method is that of a special water-cooling arrangement which also makes use of the internal circuit construction.*

*Examples of laboratory tubes are illustrated, including a radiation-cooled tube which will deliver fifty watts at 550 megacycles and a water-cooled tube which will deliver 100 watts at 600 megacycles.*

(18 pages; 16 figures)

---

\* Decimal Classification: R355.9.

† *Proc. I. R. E.*, August, 1936.

## A PUSH-PULL ULTRA-HIGH-FREQUENCY BEAM TETRODE\*†

BY

A. K. WING

RCA Manufacturing Company, Inc.,  
Harrison, N. J.

### Summary

*The design of a vacuum tube capable of delivering 10 watts useful power output at frequencies of the order of 250 megacycles and with a d-c plate voltage of 400 volts and good economy of space and cathode power, is discussed. In order to keep the physical dimensions of the tube small and to make it adaptable to straightforward circuit arrangements, the tube was designed as a push-pull beam tetrode. Unusual constructional features include the use of short, heavy leads sealed directly into the moulded glass bulb.*

*Characteristics of the tube are given. Tests show that the tube will operate as a stable Class C amplifier at frequencies up to 250 megacycles. At that frequency a power output of the order of 13 watts with an efficiency of 45 per cent has been obtained. Satisfactory operation as a frequency multiplier is possible in the same frequency range. Oscillator operation has been obtained at considerably higher frequencies. The variation of output and efficiency with frequency is shown.*

*(11 pages; 6 figures)*

---

\* Decimal Classification: R334.

† RCA Review, July, 1939.

## THE ANODE-TANK-CIRCUIT MAGNETRON\*†

BY

ERNEST G. LINDER

RCA Manufacturing Company, Inc.,  
Camden, N. J.

### Summary

*A new type of magnetron is described in which the split cylindrical anode is made approximately one-quarter wave in length, the two segments being short-circuited at one end. The anode resonates and acts as a tank circuit. Thus difficulties due to interelectrode capacitance and tube lead inductance are circumvented and a much greater heat radiating area is provided. An output of 20 watts at 3750 megacycles (8 centimeters wavelength) and an efficiency of 22 per cent is obtainable. The theory of the anode tank circuit is developed, and expressions are given for wavelength, internal resistance, and logarithmic decrement.*

*(7 pages; 8 figures; 2 tables)*

---

\* Decimal Classification: R183X355.5.

† Proc. I. R. E., November, 1939.

# RECENT DEVELOPMENTS IN MINIATURE TUBES\*†

By

BERNARD SALZBERG AND D. G. BURNSIDE

RCA Radiotron Division, RCA Manufacturing Company,  
Harrison, N. J.

**Summary**—The development of two indirectly heated miniature tubes, a triode and a sharp cut-off amplifier pentode especially suited for use at high frequencies, is described. The electrical and mechanical factors involved in the design and application of these tubes are discussed and their novel structural appearance is described.

Because of their decreased lead impedances, interelectrode capacitances, and transit times, these miniature tubes allow considerable improvement to be made in high-frequency receiving equipment. It is possible to operate the triode as an oscillator in a conventional circuit down to a wavelength of approximately 40 centimeters. The pentode can be operated as a radio-frequency amplifier down to a wavelength of approximately 70 centimeters. It is practicable to obtain stable gains with it of from ten to fifteen at three meters, a wavelength at which standard tubes are almost entirely ineffectual. Both tubes can be used, down to much lower wavelengths, in exactly the same manner and for the same applications that the corresponding conventional tubes are used; i.e., as oscillators, amplifiers, detectors, converters, and as negative-resistance devices.

The small size of the tubes and their novel structural design allow compact and convenient receiving equipment to be built. Even at the longer wavelengths, they are applicable to a large number of uses for which their excellent characteristics, small size, and low weight make them particularly useful.

## INTRODUCTION

EARLY work on the extension of the high-frequency limit of receiving equipment, which made use of conventional radio-frequency amplifier circuits built up around standard tubes, indicated that the amplifier section of the receiver became less and less effective as the signal frequency was increased and that ultimately, at frequencies of the order of one hundred megacycles, the amplifier was virtually useless. Similarly, the detector section and the oscillator section (when one was employed) of the receiver became more and more ineffectual as the frequency was raised and although they continued to operate beyond the limiting frequency of the amplifier, they too ultimately became inoperative. Improvements in the circuits proper resulted in only relatively slight improvements in the over-all performance of the receiver, so that it became apparent that the tubes themselves limited the operation of the equipment.

Recourse was then possible only to positive-grid operation of the available tubes, either in the oscillating state (Barkhausen-Kurz or

---

\* Decimal classification: R330.

† Reprinted from *Proc. I.R.E.*, October, 1935.

Gill-Morrell), or in the nonoscillating state (Hollmann or Carrara). These methods were not entirely satisfactory, however. With them, no cascaded amplification was obtainable at the carrier frequency, operation was invariably attended by high internal tube noise, over-all sensitivity was poor, careful adjustments were required, and the equipment was generally unreliable, at least for anything more than experimental use.

B. J. Thompson realized that the limitations of the conventional tubes were the result of their size. G. M. Rose, Jr. and he built small tubes and with them conclusively demonstrated that the limitations to the successful operation of vacuum tubes at the higher frequencies may be overcome by reducing the dimensions of the tubes.<sup>1,2</sup>

The possibilities of such tubes aroused an interest sufficiently widespread to warrant further development, and the "acorn" tubes are the present results of this development work.<sup>3</sup>

#### FACTORS INVOLVED IN THE DESIGN OF MINIATURE TUBES

The essential principle upon which these tubes are based is the Model Theorem, or the Principle of Similitude. It is possible to show from the fundamental differential equations and the boundary conditions involved that if all of the linear dimensions of a tube structure are divided by a constant factor, say  $n$ , then the electrode currents, transconductance, amplification factors, and plate resistance will remain substantially constant, but the lead inductances and capacitances, the tube capacitances, and the time of passage of the electrons between the various electrodes will be divided by  $n$ . The direct-current lead resistances will be multiplied by  $n$ , but the alternating-current lead resistances will ordinarily be increased by something less than this factor. The allowable plate dissipation and the available emission of the tube, however, will be divided by  $n^2$ , and the current densities will be multiplied by  $n^2$ . The latter considerations are important in any application of this principle to power amplifier or transmitter tubes. Physically, the tube will be reduced in its over-all dimensions by a factor  $n$ , and its weight by a factor  $n^3$ .

For mechanical reasons, however, it is not feasible to reduce all of the tube dimensions to the same degree. For example, a reduction by a factor of four of all of the linear dimensions of the type 56 tube would require grid side rods of  $6\frac{1}{4}$  mils diameter, grid wire of 0.83 mil

<sup>1</sup> B. J. Thompson, "Tubes to fit the wavelength," *Electronics*, August, (1933).

<sup>2</sup> B. J. Thompson and G. M. Rose, Jr. "Vacuum tubes of small dimensions for use at extremely high frequencies," *Proc. I.R.E.*, vol. 21, pp. 1707-1721; December, (1933).

<sup>3</sup> Bernard Salsberg, "Design and use of 'acorn' tubes for ultra-high frequencies," *Electronics*, September, (1934).



diameter, a cathode sleeve of  $12\frac{1}{2}$  mils diameter, and a cathode coating of approximately 0.75 mil thickness. Parts of such minute dimensions would be extremely difficult to manufacture with present-day equipment. Consequently, as is usual in many engineering problems, it is necessary to arrive at a practical solution which will give the essential results.

In addition to the limitations imposed upon design by consideration of the internal structure, a number of electrical requirements must be considered in the design of such miniature tubes. For example, the tubes should not only be suitable for high-frequency work, but because their reduced size and weight are frequently advantageous at lower frequencies, it is desirable that they be suitable for practically any use to which the standard tubes can be put. They should be adaptable to either battery or alternating-current operation, and should require a minimum of heater power. Their electrode voltage and current ratings should be such as to fit, in so far as possible, existing auxiliary circuit equipment. A reasonable life expectation and good stability of characteristics during life are also essential requirements. As regards external structure, it is imperative that the basing designs be such as to permit the aging and testing operations incidental to the manufacture of the tubes to be carried out conveniently, and to allow easy insertion of the tube in circuit equipment without introducing undue losses. The lead terminals should be placed so that they permit short connections between the tubes and the associated circuits. Finally, it is desirable that the tube designs be suitable for economical production maintainable within reasonably close electrical limits.

Considerations such as these circumscribe the design of the tubes. Their static characteristics must be set by a study of the various uses to which the tubes might be put and by a careful weighing of their relative importance. For the triode, such considerations indicated the desirability of obtaining a plate resistance of the order of ten to fifteen kilohms and an amplification factor above fifteen, together with a ratio of grid-plate transconductance to plate current as high as possible. For the sharp cut-off pentode, it was desirable to obtain under amplifier operating conditions a plate resistance of over one megohm and a transconductance of at least 1000 micromhos.

To effect a significant improvement in high-frequency behavior, and yet have tubes which could be manufactured, it was decided to reduce the electrode spacings to minimum distances of the order of five mils. This reduction would extend the upper frequency limit of operation beyond that of existing commercial tubes by a factor of approximately four, and at the same time would keep the design of the tubes within the realm of attainable manufacturing technique.

To make the tubes suitable for general battery and alternating-current use, the heater voltage was set at 6.3 volts. It was decided to use a conventional cylindrical cathode of the smallest practical diameter in order to realize the minimum heater power. Its length was so chosen that the desired static characteristics could be obtained with low interelectrode capacitances. Maximum plate voltages of 180 volts for the triode and 250 volts for the pentode were chosen as consistent with the requirements of low transit time and good life performance.

To obtain short leads, low losses, suitable means for effective bypassing at the higher frequencies, and a practical form of base, it was necessary to abandon the conventional form of pinch stem and standard base assembly. Instead, the tube elements were connected to heavy leads suitably positioned and fastened to mica spacers; these leads were then sealed in and used as base pins.

Except for transit-time considerations, the actual calculations involved in the design of these tubes are similar in all respects to the usual tube structure calculations. These are of a semiempirical nature, based in part upon known derivations of the space-charge-limited current between the elements of diodes of simple geometrical shape, and in part upon approximate analyses of the electrical field of tubes of ideal configurations.<sup>4,5,6,7</sup> As regards the transit time between the various electrodes, it is important for our purposes to keep the distances traversed by the electrons as short as possible, and to get them moving as fast as possible (by making the effective potentials in the planes of the various electrodes as high as possible)

#### DESCRIPTION OF THE TUBES

The tubes are shown in Fig. 1, and their size can be judged from the size of the golf ball which is included in this group photograph. The remarkable resemblance of the triode to an acorn, both in size and shape, has resulted in the trade designation for these tubes as the "acorn" series. One of the practical difficulties which arose as a result of the small size of the tubes was the difficulty of etching the usual trade name and type number on the bulb.

<sup>4</sup> I. Langmuir and K. T. Compton, "Electrical discharges in gases. Part II, Fundamental phenomena in electrical discharges," *Rev. Mod. Phys.*, vol. 3, p. 191; April, (1931).

<sup>5</sup> F. B. Vogdes and F. R. Elder, "Formulas for the amplification constant for three-element tubes in which the diameter of grid wires is large compared to the spacing," *Phys. Rev.*, vol. 24, p. 683, (1924).

<sup>6</sup> Bernard Salzberg, "Application of conformal transformation to some problems in vacuum tube engineering," Thesis for M.E.E. degree, Polytechnic Institute of Brooklyn, 1933.

<sup>7</sup> S. Koizumi, "On the amplification constants of multi-electrode tubes," *Jour. I. E. E. (Japan)*, Abstracts, vol. 10, p. 18, (1934).

The internal structures of the tubes are shown in Figs. 2 and 3. Both tubes are provided with a cylindrical cathode, inside of which is inserted a folded type of insulated heater. Fig. 4 illustrates the relative dimensions of this heater-cathode assembly and a common variety of pin. This gives some idea of the size of the parts and the precision and care required in the fabrication of such tubes. The No. 1 grids are elliptical in order to reduce the otherwise severe control effects of the side rods. The suppressor grid of the pentode is particularly useful in reducing the reaction between control grid and plate. The various elements are spaced very closely along the minor axis of the grids—where the cathode emission is most useful—in order to reduce the

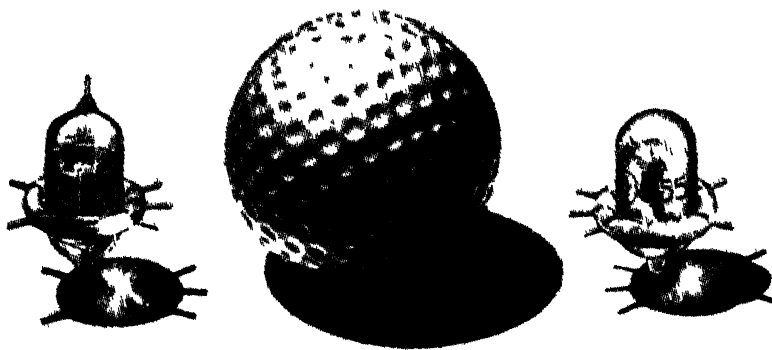


Fig. 1—Miniature triode and pentode compared with golf ball.

transit time and increase the transconductance, and somewhat less closely along the major axis in order to decrease the capacitances and increase the structural strength.

In both tubes, two accurately punched mica spacers serve to hold the elements in position. In the triode, the whole assembly is fastened in place by means of small lugs which are bent out from the ends of the plate. In the pentode, an additional mica spacer is used to insulate the plate lugs from the shielding structure, the latter being held in place by means of two support rods. In both tubes, one of the mica spacers is used as a sort of a stem, the heavy base pins and the lighter leads to the electrodes being fastened around its periphery. The "getter" material is enclosed within a flat tab welded, in the triode, to one of the plate lugs, and in the pentode, to the shielding structure.

The mount, in each case, is placed within a bulb which consists initially of two cup-shaped heavy preformed glass sections, the shallower one of which has an exhaust pipe attached to it. The main seal,

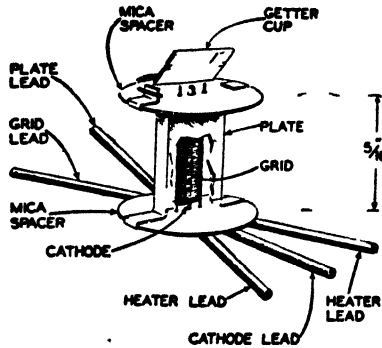


Fig. 2—Internal Structure of the triode.

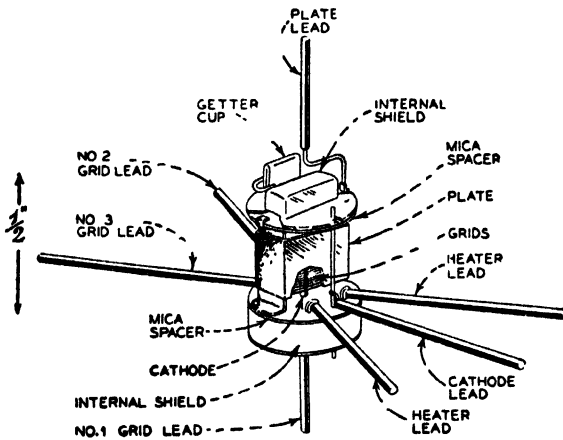


Fig. 3—Internal structure of the pentode.

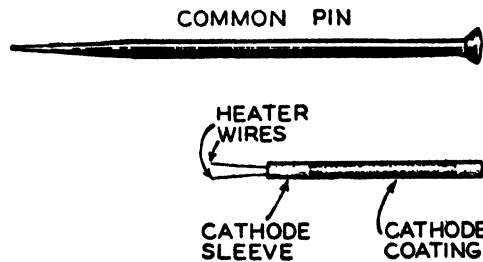


Fig. 4—Comparison of heater cathode assembly and an ordinary pin.

and in the case of the triode the only seal, is of the joined-flare type, made at the plane of the tube leads between the two glass sections. After the sealing-in operation, these leads are cut quite short, the com-

bination of the heavy glass of the joined-flare seal and the stub pins constituting a practical and extremely sturdy base. This arrangement obviates the need for soldering the tube to the circuit elements and also avoids the deleterious effects of the conventional base. The leads themselves are radial, the two heater leads being symmetrically placed 30 degrees on either side of the cathode lead, the grid and plate leads (in the triode), 60 degrees apart on the same diameter as the heater leads. In the pentode, the latter two leads are replaced by the numbers 3 and 2 grid leads, respectively, and the plate and control-grid leads are brought out at opposite ends of the bulb, a very convenient circuit arrangement. These lead arrangements provide the necessary separation between the active radio-frequency leads and the grounded radio-frequency leads. In the pentode, the control-grid lead is brought out through the exhaust pipe, an innovation in tube manufacture: incidentally, the resultant tube is thus a very special form of the "tipless" variety. The getter flash in this tube is of the directed beam type, necessary because of the small size of the structure in order to avoid leakage between elements. The inside surface of the pentode bulb is coated with carbon to reduce the emission of secondary electrons which results from the bombardment of this surface by primary electrons which escape through the interstices between the mica spacer and plate. This is particularly important at the lower frequencies, where it is desirable to keep the high load impedances from being shunted by the additional plate losses introduced by such effects.

## CHARACTERISTICS OF THE TUBES

### *I. Static and Low-Frequency Characteristics*

The heaters of both tubes are rated at 6.3 volts, making them suitable for both battery and alternating-current operation. The tubes themselves were designed so that the electrode voltages could be set at "preferred" values.

A typical plate family for the triode is shown in Fig. 5. Because of the reduced allowable plate dissipation, such miniature tubes are not especially suited for use as audio power amplifiers. Within maximum ratings, however, this tube is entirely suitable for audio-frequency amplifier and high-frequency oscillator uses. Operated as a class A audio amplifier with a load of approximately 19,000 ohms, the triode delivers an undistorted power output of 130 milliwatts. Table I shows the comparative characteristics of the miniature triode and a standard triode, type 76. It will be observed that at the same electrode voltages, not only is the miniature triode not *inferior* to the conventional tube,

but it is actually superior to it. One point not specifically tabulated is the electron grid current which flows from the grid due to thermionic emission. This is negligible, even with abnormal heater voltages, due to a combination of methods which reduce the temperature of the grid and otherwise reduce the tendency of the grid to emit. The lower

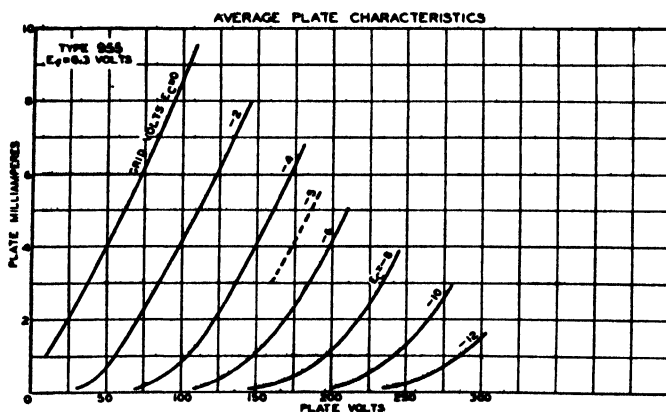


Fig. 5—A typical plate family for the triode.

capacitances of the miniature tube are very desirable at the lower frequencies, as well as the higher frequencies, because they allow higher gain over wider frequency spans. Laboratory tests of tubes of this type made up to the present writing have indicated over 1000 hours of continuous and useful life.

TABLE I  
COMPARATIVE CHARACTERISTICS

	RCA-76 Conventional Triode	RCA-955 Acorn Triode	
Heater Voltage	6.3	6.3	volts
Heater Current	0.30	0.15	amp
Plate Voltage	180	180	volts
Grid Voltage	-9.8	-5.0	volts
Plate Current	3.2	4.5	ma
Amplification Factor	13.8	25	
Plate Resistance	11200	12500	ohms
Grid-Plate Transconductance	1200	2000	$\mu$ mhos
Input Capacitance	3.5	1.0	$\mu$ f
Output Capacitance	2.5	0.6	$\mu$ f
Grid-Plate Capacitance	2.8	1.4	$\mu$ f

Figs. 6 and 7 illustrate typical plate and transfer families, respectively, for the miniature pentode. It will be observed that these static characteristics are similar to the usual characteristics obtained with conventional tubes of this type; i.e., high grid-plate transconductance,

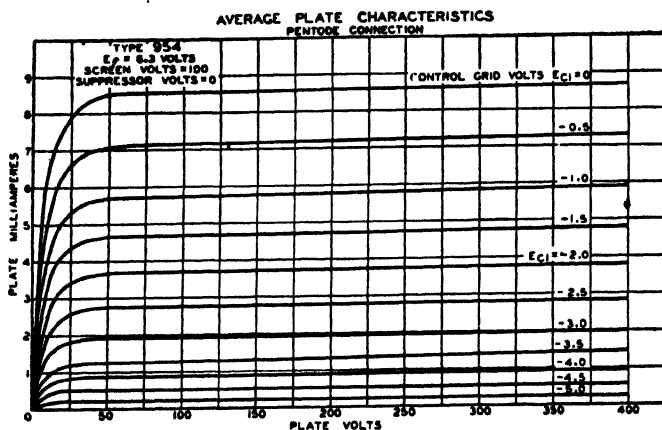


Fig. 6—A typical plate family for the pentode.

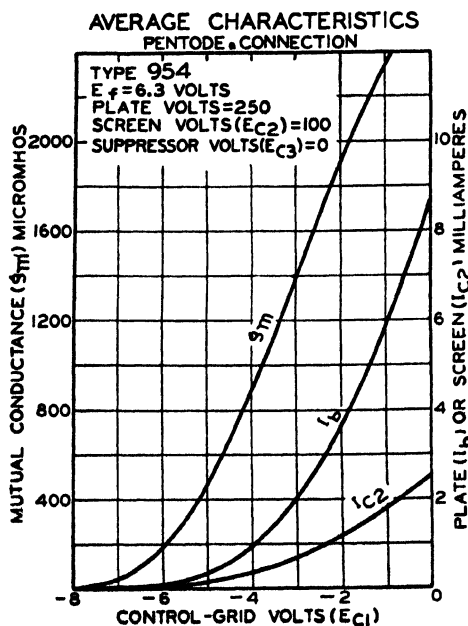


Fig. 7—A typical control-grid plate transfer family for the pentode.

high plate resistance, and sharp cutoff. Table II shows the comparative characteristics of the miniature pentode and a standard pentode, type 6C6. It will be observed, once more, that at the same electrode

voltages, the miniature pentode is actually superior to the conventional pentode, even on a strictly static comparison basis.

TABLE II  
COMPARATIVE CHARACTERISTICS

	RCA-6C6 Conventional Pentode	954 Acorn Pentode	
Heater Voltage	6.3	6.3	volts
Heater Current	0.30	0.15	amp
Plate Voltage	250	250	volts
Screen Voltage	100	100	volts
Suppressor Voltage	0	0	volts
Control-Grid Voltage	-3.0	-3.0	volts
Plate Current	2.1	2.0	ma
Plate Resistance	1.5	1.5	megohms
Control-Grid—Plate Transconductance	1225	1400	$\mu$ mhos
Input Capacitance	5.0	3.0	$\mu$ f
Output Capacitance	6.5	3.0	$\mu$ f
Control-Grid—Plate Capacitance	0.010	0.005	$\mu$ f

## II. High-Frequency Characteristics

The reduction in size of these tubes has allowed operation of the triode as a radio-frequency feed-back oscillator in conventional circuit arrangements down to a wavelength somewhat below 40 centimeters, and the operation of the pentode as a radio-frequency amplifier, also in conventional circuit arrangements, down to wavelengths of the order of 70 centimeters.

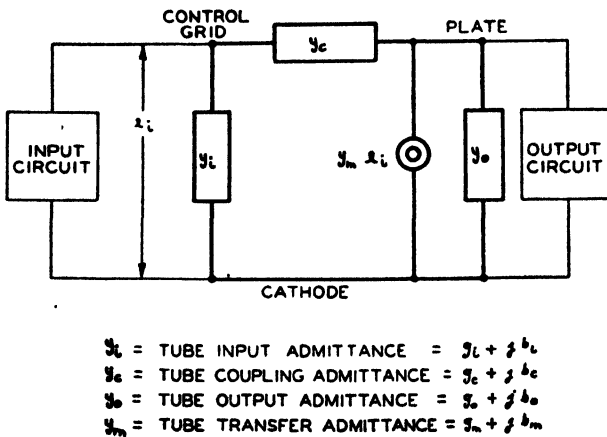


Fig. 8—The schematic first order equivalent amplifier circuit representation of an amplifier tube.

Fig. 8 shows the schematic first order equivalent amplifier circuit representation of an amplifier tube. In order to specify completely the



behavior of such a tube at any frequency, it is necessary to specify the input, output, coupling, and transfer admittances at this frequency. At low frequencies, the input and coupling admittances are essentially pure susceptances, capacitive in nature. The output admittance consists of the plate conductance, usually in a radio-frequency amplifier pentode quite small in magnitude, and a susceptance due to the output capacitance. The transfer admittance consists of only a real part, the familiar  $q_m$ .

At high frequencies, the input admittance, and (unless the tube is well screened electrically) also the coupling admittance, acquire a real part and an altered imaginary part. In addition, the output admittance acquires an increased conductance and an altered susceptance. The transfer admittance also acquires an imaginary part. The increase in the conductance components of the input, output, and coupling admittances tends to reduce the gain which can be built up by the amplifier, and ultimately to limit its effectiveness. The change in the susceptance components of these admittances alters the tuning of the associated circuits, and in the case of an oscillator provides a potential form of frequency variation. The phase shift in the transfer admittance makes conditions for stability more favorable, but also affects the gain.<sup>8</sup> These admittances are functions of the time of passage of the electrons between the various electrodes. B. J. Thompson and W. R. Ferris of the RCA Radiotron Laboratory have already discussed the loading effects due to the increase of the input conductance of tubes at high frequencies,<sup>9</sup> and W. R. Ferris and D. O. North, also of the same laboratory, have made experimental and theoretical studies of this effect.<sup>10</sup>

Typical results of measurements of the equivalent shunt input resistance of the "acorn" pentode and the RCA-6C6 are shown in Fig. 9. This is the component of resistance which is due to the actual electronic flow past the control grid. The heavy section of the curve indicates the range over which measurements were made. The light line continuations are extrapolations. There is some justification for this extrapolation procedure because theory indicates that for small values of transit angle the conductance varies as the square of the frequency. The curves indicate that even at thirty meters, where it is perfectly feasible to build up a resonant circuit impedance of 150,000 ohms, the shunting effect of the conventional tubes is serious. At three meters, it

<sup>8</sup> Bernard Salasberg, "Notes on the theory of the single stage amplifier," to be published.

<sup>9</sup> B. J. Thompson and W. R. Ferris, "Grid circuit losses in vacuum tubes at very high frequencies," presented before joint U.R.S.I.-I.R.E. meeting, Washington, D. C. April 27, 1934; Abstract published *Proc. I.R.E.*, vol. 22, p. 683; June, (1934).

<sup>10</sup> To be published.

amounts for conventional tubes to approximately 1600 ohms; this explains why the gain is so low at this wavelength when standard tubes are used.

In addition to the shunting which is due to the finite time of passage of the electrons between the various electrodes, there is an additional loss incurred as a result of the dielectric losses in the tube-lead support—glass, socket, etc.—and as a result of the capacitive currents which flow by way of the lead wires through the tube capacitances. The latter

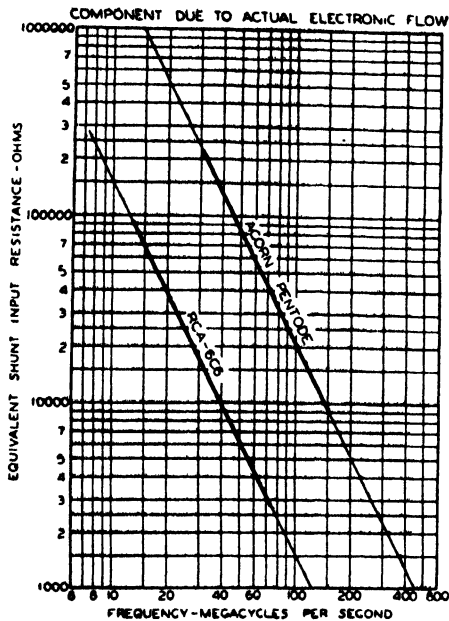


Fig. 9—The equivalent shunt input resistances of the "acorn" pentode and the RCA-6C6 as a function of the frequency. This is the component of resistance which is due to the actual electronic flow past the control grid.

cause assumes importance at the high frequencies, as shown by the curves of Fig. 10. Here is shown the shunting which takes place in the output circuit of a standard tube and of an early developmental "acorn" pentode which was used to study this effect. The losses are due partly to the dielectric loss, but mainly to the capacitive currents which passed through the leads. The same leads and by-pass condensers were used for both tubes. These curves are shown for the purpose of illustrating how significant this effect may become, and therefore how important it is to keep the radio-frequency losses in the connecting wires and the by-pass capacitors as low as possible. As seen from the

curves, this loss at the higher frequencies completely overshadows the shunting effect of the static or low-frequency plate resistance.

The measurements of the input and output admittances of tubes were made by a substitution method. A resonant circuit was coupled to a high-frequency oscillator and the voltage developed across this circuit at resonance was measured by means of an "acorn" pentode voltmeter, of the type shown in Fig. 13. The tube was operated at small space currents to reduce the electronic loading effects to a minimum.

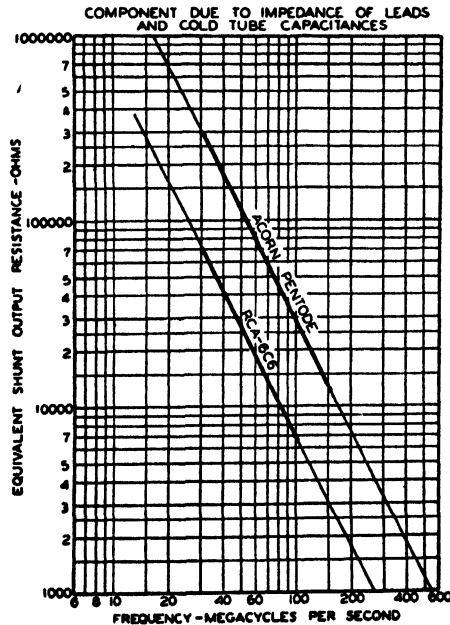


Fig. 10—The equivalent shunt output resistance of an early developmental "acorn" pentode and the RCA-6C6. This is the component of resistance which is due to the cold resistance of the tubes and the associated connecting wires.

This measurement circuit was calibrated by placing resistors, whose value at the operating frequency had been checked previously by a reactance substitution method, across the resonating capacitor, re-tuning to resonance and plotting the resulting resonant voltage against resistance. The conductance component of the admittance of a tube under test was then indicated by the value of the resonant voltage. The susceptance component was given by the frequency and the change (of the tuning capacitor) required to establish resonance.

The effects of the tube conductances on the associated input and output circuits may be minimized by matching the tube impedances

to these circuits. This may be done in a variety of ways, perhaps the simplest of which consists merely in connecting the tube at an intermediate point on the coil. It should be emphasized that since the shunt-

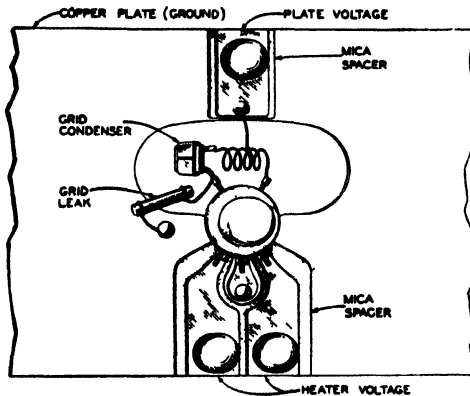


Fig. 11—A typical triode oscillator set-up.

ing effects are considerably less for the miniature tubes, there is less need for circuit arrangements of this type for these tubes. However, even for them, it becomes desirable ultimately to make use of such schemes.

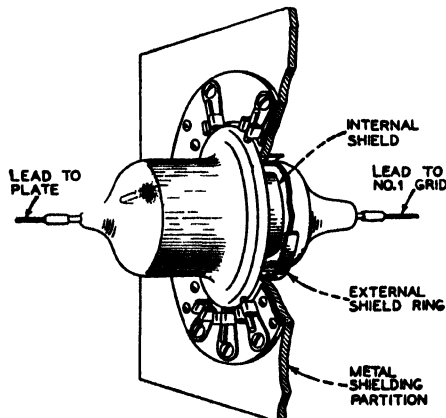


Fig. 12—A typical shielding arrangement for the miniature pentode.

Field measurements of noise developed in tubes at high frequencies indicate that the miniature tubes are definitely superior to the conventional tubes. Although elementary theory indicates that the shot noise in the plate circuit of a tube decreases with increasing interelectrode

transit angle, the initiation of a noise component in the grid circuit which is a function of the cathode-grid and of the grid-screen transit angle results in an increase in the over-all noise.<sup>11</sup>

Figs. 11 and 12 illustrate how conveniently these tubes fit in with high-frequency circuit requirements. In the triode, the leads are arranged so that the active radio-frequency leads are on the opposite side of the flare seal from the radio-frequency grounded leads. In the pentode, the grounded radio-frequency leads are all brought out in the

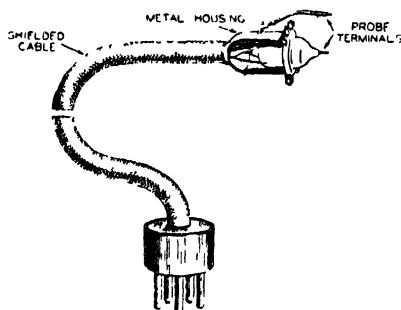


Fig. 13—A probe voltmeter using a miniature pentode.

plane of the flare seal, so that this may be used as a ground reference plane. The two active radio-frequency leads are brought out at the ends of the tube, which permits a very natural arrangement for connecting the tube to the input and to the output circuit. At high frequencies, it is usually desirable to bring all ground-return connections to one point, to avoid radio-frequency circulating currents in common impedances formed by shields.

Fig. 13 shows one of the many very useful miscellaneous applications of these tubes. A pentode is mounted at the head end of a shielded flexible cable and used as a probe voltmeter, thus permitting the measurement of voltages at their source.

### CONCLUSIONS

Because of their decreased lead impedances, interelectrode capacitances and transit times, these miniature tubes allow considerable improvement to be made in high-frequency receiving equipment. It is possible to operate the triode as an oscillator in a conventional circuit down to a wavelength of approximately 40 centimeters. The pentode can be operated as a radio-frequency amplifier down to a wavelength of approximately 70 centimeters. It is practicable to obtain stable gains of

<sup>11</sup> Stuart Ballantine, "Schrot-effect in high-frequency circuits," *Jour. Franklin Inst.*, vol. 206, no. 2, p. 159, (1928)

ten to fifteen at three meters, a wavelength at which the standard tubes are almost entirely ineffectual. Both tubes can be used, down to much lower wavelengths, in exactly the same manner and for the same applications that the corresponding conventional tubes are used; i.e., as oscillators, amplifiers, detectors, converters, and as negative-resistance devices.

The small size of the tubes and their novel structural arrangements allow compact and convenient receiving equipment to be built. Even at the higher wavelengths, they are applicable to a large number of uses for which their size, low weight, and excellent characteristics make them particularly useful.

#### ACKNOWLEDGMENT

The development of these tubes required a considerable refinement in existing tube manufacturing technique. In this connection, we wish to acknowledge the coöperation of Messrs. S. M. Reed and H. R. Seelen of the Radiotron Developmental Factory. We also wish to acknowledge the contributions of Mr. T. M. Shrader, made during the developmental period of these tubes.

# A NEW TUBE FOR USE IN SUPERHETERODYNE FREQUENCY CONVERSION SYSTEMS\*†

By

C. F. NESSLAGE, E. W. HEROLD, AND W. A. HARRIS

RCA Radiotron Division, RCA Manufacturing Company, Inc.,  
Harrison, N. J.

**Summary**—The major disadvantage of existing methods of frequency mixing is found in high-frequency operation with comparatively low intermediate frequencies, where serious coupling exists between oscillator and signal circuits in spite of electrostatic screening. Suppressor modulation of a radio-frequency pentode largely overcomes many of the defects but the oscillator voltage required is large and the low plate resistance limits the gain. For these reasons, a new tube has been developed (designated the 6L7) wherein the above disadvantages are largely overcome. The new tube contains five grids: the first grid is a remote cutoff signal grid, the second and fourth are screens, the third is used as the modulator grid controlled by a separate oscillator tube, and the fifth grid is a suppressor. The ideal characteristics of such a tube are derived. The actual characteristics of the tube developed are shown and a brief discussion of the results obtained is given. A discussion of the flow of electron current to a negative grid due to an unusual transit-time effect at high frequencies is given and it is shown that operation with sufficient grid bias reduces the phenomenon.

The characteristics of this tube also make it particularly suitable for use as a radio-frequency amplifier in receivers where the available automatic volume control or detector voltage is low; in this case the automatic volume control voltage is applied to both No. 1 and No. 3 grids.

Although not primarily intended for the purpose, the tube is also suitable for use in the volume expansion of recorded music. Such application provides for an effective means of emphasizing the crescendos and diminuendos of the music. A brief description of a method of accomplishing this is given.

## INTRODUCTION

IN A previous discussion by one of the authors of this paper,<sup>1</sup> it was pointed out that with the present usual procedures for obtaining frequency mixing, considerable loss in gain at high frequencies was experienced because of space charge and other coupling between oscillator and radio-frequency signal circuits. It was also shown that suppressor modulation of a radio-frequency pentode largely overcomes these difficulties, but has the serious disadvantages of large oscillator voltage requirements and low plate resistance. It is the purpose of this paper to describe the development of a tube which overcomes these latter faults and yet retains the advantages of outer-grid modulation.

\* Decimal classification: R330 × R361.

† Reprinted from *Proc. I.R.E.*, February, 1936.

<sup>1</sup> W. A. Harris, "The application of superheterodyne, frequency conversion systems to multirange receivers," *Proc. I.R.E.*, Vol. 23, pp. 279-294; April (1935).

## GENERAL DISCUSSION OF MIKER OPERATION

Referring to Fig. 1, it is seen that the tube consists of a cathode, an anode, and five grids having the following functions:

The first grid is the radio-frequency or control grid of the tube. It is of the remote cutoff type, thus minimizing radio-frequency distortion, cross modulation, and affording the conveniences of automatic volume control. The transconductance of this grid to the plate is made as high as possible without abnormal electrode spacings.

The purpose of the second grid is to accelerate the electrons similarly to a space-charge grid and also to provide screening between the first grid and the other electrodes of the tube.

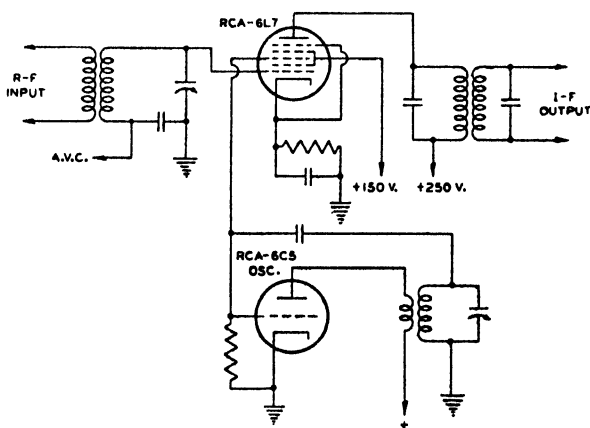


Fig. 1—Typical mixer circuit using 6L7 tube.

The third grid is modulated by the separate oscillator signal. In order to eliminate the disadvantages of large oscillator-signal requirements noted on existing pentodes, it has been made with a fairly high amplification factor.

The fourth grid is a screen internally connected to the second grid and serves as a means of securing high plate resistance to prevent the reduction in plate resistance noted in the case of the radio-frequency pentode with suppressor modulation.

The fifth grid is connected internally to the cathode and serves as a suppressor of secondary emission. This grid is included to assure high  $r_p$  and to permit operation at low plate voltages.

Since the No. 3, or modulator, grid is the most important element in overcoming the disadvantages of present pentodes in suppressor-modulation circuits, an analysis of its specific characteristics will be given at this point. To do so, it is necessary to review and analyze some converter theory.



Frequency conversion in a tube of the type considered may be regarded as a process of modulating the oscillator frequency by the signal frequency, the percentage modulation being very small in the usual case of large oscillator and small signal-frequency components in the plate current. Stated in other words, the amplitude of the oscillator-frequency component of the plate current is varied slightly at the signal frequency, one of the resulting side bands being the desired intermediate frequency. Because of the assumption that the modulation is small, high order nonlinear effects may be neglected. As is well known, the amplitude of one of these side bands is exactly one half the fractional modulation multiplied by the normal carrier amplitude (in this case the oscillator-frequency amplitude). Therefore, the intermediate-frequency component of the plate current is given by

$$I_{if} = \frac{m}{2} I_{osc}.$$

Now the change in oscillator-frequency amplitude is the product of the rate of change of this amplitude with signal voltage and the signal voltage, so that the change in oscillator-frequency amplitude is

$$\text{change in } I_{osc} = \frac{\partial I_{osc}}{\partial E_{c1}} eg_1$$

and hence the fractional change  $m$  is

$$m = \frac{1}{I_{osc}} \frac{\partial I_{osc}}{\partial E_{c1}} eg_1.$$

Thus,

$$I_{if} = \frac{1}{2} \frac{\partial I_{osc}}{\partial E_{c1}} eg_1.$$

Defining the conversion conductance as

$$s_c = \frac{I_{if}}{eg_1}$$

it is seen that

$$s_c = \frac{1}{2} \frac{\partial I_{osc}}{\partial E_{c1}}.$$

If the plate current of this tube be expanded by Fourier analysis, it can be shown that the amplitude of the oscillator-frequency component is

$$I_{osc} = \frac{1}{\pi} \int_{-\pi}^{+\pi} I_b \cos \omega t d(\omega t)$$

where  $\omega$  is the angular velocity of the oscillator.

Taking the partial derivative of this with respect to the control-grid voltage, we have

$$\begin{aligned}\frac{\partial I_{osc}}{\partial E_{c_1}} &= \frac{1}{\pi} \int_{-\pi}^{+\pi} \frac{\partial I_b}{\partial E_{c_1}} \cos \omega t d(\omega t) \\ &= \frac{1}{\pi} \int_{-\pi}^{\pi} s_{m_1} \cos \omega t d(\omega t)\end{aligned}$$

where  $s_{m_1}$  is the transconductance between No. 1 grid and plate.

It is therefore seen that the conversion transconductance

$$s_o = \frac{1}{2\pi} \int_{-\pi}^{\pi} s_{m_1} \cos \omega t d(\omega t).$$

If the conversion conductance is required to be a maximum, the tube should operate only when  $\cos \omega t$  is positive, that is, only when the oscillator swings from  $-\pi/2$  to  $\pi/2$ . The  $s_m$  should be cut off during other angles because the change in sign of  $\cos \omega t$  then would decrease

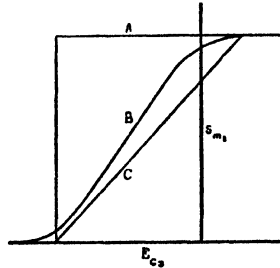


Fig. 2—First grid-to-plate transconductance as a function of third grid bias: A, ideal; B, actual; C, limiting case.

the integral. Again, during the interval  $-\pi/2$  to  $\pi/2$ ,  $s_{m_1}$  should remain at its maximum. Thus maximum conversion conductance

$$s_{o \max} = \frac{1}{2\pi} \int_{-\pi/2}^{\pi/2} s_{m \max} \cos \omega t d(\omega t) = \frac{s_{m_1 \max}}{\pi}.$$

This means that the conversion conductance of a mixer tube cannot exceed  $1/\pi$  times the maximum  $s_m$  between the control grid and output element. In terms of the proposed mixer-tube parameters, it indicates that the shape of the  $s_{m_1}$  vs.  $E_{c_3}$  curve should be that of curve (A) of Fig. 2. Actually it is almost impossible to obtain a curve of this shape in a tube, but it is possible to obtain an S-shaped curve similar to (B) in the diagram. As a limiting factor, then, we may inspect the  $s_o$  in

the case where  $s_{m_1}$  varies directly with  $E_{c_2}$  as indicated in curve (C) of the same diagram. Applying the expression for  $s_{m_1}$  in this case to the above formulas for  $s_c$ , it can be shown that

$$s_c = \frac{s_{m_1 \max}}{4}.$$

Assuming then that the oscillator voltage is sufficient to swing the No. 3 grid from cutoff through maximum  $s_{m_1}$  back to cutoff in the interval  $-\pi/2$  to  $\pi/2$ , it will be found that the  $s_c$  of the tube will lie between

$$\frac{s_{m_1 \max}}{4} \text{ and } \frac{s_{m_1 \max}}{\pi}.$$

From a receiver application standpoint,

it is desirable to keep this oscillator voltage requirement as low as possible, so that the No. 3 grid characteristic should have a high value of  $s_{m_1}$  at the maximum positive swing, be fairly saturated, and cut off as sharply as possible.

The tube embodying these refinements in outer-grid modulation has been designated as the 6L7. The characteristics of an average 6L7 together with typical operating conditions may briefly be tabulated:

6L7 CONVERTER OPERATION			
	$E_f = 6.3$	$I_f = 0.300$	
$E_{c_1}$	-3	-6	
$E_{c_2,4}$	100	150	
$E_{c_3}$	-10	-15 (oscillator voltage superimposed)	
$E_b$	250	250	
Peak Osc. Volts	12	18	
$s_c$	360 $\mu$ mhos	360 $\mu$ mhos	
$r_p$	1 meg +	1 meg +	
$I_{c_2,4}$	6.2 ma	8.3 ma	
$I_b$	2.4 ma	3.2 ma	

It will be noticed that one of the recommended screen voltages is 150 volts and is used with a normal bias of -6 volts. These values are higher than those usually employed. The reason for the choice of these voltages lies in an unusual phenomenon found at very high frequencies in the use of these tubes where a few microamperes positive grid current flows in the No. 1 grid circuit, even though this grid is biased negatively. This current was first observed by V. D. Landon of the RCA Victor Division in a typical converter circuit where 100 volts on the screen and -3 volts on the control grid were used. This effect is not to be confused with the space-charge coupling observed in pentagrid converters but is caused by forces acting on the electrons during their time of transit and may be explained as follows:

When the No. 3 grid is swinging slightly negative, part of the electrons approaching it is turned back towards the positive No. 2 grid. During their time of transit, that is, before they reach the No. 2 grid

on the way back, the No. 3 grid swings more negative. This increases the potential gradient in the No. 2 grid to No. 3 grid region, and an additional force is exerted on the returning electrons. When the frequency is high, this is sufficient to cause some of those electrons which pass through the No. 2 grid wires to overcome the retarding field near the No. 1 grid and flow through that circuit. When calculations are made on this additional imposed force on the electrons in terms of the No. 2 to No. 3 grid distance, the No. 3 grid frequency, and voltages

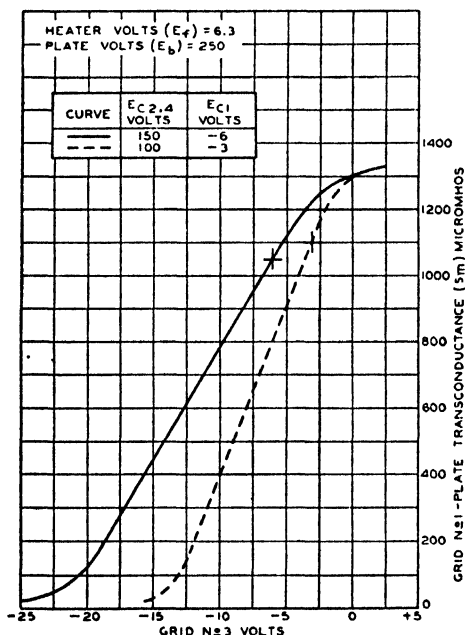


Fig. 3—First grid-to-plate transconductance characteristics for the 6L7.  $E_{a1}$  held constant.

under conditions resulting in grid current, it is found that the force imposed on the electrons during one trip is insufficient to overcome the retarding field near the No. 1 grid. It must, therefore, be assumed that the electrons make several trips through the No. 2 grid, those electrons which pass between the No. 2 grid wires picking up a small amount of energy each time until they acquire the amount necessary to enable them to reach the No. 1 grid. The additional force applied to the electrons by this effect is found to be proportional to the oscillator frequency, the transit time of the electrons, and the oscillator amplitude. Measurements at thirty megacycles using a fifteen-volt oscillator signal indicate that -6 volts bias on the No. 1 grid is sufficient to cut off the grid current. For this reason, it is recommended that for the use of the

6L7 in the short-wave bands a minimum bias of  $-6$  volts be used on the No. 1 grid. When this bias is used, the screen voltage may be increased to 150 volts to increase the conversion gain. At still higher frequencies, grid current may be avoided by further increase in bias or by reduction of the oscillator voltage, but the screen voltage should not exceed 150 volts.

The characteristic curves of an average tube which are of importance in converter operation are the  $s_{m1}$  vs.  $E_{c3}$  curves, which determine

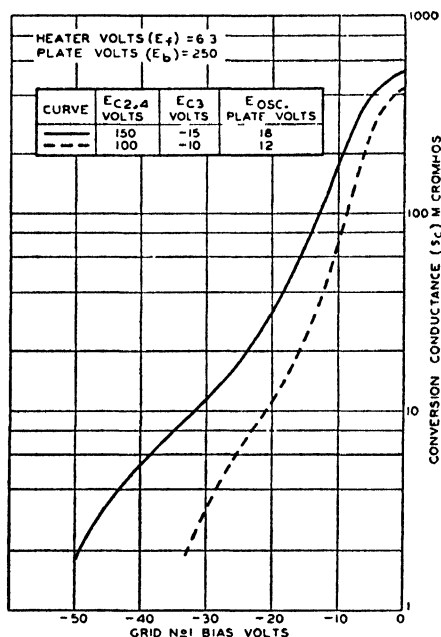


Fig. 4—Operation characteristics for type 6L7.

the  $s_c$  as outlined above, and the  $s_c$  vs.  $E_{c1}$  curve, which shows the control action and cross-modulation characteristics: The former curve is shown in Fig. 3 for a screen voltage of 150 volts and also for 100 volts. It will be observed that the latter voltage permits just as high  $s_c$  as the former (since the maximum  $s_m$  is about the same) and requires considerably less oscillator voltage. Inasmuch as the cathode current is also lower under this condition it may be advisable to use it when the upper frequency limit is twenty megacycles or less. For higher frequencies than this, enough advantage is usually obtained from the 150-volt screen operation to justify its use.

The  $s_c$  vs.  $E_{c1}$  curves of an average tube are shown in Fig. 4. This cuts off at approximately  $-50$  for 150 volts on the screen and at  $-35$

for 100 volts on the screen as shown. The curves are plotted semilog to illustrate the remote cutoff characteristics.

The performance of the tube with variation in oscillator voltage is shown on Fig. 5, where the  $s_c$  is plotted against  $E_c$  for various values of oscillator voltage. An inspection of the curves shows that the highest

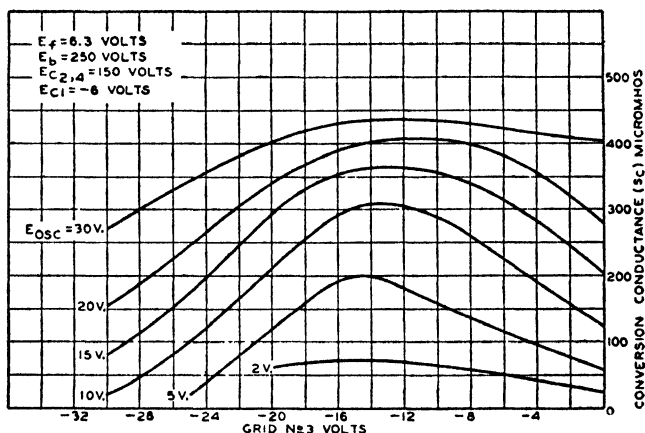


Fig. 5—Operation characteristics of type 6L7 as a mixer.

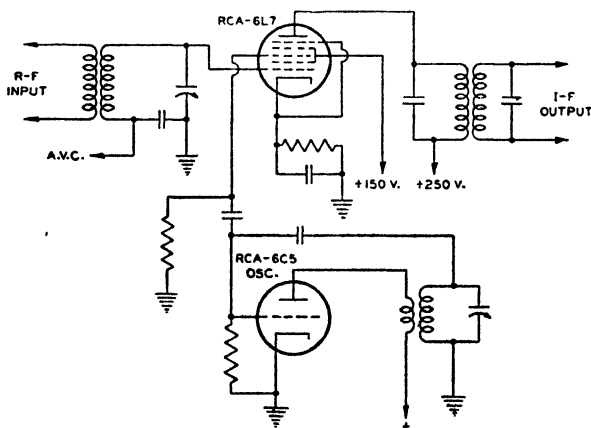


Fig. 6—Another typical mixer circuit for the type 6L7.

$s_c$  is obtained by using a large oscillator signal. It will also be noted that for best results, the peak oscillator voltage exceeds the bias of the No. 3 grid, causing current to flow between this grid and cathode. This makes it convenient to obtain the biasing voltage  $E_c$ , as the drop resulting from the flow of grid current through a grid-leak resistor. In Fig. 1, the bias is obtained by current through a grid leak common to the oscillator and 6L7 tubes. In Fig. 6, the bias is obtained by current

flowing through a separate leak for the No. 3 grid. The latter circuit permits connecting the No. 3 grid to any point in the oscillator circuit (for example, the plate) and is also helpful in reducing the effect of the No. 3 grid-to-ground capacitance of the 6L7 on the oscillator tuned circuit.

Some measured advantages<sup>2</sup> of the 6L7 over pentagrid converters in typical mixer circuits were found to be the following:

1. An increase in gain of between 5 and 8 to 1 at twenty megacycles.
2. Appreciably less required oscillator power, resulting in greater stability of the oscillator circuit.
3. Improved selectivity and increased gain in the first intermediate-frequency circuit because of the high  $r_p$ .
4. Easier alignment of tuned circuits due to less reaction between radio-frequency and oscillator components.
5. A greater range of operating frequencies. Good results have been obtained at 60 megacycles, whereas A7 type tubes will not operate well at frequencies above forty megacycles even when a separate oscillator is used. At forty megacycles, the improvement in sensitivity was measured as a 20-to-1 ratio over that of the pentagrid converter circuit.

The application of the 6L7 tube to radio receivers is not confined to converter operation alone, as the following discussion will show.

#### APPLICATION OF THE TUBE AS A RADIO-FREQUENCY AMPLIFIER

If a curve of  $s_{m_1}$  vs.  $E_{c_1}$  is plotted for various negative potentials on the No. 3 grid, it will be noted that at more negative biases on the No. 3 grid, lower No. 1 grid-plate transconductance is obtained (Fig. 7). This phenomenon may be utilized in the circuit shown on the diagram. In this case, the tube is used as a radio-frequency amplifier with the automatic volume control voltage applied to the No. 1 grid and also to the No. 3 grid. The dotted line on the curves indicates the cutoff characteristic of  $s_m$  vs. automatic volume control voltage. It will be seen that, for a given automatic volume control voltage, a wide control of gain can be effected. This connection is particularly useful in midget sets where the voltage at the detector is limited, and affords a means of securing sharper automatic volume control action than is now possible with existing pentodes in these sets. Since the signal swings over the solid curves and operating points are determined by their intersections with the dotted curve, the cross modulation and

\* We are indebted to the RCA Victor Division for these figures.

radio-frequency distortion are approximately the same as with conventional tubes. The extremely low No. 1 grid-plate capacitance is an

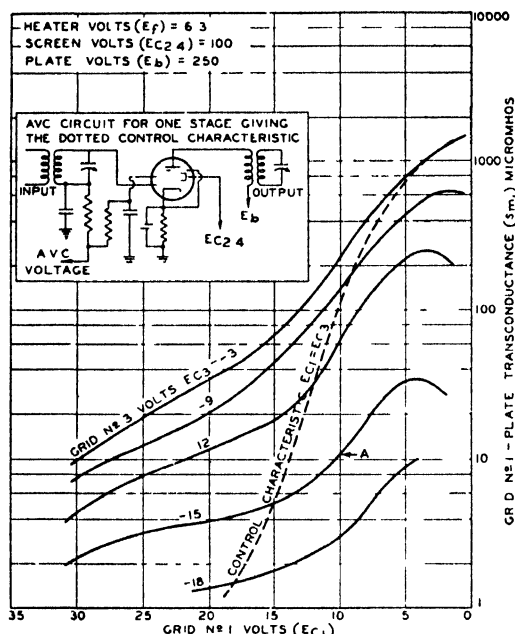


Fig. 7—First grid-to-plate transconductance characteristics of the type 6L7.

advantage in many applications. Typical operating conditions for the tube as a radio-frequency amplifier are shown below:

6L7 AS RADIO-FREQUENCY AMPLIFIER

Heater voltage	( $E_f$ )	6.3 volts
Heater current	( $I_f$ )	0.3 amperes
Plate voltage	( $E_b$ )	250 max. volts
Control-grid voltage	( $E_{c1}$ )	-3 volts
Control-grid voltage	( $E_{c3}$ )	-3 volts
Screen voltage	( $E_{c2,4}$ )	100 volts
Transconductance	( $S_m$ )	1100 micromhos
Plate current	( $I_b$ )	5.3 milliamperes
Screen current	( $I_{c2,4}$ )	5.5 milliamperes
Plate resistance	( $r_p$ )	0.8 megohms
Direct Interelectrode Capacitances:		
Input	80 $\mu\mu\text{f}$	
Output	12.5 $\mu\mu\text{f}$	
Grid-plate	0.0005 max. $\mu\mu\text{f}$	

### APPLICATION OF THE TUBE IN VOLUME EXPANSION CIRCUITS

Considerable interest has been shown recently in methods of compensating for the necessary contraction of volume range in practical systems for reproducing music. Although not primarily intended for the purpose, the 6L7 has been found adaptable to this application. The



simplest system for accomplishing this "volume-expansion" consists in increasing the gain of an amplifier tube in the audio system by means of a direct voltage proportional to the average level of the music.<sup>3</sup> One method of effecting this with the 6L7 tube is to connect the signal to the No. 1 grid and to apply the volume controlling voltage to the No. 3 grid; the controlling voltage is obtained from a separate amplifier and diode rectifier whose input is connected to the signal (Fig. 8).

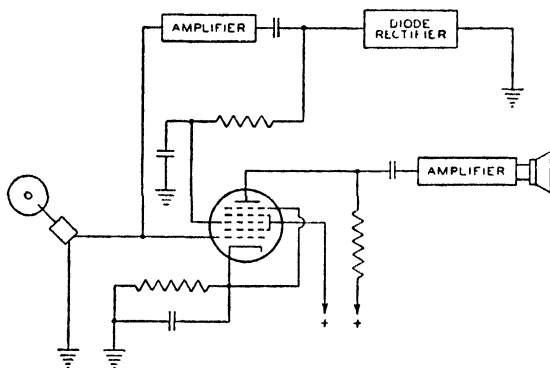


Fig. 8—Volume expander circuit.

The No. 3 grid of the 6L7 is initially biased to some low transconductance point as for example the point A on the  $s_m$  curves of Fig. 7. When the signal is applied, the diode raises the No. 3 grid potential so as to increase the gain over the zero value. The amount of increase in the gain is approximately proportional to the diode voltage and hence to the signal level.

The distortion of the audio signal by the curvature caused by the remote cutoff nature of the first grid is appreciable for large signals. The tube must therefore be used at small signal values such as are obtained from a phonograph pickup. Since the  $s_m - E_c$  characteristic is nearly exponential in shape over small regions, the second harmonic distortion produced is approximately given by

$$\text{per cent 2nd} = (1/4)bE \times 100$$

where  $b$  is the slope of the  $s_m, E_c$  curve on semilog paper and  $E$  is the peak input voltage.

For the 6L7 operated at point A on Fig. 7,  $\frac{1}{4}b \times 100 = 6$  so that about six per cent second harmonic per volt peak is encountered.

<sup>3</sup> The pioneer work which led to the system described here was done by J. F. Dreyer, Jr.

## CONCLUSION

The 6L7 tube provides a very efficient means of obtaining frequency mixing in superheterodyne receivers, particularly at high frequencies. The tube is also suited for use in radio-frequency amplification where a steep control characteristic may be obtained without sacrificing the advantages of remote cutoff tubes. In addition, the tube may be used in other circuits where a tube having two control grids is advantageous.

# BEAM POWER TUBES\*†

BY

O. H. SCHADE

RCA Radiotron Division, RCA Manufacturing Company, Inc.,  
Harrison, N. J.

**Summary**—*The general characteristics of the ideal output tube for broadcast receivers are discussed briefly with respect to specific electrical and acoustical requirements.*

*Considerations of practical power-tube design indicate that the tube most nearly approaching the ideal characteristics is one having an accelerating grid (screen) and a control grid which does not require power. The limitations of conventional output tetrodes and pentodes with respect to the ideal are treated and are illustrated by means of oscillograms and models showing field-potential distributions. It follows that homogeneous potential fields and directed electron beams having high electron density can be utilized to minimize these limitations. These design features indicate the feasibility of a tube suitable for operation as a class A amplifier having substantially second-harmonic distortion only and capable of high power output, high efficiency, and high power sensitivity.*

*The theoretically proper geometric structure for beam power tubes is developed. The theory is substantiated by performance data obtained from actual tubes.*

## I. INTRODUCTION

DEVELOPMENTS in the art of transmitting and reproducing sound by electrical means point toward systems of higher fidelity capable of reproducing faithfully the tremendous range of volume of the symphony orchestra without altering the infinite variety in combinations of tones and overtones. In the achievement of this ideal, radio tubes have an important part. A brief résumé of audio-frequency power-amplifier requirements will help in formulating the specifications of an ideal power tube for loud-speaker operation.

## II. FUNDAMENTAL REQUIREMENTS FOR HIGH-FIDELITY SOUND REPRODUCTION

The audio-frequency amplifier in the receiving unit must cover a frequency range of more than eight octaves for true reproduction of music. To accomplish this, it is necessary that the amplifier tubes themselves do not generate tones of substantial magnitude within the desired range.

---

\* Decimal classification: R330.

† Reprinted from *Proc. I.R.E.*, February, 1938.

The science of music teaches us that pure octaves, i.e., tones of second-, fourth-, and eighth-harmonic order, are always harmonious, and, therefore, are least objectionable when introduced by *harmonic distortion* in amplifiers.

The third harmonic is the octave of the pure musical "fifth." It is harmonious to single tones but causes dissonance as a harmonic of some of the component tones in musical chords of relative purity. Small magnitudes of third harmonic generated in the amplifier can be tolerated but should not exceed a few per cent of the fundamental tones. The fifth harmonic is the pure "second" to the double octave of the fundamental tone. Harmony conditions are somewhat similar to those of the third harmonic. The larger pitch difference, however, reduces masking effects<sup>1</sup> produced by the fundamental tones so that the permissible maximum value is considerably smaller than for the third harmonic. Higher-order harmonics of odd number, seventh, ninth, etc., are disharmonious and thus increasingly objectionable. High-order harmonics in general are so much different in pitch from the fundamental tone that magnitudes much smaller than one per cent may be noticed as a disagreeable sharpness of tone or a hissing sound. They are generated especially in amplifiers having dynamic characteristics with sudden changes of curvature.

In the preamplifier stages it is not difficult to limit harmonic distortion to satisfactory values if the required output power or voltage is substantially less than the obtainable maximum value. The output stage, however, must not only be operated efficiently but must also supply maximum power output at low distortion.

The *peak output power* required for reproduction is at least 10 to 25 times the average power output and still larger for amplifiers with volume expansion. Thus, an average volume level of one watt of electrical power demands the undistorted reproduction of peaks as high as 20 to 30 watts. If this power is to be obtained at reasonable cost, the output tube must have not only a high plate efficiency, but also a good "circuit" efficiency.

The *plate load* of the power stage is not a pure resistance. The motional impedance of commercial dynamic cone loud-speakers for receiving sets varies considerably with frequency due to the low coefficient of electromechanical coupling. Due to the loose coupling, the mechanical circuit reflects its reactance and resistance efficiently only at the resonant frequency as illustrated in Fig. 1, which shows the electrical characteristics of a typical speaker. The increase of the normal<sup>2</sup> resistance to 96.7 ohms indicates an efficiency of close to 90 per

<sup>1</sup> Harvey Fletcher, "Speech and Hearing," D. Van Nostrand Co., (1929).

<sup>2</sup> See 1933 Report of the Standards Committee of the I.R.E., page 36.

cent at the resonant frequency, while only about five per cent of the input power is transferred to the secondary system at other frequencies.

The reactance of the moving coil is responsible for the normal impedance rise at high frequencies. This impedance rise is quite easily corrected over the entire *high-frequency* range by the much-used series-resistance-capacitance shunt on the reflected load. This compensation is absolutely necessary to provide good quality and to avoid high transient voltages when the output tubes have high internal impedance ( $r_p$ ), but it may be omitted with low-impedance tubes.

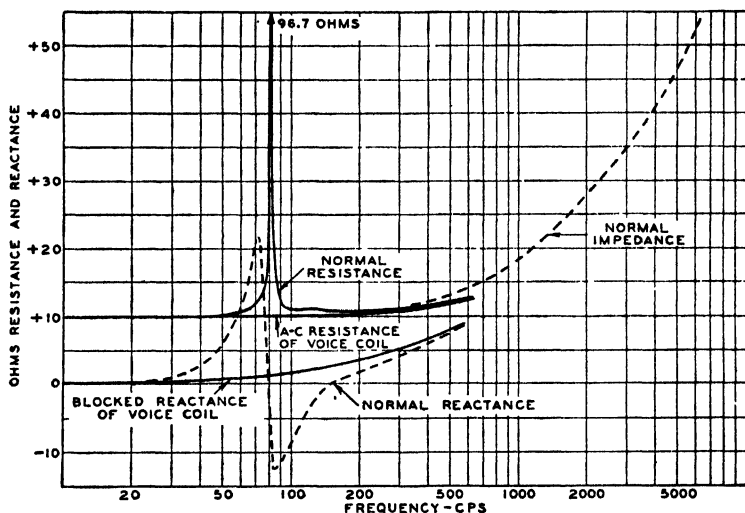


Fig. 1—Electrical characteristics of a dynamic loud-speaker.

### Loud-Speaker Damping

The internal impedance of the power tube shunts the plate load. If the plate load ( $R_p$ ) is high compared to the tube impedance, the  $Q$  ratio of a parallel-tuned plate load is decreased by the tube shunt which acts to prevent a large resonance rise. The mechanical resonance of the dynamic speaker appears over a short frequency range in the primary substantially as a high-impedance parallel-tuned circuit (compare Fig. 1). This circuit is damped by low-impedance tubes but affected little by high-impedance tubes. But even if the reflected electrical circuit resonance is almost completely damped by low tube impedance, the sound output still rises above normal due to the high energy transfer into the mechanically resonant secondary circuit.

If a resonant-voltage rise of 5 on the voice coil is assumed and the equivalent increase in efficiency is considered as from 5 to 81 per cent, a calculation yields the following results: High-impedance sources as

represented by pentodes in class A service with  $r_p = 10R_p$  permit a 16.4-decibel sound-output rise at resonance; triodes with  $r_p = \frac{1}{2}R_p$ , a 7.8-decibel rise. For  $r_p = 0$ , the rise is still 5.1 decibels.

Electrical damping cannot completely eliminate resonance "boom" and prevent overload of the speaker at resonance. This must be done by power-absorbing circuits or in the loud-speaker design.

### III. GENERAL PROBLEM OF POWER-TUBE DESIGN

The design of a desirable tube begins with the formulation of ideal-type characteristics. An analysis of the electrical characteristics of an idealized tube follows in order that the most suitable design principle may be selected on the basis of both tube development and practical operation. The theoretical investigation of the electrical principles involved points out the direction of research, and assists in formulating the specific design problem.

According to the preceding discussion, the general specifications for an ideal power tube are as follows:

#### A. General Specifications for an Ideal Power Tube

1. *Low distortion* mostly of second-harmonic order. A small percentage of third harmonic can be tolerated. Higher-order harmonics must be negligible.

2. *Good power sensitivity* to permit low-level operation of the pre-amplifier stage.

3. *High power output* obtainable with self-bias and supply circuits having the voltage regulation of conventional broadcast receivers. Exceptionally large power output with good quality for limited high-frequency response with supply circuits of moderately good regulation.

4. *Maximum efficiency* in both tube and associated circuits with respect to power dissipation as well as cost.

5. *Effective damping* of resonant loads.

#### B. Analysis of Tube Types and Design Possibilities on the Basis of the Required Electrical Characteristics

##### 1. Triodes

##### (a) The Required Characteristic for Negative-Control-Grid Operation

The distortion from present class A output triodes is low and contains only small magnitudes of higher-order harmonics. The 2A3 is a large power triode for receivers. It is a filament type, having a large effective cathode area which does not require as much heater power as a unipotential cathode of equivalent area. However, it is not feasible at present to construct at reasonable cost a triode having much higher

power sensitivity, higher efficiency, and larger power output than the 2A3 for a 300- or 400-volt plate supply. The necessary large cathode area would be quite expensive and would present difficult constructional and operating problems due to grid emission. The relatively low efficiency of low- $\mu$  class A triodes is a serious objection from the standpoint of tube dissipation, and cost of power supply for increased output power.

A plate efficiency approaching 50 per cent without grid current in class A service is not impossible even for existing triodes, but the power output for medium voltages is very small with respect to the size of the tube. The *hypothetical* triode must have a sharp cutoff, substantially constant  $\mu$  at all plate voltages, and high transconductance,

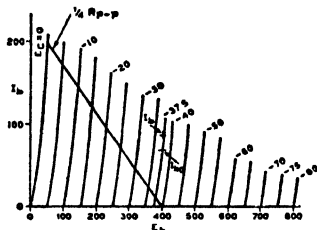


Fig. 2—Plate family of hypothetical triode.

Conditions for push-pull operation

$E_c = -37.5$  volts fixed

$E_b = 400$  volts fixed

$I_{b0} = 71$  milliamperes

$I_b = 85$  milliamperes

Power output = 35 watts (two tubes)

Efficiency  $\approx 51.2$  per cent

$R_{p-p}$  = plate-to-plate load

i.e., a very steep rise of current versus applied potential, as shown in Fig. 2. This plate characteristic is ideal on a theoretical basis. The characteristic family is constructed by parallel displacement of the zero-bias characteristic. This constant  $\mu$  (it is shown to be 10) is approached in an actual tube by using a fine-mesh control grid at relatively large distances from cathode and plate. The effective grid potential at  $E_b = +50$  volts and  $E_c = 0$  volts is thus approximately five volts, which must be sufficient to cause an electron current of 200 milliamperes. We know that this is possible only by the use of a *very large cathode area* even for considerably lower  $\mu$  values. Furthermore, this large cathode should radiate little heat to the grid in order to avoid grid emission.

A cathode of large area may be produced with an auxiliary positive grid. The "virtual cathode" of the space-charge-grid tube seems a good solution. The virtual cathode, however, must have an *electron reserve capable of supplying the peak current* demanded from it. The space-

charge-grid tube thus requires a larger cathode current and consequently a larger B power supply in comparison with other tubes to be discussed and, therefore, does not meet the requirements for circuit efficiency.

### (b) Triodes with Positive-Grid Operation

The control grid itself may be permitted to swing positive, in order to accelerate the electrons and obtain a steep current rise at low plate voltages. This method has certain disadvantages. The grid current in conventional triodes is of substantial magnitude and considerably decreases the expected plate-current rise, especially at low plate voltages.

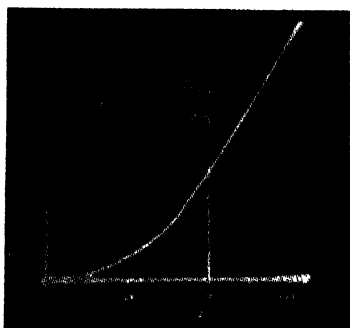


Fig. 3—Transfer characteristic of a positive-operated-grid output tube with conductively coupled driver.

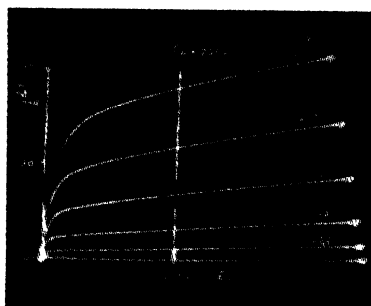


Fig. 4—Resultant plate family of a positive-operated-grid output tube with conductively coupled driver.

This action causes increased distortion. A second complication arises from the fact that there are now two positive electrodes in the tube so that secondary electrons from one electrode may not fall back to the plate but instead may travel to the other positive electrode.

*Secondary emission* occurs whenever electrons hit an obstacle which, aside from transit-time effects, must be at positive potential. The liberation of normal<sup>3</sup> secondaries begins substantially at a positive voltage of about ten volts and thus causes a break in the grid-current curve. The performance of present-day class B triodes shows fairly good success in smoothing out the grid-current "kinks" in their reaction on the plate current, by bettering the ratio of plate current to grid current through the use of specially designed high-impedance triodes. These high-impedance tubes have a plate family very similar to pentodes and thus give a performance similar to a pentode. Unlike the pentode, they require driving power and, therefore, demand care-

<sup>3</sup> H. Barkhausen, "Electronenroehren," vol. 1.



fully designed low-impedance preamplifiers. Because only drivers with zero internal resistance and ideal coupling devices eliminate grid-circuit distortion, the "kinks" and consequent higher-order harmonics cannot be completely suppressed in practical systems. That this is the case is shown by the transfer characteristic of Fig. 3. The plate load has little effect on the break in the characteristic.

In push-pull operation, tubes with positive grids operate with considerable plate efficiency. They may be designed to require no biasing voltage. The *distortion* of high-impedance triodes operating with positive grid voltages is naturally higher than that of pentodes operated without control-grid current, because distortion is increased in all

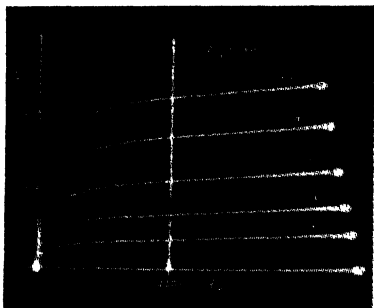


Fig. 5—Plate family of a typical power pentode.

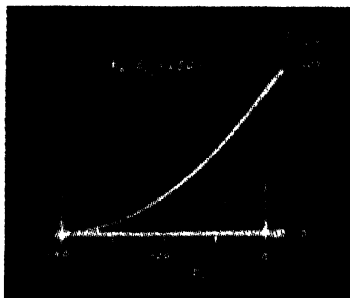


Fig. 6—Transfer characteristic of a typical power pentode.

practical cases by harmonics including those of high orders arising from the irregularities of the grid-current characteristic.

In class A operation, single high-impedance tubes operated with positive control-grid voltages and conductively coupled driver stages present no advantage in output performance over conventional pentodes. The resultant plate family is very similar to that of a pentode and consequently the plate-circuit performance with regard to distortion, efficiency, and load variation is also similar (Figs. 4 and 5). The transfer characteristic of pentodes operated without grid current is inherently a smooth curve (Fig. 6).

## 2. Pentodes

### (a) Characteristics of Conventional Pentodes

Power output and efficiency of commercial pentodes are considerably higher than those of conventional triodes operated without grid power. The screen-grid potential remains fixed and highly positive at all plate-voltage values. This feature eliminates the necessity of a large cathode area for obtaining a steep plate-current rise with low

plate potentials. *Overbiased pentodes* in push-pull operate with an overall efficiency which compares favorably with that of good class B triodes, and in addition have the considerable advantage of operating without grid current. This guarantees negligible high-order harmonics and a simple preamplifier design.

It can be shown that *overbiased operation* of push-pull pentodes is, in fact, *necessary* in order to obtain distortion values of less than three per cent consisting mainly of third-harmonic distortion and having less than one per cent of fifth harmonic. The attainment of a high plate efficiency of 70 per cent and a total B supply power efficiency of approximately 60 per cent are accompanied by considerable increases in the current demand for an applied signal. In order to maintain correct operating conditions for all signal levels, it is necessary to provide a well-regulated bias and B voltage supply. A study of modern receivers shows, however, that the power stage is generally designed to have at most a two-to-one increase in plate current due to a signal and is operated with self-bias or semi-self-bias. In many instances better performance with respect to distortion and efficiency is sacrificed to obtain partial class A performance and with it supply circuits not requiring good regulation.

It has been indicated that the desirable power tube could not be built economically as a triode, because three-electrode tubes with positive signal grids were ruled out for distortion reasons. It will also be shown later that the operation of triodes having high power sensitivity places severe requirements on the circuit. Because of these limitations the solution will be sought in a four- or five-electrode tube having a separate positive accelerating grid.

#### (b) Characteristics of a Desirable Power Pentode or Tetrode

The first requirement in our specifications for an ideal power tube is *low distortion of substantially second-harmonic order*. The practical solution is a square-law curvature of the transfer characteristic and a plate family which is substantially linear over the entire useful plate-current—plate-voltage characteristic.

The second requirement is *good power sensitivity*. This demands fine-mesh grids, and an efficient cathode with close control-grid spacing to obtain high transconductance.

The third and fourth requirements are *high power output and efficiency*. These require the extension of the straight section of the plate family down to very low plate-voltage values and a low percentage of screen-grid current at all plate voltages in the useful range.

The fifth requirement is *low plate impedance*. This is in conflict with the second, third, and fourth requirements. The screen-current rise

with decreasing plate voltage is considerably larger in pentodes or tetrodes of low plate impedance than in pentodes with high plate impedance whether the curves are ideally straight or not, provided good screening of the plate field with resultant good cutoff is maintained. The large increase of screen-grid dissipation with signal in low-impedance pentodes decreases efficiency and power-output capability, while the plate impedance obtainable is hardly low enough to effect a substantial damping of a resonant load.

It is, therefore, reasonable to depart in this one point from the ideal if a power tube can be designed which satisfies all other requirements. It will be shown later that the characteristic of such a tube can be changed into that of a very good low-impedance triode by the use of an inexpensive circuit.

An analysis of screen-grid tubes with respect to potential conditions encountered by electrons in their flight is necessary to recognize limitations in existing tubes. It will be shown that these limitations can be overcome by directed electron beams.

#### IV. ANALYSIS OF SCREEN-GRID TUBES—ESPECIALLY THE ELECTRON CURRENT IN SPACE BETWEEN ACCELERATING GRID AND PLATE

##### A. Effect of Space Charge

###### (1) *Space-Charge Effects in Diodes*

Let us assume a parallel-plane diode for the purpose of illustrating electron effects in space. Without the presence of electrons, the potential between cathode and plate increases linearly with distance (Fig. 7). This constant gradient is changed if electrons are present. The effect of the negative charge of electrons in space, the "space charge," is to reduce the space potential. Because the density of electrons in a given current is inversely proportional to their velocity, the *potential gradient* is thus zero at the cathode if the initial velocity of the electrons is neglected, and increases cumulatively with distance. An increasing number of *secondary electrons* are liberated at the plate at plate voltages over ten volts approximately. These electrons fly back a short distance towards the cathode but as their volt-velocity is much smaller than that of the primary electrons, they soon come to a stop and return to the plate. The plate current is thus not affected directly. A noticeable decrease in plate current may, however, be caused by an increased space-charge density in the space  $X-P$  (Fig. 7) due to secondary space charge in cases of large secondary emission.

## 2. Space-Charge Effects in Tubes with Accelerating Grid

The potential distribution in a triode with positive grid and plate is shown in Fig. 8 for the theoretical case of uniform electron velocity, uniform path length, and the absence of secondary emission. We as-

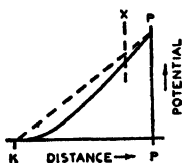


Fig. 7—Effect of space charge on potential distribution in a diode.

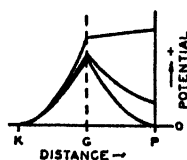


Fig. 8—Potential distribution in a tube with positive grid and plate.

sume again a parallel-plane structure and also low current absorption by the fine-mesh grid in both directions. For a distance  $d_{K-G} = d_{G-P}$  and zero plate voltage, the potential distribution is symmetrical on both sides of the positive grid. The electrons just reach the plate because they are decelerated to zero velocity at zero voltage and zero gradient. More positive plate voltages change potential distribution and gradients as indicated. This will be discussed in more detail later on. All electrons passing the grid reach the positive plate.

The *theoretical tetrode* having a control grid inserted between cathode and screen grid should thus have the desired plate characteristic

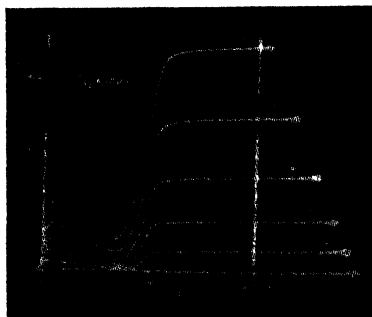


Fig. 9—Plate family of a typical tetrode with low space-charge density.

of parallel straight lines, the plate current rising abruptly at zero plate voltage to a value constant for all positive plate voltages.

In the practical case, however, *secondary electrons* are liberated at the plate and find a positive gradient in the direction of the screen grid at all plate voltages substantially lower than the screen-grid voltage (see Fig. 8). The secondaries thus fly to the screen grid. This action decreases the plate current and increases the screen current.

As the number reaching the plate decreases at very low plate voltages, the well-known plate-current curve shown in Fig. 9 is obtained. Note the plate voltage at which substantial secondary emission begins.

## B. The Suppression of Secondary-Emission Effects and the Suppressor Grid

The tetrode characteristic of Fig. 9 will approach the ideal characteristic if it is possible to prevent secondary emission or to suppress its effects. Most secondary electrons have a relatively low velocity of emission. They are forced to return to the plate if the potential between the positive grid and the plate is decreased at some point ap-

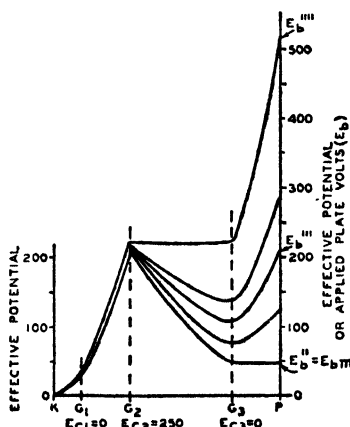


Fig. 10—Calculated effective potentials in a typical power pentode.

proximately ten to twenty volts below the plate voltage. Such a potential "minimum" will prevent the large loss of plate current due to secondary electrons. It can be produced by insertion of a low-potential electrode, the "suppressor" grid in pentodes.

As illustrated in Fig. 10, a potential minimum is formed for plate voltages higher than  $E_{bm}$ . This forces secondary electrons back to the plate. The percentage of primary electrons arriving at the plate is found, however, to decrease considerably in actual tubes when the plate potential is decreased to the value  $E_{bm}$ . This plate-current loss is caused partly by the *nonuniform potential* in the plane of the suppressor grid  $G_3$ . The wires of  $G_3$  are always at zero potential while only the space between wires have a positive potential of varying magnitude caused by the penetrating positive screen-grid and plate fields. This "bumpy" field causes the value  $E_{bm}$  to represent a range of voltages instead of a single value and thus rounds off the theoretical sharp knee at  $E_{bm}$ .

The plate-current loss at low voltages is caused by *velocity differences of electrons in the normal direction* produced mainly by distortion of the potential field due to grid wires, side rods, and nonuniform distances of electrodes. Such velocity differences between screen and plate result in oversuppression in some sections in the plate-current path, while secondaries are just sufficiently suppressed in other sections.

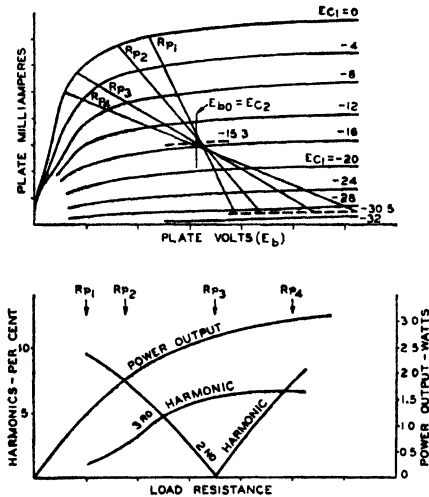


Fig. 11—Performance characteristics of a typical power pentode.

### C. Pentode Performance Resulting from Nonuniform Potential Distribution

The round "knee" of the plate-current characteristic of conventional pentodes produces in class A operation the distortion-versus-load characteristic shown in Fig. 11. With low loads ( $R_{p1}$  and  $R_{p2}$ ) the distortion is mainly of second-harmonic order but the plate efficiency is low. Higher loads give better efficiency but cause a relatively large third-harmonic distortion. Components of higher order are small for reasons discussed later.

From the standpoint of distortion, operation with a low plate load is much preferred. Although the percentage of the second harmonic is large in single-tube operation, it is much less objectionable than a considerably smaller percentage of third-harmonic distortion. It is difficult by comparison with speech or music to detect a difference in quality of sound output between tubes having five and ten per cent second-harmonic distortion.

In push-pull operation, even harmonics generated in each power

tube cancel; odd harmonics do not cancel. Odd harmonics may be reduced by the loading conditions made possible in class AB operation.

#### D. Current Distribution as a Function of the Potential Field Between Screen and Plate

##### 1. The Potential Field

We now investigate the causes of the plate-current loss in pentodes at plate voltages lower than the screen-grid voltage. The field between

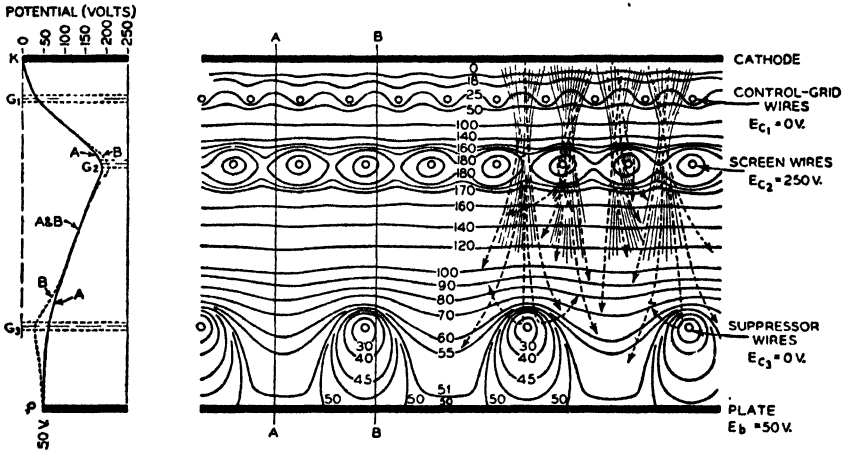


Fig. 12—Plot of potential distribution in a typical power pentode.

screen grid and plate is a decelerating field at medium and low plate voltages. The *percentages of electrons arriving at the plate* out of the total number which leave the cathode is a *function of the shape of the potential field* in the tube which determines the electron path and velocity component in the direction of the plate. According to Fig. 10, the entire electron current passing the screen-grid wires should reach the plate for the condition when  $E_b > E_{dm}$ , but this is only true if the potential field is homogeneous and only for electrons having a normal direction and equal velocities. The actual potential field of a pentode at  $E_b = E_{dm} = 50$  volts is shown in Fig. 12. The field is obviously not uniform. The wires of the grids in the tube disturb the homogeneity of the field.

The action of electrons in this field can be mechanically illustrated by means of the topographic model shown in Fig. 13. In this model, the electrostatic force is replaced by a component of gravitational force depending on the slope of the model at any particular point. The slope is analogous to the potential gradient of the electrostatic field (see left side of Fig. 12). Each lamination represents a potential

step of ten volts, the lower levels corresponding to more positive potentials. The No. 1 and No. 3 grid wires are thus mountain peaks. The electrons may be compared to frictionless balls rolling down from the elevation of the cathode (zero volts) into the valley of the screen grid (+200 to +250 volts). A certain percentage missing the wires of  $G_2$  (the holes) are carried by their momentum up the incline to the plate. Those that pass near the center between screen-grid wires follow a fairly straight path toward the plate. Some of them, are, however, diverted by the curved contour of the suppressor-grid hills, lose velocity and return in an arc toward the screen-grid valley; others traverse the gap between the suppressor hills and reach the plate on the other side.

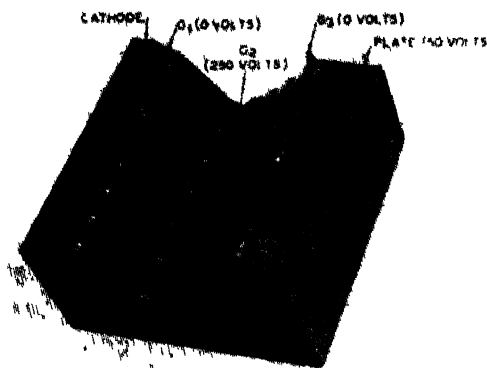


Fig. 13—Topographic model of potential distribution shown in Fig. 12.

A number of the balls coming from the cathode pass close to the screen-grid "holes," and thus are deflected from a straight path because they obtain a tangential-velocity component in the conical field near the screen-grid wires. Their chances of reaching the plate are less than for balls rolling in a straight path toward the suppressor-grid hills. A certain percentage of electrons is headed directly toward the screen-grid holes and does not get through at all. Neglecting this percentage at present, it is easily understood from the analogy that the number of electrons reaching the plate increases when the "gap" between the suppressor-grid hills is deepened by lowering the elevation of the plate because fewer electrons are turned back to the screen grid. Electrically, the gap between the suppressor wires is deepened by an increase of plate potential. The steepness of the current rise with plate voltage thus depends on the manner in which the gap width, i.e., the shape and gradient of the decelerating potential field, affects the tan-



gential component of electrons. As pointed out later, the actual potential distribution may be altered considerably by space charge which is neglected in this model.

The plate current is thus a function of the potential distribution between screen grid and plate within the range of decelerating potentials. Fig. 14(a) shows the plate current of a pentode plotted against the square root of the plate voltage. The curve has several linear sections and shows four significant plate-voltage values at which the factor of proportionality for current increments changes. Calculation of resultant potentials in the planes of the various electrodes disclosed that *significant potential-field or gradient changes* occur between screen grid and plate at the values  $E_b = E''$ ,  $E'''$ , and  $E''''$ , indicated in Fig. 10.

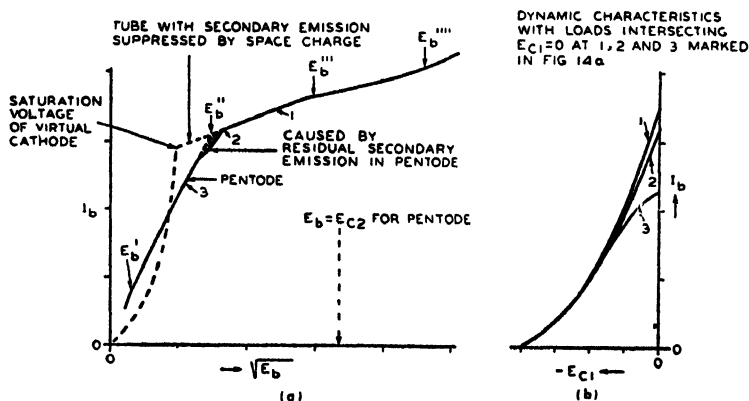


Fig. 14

- (a)—Proportionality of current increments to the square root of plate voltage between successive group-saturation values in a typical power pentode.
- (b)—Dynamic characteristics of a typical power pentode with loads intersecting  $E_{C1}=0$  at points 1, 2, and 3 marked in (a).

We term these specific values "group-saturation" voltages, as certain groups of electrons have then arrived at the plate.

## 2. Group-Saturation Potentials

At  $E_b = E_b'$  only the electrons following a normal path have reached the plate.

At  $E_b = E_b''$  the potential line of plate-voltage value has just penetrated completely between the suppressor wires, and has touched the plate. This occurs quite suddenly as observed in the electrolytic tank (compare Fig. 12). The average field gradient between  $G_2$  and plate has become zero. At plate voltages  $E_b > E_b''$ , the field between plate and  $G_2$  becomes accelerating.

At  $E_b = E_b''$ , the acceleration in the plate field has become equal in magnitude to the deceleration in the screen-grid field.<sup>4</sup>

The fourth and less distinct group-saturation value occurs when the penetrating plate-potential line extends as far as the screen grid. This is the case at  $E_b = E_b'''$ ; the entire field between  $G_2$  and plate has become accelerating so that no electrons are returning to the screen. The partial saturation voltages are easily expressed in terms of electrode potentials and forward- and reverse- $\mu$  values.

The apparent *one-half-power proportionality of current increments* to the plate voltage observed in three sections of the  $I_b - E_b$  characteristic is of particular interest. The electron "spray" in the decelerating suppressor field is caused by tangential-velocity components (compare Fig. 12). The deflecting force on electrons of given velocity having a tangential component decreases proportionately to the decelerating gradient.

The effective area enclosed by a penetrating potential line in and close to the plane of grids increases over a considerable voltage range substantially proportional to the one-half power of the voltage applied to the source or sources of the potential line. In the considered case the applied voltages  $E_{c1}$ ,  $E_{c2}$ , and  $E_{c3}$  are constant and the decelerating field is controlled by the plate voltage. Thus,  $\Delta i_p = KE_b^{1/2}$ . The factor  $K$  changes its magnitude at every partial saturation point.

Under *dynamic conditions*, the potential fields on each side of the screen grid are controlled by two respective voltages. Grid voltage and plate voltage vary with opposite signs. The plate-current increases with the three-halves or four-halves power of the grid voltage and approximately with the minus one-half power of the plate voltage (decreasing). As the plate-load value governs the plate-voltage change, it is possible to obtain sections with three-halves-, two-halves-, or one-half-power increments of current in the decreasing plate-voltage range as shown by the dynamic curves in Fig. 14(b). Due to this fact, pentodes are substantially free from high-order harmonic distortion when loaded properly.

#### E. Effects of Space Charge Between Screen and Plate of Power Pentodes

If the mesh of the suppressor grid  $G_3$  is made very fine (oversuppression), the plate current is decreased considerably at lower plate

<sup>4</sup> The value of  $E_b''$  was found to be approximately equal to the effective screen-grid potential in a number of pentodes. In tetrodes the minimum occurs in the center of the space between the screen grid and plate at  $E_b = P_{c2}$ . In pentodes, it does not necessarily occur in the plane of  $G_2$  due to space-charge effects which thus affect the value of  $E_b''$ .

voltages due to the low effective positive potential and its area in the plane of  $G_3$  (a high  $\mu$ -factor of the suppressor in both directions causes low plate impedance in the decelerating potential range). With a suppressor of coarser mesh, the effective positive potential area is increased and, consequently, the plate current and plate impedance are increased at low plate voltages. At the same time, however, the range  $E_p'$  to  $E_p''$  in which secondary-emission effects occur is moved to higher plate voltages and the potential minimum is reduced. The mesh of  $G_3$  is adjusted in practice so as just to eliminate secondary-emission effects under normal cathode-operating conditions (Fig. 5). The same tube, however, shows larger secondary-emission effects (under suppression) if operated with a temperature-limited (under-heated) cathode as shown in Fig. 15. This points out that *the electron*

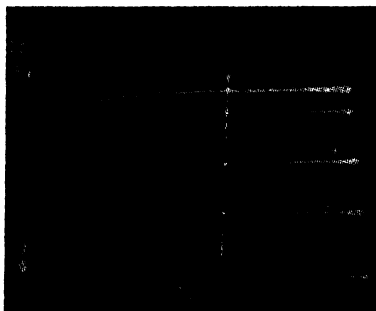


Fig. 15—Plate characteristics of typical power pentode operated with temperature-limited cathode ( $E_c = 0.4$  normal volt).

*space charge* near and between the grid wires of  $G_3$  under normal conditions reduces the space potential and *contributes to the suppression of secondary-emission effects*.

If the electron density is further increased, it does by itself become sufficiently large to produce a minimum potential in space between plate and screen, and thus suppresses secondary-emission effects without the help of a physical low potential source.

When the suppressor grid is replaced by space charge, the potential gradient at and in the direction of the plate never becomes negative in correctly designed tubes; thus, the curved section between  $E_p'$  and  $E_p''$  is eliminated as indicated by dashed lines in Fig. 14(a).<sup>5</sup>

<sup>5</sup> Some development work on replacement of the suppressor grid by space charge has been done in Europe, especially by Electric and Musical Industries, Ltd., in England. They have worked on tubes in which the suppression of secondary-emission effects is accomplished by space charge.

## V. THEORY AND DESIGN OF BEAM POWER TUBES WITH SPACE-CHARGE SUPPRESSION OF SECONDARY-EMISSION EFFECTS

### A. Plate-Current Characteristics of Tetrodes with Potential Minimum

Potential conditions in a decelerating field have been treated in a paper by Fritz Below.<sup>6</sup> The theory applies with modifications to the screen-plate section in tetrodes and pentodes, where we are interested especially in a definite and low saturation potential. Space-charge conditions at higher plate voltages are of equal importance in the design of power tubes. We shall thus examine the potential distribution in space with this specific purpose in mind.

#### 1. The Potential Minimum in Space

The space-charge density in a given electron current depends on the cross section of the electron path and the electron velocity. The potential distribution in space between positive grid and plate varies with distance as shown in Fig. 16(a). There are assumed constant cross section, constant current, and fixed electrode potentials as shown. The transit time of each electron is increased with greater distance between electrodes; hence, the number of electrons in the space between grid and plate is also increased and, consequently, the total negative electron charge which reduces the space potential. In the illustrated case the potential gradient at the plate becomes zero for  $d = d_2$ . For distances greater than  $d_2$ , a potential minimum is formed near the plate; the potential gradient at the plate has reversed sign and the field at the plate accelerates primary electrons. For the still larger plate distance  $d_4$  the potential value at the minimum  $M$  has decreased to zero.

The theoretical minimum distance  $d_{g-p}$  for the existence of a potential minimum at zero value in the ideal parallel-plane triode is equal to the cathode-grid distance, as illustrated in Fig. 8. It is seen that the minimum of zero value occurs at zero plate voltage and that no potential minimum is formed at low positive plate voltages. Hence, this distance is too short for suppression of secondary-electron effects.

The potential distribution with greater plate distances for a given current is shown versus plate voltage in Figs. 16(b) and 16(c). The minimum of zero value forms at  $E_b = E_m$ . Sufficient potential minima of positive value for suppressor purposes are produced with plate potentials having values between  $E_m$  and  $E_{b1}$ . For the shorter distance (Fig. 16(b)), the value  $E_{b1}$  is lower in potential than the accelerating-grid potential. The potential difference between plate and minimum is insufficient to repel secondary electrons from the plate for voltages be-

<sup>6</sup> "The theory of space-charge grid tubes," *Zeit. für Fernmeldetechn.*, vol. 9, pp. 113-118; August 29, (1928).

tween  $E_{b1}$  and  $E_{b2}$ . Secondary-electron effects are thus to be expected in this plate-voltage range, and are indicated in the corresponding plate characteristic. For the larger distance (Fig. 16(c)) a larger minimum of positive value is formed up to plate potentials higher than the accelerating-grid potential. The minimum potential in this case remains sufficiently lower with respect to the plate voltage to repel secondary electrons liberated at the plate.

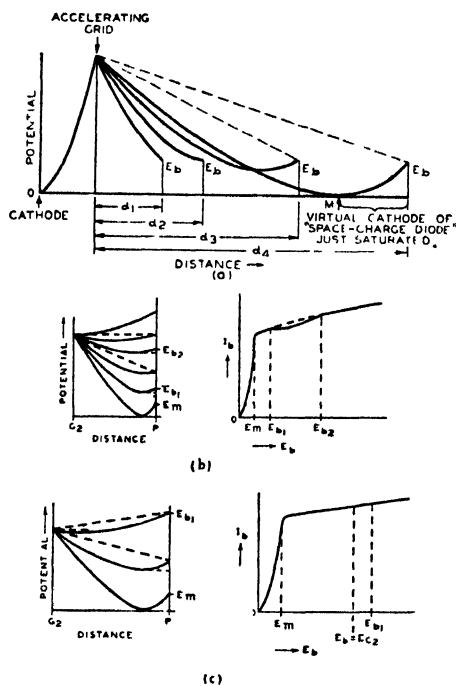


Fig. 16

- (a)—Potential distribution in space between accelerating grid and plate as a function of the distance between them (constant current to accelerating grid).  
 (b)—Plate current and space potential between accelerating grid and plate as a function of plate voltage for conditions where insufficient minima are formed.  
 (c)—Same as for (b), but for conditions where sufficient minima are formed.

Hence, the minimum plate distance for good suppressor action by the space charge is the distance for which the potential minimum remains at least ten to twenty volts lower than the plate potential. The minimum ratio of screen-plate distance to screen-cathode distance is  $\rho m = d_{g-p}/d_{g-k}$ . This ratio is considerably larger than unity for struc-

<sup>7</sup> B. Salsberg and A. V. Haef, "Effects of space charge in the grid-anode region of vacuum tubes," *RCA Rev.*, vol. 2, pp. 336-374; January, (1938).

tures with parallel or divergent electron beams, i.e., constant or increasing electron-path cross section in the direction of the plate. The actual value of  $\rho m$  depends on the electron density; hence,  $\rho m$  is larger for a larger angle of divergence and also larger for smaller values of plate current. In the equivalent triode, the ratio of  $\rho m$ , therefore, does not have one fixed value because it is a function of potentials and current. In the beam power tube, the *optimum* distance ratio has the value 2.9.

## 2. The Virtual Cathode

Assume that a constant supply of electrons having uniform velocity and perpendicular direction is maintained through a fine-mesh accelerating grid. All of these electrons reach the plate for voltages  $E_b > E_m$ : the primary electron plate current is constant. The plate saturation current may be decreased by a secondary-electron current in cases of insufficient potential minimum in space (Fig. 16(b)). In practical cases the electron supply to the screen increases with plate voltage, and causes a characteristic of finite impedance value for  $E_b > E_{bm}$ .

At  $E_b = E_{bm}$ , the electrons are just decelerated to zero velocity at zero potential. The condition in space at  $M$  (Fig. 16(a)) is termed "virtual cathode" as it has the criteria of a real cathode, i.e., zero potential and zero electron velocity. The virtual cathode is saturated and disappears at  $E_{bm}$  because the positive value of  $M$  for  $E_b > E_m$  indicates a finite velocity of all electrons which are able, therefore, to reach the plate.

A decrease in plate voltage to  $E_b < E_m$  seems to require a potential minimum of negative value. For zero electron velocity of emission at the real cathode, a minimum of negative value would stop the entire electron current to the plate; but electrons of zero initial velocity cannot form a space charge of negative potential value. The condition  $M=0$  at  $E_b < E_m$  can exist, however, for a lower plate current. The excess electrons at the virtual cathode are forced to return to the accelerating grid and increase the space charge between  $M$  and the screen grid. The consequent decrease in space potential causes the virtual cathode to recede from the plate. The plate current is space-charge limited in the voltage range  $E_b < E_m$ .

We are justified in treating the section consisting of virtual cathode and plate as a diode and in drawing the following conclusions:

- i. The steepness of the diode-current (plate-current) rise with plate voltage depends on the area of the virtual cathode and its distance from the plate. Close spacing or a large area of the virtual

diode causes high conductance with consequent low saturation potential, i.e., a "knee" of the plate-current curve at a low plate voltage.

ii. If a sharp knee is desired, the virtual cathode must saturate at a single plate-voltage value over its entire area. This requires uniform distance from the plate, as well as uniform density and velocity of all electrons forming the virtual cathode.

iii. The plate current is space-charge limited for plate voltages lower than the value necessary to saturate the virtual cathode and thus cause its disappearance.

(a) Virtual-Diode Spacing and Saturation Voltage  $E_m$ —Functions of Electrode Voltages

The electron supply to the virtual cathode can be varied in tetrodes by the control-grid voltage  $E_{c1}$  without altering the voltage on the

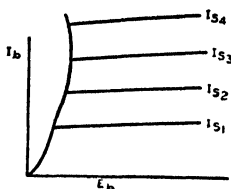


Fig. 17—Generalized "virtual-diode" characteristic.

positive grid  $G_2$ , or on the plate. The virtual-diode spacing is increased with larger currents (due to the higher space charge) and is decreased with smaller currents with corresponding changes of the saturation potential  $E_m$ . This change in perveance of the virtual diode as a function of the real cathode current explains the possible *crossover of the plate characteristics* at low  $E_b$  values for different values of the control-grid voltage at fixed screen potential (Fig. 20) and for different values of screen voltage with fixed control-grid voltage.

(b) The General Virtual-Diode Characteristic in Tetrodes

Although space-charge limited, the current does not increase in the range below  $E_m$  with the three-halves power of the plate voltage as in diodes with a real cathode, but follows a more complicated relationship as shown by the curve in Fig. 17. The conductance of the characteristic increases at some point to infinity and then becomes negative. Depending on the electron reserve and spacing, the virtual diode may saturate at any current value of the generalized curve. The peculiar relation of current and voltage is produced by the fact that the virtual-diode spacing is not fixed as in diodes with real cathodes. These conditions are analyzed in Figs. 18(a), (b), and (c).





and potential depression in the grid-plate space is decreased by the plate current and the equivalent decrease in reverse current due to fewer returning electrons. Hence the virtual cathode moves toward a position satisfying the decreased potential depression  $E_{v1}$ , which is a position closer to the plate. As the virtual-diode spacing is decreased, the plate current increases simultaneously and causes a further decrease of distance until a stable position is reached, shown as  $V_1$  in Figs. 18(a) and 18(b). If the electron reserve is not as large as shown, the virtual cathode will eventually saturate in such a stable position ( $I_{s1}$  and  $I_{s2}$  in Fig. 17). The case of a large saturation current is considered in the following, because it occurs with positive values of  $E_{c1}$  in the beam power tube (see Fig. 35).

The potential distribution (curve II in Fig. 18(a)) at  $E_b = E_2$  is critical.  $V_2$  has approached the plate sufficiently, so that the slightest increase in current starts a cumulative effect.  $V$  moves from position  $V_2$  towards the plate, an action which increases the perveance and, hence, the plate current until saturation occurs somewhat before reaching the position  $V_3$  (Figs. 18(a) and 18(b);  $E_2$  is higher than  $E_m$ ). Inasmuch as a stable minimum of zero value cannot be maintained by the plate voltage  $E_2$  (only by the lower voltage  $E_m$ ), the potential distribution changes to the stable curve III with a minimum  $M_2$  of positive value. The jump of the minimum from zero to  $M_2$  causes a plate-current increase  $\Delta I_b$  (Fig. 18(c)), which is not the case under ideal conditions, but always true in practical tubes. Some electrons have lower velocities than others, due to differences in initial velocity at the real cathode, and especially due to tangential components obtained during their flight through the structure. These slower electrons are unable to pass a minimum of low absolute potential but gradually reach the plate as the plate voltage is increased. A further cause is the finite value of the amplification factor  $\mu = -\partial e_p / \partial e_g$ .

With further increased plate voltage, the minimum recedes from the plate (see Figs. 18(a) and 18(b)). It occurs near the center (exactly at the center in ideal parallel-plane tubes) for  $E_b = P_{\sigma 2}$  and then disappears for voltages higher than  $E_6$ .

When the plate voltage is decreased, the plate current remains at saturation value and is stable until the minimum potential reaches zero value ( $M_0$ ). This occurs with  $E_b = E_m$ , and is shown by curve IV in Fig. 18(a). A virtual cathode forms; the slightest decrease of plate current forces  $V$  to move away from the plate. This action becomes cumulative until the stable position  $V_4$  (Fig. 18(b)) of high space-charge density is reached. The plate current drops suddenly to the value marked  $V_4$  in Fig. 18(c).

## (c) Optimum Plate Distance in Power Tetrodes

The control-grid voltage in power tetrodes varies the saturation current. It is best to saturate the virtual cathode at the value  $I_{s3}$  of Fig. 17 for zero control-grid voltage because the potential minimum  $M_0$  is then stable and occurs close to the plate. The saturation potential  $E_m$  of the virtual diode in power tetrodes is the plate-voltage value at which the "knee" occurs. At plate voltages  $E_b > E_m$  but  $< E_{c2}$ , a potential minimum of a least ten to fifteen volts less than plate potential must be formed between screen and plate in order to suppress secondary-emission effects. The virtual cathode is not a necessity for suppressor action but is formed eventually in all cases where a potential minimum is obtained at higher voltages.

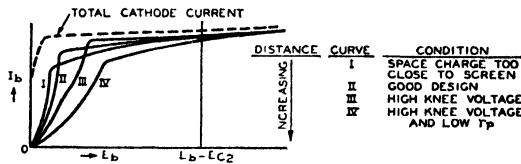


Fig. 19—Effects of plate-to-screen-distance variation on the plate characteristic in tetrodes having electrons with tangential components.

High plate currents at low plate potentials with respect to the screen potential require that the distance from virtual cathode to plate be short and uniform in order to obtain saturation at *one low plate-voltage value*. The plate distance can be made longer, if the area of the virtual cathode is increased which would indicate the use of a divergent electron path (wide beam angle) and circular structures. The potential *minimum after saturation should occur, however, closer to the plate* than to the screen and *should not be of large cross-sectional area*, to prevent a steep decelerating field. The latter undesirable condition is obtained either with very short plate distances and extreme electron densities or in circular structures with wide-angle electron beam and moderate electron densities. It causes high screen current and low plate impedance similar to high forward- $\mu$  suppressor grids located in pentodes too close to the screen grid. For these reasons circular structures with larger plate distances have been found unsatisfactory. The design of the structure for the saturation current  $I_{s3}$  in Fig. 17 results in a low saturation potential with high current due to the high diode conductance and causes the formation of a potential minimum sufficient for suppression of secondary-emission effects. The optimum distance ratio for the beam power tube (see page 156) is  $\rho_{opt} = 2.9$ . The beam angle is approximately 60 degrees. The curves I to IV in Fig. 19 illustrate the effects of plate-to-screen-distance varia-

tion in tubes having electrons with tangential components. The curves are understood from the aforesaid. Oscillogram checks for plate diameter changes in the beam power tube are shown in Fig. 20.

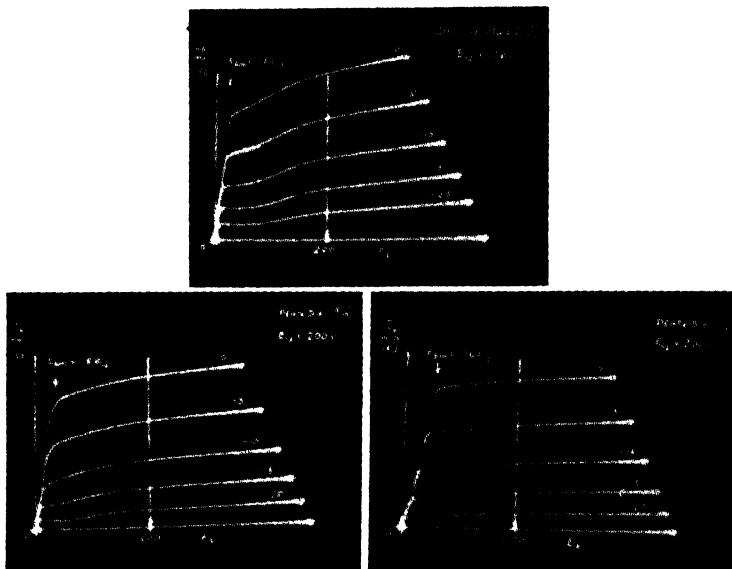


Fig. 20—Oscillograms showing plate characteristics for beam power tubes having different plate diameters.

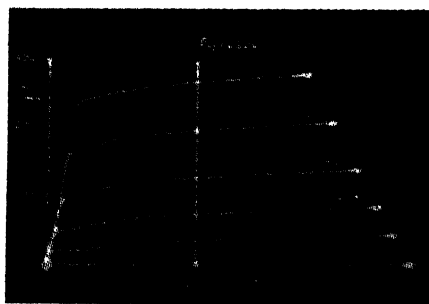


Fig. 21—Plate family of type 6L6 beam power tube.

## B. Beam Formation and Structure of the Beam Power Tetrode

### 1. The Electron Beam in a Radial Plane

#### (a) The Beam between Accelerating Grid and Plate

It is essential to maintain electron direction and *density perfectly uniform* in any cross section of the electron path at any distance from

cathode or plate to approach the theoretical performance discussed in the preceding section. The electron current is thus formed into a beam with definite properties.

The beam density at saturation current for the condition  $I_{s3}$  in Fig. 17 was found to be 28 milliamperes per square centimeter at the plate for  $E_{c2}=250$  volts and  $E_{c1}=0$  volts. The restriction of the electron beam to a section of a cylindrical structure with large radius is necessary to obtain high plate impedance and low screen current.

A series of tests has shown that the desirable relatively short plate distance will invariably cause a serious loss of plate current, a badly rounded "knee," or give rise to secondary-emission effects, unless the *utmost care is taken* in the design of the entire electrode structure to produce and maintain at low plate voltages a uniform electron beam that neither spreads nor compresses and has the required density and

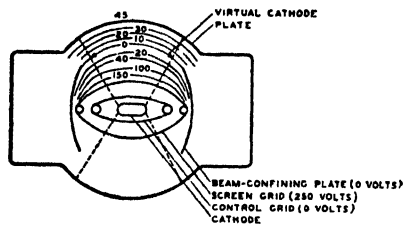


Fig. 22—Cross section and potential plot of beam power tube.

cross section when decelerated. The horizontal-beam cross section and location of the virtual cathode at saturation voltage in the beam power tube are indicated in the sectional view of the beam power-tube structure in Fig. 22.

In the screen-plate space, the electron beam in a radial plane is confined to a sector by two "beam-confining" plates at cathode potential. Virtual cathode and potential minimum stop secondary electrons from the plate. The beam-confining plates continue this potential barrier outside of the electron stream and prevent the return of secondary electrons along the sides of the beam. Ideal beam-confining plates should terminate all potential lines abruptly without distorting their uniformity. Shape and spacing of the actual plates is thus adjusted for best termination of the potential lines on the beam borders at low plate-voltage conditions. The edges of the plates point to the zero-potential plane of the virtual cathode at saturation potential: A mechanical analogy for explaining the shape of the radial field would be a tapered chute with bent-up sides and a curved bottom. The model in Fig. 25(b) shows the smooth bottom of this "chute."

### (b) The Beam between Cathode and Screen Grid

Having provided a suitable radial path for the electrons beyond the screen, we must further supply an electron stream of uniform density and velocity to the plane of the screen. Starting at the cathode, we must maintain the electron-beam density at any distance from the cathode substantially constant over the sector width by adjusting the *radius of curvature of the grids*. The sectional view in Fig. 22 shows that the radius of curvature of the electrodes is *decreasing* with distance. This is because a radius correction is necessary to compensate for

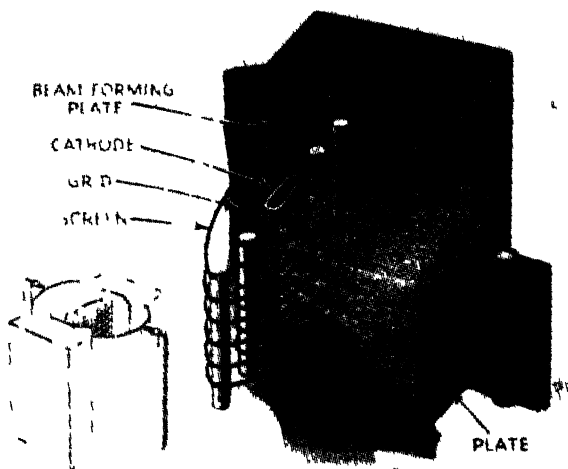


Fig. 23—Beam formation in type 6L6 beam power tube.

side-rod effects. The *flattened cathode* gives a more uniform and larger effective area than a round cathode with consequent gain in transconductance and power sensitivity. Spacing and cross section of the *grid side rods*, especially of the control grid, determine the beam angle and thus are fixed for a given current density in the decelerating field. With negative control-grid voltages, the beam angle is reduced by the control-grid side-rod field and thus some secondary electrons from the plate travel to the screen grid along the edges of the beam. This can be prevented but is unnecessary in a power tube.

### 2. The Beam Formation in a Longitudinal Plane

#### (a) Subdivision of Cathode Current by Grid Wires into Directed Beams of Disk-Sector Shape

If the resultant field in the control-grid plane is positive, electrons leave the space-charge cloud at the cathode and travel with increasing

velocity in a path which approaches the position of a flux line. In tubes with negative control-grid voltage, the entire electron stream is divided into definite beams. In conventional tubes, no attempt is made to direct these beams, with the result that the electron streams have varying density and direction (see Fig. 12). These undirected beams of emission are responsible for a considerable absorption of electrons at the screen and a large variation of electron direction in the decelerating field beyond the screen, which causes gradual saturation no matter how uniform the electrostatic field is made in the space between screen and plate.

The misalignment of grid wires (see Fig. 12) in conventional pentodes permits electrons to pass at any point between the screen wires; the potential in the plane of  $G_2$  varies more than 50 volts. In the case shown, four beams are formed within one period of grid-wire alignment. The main beam area is shaded. Two of the main beams pass between the wires of  $G_2$  and only stray electrons are intercepted directly. The other two beams, however, hit the wires of  $G_2$  which intercept approximately 25 per cent of the beam current. The screen current intercepted directly is thus approximately 12.5 per cent of the cathode current. This value is obtained only at high plate voltages where all electrons passing the screen are collected by the plate. At lower plate voltages, electrons with tangential components fall back into the screen grid. For the particular tube and voltage shown, they amount to 20 per cent of the cathode current. Thus, the screen collects approximately one third of the total cathode current for the condition shown. To prevent serious overheating of the bombarded screen wires, the grids are wound with opposite thread so that the bombarded length of wire per turn is reduced and so that the total bombarded length is distributed over more turns.

*Directed electron beams are formed* when the entire length of all screen wires in the electron current is positioned in the electrical shadow of the control-grid wires. Certain distance relations are necessary to maintain a narrow beam width between the wires of  $G_2$  within the range of the variable control-grid voltage of power tubes in order to minimize screen current, and prevent serious divergence of electron paths at low plate voltages in the decelerating field beyond the screen.

The control-grid voltage governs the focal length of the beams, and thus their divergence for given electrode and grid-wire distances. Simultaneous adjustments must be made when designing the tube structure because control-grid voltage, plate current, and beam focus depend on the same physical space relations between grid wires, grids, and cathode.

## (b) Advantages of Directed Beam Formation

i. Substantially uniform current density and electron direction at the virtual cathode in a direction parallel to the cathode axis is obtained. (The beams meet. See Fig. 24.)

ii. The low screen dissipation increases the efficiency of the tube.

iii. The low screen current gives an unusual flexibility of operating conditions, as the screen voltage can be stabilized with bleeders of low power dissipation.

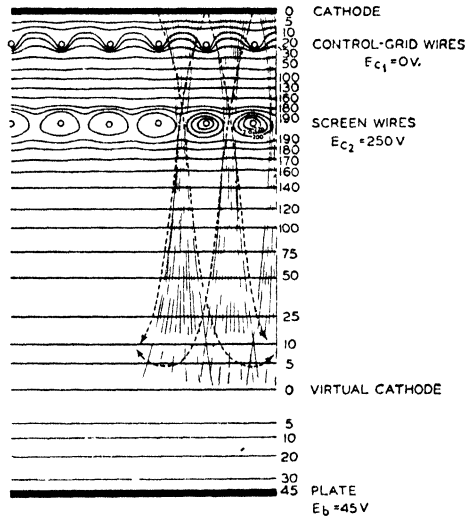


Fig. 24—Potential field of type 6L6 beam power tube for the condition of virtual-cathode saturation.

iv. Higher screen-voltage ratings are permitted with consequent increase in power output.

v. The power sensitivity can be increased without danger of grid emission, because the screen temperature is low.

vi. The field distribution parallel to the axis of the cathode is more uniform at the cathode than in tubes with grids of different pitch and periodic misalignment of grid wires. This uniformity permits obtaining higher transconductance values with good plate-current cutoff.

## (c) The Beam Formation in the Beam Power Tube

Developmental power tubes have been constructed with individual beams of long focal length formed by negative grid wires and sharply focused between the positive screen wires. The screen-grid current at the operating point was reduced to less than two per cent of the plate-

current value. The spacing requirement is, however, not suitable for high power sensitivity.

The distance between control grid and cathode is determined by the power sensitivity, and the control-grid pitch and wire size by the cutoff characteristic, as explained later. *The formation of directed beams requires equal pitch of control and screen grid.* Hence, for a given set of the above conditions, the distance ratio of  $d_{G1-G2}$  to the pitch distance is the main variable. It determines the focal length of the beams and also plate-current, screen-current, and control-grid voltage. In order to satisfy also the requirements for grid side-rod spacing, radius of curvature, power-dissipation capability of the plate, and low grid emission, a balance of the various tube properties is necessary to result in a generally desirable structure.

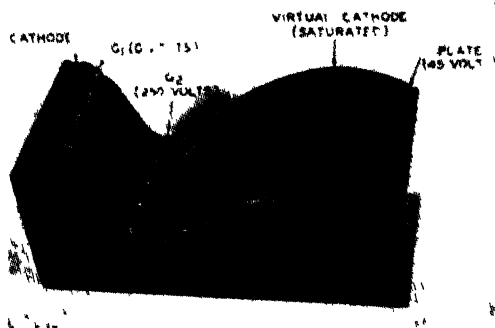


Fig. 25—Topographic model of potential field shown in Fig. 24.

An artist's sketch of the total beam formation in the beam power tube at a low plate voltage is shown in Fig. 23. The control-grid beams have the form of sheets. The dense area near the plate indicates the location of the virtual cathode also shown in Fig. 22. The cathode current is split up into two groups of 43 narrow beams. The ratio of the grid distance ( $d_{G1-G2}$ ) to the grid-wire spacing is 1.4.

The potential field of the beam power tube and a topographic model are shown in Figs. 24 and 25. The uniformity of the field between screen grid and plate is apparent. The plate voltage shown is the saturating potential (45 volts) of the virtual cathode (knee), and thus the hill in front of the plate has an elevation just equal to that of the cathode. The control-grid mountain peaks (shown for zero grid voltage) direct the electron "balls" towards the narrow ridge between the screen-grid holes. Less than nine per cent of the electrons at the sides of the beams is deflected from a linear path by the conical holes, loses radial velocity,



and turns back from the virtual-cathode hill to the screen. About three per cent of stray electrons is intercepted directly. All others have just sufficient momentum to roll over the virtual-cathode hill to the plate. With increased plate voltage ( $E_b > 45$  volts), the elevation of the plate decreases (in the model) as does also that of the potential minimum in front of the plate. The electrons including those with tangential components pass easily over the lower hill in front of the plate but hit the plate with considerably more impact. The hill in front of the plate, however, prevents them from bounding back and rolling back to the screen valley. In an actual tube, however, the primary electrons stay bound at the plate, but secondary electrons are knocked off and are the ones which are prevented from reaching the screen valley.

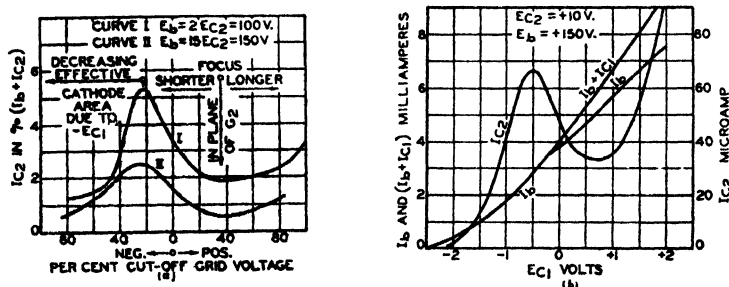


Fig. 26

- (a)—Changes of beam focus and current intercepted by the screen as a function of control-grid voltage in a beam power tube.  
 (b)—Current distribution in a beam power tube as a function of control-grid voltage.

The beams come to a focus in the plane of the screen grid with a positive control-grid voltage, and cause a screen-current minimum (see Figs. 26(a) and 26(b)). The focal length is decreased with increased negative control voltages. Consequently, the beam width in the plane of  $G_2$  is increased. The increase of  $I_{c2}$  is, however, checked by the decrease in effective cathode area opposite the grid-wire space due to cutoff conditions. This narrows the convergent angle so that the divergence and beam width beyond the focus actually reduce for high bias values with consequent low current absorption. A low screen voltage and high plate voltage were used in obtaining the curves of Figs. 26(a) and 26(b) to minimize secondary-emission effects from the screen.<sup>a</sup>

<sup>a</sup> I am indebted to Mr. H. C. Thompson, who has studied beam principles for many years in our laboratory, for his explanation of beam theory. His paper, "Electron beams and their applications in low voltage devices," appeared in the Proc. I.R.E., vol. 24, pp. 1276-1297; October, (1936).

The transfer characteristic of the tube follows the square law in order to reduce third-harmonic distortion. The control-grid-wire distance from the cathode was made shorter than the grid-wire spacing (ratio 2 to 3) so as to cause the effective area of the control potential to vary substantially with the one-half power of the applied control-grid voltage as pointed out in the discussion of the pentode plate char-

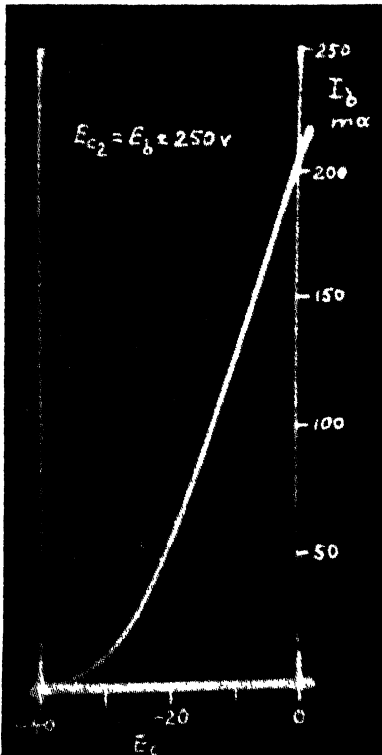


Fig 27—Transfer characteristic of type 6L6 beam power tube

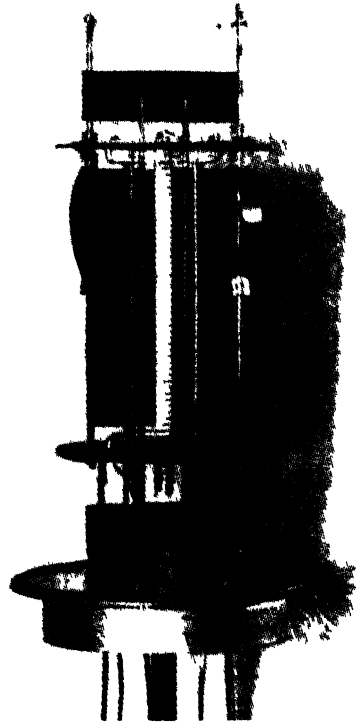


Fig. 28—Type 6L6 with cutaway plate to show grid-wire alignment.

acteristic. The desired result is obtained because the positive potential source (the screen) remains at a fixed potential and because side-rod effects are compensated for by electrode shape adjustment. An oscillogram of the transfer characteristic is shown in Fig. 27.

The *plate characteristics* of the beam power tube are shown in the oscillogram in Fig. 21. Insufficient minimum potentials are indicated at highly negative grid voltages by the presence of secondary-emission effects but they have no harmful consequences inasmuch as this section of the plate characteristics is not utilized in practical operating

conditions. Although the beam power tube was designed for operation with screen voltages between 250 and 300 volts, it may be operated within a wide screen-voltage range without substantial performance loss.

The beam power tube is the first tube in large quantity production to utilize grids in register. The alignment is held at present within 0.004 inch for all grid wires. This corresponds to a screen-current variation of from four to ten per cent of the plate current at the normal operating point. In the side view with cutaway plate in Fig. 28, the tube appears to have only a single grid on account of the exact alignment of the two grids. This precision is obtained by means of a high degree of accuracy in maintaining a constant pitch angle in the manufacture of both grids. The grids are aligned mechanically and all side rods are anchored to weld lugs clamped in a "terminal board" mica which positions and supports the electrodes rigidly. Two heat radiators maintain the control-grid temperature at a low value to minimize grid emission under all operating conditions within the rating of the tube.

It is thus found that directed electron beams obtained by electrical focusing with properly chosen grid wires, grid side rods, beam-confining plates, and electrode shapes will produce an electron stream of nearly ideal properties with respect to uniformity of electron direction and velocity, and that substantially theoretical performance may be obtained with tubes in which these beams are used. In the beam power tube, slow electrons and those having large tangential components are substantially prevented by beam formation; hence, large plate spacings are not required, wasteful screen current is avoided, and improved plate efficiency is obtained. In this beam power tube it was found practical to suppress secondary-emission effects by space charge.

Tubes which do not utilize carefully directed electron beams, but use the space-charge type of secondary-emission suppression, require long distances between screen grid and plate for satisfactory results and have been found to show little improvement over existing commercial pentodes. Such tubes with a large screen-to-anode distance, may be made to have a characteristic with a fairly defined knee occurring at somewhat higher voltages than in a beam tube, but the magnitude of the screen current at lower plate voltages prevents highly efficient tube operation. Tubes of this type with long distance between screen grid and anode have been discussed by J. H. O. Harries<sup>9</sup> of London, England, in recent articles.

<sup>9</sup> "Critical distance tubes," *Electronics*, vol. 9, p. 33; May, (1936).

## VI. THE PERFORMANCE OF THE BEAM POWER TUBE

### A. Single-Tube Operation

#### 1. Distortion, Efficiency, and Ratings

The harmonic distortion of a single tube is of substantially second-harmonic order, and decreases linearly with signal according to theory. Higher orders than the third are negligible (see Figs. 29(a) and 29(b)). The percentage of second harmonic is comparatively large if the grid

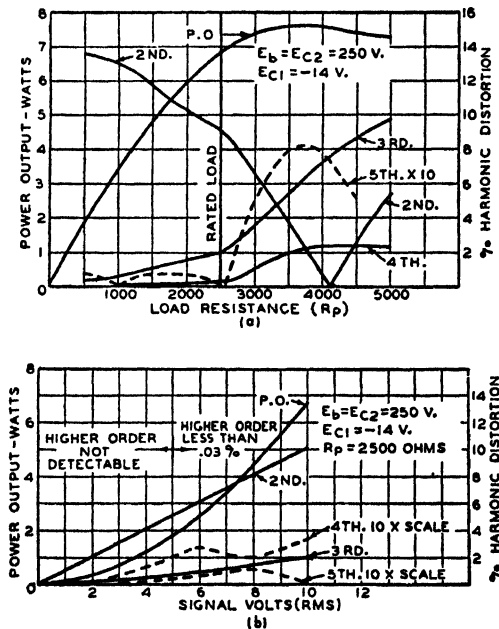


Fig. 29

- (a)—Harmonic distortion and power output as a function of load resistance for type 6L6 at peak input signal volts equal to the grid-bias voltage.  
 (b)—Harmonic distortion and power output as a function of input signal voltage for type 6L6 with 2500-ohm load.

bias is selected for high efficiency as shown in Fig. 30(a) by the values calculated from the ideal characteristic of parallel straight lines with square-law spacing. A comparison of actual tube performance (Fig. 30(b)) with these values shows better efficiency at the same values of second-harmonic distortion because a small value of third-harmonic distortion has been intentionally allowed by designing the plate characteristic as shown by curve II in Fig. 19.

Various measurements have proved that it is always possible to reduce the total distortion to six per cent or less with resistance-coupled

preamplifiers (triodes or pentodes) by generating in these amplifiers operated with reduced plate loads a canceling second harmonic of sufficient magnitude. A third harmonic produced in preamplifiers is usually additive to the third harmonic in the output stage except in special operation of push-pull preamplifiers.

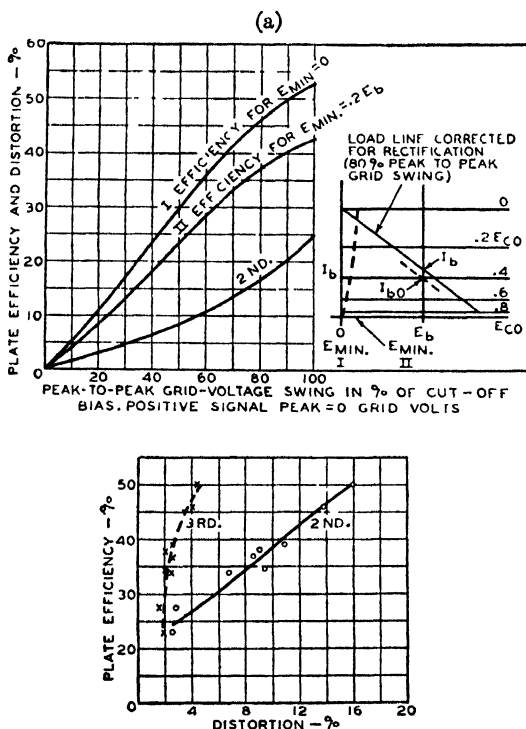


Fig. 30

- (a)—Performance of hypothetical screen-grid tube with linear characteristics and square-law transfer characteristic.
- (b)—Performance of beam power tube for various operating conditions at maximum signal input without grid current.

The flexibility of screen-voltage values permitted by the low screen current results in large power-output ratings as well as high power sensitivity as tabulated in Table I.

In contrast to standard practice for pentodes, the plate load is not selected for minimum total distortion (Fig. 29(a)), but for a minimum of higher-order distortion in accordance with the previous discussions, because the design of the tube allows nearly maximum power output to be obtained with such loads.

TABLE I

Static and Dynamic Characteristics						
Heater voltage	6 3 volts					
Plate voltage	250 volts					
Screen voltage	250 volts					
Grid voltage	-14 volts					
Amplification factor	135					
Plate resistance	22500 ohms					
Transconductance	6000 micromhos					
Plate current	72 milliamperes					
Screen current	5 milliamperes					
Single-Tube Class A1 Amplifier*						
Plate voltage	375 max volts					
Screen voltage	250 max volts					
Plate and screen dissipation (total)	24 max watts					
Screen dissipation	3 5 max. watts					
Typical operation						
Heater voltage	6 3		6 3		6 3	
Plate voltage	375		250		300	
Screen voltage	125		250		200	
	<i>Fixed Bias</i>	<i>Self-Bias</i>	<i>Fixed Bias</i>	<i>Self-Bias</i>	<i>Fixed Bias</i>	<i>Self-Bias</i>
Direct grid voltage	-9	—	-14	—	-12 5	—
Self-biasing resistor	—	365	—	170	—	220
Peak audio-frequency grid voltage	8	8 5	14	14	12 5	12 5
Zero-signal direct plate current	24	24	72	75	48	51
Max-signal direct plate current	26	24 3	79	78	55	54 5
Zero-signal direct screen current	0 7	0 7	5	5 4	2 5	3
Max-signal direct screen current	2	1 8	7 3	7 2	4 7	4 6
Load resistance	14000		2500		4500	
Distortion						
Total harmonic	9		10		11	
2nd harmonic	8		9 7		10 7	
3rd harmonic	4		2.5		2.5	
Max-signal power output	4 2		6.5		6.5	
Plate and screen efficiency (total) . . .	42 43		30		37 2	
					43 per cent	

\* Suffix 1 indicates that grid current does not flow during any part of the input cycle.

## 2. Overload Characteristics

In all ideal audio-frequency amplifier tubes, whether triodes or pentodes, the efficiency has reached the maximum value of 50 per cent with normal operating conditions and zero peak grid volts. A so-called "smooth overload" characteristic as obtained in tubes having low efficiency at the rated output value is thus not obtainable in class A operation for audio-frequency purposes. An analysis of the ideal triode characteristic shown in Fig. 2 shows that distortion at the grid-current point is very small and rises steeply for further increases in signal voltages because the plate voltage at the current maximum can only increase 50 volts at most. This fact is not altered by the assumption of a control grid which draws no current even with high positive grid voltages.

The plate-current knees in the beam power tube occur at a low plate voltage. A high plate load intersects a knee of a negative-control-grid-voltage line. The corresponding peak swings of voltage and current do

not increase any further with larger grid signals, although these may be negative. Power output and efficiency are increased but at the expense of higher distortion because plate-efficiency values over 50 per cent require that the wave approach a "flat-topped" or square form.

## B. Push-Pull Operation

### 1. General Discussion of Push-Pull Amplifiers Having High Power Sensitivity.

Push-pull amplifiers are used in radio receivers not only for balancing out various current components in transformers and load, but also to obtain low distortion and increased efficiency of tube and circuit operation. It is highly important to analyze the performance of hypothetical tubes with high power sensitivity in amplifier circuits having commercially obtainable power supply regulation.

#### (a) Triodes

The dynamic characteristic of triodes having a constant  $\mu$  and a plate impedance much lower than the plate load (as, for instance, the ideal tube shown in Fig. 2) is substantially linear. The resultant characteristic of two tubes in a push-pull circuit is thus represented by the geometric addition of two straight lines. Fig. 31 shows the joined characteristics for five distinct operating points. Dotted lines mark the grid-current point. Conditions 1 and 2 show class A1 operation; condition 2 is for class A1 operation with minimum plate current. Both conditions give zero distortion. The power output and efficiency of condition 1 is naturally less than for condition 2 which is limited to 50 per cent efficiency. Class AB1 operation, as shown in condition 3, has still higher efficiency because  $I_{b0}$  is lower than  $\frac{1}{2} I_{max}$ . The breaks in the curve, however, cause distortion including high orders. Condition 4 shows the very critical class B1 operation having zero distortion and a maximum theoretical efficiency for ideal audio amplifiers of 78.6 per cent.

In practical amplifiers the supply voltages vary with current increments because of imperfect regulation. The operation of ideal triode amplifiers is thus limited to class A conditions. A pair of hypothetical triodes (Fig. 2) operated as push-pull class A1 amplifiers at maximum efficiency as in Fig. 31, condition 2, requires a direct grid voltage ( $E_c$ ) of -37.5 volts and a plate voltage ( $E_b$ ) of 400 volts for 35 watts output with 51 per cent plate efficiency and negligible distortion. The characteristic (Fig. 2) of these hypothetical tubes was constructed to obtain a performance approximately equal to the beam power tube. Because of the high triode conductance, the plate-current increment due to signal is sufficient to shift the operating point to zero plate

current (Fig. 31, condition 4), if the plate-voltage regulation is 6.25 per cent.

It can be shown that self-biased operation of these tubes requires a minimum plate current of 85 milliamperes per tube in order to prevent complete cutoff (condition 5) at full signal. The rectification in actual tubes would be larger and the obtainable efficiency would be reduced

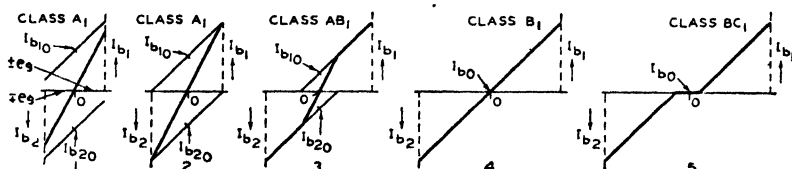


Fig. 31—Push-pull characteristics for triodes having linear dynamic characteristics.

to the order of 35 per cent because the required operating condition would necessitate a higher plate current and cause higher plate dissipation.

#### (b) Pentodes and Beam Power Tubes

For equal power sensitivity the stability of the operating point is considerably better in tubes with accelerating grid. The screen prevents the control of the plate voltage over the plate current and thus the required transconductance for equally good efficiency and power sensitivity is considerably lower than in triodes.

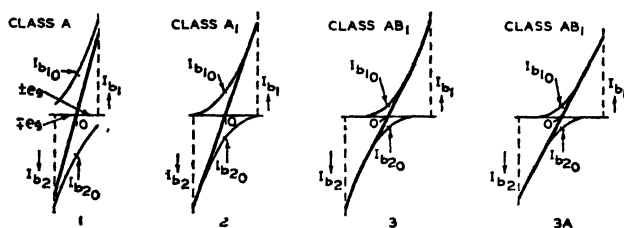


Fig. 32—Push-pull characteristics for ideal pentodes having square-law dynamic characteristics (sketches 1, 2, and 3); push-pull characteristic of beam power tube (sketch 3A).

The dynamic transconductance obtained with two of the new beam power tubes in push-pull is 4000 micromhos per tube while that of the equivalent hypothetical triode would have to be 56,000 micromhos.<sup>10</sup>

<sup>10</sup> It can be shown that for a triode power tube to equal the performance of a pentode power tube the following ratio holds:

$$\frac{g_m (\text{triode})}{g_m (\text{pentode})} = \frac{2(E_{b0} - E_{bm})}{E_{bm}}$$

For  $E_{b0} = 400$  volts and  $E_{bm} = 50$  volts, we obtain  $g_m (\text{triode}) = 14 g_m (\text{pentode})$ .



The curvature of a high-impedance plate characteristic is *not* straightened out by the plate load. This permits operation with smaller quiescent plate currents and thus higher efficiency, as illustrated in Fig. 32. The resultant characteristic from two square-law curves is linear for the class A1 operating conditions 1 and 2. The overbiased operation in condition 3 does not cause high-order distortion because the curve does not have sharp breaks.

In the design of the beam power tube the plate characteristics in the low plate-voltage range are so adjusted that the distortion minimum (0.8 per cent) is obtained in push-pull class AB1 operation with a quiescent plate current of 28 milliamperes per tube, i.e.,  $I_{b0} = 0.14 I_{max}$  at  $b_{c1} = 0.625 \phi E_c$ . The high-current end of each individual dynamic characteristic is straightened out by the plate load so that only the square-law sections of the individual characteristics have to be overlapped (3A in Fig. 32). Class A1 operation of these tubes causes an increase in distortion to two per cent which, due to the absence of higher orders, is not objectionable. Plate-current increments above the knee are substantially proportional to the one-half power of the plate voltage over the range in which a potential depression is caused by space charge between  $G_2$  and the plate.

## *2. Performance of Beam Power Tubes in Conventional Push-Pull Service*

The new all-metal beam power tube is designed for class A1 and class AB1 operation.<sup>11</sup> Two self-biased tubes in push-pull class AB1 are capable of delivering without grid current a power of 32 watts with 58 per cent plate-plus-screen-power efficiency, and 54 per cent direct-current-power efficiency including self-biasing power. Including heater power, the total circuit efficiency is 45 per cent. Distortion has the small value of one to two per cent and is of substantially third-harmonic order. Other harmonics are small fractions of one per cent, no larger or of higher order than found in the output of push-pull low-impedance triodes.

With only 350 milliwatts peak grid power, a power output of 60 watts with two per cent plate distortion and with efficiency similar to that just given is obtained in class AB2 operation for use in large sound systems. Operation with grid current is not recommended for high quality reproduction due to the generation of higher harmonics in the grid circuit. The small grid power permits a driver design of low distortion.

The cathode is of the indirectly heated type operating with 6.3 volts alternating or direct current and 0.9 ampere, i.e., 5.7 watts.

<sup>11</sup> The tube has been made available under the type number 6L6.

Correct self-bias operation is highly efficient and does not require good supply-voltage regulation, as may be seen from the table comparing fixed-bias and self-bias operation in Table II. The self-bias

TABLE II

Push-Pull Class AB1 Amplifier					
Plate voltage.....					400 max. volts
Screen voltage.....					300 max. volts
Plate and screen dissipation (total).....					24 max. watts
Screen dissipation.....					3.5 max. watts
Typical operation—2 tubes:					
Values are for 2 tubes					
Heater voltage.....	6.3	6.3	6.3	6.3	6.3 volts
Plate voltage.....	400	400	400	400	400 volts
Screen voltage.....	250	250	300	300	300 volts
	Fixed	Fixed	Self-	Self-	Fixed
	Bias*	Bias	Bias	Bias	Bias*
Direct grid voltage.....	-20	-20	-25	—	-25 volts
Self-biasing resistor.....	—	—	—	200	— ohms
Peak audio-frequency grid-to-grid voltage.....	40	40	43.8	50	57
Zero-signal direct plate current.....	88	88	96	102	112
Max.-signal direct plate current.....	126	124	110	152	128
Zero-signal direct screen current.....	4	4	4.6	6	7
Max.-signal direct screen current.....	9	12	10.8	17	16
Load resistance (plate to plate).....	6000	8500	—	6600	3800
Distortion:					
Total harmonic.....	1	2	—	2	0.6 per cent
3rd harmonic.....	1	2	—	2	0.6 per cent
Max.-signal power output.....	20	26.5	24	34	32
Plate and screen efficiency (total).....	38	50.5	52	51.5	58
					23 watts
					35 per cent

\* Plate load decreased to permit operation with grid current.

resistor is selected such that the plate and the screen rectification at full signal do not shift the bias beyond the value of minimum distortion and highest efficiency. Because of the high power sensitivity, the voltage changes are small causing but a slight decrease in power output. The amplitude distortion of  $-0.8$  decibel in input voltage due to the self-bias shift is not detectable by the ear.

The advantages offered by push-pull amplifiers utilizing tubes with accelerating screen grids are augmented by the use of beam power tubes. Owing to their characteristics and their precision of manufacture, it is possible to obtain substantially the same performance in the practical use of beam power tubes as is obtained under ideal conditions. No matching of beam power tubes is required.

## C. Circuits with Inverse-Voltage Feedback for Adjustment of Tube Impedance

### 1. Theory

Low plate impedance has been shown to be inconsistent with regard to design and operation of practical highly efficient power tubes. As low plate impedance is, however, one of the specified properties of an ideal power tube, circuit means for changing the effective plate impedance of tubes were investigated.

The plate impedance of a vacuum tube is defined as  $r_p = d_{e_p}/d_{i_p}$  and measured by the ratio  $\Delta e_p/\Delta i_p$ . If the increment  $\Delta e_p$ , or a percentage of  $\Delta e_p$ , in the plate circuit is coupled back into the grid circuit, it will increase or decrease the plate-current change  $\Delta i_p$ , depending on the phase of the feedback. If, furthermore, the phase of the feed-back voltage is in opposition, i.e., "inverse," to the grid-voltage change which causes the plate-voltage change  $\Delta e_p$ , stable operation is obtained; the circuit is not regenerative.

The circuit in Fig. 33(a) has 100 per cent inverse-voltage feedback. If a voltage increment  $+\Delta e_p$  is produced in the circuit branch normally containing the load resistance, the plate-current increment without

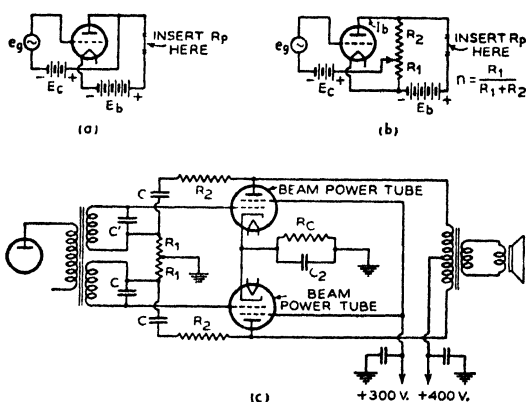


Fig. 33

- (a)—Circuit for 100 per cent conductive feedback ( $n=1$ ).  
 (b)—Circuit with adjustable conductive inverse feedback ( $n < 1$ ).  
 (c)—Practical inverse-feed-back circuit utilizing push-pull beam power tubes.

$R_1 = 10,000$  } or  $5000$  } for 10 per cent feedback  
 $R_2 = 90,000$  }

$R_G$  = self-bias resistor

$C = 0.1$  microfarad or larger

$C'$  = value depends on secondary impedance of transformer and should be determined by test. Large values require a series resistor to prevent transients.

$C = 35$ -volt electrolytic condenser (50 microfarads).

feedback is  $+\Delta i_{p1} = +\Delta e_p/r_p$ . Due to the feed-back connection, however, the grid voltage is changed simultaneously by the increment  $+\Delta e_g = +\Delta e_p$ . This causes a further plate-current change  $+\Delta i_{p2} = \Delta e_g \times g_m$ , and thus

$$\Delta i_p = \Delta i_{p1} + \Delta i_{p2} = \Delta e_p (1/r_p + g_m).$$

The resultant value of plate resistance is thus

$$r_{p(r)} = \frac{1}{1/r_p + g_m} = \frac{r_p \times 1/g_m}{1/g_m + r_p} = r_p \parallel 1/g_m.$$

The feedback causes an effective shunt  $r_p' = 1/g_m$  across the actual plate impedance. The new resultant value  $r_{p(r)}$  in this circuit requires a change in magnitude of amplification factor in order to satisfy the tube equation  $\mu = g_m \times r_p$ . Because the plate and grid circuit do not contain any common resistances,  $g_m$  remains constant and thus the resultant amplification factor ( $\mu_r$ ) is

$$\mu_{(r)} = g_m \times r_{p(r)}$$

which can be written

$$\mu_{(r)} = \mu / (1 + \mu).$$

The feedback  $n$  in this circuit is unity. Less feedback ( $n < 1$ ) results in smaller changes of  $r_p$  and  $\mu$ , because in general

$$r_{p(r)} = r_p \parallel \frac{1}{n \times g_m}$$

where  $n$  = feed-back factor, and

$$\mu_{(r)} = \frac{\mu}{1 + n\mu}.$$

The distortion in circuits with 100 per cent inverse feedback has been investigated by F. H. Shepard, Jr., of the RCA Radiotron Division. He found it to be extremely low, because it is reduced approximately by the same factor by which the required grid signal must be increased. Circuits with unity feedback ( $n = 1$ ) require a grid signal equal to the sum of plate and grid-signal voltage and thus have very low power sensitivity.

A modification of the circuit for obtaining fractional feed-back values ( $n < 1$ ) is shown in Fig. 33(b), in which the feed-back value  $n = r_1/(r_1 + r_2)$  may be adjusted at will. The circuit shown has a conductive feed-back connection, which permits the plotting of the resultant plate characteristic of the tube with feedback by any conventional method.

Oscillograms of feed-back characteristics of the beam power tube taken with a cathode-ray curve tracer for 10, 20, and 30 per cent inverse feedback are shown in Fig. 34. Because the oscillograms require a flat frequency characteristic with zero phase distortion from 10 to approximately 10,000 cycles, they prove the frequency stability of the circuit. The decrease of  $r_{p(r)}$  and  $\mu_{(r)}$  with increased feedback is obvious.

## 2. Graphic Construction of Feed-Back Characteristic

The construction of the characteristic with feedback from the original characteristic is not difficult. As illustrated in Fig. 35, it is obtained by simply adding  $-n E_b$  to all grid-voltage values and draw-

ing curves through all points  $-(E_{c1} + nE_b) = -E_{c1(r)}$  of equal voltage.

The construction furnishes the correct resultant values of  $\mu_{(r)}$  and  $r_{p(r)}$  ( $g_m$  is unchanged) at any point of the feed-back characteristic. The original

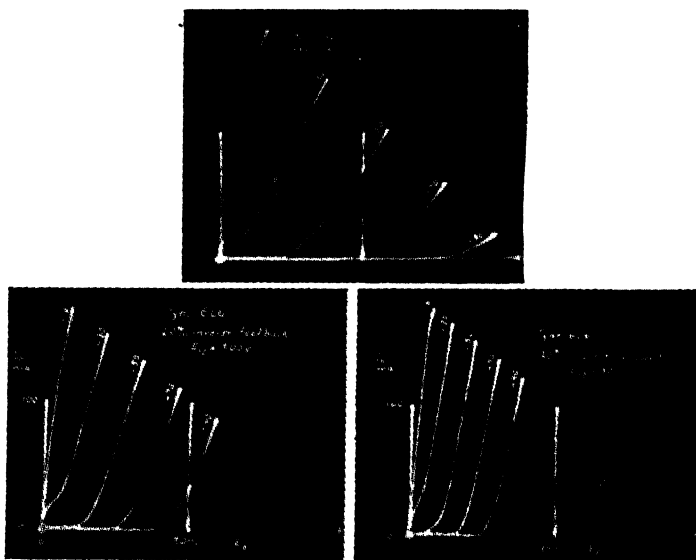


Fig. 34—Oscillograms showing effects of inverse feedback on plate characteristics of a beam power tube. Oscillograms taken with the curve tracer using circuit of Fig. 33(b).

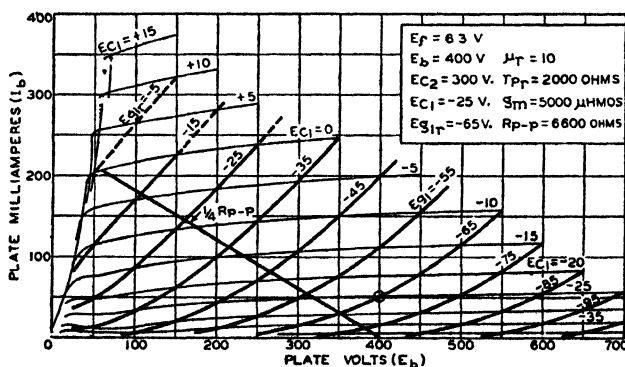


Fig. 35—Inverse feed-back plate characteristics for  $n=0.1$  constructed from the static plate family of the 6L6 beam power tube.

zero-bias line is the envelope of all values without grid current. It is further seen that the position of the optimum plate load and the power output, as determined for all normal operating conditions, remains

unchanged. Distortion analysis, however, will show a reduction of distortion in approximate proportion to the required signal increase.

### 3. Performance of Beam Power Tubes in Practical Circuits with Inverse-Voltage Feedback

Conductive feedback is unnecessary in audio-frequency amplifiers. The correct phase relation is least disturbed by a resistance-capacitance coupling as shown in the practical circuit of Fig. 33(c). The blocking condensers  $C$  eliminate direct-current feedback and thus make it unnecessary to change the original grid-biasing voltage. *This measure avoids at the same time possible plate-current cutoff due to rectification*, because the direct-current plate conductance is not increased to the high value of a real triode.

The high power sensitivity of the beam power tube requires the value of only 10 per cent feedback to effect a *loud-speaker damping equal to that obtained with class A1-operated low-impedance triodes*. The required grid signal as obtained from the push-pull operating condition illustrated in the feed-back characteristics of Fig. 35 is 60 peak volts at the grid-current point. The operating bias ( $E_{g1}$ ) is  $-65$  volts which would be the direct-current bias value for the conductive feed-back connection. Since the practical feed-back connection contains a blocking condenser, the direct-current bias on the tube is  $-25$  volts. The power output remains 32 watts, a small percentage of which is dissipated in the potential divider. The distortion is reduced to approximately 0.6 per cent. The high circuit efficiency is substantially unaltered.

A possible phase reversal due to leakage-reactance tuning of the input transformer is prevented by connecting small condensers across each secondary winding. Plate-load compensation is unnecessary due to the low effective plate impedance of the tubes. The low  $r_{p(r)}$  of the tubes will give less trouble from hum than triodes, due to better stability of the operating point, but naturally requires a better filtered B supply voltage as compared to pentode operation.

*Circuits with un-bypassed cathode resistor* are also inverse-feed-back circuits. In single-tube operation such circuits will reduce the distortion of the beam power tube to approximately one half of its normal value while the required grid signal will be doubled and the output power reduced approximately 10 per cent by the loss in the cathode resistor. It can be shown that this feed-back method *increases the effective plate impedance of the tube with respect to a separate plate-circuit load and decreases the tube impedance with respect to the cathode resistor*. For damping purposes, therefore, this method is efficient only for 100 per cent inverse feedback, i.e., if  $R_p$  is located in the cathode lead.

### CONCLUSION

By the use of new principles in design and application of power tubes, we have in the beam power tube closely approached ideal power-tube characteristics and performance. The development of this tube has been made possible by the splendid co-operation and specific knowledge of many fellow engineers, to whom I want to express my sincere appreciation.

# REVIEW OF ULTRA-HIGH-FREQUENCY VACUUM-TUBE PROBLEMS\*†

BY

B. J. THOMPSON

RCA Radiotron Division, RCA Manufacturing Company, Inc.,  
Harrison, N. J.

*Summary*—The effects of electron transit time and of lead inductance and interelectrode capacitance which become of importance at ultra-high frequencies are reviewed. It is shown that, in radio-frequency amplifier tubes for use in receivers, the most serious effect is the high ratio of input conductance to transconductance, which is independent of the transconductance and is proportional to the square of the frequency. This ratio may be reduced by reducing the electron transit time, the lead inductances, and the interelectrode capacitances. In power amplifiers and oscillators for transmitters, the important effects are much the same as in receiving tubes. The solution is complicated, however, by the problem of obtaining sufficient power output in a small structure.

## I. INTRODUCTION

THE intensive use of all longer radio wavelengths by established services has forced new services and expansions of the old into the shorter wavelength portion of the radio spectrum. Fortunately, it has been found that these shorter wavelengths have advantages over the longer for many applications. In fact, the known or expected advantages of the very short wavelengths have brought about the use, or proposed use, of wavelengths from 7 meters to 10 centimeters, even though the spectrum of longer wavelengths is not saturated. Among these advantages are limited transmission range, making possible the multiple use of one wavelength or providing secrecy; wide available band width for a single channel, necessary for television; high directivity attainable with small antenna systems, including the possibility of using "wave guides"; and high resolving power of the waves, making possible, for example, navigational aids for ships and airplanes.

As shorter and shorter wavelengths have been used, it has been found that the vacuum tubes of the transmitters and receivers place a serious limitation on the attainable performance. Ultimately, improved performance can only be attained by radical improvements in vacuum-tube design or by radical departures from conventional modes

---

\* Decimal Classification: R339.2.

† Reprinted from *RCA Review*, October, 1938.



of vacuum-tube operation. It may be said that the problem of the development of satisfactory apparatus for the ultra-short wavelengths, on which depends the development of this promising field, is identical with the problem of designing better vacuum tubes for ultra-high-frequency operation.

In recent years very considerable advancements have been made in the design of vacuum tubes for high-frequency use. Most noteworthy has been the trend toward the use of conventional modes of operation at frequencies where formerly such operation was not considered feasible. This has been the result of improved design based on increased theoretical knowledge of the limitations to high-frequency tube performance and on the development of new manufacturing techniques. Noteworthy advances have also been made in the performance of some of the unconventional types of vacuum tubes. These advances naturally focus attention on the question of what may be expected in the future.

Foretelling the future is a dangerous though fascinating game. We shall be on surer ground if we confine ourselves to an attempt to understand the nature of the limitations which restrict the design and operation of present ultra-high-frequency tubes. Such an understanding should indicate the directions in which progress may be expected.

## II. FUNDAMENTAL CONSIDERATIONS

At low frequencies any effects of electron transit time or electrode leads are usually ignored. At the higher frequencies which we are discussing, this may no longer be done. The limitations imposed on the performance of high-frequency tubes are so largely the result of lead and transit-time effects that we must consider these in some detail.

The current flowing to an electrode in a vacuum tube is frequently viewed as resulting from the arrival of electrons at the electrode and as being, therefore, proportional to the instantaneous rate of arrival. This viewpoint is fairly satisfactory at frequencies where the electron transit time is a vanishingly small part of the period, but it is completely misleading at higher frequencies where the transit time becomes appreciable.

A useful and satisfactory viewpoint is to consider the current flow to an electrode the result of the motion of charges in the space between electrodes. Consider two infinite parallel-plane electrodes as in Figure 1 with a voltage  $E$  applied between them. The electric field  $F$

between the electrodes is simply  $\frac{E}{d}$  where  $d$  is the distance between

electrodes. If a small positive electric charge  $q$  is placed between the plates very close to the positive plate there will be an increase in the charge of the positive plate of amount  $-q$  and no increase in the charge of the negative plate. There will be a force acting on the charge of magnitude  $Fq$  tending to move it toward the negative plate. If the charge is allowed to move, the work done on it by the field is equal to  $Fqx$  where  $x$  is the distance the charge has moved. Now, the work done on the charge is supplied from the battery. The work done by the battery is equal to the product of its voltage  $E$  and the change

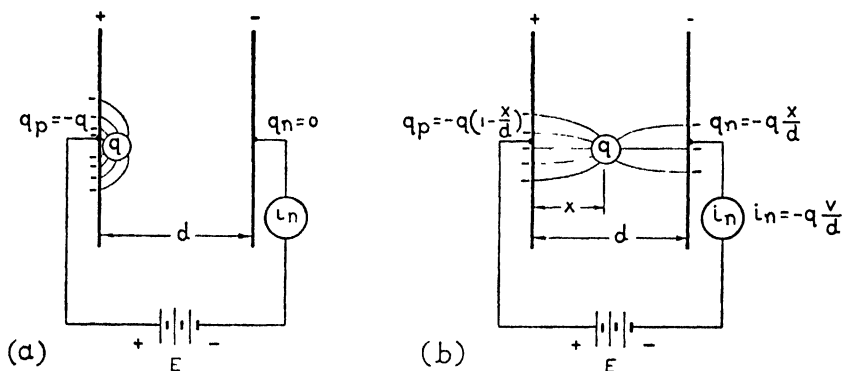


Fig. 1—Distribution of induced charge and current flow between parallel planes as a charge  $q$  moves between the planes. (a) illustrates the condition where the charge is an infinitesimal distance from the positive plane. (b) represents the condition where the charge has moved a distance  $x$  away from the positive plane and is moving at a velocity  $v$ .

in charge induced on one of the plates. If  $q_n$  represents the charge induced on the negative plate, we may write

$$-Eq_n = Fqx$$

$$= \frac{Eqx}{d}$$

or

$$q_n = -q \frac{x}{d}.$$

In other words, the charge induced on the negative plate is proportional to the charge in the space and to the fraction of the total distance between plates which the charge has covered. Of course, the

charge  $q_p$  induced on the positive plate is equal to the difference between the space charge and the charge induced on the negative plate, since the total charge induced on the two plates is always equal in magnitude and opposite in sign to the space charge.

The current flowing to the negative plate as a result of the motion of the charge  $q$  is equal to the rate of change of the charge  $q_n$ . This is simply

$$i_n = \frac{dq_n}{dt} = - \frac{q}{d} \frac{dx}{dt} = -q \frac{v}{d}.$$

In other words, the current flowing as a result of the motion of a charge between two plates is equal to the product of the charge times its velocity divided by the distance between the plates. Of course, the current flow to the positive plate is always instantaneously equal in magnitude to the current to the negative plate.

The important conclusion which we may draw from this simple analysis is that in a vacuum tube the current produced by the passage of an electron does not flow simply at the instant the electron reaches the electrode, but flows continuously in all adjacent electrodes while the electron is in motion. If the electron moves between parallel plates, the current flow does not depend on the position of the electron, but only on its velocity.

The total current flowing to an electrode may be determined by adding up all the minute currents produced by individual electrons, or more analytically by integrating the currents produced by infinitesimal strips of space charge.

In a steady-state condition, the current flow determined by such integration (or the measured value) is exactly equal to the rate of arrival of electrons at the electrodes. When the current is varying with time—as in the case of an amplifier tube with an alternating voltage applied to the grid,—the rate of arrival of electrons at the electrode may be greater or less than the actual current flowing because of the finite transit time of the electrons. If the current is momentarily increasing, the rate of arrival of electrons is less at any instant than corresponds to the flow of electrons in the space.

These considerations show that the current flowing to an electrode may be different from the rate of arrival of electrons at the electrode. It is also possible to have a current flowing to an electrode at which no electrons arrive, if the number or velocity of the electrons approaching the electrode is instantaneously different from the number or velocity of those receding from it.

From these elementary considerations we may understand qualitatively the various transit-time effects which are observed in high-frequency vacuum tubes.

The transit-time effects in the grid circuit are of most interest to us because they are the only effects in that circuit when no electrons or ions reach the grid. Because of the instantaneous difference between the rates at which electrons approach the grid and recede from it, there is an alternating current flowing to the grid which is proportional to the transconductance, to the alternating grid voltage, to the frequency, and to the electron transit time. This current leads the alternating grid voltage by 90 degrees. Hence, one may say that there is an electronic component of grid capacitance which is proportional to the transconductance and to the transit time. This capacitance is the well-known increase in "hot" capacitance over "cold" capacitance. While it is a transit-time effect, the equivalent capacitance does not vary appreciably with frequency, though, of course, the capacity current is proportional to the frequency.

Because of the electron transit-time, there is a shift in the originally 90-degree phase relation between grid voltage and grid current with increasing frequency. This phase shift results in an equivalent shunt resistance between grid and cathode which is inversely proportional to the transconductance and to the square of the frequency and of the transit time. This resistance, which is normally very high at frequencies of the order of 1 megacycle, may become as low as several thousand ohms at a frequency of 50 megacycles in conventional receiving tubes.

There are also transit-time effects in the plate circuit. First, there is a phase lag between plate current and grid voltage which is proportional to the frequency and to the transit time. The relation between plate current and grid voltage is normally expressed as the transconductance. Of course, properly speaking, conductance can refer only to the component of alternating plate current which is in phase with the grid voltage. The quotient of the total alternating plate current divided by the alternating grid voltage is therefore called the transadmittance.

Second, the magnitude of the transadmittance decreases somewhat as the frequency is increased. This effect is normally quite small at the maximum frequency at which a given tube may be used.

Third, there is a decrease in the internal plate resistance of the tube as the frequency is increased. This is also usually quite small.

These are the principal transit-time effects. Lead effects are also of importance.

Consider the simple triode shown in Figure 2 with inductance in the cathode and plate leads and with capacitance between grid and cathode and grid and plate. The plate has no external load and the frequency of the voltage applied to the grid is well below that at which resonance between lead inductances and interelectrode capacitances occurs. If  $L_k$  is equal to  $L_p$ ,  $C_{gk}$  to  $C_{gp}$ , and  $i_1$  to  $i_2$ , it can readily be seen that  $i_g$  is not influenced by the lead inductances, for the triode is then a bridge in perfect balance. But if any one of these qualities is upset (more exactly, if  $i_1 L_k C_{gp}$  is not equal to  $i_2 L_p C_{gk}$ ), there appears a conductive component in the grid current  $i_g$ . If  $i_1 L_k C_{gk}$  is greater

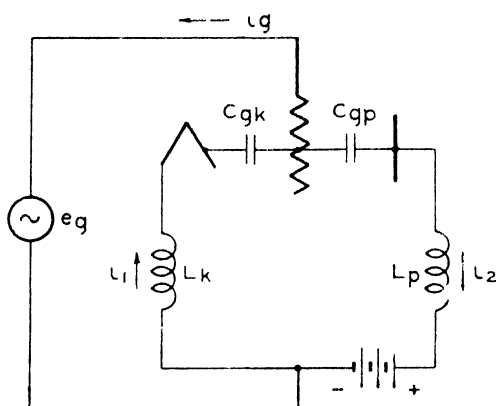


Fig. 2—Schematic diagram of triode without plate-load impedance.  $L_k$  and  $L_p$  represent the self-inductances of the cathode and plate leads.

than  $i_2 L_p C_{gp}$ , this component is positive and represents an input loading in addition to the electronic loading. It is most interesting to observe that the effective resistance shunted between grid and cathode which corresponds to this lead-effect loading is inversely proportional to the transconductance and to the square of the frequency, exactly as was the case for electronic loading.

Normally it is not feasible to balance out the two lead effects. Especially is this true in screen-grid tubes where the screen-grid current is a small fraction of the cathode current. Therefore, the lead-effect loading is often very important.

### III. RECEIVING TUBES

For almost any application of ultra-short waves, both transmitting and receiving apparatus are required. While it may seem that transmission logically comes first, the problems of receiving tubes are such that the discussion of them will serve as background for the discussion of transmitting tubes.

It is conventional practice at lower frequencies to amplify the received signal at the radio frequency, then to convert it to a lower intermediate frequency at which additional amplification takes place, and finally to detect the signal, or to omit the intermediate frequency and detect the radio-frequency signal directly. Where intermediate-frequency amplification is used, radio-frequency amplification is desirable to prevent radiation at the local-oscillator frequency from the receiving antenna, to reduce the response to the unwanted frequency which differs from the local-oscillator frequency by the same amount as the wanted frequency, and to increase the signal-to-noise ratio for weak signals. Where intermediate-frequency amplification is not used, radio-frequency amplification is required to achieve selectivity and sensitivity with high signal-to-noise ratio. While special applications of ultra-short waves may not impose such severe requirements on the receiver, it is reasonable to suppose that equivalent performance will be desired in other applications. We shall, therefore, wish to discuss all pertinent limitations of receiving tubes.

The maximum voltage amplification per stage which may be obtained from a vacuum-tube amplifier depends on the magnitudes of the transadmittance, the internal grid conductance, the internal plate resistance, the grid and plate capacitances to ground, and the band width to be passed by the amplifier. The phase angle of the transadmittance is unimportant in an amplifier. There is ordinarily no serious problem in obtaining suitable external circuits at even the highest frequencies. Where ordinary lumped circuits may not be used, distributed circuits, such as concentric transmission lines, are suitable.

As was stated earlier, the reduction in magnitude of transadmittance with increasing frequency is usually not serious. The internal plate resistance may or may not be importantly reduced at high frequencies. When it is, the trouble is not usually fundamental, but is likely to be a matter of bulb effects such as electron bombardment or surface film resistance. Such effects may be hard to isolate and to eliminate, but they will certainly not be an ultimate limitation.

For wide-band amplification, the interelectrode capacitances may be a limiting factor in determining the maximum attainable amplification at moderately high frequencies. However, as the frequency is increased, the input conductance becomes rapidly larger until the effective impedance of the circuit connected to the grid becomes lower, in general, than the value required for wide-band amplification. The problem of increasing the frequency at which some voltage amplification may be obtained is, therefore, the problem of increasing the ratio of transadmittance to input conductance.

Because for given spacings and operating voltages the ratio of transadmittance to input conductance at a definite frequency is fixed, increase in this ratio may be attained in a straightforward manner only by reducing spacings or increasing voltages. As the latter method is usually impractical, reduced spacings is the obvious alternative. This is the method followed in the design of acorn tubes. There are possibilities of more or less radically new kinds of amplifying tubes which may give better performance without smaller structures. Speculation as to the nature of such tubes is beyond the scope of the present paper; one may be sure, however, that the improvement will be in the ratio of transadmittance to input conductance.

Satisfactory performance at higher frequencies than those at which vacuum-tube amplifiers will give a voltage gain appears to be possible only if one is satisfied to do without radio-frequency amplification. Detectors will operate at much higher frequencies than present amplifiers or oscillators. Superheterodyne operation at as high as 3,000 megacycles does not seem impossible with the use of a harmonic of a lower-frequency local oscillator.

#### IV. TRANSMITTING TUBES

The performance requirements for transmitting tubes for ultra-high-frequency operation are substantially the same as those for lower frequencies. Only where such requirements cannot be met will inferior performance be accepted. These requirements stated briefly are: oscillators having good frequency stability; efficient power amplifiers which have good modulation characteristics; and as much power output as can be attained. It appears that the requirements of power amplification and good modulation characteristics may not readily be met by such tubes as magnetrons and Barkhausen-Kurz oscillators. It is not surprising, therefore, that the trend has been toward conventional negative-grid tubes at all frequencies much below 3,000 megacycles.

The fundamental electronic theory of the operation of negative-grid transmitting tubes at high frequencies is, naturally, the same as that of receiving tubes. If power output were not a consideration, transmitting tubes would not differ from receiving tubes. The demand for large power outputs with low interelectrode capacitance and close spacings, three requirements mutually in opposition, naturally requires a compromise in design about which one might not be optimistic. Actually, however, the situation is not so bad as it might appear at first. Because transmitting tubes are normally operated with much

higher voltages than receiving tubes and, further, because the grid usually swings quite positive over a portion of the cycle to cause the current to flow for a half-cycle or less, the electron velocity is much higher and therefore the spacings may be greater than in the case of receiving tubes. The fact that current flows for only part of a cycle causes the average grid conductance over the cycle to be lower.

Oscillators have one important advantage over power amplifiers. Lead-inductance effects are not serious because the feed-back from cathode to grid may be more than compensated by feed-back from plate to grid. They also have a disadvantage in that the phase angle of the transconductance is of importance in the simple feed-back circuits which are most convenient to use. The net result is that properly designed power amplifiers may be expected ultimately to equal or to exceed the performance of oscillators with respect to obtainable power output at a given frequency.

The limitation in power output at a given frequency of either oscillators or power amplifiers is set by the limitation in cathode-emission density and in anode and grid-dissipating ability which are properties of the materials used or of the methods of cooling. If unlimited emission could be obtained in a small space and the resultant unlimited-power dissipation accommodated, the problem would become simply one of handling the output power in the plate lead.

The limitation in frequency for a given power output is set by the transit times which result from the operating voltages, anode area, and spacings determined by the permissible anode dissipation per unit area and interelectrode capacitance.

The limitation in highest operating frequency without regard for power output is set by how small and how closely spaced it is considered feasible to make tubes, exactly the same limitation as for receiving tubes.

Improvements in both power output and maximum frequency may be expected from further refinements of design and construction. Greater improvements may be expected to result if new anode, grid, and cathode materials are found which will withstand greater dissipation density and afford greater emission density. As it is not to be expected that very great improvements may be attained in this direction, it appears that other means of generation must be found if power outputs as great as will be demanded are to be obtained.

The substantial progress which has been made in ultra-high-frequency vacuum-tube performance in the past few years is very encouraging. It will be interesting to watch the developments in the next few years. The requirements are definite and the demands press-



ing; the limitations are great and well recognized. Engineering and scientific ingenuity seem to be most active under such circumstances.

#### BIBLIOGRAPHY

D. O. North, "Analysis of the Effects of Space Charge on Grid Impedance", *Proc. I.R.E.*, Vol. 24, No. 1, pp. 108-136; January (1936).

W. R. Ferris, "Input Resistance of Vacuum Tubes as Ultra-High-Frequency Amplifiers", *Proc. I.R.E.*, Vol. 24, No. 1, pp. 82-107; January (1936).

F. B. Llewellyn, "Phase Angle of Vacuum-Tube Transconductance at Very High Frequencies", *Proc. I.R.E.*, Vol. 22, No. 8, pp. 947-956; August (1934).

M. J. O. Strutt and A. van der Ziel, "The Causes for the Increase of the Admittances of Modern High-Frequency Amplifier Tubes on Short Waves", *Proc. I.R.E.*, Vol. 26, No. 8, pp. 1011-1032; August (1938).

B. J. Thompson and G. M. Rose, Jr., "Vacuum Tubes of Small Dimensions for Use at Extremely High Frequencies", *Proc. I.R.E.*, Vol. 21, No. 12, pp. 1707-1721; December (1933).

B. Salzberg and D. G. Burnside, "Recent Developments in Miniature Tubes", *Proc. I.R.E.*, Vol. 23, No. 10, pp. 1142-1157; October (1935).

C. E. Fay and A. L. Samuel, "Vacuum Tubes for Generating Frequencies Above One Hundred Megacycles", *Proc. I.R.E.*, Vol. 23, No. 3, pp. 199-212; March (1935).

A. L. Samuel, "Extending the Frequency Range of the Negative Grid Tube", *Journal of Applied Physics*, Vol. 8, No. 10, pp. 677-688; October (1937).

W. G. Wagener, "The Developmental Problems and Operating Characteristics of Two New Ultra-High-Frequency Triodes", *Proc. I.R.E.*, Vol. 26, No. 4, pp. 401-414; April (1938).

L. S. Nergaard, "Electrical Measurements at Wavelengths Less Than Two Meters", *Proc. I.R.E.*, Vol. 24, No. 9, pp. 1207-1229; September (1936).

# DEVELOPMENT AND PRODUCTION OF THE NEW MINIATURE BATTERY TUBES\*†

By

NEWELL R. SMITH AND ALLEN H. SCHOOLEY

RCA Radiotron Division, RCA Manufacturing Company, Inc.,  
Harrison, N. J.

**Summary**—A new line of miniature battery tubes, including a converter, a radio frequency amplifier, a diode-pentode and a power output pentode has been made available. These new tubes are designed to operate efficiently on a 45-volt "B" supply with the filament operating directly from a single dry cell. The tubes are about two inches long and less than three quarters of an inch in diameter.

A feature of this new line of tubes is a decrease in size without an increase in cost. This is accomplished by using a simplified envelope design which in the majority of cases permits standard size electrodes to be assembled using conventional manufacturing procedure. A new button stem in which the external leads serve as base connections contributes materially to the reduction in tube dimensions.

The small size and efficient operating characteristics of the new miniature tubes make them especially applicable to compact communication equipment as well as portable broadcast receivers. Also they may find application in special fields such as hearing aids, meteorological service, or other places where size and weight are a consideration.

THE trend in radio receiver design, during the past two years has been toward small, low-priced models. This, together with the increasing popularity of portable, self-contained, battery receivers, has created a demand for smaller and less expensive radio tubes. The new miniature tubes, with their simplified construction and great reduction in size, provide a logical answer to this demand.

Although several types of small tubes are now available, these, in general, use very small parts with close electrode spacing requiring slow, careful, assembly by highly skilled operators and special fabricating processes. Such tubes have application wherever the requirement for special characteristics warrant their increased cost. However, the inherently higher cost of producing tubes of this character is sufficient to prohibit their general use in popular-priced broadcast receivers. Consequently, the problem of obtaining a small, low-cost tube depends for its solution upon the selection of a satisfactory design of simplified construction which will not only offer the desired reduction in size, but also lend itself to usual manufacturing operations.

In the design of this new line of tubes every effort has been directed toward producing the smallest glass tubes which can feasibly be manufactured by present high-speed methods of fabrication. The variations required in manufacturing technique have, therefore, been carefully restricted to procedures which have been proven by prior experience.

---

\* Decimal Classification: R331.

† Reprinted from RCA Review, April, 1940.

In so far as possible, all parts and materials which serve no functional purpose in the completed tube have been eliminated.

The new miniature line consists of four tubes, the RCA-1R5, converter; RCA-1T4, radio-frequency pentode; RCA-1S5, diode-pentode; and RCA-1S4, power-output pentode; and provides a complete complement for receiver design. All of the tubes operate efficiently from a small, 45-volt "B" battery and their filaments are designed for operation at 50 milliamperes (except the RCA-1S4 which requires 100 milliamperes) supplied directly from a single dry-cell.

The reduction in tube dimensions accomplished by the new design is illustrated by the photograph, Figure 1, in which a miniature tube is

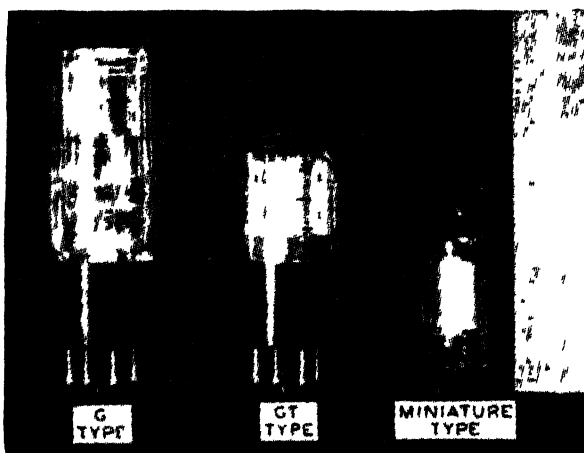


Fig. 1—New Miniature Tube compared with smallest present equivalent types.

compared with a G-type and a GT-type having similar characteristics. It is interesting to note that the miniature tube is about two inches long and less than  $\frac{3}{4}$  inch in diameter and only displaces about 20 per cent of the receiver space required by the GT-type equivalent. This large reduction in volume should recommend these new tubes for those applications where compactness is essential. They should be especially desirable in the design of portable broadcast receivers, pocket receivers and police equipment. They may prove useful in meteorological work, hearing-aid and other special applications where size, weight and cost must be considered.

The manner in which the reduction in size has been effected together with the various special features of design and manufacturing technique employed in the production of the new miniature tubes are discussed in the ensuing paragraphs.

## STEM DESIGN

In Figure 2 (top) the various parts and an assembled unit of a conventional-type stem are shown. In this stem, the electrode leads are located in a single plane through the center of the preformed flare and the vacuum seal is made by pinch-pressing the molten glass onto the short sections of special seal wire. The particular stem shown in Figure 2 (top) is representative of one of the shortest stems in general use. In this case the length of the glass flare from the sealing line to the top of the press is approximately 14 millimeters (0.55 inch). To

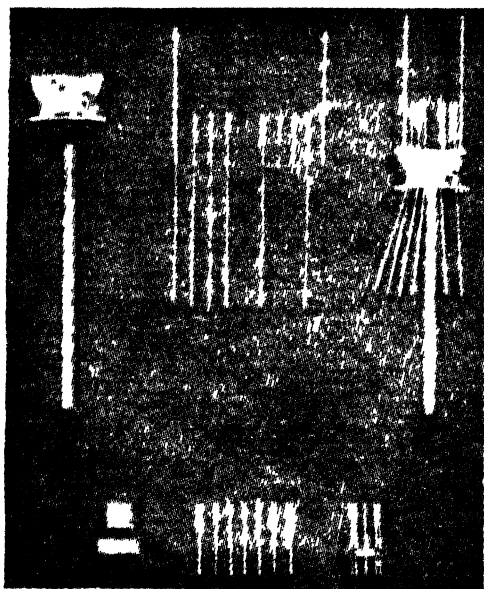


Fig. 2—(Top)—Parts and an assembled unit of a conventional stem.  
(Bottom)—Miniature button stem and component parts.

this value must be added sufficient length to provide for trimming and forming the leads and making the welds of the leads to the tube electrodes. This additional length of approximately 10 millimeters (0.39 inch) makes the total distance from the point of sealing to the lower edge of the mount approximately 24 millimeters (0.94 inch). It will be evident that this long length is non-essential to the electrical characteristics, but results from the mechanical limitations of this type of stem design. The stem length has been greatly reduced in the design of the miniature button stem by making the sealing position to the enclosure coincident with the vacuum seal line as shown in Figure 2 (bottom). The distance from the sealing line to the lower edge of the

mount has by this construction been reduced by 65 per cent and results in shortening the overall length of the finished tube by 14 to 15 millimeters (.55 to .59 inch).

The use of the "button-type" stem also contributes to a reduction in tube diameter. The conventional-type stem shown in Figure 2 (top) requires a flange diameter which exceeds the width of the stem press. In the GT-type tube of Figure 3, the flange diameter is approximately 1 inch and a bulb diameter of  $1\frac{1}{8}$  inches is, therefore, required for successful assembly. In comparison, the miniature type has seven leads located on a  $\frac{3}{4}$  inch circle in a glass button only  $\frac{6}{10}$  inch in diameter. This stem can be sealed into a bulb having an outside dimension of approximately  $1\frac{1}{16}$  inch.

Although the diameter of the tube is reduced, the lead spacing has

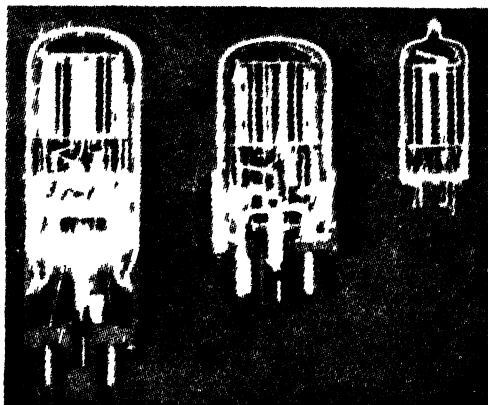


Fig. 3—Cut-away view of G-Type (left), GT-Type (center), and Miniature Type (right).

been improved by use of the button-type stem. For example: seven leads sealed into a conventional-type stem cannot have an average spacing much in excess of 0.110 inch between leads. In the miniature-tube design seven leads are spaced  $45^\circ$  apart on a circle 0.375 inch in diameter. Thus, the leads are spaced 0.147 inch apart, an increase of 33 per cent more than can be obtained by use of the larger conventional-type stem. From this explanation, it is evident that in those instances where three or more leads are required, a much smaller diameter stem of the button type can be designed to have a greater lead spacing than would be possible with the conventional flat-press stem. The wider spacing reduces the possibility of electrical leakage and minimizes capacitance coupling between leads.

It is evident that in addition to the reduction in size realized through

the use of the miniature button stem that a considerable saving in materials has also been achieved by departing from the conventional pinch-press stem. For example: only about  $\frac{1}{5}$  of the amount of glass used by the small conventional type stems is required for the miniature stem. The glass does not need to be preformed, but is cut directly from tubing of the correct diameters to the short lengths required. All leads used in the miniature stem are identical regardless of tube type. Only three types of parts are required to produce the miniature stems as compared to six types of parts for the conventional stem. This standardization of parts is a decided advantage in manufacture.

Since the miniature stem was designed for fabrication on the same

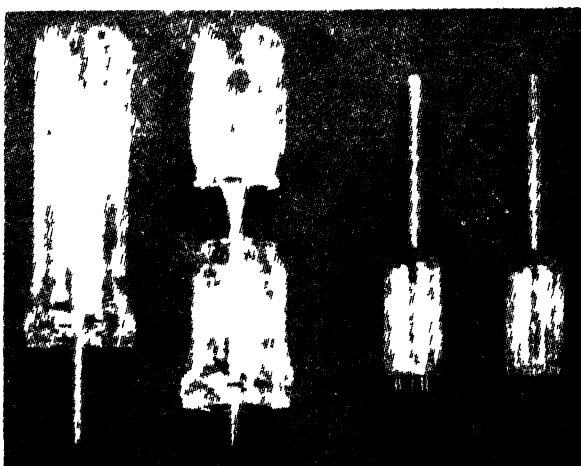


Fig. 4—(Left Half)—Conventional type tube before and after sealing, with discarded collet.  
(Right Half)—Miniature-type tube before and after sealing, with no collet.

equipment and under the same technique employed for the production of metal-tube button stems, only slight modifications of existing equipment were required.

#### BULB

The miniature bulb (shown as part of Figure 4) is molded from glass tubing and has no collet. This method of fabrication is economical in that no glass is wasted and close tolerances in the bulb and the stem combine to make sealing a relatively simple operation.

The miniature stem has no tubulation and it is, therefore, necessary to provide an exhaust tubing in the bulb. This is done by reviving the bulb seal-off which was used by the incandescent lamp and radio tube industries for many years.

## MOUNT

In the past, the designers of small tubes have concentrated upon obtaining a reduction in mount size by close electrode spacings and very small parts, the primary reason being to reduce inter-electrode capacity and lead inductance in order to improve high frequency operation. Tubes of this design are difficult and slow to assemble in the factory and must necessarily be expensive to produce. Examination of

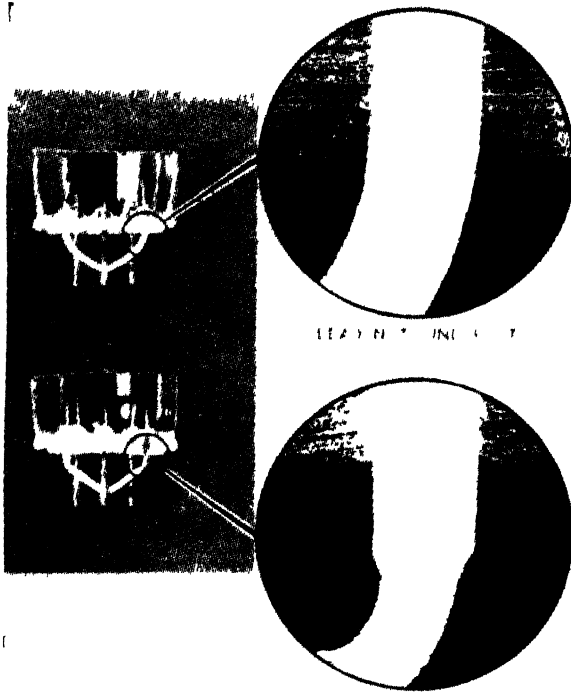


Fig. 5—Photographs showing how undercutting leads of miniature stems protects the glass seal under extreme conditions of bending.

the three tubes shown in Figure 3 will disclose that the mounts in all three types are identical for mount parts and electrode spacings except, in the case of the miniature, that the anode has been changed to a simple cylindrical sleeve so as to permit insertion into the bulb. In the miniature tube, the getter has been mounted above the top mica to eliminate any possibility of leakage across the stem due to getter. Maintenance of mount dimensions identical to those used on other types of receiving tubes, provides standardization of parts and materials and facilitates factory operations by permitting assembly on common fixtures and at usual mounting speeds.

## BASELESS CONSTRUCTION

From a comparison of the tubes shown in Figure 3, it will be apparent that the reduction in size of the miniature tubes has been obtained almost entirely from the stem and enclosure, either by redesign or elimination of parts. Some of these changes may be considered as elimination of safeguards previously considered essential to tube construction. For instance, the tubulated bulb used in early incandescent lamp and radio tube practice has been incorporated in the miniature design. The bakelite base with its rigid pins for socket contacts separated by intermediate flexible connectors from the vacuum seal has been replaced by short pins sealed directly into the glass of the stem. Although laboratory tests have indicated that the glass seal is sufficiently strong to withstand the normal pressures which will be exerted on the base pins in various applications, it has been deemed advisable until experience can be obtained from the field to incorporate an additional safety factor of undercut pins as illustrated in Figure 5. This device consists of reducing the diameter of a short length of the pin at some point below the glass so that in case the lead is accidentally deflected from its normal position the bending will be localized in the weakened part of the pin and the vacuum seal will not be affected. If a solid lead is bent, the fulcrum point of the bend is located at the edge of the glass seal as is shown in Figure 5 (top). This causes chipping of the glass and may result in a ruptured seal. An undercut pin which is similarly bent (Figure 5 bottom) has absorbed the distortion entirely in the weakened section and has not disturbed the vacuum seal. The advantage of this artifice is that the strength of the contact pin can be reduced to well within the safe limits permitted by the strength of the glass seal. The amount of this lead under-cutting can be varied or eliminated entirely without altering the contact diameter of the pins.

This development provides a new line of small tubes having very efficient operating characteristics at low battery voltages. These tubes are designed especially for use in compact, lightweight, portable equipment.

The co-operative efforts of the many engineers involved in this development are recognized and appreciated, although it is impractical to acknowledge the contributions individually.



## RECENT TRENDS IN RECEIVING TUBE DESIGN\*†

By

J. C. WARNER, E. W. RITTER AND D. F. SCHMIT

Research and Development Laboratory,  
RCA Radiotron Company,  
Harrison, N. J.

*Summary*

*This paper gives a brief summary of the important steps in receiving tube design over the past ten years. The significance of new forms of grids and in particular the suppressor grid are discussed. Characteristics of new radio-frequency tubes containing suppressor grids are shown. Improvements in cathode and grid designs are illustrated by the characteristics of a new triode as well as two triple-grid tubes. A new tube for class B audio amplification is described together with a mercury vapor rectifier for supplying power to the class B amplifier.*

*(16 pages; 17 figures)*

---

\* Decimal classification: R330.

† Proc. I.R.E., August 1932.

VACUUM TUBES OF SMALL DIMENSIONS FOR USE  
AT EXTREMELY HIGH FREQUENCIES\*†

By

B. J. THOMPSON AND G. M. ROSE, JR.

RCA Radiotron Company, Inc.,  
Harrison, N. J.

*Summary*

*This paper describes the construction and operation of very small triodes and screen-grid tubes intended for reception at wavelengths down to 60 centimeters with conventional circuits.*

*The tubes represent nearly a tenfold reduction in dimensions as compared with conventional receiving tubes, but compare favorably with them in transconductance and amplification factor. The interelectrode capacitances are only a fraction of those obtained in the larger tubes.*

*The triodes have been operated in a conventional feed-back oscillator circuit at a wavelength of 30 centimeters with a plate voltage of 115 volts and a plate current of 3 milliamperes.*

*Receivers have been constructed using the screen-grid tubes which afford tuned radio-frequency amplification at 100 centimeters and 75 centimeters, a gain of approximately four per stage being obtained at the longer wavelength.*

*(15 pages; 15 figures)*

---

\* Decimal Classification: R331.

† Proc. I. R. E., December, 1933.

## A NEW CONVERTER TUBE FOR ALL-WAVE RECEIVERS\*†

By

E. W. HEROLD, W. A. HARRIS AND T. J. HENRY

RCA Radiotron Division, RCA Manufacturing Company, Inc.,  
Harrison, N. J.

### *Summary*

*The need for a more efficient converter tube for use in all-wave receivers is pointed out. A new tube, the 6K8, which gives considerable better performance than previously used tubes, is described. The tube functions both as an oscillator and mixer. Constructional details as well as performance characteristics are given. Some modification is required in conventional circuits in order to obtain optimum performance of the 6K8.*

*(11 pages; 5 figures)*

---

\* Decimal Classification: R335 × R331.

† RCA Review, July 1938.

# THE SECONDARY EMISSION MULTIPLIER — A NEW ELECTRONIC DEVICE\*†

BY

V. K. ZWORYKIN, G. A. MORTON, AND L. MALTER

RCA Manufacturing Company,  
Camden, N. J.

*Summary*—This paper describes the construction, theory, and performance of various types of fixed field secondary emission multipliers. Detailed consideration is given of multiplier phototubes employing crossed electrostatic and magnetic fields and of electron multipliers using electrostatic focusing alone, to serve as coupling and amplifying units for cathode-ray tubes such as the "Iconoscope."

It is shown that while the power required for the operation of the secondary emission multiplier is about the same as that for the conventional amplifier, it is superior to the latter from the standpoint of noise. In the case of the multiplier phototube the signal-to-noise ratio is essentially determined by the shot noise of the photoemission, and is therefore sixty to one hundred times greater than that for a thermionic amplifier and phototube under conditions of low light intensity.

Multiplier phototubes have been built with an amplification factor of several millions and serve to replace the conventional phototube and accompanying amplifier system.

Their low "noise" level, together with their excellent frequency response and extreme simplicity, make these electron multipliers a very satisfactory form of amplifier.

## INTRODUCTION

FOR MORE than thirty years it has been known that when certain surfaces are bombarded with cathode rays they emit electrons. This effect, known as secondary emission, has, from an early date, been extensively studied by a large number of workers such as Lenard, Hull, Von Bayer, etc.

The study of this phenomenon revealed that the number of electrons emitted is proportional to the bombarding current, the factor of proportionality ranging from a mere fraction to ten times as many secondary as primary electrons. The value of this ratio depends upon the surface used and on the velocity of the bombarding electrons. Although these facts have been known for a long time, the effect was not put to any useful work, except in the case of the dynatron invented by A. W. Hull. In fact, secondary emission had chiefly been looked upon as a serious obstacle in the design of thermionic vacuum

---

\* Decimal classification: R585.38.

† Reprinted from *Proc. I.R.E.*, March, 1936.

tubes, and much research was carried on with an aim towards suppressing and reducing it.

During the past fifteen years it became recognized that secondary emission could be used as a means of amplifying a small initial electron current and a number of workers began investigating this field. Patents on methods of carrying out this idea were filed as early as 1919 by Slepian<sup>1</sup> and later by such workers as Jarvis and Blair,<sup>2</sup> Iams,<sup>3</sup> Farnsworth and others.

The general method involved is to allow the initial electron stream to impinge upon a target which has been sensitized for secondary emission. The secondary electrons from this target are directed on to a second target, producing still further electrons, the multiplication being repeated as many times as is desired. Reference to Fig. 1 will make this process clear. In this figure, electrodes *A*, *B*, *C*, etc., represent a number of plane targets having a high secondary emission ratio. These electrodes are connected to successively higher positive potentials. The stream of electrons to be multiplied is directed against *A*. This target gives rise to secondaries which go to target *B*, in turn giving rise to secondary electrons which are directed against *C*. After this process has been repeated a sufficient number of times to give the desired over-all multiplication, the electrons from the final target are collected on collector *O*. If *R* be the number of secondary electrons per primary for each stage and *n* the total number of stages, then the initial current *I*<sub>0</sub> will be multiplied up to an output current

$$I = I_0 R^n. \quad (1)$$

Clearly, the over-all gain will be *R*<sup>*n*</sup> times. It will be seen that the over-all gain becomes very large indeed as the number of stages is increased if the secondary emission ratio of the targets is large (e.g., between five and nine).

A second class of multipliers has been described by P. T. Farnsworth,<sup>4</sup> in which the electrons are made to go back and forth between a single pair of targets receiving their energy from a high-frequency electric field. Of these two classes of multipliers, only the type using successive targets, wherein the number of impacts can be rigorously controlled and the stability, consequently, is very great, will be discussed in this paper.

<sup>1</sup> Slepian, Patent No. 1,450,265, April 3, 1923 (1919).

<sup>2</sup> Jarvis and Blair, Patent No. 1,903,569, April 11, 1933 (1926).

<sup>3</sup> Iams and Salzberg, "The secondary emission phototube," *Proc. I.R.E.*, vol. 23, pp. 55-64; January, (1935).

<sup>4</sup> P. T. Farnsworth, "Television by electron image scanning," *Jour. Frank. Inst.*, vol. 218, pp. 411-444; October, (1934); also see *Electronics*, vol. 7, pp. 242-243; August, (1934).

The problem of making a multiplier which gives high gain is not, however, so simple as it might seem at first sight. A simplified multiplier constructed in accordance with the diagram (Fig. 1) would be almost completely inoperative, for the reason that practically all the electrons leaving any target would not go to the following one, but would merely go down the length of the tube and be collected at the final collector with almost no multiplication. In order to construct a successful multiplier, not only must the targets have a high secondary emission ratio, but also means must be provided to focus the electrons on to each target, and to draw away secondary electrons from one target preparatory to focusing them on to the next succeeding target.

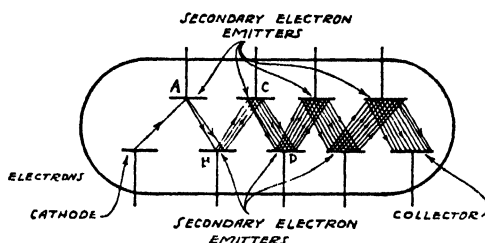


Fig. 1—Simplified secondary emission multiplier.

Before methods of electron focusing employed in specific multipliers are considered, there are certain general aspects of fixed field multipliers that should be discussed.

## I. GENERAL CONSIDERATIONS

### 1. Secondary Emission

Since the successful operation of these multipliers depends upon a high secondary emission from the targets, it is of prime importance to discover the most suitable surfaces to use. In our search for good emitters, very little aid can be obtained from the theoretical physicist.

The most complete treatment of the theoretical aspect of secondary emission in the light of quantum mechanics was done by H. Fröhlich<sup>5</sup> in 1932. In this discussion he calculates the probability of the transfer of energy between an incoming primary electron and a conduction electron moving in the periodic potential field of the metal, where the exchange is such as to give the conduction electron sufficient momentum to escape from the metal. On this basis, he concludes that metals with a crystal structure having a large lattice spacing and with a low work function should be the best secondary emitters. However, this treatment applies only to simple metal surfaces.

<sup>5</sup> H. Fröhlich, *Ann. der Phys.*, Band 13, no. 2, pp. 229-248, (1932).

Experimentally, it has been found that the emission ratio from simple metal surfaces is invariably below that obtained from composite surfaces just as is the case with photoelectric emission. Since the theoretical knowledge of secondary emission does not extend to these composite surfaces, it is necessary to go ahead more or less empirically on the basis that, other things being equal, a surface of low work function is the most likely to be a good emitter. A large number of low work function surfaces were, therefore, studied having as a base metal, Ag, Be, Ta, Ni, Al, Zr, Ca, W, Cr, etc., and Na, K, Rb, and Cs as a surface layer. Of these, the most satisfactory to date have been oxidized Ag, Be, or Zr with a surface layer of cesium. These surfaces have a maximum secondary emission ratio of from eight to ten, occurring at a bombarding velocity of from 400 to 600 volts.

A curve showing the secondary emission ratio of Cs-CsO-Ag surface for various bombarding voltages is illustrated in Fig. 2. This is typical of the type of surfaces frequently used in the multipliers to be described later.

The method of preparation of this surface is very similar to that used in the preparation of the photoelectric cathode for a high vacuum cesium photocell. A matte silver sheet is oxidized to the second yellow by passing an electrical discharge through oxygen at low pressure. Then, after removing the oxygen from the vacuum system, cesium is admitted. The amount of cesium required is slightly less than that necessary to give maximum photosensitivity. The surface is then baked at 200 degrees centigrade for a few minutes to promote the reaction between the cesium and the silver oxide. This surface, when cooled, should be an excellent emitter.

## 2. Multiplier Efficiency

There are two ways of considering the efficiency of a multiplier. The first is the efficiency of secondary emission as a source of electrons, in terms of amperes per watt power supplied, while the second considers gain obtainable for a given over-all voltage as a function of the number of stages and voltage per stage. The second of these two considerations is more important from a practical standpoint, but both are worthy of some discussion.

Considering, first, the power efficiency, we have a target bombarded with a primary current  $I_0$  at  $V_0$  volts velocity. The power supplied by the primary beam is  $V_0 I_0$  and, if the secondary emission ratio is  $R$ , the current  $I$  emitted is  $I_0 R$ . Therefore, the current per watt is

$$\frac{I}{W} = \frac{R}{V_0} \frac{I_0}{I_0} = \frac{R}{V_0}. \quad (2)$$

Hence the most efficient point of operation is that at which the secondary emission curve shows the greatest gain per volt.

From Fig. 2 the curve of the gain per volt plotted against bombarding voltage, as shown in Fig. 3, can readily be calculated. This curve shows that at its maximum around thirty volts the emission is sixty milliamperes per watt, dropping to forty-five milliamperes per watt

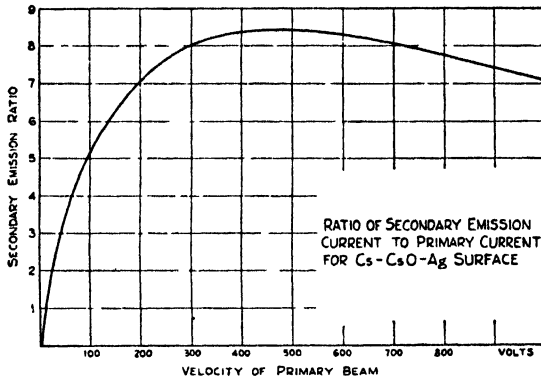


Fig. 2

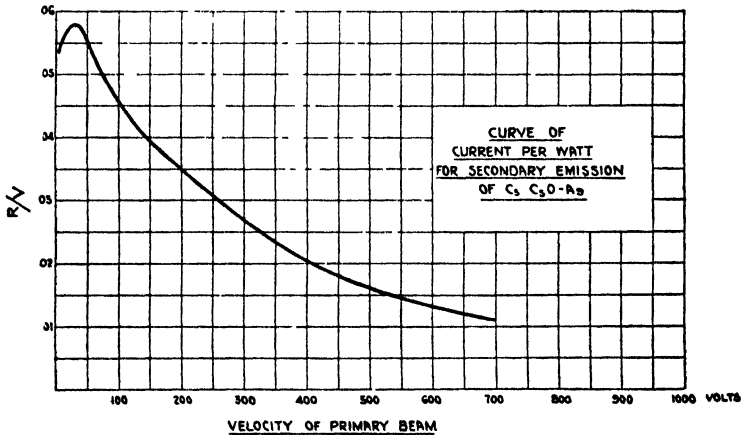


Fig. 3

at 100 volts, and seventeen milliamperes per watt at 500 volts. For comparison, it might be mentioned that a good thoriated tungsten thermionic cathode will deliver from fifty to seventy-five milliamperes per watt, while a very good oxide-coated cathode may run as high as one hundred milliamperes per watt. Thus, while secondary emission is not the most efficient way of obtaining an electron current, it compares rather favorably with other methods.

It is, of course, desirable to operate a multiplier under conditions such that maximum gain is had for a given over-all voltage. This condition may be determined as follows: Let  $R$  be the gain per stage,  $V_0$  the voltage per stage,  $n$  the number of stages, and  $V = nV_0$  the over-all voltage. The total gain is

$$G = R^n.$$

We can find the condition of maximum gain as  $n$  or  $V_0$  is changed; i.e.,

$$\frac{dG}{dV_0} = R^{(V/V_0)-1} \left( \frac{V}{V_0} \frac{dR}{dV_0} - \frac{V}{V_0^2} R \log_e R \right) = 0. \quad (3a)$$

In other words, the maximum occurs when

$$\frac{dR}{dV_0} = \frac{R}{V_0} \log_e R. \quad (3b)$$

It is interesting to compare this with the slope of the emission curve when the power consumption is a minimum as obtained from (2)

$$\frac{dR}{dV_0} = \frac{R}{V_0}. \quad (4)$$

For cesiated silver, these two points are fairly close together, so that a multiplier built to give close to the maximum gain also is fairly efficient from the standpoint of power consumption.

The question of maximum over-all gain will be made clearer by reference to Fig. 4. This family of curves shows the gain that can be obtained from multipliers with various numbers of stages plotted against voltage. These curves show that the most efficient multiplier is one operated with from forty to fifty volts per stage. Run in this way, very high gains may be obtained. For example, a ten-stage multiplier at 500 volts will have a gain of 30,000, while a fifteen-stage multiplier at 800 volts will multiply the initial current ten million times. It should be noted that the curves in Fig. 4 and the over-all voltages given do not include the voltage between the collector and the last target, as this will depend upon the use to which the tube is to be applied.

### 3. "Noise" in Multiplier Output

Regarding the question of "noise" in these multipliers, the first consideration will be that of the statistical fluctuation of the useful electron current through the tube. Assume that we have a source of electrons, for example a photoelectric cathode, and that the electrons



from it impinge upon a secondary emitting target. The noise from the secondary electrons emitted will consist of two parts: first, the multiplied shot noise in the initial beam, and second, the fluctuation noise of the secondary emission from the target. For every target in the multiplier we shall have these two effects occurring simultaneously.

As yet, very little work has been done on the question of statistical fluctuation in secondary emission, either from a theoretical or an experimental standpoint, and there is some disagreement among the few

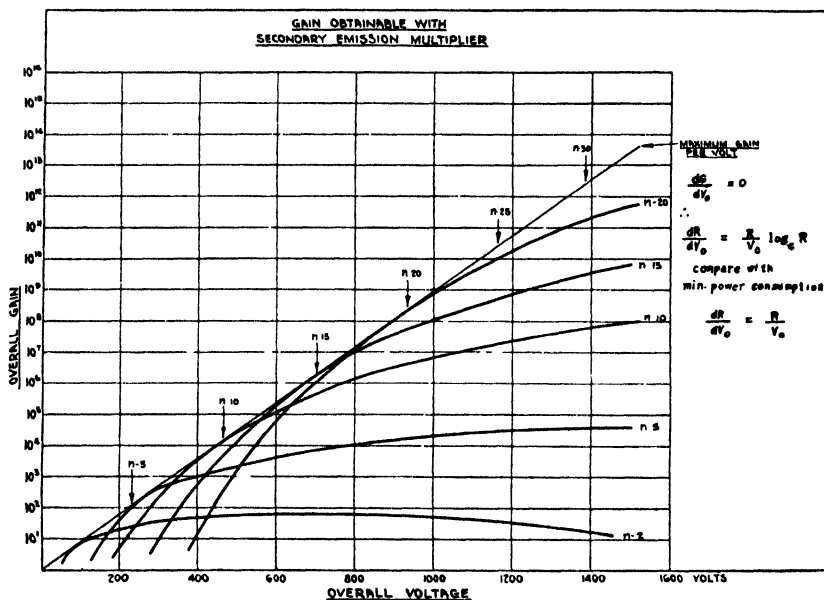


Fig. 4

experimental results available. However, these results indicate that the general magnitude of the effect is the same as the temperature limited shot noise from a thermionic cathode delivering a current equal to the secondary emission current.\*

Let us, then, make the two following assumptions:

1. Shot noise from an emitter is multiplied by the subsequent stages in the same way in which an ordinary signal is multiplied.
2. Secondary emission from a target is subject to shot effect such that

$$i_n^2 = KI$$

\* A. W. Hull and N. H. Williams, *Phys. Rev.*, vol. 25, p.147 (1925); Penning and Kruithof, *Physica*, vol. 2, pp. 793-804; August, (1935); L. J. Hayner, *Physica*, vol. 6, pp. 323-333; October, (1935).

where,

$I$  is the output current,

$K = 2eF$ ,

$e$  = the charge on an electron,

$F$  = frequency band over which noise is measured.

On the basis of these two assumptions, the total noise output from a phototube multiplier having an over-all gain  $G$  and  $n$  stages of uniform gain per stage, would be

$$i_n^2 = \frac{G^{(n+1)/n} - 1}{G^{1/n} - 1} 2eFI = K'I. \quad (5)$$

The table given below indicates the agreement between the measured noise output of several types of multipliers, and the values calculated from (5).

TABLE I

No of Stages	Gain	$K'/K$ Observed	$K'/K$ Calculated
3	60	77	80
3	28	40	41
3	6 8	12 1	12 3
2	29 5	36 2	36 0
1	6 0	7 2	7 0

This agreement is sufficiently close to indicate that (5) based on the two assumptions made above is accurate to the extent necessary for any practical noise calculation.

Rewriting (5) in terms of  $R$  and neglecting 1 in the numerator in comparison with  $G$  we have

$$i_n^2 = \frac{R^{n+1}}{R - 1} 2eFI$$

or in terms of the original photoelectric current

$$i_n^2 = \frac{R^{2n+1}}{R - 1} 2eFI_0. \quad (5a)$$

Let us compare the noise output with the signal output, where the light producing the original photocurrent is modulated so as to produce a signal  $i_s = kI$ ,  $k$  being the modulation factor. Under these conditions, the signal-to-noise ratio  $S_M$  is given by

$$\begin{aligned}
 S_M^2 &= \frac{i_s^2}{i_n^2} = k^2 \left( \frac{R^{2n}}{\frac{R^{2n+1}}{R - 1} 2eF} \right) I_{\text{cathode}} \\
 &= \frac{k^2}{2eF} \frac{R - 1}{R} I_{\text{cathode}}.
 \end{aligned} \quad (6)$$

The signal-to-noise ratio  $S$  for the original photocurrent is obviously given by

$$S^2 = \frac{i_s^2}{i_n^2} = \frac{k^2}{2eF} I.$$

The signal-to-noise ratio from the multiplier, therefore, only differs from the fundamental limit imposed by the photoelectric emission, by the factor

$$\sqrt{\frac{R-1}{R}}. \quad (7)$$

It should be pointed out here that if, instead of assuming that the shot noise due to secondary emission was the same as that from a saturated thermionic emission, we had assumed

$$i_n^2 = p2eFI$$

where  $p$  is some factor which has a value near unity, (7) becomes

$$\frac{R-1}{R-(1-p)}. \quad (7a)$$

From these equations it is evident that if  $R$  is large, the signal-to-noise ratio obtainable from these multipliers is practically that determined by the shot effect in the original photoelectric current.

Let us consider the improvement obtainable over the conventional amplifier by the use of a phototube multiplier. In the case of the thermionic amplifier, the noise limit is determined by the thermal noise in the first coupling impedance. The noise voltage input to the first tube is

$$e_n^2 = 1.6 \times 10^{-20} Fr$$

$$r = \text{input resistance}$$

while the signal will be

$$e_s^2 = k^2 r^2 I^2$$

and the signal-to-noise ratio

$$S_A = \sqrt{\frac{e_s^2}{e_n^2}} = k \sqrt{\frac{r}{1.6 \times 10^{-20} F}} I.$$

This is to be compared with the corresponding ratio for the multiplier

$$S_M = k \sqrt{\frac{R-1}{R 2eF}} I.$$

For example, let us calculate the value of photoelectric current in each case which will give a signal-to-noise ratio of five when  $k=1/2$ . Using the following condition (typical of those met with in television practice):

$$F = 10^6 \text{ cycles}$$

$$r = 10^4 \text{ ohms}$$

$$R = 5 \text{ per stage}$$

we find the current must be

$$8 \times 10^{-9} \text{ amperes}$$

when a conventional amplifier is used; whereas the current need only be

$$4 \times 10^{-11} \text{ amperes}$$

in the case of the multiplier photocell. Thus, it is seen that only 1/200 of the light is required to produce this signal-to-noise ratio when a multiplier photocell is used.

It is interesting to consider the case where the secondary emission ratio is not the same for every stage. If the gains per stage be  $R_1, R_2, R_3, R_4 \dots R_n$ , the total gain will be the product of these factors, while the noise output will be

$$i_n^2 = 1 + R_n(1 + R_{n-1}(1 + \dots (1 + R_1)))2eF I_0$$

and the signal-to-noise ratio is therefore

$$S_M = \left\{ 1 + \frac{1}{R_1} \left( 1 + \frac{1}{R_2} + \frac{1}{R_2 R_3} + \dots \right) \right\}^{-1/2} \left( \frac{I}{2eF} \right)^{1/2}. \quad (8)$$

In this expression  $R_1$  is the most important factor determining the signal-to-noise ratio. A multiplier which is to combine high signal-to-noise ratio with very efficient voltage operation should, therefore, be run with a high gain for the first one or two stages and the remaining stages set for greatest over-all gain per volt.

Where a multiplier is to be used in connection with an electron source other than a photoelectric cathode, as for example a television transmitting tube or "iconoscope," the noise output will be

$$i_n^2 = m^2 G^2 + \frac{G - 1}{G^{1/a} - 1} 2peFI \quad (9)$$

where  $m$  is the root-mean-square fluctuation on the cathode-ray beam to be multiplied. The second term is, of course, the noise generated in the multiplier and is in general much lower than the first term.

There are two other factors which limit the sensitivity of these multipliers. The first of these is thermionic emission from the secondary emission targets. Since all good secondary emitters have a low work function, they emit electrons in appreciable numbers even at room temperature. This difficulty may be overcome by running the tube at low temperature. However, this precaution need only be taken when the device is being used to detect an absolute minimum of current. Under any ordinary condition of operation, even where a gain of several millions is employed, the tube can be satisfactorily run at room temperature.

The final factor to be considered is noise due to positive ions. The magnitude of this effect will depend upon the configuration of the tube, the degree of exhaust, and the temperature of the walls of the tube. The last two factors mentioned, while troublesome, can be overcome if proper precautions are taken. Therefore, it may be said that the shot noise of electron emission sets the fundamental limit to the sensitivity of the secondary emission multiplier.

#### 4. *Frequency Response*

The frequency response of the secondary emission multiplier is flat over a very wide range of frequencies. As far as the lower limit of frequency response is concerned, the multiplier performs equally well at very low frequencies (including direct current) as at an intermediate frequency. A number of factors influence the high-frequency response. Basically, the limits are due to the spread of the time of flight of electrons in the tube and to the time of secondary emission. This will set an upper limit at many hundreds of megacycles. In addition to this, the upper limit is determined by the nature of the voltage supply for the targets and the output circuit. The latter factors are controllable and can be made as high as desired. Between the upper limit and a direct-current signal, the frequency response is essentially uniform.

## II. MAGNETIC SECONDARY EMISSION MULTIPLIER

### 1. *Theory of Operation*

The magnetic multiplier is based upon the use of a crossed magnetic and electrostatic field to separate and focus the secondary electrons from one target to the next. This configuration of fields and electrodes was first suggested by Slepian in 1919, for use as a high current cathode.

The general arrangement of a multiplier based on this principle is shown in Fig. 5. It consists of two rows of electrodes, the bottom row being secondary emitters, while the upper row serves solely to maintain a transverse electrostatic field between the two sets of elements.

Each target in the bottom row is made positive with respect to the preceding one so that it will produce secondary electrons when struck by electrons originating from the latter. A magnetic field is established in the tube at right angles to its axis and to the field between the two rows of plates. Electrons leaving any of the lower plates are bent by

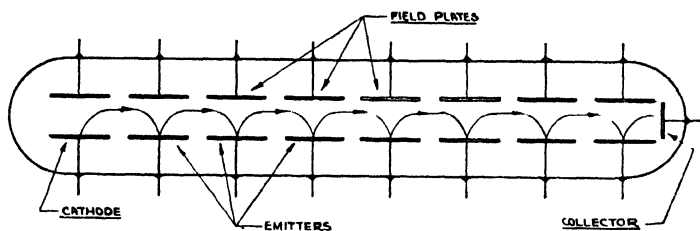


Fig. 5—Magnetic secondary emission multiplier.

the combined fields in such a way that they strike the next target, giving rise to secondary electrons which are in turn deflected on to another target, and so on through the tube.

This will be made clear by a consideration of the paths of the electrons under the influence of crossed fields. Let us assume, as a first approximation, that the potential difference between successive tar-

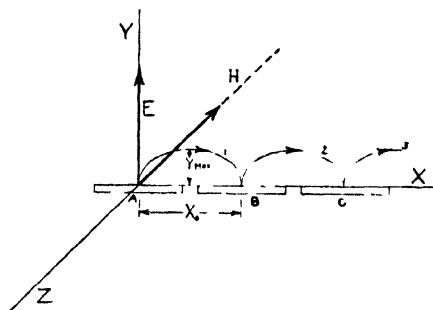


Fig. 6

gets is small compared with the potential between the targets and the top plates. Also, assume that the initial velocities are zero. The system as described can be represented by a rectangular co-ordinate system shown in Fig. 6, the targets lying along the axis of the tube, the electrostatic field  $E$  between the two rows of plates being in the  $y$  direction and the magnetic field  $H$  being in the negative  $z$  direction. The equations of motion of the electrons are therefore

$$\begin{aligned}
 m\ddot{x} &= eH\dot{y} \\
 m\ddot{y} &= eE - eH\dot{x} \\
 m\ddot{z} &= 0.
 \end{aligned}
 \tag{10}$$

A solution of these equations of motion leads to the following expression for the electron paths

$$\begin{aligned}
 x &= \frac{E}{H^2} \frac{m}{e} \left( \frac{eHt}{m} - \sin \frac{eHt}{m} \right) \\
 y &= \frac{E}{H^2} \frac{m}{e} \left( 1 - \cos \frac{eH}{m} t \right) \\
 z &= 0.
 \end{aligned}
 \tag{11}$$

These are the equations of a cycloid. The paths of the electrons will, therefore, appear as shown in Fig. 6, leaving cathode *A* along path 1, then after striking target *B* cause electrons to leave along path 2 following a cycloidal trajectory to target *C*.

From these equations it can be seen that the distance between points of impact will be

$$X_0 = 2\pi \frac{E}{H^2} \frac{m}{e} \tag{12}$$

while the maximum vertical displacement will be

$$Y_0 = \frac{2E}{H^2} \frac{m}{e}. \tag{13}$$

Actually, the conditions we have used in making these calculations are not exactly those found to exist in the tube, for under the conditions assumed the electrons would reach each target with zero velocity. In the multiplier tube, the targets are made successively more positive, so that the electrons will strike them with sufficient velocity to produce secondary electrons. In order to maintain an equal field between each target and its top plate, it is necessary also to make the top plates successively positive with respect to each other. This introduces a component of electric fields in the *x* direction. Furthermore, the fields in the *x* and *y* directions are not constant, but become, under operating conditions, very complicated indeed. It is not possible to determine analytically the electron paths in the fields actually known to exist in these multipliers; therefore, for the present, we must base our calculations on the approximations given above.

So far, we have neglected the effect of initial velocities on the trajectories. If the initial velocities  $\lambda_0$ ,  $\mu_0$ , and  $\nu_0$  in the *x*, *y*, and *z*

directions are introduced as boundary conditions into the solution of (10), the equations of the paths become

$$x = \alpha\beta t + \frac{\mu_0}{\alpha} - \beta' \sin(\alpha t + \theta) \quad (14)$$

$$y = \beta - \frac{\lambda_0}{\alpha} - \beta' \cos(\alpha t + \theta) \quad (15)$$

$$z = v_0 t \quad (16)$$

where,

$$\alpha = \frac{e}{m} H$$

$$\beta = \frac{1}{\alpha} \frac{E}{H} = \frac{E}{H^2 e/m}$$

$$\beta' = \left( \beta - \frac{\lambda_0}{\alpha} \right)^2 + \left( \frac{\mu_0}{\alpha} \right)^2$$

$$\theta = \tan^{-1} \frac{\mu_0/\alpha}{\beta - (\lambda_0/\alpha)}$$

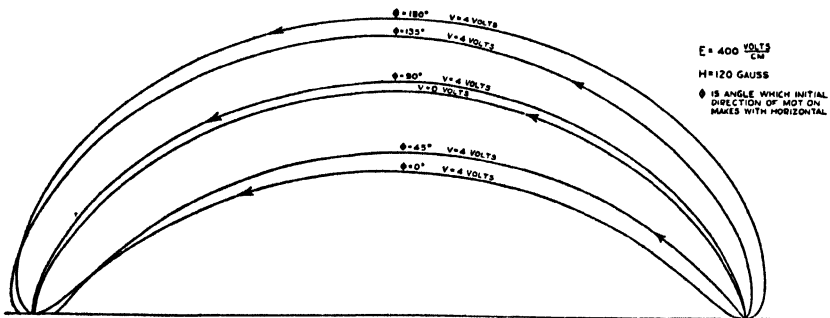


Fig. 7

These equations represent trochoidal paths, which degenerate into cycloids when the initial velocities become zero. Fig. 7 shows a family of these paths traced out by electrons having four volts initial velocity and emitted in various directions in the  $x, y$  plane.

It will be seen that the defocusing even at its maximum is only a very small fraction of the distance between points of impact. A general expression for the fractional defocusing (i.e., the distance  $\Delta X$  that an electron with a given initial velocity strikes the target from the point where an electron with zero initial velocity impinges divided by the



total path distance  $X_0$  along the  $x$  axis) can be derived from (10) and (14). This equation takes the form

$$\frac{\Delta X}{X_0} = \frac{1}{\pi} \left( \frac{\mu_0}{\alpha\beta} - \theta \right) \quad (17)$$

and can be used to calculate the axial defocusing for any value of initial velocity.

From (16) it can be seen that there will be a transverse defocusing if the initial velocity in the  $z$  direction is not zero. This transverse spreading can be calculated by substituting the time of flight between two stages into the equation

$$z = v_0 t.$$

This leads to an equation for the displacement  $\Delta Z$  from the center of the targets as follows

$$\frac{\Delta Z}{X_0} = \frac{H}{2E} \sqrt{2V_{0z}e/m} \quad (18)$$

where  $V_{0z}$  is the initial velocity of the electron in the  $z$  direction expressed in units of potential.

It should be noted that the transverse displacement is cumulative from stage to stage. However, due to the statistical nature of the effect, the spreading of all the electrons as they traverse the tube will be proportional to the square root of the number of stages, rather than to the number of stages.

It was shown that the ratio of maximum height that the electrons rise above the targets is

$$\frac{Y_{\max}}{X_0} = \frac{1}{\pi}$$

in the case where the initial velocities are zero. The existence of initial velocities increase the maximum height slightly. Using (10) and (15), it can be shown that the equation for the maximum becomes

$$\frac{Y_{\max}}{X_0} = \frac{\beta + \beta' - (\lambda_0/\alpha)}{2\pi}. \quad (19)$$

As yet, no accurate measurement has been made on the velocity distribution for secondary emission from cesiated surfaces; however, measurements have been made which show that 85 per cent of the electrons leaving a target have less than three volts initial velocity.

Using the value  $V_0 =$  three electron volts to calculate the defocusing in an actual multiplier operated under the following conditions

$$E = 400 \text{ volts per centimeter}$$

$$H = 120 \text{ gauss}$$

$$V_0 = 3 \text{ volts}$$

we find,

$$\frac{\Delta X}{X_0} = 0.02$$

$$\frac{\Delta Z}{X_0} = 0.3$$

$$X_0 = 0.97 \text{ centimeter.}$$

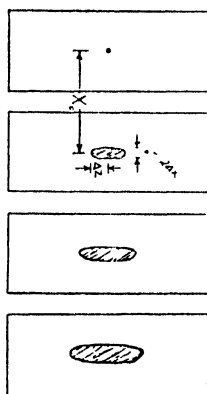


Fig. 8

This means that electrons leaving from a point on the cathode spread into an elliptical spot on the first target. This in turn is spread into a larger ellipse on the second target, the size of the spot increasing as the electrons progress down the tube. This is illustrated schematically in Fig. 8.

Eventually, the spot becomes so large that some of the electrons miss the target entirely, and there is a dropping off of the efficiency of the subsequent stages. The transverse spreading is such that there would be a serious loss after a comparatively few stages unless special precautions, that will be described later, are taken to prevent this type of defocusing.

Finally, the relative height above the targets to which the electrons rise will be

$$\frac{Y_{\max}}{X_0} = 0.4.$$

Thus the top row of plates must be placed at a distance slightly greater than this above the targets, to avoid collecting any current. The actual spacing used is one half the distance between target centers.

## 2. Design and Construction of Magnetic Multiplier

A schematic diagram of the actual application of the principles, described above, to a multiplier phototube is shown in Fig. 9. Photoelectrons are focused upon a target 2a. Secondary electrons from this electrode will be focused on target 3a giving rise to further electrons, and so on, for as many stages as are desired.

The plates are mounted in the tube in such a way that the upper and lower plates are as close together as is possible in order to make  $E_y$  large and thus increase the current that can be drawn away from a target before space-charge limitations occur. This minimum spacing, as was shown above, is half the distance between centers of successive targets. With this construction it is found that the current that can be drawn from the tube is limited only by the power that can be dissipated from the final stages in overcoming the heat generated by electron impacts.

In order to limit the sidewise spreading, the electrodes are mounted on vertical strips of mica. Charges which accumulate on these vertical walls so alter the field as to introduce an additional lens action which limits sidewise spreading. With this arrangement, the limit to the number of stages which may be used is set by the axial defocusing. However, this defocusing is so small as to permit the use of a great many stages. The upper limit to the number of stages has not been determined experimentally although multipliers employing as many as twelve stages without a decrease in gain per stage have been constructed.

When multipliers are operated at high gains into high impedance loads, some difficulty is encountered from oscillation. This can be eliminated by surrounding the collector electrode with a shield grid as shown in Fig. 9. The grid serves as an electrostatic shield and prevents changes of collector potential from reacting upon earlier stages. It also results in the alteration of the output characteristic from that of a triode to that of a conventional screen-grid tetrode.

For operation of the device, it is necessary that the upper electrodes be at a fixed positive potential with respect to the corresponding lower electrode, and that the voltage steps between adjacent electrodes be equal. In order to decrease the number of leads required, it has been found advantageous to connect upper electrodes to lower targets farther down in the tube. Satisfactory results have been attained when

each upper electrode is connected to the next succeeding lower target.

Since the first few targets draw almost no current, their potential can be supplied very satisfactorily from a voltage divider or bleeder. In order to decrease further the number of leads in a multiplier employing many stages, it has been found practicable to incorporate the bleeder for the initial stages inside the tube. Resistors for this purpose must be able to withstand the evacuating, baking, and activating processes involved in the tube construction. In the case of the tube shown in Fig. 9, the first five stages are supplied from an internal divider. The remaining stages may be supplied from an external bleeder. However, for the sake of economy in power required for operation, it may be well to supply the output stage and the last few targets from

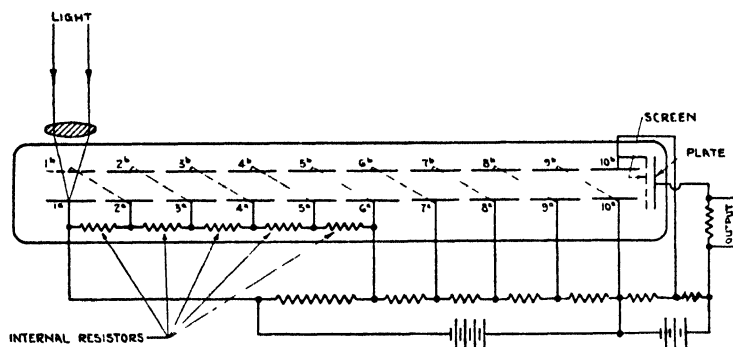


Fig. 9

a separate voltage supply, as the target currents may become quite high. In Fig. 9, the output is supplied from a separate source, the other stages being supplied from resistance voltage dividers.

It has been found possible to operate the device with alternating voltages on the electrodes. The operation will, of course, occur over only a portion of each cycle. The frequency of the applied alternating current must exceed the highest frequency which the multiplier is to transmit.

As a means of supplying the requisite magnetic field, permanent magnets have been found to be very satisfactory. These are superior to electromagnets from the standpoint of size and the fact that no external power is required.

In Fig. 10 is shown the effect of varying the magnetic field, while Fig. 11 is a similar curve for the effect of the over-all voltage. Both of these curves exhibit secondary maxima as well as the major peak. The secondary maxima are caused by more complex electron paths

where one or more of the lower electrodes are missed by the electron stream.

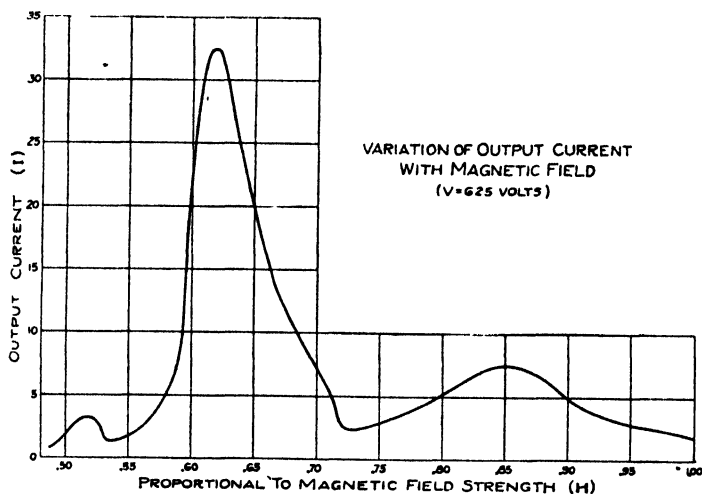


Fig. 10

The primary maximum is sufficiently broad so that ordinary fluctuations in line voltage do not result in appreciable variations in the

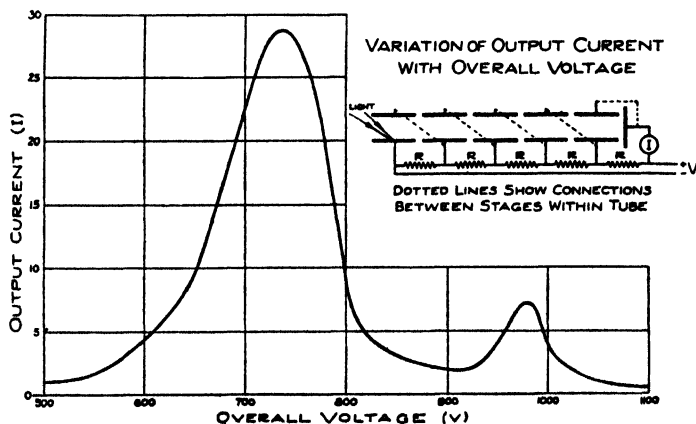


Fig. 11

output from the multiplier. If the current to any one stage is plotted as a function of the voltage to that stage alone or as a function of over-all voltage, characteristic curves are obtained similar to those of Fig. 11.

A photograph of the internal structure of a twelve-stage multiplier in which the voltage divider for the first five stages is incorporated in the tube, is shown in Fig. 12.



Fig. 12

### III. ELECTROSTATIC MULTIPLIER

Where the application of a secondary emission multiplier does not permit the use of a magnetic field, it is necessary to use a multiplier in which the electrons are focused by electrostatic fields alone.

The problems involved in designing the focusing system for such a multiplier are similar to many of those encountered in an electron microscope. It can be shown that in general a radially symmetric electrostatic field will have the properties of a lens over portions of the

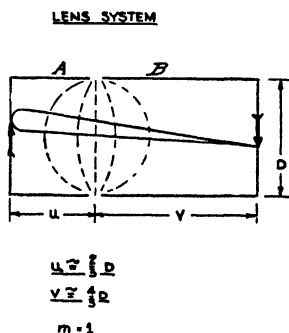


Fig. 13

field near the axis of symmetry. The radial distance from the axis over which this condition applies will depend upon the field configuration. The focusing system of the electrostatic multiplier is based on the field between two coaxial cylinders. Since it is desirable to have a minimum of separate voltages to operate the tube, one cylinder is made part of one target, while the other is connected to the next succeeding emitter. The configuration is made such that electrons from an area in the center of the first target will come to a focus at the center of the next

target and that the magnification of the electron image formed will be unity.

This electron "optical" system will be made clearer by reference to Fig. 13. In this diagram the lens is formed between the cylinders *A* and *B*, *A* being at ground potential, while *B* is at the potential *E*. The electrons are emitted from the cathode in *A* with a very low velocity, are deflected by the "lens" formed between the two cylinders, and are focused on to the screen or electrode in *B* striking it with a velocity of *E* electron volts. The magnification of this system will depend upon the object and image distance from the lens, but instead of  $m=v/u$ , we have, from the varying index of refraction of the medium along the "optical" path (i.e., electron path),  $m=v/2u$ .

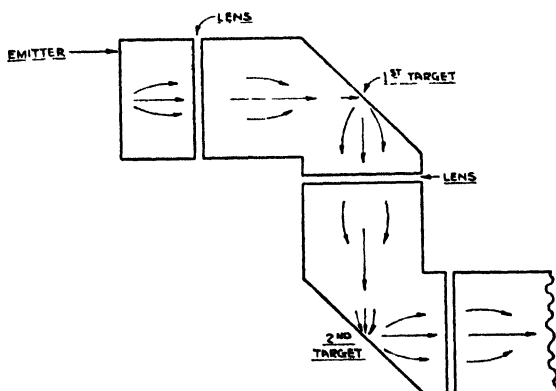


Fig. 14—L type multiplier.

The focal length is independent of the voltage between *A*, *B*, but is dependent on the diameter of the cylinders. It is found that in order to get good focus and unity magnification, the dimensions should be

$$u + v = 2D$$

with,

$$u = \frac{2D}{3} \quad \text{and} \quad v = \frac{4D}{3}.$$

The dimensions are only approximate, as the exact dimensions depend also upon the separation between cylinders. There will be some defocusing and lack of sharpness resulting from the initial velocities of the electrons (i.e., "chromatic" aberration) and also from aberrations in the lens system. This is not serious when the arrangement is used in a multiplier unless a very large number of stages is to be used.

The application of this optical system leads to the so-called L type multiplier whose construction is shown in Fig. 14. This multiplier is

quite satisfactory from the standpoint of focus. However, the field at each target drawing away the secondary electrons is rather weak and the multiplier becomes space-charge limited at rather small current values. Further, the emitting spot on the initial cathode must be small if accurate focus is to be maintained.

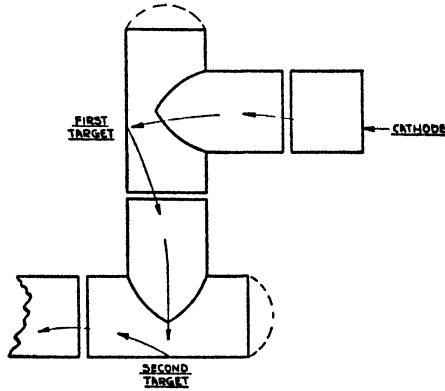


Fig. 15—T type multiplier.

A second type of multiplier has been designed which does not depend upon so sharp a focus and which has a higher collecting field at the targets. This is the T type multiplier which is shown in Fig. 15. This multiplier is built so that the cylindrical exits from the targets are as short as possible and yet long enough so that electrons entering

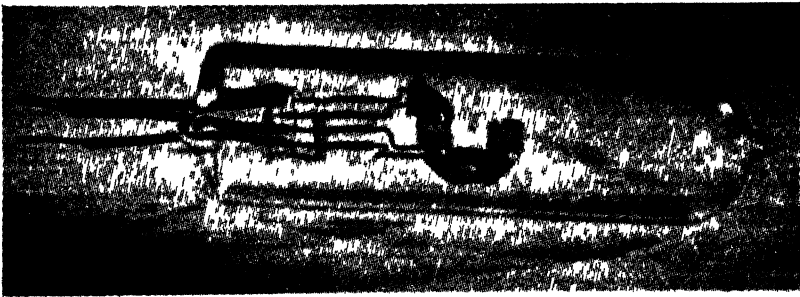


Fig. 16

through the stem of the T will not be deflected sufficiently by the field from the succeeding electrode to miss the target. The targets are formed by sensitizing the whole inside of the cylindrical crossarm of the T. Even with this arrangement, where currents of the order of a milliampere are to be used, it is necessary to operate the multiplier at a



fairly high voltage per stage, that is, 200 to 400 volts, if space-charge effects are to be avoided. Figs. 16 and 17 show multiplier phototubes of the L and T type.

#### IV. APPLICATIONS

The most obvious application of these multipliers is as a photoelectric amplifier. This use is very much simplified in view of the similarity between the photoelectric and secondary emissive surfaces. The most convenient type of multiplier to use for this purpose is the one combining electrostatic and magnetic fields. This is because of its excellent focusing characteristics and because of the high current output obtainable. A tube of this type having a gain of several millions or an output of ten or more amperes per lumen is but little larger than an ordinary receiving tube. A voltage of about 1500 volts is required

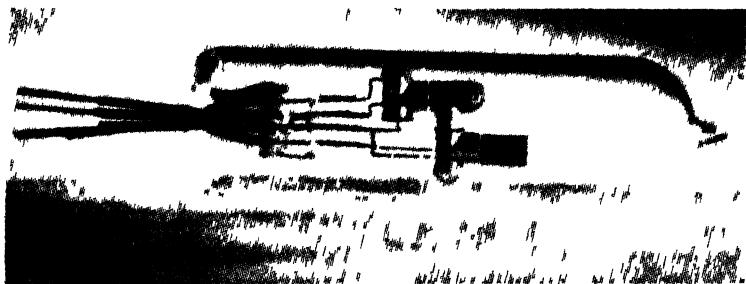


Fig 17

for operation, and since the current consumed is small, may be supplied from a small socket power unit.

Since the tube serves to replace not only a phototube but also its accompanying amplifier, there is obviously a great gain in simplicity and a saving in bulk. In addition, these multipliers are very stable, are insensitive to external interference, and have an excellent frequency characteristic. An even more important factor is that the noise output is determined by the shot noise of photoelectric effect and therefore allows an increase of sixty to one hundred times in signal-to-noise ratio under ordinary operating conditions for extremely low values of light. These facts combine to make this type of multiplier a very excellent means of converting a light signal into an electrical signal. In order to compare the size of this tube with that of a conventional receiving tube Fig. 18 is included comparing a ten-stage multiplier with an RCA 59.

The applications of multiplier phototubes are extensive including

in particular pickup from sound film, facsimile, automatic door control, alarm systems, automatic sorting machines, etc.

Although at present the most important application of the secondary emission multiplier is as a phototube it has a number of other applications which may become increasingly important. In general, these multipliers can be used in connection with any device where the signal to be amplified is generated in the form of an electron current. This use includes types of electron commutator tubes such as are used for high speed switching, secret sound systems, and frequency multi-

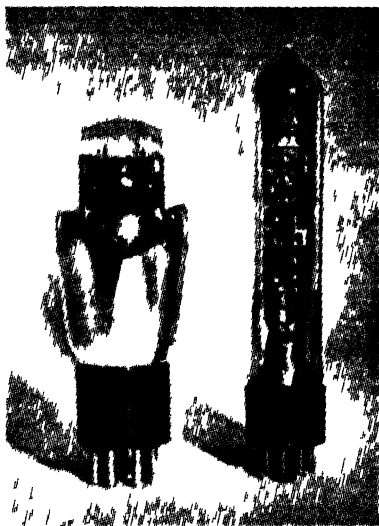


Fig. 18

pliers. One use in particular should be mentioned; that is, the application of the multiplier to the "iconoscope." For this purpose, an electrostatic multiplier is found to be the most satisfactory in that it avoids the use of a magnetic field which interacts detrimentally with the low velocity electrons in the tube. A multiplier used in this way serves not only as a very efficient means of coupling the tube to the television terminal equipment, but also replaces part or all of the picture amplifier.

As a voltage-controlled amplifier, the device does not lend itself so readily. This is because, in general, to couple the input of a voltage-controlled amplifier to its external circuit, it is necessary to use some form of coupling impedance and this, as in the case of a conventional thermionic amplifier, will limit the signal-to-noise ratio obtainable.

If the conventional type of thermionic cathode and control grid are used in connection with a multiplier, the problem of securing results superior to those obtainable with an ordinary vacuum tube presents considerable difficulties. There is the possibility of obtaining a higher per cent control per volt applied to the grid by deliberately throwing away a large fraction of the cathode current to gain this control, then using a multiplier to bring the average current back to a higher level. This is still in its initial experimental stages, and it is too early yet to say what the outcome will be. It should be noted also that this type of tube offers excellent opportunities to be used as a multiple-duty tube by using the control obtainable at various targets operated on different parts of their emission or focusing characteristics.

The secondary emission multiplier is too new an instrument to be able to foretell the full extent of its application; however, even now there is evidence that it may become a serious rival to the thermionic amplifier in many of the fields which that device has occupied alone for so long, and may also open up new fields in the realm of the electronics of small currents.

#### ACKNOWLEDGMENT

The authors wish to express their appreciation for the valuable assistance rendered by the other members of the Electronic Research Laboratory.

# ELECTRON OPTICS OF AN IMAGE TUBE\*†

By

G. A. MORTON AND E. G. RAMBERG

RCA Manufacturing Company, Inc.,  
Camden, N. J.

**Summary**—(1). *Introduction: Description of fixed-focus and variable-focus electrostatic image tube; scope of paper.* (2). *Focusing properties: Measurement of the variation of image distances and magnification with object distance and ratio of applied voltages for both types of tubes; calculation of potential distributions and electron paths; comparison of experimental and theoretical results.* (3). *Aberrations: Classification of aberrations; measurement of tangential and sagittal image surfaces for fixed-focus tube; calculation of axial (chromatic and spherical) aberrations; calculation of field aberrations; comparison between measurements and calculation; reduction of field aberrations by curving the cathode.*

## 1. INTRODUCTION

IN a recent paper, Drs. Zworykin and Morton<sup>1</sup> have described several electron optical systems for producing, on a fluorescent screen, slightly magnified or unmagnified images of extended objects, such as photosensitive surfaces on which light images are projected. The combination of such a photocathode, a suitable electron lens system and a fluorescent screen for observing the electron image, we shall call an "image tube." In the image tubes considered in the paper referred to above, the focusing of the electrons was accomplished by purely electrostatic means. The simplest ("fixed-focus") type of tube (Fig. 1, a) consisted of two narrowly separated cylinders of equal diameter at cathode and screen potential, respectively, the juncture of the two being described as the "lens." By replacing the cathode cylinder by a system of rings at uniformly increasing or decreasing potential (Fig. 1, b), simulating a resistive cylinder between whose ends a voltage is applied, it was found possible to obtain exact focusing for a given object and image distance by varying the ratio of the voltages applied across the system of rings ( $V_2$ ) and that between the anode and cathode ( $V_1$ ). Finally, it was found that, in either case, giving the cathode a curvature such that its center of curvature falls into the lens (Fig. 1, c), greatly improves the quality of the image, especially in the peripheral portions.

\* Decimal Classification: R138.3.

† Reprinted from *Physics*, December, 1936.

<sup>1</sup> V. K. Zworykin and G. A. Morton, *J. Opt. Soc. Am.*, 26, 181 (1936).

In the present paper, a more detailed experimental and theoretical study of the focusing properties and image defects of the above image tubes will be presented. It is hoped that such a study may help to outline the scope of these image tubes by pointing out the natural limits imposed by the focusing characteristics and aberrations, and suggesting in what directions future improvement must be sought.

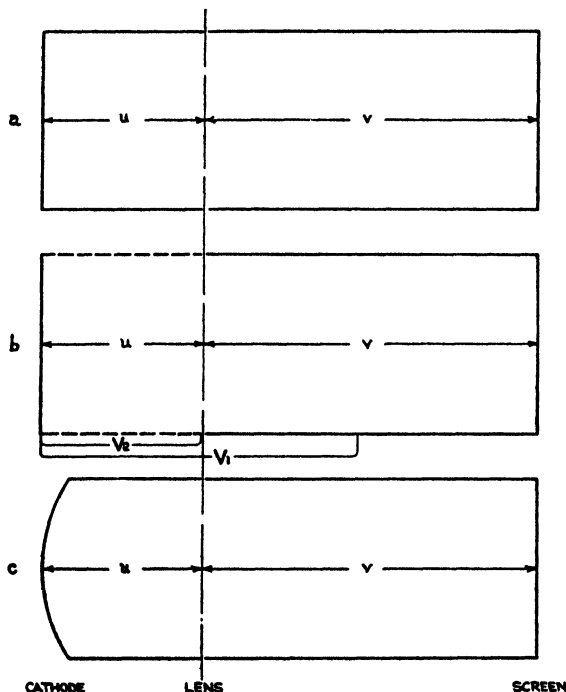


Fig. 1—Schematic diagram of image tubes.

## 2. FOCUSING PROPERTIES

In order to measure the variation of image distance  $v$  with object distance  $u$ , both measured from the "lens," in the fixed-focus type of tube, the tube shown in Fig. 2 was constructed. The cathode and screen are movable and can be shifted by tilting the tube. Catches are provided which hold the cathode in place when the tube is tilted in one position, and the screen in place when it is rotated about its axis through  $180^\circ$ . This allows the two elements to be moved independently. The lens-to-image distance  $v$ , for which the center of the image appeared sharp, as well as the corresponding magnification  $m$ , were measured for a set of cathode-to-lens distances  $u$ .

Fig. 3 shows a corresponding modification of the focusing ring

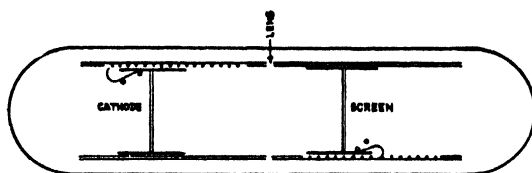


Fig. 2—Experimental tube with movable cathode and screen.

type tube shown in Fig. 1, b. Here, the screen is made movable, and the cathode fixed at a distance of 1.8 lens radii from the lens, the image distance and magnification being measured for different values of  $V_2/V_1$ , the ratio of the voltage applied between the cathode and outermost ring, and that applied between the cathode and anode.

To obtain similar information by calculation, it is necessary first to find the variation of the refractive index  $n$ , of the medium, which is conveniently given by the square root of the potential, if we choose the latter to be zero at points where the velocity of the electrons vanishes (e.g., at the cathode if we neglect the initial velocities).<sup>2</sup> Then, with the aid of Fermat's law,

$$\delta \int n ds = 0, \quad (1)$$

$ds$  being an element of path of the ray considered, and the variation applying to paths with fixed endpoints, the paths actually taken by electrons emitted from the cathode and, hence, the position and magnification of the image can be determined.

The variation of potential within the tube is governed by Laplace's equation and conditions imposed at the boundaries, i.e., the potentials applied to the cylinders and the cathode. We shall, for convenience, imagine the anode cylinder to be extended to infinity. This introduces no appreciable error, as electrons which have entered the anode cylinder, owing to their high velocities, are but slightly affected by any "end-effects," including among these the presence of the fluorescent screen.

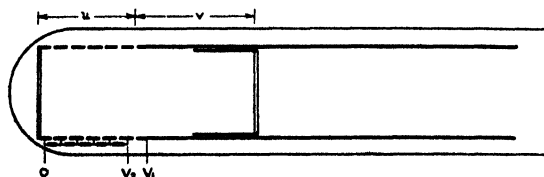


Fig. 3—Variable focus tube with movable screen.

<sup>2</sup> See e.g., E. Brüche and O. Scherzer, *Geometrische Elektronenoptik* (Springer, 1934), p. 3.

Cylindrical coordinates, with their origin at the center of the cathode, are most convenient.  $z$  will denote the distance from this point along the axis of symmetry, and  $r$  the separation of any point from this same axis. The radius of the focusing cylinders ("lens radius") will be taken as unit of length. The substitution

$$\chi(r, z) = F(z) \cdot G(r) \quad (2)$$

in Laplace's equation

$$\nabla^2 \chi = 0 \quad (3)$$

reduces its solution to that of the two ordinary differential equations.

$$(1/F) (d^2 F/dz^2) = -k^2, \quad (4a)$$

$$(1/rG) (d/dr) (r dG/dr) = k^2, \quad (4b)$$

$k^2$  being a separation parameter, with the general solutions

$$F = ae^{ikz} + be^{-ikz}, \quad (5a)$$

$$G = cJ_0(ikr) + dN_0(ikr). \quad (5b)$$

The solution for the potential must have the form of a linear combination of products of such functions with the same value of  $k$ , which may be any value in the complex plane. The requirement that the potential remain finite as  $z \rightarrow \infty$ , eliminates terms with complex  $k$ . Furthermore, the condition that it be finite on the axis, eliminates those containing the Neumann function  $N_0$ . Finally, the fact that the potential vanishes (in the case of the flat cathode) all over the cathode plane, limits the trigonometric functions to be considered to sines. The solution for the potential thus becomes

$$\varphi(r, z) = \int_0^\infty b_k J_0(ikr) \sin k z dk. \quad (6)$$

The coefficient  $b_k$  can be evaluated by substituting the values of  $\varphi(r, z)$  for  $r = 1$  by the usual methods used for evaluating Fourier coefficients. For the fixed-focus tube, assuming the gap between the cathode and anode cylinders to be negligible, the potential along the axis becomes

$$\Phi(z) = \varphi(0, z) = -\frac{2}{\pi} \int_0^\infty V_1 \frac{\cos ku}{k} \frac{\sin kz}{J_0(ik)} dk, \quad (7)$$

the first two derivatives being given correspondingly by

$$\Phi'(z) = \frac{2}{\pi} \int_0^\infty V_1 \cos ku \frac{\cos kz}{J_0(ik)} dk, \quad (7')$$

$$\Phi''(z) = \frac{-2}{\pi} \int_0^\infty V_1 k \cos ku \frac{\sin kz}{J_0(ik)} dk. \quad (7'')$$

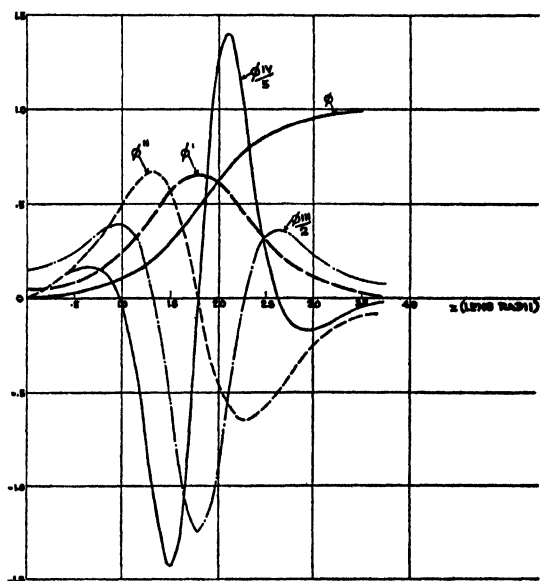


Fig. 4—Axial potential for fixed-focus tube and its first four derivatives.

Fig. 4 shows the axial potential distribution of the fixed-focus type of tube with  $u = 1.8$ , together with its first four derivatives.

Similarly, for the focusing ring type tube, replacing the set of rings by a cylinder of uniformly increasing or decreasing potential, the result for the potential along the axis is

$$\Phi(z) = \frac{2}{\pi} \int_0^\infty \left( \frac{V_2}{u} \frac{\sin ku}{k^2} + (V_1 - V_2) \frac{\cos ku}{k} \right) \frac{\sin kz}{J_0(ik)} dk. \quad (8)$$



For any given object distance  $u$ , it is thus possible, by numerical or graphical quadrature of the above integrals, to find the potential along the axis for different values of  $z$ . Furthermore, the potential off the axis is given in terms of the axial potential and its derivatives by the relation<sup>3</sup>

$$\varphi(r, z) = \Phi(z) - \frac{r^2}{4} \Phi''(z) + \frac{r^4}{64} \Phi^{IV}(z) - \dots \quad (9)$$

Replacing, temporarily, the cylindrical ordinates  $r, \theta$  by Cartesian coordinates  $x, y$  ( $r^2 = x^2 + y^2$ ), Fermat's law can be written

$$\delta \int F(x, y, x', y', z) dz = \delta \int \{ \varphi(x, y, z) \times [x'^2 + y'^2 + 1] \}^{\frac{1}{2}} dz = 0, \quad (10)$$

where a prime denotes differentiation with respect to  $z$ . The corresponding Euler equations for the electron paths,

$$(d/dz) F_{x'} - F_x = 0, \quad (11a)$$

$$(d/dz) F_{y'} - F_y = 0, \quad (11b)$$

thus become

$$x'' = \frac{x'y'y''}{1+y'^2} - \frac{1}{2\varphi} x' \left( 1 + \frac{x'^2}{1+y'^2} \right) \times \left( \frac{\partial \varphi}{\partial r} \left[ \frac{x'x + y'y}{r} \right] + \frac{\partial \varphi}{\partial z} \right) + \frac{(1+x'^2+y'^2)^2}{1+y'^2} \frac{x}{r} \frac{1}{2\varphi} \frac{\partial \varphi}{\partial r}, \quad (12a)$$

$$y'' = \frac{x'y'x''}{1+x'^2} - \frac{1}{2\varphi} y' \left( 1 + \frac{y'^2}{1+x'^2} \right) \times \left( \frac{\partial \varphi}{\partial r} \left[ \frac{x'x + y'y}{r} \right] + \frac{\partial \varphi}{\partial z} \right) + \left( \frac{1+x'^2+y'^2}{1+x'^2} \right)^2 \frac{y}{r} \frac{1}{2\varphi} \frac{\partial \varphi}{\partial r}. \quad (12b)$$

When the rays considered are in meridian planes only, attention may be confined to the first of these equations, and  $x$  may be replaced

<sup>3</sup> Reference 2, p. 66, Eq. (16).

throughout by  $r$ ,  $y$  being set equal to zero. If, finally, the expression (9) is substituted for  $\varphi$  we may drop, for "paraxial rays," i.e., such that deviate infinitesimally from the axis of the system, all terms involving higher powers than the first of  $r$  and  $r'$  yielding:

$$r'' = -(\Phi'/2\Phi)r' - (\Phi''/4\Phi)r. \quad (13)$$

If the radial distance from the center of the cathode to the starting point of an electron ray,  $r(0)$ , and its initial slope,  $r'(0)$ , are given, this equation, by a process of numerical integration, enables us to find the distance of the ray from the axis,  $r(z)$ , for any value of  $z$ .

To locate the image position, we shall consider the path of an electron leaving the center of the cathode with an infinitesimal initial radial velocity. The determination of the path is simplified by introducing, as dependent variable,

$$b = 1/2z - 1/r(dr/dz). \quad (14)$$

which reduces Eq. (13) to a first-order equation. The term  $-(dr/dz)/r$  is the convergence of the ray at the point  $z$ , i.e., the reciprocal of the segment of the axis measured from the abscissa of the point considered to the intersection with the tangent to the ray;  $-1/2z$ , on the other hand, is the initial convergence of the ray, which describes a parabola of the form  $r^2 = pz$  ( $p = a$  constant) in the uniform field immediately in front of the cathode. The convergence variable,  $b$ , is thus chosen so as to vanish for  $z = 0$ , where the convergence itself becomes negatively infinite.

Substituting (14) in (13), the equation governing  $b$  becomes

$$\frac{db}{dz} = b^2 - b \left( \frac{1}{z} + \frac{\Phi'}{2\Phi} \right) + \frac{\Phi''}{4\Phi} + \frac{1}{2z} \left( \frac{\Phi'}{2\Phi} - \frac{1}{2z} \right). \quad (15)$$

This equation, again, cannot be integrated analytically but must be evaluated numerically. The value of  $b$  is determined by a step-by-step process of integration, for some particular value of  $z$ , far enough to the right of the lens so that the ray path is essentially a straight line. From the convergence of the ray at this point the image position is located.

To determine the magnification, as illustrated in Fig. 5, the point of intersection of the image plane, as determined above, and the path of an electron leaving the cathode, with zero initial velocity, at a radial distance "O" from the center of the cathode, is located. The

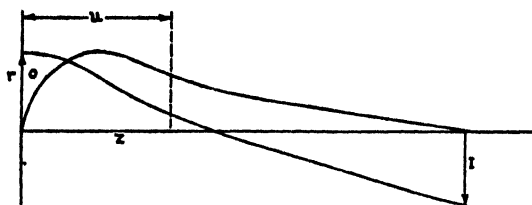


Fig. 5—Electron paths.

radial distance "I" of this intersection, divided by the distance "O," gives the magnification. To calculate this path Eq. (13) must be used.

A comparison of the results of the measurements and calculations for the fixed and variable focus type tubes is given by Figs. 6 to 9. The relatively large deviations for very small image distances,  $v$ , may be ascribed to the interference of the screen with the field distribution within the lens. The closeness with which the magnification is given by  $v/2u$  is striking for both types of tubes.

### 3. ABERRATIONS

The aberrations which detract from the quality of the electron image observed on the fluorescent screen can conveniently be separated into two classes; axial aberrations and field aberrations. The former, chromatic and spherical aberration in the customary nomenclature, affect the quality of the image on the axis, as well as in other

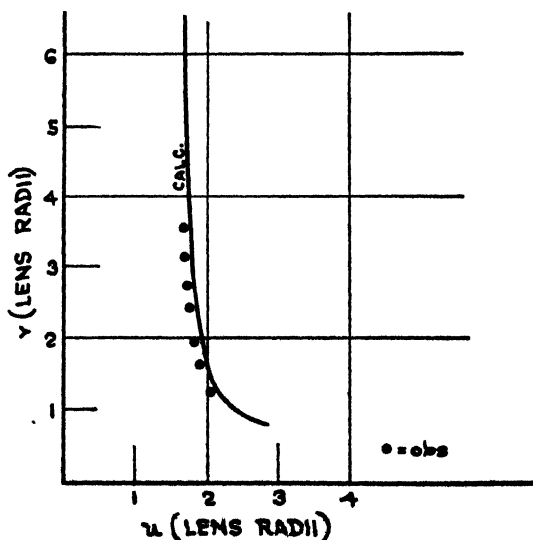


Fig. 6—Focusing relation (fixed focus).

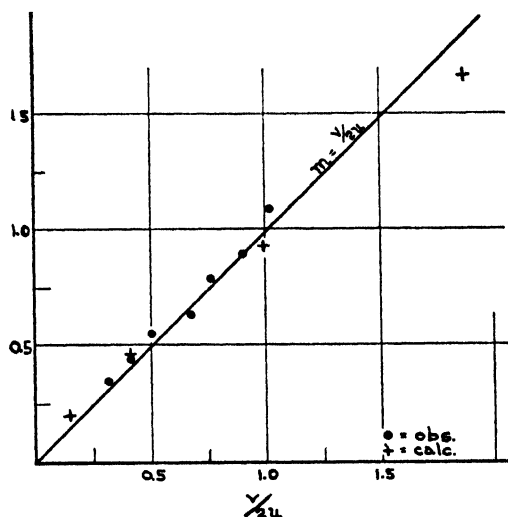


Fig. 7—Magnification (fixed focus).

parts of the field, while the latter, in first line astigmatism and curvature of field, become noticeable only in the outer portions of the image. It will be seen that these constitute the most serious defects of the systems here studied.

An experimental investigation of all the image defects of electron optical systems has been carried out for a point source by Diels and

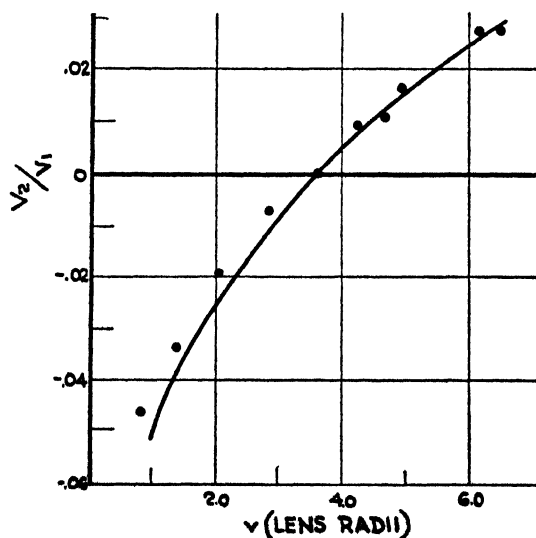


Fig. 8—Focusing relation (variable focus).

Knoll,<sup>4</sup> to demonstrate their identity with the aberrations encountered in light optics. H. Johansson<sup>5</sup> has made a special study of the aberrations of the electron microscope. On the theoretical side, Glaser<sup>6</sup> has developed the theory of electron optical aberrations very completely, though not in the form in which it is directly applicable to our case, where the electrons enter the refracting field with infinitesimal velocities. Henneberg and Recknagel<sup>7</sup> have, making suitable simplifying assumptions, given a theoretical treatment of the chromatic (and spherical) aberrations of various types of image tubes.

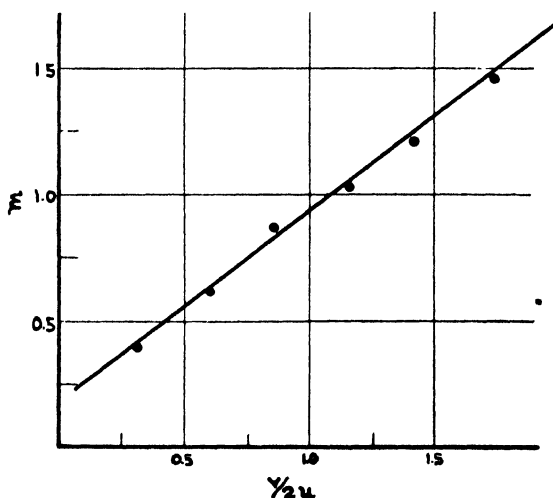


Fig. 9—Magnification (variable focus).

It was not practical, in the present case, to carry out measurements of the axial aberrations, as these are not of sufficient magnitude to be readily determined except for so low accelerating voltages that no bright images could be obtained on the screen. For the measurement of the field aberrations, curvature and astigmatism, the procedure was the following. In the tube of Fig. 2 the object distance was kept fixed at the value  $u = 1.8$  and pictures were taken of the image on the fluorescent screen at various distances from the lens; such a series of photographs is shown in Fig. 10. The object consisted of a grid of fine vertical lines superposed on an array of black squares. The point along a vertical line through the optical axis of the system at which the fine

<sup>4</sup> K. Diels and M. Knoll, *Zeits. f. Tech. Physik* 16, 617 (1935).

<sup>5</sup> H. Johansson, *Ann. d. Physik* 18, 385 (1933); 21, 274 (1934).

<sup>6</sup> W. Glaser, *Zeits. f. Physik* 80, 451; 81, 647; 83, 104 (1933); 97, 177 (1935); *Ann. d. Physik* 18, 557 (1933).

<sup>7</sup> W. Henneberg and A. Recknagel, *Zeits. f. Tech. Physik* 16, 230 (1935).

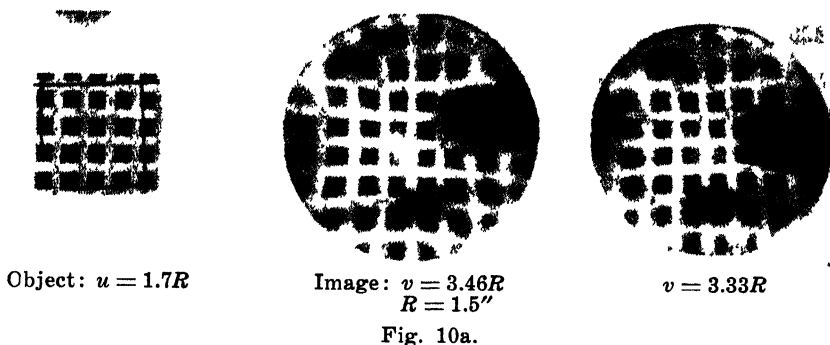


Fig. 10a.

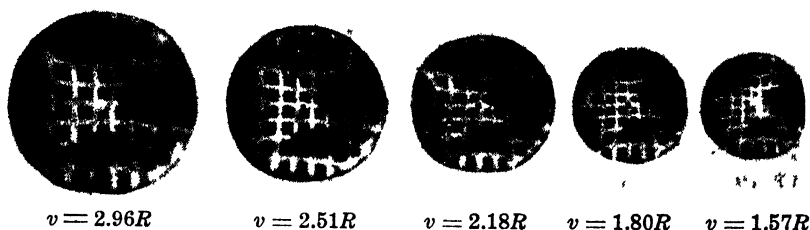


Fig. 10b.

Fig. 10—Sections through image space of flat cathode tube for various distances from lens  $v$ .

lines appear sharpest, indicates the location of a sagittal, that along a horizontal line through the axis where they appear sharpest, that of a tangential image point, just as in ordinary optics. Having located the sagittal and tangential image points in every plane, it is possible to construct also the sagittal and tangential images surfaces.

In order to calculate the axial aberrations, we consider pencils of rays leaving the center of the cathode with a fixed initial kinetic energy  $e\Delta\Phi$  under different angles, e.g.,  $0^\circ$ ,  $45^\circ$ , and  $90^\circ$ , and find their points of convergence on the axis.

To treat the first case,  $\theta = 0$ , we place  $\Phi$  in Eq. (13) by  $\Phi + \Delta\Phi$  and then introduce as new dependent variable (which vanishes for  $z = 0$ ):

$$b. = \frac{1}{2 \left( \left[ z + \frac{\Delta\Phi}{\Phi'(0)} \right] - \left[ \frac{\Delta\Phi}{\Phi'(0)} \left[ z + \frac{\Delta\Phi}{\Phi'(0)} \right] \right)^{\frac{1}{2}}} - \frac{1}{r} \frac{dr}{dz}. \quad (16)$$

If  $b_0$  is a solution of Eq. (15) corresponding to the case of zero initial velocity and  $\Delta b = b - b_0$  is small up to the point where ray paths become substantially straight ( $z = z_1$ ), we can write for  $\Delta b(z_1)$ :

$$\Delta b(z_1) = \int_0^{z_1} B(z') \exp\left(\int_{z'}^{z_1} A(z'') dz''\right) dz', \quad (17)$$

$$\text{where} \quad A = (1/z + \Phi/2\Phi) + 2b_0, \quad (18)$$

$$B = \frac{\Delta\Phi}{\Phi} \left( b_0^2 - \frac{db_0}{dz} - \frac{b_0}{z} - \frac{1}{4z^2} \right) - \frac{1}{4z^2} \left( \frac{\Delta\Phi}{\Phi'(0)z} \right)^{\frac{1}{2}} \\ \times \left( 1 - \left( \frac{\Delta\Phi}{\Phi'(0)z} \right)^{\frac{1}{2}} \right) - \frac{b_0}{z} \left( \frac{\Delta\Phi}{\Phi'(0)z} \right)^{\frac{1}{2}} + \frac{\Phi'}{4z\Phi} \left( \frac{\Delta\Phi}{\Phi'(0)} \right)^{\frac{1}{2}}.$$

To find the solutions for rays with finite initial lateral velocity components, we introduce the variable  $\Delta r = r - r_0$  where  $r_0$  is the solution of the paraxial Eq. (13) for an equal initial lateral velocity and integrate the equation

$$\Delta r'' = - \frac{\Phi''}{4(\Phi + \Delta\Phi)} \Delta r - \frac{\Phi'}{2(\Phi + \Delta\Phi)} \Delta r' \\ - r_0 \frac{\Phi''}{4(\Phi + \Delta\Phi)} \left[ r_0^2 \left( \frac{\Phi''}{4(\Phi + \Delta\Phi)} - \frac{\Phi^{IV}}{8\Phi''} \right) + 2r_0'^2 \right] \\ - r_0' \frac{\Phi'}{2(\Phi + \Delta\Phi)} \left[ r_0^2 \left( \frac{\Phi''}{4(\Phi + \Delta\Phi)} - \frac{\Phi'''}{4\Phi'} \right) \right. \\ \left. - r_0 r_0' \frac{\Phi''}{2\Phi} + r_0'^2 \right] - r_0'' \frac{\Delta\Phi}{\Phi + \Delta\Phi}. \quad (19)$$

This is obtained from Eq. (12a) if terms involving third powers of  $r$  and  $r'$  are retained. The proper initial conditions follow in every case from the form of the parabolic path described by the electron in the uniform accelerating field immediately in front of the cathode.

For the case of the fixed-focus tube with unity magnification and with  $\Delta\Phi/V_1 = 0.001$  (e.g.,  $\Delta\Phi = 0.4$  volt,  $V_1 = 4000$  volts), the axial deviations from the focal point corresponding to infinitesimal initial velocities are found to be 0.44, 0.24, and  $-0.03$  lens radii for  $\theta = 0^\circ$ ,  $45^\circ$ , and  $90^\circ$  respectively. As the solution of Eq. (18) for our particular case indicates that the vertex angle of a beam, with initial lateral velocity  $[2(e/m)\Delta\Phi_r]^{\frac{1}{2}}$ , is equal to  $2.17(\Delta\Phi_r/V_1)^{\frac{1}{2}}$  the diameter

$\Delta$  of the circle of least diffusion is found to be about 0.003 lens radii, or 0.004" (= 0.1 mm), increasing approximately in proportion to the initial energy of the electrons. The formula given by Henneberg and Recknagel<sup>7</sup> yields  $\Delta = 2m\Delta\Phi/\Phi'(0) = 0.004$  lens radii or 0.006" (= 0.15 mm). It is based on considering the image tube field as consisting of a uniform initial field terminated by a short lens. It is seen that the axial aberrations, while not important in the present case, may be of significance when the field before the cathode is reduced (as when a very small image is desired), or in cases when the initial velocities are on the average substantially larger and the accelerating voltage is reduced.

Of greatest importance are, however, the field aberrations, image curvature and astigmatism. To calculate these, the paths of a set of principal rays, corresponding to electrons starting from rest on the cathode at various distances from the axis, must first be obtained by integrating the equation

$$r'' = -\frac{r\Phi''}{4\Phi} \left[ 1 + r^2 \left( \frac{\Phi''}{4\Phi} - \frac{\Phi^{IV}}{8\Phi''} \right) + 2r'^2 \right] - \frac{r'\Phi'}{2\Phi} \left[ 1 + r^2 \left( \frac{\Phi''}{4\Phi} - \frac{\Phi'''}{4\Phi'} \right) - r \frac{r'\Phi''}{2\Phi'} + r'^2 \right], \quad (20)$$

which is found by substituting Eq. (9) in Eq. (12a), retaining terms up to the third power in  $r$  and  $r'$ . Pencils of rays starting from the same point on the cathode, with infinitesimal lateral velocities, will in general come to a focus only if they lie either in the meridional plane or a plane normal thereto, the focal points being termed the tangential and sagittal image points, respectively. These image points, corresponding to all possible principal rays, form the tangential and sagittal image surfaces which are the object of the calculation. The separation of the two surfaces gives a measure of the astigmatism, their curvature determines the image curvature. Fig. 11 illustrates the tangential and sagittal pencils belonging to a particular principal ray, as well as the two image surfaces  $T$  and  $S$ .

To obtain the tangential image point corresponding to a given principal ray  $r_0(z)$ , which is a solution of Eq. (20) for  $r'_0(0) = 0$ , we introduce the difference variable  $\Delta r = r - r_0$  and, furthermore, the convergence variable

$$b = 1/2z - (1/\Delta r)\Delta r', \quad (21)$$



which obeys the equation

$$\begin{aligned} \frac{db}{dz} = & -\frac{1}{4z^2} + \frac{\Phi''}{4\Phi} \left[ 1 + 3r_0'^2 \left( \frac{\Phi''}{4\Phi} - \frac{\Phi^{IV}}{8\Phi''} \right) \right. \\ & \left. + 2r_0'r_0'' \left( \frac{\Phi'}{2\Phi} - \frac{\Phi'''}{2\Phi''} \right) + r_0''^2 \right] \\ & + \frac{\Phi'}{2\Phi} \left( \frac{1}{2z} - b \right) \left[ 1 + r_0'^2 \left( \frac{\Phi''}{4\Phi} - \frac{\Phi'''}{4\Phi'} \right) \right. \\ & \left. + r_0'r_0'' \frac{\Phi''}{\Phi'} + 3r_0''^2 \right] - \frac{b}{z} + b^2. \quad (22) \end{aligned}$$

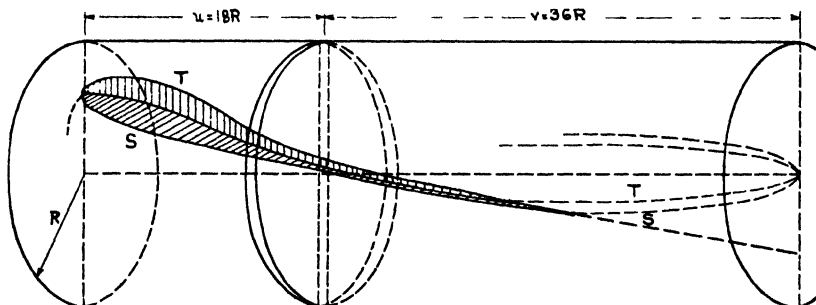


Fig. 11—Schematic diagram of lens structure and sagittal and tangential pencils.

This can be integrated numerically in the same fashion as Eq. (15) giving the tangential image point on the principal ray. The calculation of the tangential image curvature on the axis can readily be reduced to quadrature if  $\Delta b = b - b_0$ , where  $b_0$  is the solution of Eq. (15), is introduced in Eq. (22).

To find the sagittal image point, the second Euler equation, (12b), is utilized, considering the displacement  $y$  as infinitesimal; then Eq. (12b) becomes

$$y'' = y' \left[ \frac{r_0'r_0''}{1 + r_0'^2} - \frac{1}{2\Phi} \left( \frac{\partial\Phi}{\partial r} r_0' + \frac{\partial\Phi}{\partial z} \right) \right] + \frac{(1 + r_0'^2)}{2\Phi r_0} \frac{\partial\Phi}{\partial r} y. \quad (23)$$

Introducing

$$b = 1/2z - (1/y)y', \quad (24)$$

as well as the expansion of the potential (9), a convergence equation analogous to (22) is obtained:

$$\begin{aligned} \frac{db}{dz} - \frac{1}{4z^2} + \frac{\Phi''}{4\Phi} \left[ 1 + r_0'^2 \left( \frac{\Phi''}{4\Phi} - \frac{\Phi^{IV}}{8\Phi''} \right) + r_0'^2 \right] \\ - \frac{r_0' r_0''}{2z} + \frac{\Phi'}{2\Phi} \left( \frac{1}{2z} - b \right) \left[ 1 + r_0'^2 \left( \frac{\Phi''}{4\Phi} - \frac{\Phi'''}{4\Phi'} \right) \right. \\ \left. - r_0' r_0' \frac{\Phi''}{2\Phi'} \right] + b r_0' r_0'' - \frac{b}{z} + b^2. \end{aligned} \quad (25)$$

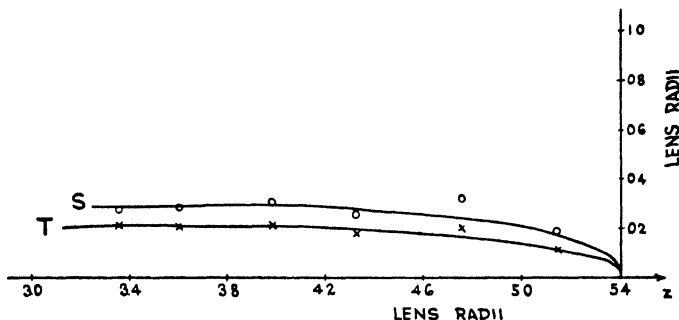


Fig. 12—Curvature of image field. *S*, calculated sagittal image surface; *T*, calculated tangential image surface; *o*, measured sagittal image points; *x*, measured tangential points.

The numerical work and the obtention of the sagittal radius of curvature on the axis proceed as in the case of the tangential pencil.

In Fig. 12, the measured image points are compared with the calculated image surfaces, computations being made for object points on the cathode separated by 0.2, 0.4 and 0.6 lens radii from the axis, as well as for the radii of curvature on the axis. Vertical and horizontal scales are identical so that the figure gives a true picture of the appearance of the image surfaces. Fig. 13 gives the corresponding large diameters of the ellipses of diffusion in the plane of the paraxial image point neglecting axial aberrations. The axial radii of curvature of the tangential and sagittal image surfaces are only 0.044 and 0.075 lens radii, or 1.7 and 2.9 mm, respectively.

It was found as already reported in the earlier paper,<sup>1</sup> that this very serious defect could be largely removed by giving the cathode a curvature such that its center of curvature fell, approximately, into the center of the lens. The comparison of the images given by the flat and

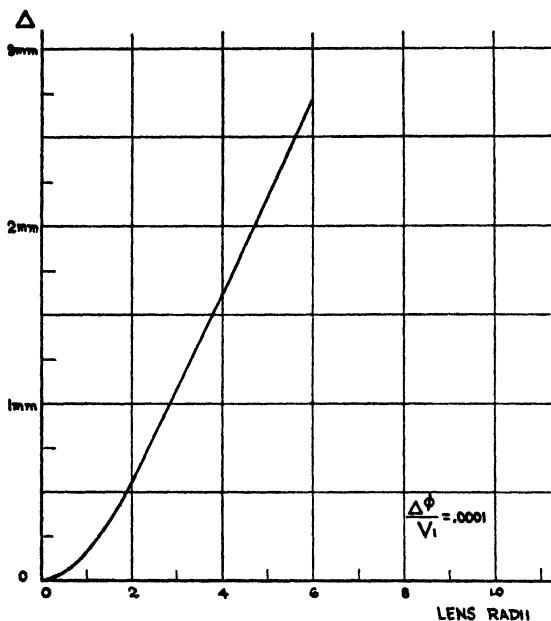


Fig. 13 — Large diameter of ellipse of diffusion due to curvature of field as function of radial distance of object point.

the curved cathode tube, shown in Fig. 14, brings this out strikingly. Without, as yet, giving a quantitative treatment of the curved cathode tube, the main reason for the improvement may readily be pointed out. By curving the cathode in the above mentioned fashion, the principal rays are practically undeflected in the first part of their path, and the sagittal and tangential pencils of all the rays encounter practically identical variations of potential. As, due to the low velocities of the electrons in this region, their paths are most easily influenced in the early portion of their transit, it is clear that this must minimize the astigmatism, i.e., the difference between the convergence of the tangential and sagittal rays, and similarly reduce the curvature due to the similar conditions along different principal rays.

In conclusion, the authors wish to express their thanks to Dr. V. K. Zworykin, the director of the Electronic Research Laboratory, and to the members of the laboratory staff whose cooperation made this work possible.

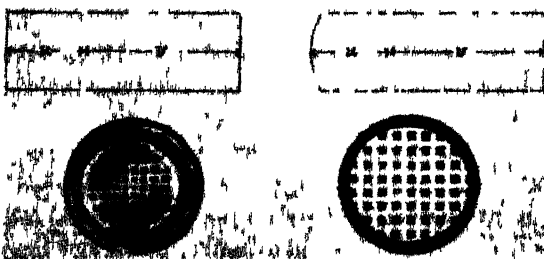


Fig. 14 — Comparison of images from tubes with flat (left side) and curved (right side) cathodes.

# A REVIEW OF THE DEVELOPMENT OF SENSITIVE PHOTOTUBES\*†

BY

ALAN M. GLOVER

RCA Manufacturing Company, Inc.,  
Harrison, N. J.

*Summary*—The development of phototubes is traced from early investigations of the nature of the photoelectric effect to the development of modern sensitized photosurfaces. The photoelectric properties of such surfaces are contrasted with those of pure metals. A discussion is given of the technical developments which have contributed to the importance of modern phototubes. A comprehensive bibliography covering both general and specific references on the subject of photoelectricity with emphasis on photoemissive surfaces is included.

## HISTORICAL INTRODUCTION

THE TERM "photoelectric cell" may be applied to three different devices which respond to the incidence of light or other electromagnetic radiation by the flow of an electric current. Of these three, the photoemissive cell or phototube is historically the most recent. In 1839, Becquerel<sup>1,2</sup> discovered that the illumination of one of two silver electrodes in an electrolytic or voltaic cell resulted in the production of an electromotive force which thus caused a current to pass through the cell. Such cells are now known as photovoltaic cells because the generation of the electromotive force was long thought to be the primary mechanism involved. The discovery that the resistance of selenium is altered upon illumination has been attributed to W. Smith who, in 1873<sup>3</sup>, was engaged in developing materials for use in the transatlantic cable. Light-sensitive materials in which a change in current is thus produced are known as photoconductive cells. In general, such substances are found to be semiconductors, although insulators exhibit a small photoconductive effect.

---

\* Decimal Classification: 535.38.

† Reprinted from *Proc. I.R.E.*, August, 1941.

<sup>1</sup> E. Becquerel, "Recherches sur les effets de la radiation chimique de la lumiere solaire, au moyen des courants electriques," *Compt. Rend.*, Vol. 9, pp. 144-149; July, 1839.

<sup>2</sup> E. Becquerel, "Memoire sur les effets electriques produits sous l'influence des rayons solaires," *Compt. Rend.*, Vol. 9, pp. 561-567; November, 1839.

<sup>3</sup> S. Bidwell, "On the sensitiveness of selenium to light, and the development of a similar property in sulphur," *Phil. Mag.*, Vol. 20, pp. 178-190; August, 1885.

In 1887, Hertz<sup>4</sup> was engaged in an experiment which demonstrated the validity of Maxwell's prediction that energy should be radiated from a conductor in which a rapidly changing current flows. Hertz discovered that when a spark discharge took place in a circuit, a small spark was observed at a gap in a similar neighboring circuit. Incidentally, this experiment laid the basis for the development of radio. In the course of the experiment, Hertz found that the length of the spark induced in the auxiliary circuit was reduced if the light from the primary spark was not allowed to fall upon the second gap. The effect was traced to the ultraviolet light from the spark and was found to be primarily due to the illumination of the negative electrode. The investigations of Hallwachs<sup>5</sup> showed that negative electricity was released from a negatively charged zinc plate under the influence of ultraviolet light. This current was identified in 1899 by Lenard<sup>6</sup>, and by J. J. Thomson<sup>7</sup> with the electrons which constituted the current in the discharge of a Geissler tube. Elster and Geitel<sup>8</sup> showed in 1899 that certain metals such as potassium and sodium, when amalgamated with mercury, were sensitive even to visible light. Within a short time, they realized that a considerably enhanced and more stable emission current could be obtained if the negative element and a positive collector were enclosed in an evacuated bulb<sup>9,10</sup>. Hence, the phototube may be considered as one of the first of the family of electronic tubes. As early as 1892 Elster and Geitel<sup>11,12</sup> devised an instrument which incorporated a photosensitive surface for measuring the ultraviolet light from the sun.

---

<sup>4</sup> H. Hertz, "Ueber einen Einfluss des ultravioletten Lichtes auf die electrische Entladung," *Ann. der Phys.*, Vol. 31, No. 8(B), pp. 983-1000; 1887.

<sup>5</sup> W. Hallwachs, "Ueber den Einfluss des Lichtes auf electrostatisch geladene Korper," *Ann. der Phys.*, Vol. 33, No. 2, pp. 301-312; 1888.

<sup>6</sup> P. Lenard, "Erzeugung von Kathodenstrahlen durch ultraviolettes Licht," *Ann. der Phys.*, Vol. 2, No. 6, pp. 359-375; 1900.

<sup>7</sup> J. J. Thomson, "On the masses of the ions in gases at low pressures," *Phil. Mag.*, Vol. 48, pp. 547-567; December, 1899.

<sup>8</sup> J. Elster and H. Geitel, "Notiz ueber die Zerstreuung der negativen Electricitat durch das Sonnen und Tageslicht," *Ann. der Phys.*, Vol. 38, No. 9, pp. 40-41; 1889.

<sup>9</sup> J. Elster and H. Geitel, "Ueber die Verwendung des Natriumamalgames zu lichtelectrischen Versuchen," *Ann. der Phys.*, Vol. 41, No. 10, pp. 161-176; 1890.

<sup>10</sup> J. Elster and H. Geitel, "Notiz ueber eine neue Form der Apparate zur Demonstration der lichtelectrischen Entladung durch Tageslicht," *Ann. der Phys.*, Vol. 42, No. 4, pp. 564-567; 1891.

<sup>11</sup> J. Elster and H. Geitel, "Beobachtungen des atmospharischen Potentialgefalles und der ultravioletten Sonnenstrahlung," *Ann. der Phys.*, Vol. 48, No. 2, pp. 338-373; 1893.

<sup>12</sup> J. Elster and H. Geitel, "Ueber die Vergleichung von Lichtstarken auf photoelectrischen Wege," *Ann. der Phys.*, Vol. 48, No. 4, pp. 625-635; 1893.

The photoelectric current was also shown to be directly proportional to the intensity of the light producing it. However, the kinetic energy of the released electrons was found to be independent of the intensity of the light, but to be dependent upon the frequency of the light<sup>6</sup>. These facts, which were inconsistent with a wave theory of the nature of light, led Einstein<sup>13</sup> to postulate that light was corpuscular in nature and that each light corpuscle or "quantum" could give up its energy to an electron of the metal. He assumed that the energy of each quantum of light of a given frequency was proportional to the frequency and was equal to  $h\nu$  where  $\nu$  is the frequency and  $h$  is Planck's constant. The kinetic energy  $E$  of the electron released would then be equal to  $h\nu$  less any energy lost by the electron in passing through the surface. This latter amount is usually expressed in terms of the potential which the electron must overcome in leaving the surface and is called the work function of the surface  $\phi_p$ . Hence,  $E = h\nu - \phi_p e$  where  $e$  is the charge carried by one electron.

The immediate implication of this equation is that no current will be produced for light frequency such that  $h\nu$  is less than  $\phi_p e$ . This conclusion has been verified in many experiments, although in recent years some modification of the interpretation of  $\phi_p$  has been required. For pure metals,  $\phi_p$  has been found to be related to the position of the metal in the periodic table being, in general, small for the alkali metals, and decreasing with increasing atomic weight.  $\phi_p$  has also been shown to be equal or very nearly equal to  $\phi_r$ , the thermionic work function involved in Richardson's equation for the emission of electrons from heated bodies. The surface photoelectric effect has proved to be basic in the development of the quantum theory of light as well as in the development of modern theories of the structure of metals. The large number of photoelectrons released from metals is attributed to the presence of "free" electrons within the metal which are relatively free to move within the metal lattice. These electrons are responsible for the high conductivity of metals. A smaller surface photoelectric effect is also found for insulators but the absence of conductivity makes it difficult to obtain a continuous emission since the insulator eventually assumes a positive charge. The reaction of the light quantum with the electron is now thought to be the primary mechanism involved in the "photoconductive" as well as in the "photovoltaic" effect.

All three of these effects are now incorporated in commercial photoelectric cells. Their respective advantages and limitations have resulted

---

<sup>13</sup> A. Einstein, "Ueber einen die Erzeugung und Verwandlung des Lichtes betreffenden heuristischen Gesichtspunkt," *Ann. der Phys.*, Vol. 17, No. 6, pp. 132-148; 1905.

in widely different fields of application. The current sensitivity of the photoconductive cell considerably exceeds that of the other types but disadvantages such as a large time lag have limited its use. Since no external source of voltage is required with the photovoltaic cell, one variety of this type, "the barrier-layer" or "blocking-layer" cell has found wide use in connection with low-resistance current meters in light-measuring devices such as photographic exposure meters. The photoemissive tube, or phototube, on the other hand is a high-resistance device ideally suited for use with a modern thermionic amplifying tube either of the high-vacuum or gas-filled type, the combination being capable of controlling large amounts of power. Close relatives of the phototube are the electronic "pickup" tubes used in television; these utilize large multielement photoemissive surfaces.

#### THE PHOTSENSITIVITY OF PURE METALS

Returning to the investigations of Hallwachs<sup>5</sup>, it will be remembered that the initial experiments on the surface photoelectric effect were made in air and that in this case ultraviolet light was required to produce the electric current. As further experiments were made and as an explanation of the effect was developed based on Einstein's equation, the wavelength threshold, that is, the longest wavelength radiation which will liberate photoelectrons, was moved into the visible region of the spectrum. As the metals which possess the lowest surface work function are sensitive to visible light, continual attempts were made to obtain surfaces of lower work function. Since a low work function has been found to be intimately associated with high chemical activity, the alkali metals which possess these properties must be examined under the best vacuum conditions. The difficulties which beset the early experimenters must be considered as being tremendous compared with experiments made today with modern vacuum pumps. However, the alkali metals were soon found to be the materials most photoelectrically sensitive to visible radiation.

The early investigators believed that the presence of gas might even be required for the passage of the photocurrent. Elster and Geitel<sup>11,12</sup> indeed found that a maximum current could be obtained if the envelope contained hydrogen at a certain optimum pressure. Such a device may be said to be the first gas-filled phototube. The photoelectric effect, however, was eventually found to be independent of anything but the nature of the metal surface and the character of the incident radiation. However, a subsequent amplification of this current could be obtained by ionization of a gaseous atmosphere included

in the envelope. Since the active sensitive surface would be destroyed by anything other than an inert gas, such gases are always employed in gas-filled phototubes. Argon is most suitable since it possesses a low ionization potential and is relatively cheap. The value of  $\phi_p$  for a given metal differs widely, however, depending upon the condition of the surface. Contaminations such as occluded gases or the presence of thin oxide layers change the work function markedly. The values of  $\phi_p$  for many gas-free pure-metal surfaces have gradually been established and the maximum wavelengths for their photoelectric emission measured. The response of a metal surface to light of frequency greater than the threshold value increases until a maximum is reached. This effect was formerly attributed to the loss of energy by electrons coming from deep within the metal but is now believed to be due to the distribution of energy among the free electrons of the metal, the faster electrons being more readily emitted. Wentzel<sup>14</sup>, followed by others<sup>15-19</sup>, has computed the form of the spectral-distribution curve to be expected based on wave mechanics and a Fermi-Dirac distribution of the energies of the free electrons. Fair agreement with experiment has been obtained. The spectral-distribution curves for the alkali metals<sup>20</sup> are shown in Fig. 1, which gives the relative spectral response as a function of the wavelength of the incident light. Caesium may be seen to possess the longest wavelength sensitivity being sensitive even to red radiation. For the measurement of ultraviolet radiation, various metal surfaces whose thresholds lie within that region have been used. It is frequently advisable that an ultraviolet sensitive phototube be insensitive to visible radiation; hence, the use of such metals as tantalum, titanium, and thorium<sup>21</sup>, the spectral curves for which are shown in Fig. 2.

---

<sup>14</sup> G. Wentzel, in "Probleme der Modernen Physik," Sommerfeld Festschrift, p. 79; 1928.

<sup>15</sup> W. V. Houston, *Rev. Mod. Phys.*, Vol. 5, p. 41; January, 1933.

<sup>16</sup> I. Tamm and S. Schubin, "Zur theorie des Photoeffektes an Metallen," *Zeit. für Phys.*, Vol. 68, pp. 97-113; March 11, 1931.

<sup>17</sup> H. Fröhlich, "Zum Photoeffekt an Metallen," *Ann. der Phys.*, Vol. 7, pp. 103-128; October 23, 1930.

<sup>18</sup> W. G. Penney, "The photoelectric effect in thin metallic films," *Proc. Roy. Soc.*, Vol. A133, pp. 407-417; October, 1931.

<sup>19</sup> K. Mitchell, "The theory of the surface photoelectric effects in metals," *Proc. Roy. Soc.*, Vol. A146, pp. 442-464; September, 1934.

<sup>20</sup> E. F. Seiler, "Colour sensitiveness of photoelectric cells," *Astrophys. Jour.*, Vol. 52, pp. 129-153; October, 1920.

<sup>21</sup> H. C. Rentschler, D. E. Henry, and K. O. Smith, "Photoelectric emission from different metals," *Rev. Sci. Instr.*, Vol. 3, pp. 794-802; December, 1932.



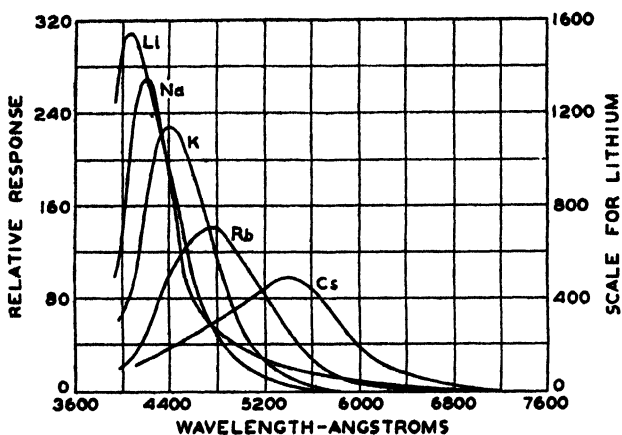
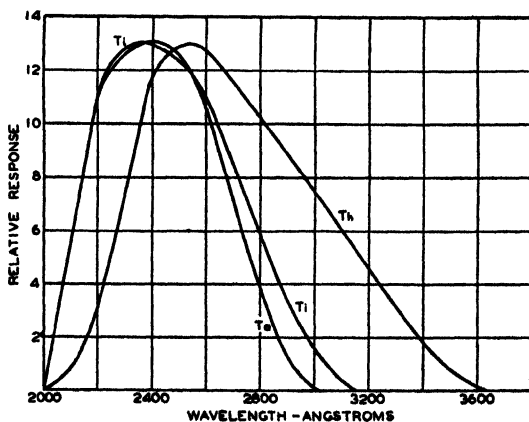


Fig. 1 — Spectral-distribution curves of the alkali metals (Miss Seiler).

#### DEVELOPMENT OF SENSITIZED SURFACES

The first successful attempt to produce an artificially enhanced photoelectric emission was that of Elster and Geitel<sup>22-24</sup> who found that upon filling a potassium cell with hydrogen, the photoemission was completely destroyed but that after the passage of a glow discharge in the hydrogen atmosphere, a considerable increase in sensitivity over

Fig. 2 — Spectral distribution of tantalum, titanium, and thorium in ultra-violet-transmitting glass (Courtesy of Lamp Division, Westinghouse Electric and Manufacturing Co.).



<sup>22</sup> J. Elster and H. Geitel, "Ueber gefärbte Hydride der Alkalimetalle und ihre photoelektrische Empfindlichkeit," *Phys. Zeit.*, Vol. 11, pp. 257-262; April, 1910.

<sup>23</sup> J. Elster and H. Geitel, "Bemerkungen ueber die Natur der durch elektrische Entladungen auf Alkalimetallen in Vacuumrohren gebildeten farbigen Schichten," *Phys. Zeit.*, Vol. 11, pp. 1082-1083; November, 1910.

<sup>24</sup> J. Elster and H. Geitel, "Weitere Untersuchungen an photoelektrischen Zellen mit gefärbten Kaliumkathoden," *Phys. Zeit.*, Vol. 12, pp. 609-614; August, 1911.

that of pure potassium was obtained. The hydrogen was then pumped out and argon introduced. Various improvements on this process have been made<sup>25-28</sup> and indeed until about 1925, practically all commercial phototubes were of this general type. In Fig. 3 are shown the spectral-sensitivity curves for potassium (K) and potassium hydride (K-H) as the surface is commonly called. The maximum sensitivity of the potassium-hydride surface is located in the blue portion of the spectrum, this maximum occurring at 4350 angstroms, the long-wavelength threshold occurring at 5900 angstroms. A sensitivity of 1 to 2 microamperes per lumen to a tungsten incandescent light operating at a color temperature of 2870 degrees Kelvin is obtained. Gas filling is employed to increase this value about ten to twenty times.

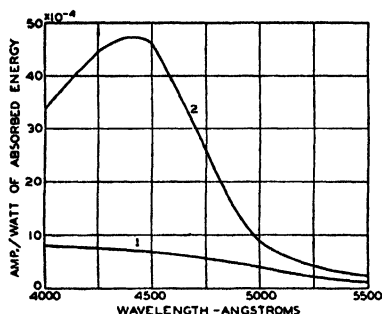


Fig. 3—Sensitization of potassium by glow discharge in hydrogen. Curve 1—potassium before sensitization. Curve 2—potassium sensitized with hydrogen (Campbell and Ritchie).

from the water vapor. Suhrman and Theissing<sup>30</sup> have also reported the same observation. Sensitivities for tubes made under careful control have been reported with values as high as 10 microamperes per

Very recently Tykociner, Kunz, and Garner<sup>29</sup> have reported the development of an improved form of the potassium-hydride surface. A reaction with carefully purified hydrogen was found to be incapable of increasing the sensitivity of a potassium tube even when the tube was submitted to a glow discharge according to common practice. This effect was traced to the absence of water vapor. Further analysis revealed that the necessary constituent for maximum sensitivity was atomic hydrogen which was derived

<sup>25</sup> R. Pohl and P. Pringsheim, "Bemerkung ueber die lichtelektrischen effekte an kolloidalen Alkalimetallen," *Verh. der Deutsch Phys. Ges.*, Vol. 13, pp. 219-223; March, 1911.

<sup>26</sup> R. Pohl and P. Pringsheim, "Der selektive Photoeffekt bezogen auf absorbierte Lichtenergie," *Verh. der Deutsch Phys. Ges.*, Vol. 15, pp. 173-185; March, 1913.

<sup>27</sup> W. B. Nottingham, "Manufacture of potassium-hydride photoelectric cells," *Jour. Frank. Inst.*, Vol. 205, pp. 637-648; May, 1928.

<sup>28</sup> N. R. Campbell, "Wasserstoff und die photoelektrische Emission aus Kalium," *Phys. Zeit.*, Vol. 30, pp. 537-538; September, 1929.

<sup>29</sup> J. T. Tykociner, J. Kunz and L. Garner, "Photoelectric sensitization of alkali surfaces by means of electric discharges in water vapor," University of Illinois, Bulletin Series No. 325; 1940.

<sup>30</sup> R. Suhrmann and H. Theissing, "Influence of hydrogen on the photoelectric emission of potassium," *Zeit. für Phys.*, Vol. 52, No. 7-8, pp. 453-463; 1928.

lumen (light-source color temperature not stated). This sensitivity is several fold that previously reported for potassium-hydride surfaces.

During the preparation of alkali-metal tubes, the presence of the volatile alkali vapor results in a condensation of a thin film of the metal on all the exposed parts of the tube such as the glass press or even the anode. The photocurrents arising from these films are often found to be comparable in size to the main photocurrent. Ives<sup>81</sup> and Suhrman and Theissing<sup>82</sup> have investigated films of this sort, for example, potassium or sodium deposited on platinum. Ives found that as the thickness of the film was increased, a shift in the threshold to the red to a point beyond that of the alkali metal in bulk took place. As the thickness was further increased, the threshold decreased until it approached that of the alkali in bulk. While surfaces of this type have had no commercial significance, the study of the effect has led to a better understanding of the modern thin-film surface to be discussed shortly. Ives and Olpin<sup>83</sup> determined the maximum excursion of the long-wavelength threshold to be equal to the first line of the primary series or resonance line of the element in question. Although this correlation has been shown to be true for the alkali metals, it has not contributed materially to an understanding of the effect. Later measurements by Brady<sup>84</sup> indicate that such a correlation may be invalid. The spectral selectivity found with surfaces of this sort has recently been interpreted by Ives and Briggs<sup>85</sup> in terms of the optical constants of the alkali-metal films. The maximum sensitivity is found to occur at that wavelength at which the electromagnetic-energy density at the surface in the standing wave which is set up in the film by interference is a maximum. The necessity for the dual relation between the wave theory and the corpuscular theory of light is nowhere more clearly required than in this aspect of photoemission.

As might be expected from the close relation between thermionic emission and photoemission, the attention of experimenters was given to the materials used for cathodes in radio receiving tubes. An early

---

<sup>81</sup> H. E. Ives, "Photoelectric properties of thin films of alkali metals," *Astrophys. Jour.*, Vol. 60, pp. 209-230; November, 1924.

<sup>82</sup> R. Suhrmann and H. Theissing, "Selective photoelectric effect with thin layers of potassium absorbed on polished platinum," *Zeit. für Phys.*, Vol. 55, No. 11-12, pp. 701-716; 1929.

<sup>83</sup> H. E. Ives and A. R. Olpin, "Photoelectric long wave limit of the alkali metals," *Phys. Rev.*, [2], Vol. 34, pp. 117-128; July, 1929.

<sup>84</sup> J. J. Brady, "The photoelectric properties of alkali metal films as a function of their thickness," *Phys. Rev.*, [2], Vol. 41, p. 613; September, 1932.

<sup>85</sup> H. E. Ives and H. B. Briggs, "Optical properties and photoelectric emission in thin alkali metal films," *Jour. Opt. Soc. Amer.*, Vol. 28, pp. 330-338; September, 1938.

phototube of this type was the barium tube developed by T. W. Case<sup>36</sup>. Huxford<sup>37</sup> has measured the spectral sensitivity of barium-strontium-oxide cathodes which is shown in Fig. 4. It is apparent that the barium-strontium cathode so widely used today in receiving tubes is quite photosensitive to visible light. A shift in threshold with applied voltage is quite marked. During the life of the tube, some of this material may be evaporated on to the control grid. When such tubes are used for the measurement of extremely small amounts of current, the light from the filament may create a troublesome source of undesirable grid current.

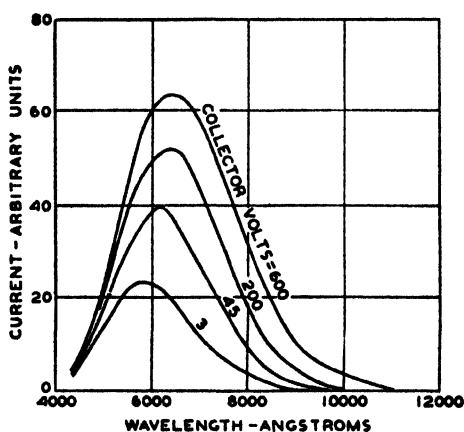


Fig. 4 — Spectral-distribution curve of oxide-coated cathode as a function of the collector voltage (W. S. Huxford).

The investigations of Langmuir and Kingdon<sup>38</sup> showed that a thin film of volatile metal, such as caesium, may be bound to a base metal such as tungsten at temperatures far above that at which the caesium would normally be evaporated from caesium metal in bulk. Such films were found to possess a very high thermionic emission. It was further found that oxidation of the tungsten before deposition of the caesium intensified the

binding forces. The value of the thermionic work function for caesium on oxygen on tungsten is given by Dushman<sup>39</sup> as being  $\phi_r = 0.695$  volt. While this value is not necessarily equal to the photoelectric threshold, the low value of  $\phi_r$  would indicate the probability of high photoelectric sensitivity. A photosurface of similar nature was developed by Zworykin and Wilson<sup>40</sup> by the deposition of caesium upon a magnesium base. The excess caesium was then driven off by heating and the resultant

<sup>36</sup> T. W. Case, "New strontium and barium photoelectric cells," *Phys. Rev.*, [2], Vol. 17, pp. 398-399; March, 1921.

<sup>37</sup> W. S. Huxford, "Effect of electric field on emission of photoelectrons from oxide cathodes," *Phys. Rev.*, [2], Vol. 38, pp. 879-395; August, 1931.

<sup>38</sup> I. Langmuir and K. H. Kingdon, "Thermionic effects caused by vapors of alkali metals," *Proc. Roy. Soc.*, Vol. A107, pp. 61-79; January, 1925.

<sup>39</sup> K. Dushman, "Thermionic emission," *Rev. Mod. Phys.*, Vol. 2, pp. 381-476; January, 1930.

<sup>40</sup> V. K. Zworykin and E. D. Wilson, "Caesium-magnesium photocell," *Jour. Opt. Soc. Amer.*, Vol. 19, pp. 81-89; August, 1929.

photosurface was found to have a high sensitivity with a peak at 4850 angstroms. The maximum response was about 2 microamperes per lumen to a tungsten lamp at 2870 degrees Kelvin. The spectral response is shown in Fig. 5. Gas filling has usually been employed to increase the sensitivity. It may be noted that this surface could withstand a temperature of 150 degrees centigrade and that its life is indefinite under very severe operating conditions.

At about the same period, Bainbridge and Charlton<sup>41</sup> developed a surface of a somewhat similar nature in which silver was employed as the base metal. It was later found if oxygen was admitted to the

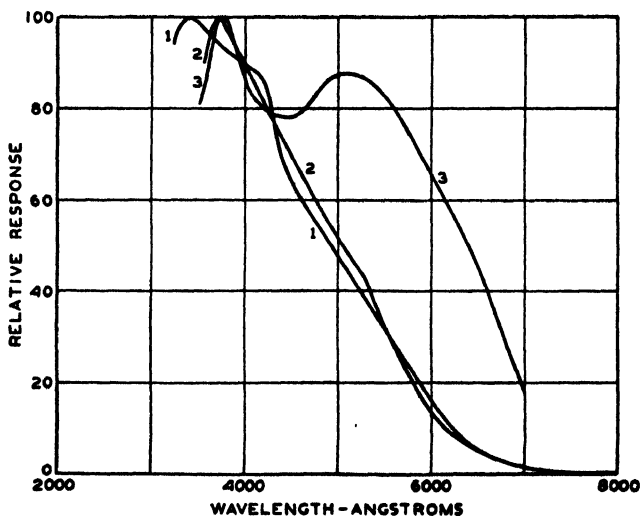


Fig. 5—Spectral-distribution curves for several sensitized surfaces. Curve 1—caesium-magnesium (Zworykin). Curve 2—sodium-sulphur (Olpin). Curve 3—sodium-oxygen-sulphur (Olpin). (Curve 1 used by permission of John Wiley and Sons, Inc.)

envelope after the silver layer was prepared, the tube heated, and then the oxygen pumped out, that subsequent distillation of caesium on to the surface gave a more reliable and uniform result. The surface is usually denoted as a caesium-silver surface since no reaction between the oxygen and the silver was promoted other than absorption. The spectral curve is shown in Fig. 6, curve 1. Development by Koller<sup>42</sup> and by Campbell<sup>43</sup> showed that if the silver was superficially oxidized

<sup>41</sup> Bainbridge and Charlton, see reference 42, page 1639.

<sup>42</sup> L. R. Koller, "Photoelectric emission from thin films of caesium," *Phys. Rev.*, [2], Vol. 36, pp. 1639-1647; December, 1930.

<sup>43</sup> N. R. Campbell, "Photoelectric emission of thin films," *Phil. Mag.*, Vol. 12, pp. 173-185; July, 1931.

by a glow discharge in an atmosphere of oxygen at a pressure of 1 or 2 millimeters the sensitivity was found to be markedly increased. This surface will be identified subsequently as caesium-oxygen-silver, including the many modifications which may be obtained by varying the proportions of the constituents. A peak in the spectral sensitivity was then found in the red and near infrared. The long-wavelength limit was extended to 10,000 to 12,000 angstroms, and sensitivities as high as 30 microamperes per lumen have been obtained. This surface is the most widely used commercially today. Various modifications of the process have been made which have led to an understanding of the mechanism involved. A solid-silver cathode or a copper cathode on which silver has been electroplated usually serves as the base for the surface. Other metals may be employed but silver is found to be the most satisfactory. Campbell found that the surface could be further

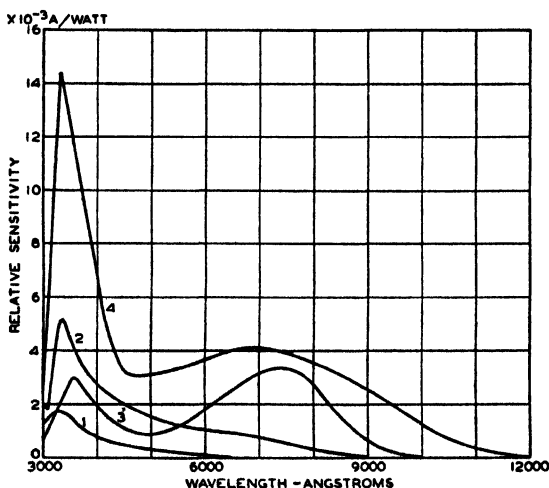


Fig. 6—Spectral-distribution curves of sensitized caesium surfaces. Curve 1—caesium-silver (Koller). Curve 2—caesium-oxygen-silver (deficiency of caesium) (Campbell and Ritchie). Curve 3—caesium-oxygen-silver (excess of caesium) (Ritchie). Curve 4—silver-caesium-oxygen-silver (Asao and Suzuki).

sensitized by a glow discharge in argon for a short period of time, although continued bombardment would destroy the surface. Prescott and Kelly<sup>44</sup> have published a detailed account of one procedure giving very satisfactory results in which great care was taken to obtain a careful balance between the amount of oxygen and the amount of caesium employed.

N. R. Campbell<sup>45</sup> established that the amount of caesium required to obtain maximum sensitivity was proportional to the amount of oxidation of the silver. Two types of such surfaces are shown in Fig. 6, curves 2 and 3, in which the ratio of caesium to oxygen is larger

<sup>44</sup>C. H. Prescott, Jr. and M. J. Kelly, "The caesium-oxygen-silver photoelectric cell," *Bell Sys. Tech. Jour.*, Vol. 11, pp. 384-367; July, 1932.

for the surface of curve 3. Campbell believes that surfaces of this type may be considered as consisting of a layerlike structure in which a thin film of alkali, probably monatomic in nature, is superimposed on a matrix of an oxide of caesium which is in turn built upon the silver base by reduction of the silver oxide. The nature of the oxide of caesium is rather indeterminate. Probably the intermediate layer is a mixture of various oxides of caesium, unreduced silver oxide, and free silver. According to deBoer and Teves<sup>45</sup> the presence of a certain amount of free silver enhances the sensitivity by providing a source of conductivity in an otherwise poorly conducting layer. They assume that the electrons emitted are the result of a photoionization of the surface caesium atoms. By a partial reduction of the silver oxide in a hydrogen atmosphere, they obtain the presence of a certain amount of free silver. By such a technique, surfaces have been obtained in which the sensitivity extends into the infrared region to 17,000 angstroms. Asao and Suzuki<sup>46</sup> have shown that it is possible to enhance the sensitivity by evaporating a thin film of silver upon the surface subsequent to the normal procedure outlined above (see Fig. 6, curve 4). Caesium will probably distill through the silver to reform a monatomic film on the surface, especially if the surface is subjected to a subsequent baking. The evaporation of silver is also used to alter the spectral sensitivity of the iconoscope and orthicon, types of television pickup tubes employing this surface<sup>47</sup>. In this case silver is evaporated upon the completed surface without any subsequent baking. A reduction of the infrared peak with improved sensitivity in the blue and green regions of the spectrum is thus obtained. In a discussion of forms of the caesium-oxide-silver surface, deBoer and Teves suggest various complicated structures to explain the different types of sensitivity and spectral response obtained. There seems to be little question that the presence of an electronegative element is the essential constituent in producing a reduction of the work function of the metal surface. Others have substituted sulphur for the oxygen with somewhat similar results, although the sensitivity reported has not been as high. Campbell interprets the sensitivity in terms of a transmission of electrons through a surface potential barrier consisting of a series of maxima and minima in the potential as a function of the distance from the

---

<sup>45</sup> J. H. deBoer and M. Teves, "Electron Emission and Absorption Phenomena," The Macmillan Company, Cambridge, England, 1935, p. 330.

<sup>46</sup> S. Asao and M. Suzuki, "Improvement of thin film caesium photoelectric tube," *Proc. Phys. Math. Soc. (Japan)*, Series 3, Vol. 12, pp. 247-250; October, 1930.

<sup>47</sup> E. B. Janes and W. H. Hickok, "Recent improvements in the design and characteristics of the iconoscope," *Proc. I.R.E.*, Vol. 27, pp. 535-540; September, 1939.

surface. On a wave mechanical theory, such a potential barrier will have a selective transmission for electrons of certain energies. Olpin<sup>48</sup> has computed the atomic spacing which would be expected to give a selective transmission on the basis of a crystalline structure, through which the electrons would pass according to the wave mechanical theory. He shows that such distances as computed from the observed wavelengths of the spectral maximum show a direct ratio to the atomic diameters of the atoms involved and that the correlation is remarkable considering the uncertainties in the theory and in the experimental quantities involved. Olpin's results are probably somewhat fortuitous as pointed out by Zachariasen<sup>49</sup>.

An extensive series of investigations on the sensitization of alkali surfaces has been carried out by Olpin<sup>50</sup>. Among various inorganic substances, Olpin tried oxygen, water vapor, and sulphur. Among the organic materials tested were benzene, acetone, and organic dyes such as are used for sensitization in photography, for example eosine, kryptocyanine, and dicyanine. Olpin found that practically every substance tried increased the sensitivity of the alkali metal to red light. He concluded that a contamination common to all the substances might be the cause and suggested water vapor. A more reasonable explanation now appears to be that the presence of any electronegative element in the surface layer is sufficient to distort the potential barrier so as to increase the threshold wavelength. Hence, oxygen or sulphur may be the most likely sources of the increased sensitivity in all the above cases. Olpin notes the effect of depositing a thin film of sodium on a surface of sodium already exposed to sulphur. A surface very similar to the caesium-oxygen-silver in structure is probably obtained. Curves showing the spectral sensitivities for some of the surfaces produced by Olpin are shown in Fig. 5. The commercial importance of these discoveries has been limited by the widespread use of the caesium-oxygen-silver types of surface, but as in the case of Ives' work on thin films, the general conclusions obtained have been very valuable in forming a picture of the type of surface most likely to result in a high sensitivity within the visible region of the spectrum and in the near-infrared region in which much of the energy radiated from a tungsten lamp is concentrated.

---

<sup>48</sup> A. R. Olpin, "An interpretation of the selective photoelectric effect from two component cathodes," *Phys. Rev.*, [2], Vol. 38, pp. 1745-1757; November, 1931.

<sup>49</sup> W. H. Zachariasen, "On the interpretation of the selective photoelectric effect from two component cathodes," *Phys. Rev.*, [2], Vol. 38, p. 2290; December, 1931.

<sup>50</sup> A. R. Olpin, "Method of enhancing the sensitiveness of alkali metal photoelectric cells," *Phys. Rev.*, [2], Vol. 36, pp. 251-295; July, 1930.



As the development of the caesium-oxygen-silver photosurface progressed, sensitivities as high as 50 microamperes per lumen (to tungsten light at 2870 degrees Kelvin) have been obtained. However, the average sensitivity is about 15 to 25 microamperes per lumen. Gas filling of caesium-oxygen-silver phototubes permits of an increase in the sensitivity to 100 to 150 microamperes per lumen with the increase obtained somewhat at the expense of constancy and stability. The yield obtained from caesium-oxygen-silver when expressed in terms of electrons per incident quantum of the light is very low, being only 0.6 per cent (for a sensitivity of 40 microamperes per lumen) at the peak in sensitivity in the infrared. At the peak in the near ultraviolet, the value is somewhat higher, being about 1.6 per cent.

Glover and Janes<sup>51</sup> have reported the development of a composite caesium photosurface in which the sensitive surface is formed upon a metal base such as nickel. The spectral maximum for this surface is found to occur at 3750 angstroms and is accompanied by a long-wavelength threshold in the neighborhood of 6300 angstroms. Sensitivity as high as 90 microamperes per lumen (to tungsten light at 2870 degrees Kelvin) has been obtained which corresponds to a quantum efficiency as high as 26 per cent at the wavelength of peak sensitivity. This surface is found to be very stable at conditions under which the caesium-oxygen-silver surface is subject to loss of sensitivity. The spectral sensitivity for this surface enclosed in a lime-glass bulb is shown in Fig. 7. The sensitivity in the ultraviolet region between 2000 and 3000 angstroms is undoubtedly higher than for any surface yet available.

Görlich<sup>52</sup> has reported the development of a transparent surface in which the sensitivity is largely limited to the blue and green region of the spectrum, but for which the yield is remarkably high in this region. The surface is obtained by the deposition of a layer of antimony upon the glass envelope. The antimony is then treated with oxygen and subjected to caesium vapor. This surface may be deposited in a transparent layer sufficiently thin so that the sensitivity may be obtained by light incident upon the surface from the side opposite to that from which the current is collected. Görlich reports that the selective maximum lies between 4000 and 6000 angstroms and that the position of the maximum is largely unaffected by the substitution of sodium, potassium, rubidium, or lithium in place of the caesium.

---

<sup>51</sup> A. M. Glover and R. B. Janes, "A new high-sensitivity photosurface," *Electronics*, Vol. 13, pp. 26-27; August, 1940.

<sup>52</sup> P. Görlich, "Sensitization of transparent compound photocathodes," *Zeit. für Tech. Phys.*, Vol. 18, pp. 460-462; November, 1937.

Gopstein and Khorosh<sup>53</sup> report measurements on such surfaces and upon surfaces in which the antimony is replaced by bismuth and arsenic for illumination both from the front and from the rear of the surface. They quote values for the sensitivity as:

antimony-caesium	60-70 microamperes per lumen
bismuth-caesium	10-15 microamperes per lumen
silver-caesium	20-40 microamperes per lumen

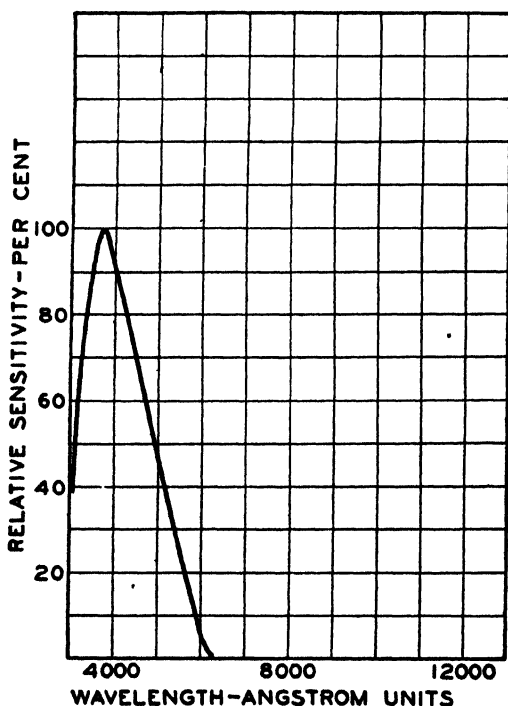


Fig. 7—Spectral-distribution curve of composite caesium surface in lime-glass bulb (Glover and Janes).

The color of these surfaces is a burnt red, indicating a possible correlation between the photoemission and the optical absorption of the surface<sup>54</sup>. Further development<sup>52</sup> has included the sensitization of these surfaces by controlled amounts of oxygen to produce a shift of the wavelength of the peak sensitivity towards the red end of the spectrum. The spectral-sensitivity curve for the caesium-antimony surface reported by Görlich is shown in Fig. 8.

#### TECHNICAL DEVELOPMENT

The development of commercial phototubes has, of course, accompanied the development of radio receiving tubes. Thus, improvements

<sup>53</sup> N. M. Gopstein and D. M. Khorosh, "Photoeffect and secondary emission with alloy cathodes," *Jour. Tech. Phys.* (U.S.S.R.), Vol. 8, pp. 2103-2106; 1938.

<sup>54</sup> P. Lukirsky and N. N. Lusheva, "Photosurfaces with high selective sensitivity," *Jour. Tech. Phys.* (U.S.S.R.), Vol. 7, pp. 1900-1904; 1937.

in the latter, both of technical and of economic significance, have been largely incorporated in the manufacture of phototubes. Some of these are so obvious as to need no mention but others may be of some interest. In general, it may be said that the surface of a phototube is more sensitive to contamination than the cathode of a receiving tube. The cathode surface of a receiving tube is believed to be covered with a thin film of barium which is replenished during the life of the tube by transfer of barium toward the surface of the cathode by electrolysis. The result is that as traces of residual gas react with the metallic barium on the surface, this gas is gradually cleaned up until insufficient to do any further harm. On the other hand, the alkali elements which are usually present in phototubes and which are also

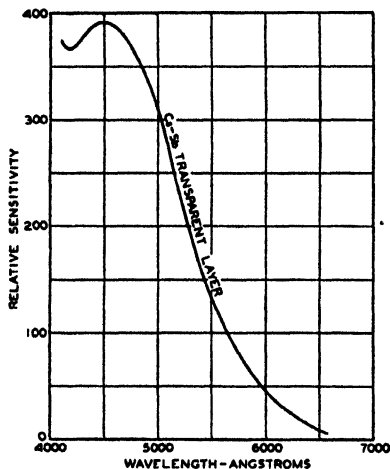


Fig. 8 — Spectral-distribution curve of transparent caesium-anitmony alloy (Görlich).

very active chemically react during processing with residual gases present in the tube or released from the walls and parts by electron bombardment. No electrolysis of alkali atoms toward the surface takes place subsequent to formation of the surface. Hence, if the surface should be contaminated there would be no additional supply of alkali available to replenish the surface atoms. The sensitivity obtained thus would be decreased. As a consequence, phototubes require special care on exhaust procedure. A getter is not generally used because of the high activity of the alkali elements since the free alkali present during the formation of the surface pro-

vides the final gettering. On the other hand, once a sensitive surface has been formed, its life is practically indefinite since the cathode is operated at low temperature with no loss of material by evaporation. If an inert gas is used to provide amplification of the electron current, it must be one of the noble gases, such as helium, argon, or neon. The gas is usually purified by an electrical discharge to misch-metal or some other active surface in a bulb containing the supply of gas. Argon is usually used because of its low cost and relatively low ionization potential. Vacuum diffusion pumps of good quality are universally used in conjunction with liquid-air traps to remove traces of water vapor and other condensable gases.

If the active surface is a pure metal, this may be prepared by cathode sputtering or by evaporation of the metal in vacuo. The latter method is being used widely for the preparation of metal surfaces sensitive to the ultraviolet. In early phototubes in which the presence of an alkali metal was desired, the alkali was usually obtained by distillation from bulk metal contained in a side tube. This method is tedious and unsuited to large-scale production. Burt<sup>55</sup> found that sodium could be electrolytically formed upon the inner surface of a soda-glass bulb, if the bulb were placed in an electrolytic bath which would furnish the sodium ion to the glass. Zworykin used a potassium-containing glass for the purpose of obtaining a potassium surface in similar fashion. In recent years, the alkali metal has been obtained by the reduction of a suitable salt. A reducing element is provided with the salt incorporated in a pellet which is brought to high temperature usually by high-frequency induction. For obtaining caesium, it is usual to employ a mixture of caesium dichromate and silicon. An alternative mixture is a combination of caesium chromate, aluminum, and tantalum. This method is convenient and provides a controlled amount of the desired alkali directly within the tube. Hydrogen which is required for the potassium-hydrogen cell may be obtained by heating palladium in a side tube or by dosing from a bottle of gas connected to the exhaust system.

In the preparation of the caesium-oxygen-silver or similar surfaces, an excess of alkali is useful in the preparation of the surface. This excess must then be removed in order to prevent electrical leakage across any films condensed upon the stem press or interior of the bulb surface. The removal may be accomplished by the introduction of a compound such as oxidized copper or stannic oxide or by the reaction of the excess caesium with the lead of the glass stem press. Since this reaction causes a darkening of the glass, the bulbs of alkali-containing phototubes must be of lead-free glass such as lime glass or one of the borosilicate glasses.

For convenience, it is usually desirable that the cathode surface be formed upon a metal element which may be directly connected to one of the lead-in wires in the stem press. This metal support may be of nickel, copper, or even be of solid silver. The last is used frequently in the preparation of the caesium-oxygen-silver surface. The anode is usually a nickel wire also directly connected to a lead-in wire in the press and, then, to one of the base pins. For many purposes, however, it is desirable to provide an exceptionally high-resistance

---

<sup>55</sup> R. C. Burt, "Sodium by electrolysis through glass," *Jour. Opt. Soc. Amer. and Rev. Sci. Instr.*, Vol. 11, pp. 87-91; July, 1925.

path between anode and cathode. This is accomplished by sealing the anode connection through the glass envelope separately. A guard ring consisting of a strip of metallic paste painted on the glass between the anode connection and the cathode connection is also of use in bypassing undesirable leakage currents from the measuring circuit. Surface leakage may also be reduced by coating the bulb surface with a nonhygroscopic wax such as ceresin.

For many years, applications of phototubes were limited to the scientific laboratory because of the small size of the currents obtained and because of the delicate nature of the instruments required for measuring such currents. The development of the vacuum tube, however, has changed the situation completely. Because of the high-resistance characteristic of phototubes, the small current output of a phototube may be converted into a voltage of sufficient size to be used as the grid voltage of a commercial radio tube. No extraordinary precautions need be taken other than to insure that base and socket leakages be kept to a minimum and that a suitable amplifying tube be used. (A tube with a top grid cap is normally desirable because of the increased grid resistance thus provided.) For the detection or measurement of extraordinarily small amounts of light, amplifying tubes have been developed in which all sources of extraneous grid current have been minimized by providing high internal-leakage paths and by adjusting the operating characteristics so that the applied voltages are insufficient to ionize any residual gas present in the tube after manufacture<sup>56,57</sup>. These tubes have largely replaced the delicate laboratory electrometer and are, therefore, frequently referred to as electrometer tubes. Balanced bridge circuits<sup>58</sup> have also been employed to decrease the effect of changing conditions of light and fluctuations due to changes in battery or line voltages.

The limited sensitivity of the phototube may be partially overcome by gas filling. Campbell<sup>59</sup> has studied the performance of tubes for varying gas pressures. He shows that the voltage at which the tube breaks down, that is, the voltage at which the ionization becomes cumulative, is a function of both the amount of light and the pressure of gas used. The effect of the gas upon the frequency response of such

---

<sup>56</sup> G. F. Metcalf and B. J. Thompson, "A low grid current vacuum tube," *Phys. Rev.*, Vol. 36, pp. 1489-1494; November 1930.

<sup>57</sup> H. Nelson, "A vacuum tube electrometer," *Rev. Sci. Instr.*, Vol. 1, pp. 281-284; May, 1930.

<sup>58</sup> L. A. DuBridge and H. Brown, "An improved d.c. amplifying circuit," *Rev. Sci. Instr.*, Vol. 4, pp. 582-586; October, 1933.

<sup>59</sup> N. R. Campbell and D. Ritchie, "Photoelectric Cells," Sir Isaac Pitman and Sons, Ltd., London, England, 1934, p. 66.

tubes is shown in Fig. 9. A portion of this effect has been attributed to the finite time required for positive ions of the inert gas to reach the cathode. Also, the positive ions on reaching the cathode, release secondary electrons which contribute to the current. The amount of this secondary emission is quite high for the caesium-oxygen-silver surface as compared with the potassium-hydrogen surface. A more rapid increase in current with an increase in applied voltage is thereby found (see Fig. 10). Kingdon and Thompson<sup>60</sup> attributed the major portion of the effect to the time required for neutralization of the positive ion after it reaches the cathode. They assumed that during this interval, the work function of the cathode will be lowered and that increased secondary emission would be expected. Skellet<sup>61</sup> has shown

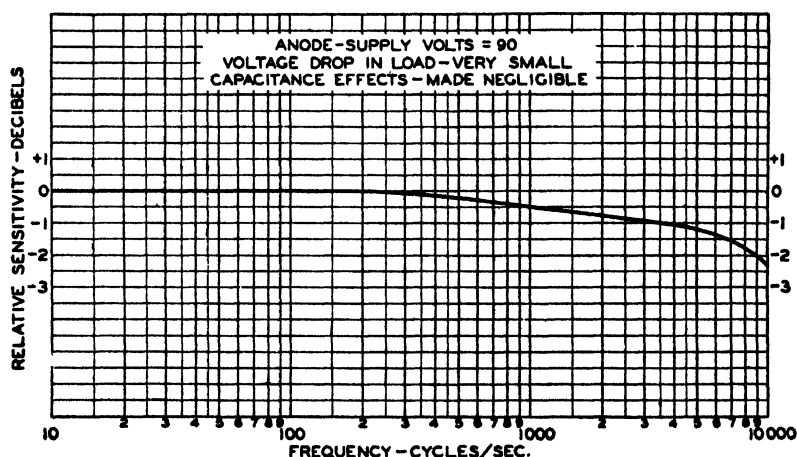


Fig. 9—Frequency response of gas-filled phototube (Courtesy of RCA Manufacturing Co.).

a definite correlation between the time lag and the geometry of the tube, indicating the importance of the first factor. More recently, Huxford<sup>62</sup> and Kruithof<sup>63</sup> have shown that the presence of metastable atoms can explain the excessive lag at low frequencies. The increased

<sup>60</sup> K. H. Kingdon and H. Thompson, "Some experiments with gas-filled Cs-O-Ag photoelectric cells," *Physics*, Vol. 1, pp. 343-351; 1931.

<sup>61</sup> A. Skellet, "Time lag in gas-filled photoelectric cells," *Jour. Appl. Phys.*, Vol. 9, pp. 631-634; October, 1938.

<sup>62</sup> W. S. Huxford, "Townsend ionization coefficients in Cs-Ag-O phototubes filled with argon," *Phys. Rev.*, [2], Vol. 55, pp. 754-762; April, 1939.

<sup>63</sup> A. A. Kruithof, "Time lag phenomena in gas-filled photocells," *Philips Tech. Rev.*, Vol. 4, pp. 48-55; February, 1939.

lag when helium is used is then readily explained since the probability of excitation of metastable atoms is known to be greater for helium than for argon. While the poorer frequency response of a gas-filled tube, as compared with a high-vacuum tube, is annoying, the falling off at higher frequencies is readily compensated by adjustment of the amplifier characteristics. The effect, therefore, has been no bar to the use of such tubes in the motion-picture industry.

In an attempt to avoid the disadvantages which accompany the use of gas to increase the sensitivity, amplification by the use of secondary-emission currents released by electron bombardment of auxiliary electrodes has been employed. Secondary emission is an effect whose presence has been noted in receiving tubes for many years. In general, the secondary emission obtained from pure metals is low; however, at a few hundred volts, release of as many as 6 to 8 electrons per primary electron has been obtained from caesium-oxygen-silver surfaces, and somewhat lower ratios are readily obtained from oxides. The emission varies rapidly with voltage and passes through a maximum for a value of a few hundred volts on the bombarded electrode. The emission is stable at the current densities encountered in phototubes but in order to obtain a maximum benefit, several stages of amplification are desirable. A scheme for directing the electron streams to successive electrodes has been devised<sup>64</sup>. This method employs the

focusing effect of the combined action of crossed electrostatic and electromagnetic fields. A somewhat simpler arrangement dispenses with the magnetic fields by the use of a number of secondary-emissive grids arranged in a row<sup>65</sup>. A large portion of the current passes directly through each grid, however, thus reducing the over-all ampli-

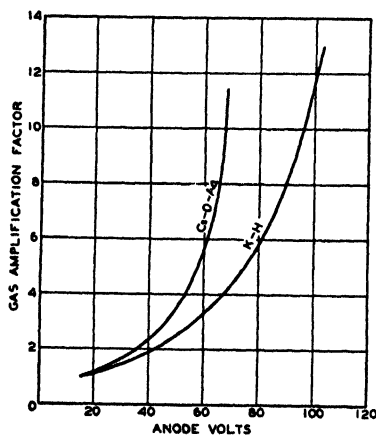


Fig. 10 — Amplification by gas filling with caesium-oxygen-silver and potassium-hydride surfaces (Campbell and Ritchie).

<sup>64</sup> V. K. Zworykin, G. Morton, and L. Malter, "The secondary emission multiplier," *Proc. I.R.E.*, Vol. 24, pp. 351-375; March, 1936.

<sup>65</sup> W. Kluge, O. Beyer, and H. Steyskal, "Photocells with secondary emission amplification," *Zeit. für Tech. Phys.*, Vol. 18, No. 8, pp. 319-228; 1937.

fication. Pierce<sup>66</sup> and Zworykin and Rajchman<sup>67,68</sup> have employed mechanical models to develop all-electrostatic focusing structures which conserve all the electrons available and give maximum amplifications. In addition, the structure of Zworykin and Rajchman is so designed that it is difficult for positive ions, formed in the inevitable residual gas, to reach the photocathode and thus produce unwanted currents which might lead to uncontrolled regeneration. An electron multiplier employing this principle has recently been described by Janes and Glover<sup>69</sup>, the construction of which is shown in Fig. 11. A gain of 250,000 is readily obtainable at a total of 1250 volts between the collecting anode and the photocathode. Considerably higher figures have been obtained in laboratory models. The size of the tube is no greater than that of a simple phototube.

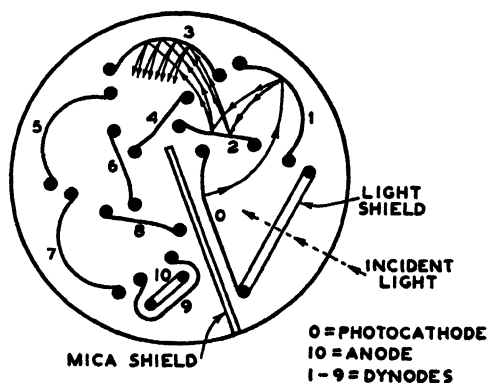


Fig. 11—Electrode structure of electrostatically focused electron multiplier (Janes and Glover).

The phototube is the heart of most sound-picture systems. Its use is also general in "facsimile" systems which accomplish the transmission of pictures by wire or wireless. For this service, the picture is broken up into a series of elements in a fashion somewhat similar to that of a half tone and the light reflected from each element is directed successively to a phototube by some mechanical means. The time

required to transmit a reproduction of a page of this size may be several minutes. For television, the requirement is, of course, to transmit the reproduction almost instantaneously.

For this purpose, a two-dimensional system is required; that is, all elements of a picture or a live scene must be scanned and transmitted within a time sufficiently short for the eye to recreate by persistence

<sup>66</sup> J. R. Pierce, "Electron multiplier design," *Bell Lab. Rec.*, Vol. 16, pp. 305-309; May, 1938.

<sup>67</sup> V. K. Zworykin and J. Rajchman, "The electrostatic electron multiplier," *Proc. I.R.E.*, Vol. 27, pp. 558-565; September, 1939.

<sup>68</sup> J. A. Rajchman and R. L. Snyder, "An electrically focused multiplier phototube," *Electronics*, Vol. 13, pp. 20-23, 58-60; December, 1940.

<sup>69</sup> R. B. Janes and A. M. Glover, "Recent developments in phototubes," *RCA Review*, Vol. 6, pp. 43-54; July, 1941.



of vision the original picture from light signals supplied by the reproducing mechanism to the eye. A photosurface consisting of a multitude of sensitive elements is one answer to this problem<sup>70</sup>. The caesium-oxygen-silver surface used is obtained by methods analogous to those previously described. However, the surface is broken up into a large number of individual elements by depositing the silver in a thin film upon a sheet of mica and heating the film until it coagulates into hemispherical lumps of silver. The process from this point on is very similar to that used in phototubes. To obtain good resolution, no excess caesium may be left upon the mica, however, so that an amount less than that required for obtaining a maximum photosensitivity is usually employed. The surface may be processed further to match its characteristics more nearly to the spectral response of the eye by the subsequent deposition of a very thin film of silver<sup>71</sup>. In other television pickup devices, it has been found desirable to make use of semitransparent photocathodes deposited either upon the wall of the glass envelope or upon a thin transparent sheet of mica<sup>71,72</sup>. The caesium-oxygen-silver surface is again most universally used, although in this case the film is usually continuous.

Little mention need be made of the countless applications of phototubes in which the various surfaces described above have been incorporated. In general, it may be said that a trend toward a more compact design is apparent. Uniformity of construction and of characteristics is a much-sought-after goal, toward which considerable progress has been made.

The phototube has thus become a tool suitable for commercial use as a rugged, reliable, light-sensitive device. The considerable quantity of phototubes used by the motion-picture industry is evidence of this. For this application and, of course, for many others, the incandescent lamp has been the most suitable light source available. For use with this light source, the caesium-oxygen-silver surface is highly desirable, particularly if the lamp is operated at reduced voltage in order to provide increased life. On the other hand, for many applications, daylight is the source of light to be detected, and in many chemical processes or in color sorting, blue or green light is the predominant

---

<sup>70</sup> V. K. Zworykin, G. A. Morton, and L. E. Flory, "Theory and performance of the iconoscope," *Proc. I.R.E.*, Vol. 25, pp. 1071-1093; August, 1937.

<sup>71</sup> C. C. Larson and B. C. Gardner, "Image dissector," *Electronics*, Vol. 12, pp. 24-27; October, 1939.

<sup>72</sup> Albert Rose and Harley Iams, "Television pickup tubes using low-velocity electron-beam scanning," *Proc. I.R.E.*, Vol. 27, pp. 547-555; September, 1939.

color. In late years, several new sources of illumination have appeared such as the sodium-vapor lamp<sup>73</sup>, the high-pressure mercury arc, and fluorescent lamps. Since the available output from the phototube at a given wavelength is the product of the emission of the source and the sensitivity of the phototube at that wavelength, the over-all sensitivity curve of the combination may be measured or computed. The effect of the light source on the response of caesium-oxygen-silver and a potassium-hydrogen cell is given in Fig. 12, showing the relatively high sensitivity of the caesium-oxygen-silver surface with an incandescent-light source. For many applications, a phototube whose sensitivity matches that of the eye would be desirable. A close approach to this requirement has been obtained with various types of barrier-layer photovoltaic cells. However, when amplification of the output current

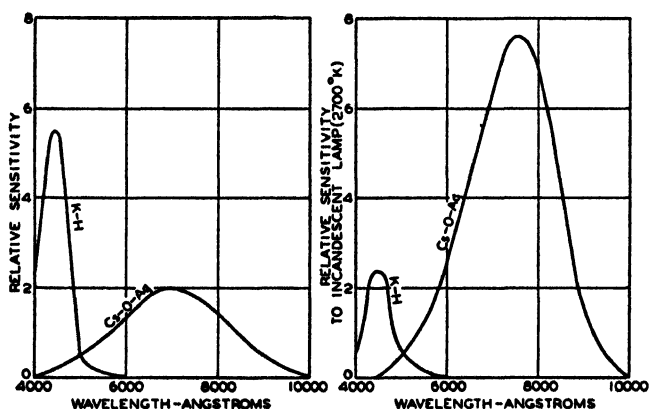


Fig. 12—Effect of light source upon the response of phototubes (Walker and Lance).

is required, this type of cell is seldom suitable. In this case, the use of a phototube, together with the proper choice of filter, will be the more satisfactory solution.

## BIBLIOGRAPHY

A complete bibliography of the development of photoemissive surfaces is, of course, out of the question. However, an attempt has been made to list sufficient references to indicate both the trend of the development, and the names of those most active in the field. From these as a start, it should be possible to trace through the literature subsequent references to any item of particular interest. There are also listed several representative texts to which reference may be made as well as comprehensive summaries

<sup>73</sup> L. J. Buttolph, "High efficiency mercury and sodium vapor lamps," *Jour. Opt. Soc. Amer.*, Vol. 29, pp. 124-130; March, 1939.

which are available for a survey of the theory of the photoelectric effect. In addition, several surveys are listed on the photoconductive and photovoltaic effects which should be of value to anyone interested in the subject of photoelectricity.

- (1) A. L. Hughes and L. A. DuBridge, "Photoelectric Phenomena," McGraw-Hill Book Co., Inc., New York, N. Y., 1932.
- (2) N. R. Campbell and D. Ritchie, "Photoelectric Cells," Sir Isaac Pitman and Sons, Ltd., London, England, 1934.
- (3) B. Lange, "Die Photoelemente und ihre Anwendung," J. A. Barth-Verlag, Leipzig, Germany, 1936.
- (4) F. Seitz, "Modern Theory of Solids," McGraw-Hill Book Co., Inc., New York, N. Y., 1940.
- (5) K. T. Compton and I. Langmuir, "Electrical Discharges in gases," *Rev. Mod. Phys.*, Vol. 2, pp. 123-242; April, 1930.
- (6) L. B. Linford, "Recent developments in the study of the external photoeffect," *Rev. Mod. Phys.*, Vol. 5, pp. 34-61; January, 1933.
- (7) F. C. Nix, "Photoconductivity," *Rev. Mod. Phys.*, Vol. 4, pp. 723-766; October, 1932.
- (8) L. O. Grondahl, "The copper-cuprous oxide rectifier and photoelectric cell," *Rev. Mod. Phys.*, Vol. 5, pp. 141-168; April, 1933.
- (9) G. Déjardin, "Procédés modernes de fabrication des cellules photoélectriques," *Rev. Gen. de l'Elect.*, Vol. 33, p. 3, p. 36; 1933.
- (10) "Photoelectric cells and their applications," (A joint discussion with many contributed papers); *Trans. Opt. Soc.*, Vol. 314, pp. 233-240; 1929-1930.

## THE SECONDARY EMISSION PHOTOTUBE\*†

BY

HARLEY IAMS AND BERNARD SALZBERG

RCA Radiotron Company, Inc.,  
Harrison, N. J.*Summary*

*A type of phototube is described in which the secondary electron emission from an auxiliary cathode (bombarded by the photoelectrons) is utilized to obtain amplification of the primary photocurrent. Phenomena of secondary emission, particularly as applied to the vacuum phototube, are discussed. The operating performance of a typical developmental embodiment is illustrated, and it is shown that its static sensitivity is comparable with that of a corresponding gas phototube; that as regards fidelity, it retains the freedom of the vacuum phototube from the considerable loss in response at the higher audio frequencies which is inherent in the gas phototube; and that on the basis of noise produced by the microscopic fluctuations of its current, it is somewhat superior to the comparable gas tube, and approximately equivalent to a vacuum phototube having the same emission and followed by an amplifier having an over-all gain equivalent to the secondary emission amplification. Life tests indicate that the stability of these tubes is entirely comparable with that of the vacuum phototube, both as regards secondary emitter and photocathode behavior. In addition to the usual applications, various incidental uses of these phototubes are suggested.*

*(10 pages; 6 figures)*

\* Decimal Classification: 535.38.

† *Proc. I. R. E.*, January, 1935.DEVELOPMENT OF CATHODE-RAY TUBES FOR  
OSCILLOGRAPHIC PURPOSES\*†

BY

R. T. ORTH, P. A. RICHARDS, AND L. B. HEADRICK

RCA Manufacturing Company, Inc.,  
Harrison, N. J.*Summary*

*Some typical electrical characteristics of a cathode-ray-tube electron gun are shown and the function of the various gun elements described. Light output, luminescent screen efficiency, space distribution of radiation, as well as decay and spectral distribution characteristics of willemite screens, are shown and the relations of the various factors discussed. The*

\* Decimal Classification: R388.

† *Proc. I. R. E.*, November, 1935.

starting and dynamic characteristics of the tube are discussed. Magnetic and electrostatic deflection are discussed with regard to sensitivity, frequency range of application, and impedance of deflection plates. In conclusion, a few general precautions in the operating of cathode-ray tubes are given.

(16 pages; 14 figures)

## THE ELECTRON-IMAGE TUBE, A MEANS FOR MAKING INFRARED IMAGES VISIBLE\*†

By

G. A. MORTON

RCA Manufacturing Company, Inc.,  
Camden, N. J.

### Summary

*The construction and theory of operation are described of the electron-image tube, which consists of a photosensitive cathode, a fluorescent screen, and an electron-optical system which focuses the electron "image" from the cathode upon the viewing screen. Due to the wide spectral response of the cathode, the tube can be used to convert infrared, visible, or ultraviolet images into visible images upon the fluorescent screen.*

*The electron optical system is discussed and its analogy to the conventional optical system is shown. To reproduce an image faithfully the electron "lens" system must be corrected for various aberrations. Methods of making these corrections are indicated, and applications of the device are described.*

(10 pages; 12 figures)

---

\* Decimal Classification: R339.

† Jour. Soc. Mot. Pic. Eng., September, 1936.

## THEORETICAL LIMITATIONS OF CATHODE-RAY TUBES\*†

By

DAVID B. LANGMUIR

RCA Manufacturing Company, Inc.,  
Harrison, N. J.

### Summary

*The current density in a focused beam of cathode rays is shown to have an upper limit defined by  $I = I_0 (Ee/kT + 1) \sin^2 \phi$ , where  $I$  is the maximum current density obtainable in the focused spot,  $I_0$  is the current density at*

---

\* Decimal Classification: R388.

† Proc. I. R. E., August, 1937.

the cathode,  $E$  is the voltage at the focus relative to the cathode,  $T$  is the absolute temperature of the cathode,  $e$  is the electronic charge,  $k$  is Boltzmann's constant, and  $\phi$  is the half angle subtended by the cone of electrons which converge on the focused spot. The cases in which the focused spot is an image of the cathode, and in which it is a pupil, or "crossover", are considered separately, and the above formula is shown to apply to both. The necessary initial assumptions are (1) that electrons leave the cathode with a Maxwellian distribution of velocities, and (2) that the focusing system is free from aberrations and obeys the law of sines. Aberrations may reduce the current density, but nothing can raise it above the value defined.

In the Appendix the focusing properties of a uniform accelerating field are calculated. The virtual image of a plane cathode formed by such a field suffers from spherical aberration. The diameter of the circle of least confusion formed by electrons from a single point is approximately equal to the distance the electrons can travel against the field by virtue of their initial velocities. This aberration may be the factor which limits the resolving power of some kinds of electron microscopes.

(15 pages; 6 figures; 1 table; 1 appendix)

## VACUUM-TUBE ENGINEERING FOR MOTION PICTURES\*†

BY

L. C. HOLLANDS AND A. M. GLOVER

RCA Manufacturing Company, Inc.,  
Harrison, N. J.

### Summary

Manufacturing and developmental technics of vacuum tubes are described with particular reference to their use in motion picture equipment. A brief discussion of how application requirements affect the choice of materials, structural design, and electrical characteristics of phototubes and amplifiers of both power and voltage types is included. How tubes are designed to meet specific needs is illustrated by reference to recent tube developments. Work on producing tubes having low-hum, low-microphonics, and low-noise characteristics is described as of special interest to the motion picture engineer. The paper closes with recommendations as to how to use tubes to best advantage.

(20 pages; 6 figures; 1 table)

---

\* Decimal Classification: R381.

† Jour. Soc. Mot. Pic. Eng., January, 1938.

## THE ELECTROSTATIC ELECTRON MULTIPLIER\*†

BY

V. K. ZWORYKIN AND J. A. RAJCHMAN

RCA Manufacturing Company, Inc.,  
Camden, N. J.*Summary*

*This paper describes the design of improved types of electron multipliers in which the electrodes are so shaped and positioned as to provide accurate electrostatic focusing and to minimize space-charge limitations. The first section of the paper describes the general methods available for determining electron trajectories in electrostatic fields. The second section describes the details of design of several experimental self-focusing electron-multiplier tubes.*

*(9 pages; 13 figures)*

---

\* Decimal Classification: 535.38.† *Proc. I. R. E.*, September, 1939.AN ELECTRICALLY-FOCUSED MULTIPLIER  
PHOTOTUBE\*†

BY

J. A. RAJCHMAN AND R. L. SNYDER

RCA Manufacturing Company, Inc.,  
Camden, N. J.*Summary*

*A compact secondary-emission multiplier structure using curved targets or "dynodes" is described which develops a maximum current gain of over a million and a luminous sensitivity of over ten amperes per lumen, with signal-to-noise ratio considerably better than conventional phototubes. This is a practical tube useful in sound-track reproduction, light-operated relays and the like.*

*(6 pages; 10 figures)*

---

\* Decimal Classification: 535.38.† *Electronics*, December, 1940.

## THE BEHAVIOR OF ELECTROSTATIC ELECTRON MULTIPLIERS AS A FUNCTION OF FREQUENCY\*†

By

L. MALTER

RCA Manufacturing Company, Inc.,  
Harrison, N. J.

### Summary

*This paper consists of a theoretical and experimental study of the frequency variation of transconductance of electrostatic electron multipliers. It is shown that the decrease of transconductance with frequency up to 500 megacycles, the highest frequency studied, can be ascribed to a spread in transit angle resulting from the emission velocities of secondary electrons and the varying paths of electrons through the stages of the multiplier. The spread in transit angle may be represented by an equivalent angle that is linearly related to the total transit angle unless the latter is quite large.*

*For a given scale and with multipliers of the form herein studied an upper limit can be set upon the frequency at which multipliers may be profitably employed. A brief analysis of the effect of leads within the tube is included.*

*An upper limit of  $2 \times 10^{-9}$  second was set upon the time taken for the phenomenon of secondary emission to occur.*

(12 pages; 16 figures)

---

\* Decimal Classification: R139.

† *Proc. I. R. E.*, November, 1941.

## THE ORBITAL-BEAM SECONDARY-ELECTRON MULTIPLIER FOR ULTRA-HIGH-FREQUENCY AMPLIFICATION\*†

By

H. M. WAGNER AND W. R. FERRIS

RCA Manufacturing Company, Inc.,  
Harrison, N. J.

### Summary

*A developmental ultra-high-frequency receiving tube in which secondary-emission electron multiplication has been applied to a conventional high-transconductance tube structure to increase the transconductance without a corresponding increase in interelectrode capacitances and input conductance is described. It was designed primarily for wide-band amplification at a frequency of approximately 500 megacycles, as required for television radio relay systems. The tube uses conventional circuits and requires a power supply of less than 400 volts. The structure adopted permits the most efficient use of the secondary-emission multiplier consistent with satisfactory life and good high-frequency performance. The*



structure also permits the use of beam deflection to provide a convenient gain-control method, free from the input capacitance and conductance variations attending the usual grid-bias control. A novel method of measuring interstage gain, involving the use of transmission lines, is discussed.

(6 pages; 7 figures)

---

\* Decimal Classification: R330×R262.4.

† *Proc. I. R. E.*, November, 1941.

## VOLTAGE-CONTROLLED ELECTRON MULTIPLIERS\*†

BY

B. J. THOMPSON

RCA Manufacturing Company, Inc.,  
Harrison, N. J.

### Summary

The application of secondary-emission multiplication to conventional grid-controlled amplifier tubes is discussed from the viewpoints of practical voltage gain per stage of amplification, signal-to-noise ratio, and ultra-high-frequency applications. It is pointed out that the gain per stage is limited by the practical output current and the quotient of transconductance by current ( $N$ ) and that electron multiplication increases the gain only as it permits the attaining of higher values of  $N$ . If the output current is assumed to be 20 milliamperes and  $N$  is taken as 1 milliamperes per volt per milliamperes, the output transconductance would be 20 milliamperes per volt—little, if any, better than could be achieved without multiplication. If  $N$  is assumed to be 11.6 (the theoretical maximum for conventional grid control with a cathode temperature of 1000 degrees Kelvin) the output transconductance could be greater than 200 milliamperes per volt per milliamperes. Higher values of  $N$  might be attained by some other method of control. In this case, the ultimate limit of transconductance would be set by the difficulty in stabilizing the effective control-electrode bias voltage.

The signal-to-noise ratio of the voltage-controlled multiplier is determined chiefly by the input system of the multiplier, the multiplier being a relatively noiseless amplifier following this input system. The noise level of the input system is determined by the input transconductance. If the use of a multiplier leads to reduced input transconductance, the noise level will be increased as compared with conventional tubes.

The principal advantages to be attained from the use of the multiplier are found in ultra-high-frequency applications where input loading and input capacitance are serious. The reduction in transconductance of the input system for a given over-all gain which is permissible leads to a corresponding reduction of input conductance (whether arising from electron-transit-time or lead effects) and input capacitance.

(5 pages; 6 figures; 1 appendix)

---

\* Decimal Classification: R132.

† *Proc. I. R. E.*, November, 1941.

## APPENDIX I

---

### ELECTRON TUBES

#### A Bibliography of Technical Papers

by RCA Authors

(1919-1941)

---

This listing includes some 400 technical papers on electron tubes, thermionics, and related subjects, selected from those written by RCA Authors and published during the period 1919-1941.

Papers are listed chronologically except in cases of multiple publication. Papers which have appeared in more than one journal are listed once, with additional publication data appended.

Abbreviations used in listing the various journals are given on the following pages.

Any requests for copies of papers listed herein should be addressed to the publication to which credited. However, *RCA Licensee Bulletins* are not published and are issued only as a service to licensees of the Radio Corporation of America.

---

## ABBREVIATIONS

(Note—Titles of periodicals not listed below,  
as well as book titles, are not abbreviated.)

<i>Amer. Jour. Phys.</i> .....	AMERICAN JOURNAL OF PHYSICS
<i>Amer. Rev.</i> .....	AMERICAN REVIEW
<i>An. Amer. Acad. Polit. Soc. Sci.</i> .....	ANNALS OF THE AMERICAN ACADEMY OF POLITICAL AND SOCIAL SCIENCES
<i>Broad. Eng. Jour.</i> .....	BROADCAST ENGINEERS JOURNAL (A.T.E. JOURNAL)
<i>Comm. and Broad. Eng.</i> .....	COMMUNICATION AND BROADCASTING ENGINEERING
<i>Elec. Eng.</i> .....	ELECTRICAL ENGINEERING (TRANSACTIONS A.I.E.E.)
<i>Electronic Ind.</i> .....	ELECTRONIC INDUSTRIES
<i>FM and Tele.</i> .....	FM AND TELEVISION
<i>G.E. Review</i> .....	GENERAL ELECTRIC REVIEW
<i>Ind. Eng. Chem.</i> .....	INDUSTRIAL AND ENGINEERING CHEMISTRY
<i>Ind. Standard.</i> .....	INDUSTRIAL STANDARDIZATION (AMERICAN STANDARDS ASSOCIATION JOURNAL)
<i>Inter. Project</i> .....	INTERNATIONAL PROJECTIONIST
<i>Jour. Acous. Soc. Amer.</i> .....	JOURNAL OF THE ACOUSTICAL SOCIETY OF AMERICA
<i>Jour. A.I.E.E.</i> .....	JOURNAL OF THE AMERICAN INSTITUTE OF ELECTRICAL ENGINEERS
<i>Jour. Appl. Phys.</i> .....	JOURNAL OF APPLIED PHYSICS
<i>Jour. Amer. Ceramic Soc.</i> .....	JOURNAL OF THE AMERICAN CERAMIC SOCIETY
<i>Jour. Bacteriology</i> .....	JOURNAL OF BACTERIOLOGY
<i>Jour. British Inst. Cine.</i> .....	JOURNAL OF THE BRITISH INSTITUTE OF CINEMATICS
<i>Jour. Chem. Phys.</i> .....	JOURNAL OF CHEMICAL PHYSICS
<i>Jour. Eng. Educ.</i> .....	JOURNAL OF ENGINEERING EDUCATION
<i>Jour. Frank. Inst.</i> .....	JOURNAL OF THE FRANKLIN INSTITUTE
<i>Jour. Opt. Soc. Amer.</i> .....	JOURNAL OF THE OPTICAL SOCIETY OF AMERICA
<i>Jour. Sci. Inst. (Brit.)</i> .....	JOURNAL OF SCIENTIFIC INSTRUMENTS (BRITISH)
<i>Jour. Soc. Mot. Pic. Eng.</i> .....	JOURNAL OF THE SOCIETY OF MOTION PICTURE ENGINEERS
<i>Jour. Tele. Soc. (Brit.)</i> .....	JOURNAL OF THE TELEVISION SOCIETY (BRITISH)
<i>Phys. Rev.</i> .....	PHYSICAL REVIEW
<i>Proc. Amer. Phil. Soc.</i> .....	PROCEEDINGS OF THE AMERICAN PHILOSOPHICAL SOCIETY
<i>Proc. I.R.E.</i> .....	PROCEEDINGS OF THE INSTITUTE OF RADIO ENGINEERS
<i>Proc. Nat. Elec. Conf.</i> .....	PROCEEDINGS OF THE NATIONAL ELECTRONICS CONFERENCE

## ABBREVIATIONS (Continued)

<i>Proc. Rad. Club Amer.</i> .....	PROCEEDINGS OF THE RADIO CLUB OF AMERICA
<i>Project. Jour. (Brit.)</i> .....	PROJECTIONISTS JOURNAL (BRITISH)
<i>Product Eng.</i> .....	PRODUCT ENGINEERING
<i>Project. Eng.</i> .....	PROJECTION ENGINEERING
<i>QST</i> .....	QST (A.R.R.L.)
<i>Radio and Tele.</i> .....	RADIO AND TELEVISION
<i>Radio Eng.</i> .....	RADIO ENGINEERING
<i>Radio Tech. Digest</i> .....	RADIO TECHNICAL DIGEST
<i>RCA Rad. Serv. News</i> .....	RCA RADIO SERVICE NEWS
<i>Rev. Mod. Phys.</i> .....	REVIEWS OF MODERN PHYSICS
<i>Rev. Sci. Instr.</i> .....	REVIEW OF SCIENTIFIC INSTRUMENTS
<i>RMA Eng.</i> .....	RMA ENGINEER
<i>Sci. Monthly</i> .....	SCIENTIFIC MONTHLY
<i>Sci. News Ltr.</i> .....	SCIENCE NEWS LETTER
<i>Short Wave and Tele.</i> .....	SHORT WAVE AND TELEVISION
<i>TBA Annual</i> .....	ANNUAL OF THE TELEVISION BROADCASTERS ASSOCIATION
<i>Teleg. &amp; Teleph. Age</i> .....	TELEGRAPH AND TELEPHONE AGE
<i>Tele. News</i> .....	TELEVISION NEWS
<i>The T &amp; R Bulletin (Brit.)</i> ....	BULLETIN OF THE RADIO SOCIETY OF GREAT BRITAIN
<i>Trans. Amer. Soc. Mech. Eng.</i> ..	TRANSACTIONS OF THE AMERICAN SOCIETY OF MECHANICAL ENGINEERS
<i>Trans. Electrochem. Soc.</i> .....	TRANSACTIONS OF THE ELECTRO- CHEMICAL SOCIETY

## ELECTRON TUBE BIBLIOGRAPHY

	Year
"An Oscillation Source for Radio Receiver Investigations", J. Weinberger, <i>Proc. I.R.E.</i> (December) .....	1919
"Note on the Input Impedance of Vacuum Tubes at Radio Frequency", J. Weinberger, <i>Proc. I.R.E.</i> (August) .....	1920
"The Possibility of Pulling Electrons from Metals by Powerful Electric Fields", B. E. Shackelford, <i>Phys. Rev.</i> 15 .....	1920
"How to Choose and Use Dry Cell Tubes for Portable Vacation Sets", J. O. Smith, <i>N. Y. Eve. World</i> (June 23) .....	1923
"Practical Master Oscillator Sets", E. A. Laport, <i>QST</i> (June) .....	1924
"Design of Non-Distorting Power Amplifiers", E. W. Kellogg, <i>Jour. A.I.E.E.</i> (May) .....	1925
Additional matter in contributed discussion (June) .....	1925
"Frequency Multiplication Principles and Practical Application of Ferro Magnetic Methods", N. E. Lindenblad and W. W. Brown, <i>Jour. A.I.E.E.</i> .....	1925
"A Method for Generating and Measuring Very Weak Radio-Frequency Currents", W. van B. Roberts, <i>Jour. Frank. Inst.</i> (March) .....	1926
"Notes on the Testing of Audio Frequency Amplifiers", E. T. Dickey, <i>Proc. I.R.E.</i> (August) .....	1927
"Note on Detection by Grid Condenser and Leak", W. van B. Roberts, <i>Proc. I.R.E.</i> (September) .....	1927
"A Radio-Frequency Oscillator for Receiver Investigations", G. Rodwin and T. A. Smith, <i>Proc. I.R.E.</i> (February) .....	1928
"The Three-Electrode Vacuum Tube as Applied to the Talking Motion Picture", E. W. Kellogg, <i>Jour. Soc. Mot. Pic. Eng.</i> (September) ..	1928
"Vacuum Tube Production Tests", A. F. Van Dyck and F. H. Engel, <i>Proc. I.R.E.</i> (November) .....	1928
"The Screen Grid Tube", A. F. Van Dyck, <i>N. Y. Times</i> (May) .....	1929
"Calculating Detector Output", J. M. Stinchfield, <i>Radio Broadcast</i> (August) .....	1929
"Grid-Leak Versus Bias Detection", J. M. Stinchfield, <i>Radio Broadcast</i> (October) .....	1929
"Television with Cathode-Ray Tube for Receiver", V. K. Zworykin, <i>Radio Eng.</i> (December) .....	1929
"Novel Electrical Controls Developed in Making Radio Tubes", B. E. Shackelford, <i>Jour. Chem. and Met. Eng.</i> 36 .....	1929
"Notes on a Method for Measuring the Microphonic Sensitivity of Tubes", F. H. Engel, <i>RCA Licensee Bulletin LB-102</i> (May 10) ..	1930
"A Note on the Mathematical Theory of the Multielectrode Tube", P. Caporale, <i>Proc. I.R.E.</i> (September) .....	1930
"The RCA Photophone System of Sound Recording and Reproduction for Sound Motion Pictures", A. N. Goldsmith and M. C. Batsel, <i>Proc. I.R.E.</i> (October) .....	1930
"Specification for Vacuum Tube Test Equipment Manufactured by RCA Victor", F. H. Engel, <i>RCA Licensee Bulletin LB-109</i> (November 5) .....	1930
"Hot-Cathode Grid-Controlled Arc Tubes", F. H. Engel, <i>RCA Licensee Bulletin LB-112</i> (December 31) .....	1930
"Notes on a Method of Measuring Plate Resistance of Vacuum Tubes", E. B. Boise and F. H. Engel, <i>RCA Licensee Bulletin LB-114</i> (January 14) .....	1931
"Notes on Super-Heterodyne Design", D. Grimes, <i>RCA Licensee Bulletin LB-115</i> (January 26) .....	1931
"Circuit Considerations of the Screen Grid Radiotron RCA 235", D. Grimes and W. S. Barden, <i>RCA Licensee Bulletin LB-120</i> (March 2) .....	1931
"Notes on a Method of Measuring Plate Resistance and Mutual Conductance of Vacuum Tubes", D. Grimes and E. B. Boise, <i>RCA Licensee Bulletin LB-128</i> (June 17) .....	1931

	Year
"Maximum Amplification in Capacity-Coupled Circuits", W. van B. Roberts, <i>Electronics</i> (July) .....	1931
"High Audio Power from Relatively Small Tubes", L. E. Barton, <i>Proc. I.R.E.</i> (July) .....	1931
"What Happens Within the Bulb of a Radio Tube?", L. G. Lessig, <i>Projection Eng.</i> (August) .....	1931
"Some Thermionic Properties of Barium Films Adsorbed on Tungsten", H. Nelson, <i>Physics</i> (August) .....	1931
"Composite First Detector-Oscillator Considerations", D. Grimes and W. S. Barden, <i>RCA Licensee Bulletin LB-132</i> (September 14) ...	1931
"Notes on the '47 Power Pentode", W. S. Barden, D. Grimes and E. B. Boise, <i>RCA Licensee Bulletin LB-125</i> (September 21) .....	1931
"Radio Tube Yardsticks", L. G. Lessig, <i>Radio Eng.</i> (October) .....	1931
"A Reversed Current Feed-Back Oscillator", W. van B. Roberts, <i>QST</i> (February) .....	1932
"Gm and Rp Test Circuit", E. B. Boise, <i>RCA Licensee Bulletin LB-146</i> (March 9) .....	1932
"Class B Amplification in Radio Receivers", W. S. Barden and C. Travis, <i>RCA Licensee Bulletin LB-153</i> (April 29) .....	1932
"Application of Class B Audio Amplifiers to A-C Operated Receivers", L. E. Barton, <i>Proc. I.R.E.</i> (July) .....	1932
"The New 57 as a High-Gain Amplifier", L. C. Waller, <i>QST</i> (July) ..	1932
"Recent Trends in Receiving Tube Design", J. C. Warner, E. W. Ritter and D. F. Schmit, <i>Proc. I.R.E.</i> (August) .....	1932
"Notes on Push-Pull Circuit Considerations", C. Travis, <i>RCA Licensee Bulletin LB-163</i> (August 18) .....	1932
"New Forms of Short Wave Tubes", I. E. Mourontseff, G. R. Kilgore and H. V. Noble, <i>Electronics</i> (September) .....	1932
"A Theory of Diode Detection", C. Travis, <i>RCA Licensee Bulletin LB-167</i> (September 15) .....	1932
"Notes on Class A Prime Considerations", W. S. Barden, <i>RCA Licensee Bulletin LB-173</i> (October 21) .....	1932
"Magnetostatic Oscillators for Generation of Ultra Short Waves", G. R. Kilgore, <i>Proc. I.R.E.</i> (November) .....	1932
"Some General Principles of Frequency Conversion in Superheterodyne Receivers", D. Grimes and W. S. Barden, <i>RCA Licensee Bulletin LB-187</i> (November 11) .....	1932
"Diode Triode Delayed AVC", C. Travis, <i>RCA Licensee Bulletin LB-179</i> (November 14) .....	1932
"Triple-Grid Power Amplifier Tubes", E. W. Herold, <i>Radio Eng.</i> (December) .....	1932
"Use of The 77 as a Biased Detector With 100 Volts Plate Supply", <i>RCA Tube Dept. Applic. Note No. 1</i> (March 10) .....	1933
"Use of The 57 as a Biased-Detector Resistance-Coupled to a 2A5", <i>RCA Tube Dept. Applic. Note No. 2</i> (March 17) .....	1933
"Use and Operation of the 2A7 and 6A7 as Pentagrid Converters", <i>RCA Tube Dept. Applic. Note No. 3</i> (March 29) .....	1933
"Graphical Determination of Performance of Push-Pull Audio Amplifiers", B. J. Thompson, <i>Proc. I.R.E.</i> (April) .....	1933
"The 2B7, 6B7, 55, 75 and 85 as Resistance Coupled Audio-Frequency Amplifiers", <i>RCA Tube Dept. Applic. Note No. 4</i> (April 5) ....	1933
"The Application of the Type 79 Tube", <i>RCA Tube Dept. Applic. Note No. 5</i> (April 12) .....	1933
"Higher Voltage Ratings for The 36, 37, 38, 39-44, and 89", <i>RCA Tube Dept. Applic. Note No. 6</i> (April 12) .....	1933
"Bulletin on Pentagrid Converter", C. Travis, <i>RCA Licensee Bulletin LB-226</i> (April 12) .....	1933
"250-Volt Rating for the 79", <i>RCA Tube Dept. Applic. Note No. 7</i> (April 19) .....	1933
"The 2A6 as a Resistance-Coupled Audio-Frequency Amplifier", <i>RCA Tube Dept. Applic. Note No. 8</i> (April 26) .....	1933

	Year
"Recent Advances in Tube Design", <i>RCA Tube Dept. Applic. Note No. 9</i> (April 26) .....	1933
"Reflex Circuits in Superheterodyne Receivers", J. Yolles, <i>RCA Licensee Bulletin LB-232</i> (April 28) .....	1933
"Notes on the 2A7 and 6A7 Converter Tubes", C. Travis, <i>RCA Licensee Bulletin LB-233</i> (April 29) .....	1933
"On Electron Optics", V. K. Zworykin, <i>Jour. Frank. Inst.</i> (May) ...	1933
"Effect of Diode Detection on I-F Driver Stage Design", W. S. Barden, <i>RCA Licensee Bulletin LB-230</i> (May 2) .....	1933
"The Use and Operation of the 25Z5", <i>RCA Tube Dept. Applic. Note No. 11</i> (May 10) .....	1933
"Half-Wave Operation of the 25Z5 with Separate Load Circuits for Each Rectifier Unit", <i>RCA Tube Dept. Applic. Note No. 12</i> (May 17) .....	1933
"Recommended Operating Conditions for the 38, 41, 42, 43, and 89", <i>RCA Tube Dept. Applic. Note No. 13</i> (May 24) .....	1933
"Operating Conditions for the 53 Tube", <i>RCA Tube Dept. Applic. Note No. 14</i> (May 31) .....	1933
"Reflex Circuit Considerations", O. H. Schade and J. M. Stinchfield, <i>Electronics</i> (June) .....	1933
"The Operation of the Type 48 Tube as a Triode", <i>RCA Tube Dept. Applic. Note No. 15</i> (June 7) .....	1933
"Further Notes on Reflex Considerations", D. Grimes and W. S. Barden, <i>RCA Licensee Bulletin LB-246</i> (June 23) .....	1933
"Operation of the 2B7, or 6B7, as a Reflex Amplifier", <i>RCA Tube Dept. Applic. Note No. 16</i> (July 7) .....	1933
"Special Applications of the Type 53 Tube", <i>RCA Tube Dept. Applic. Note No. 17</i> (July 13) .....	1933
"Operation Conditions for the Type 19 Tube", <i>RCA Tube Dept. Applic. Note No. 18</i> (July 27) .....	1933
"The Application for Graphite as an Anode Material to High-Vacuum Transmitting Tubes", E. E. Spitzer, <i>Proc. I.R.E.</i> (August) ....	1933
"Tubes to Fit the Wavelength", B. J. Thompson, <i>Electronics</i> (August) .....	1933
"Operating Conditions for the 1A6 as an Oscillator-Mixer", <i>RCA Tube Dept. Applic. Note No. 19</i> (August 23) .....	1933
"An Increase in the Maximum Allowable Grid Resistor for Types 38, 41, 42, 89 and 2A6", <i>RCA Tube Dept. Applic. Note No. 20</i> (August 23) .....	1933
"Operation Characteristics of the Type 1-v and the type 12Z3 Tube", <i>RCA Tube Dept. Applic. Note No. 21</i> (August 30) .....	1933
"Operation of the 2A6, 2B7, 6B7, 55, 75, 77 and 85 as Resistance-Coupled Audio-Frequency Amplifiers", <i>RCA Tube Dept. Applic. Note No. 22</i> (September 6) .....	1933
"The Operating Characteristics of the Type 84 Tube", <i>RCA Tube Dept. Applic. Note No. 23</i> (October 5) .....	1933
"Use of the 1A6 as a Half-Wave Diode-Tetrode", <i>RCA Tube Dept. Applic. Note No. 24</i> (October 12) .....	1933
"Influence of Circuit Constants on Receiver Output Noise", <i>RCA Tube Dept. Applic. Note No. 25</i> (October 19) .....	1933
"The 37, 56, 57 and 77 Tubes as Resistance-Coupled High-Voltage Amplifiers", <i>RCA Tube Dept. Applic. Note No. 26</i> (October 26) .....	1933
"A Cathode-Ray Modulation Indicator", E. C. Ballentine, <i>Broadcast News</i> (November) .....	1933
"An Analysis of Super-Regeneration", W. van B. Roberts, <i>RCA Licensee Bulletin LB-266</i> (November 1) .....	1933
"Use of Pentagrid Converter Tubes in Multi-Range Receivers", <i>RCA Tube Dept. Applic. Note No. 27</i> (November 2) .....	1933
"Super-Regeneration and Its Application to High-Frequency Reception", D. Grimes and W. S. Barden, <i>RCA Licensee Bulletin LB-267</i> (November 8) .....	1933
"Special Applications of the Type 79 Tube", <i>RCA Tube Dept. Applic. Note No. 28</i> (November 9) .....	1933

	Year
"Cathode-Ray Tubes for Oscillograph Purposes", C. W. Taylor, L. B. Headrick and R. T. Orth, <i>Electronics</i> (December) .....	1933
"Vacuum Tubes of Small Dimensions for Use at Extremely High Frequencies", B. J. Thompson and G. M. Rose, Jr., <i>Proc. I.R.E.</i> (December) .....	1933
"Description of an Experimental Television System and the Kinescope", V. K. Zworykin, <i>Proc. I.R.E.</i> (December) .....	1933
"Notes on the Measurement of Inter-Electrode Capacities with a Tentative Standard of Procedure", C. Travis, <i>RCA Licensee Bulletin LB-270</i> (December 5) .....	1933
"Design of Audio Systems Employing Type 2A3 Power Amplifier Triodes", <i>RCA Tube Dept. Applic. Note No. 29</i> (December 29) ..	1933
"Vacuum Tubes", J. M. Stinchfield, Section of RADIO ENGINEERING HANDBOOK, Henney, McGraw-Hill Book Co., New York, N. Y. ...	1933
"Problems of Cathode-Ray Television", I. G. Maloff, <i>Electronics</i> (January) .....	1934
"The Iconoscope—A Modern Version of the Electric Eye", V. K. Zworykin, <i>Proc. I.R.E.</i> (January) .....	1934
"Characteristics of The 6F7 Tube", <i>RCA Tube Dept. Applic. Note No. 30</i> (January 3) .....	1934
"Operating Considerations of Cathode Ray Tubes 905 and 906 for Oscillographic Purposes", <i>RCA Tube Dept. Applic. Note No. 31</i> (January 11) .....	1934
"Revision of Characteristics for the Type 48 Tube", <i>RCA Tube Dept. Applic. Note No. 32</i> (January 17) .....	1934
"The RCA-800 in Class B Audio Amplifiers", <i>RCA Tube Dept. Applic. Note No. 33</i> (January 31) .....	1934
"Characteristics of the 868 Phototube", <i>RCA Tube Dept. Applic. Note No. 34</i> (February 15) .....	1934
"Triode Operation of Type 42 and Type 2A5 Pentodes", <i>RCA Tube Dept. Applic. Note No. 35</i> (February 26) .....	1934
"Voltage Multiplying Circuits", C. Travis, <i>RCA Licensee Bulletin LB-283</i> (February 26) .....	1934
"100-Volt Operation of 6C6 and 6D6 Tubes", <i>RCA Tube Dept. Applic. Note No. 37</i> (March 27) .....	1934
"Power Supply and Linear Time Axis for Cathode-Ray Oscillographs", P. A. Richards and W. L. Meier, <i>Electronics</i> (April) ..	1934
"A Simple Method for Converting Pentode Characteristics", <i>RCA Tube Dept. Applic. Note No. 38</i> (April 25) .....	1934
"The Input Impedance of Vacuum Tubes", J. Yolles, <i>RCA Licensee Bulletin LB-290</i> (April 28) .....	1934
"Improved Magnetron Oscillator for the Generation of Microwaves", E. G. Linder, <i>Phys. Rev.</i> (May 1) .....	1934
"The Design of a Voltage Supply for the 905 and 906 Cathode Ray Tubes", <i>RCA Tube Dept. Applic. Note No. 39</i> (May 11) .....	1934
"Notes on an Ionized Gas Modulator for Short Radio Waves", E. G. Linder and I. Wolff, <i>Proc. I.R.E.</i> (June) .....	1934
"High Power Output from Type 45 Tubes", <i>RCA Tube Dept. Applic. Note No. 40</i> (June 14) .....	1934
"The 1C6", <i>RCA Tube Dept. Applic. Note No. 41</i> (July 6) .....	1934
"Tube Consideration in Class-B Amplification", L. E. Barton, <i>Broadcast News</i> (August) .....	1934
"Push-Pull vs. Parallel Operation", J. L. Reinartz, <i>Radio</i> (September, December) .....	1934
"Design and Use of 'Acorn' Tubes for Ultra High Frequencies", B. Salzberg, <i>Electronics</i> (September) .....	1934
"Short-cut Method for Determining Operating Conditions of Power Output Triodes", <i>RCA Tube Dept. Applic. Note No. 42</i> (September 5) .....	1934
"Notes on Tests and Ratings of Tubes for Oscillator Service", C. Travis, <i>RCA Licensee Bulletin LB-307</i> (October 1) .....	1934



	Year
"Operating Conditions for the 6A6", <i>RCA Tube Dept. Applic. Note No. 44</i> (November 14) .....	1934
"Theory of Electron Gun", I. G. Maloff and D. W. Epstein, <i>Proc. I.R.E.</i> (December) .....	1934
"Cathode-Ray Tubes and Their Applications", J. M. Stinchfield, <i>Elec. Eng.</i> (December) .....	1934
"An Electron Oscillator with Plane Electrodes", B. J. Thompson and P. D. Zottu, <i>Proc. I.R.E.</i> (December) .....	1934
"Vacuum Tube Amplifiers", L. E. Barton, Section of ELECTRICAL ENGINEERS' HANDBOOK, Pender-McIlwain, New York, N. Y. ....	1934
"The Secondary Emission Phototube", H. Iams and B. Salzberg, <i>Proc. I.R.E.</i> (January) .....	1935
"The Use of the 57 or 6C6 to Obtain Negative Transconductance and Negative Resistance", <i>RCA Tube Dept. Applic. Note No. 45</i> (February 7) .....	1935
"The Application of Superheterodyne Frequency-Conversion System to Multirange Receivers", W. A. Harris, <i>Proc. I.R.E.</i> (April) ...	1935
"Graphical Harmonic Analysis for Determining Modulation Distortion in Amplifier Tubes", W. R. Ferris, <i>Proc. I.R.E.</i> (May) .....	1935
"Automatic Frequency Control", C. Travis, <i>RCA Licensee Bulletin LB-326</i> (May) .....	1935
"Use of the 954 as a Vacuum-Tube Voltmeter", <i>RCA Tube Dept. Applic. Note No. 47</i> (May 20) .....	1935
"Miscellaneous Applications of Vacuum Tubes", E. H. Shepard, <i>Proc. Rad. Club Amer.</i> (June) .....	1935
"The Construction of a Top-Cap Shield for Metal Tubes", <i>RCA Tube Dept. Applic. Note No. 49</i> (July 23) .....	1935
"High-Gain Audio Frequency Amplifiers", E. H. Shepard, <i>Radio Craft</i> (August) .....	1935
"Characteristics of the Photophone Light-Modulating System", L. T. Sachtleben, <i>Jour. Soc. Mot. Pic. Eng.</i> (August) .....	1935
"Operation of the 6L7 as a Mixer Tube", <i>RCA Tube Dept. Applic. Note No. 50</i> (August 19) .....	1935
"The 6F5", <i>RCA Tube Dept. Applic. Note No. 51</i> (September 25) ...	1935
"Recent Developments in Miniature Tubes", B. Salzberg and D. G. Burnside, <i>Proc. I.R.E.</i> (October) .....	1935
"Negative Resistance and Devices for Obtaining It", E. W. Herold, <i>Proc. I.R.E.</i> (October) .....	1935
"Automatic Frequency Control", C. Travis, <i>Proc. I.R.E.</i> (October) ..	1935
"Class AB Operation of Type 6F6 Tubes Connected as Triodes", <i>RCA Tube Dept. Applic. Note No. 52</i> (October 31) .....	1935
"Halation (Interference in Fluorescent Screens)", Berthold Sheffield, <i>Electronics</i> (November) .....	1935
"Development of Cathode-Ray Tubes for Oscillographic Purposes", R. T. Orth, P. A. Richards and L. B. Headrick, <i>Proc. I.R.E.</i> (November) .....	1935
"Luminescent Materials for Cathode-Ray Tubes", T. B. Perkins and H. W. Kaufman, <i>Proc. I.R.E.</i> (November) .....	1935
"Cathode-Ray Tube Terminology", T. B. Perkins, <i>Proc. I.R.E.</i> (November) .....	1935
"Anode Materials and Design for High-Vacuum Transmitting Tubes", E. E. Spitzer, <i>Elec. Eng.</i> (November) .....	1935
"Quantitative Influence of Tube and Circuit Properties on Random Electron Noise", W. S. Barden and S. W. Seeley, <i>RCA Licensee Bulletin LB-341</i> (November 7) .....	1935
"Method for Measurement of Conversion Conductance", S. W. Seeley, <i>RCA Licensee Bulletin LB-342</i> (November 16) .....	1935
"The 6L7 as a Volume Expander for Phonographs", <i>RCA Tube Dept. Applic. Note No. 53</i> (November 27) .....	1935
"Influence of Tube and Circuit Properties in Electron Noise", S. W. Seeley and W. S. Barden, <i>Electronics</i> (December) .....	1935

	Year
"Improved and Simplified Methods for Automatic Frequency Control", D. E. Foster and S. W. Seeley, <i>RCA Licensee Bulletin LB-343</i> (December 12) .....	1935
"Class AB Operation of Type 6F6 Tubes Connected as Pentodes", <i>RCA Tube Dept. Applic. Note No. 54</i> (December 20) .....	1935
"Operation of the 6A8", <i>RCA Tube Dept. Applic. Note No. 55</i> (De- cember 27) .....	1935
"Possibilities of the Iconoscope in Television", V. K. Zworykin and G. A. Morton, booklet, Geo. Newnes, Ltd., England .....	1935
"Input Resistance of Vacuum Tubes as Ultra-High-Frequency Am- plifiers", W. R. Ferris, <i>Proc. I.R.E.</i> (January) .....	1936
"Analysis of the Effects of Space Charge on Grid Impedance", D. O. North, <i>Proc. I.R.E.</i> (January) .....	1936
"Receiver Design", <i>RCA Tube Dept. Applic. Note No. 56</i> (January 15)	1936
"A New Tube for Use in Superheterodyne Frequency Conversion Systems", C. F. Nesslage, E. W. Herold and W. A. Harris, <i>Proc.</i> <i>I.R.E.</i> (February) .....	1936
"A Detector Circuit for Reducing Noise Interference in Phone Recep- tion", L. E. Thompson, <i>QST</i> (February) .....	1936
"Balanced Amplifiers", A. Preisman, <i>Comm. and Broad. Eng.</i> (Febru- ary, March, September, October, November, December) .....	1936
(January) .....	1937
"The 6L7 as an R-F Amplifier", <i>RCA Tube Dept. Applic. Note No. 57</i> (February 5) .....	1936
"The Secondary Emission Multiplier—A New Electronic Device", V. K. Zworykin, G. A. Morton and L. Malter, <i>Proc. I.R.E.</i> (March)	1936
"A High Efficiency Crystal Oscillator", J. L. Reinartz, <i>Radio</i> (March)	1936
"Intermediate Frequency Considerations", D. E. Foster and E. W. Wilby, <i>RCA Licensee Bulletin LB-349</i> (March 2) .....	1936
"Output Tubes for Radio Receivers", J. F. Dreyer, Jr., <i>Electronics</i> (April) .....	1936
"Description and Characteristics of the End-Plate Magnetron", E. G. Linder, <i>Proc. I.R.E.</i> (April) .....	1936
"Applied Electron Optics", V. K. Zworykin and G. A. Morton, <i>Jour.</i> <i>Opt. Soc. Amer.</i> (April) .....	1936
"The Electron Image Tube", V. K. Zworykin, <i>Broadcast News</i> (April)	1936
"Automatic Frequency Control for Single I-F Stage Receivers", D. E. Foster, <i>RCA Licensee Bulletin LB-355</i> (April 13) .....	1936
"Simplified Means for Determination of Converter Tube Perform- ance", C. N. Kimball and C. E. Coon, <i>RCA Licensee Bulletin LB-</i> <i>356</i> (April 27) .....	1936
"A Different Amplifier Tube", Berthold Sheffield, <i>Electronics</i> (May) ..	1936
"Operation of the 6Q7", <i>RCA Tube Dept. Applic. Note No. 59</i> (May 7)	1936
"Effect of Electron Pressure on Plasma Electron Oscillations", E. G. Linder, <i>Phys. Rev.</i> (May 15) .....	1936
"Notes on the Theory of the Single Stage Amplifier", B. Salzberg, <i>Proc. I.R.E.</i> (June) .....	1936
"A Study of Polarization Capacity and Electrode Condition", I. Wolff, <i>Jour. Chem. Phys.</i> (June) .....	1936
"Power Saving Tubes With Copper Cathodes", Berthold Sheffield, <i>Electronics</i> (June) .....	1936
"Operation of the 6L6", <i>RCA Tube Dept. Applic. Note No. 60</i> (June 10) .....	1936
"The Conversion of a 6L6 Plate Family to New Screen Voltage Con- ditions", <i>RCA Tube Dept. Applic. Note No. 61</i> (June 25) .....	1936
"Iconoscopes and Kinescopes in Television", V. K. Zworykin, <i>RCA</i> <i>Review</i> (July) .....	1936
<i>Jour. Soc. Mot. Pic. Eng.</i> (May) .....	1937
"New Developments in Audio Power Tubes", R. S. Burnap, <i>RCA</i> <i>Review</i> (July) .....	1936

	Year
"The Cathode-Ray Tube in Television Reception", I. G. Maloff, <i>TELEVISION</i> , Vol. I (July) .....	1936
"A New Operating Condition for Two Type 6F6 Tubes Connected as Pentodes", <i>RCA Tube Dept. Applic. Note No. 62</i> (July 13) ....	1936
"A High-Gain Single-Tube Phase Inverter", <i>RCA Tube Dept. Applic. Note No. 63</i> (July 30) .....	1936
"Electron Optical System of Two Cylinders as Applied to Cathode-Ray Tubes", D. W. Epstein, <i>Proc. I.R.E.</i> (August) .....	1936
"Magnetron Oscillators for the Generation of Frequencies Between 300 and 600 Megacycles", G. R. Kilgore, <i>Proc. I.R.E.</i> (August) ..	1936
"Recent Developments of the Class 'B' Audio and Radio-Frequency Amplifiers", L. E. Barton, <i>Proc. I.R.E.</i> (July) .....	1936
"Study of Cathode Loaded Drivers and Detectors", C. N. Kimball and W. S. Barden, <i>RCA Licensee Bulletin LB-371</i> (August) .....	1936
"Inverse-Feedback Circuits for A-F Amplifiers", <i>RCA Tube Dept. Applic. Note No. 64</i> (August 26) .....	1936
"The Sommerfeld Formula", W. A. Fitch, <i>Electronics</i> (September) ..	1936
"The Electron-Image Tube, a Means for Making Infra-Red Images Visible", G. A. Morton, <i>Jour. Soc. Mot. Pic. Eng.</i> (September) ..	1936
"Tuning-Indicator Circuits for the 6E5 and 6G5", <i>RCA Tube Dept. Applic. Note No. 65</i> (September 10) .....	1936
"Equal Plate and Screen Voltage Operation of the 6L6", <i>RCA Tube Dept. Applic. Note No. 66</i> (September 29) .....	1936
"Electron Motion in a Plasma", E. G. Linder, <i>Science</i> (October) .....	1936
"5-Meter Crystal Controlled Push-Pull 800 Output", J. L. Reinartz, <i>QST</i> (October) .....	1936
"Electron Beams and Their Applications in Low-Voltage Devices", H. C. Thompson, <i>Proc. I.R.E.</i> (October) .....	1936
"Multitube Oscillators for the Ultra-High-Frequencies", P. D. Zottu, <i>QST</i> (October) .....	1936
"A Study of the Characteristics of Noise", V. D. Landon, <i>Proc. I.R.E.</i> (November) .....	1936
"Application of Conventional Vacuum Tubes in Unconventional Circuits", E. H. Shepard, Jr., <i>Proc. I.R.E.</i> (December) .....	1936
"Electron Optics of an Image Tube", G. A. Morton and E. G. Ramberg, <i>Physics</i> (December) .....	1936
"An Improved Vacuum Tube Microammeter", A. W. Vance, <i>Rev. Sci. Instr.</i> .....	1936
"Vacuum Tubes", B. J. Thompson, J. M. Stinchfield, B. Salzberg, E. W. Herold, Section of ELECTRICAL ENGINEERS' HANDBOOK, Pender-McIlwain, New York, N. Y. ....	1936
"Simplified Methods for Computing Performance of Transmitting Tubes", W. G. Wagener, <i>Proc. I.R.E.</i> (January) .....	1937
"Resistance-Coupled Audio-Frequency Amplifiers", <i>RCA Tube Dept. Applic. Note No. 67</i> (January 20) .....	1937
"A 55-Watt Amplifier Using Two Type 6L6 Tubes", <i>RCA Tube Dept. Applic. Note No. 68</i> (January 20) .....	1937
"250-Volt Low-Current Operation of the 6L6", <i>RCA Tube Dept. Applic. Note No. 69</i> (February 3) .....	1937
"UHF Diode with Movable Anode", Berthold Sheffield, <i>Electronics</i> (March) .....	1937
"Low-Current, High-Power Operation of Two 6L6's Connected in Push-Pull", <i>RCA Tube Dept. Applic. Note No. 71</i> (March 3) .....	1937
"A 40-Watt Operating Condition for Two Type 6L6 Tubes", <i>RCA Tube Dept. Applic. Note No. 72</i> (March 17) .....	1937
"Operation of the 25L6 in Typical Circuits", <i>RCA Tube Dept. Applic. Note No. 73</i> (March 31) .....	1937
"A Control System for AFC Receivers with Improved Flexibility", G. Mountjoy, <i>RCA Licensee Bulletin LB-389</i> (April 20) .....	1937
"New High-Voltage Choke-Input Rating for the 5T4", <i>RCA Tube Dept. Applic. Note No. 74</i> (April 28) .....	1937

	Year
"Receiver Design", <i>RCA Tube Dept. Applic. Note No. 75</i> (May 28) . . .	1937
"A Wide-Range, Linear-Scale Photoelectric Cell Densitometer", W. W. Lindsay, Jr., and W. V. Wolfe, <i>Jour. Soc. Mot. Pic. Eng.</i> (June) . .	1937
"Mixer Circuits", A. Preisman, <i>Communications</i> (June, August) . . .	1937
"Automatic Plotting of Electron Trajectories", D. B. Langmuir, <i>Nature (Brit.)</i> (June) . . . . .	1937
"An Amplifier with No Phase Distortion", O. H. Schade, <i>Electronics</i> (June) . . . . .	1937
"Batalum, a Barium Getter for Metal Tubes", E. A. Lederer and D. H. Wamsley, <i>RCA Review</i> (July) . . . . .	1937
"A Fundamental-Reinforced Harmonic-Generating Circuit", J. L. Reinartz, <i>QST</i> (July) . . . . .	1937
"The New RCA Electronic Sweep Oscillator", O. M. Owsley, <i>RCA Rad. Serv. News</i> (July) . . . . .	1937
"Dimensions of Popular Tube Types", <i>RCA Tube Dept. Applic. Note No. 77</i> (July 14) . . . . .	1937
"Use of the Plate Family in Vacuum-Tube Power-Output Calculations", <i>RCA Tube Dept. Applic. Note No. 78</i> (July 28) . . . . .	1937
"A Circuit for Studying Kinescope Resolutions", C. E. Burnett, <i>Proc. I.R.E.</i> (August) . . . . .	1937
"Development of the Projection Kinescope", V. K. Zworykin and W. H. Painter, <i>Proc. I.R.E.</i> (August) . . . . .	1937
"Theory and Performance of the Iconoscope", V. K. Zworykin, G. A. Morton and L. E. Flory, <i>Proc. I.R.E.</i> (August) . . . . .	1937
"Television Pickup Tubes with Cathode-Ray Beam Scanning", H. Iams and A. Rose, <i>Proc. I.R.E.</i> (August) . . . . .	1937
"Theoretical Limitation of Cathode-Ray Tubes", D. B. Langmuir, <i>Proc. I.R.E.</i> (August) . . . . .	1937
"High-Current Electron Gun for Projection Kinescope", R. R. Law, <i>Proc. I.R.E.</i> (August) . . . . .	1937
"The Oscillotrol", D. E. Foster and G. Mountjoy, <i>RCA Licensee Bulletin LB-404</i> (August 2) . . . . .	1937
"Characteristics of Inverse Feed-Back Circuits," L. R. Martin, <i>Radio Eng.</i> (May) . . . . .	1937
"Analysis and Design of Video Amplifiers, Part I", C. N. Kimball and S. W. Seeley, <i>RCA Licensee Bulletin LB-406</i> (August 17) . .	1937
<i>RCA Review</i> (October) . . . . .	1937
"Frequency Changers in All-Wave Receivers", E. W. Herold, <i>Wireless Eng. (Brit.)</i> (September) . . . . .	1937
"Significance of Ratings for Power Output Tubes", <i>RCA Tube Dept. Applic. Note No. 79</i> (September 8) . . . . .	1937
"The Magnetron as a High-Frequency Generator", G. R. Kilgore, <i>Jour. Appl. Phys.</i> (October) . . . . .	1937
"Negative Peak Automatic Modulation Control for Plate-Modulated Phone Transmitters", L. C. Waller, <i>QST</i> (October) . . . . .	1937
"Some Unconventional Vacuum Tube Applications", E. H. Shepard, <i>RCA Review</i> (October) . . . . .	1937
"Problems Concerning the Production of Cathode Ray Tube Screens", H. W. Leverenz, <i>Television</i> , Vol. II (October) . . . . .	1937
"A Transformation for Calculating the Constants of Vacuum Tubes with Cylindrical Elements", W. van B. Roberts, <i>Proc. I.R.E.</i> (October) . . . . .	1937
"The Requirements and Performance of a New Ultra-High-Frequency Power Tube", W. G. Wagener, <i>RCA Review</i> (October) . . . . .	1937
"Operation of the 6V6-G", <i>RCA Tube Dept. Applic. Note No. 80</i> (October 20) . . . . .	1937
"Direct Viewing Type Cathode-Ray Tube for Large Television Images", I. G. Maloff, <i>Proc. I.R.E.</i> (November) . . . . .	1937
"Screens for Television Tubes", I. G. Maloff and D. W. Epstein, <i>Electronics</i> (November) . . . . .	1937

	Year
"Class B R-F Amplifier Chart", W. van B. Roberts, <i>Electronics</i> (November) .....	1937
"Description of the RCA Type 96A Limiting Amplifier", J. M. Brumbaugh and B. W. Robins, <i>Broadcast News</i> (November) .....	1937
"Analysis of Admittance Neutralization by Means of Negative Transconductance Tubes", E. W. Herold, <i>Proc. I.R.E.</i> (November) ....	1937
"Recent Developments in German Cathode Ray Tubes", Berthold Sheffield, <i>Electronics</i> (November) .....	1937
"A Two-Terminal Oscillator", RCA Tube Dept. <i>Applic. Note No. 81</i> (November 17) .....	1937
"Effects of Space Charge in the Grid-Anode Region of Vacuum Tubes", A. V. Haeff and B. Salzberg, <i>RCA Review</i> (January) .....	1938
"Television Cathode-Ray Tubes for the Amateur", R. S. Burnap, <i>RCA Review</i> (January) .....	1938
"Vacuum-Tube Engineering for Motion Pictures", A. M. Glover and L. C. Hollands, <i>Jour. Soc. Mot. Pic. Eng.</i> (January) .....	1938
"Wide-Angle Tuning with the 6E5, 6G5 or 6U5", RCA Tube Dept. <i>Applic. Note No. 82</i> (January 5) .....	1938
"Resistance-Coupled Amplifier Data for the 6L6, 6T7-G and 6S7-G", RCA Tube Dept. <i>Applic. Note No. 83</i> (January 5) .....	1938
"Video I. F. System Considerations", S. W. Seeley and W. S. Barden, <i>RCA Licensee Bulletin LB-417</i> (January 5) .....	1938
"Oscillator Frequency Stability in Relation to Receivers with Spread Short Wave Bands", D. E. Foster, <i>RCA Licensee Bulletin LB-418</i> (January 8) .....	1938
"The Operation of Phototubes", RCA Tube Dept. <i>Applic. Note No. 84</i> (January 12) .....	1938
"Operation of the 6AC5-G", RCA Tube Dept. <i>Applic. Note No. 85</i> (January 26) .....	1938
"Operation of the 6Y6-G", RCA Tube Dept. <i>Applic. Note No. 86</i> (January 26) .....	1938
"Beam Power Tubes", O. H. Schade, <i>Proc. I.R.E.</i> (February) .....	1938
"The 6K8—A New Converter Tube", RCA Tube Dept. <i>Applic. Note No. 87</i> (February 16) .....	1938
"Excess Energy Electrons and Electron Motion in High Vacuum Tubes", E. G. Linder, <i>Proc. I.R.E.</i> (March) .....	1938
"The New RCA-153 Service Oscillator", O. M. Owsley, <i>RCA Rad. Serv. News</i> (March) .....	1938
"Hum in Heater-Type Tubes", RCA Tube Dept. <i>Applic. Note No. 88</i> (March 9) .....	1938
"Some Notes on Video-Amplifier Design", A. Preisman, <i>RCA Review</i> (April) .....	1938
"The Monoscope and Its Uses", C. E. Burnett, <i>RCA Review</i> (April) ..	1938
"The Developmental Problems and Operation Characteristics of Two New Ultra-High-Frequency Triodes", W. G. Wagener, <i>Proc. I.R.E.</i> (April) .....	1938
"Resistance-Coupled Amplifier Data for the 6C8-G, 6F1-G, 6J5, 6J5-G and 6Z7-G", RCA Tube Dept. <i>Applic. Note No. 90</i> (April 13) ..	1938
"Operation of the Gas-Triode OA4-G", RCA Tube Dept. <i>Applic. Note No. 91</i> (April 29) .....	1938
"A New Cold-Cathode Gas Triode", W. E. Bahls and C. H. Thomas, <i>Electronics</i> (May) .....	1938
"Effect of High-Energy Electron Random Motion Upon the Shape of the Magnetron Cut-off Curve", E. G. Linder, <i>Jour. Appl. Phys.</i> (May) .....	1938
"Operation of the Improved Type 906 Cathode-Ray Tube at Low Voltages", RCA Tube Dept. <i>Applic. Note No. 92</i> (May 25) .....	1938
"Metal Evaporators", H. B. DeVore, <i>Rev. of Sci. Instr.</i> (June) .....	1938
"An Inverse-Feedback Circuit for Resistance-Coupled Amplifiers", RCA Tube Dept. <i>Applic. Note No. 93</i> (June 8) .....	1938

	Year
"Operation of the 6AF6-G", RCA Tube Dept. Applic. Note No. 94 (June 22) .....	1938
"A Discussion on Video Modulation Detection", W. S. Barden, RCA Licensee Bulletin LB-435 (June 27) .....	1938
"Teledynamic Control by Selective Ionization With Application to Radio Receivers", H. B. Deal, S. W. Seeley, and C. N. Kimball, Proc. I.R.E. (July) .....	1938
"Linear Rectifier Design Calculations", E. A. Laport, RCA Review (July) .....	1938
"A New Converter Tube for All-Wave Receivers", E. W. Herold, W. A. Harris and T. J. Henry, RCA Review (July) .....	1938
"Inverse Feedback Circuits for Output Tubes", D. E. Foster and J. A. Rankin, RCA Licensee Bulletin LB-438 (July 19) .....	1938
"Performance of 6K8 Converter in Short Wave Receivers", A. E. Newlon, RCA Licensee Bulletin LB-441 (July 19) .....	1938
"Television I-F Circuits", R. S. Holmes and E. W. Engstrom, Electronics (August) .....	1938
"Wide-Range Beat Frequency Oscillator", E. I. Anderson, RCA Licensee Bulletin LB-444 (August 11) .....	1938
"Operating Positions of Receiving Tubes", RCA Tube Dept. Applic. Note No. 95 (August 17) .....	1938
"A Voltage Regulator For D-C Power Supplies", RCA Tube Dept. Applic. Note No. 96 (August 24) .....	1938
"Method of Measuring Luminescent Screen Potential", H. Nelson, Jour. Appl. Phys. (September) .....	1938
"Single-Ended R-F Pentodes", R. L. Kelly and J. F. Miller, Electronics (September) .....	1938
"Improvements in High Frequency Amplifiers", D. E. Foster and A. E. Newlon, RCA Licensee Bulletin LB-450 (September 22) ..	1938
"A Self-Balancing Phase-Inverter Circuit", RCA Tube Dept. Applic. Note No. 97 (September 28) .....	1938
"Review of Ultra-High-Frequency Vacuum-Tube Problems", B. J. Thompson, RCA Review (October) .....	1938
"Application of an Electron Multiplier to the Production of Facsimile Test Wave-Forms", W. H. Bliss, RADIO FACSIMILE, Vol. I (October) .....	1938
"Analysis and Design of Video Amplifiers, Part II", C. N. Kimball and S. W. Seeley, Jour. Tele. Soc. (October) .....	1938
"A Video Mixing Amplifier", A. A. Barco, RCA Licensee Bulletin LB-453 (October 11) .....	1938
"The Operation of Single-Ended Tubes", RCA Tube Dept. Applic. Note No. 98 (October 19) .....	1938
"Revision of 6K8 Ratings", RCA Tube Dept. Applic. Note No. 99 (October 19) .....	1938
"Photoelectric Cells and Circuits", W. S. Thompson, International Photographer (November) .....	1938
"Operation of the 6SA7", RCA Tube Dept. Applic. Note No. 100 (December 2) .....	1938
CATHODE-RAY TUBE IN TELEVISION, I. G. Maloff and D. W. Epstein, McGraw-Hill Book Co., New York, N. Y. ....	1938
"Amplifiers and Power Supplies", W. S. Thompson, International Photographer (January) .....	1939
"A Bridge Type Set for Measuring Vacuum Tube Parameters", J. R. Pernice, Communications (January) .....	1939
"Analysis and Design of Video Amplifiers—Part II", S. W. Seeley and C. N. Kimball, RCA Review (January) .....	1939
"New Television Amplifier Receiving Tubes", A. P. Kauzmann, RCA Review (January) .....	1939
"Sweep Frequency Signal Generator", J. A. Rankin, RCA Licensee Bulletin LB-466 (January) .....	1939

	Year
"Input Loading of Receiving Tubes at Radio Frequencies", <i>RCA Tube Dept. Applic. Note No. 101</i> (January 25) .....	1939
"A Fixed-Focus Electron Gun for Cathode-Ray Tubes", H. Iams, <i>Proc. I.R.E.</i> (February) .....	1939
"An Ultra-High-Frequency Power Amplifier of Novel Design", A. V. Haeff, <i>Electronics</i> (February) .....	1939
"Light Output and Secondary Emission Characteristics of Luminescent Materials", S. T. Martin and L. B. Headrick, <i>Jour. Appl. Phys.</i> (February) .....	1939
"Simplified Derivation of the General Properties of an Electron-Optical Image", E. G. Ramberg, <i>Jour. Opt. Soc. Amer.</i> (February) .....	1939
"Using Electromagnetic-Deflection Cathode-Ray Tubes in the Television Receiver", J. B. Sherman, <i>QST</i> (February) .....	1939
"Variation of Light Output with Current Density and Classification of Willemite Phosphors", E. G. Ramberg and G. A. Morton, <i>Phys. Rev.</i> (February) .....	1939
"Circuit Design and Its Relation to Tube Performance", L. C. Hollands, <i>Electronics</i> (March) .....	1939
"Electrostatic Deflection Kinescope Unit for the Television Receiver", J. B. Sherman, <i>QST</i> (March) .....	1939
"Transmitter Circuit Design for Frequencies Above 100 Mc", O. E. Dow, <i>Proc. Rad. Club Amer.</i> (March) .....	1939
"The 6SK7 As An I-F Amplifier", <i>RCA Tube Dept. Applic. Note No. 102</i> (March 15) .....	1939
"Tubes at Work", D. Pollack, <i>Electronics</i> (April) .....	1939
"A Wide-Range Video-Amplifier for a Cathode-Ray Oscilloscope", A. Preisman, <i>RCA Review</i> (April) .....	1939
"Kinescopes for Television Receivers", L. C. Waller, <i>Communications</i> (April) .....	1939
"Measurements of Admittances at Ultra-High Frequencies", J. M. Miller and B. Salzberg, <i>RCA Review</i> (April) .....	1939
"Transient Response of Multistage Video-Frequency Amplifiers", A. V. Bedford and G. L. Fredendall, <i>Proc. I.R.E.</i> (April) .....	1939
"Rate of Evaporation of Tantalum", L. Malter and D. B. Langmuir, <i>Phys. Rev.</i> (April 15) .....	1939
"Resistance, Emissivities, and Melting Point of Tantalum", L. Malter and D. B. Langmuir, <i>Phys. Rev.</i> (April 15) .....	1939
"Operation of the 35L6-GT" <i>RCA Tube Dept. Applic. Note No. 103</i> (April 26) .....	1939
"Phenomenon of Secondary Electron Emission", H. Nelson, <i>Phys. Rev.</i> (May 15) .....	1939
"An Iconoscope Pre-Amplifier", Allen A. Barco, <i>RCA Review</i> (July) .....	1939
"A Push-Pull Ultra-High-Frequency Beam Tetrode", A. K. Wing, <i>RCA Review</i> (July) .....	1939
"Effect of Electron Transit Time on Efficiency of a Power Amplifier", A. V. Haeff, <i>RCA Review</i> (July) .....	1939
"Electron Optics", E. G. Ramberg and G. A. Morton, <i>Jour. Appl. Phys.</i> (July) .....	1939
"Luminescent Materials", H. W. Leverenz (Coauthor), <i>Jour. Appl. Phys.</i> (July) .....	1939
"Survey of Radio Tube Sales for 1938", E. W. Wilby, <i>RCA Licensee Bulletin LB-491</i> (August) .....	1939
"Contrast in Kinescopes", R. R. Law, <i>Proc. I.R.E.</i> (August) .....	1939
"Recent Improvements in the Design and Characteristics of Iconoscopes", R. B. Janes and W. H. Hickok, <i>Proc. I.R.E.</i> (September) .....	1939
"Space Charge Effects in Electron Beams", A. V. Haeff, <i>Proc. I.R.E.</i> (September) .....	1939
"Television Pickup Tubes Using Low-Velocity Beam Scanning", A. Rose and H. Iams, <i>Proc. I.R.E.</i> (September) .....	1939
"The Class A-B Push-Pull Recording Systems", C. Hawley Cartwright and W. S. Thompson, <i>Jour. Soc. Mot. Pic. Eng.</i> (September) ....	1939

	Year
"The Electrostatic Electron Multiplier", V. K. Zworykin and J. A. Rajchman, <i>Proc. I.R.E.</i> (September) .....	1939
"The Image Iconoscope", H. Iams, G. A. Morton, and V. K. Zworykin, <i>Proc. I.R.E.</i> (September) .....	1939
"Point Projector Electron Microscope", G. A. Morton and E. G. Ramberg, <i>Phys. Rev.</i> (October) .....	1939
"Television Signal-Frequency Circuit Considerations", Garrard Mountjoy, <i>RCA Review</i> (October) .....	1939
"The Orthicon, a Television Pickup Tube", A. Rose and H. Iams, <i>RCA Review</i> (October) .....	1939
"Miniature Battery Tubes", K. G. Bucklin, <i>Electronics</i> (November) .....	1939
"The Anode-Tank-Circuit Magnetron", Ernest G. Linder, <i>Proc. I.R.E.</i> (November) .....	1939
"A Direct Reading Vacuum Tube Mille-Voltmeter for Bio-Electric Studies", Walter Lyons and R. E. Heller, <i>Electronics</i> (November) .....	1939
"A Change in Maximum Ratings of Receiver Tubes", <i>RCA Tube Dept. Applic. Note No. 105</i> (November 15) .....	1939
"Performance of 6AC7 Tube as a Television Converter", A. E. Newlon, <i>RCA Licensee Bulletin LB-501</i> (December) .....	1939
"Electron Optics of Cylindrical Electrical and Magnetic Fields", Albert Rose, <i>Proc. I.R.E.</i> (January) .....	1940
"Fluctuations in Space-Charge-Limited Currents at Moderately High Frequencies—Part I", B. J. Thompson, D. O. North and W. A. Harris, <i>RCA Review</i> (January) .....	1940
"Recent Advances in Barium Getter Technique", E. A. Lederer, <i>RCA Review</i> (January) .....	1940
"Simplified Television I-F Systems", Garrard Mountjoy, <i>RCA Review</i> (January) .....	1940
"Superheterodyne Converter System Considerations in Television Receivers", E. W. Herold, <i>RCA Review</i> (January) .....	1940
"A Cathode Ray Frequency Modulation Generator", Robert E. Shelby, <i>Electronics</i> (February) .....	1940
"A Behavior of Willemite Under Electron Bombardment", G. A. Morton and E. R. Piore, <i>Jour. Appl. Phys.</i> (February) .....	1940
"Untuned Radio-Frequency Amplifiers", C. W. Finnigan, <i>RCA Licensee Bulletin LB-508</i> (February 2) .....	1940
"Wide-Band Inductive Output Amplifier", A. V. Haeff and L. S. Nergaard, <i>Proc. I.R.E.</i> (March) .....	1940
"The Formation and Maintenance of Electron and Ion Beams", L. P. Smith and P. L. Hartman, <i>Jour. Appl. Phys.</i> (March) .....	1940
"Signal Generators for Frequency Modulated Waves", J. A. Rankin and D. E. Foster, <i>RCA Licensee Bulletin LB-514</i> (March 5) .....	1940
"Design of Superheterodyne Intermediate-Frequency Circuits", F. E. Spaulding, Jr., <i>RCA Review</i> (April) .....	1940
"Development and Production of the New Miniature Battery Tubes", N. R. Smith and A. H. Schooley, <i>RCA Review</i> (April) .....	1940
"Fluctuations in Space-Charge-Limited Currents at Moderately High Frequencies—Part II", B. J. Thompson, D. O. North, and W. A. Harris, <i>RCA Review</i> (April and July) .....	1940
"Simple Methods for Checking R-F Distortion or Cross-Modulation of Pentode Amplifier Tubes", E. W. Herold, <i>Electronics</i> (April) .....	1940
"U.H.F. Oscillator Frequency Stability Considerations", S. W. Seeley and E. I. Anderson, <i>RCA Licensee Bulletin LB-524</i> (May 6) .....	1940
"A V-T Voltmeter for Coaxial Line Measurements", G. L. Usselman, <i>Electronics</i> (July) .....	1940
"Flash-Arc Currents in Transmitter Tubes", J. C. Walter, <i>Broadcast News</i> (July) .....	1940
"Optimum Efficiency Conditions for White Luminescent Screens in Kinescopes", H. W. Leverenz, <i>Jour. Opt. Soc. Amer.</i> (July) .....	1940
"Reactance Tube Frequency Modulators", M. G. Crosby, <i>QST</i> (June) .....	1940
<i>RCA Review</i> (July) .....	1940



	Year
"U-H-F Oscillator Stability Considerations", E. I. Anderson, S. W. Seeley, and W. Stuart, <i>RCA Review</i> (July) .....	1940
"Space Charge Limitations on the Focus of Electron Beams", B. J. Thompson and L. B. Headrick, <i>Proc. I.R.E.</i> (July) .....	1940
"A New High Sensitivity Photosurface", A. M. Glover and R. B. Janes, <i>Electronics</i> (August) .....	1940
"Materials Used in Vacuum Tube Manufacture", A. J. Monack, <i>Jour. Ind. Eng. Chem.</i> (August) .....	1940
"Fluctuations in Space-Charge-Limited Currents at Moderately High Frequencies—Part III", B. J. Thompson, D. O. North, and W. A. Harris, <i>RCA Review</i> (October) .....	1940
"Cathodoluminescence as Applied in Television", H. W. Leverenz, <i>RCA Review</i> (October) .....	1940
<i>Jour. Tele. Soc. (Brit.)</i> (June) .....	1941
"A New Electron Microscope", L. Morton, M. C. Banca, and J. F. Bender, <i>RCA Review</i> (October) .....	1940
"Survey of Radio Tube Sales for 1939", E. W. Wilby, <i>RCA Licensee Bulletin LB-536</i> (October 2) .....	1940
"A Mechanical Model for the Motion of Electrons in a Magnetic Field", Albert Rose, <i>Jour. Appl. Phys.</i> (November) .....	1940
"Fresnel Diffraction of Electrons as a Contour Phenomenon in Electron Supermicroscope Images", J. Hillier, <i>Phys. Rev.</i> (November) .....	1940
"Effect of Temperature on Frequency of 6J5 Oscillator", <i>RCA Tube Dept. Applic. Note No. 108</i> (November 13) .....	1940
"Operation of Fifty Milliampere Tubes by the 117N7-GT", <i>RCA Tube Dept. Applic. Note No. 109</i> (November 13) .....	1940
"An Improved Inter-Electrode Capacitance Meter", A. A. Barco, <i>RCA Licensee Bulletin LB-541</i> (November 19) .....	1940
"An Electrical-Focused Multiplier Phototube", J. A. Rajchman and R. L. Snyder, <i>Electronics</i> (December) .....	1940
"The RCA Miniature Tubes", <i>RCA Tube Dept. Applic. Note No. 106</i> .....	1940
"A Miniature-Tube Hearing-Aid Amplifier for Use With an Air-Conduction Earpiece", <i>RCA Tube Dept. Applic. Note No. 107</i> .....	1940
"A New Ultra-High Frequency Tetrode and Its Use in a One Kilowatt Television Sound Transmitter", A. K. Wing and F. E. Young, <i>Proc. I.R.E.</i> (January) .....	1941
"A Transmitter for Frequency Modulated Broadcast Service Using a New Ultra-High-Frequency Tetrode", A. K. Wing and J. E. Young, <i>RCA Review</i> (January) .....	1941
"Cascade Amplifiers with Maximal Flatness", V. D. Landon, <i>RCA Review</i> (January, April) .....	1941
"Fluctuations in Space-Charged-Limited Currents at Moderately High Frequencies—Part IV", B. J. Thompson, D. O. North and W. A. Harris, <i>RCA Review</i> (January) .....	1941
"Generation and Detection of Frequency Modulated Waves", S. W. Seeley, C. N. Kimball and A. A. Barco, <i>RCA Licensee Bulletin LB-546</i> (January 7) .....	1941
"I-F Amplifier Design for Battery Receivers", D. E. Foster and G. Mountjoy, <i>RCA Licensee Bulletin LB-544</i> (January 7) .....	1941
"Fluctuations Induced in Vacuum-Tube Grids at High Frequencies", W. R. Ferris and D. O. North, <i>Proc. I.R.E.</i> (February) .....	1941
"The Electron Optics of the Electron Microscope", J. Hillier, <i>Jour. Bacteriology</i> (February) .....	1941
"Instantaneous Plate-Voltage Capability of RCA-6L6, <i>RCA Tube Dept. Applic. Note No. 110</i> (March 4) .....	1941
"The New High-Transconductance R-F Pentode RCA 68G7", <i>RCA Tube Dept. Applic. Note No. 111</i> (March 4) .....	1941
"A New Series of Insulators for Ultra-High Frequency Tubes", L. R. Shardlow, <i>RCA Review</i> (April) .....	1941

	Year
"An Electron Microscope for Practical Laboratory Service", V. K. Zworykin, J. Hillier and A. W. Vance, <i>Elec. Eng.</i> (April) .....	1941
"Deflection and Impedance of Electron Beams at High Frequencies in The Presence of a Magnetic Field", L. Malter, <i>RCA Review</i> (April) .....	1941
"Fluctuations in Space-Charge-Limited Currents at Moderately High Frequencies—Part V", B. J. Thompson, D. O. North and W. A. Harris, <i>RCA Review</i> (April and July) .....	1941
"Recent Developments in the Electron Microscope", J. Hillier and A. W. Vance, <i>Proc. I.R.E.</i> (April) .....	1941
"Use of the RCA 6SF7", <i>RCA Tube Dept. Applic. Note No. 112</i> (April 8) .....	1941
"Characteristics of Converters for Broadcast Receivers", C. W. Finnigan, <i>RCA Licensee Bulletin LB-563</i> (June 20) .....	1941
"Recent Developments in Phototubes", R. B. Janes and A. M. Glover, <i>RCA Review</i> (July) .....	1941
"The Equivalent Characteristics of Vacuum Tubes Operating in Feedback Circuits", J. H. Pratt, <i>RCA Review</i> (July) .....	1941
"Properties of Untuned R-F Amplifier Stages", <i>RCA Tube Dept. Applic. Note No. 116</i> (July 2) .....	1941
"A Review of the Development of Sensitive Phototubes", A. M. Glover, <i>Proc. I.R.E.</i> (August) .....	1941
"Applications of the Inductive Output Tube", O. E. Dow, <i>Proc. Rad. Club Amer.</i> (August) .....	1941
"New Sensitive and Inexpensive Gas-Control Tubes", W. E. Bahls, <i>Electronics</i> (September) .....	1941
"Silver-Magnesium Alloy as a Secondary Electron Emitting Material", V. K. Zworykin, J. E. Ruedy and E. W. Pike, <i>Jour. Appl. Phys.</i> (September) .....	1941
"Low Capacitance A-C Power Supplies", G. Mountjoy and C. W. Finnigan, <i>RCA Licensee Bulletin LB-575</i> (September 3) .....	1941
"A Preliminary Report on the Development of a 300-kilovolt Magnetic Electron Microscope", V. K. Zworykin, J. Hillier, and A. W. Vance, <i>Jou. Appl. Phys.</i> (October) .....	1941
"A Discussion of the Fundamental Limit of Performance of an Electron Microscope", J. Hillier, <i>Phys. Rev.</i> (November) .....	1941
"Behavior of Electron Multipliers as a Function of Frequency", L. Malter, <i>Proc. I.R.E.</i> (November) .....	1941
"The Orbital-Beam Secondary-Electron Multiplier for Ultra-High Frequency Amplification", H. M. Wagner and W. R. Ferris, <i>Proc. I.R.E.</i> (November) .....	1941
"Voltage-Controlled Electron Multipliers", B. J. Thompson, <i>Proc. I.R.E.</i> (November) .....	1941
"Design Precaution for Oscillators Employing Filament-Type Tubes", <i>RCA Tube Dept. Applic. Note No. 117</i> (December 22) .....	1941
"Electron Optics", G. A. Morton, Section of PROGRESS OF SCIENCE, Grolier Society, Chicago, Ill. ....	1941

## APPENDIX II

### LIST OF APPLICATION NOTES (1933-1941)

While the RCA Application Notes published by the RCA Tube Department before World War II are out of print and extra copies are no longer available, the list below is included to provide a convenient additional reference source for the many organizations and engineers who have maintained files of the notes.

#### APPLICATION NOTES

NUMBER	YEAR	TITLE
AN-1	1933	Use of the 77 as a Biased Detector with 100 Volts Plate Supply
AN-2	1933	Use of the 57 as a Biased Detector Resistance-Coupled to a 2A5
AN-3	1933	Use and Operation of the 2A7 and 6A7 as Pentagrid Converters
AN-4	1933	The 2B7, 6B7, 55, 75, 77 & 85 as Resistance-Coupled Audio-Frequency Amplifiers
AN-5	1933	Application of the Type 79 Tube
AN-6	1933	Higher Voltage Ratings for the 36, 37, 38, 39/44, and 89
AN-7	1933	250-Volt Rating for the 79
AN-8	1933	2A6 as a Resistance-Coupled Audio-Frequency Amplifier
AN-9	1933	Recent Advances in Tube Design
AN-10	1933	Hum Elimination in Universal Receivers
AN-11	1933	The Use and Operation of the 25Z5
AN-12	1933	Half-Wave Operation of the 25Z5 with Separate Load Circuits for each Rectifier Unit
AN-13	1933	Recommended Operating Conditions for the 38, 41, 42, 43, and 89
AN-14	1933	Operating Conditions for the Type 53 Tube
AN-15	1933	The Operation of the Type 48 Tube as a Triode
AN-16	1933	The Operation of the 2B7, or 6B7, as a Reflex Amplifier
AN-17	1933	Special Applications of the Type 53 Tube
AN-18	1933	Operation Conditions for the Type 19 Tube
AN-19	1933	Operating Conditions for the 1A6 as an Oscillator-Mixer
AN-20	1933	An Increase in the Maximum Allowable Grid Resistor for Types 38, 41, 42, 89, and 2A5
AN-21	1933	Operation Characteristics of the Type 1-v and the Type 12Z3 Tube
AN-22	1933	The Operation of the 2A6, 2B7, 6B7, 55, 75, 77, and 85 as Resistance-Coupled Audio-Frequency Amplifiers

NUMBER	YEAR	TITLE
AN-23	1933	The Operating Characteristics of the Type 84 Tube
AN-24	1933	Use of the 1A6 as a Half-Wave Diode-Tetrode
AN-25	1933	Influence of Circuit Constants on Receiver Output Noise
AN-26	1933	The 37, 56, 57, and 77 Tubes as Resistance-Coupled High-Voltage Amplifiers
AN-27	1933	Use of Pentagrid Converter Tubes in Multi-Range Receivers
AN-28	1933	Special Applications of the Type 79 Tube
AN-29	1933	Design of Audio Systems Employing Type 2A3 Power Amplifier Triodes
AN-30	1934	Characteristics of the 6F7 Tube
AN-31	1934	Operating Considerations of Cathode-Ray Tubes 905 and 906 for Oscillographic Purposes
AN-32	1934	Revision of Characteristics for the Type 48 Tube
AN-33	1934	RCA-800 in Class B Audio Amplifiers
AN-34	1934	Characteristics of the 868 Phototube
AN-35	1934	Triode Operation of Type 42 and Type 2A5 Pentodes
AN-36	1934	Lissajou's Figures
AN-37	1934	100-Volt Operation of 6C6 and 6D6 Tubes
AN-38	1934	A Simple Method for Converting Pentode Characteristics
AN-39	1934	The Design of a Voltage Supply for the 905 and 906 Cathode-Ray Tubes
AN-40	1934	High Power Output from Type 45 Tubes
AN-41	1934	The 1C6
AN-42	1934	Short-Cut Method for Determining Operating Conditions of Power Output Triodes
AN-43	1934	Cathode-Ray Curve-Tracing Apparatus for Aligning Tuned Circuits
AN-44	1934	Operating Conditions for the 6A6
AN-45	1935	Use of the 57 or 6C6 to Obtain Negative Transconductance and Negative Resistance
AN-46	1935	The Design of Six-Volt Battery-Operated Receivers
AN-47	1935	The Use of the 954 as a Vacuum-Tube Voltmeter
AN-48	1935	Graphical Determination of the Decrease in Inductance Produced by a Coil Shield
AN-49	1935	Construction of a Top-Cap Shield for Metal Tubes
AN-50	1935	Operation of the 6L7 as a Mixer Tube
AN-51	1935	The 6F5
AN-52	1935	Class AB Operation of Type 6F6 Tubes Connected as Triodes
AN-53	1935	The 6L7 as a Volume Expander for Phonographs
AN-54	1935	Class AB Operation of Type 6F6 Tubes Connected as Pentodes
AN-55	1935	Operation of the 6A8

NUMBER	YEAR	TITLE
AN-56	1936	Receiver Design
AN-57	1936	The 6L7 as an R-F Amplifier
AN-58	1936	Receiver Design
AN-59	1936	Operation of the 6Q7
AN-60	1936	Operation of the 6L6
AN-61	1936	The Conversion of a 6L6 Plate Family to New Screen Voltage Conditions
AN-62	1936	A New Operating Condition for Two Type 6F6 Tubes Connected as Pentodes
AN-63	1936	A High-Gain Single-Tube Phase Inverter
AN-64	1936	Inverse-Feedback Circuits for A-F Amplifiers
AN-65	1936	Tuning-Indicator Circuits for the 6E5 and 6G5
AN-66	1936	Equal Plate and Screen Voltage Operation of the 6L6
AN-67	1937	Resistance-Coupled Audio-Frequency Amplifiers
AN-68	1937	A 55-Watt Amplifier Using Two Type 6L6 Tubes
AN-69	1937	250-Volt, Low-Current Operation of the 6L6
AN-70	1937	An Exposure Meter for Cathode-Ray Oscillographs
AN-71	1937	Low-Current, High-Power Operation of Two 6L6's Connected in Push-Pull
AN-72	1937	A 40-Watt Operating Condition for Two Type 6L6 Tubes
AN-73	1937	Operation of the 25L6 in Typical Circuits
AN-74	1937	A New High-Voltage Choke-Input Rating for the 5T4
AN-75	1937	Receiver Design
AN-76	1937	An Audio-Frequency Curve Tracer Using a Cathode-Ray Tube
AN-77	1937	Dimensions of Popular Tube Types
AN-78	1937	Use of the Plate Family in Vacuum-Tube Power-Output Calculations
AN-79	1937	Significance of Ratings for Power Output Tubes
AN-80	1937	Operation of the 6V6-G
AN-81	1937	A Two-Terminal Oscillator
AN-82	1938	Wide-Angle Tuning with the 6E5, 6G5, or 6U5
AN-83	1938	Resistance-Coupled Amplifier Data for the 6L5-G, 6T7-G, and 6S7-G
AN-84	1938	The Operation of Phototubes
AN-85	1938	Operation of the 6AC5-G
AN-86	1938	Operation of the 6Y6-G
AN-87	1938	The 6K8 — A New Converter Tube
AN-88	1938	Hum in Heater-Type Tubes
AN-89	1938	Receiver Design
AN-90	1938	Resistance-Coupled Amplifier Data for the 6C8-G, 6F8-G, 6J5, 6J5-G, and 6Z7-G
AN-91	1938	Operation of the Gas-Triode 0A4-G
AN-92	1938	Operation of the Improved Type 906 Cathode-Ray Tube at Low Voltages
AN-93	1938	An Inverse-Feedback Circuit for Resistance-Coupled Amplifiers

NUMBER	YEAR	TITLE
AN-94	1938	Operation of the 6AF6-G
AN-95	1938	Operating Positions of Receiving Tubes
AN-96	1938	A Voltage Regulator for D-C Power Supplies
AN-97	1938	A Self-Balancing Phase-Inverter Circuit
AN-98	1938	The Operation of Single-Ended Tubes
AN-99	1938	Revision of 6K8 Ratings
AN-100	1938	Operation of the 6SA7
AN-101	1939	Input Loading of Receiving Tubes at Radio Frequencies
AN-102	1939	The 6SK7 as an I-F Amplifier
AN-103	1939	Operation of the 35L6-GT
AN-104	1939	A Television Bibliography and RMA Television Standards
AN-105	1939	A Change in Maximum Ratings of Receiver Tubes
AN-106	1940	The RCA Miniature Tubes
AN-107	1940	A Miniature-Tube Hearing-Aid Amplifier for use with an Air-Conduction Earpiece
AN-108	1940	Effect of Temperature on Frequency of 6J5 Oscillator
AN-109	1940	Operation of Fifty Milliampere Tubes by the 117N7-GT
AN-110	1941	Instantaneous Plate-Voltage Capability of RCA-6L6
AN-111	1941	The New High-Transconductance R-F Pentode RCA-6SG7
AN-112	1941	Use of the RCA-6SF7
AN-113	1941	Precaution in Assembly of Receivers Employing Button-Base Tubes
AN-114	1941	Use of Cushioned Sockets in Small Receivers
AN-115	1941	A Discussion of Noise in Portable Receivers
AN-116	1941	Properties of Untuned R-F Amplifier Stages
AN-117	1941	Design Precaution for Oscillators Employing Filament-Type Tubes



